5. ALTERNATIVE C, YEAR 0, WINTER CONDITIONS

This section presents the results of the Alternative C, year 0, simulation under winter conditions, including a comparison with baseline winter conditions. The analysis presented utilizes the same approach presented in Section 4 for ease of comparison between simulations, and the results are very similar to those presented for summer conditions. Of note during the winter analysis period is a storm event which begins on February 24 and affects slough hydrodynamics around the whole South Bay. Under winter conditions, the reduction in tidal range is less pronounced in the far South Bay, and the increases in water levels associated with LLW are less asymmetric. During the storm event, the tidal damping in the slough channels is reduced, and the increased mixing between the sloughs and the Bay, coupled with the off-channel pond volume, help keep slough salinities high, thus reducing salinity variability in the tidal sloughs in response to temporarily high freshwater tributary inflows.

An additional dynamic occurring in the model that was not evident in the summer simulation presented in Section 4 was the re-routing of flow observed in the Eden Landing pond complex during the storm event. A portion of the high flows in the ACFCC was captured by the Eden Landing ponds and routed through the ponds and into Old Alameda Creek, increasing the tidal prism and velocities in Old Alameda Creek. This re-routing of flows could have potential flood protection benefit implications in the ACFCC as water levels and velocities did not increase appreciably in the flood control channel in response to the moderate storm event.

As discussed in Section 4, this simulation represents a hypothetical and conservative case where all tidally-restored ponds are restored at year 0 – phasing is not considered. Therefore, the results presented in this section are likely an overstatement of the potential impacts. In reality, the restoration will be phased over many years, thereby reducing the magnitude of the project's impacts.

The model predictions are analyzed using time series at stations throughout the South Bay. Figure 4-1 through Figure 4-4 show the station locations for the South Bay and three pond complexes. The model predictions are also analyzed at specific snapshots in time for the entire South Bay and the pond complexes. The sections below present the results with respect to water levels, tidal prism, salinity, circulation and bed shear stress.

5.1 Water Levels

This section presents the model results with respect to water levels in the South Bay, the tidal sloughs and the ponds under Alternative C, year 50, winter conditions. The model predictions are compared to baseline winter predictions in order to assess the short-term impacts associated with opening 90 percent of the ponds to tidal action.

5.1.1 South Bay

In the South Bay, the modeled water levels at the San Mateo and Dumbarton Bridges under Alternative C exhibit minimal change when compared with the baseline. Table 5-1 shows the water surface elevations and phase difference for the South Bay under Alternative C winter conditions. Positive water surface elevation values in Table 5-1 represent an increase in water surface elevation when compared with baseline conditions, and negative values represent a decrease in water surface elevation. Positive phase values correspond to a slower arrival time under Alternative C, or a phase lag when compared with baseline conditions, whereas negative values represent that modeled water levels under Alternative C are leading baseline conditions.

At the San Mateo Bridge (Figure 5-1), LLW increases by approximately 1 cm under both neap and spring conditions (see Table 5-1), and higher high water (HHW) decreases by approximately 1 cm. At the Dumbarton Bridge (Figure 5-2), LLW increases by approximately 2 cm under neap tide and 1 cm under spring tide, and HHW decreases by approximately 3 cm under neap tide and 4 cm under spring tide. The water level changes are relatively negligible north of the Dumbarton Bridge, and the differences are similar to the level of accuracy of the model calibration with respect to tidal amplitudes. The model predicts no noticeable change in phase relative to baseline conditions at either bridge station.

Within the far South Bay, water level and phase changes under Alternative C become more pronounced. At Channel Marker 17 (Figure 5-3), located near the mouth of Coyote Creek, LLW increases by approximately 5 cm under neap tide and 11 cm under spring tide, and HHW decreases by approximately 6 cm under neap tide and 8 cm under spring tide. When compared with summer conditions under Alternative C (see Table 4-1), the far South Bay experiences a smaller reduction in tidal amplitude, and the increase in water level associated with LLW is less pronounced.

Although the tidal amplitude changes are small, the long-term trend in reduced tidal amplitude (decrease in high water levels and increase in low water levels) would lead to an increase in the MLLW tidal datum, and a decrease in the MHHW tidal datum. Figure 5-4 depicts the change in MLLW in response to the tidal restoration. The increase in MLLW is most pronounced in the far South Bay, with the change trending toward zero just north of the San Mateo Bridge. Similar changes are seen with respect to MHHW (Figure 5-5), with the largest reduction occurring in the far South Bay, and the reduction trending toward zero just north of the San Mateo Bridge.

Harmonic analysis was performed on water levels at several stations along the main South Bay channel, and the computed phase and amplitudes of the M_2 and K_1 tidal constituents for baseline and Alternative C year 0 conditions are compared (Figure 5-6). By comparing the phase and amplitude of the two primary harmonic constituents along the centerline of the South Bay, it is possible to assess how the tidal restoration is affecting the tidal propagation within the South Bay. Figure 5-6a presents the computed phase of the M_2 and K_1 tidal constituents. Little difference is observed in the South Bay as a result of the restoration project, which is consistent with Table 5-1. Figure 5-6b presents the computed amplitude of the M_2 and K_1 tidal constituents. As the tides propagate into the South Bay, the amplitude of both tidal constituents is decreased, with a more marked difference observed in the M_2 tidal constituent in the far South Bay.

Table 5-1. South Bay Tidal Water Surface Elevation and Phase Differences under Alt C, Year 0, Winter

(Water surface elevation differences in cm, phase differences in minutes. Feb 27 = neap tide, Mar 12 = spring tide.)

Station Name	**Feb 27 LLW**		**Feb 27 HHW**		**Mar 12 LLW**		**Mar 12 HHW**	
	WSE	**Phase**	**WSE**	**Phase**	**WSE**	**Phase**	**WSE**	**Phase**
San Mateo Bridge, Figure 5-1	1	0	-1	0	1	0	-2	0
Dumbarton Bridge, Figure 5-2	1	0	-3	0	2	0	-4	0
Channel Marker 17, Figure 5-3	5	10	-6	10	39	30	-8	0

5.1.2 Tidal Sloughs

As with the summer condition simulation (Section 4), Alternative C has a significant effect on modeled tidal slough water levels within all the three pond complexes under winter conditions. This is expected as the tidally-restored ponds are breached directly to the tidal sloughs, and the volume of water exchanged through the breach represents a considerable increase over the existing, or baseline, tidal prism in the slough regardless of the increased freshwater inflow contributions occurring during winter. The overall magnitude of the effect on water levels within each slough is dependent on the baseline tidal prism, the tributary freshwater inflow, and the tidal prism added to the slough by the restored ponds. The bathymetry of the sloughs also plays an important role in determining the change in water levels. As described in Section 3.2, the bathymetry of the tidal sloughs was not altered under this simulation; therefore the sloughs are undersized relative to the newly restored flow conditions. As discussed in Section 2.3.5, some of the sloughs, particularly those in the Eden Landing and Ravenswood pond complex, are modeled with larger than actual channel widths due to limitations with respect to the grid resolution; therefore, the model results for these sloughs may underestimate the potential short-term changes in water levels.

Table 5-2 shows the water surface elevation and phase difference for the water levels under Alternative C at both upstream (landward) and downstream (near the mouth) stations in each tidal slough. Positive water surface elevation values in Table 5-2 represent an increase in water level when compared with baseline conditions, and negative values represent a decrease in water level. Positive phase values correspond to a slower arrival time under Alternative C, or a phase lag when compared with baseline conditions, whereas negative values represent that modeled water levels under Alternative C are leading baseline conditions. The neap tide period corresponds with a moderate storm event beginning February 24 and extending through February 28 when freshwater tributary inflows are higher. During this period, the change in water levels between baseline and Alternative C conditions is lessened; therefore the short-term impact of Alternative C on tidal slough water levels is less pronounced during high flow events.

Near slough mouths (downstream stations), the water level trends are similar to that seen under summer conditions (Table 4-2). For most sloughs, there is a moderate reduction of the water surface elevation at high water, and a larger increase in the water surface elevation at LLW when compared to baseline conditions. The larger increase in water levels at LLW reflects the influence of the channel geometry on the water level dynamics. At low water levels, the wetted cross-section area of the channel is small, yet it is draining a large surface area (e.g., the tidally-restored ponds). Therefore, in order to convey the larger volume of water, LLW is increased relative to baseline conditions. The relative difference between the wetted cross-sectional area under baseline and Alternative C, year 0 conditions is not as great at HHW, therefore a smaller difference is observed. Water levels downstream in Alviso Slough (Figure 5-17) provide an example of this response pattern. At both high water marks and higher low water (HLW), Alternative C predicts damping on the order of 20 – 60 cm during spring tide and by 10 – 30 cm during neap tide. In contrast, LLW is predicted to dampen by 60 – 90 cm during spring tide. The upstream stations experience similar changes in tidal amplitude relative to the downstream stations.

Phasing changes are relatively small at the downstream stations in the Eden Landing pond complex, with Alternative C lagging behind baseline conditions by approximately 30 – 40 minutes during neap and spring tides. In the Ravenswood pond complex, Alternative C lags behind baseline conditions on the order of 70 – 110 minutes during neap tide 50 – 90 minutes during spring tide downstream in Ravenswood Slough (Figure 5-28), with smaller phase lags observed upstream (Figure 5-29). In the Alviso pond complex, phase changes vary considerably depending on the volume of the freshwater tributary inflows and the increase in tidal prism. Downstream in Alviso Slough (Figure 5-17), Alternative C lags winter baseline conditions on the order of 40 – 70 minutes on spring and neap tides. In Guadalupe Slough (Figure 5-19), Alternative C lags baseline conditions on the other of 10 – 20 minutes under neap tides, with a phase lag of approximately 90 minutes on LLW under spring tide conditions.

Table 5-2. Tidal Slough Water Surface Elevation and Phase Differences under Alt C, Year 0, Winter

(Water surface elevation differences in cm, phase differences in minutes. Feb 27 = neap tide, Mar 12 = spring tide.)

Station Name	Feb 27 LLW		Feb 27 HHW		Mar 12 LLW		Mar 12 HHW	
	WSE	Phase	WSE	Phase	WSE	Phase	WSE	Phase
Eden Landing pond complex								
ACFCC Downstream, Figure 5-7	7	30	-14	40	35	30	-28	40
ACFCC Upstream, Figure 5-8	0	-10	-11	60	4	10	-31	20
Old Alameda Creek Downstream, Figure 5-9	6	10	-10	0	38	20	-16	0
Old Alameda Creek Upstream, Figure 5-10	12	30	-21	80	48	40	-38	50
Alviso pond complex								
Coyote Creek Power Tower, Figure 5-11	13	10	-17	10	62	50	-24	0
Coyote Creek Railroad Bridge, Figure 5-12	24	40	-29	70	69	80	-48	0
Coyote Creek/Island Ponds , Figure 5-13	23	40	-30	80	68	70	-53	0
Coyote Creek Upstream, Figure 5-14	24	40	-31	80	68	70	-57	0
Mud Slough Downstream, Figure 5-15	24	30	-32	70	68	70	-48	10
Mud Slough Upstream, Figure 5-16	27	50	-34	110	66	60	-65	0
Alviso Slough Downstream, Figure 5-17	25	40	-29	60	90	70	-43	40
Alviso Slough Upstream, Figure 5-18	26	80	-33	130	86	100	-78	30
Guadalupe Slough Downstream, Figure 5-19	14	20	-11	10	86	90	-16	10
Guadalupe Slough Upstream, Figure 5-20	20	80	-37	120	86	110	-69	10
Moffett Channel, Figure 5-21	20	80	-37	120	86	110	-69	10
Stevens Creek Downstream, Figure 5-22	16	30	-13	40	26	0	-21	30
Stevens Creek Upstream, Figure 5-23	14	60	-16	70	26	10	-25	70
Mountain View Slough Downstream, Figure 5-24	29	90	-10	70	69	40	-18	60
Mountain View Slough Upstream, Figure 5-25	29	90	-10	70	66	30	-17	60
Charleston Slough Downstream, Figure 5-26	16	40	-10	60	51	30	-18	70
Charleston Slough Upstream, Figure 5-27	13	30	-10	80	46	30	-18	70
Ravenswood pond complex								
Ravenswood Slough Downstream, Figure 5-28	23	70	-27	110	69	50	-41	90
Ravenswood Slough Upstream, Figure 5-29	22	40	-8	30	63	30	-12	10

5.1.3 Ponds

Under baseline conditions, only the Island Ponds in the Alviso pond complex and the Eden Landing Ecological Reserve in the Eden Landing pond complex are open to tidal inundation. Restoring additional ponds to tidal action would therefore impact water levels within these existing restoration sites. Figure 5-30 displays the water level in the center of Pond A20. Under winter conditions, Pond A20 experiences a reduction in high water levels. Low water levels remain unchanged as Pond A20 sits relatively high in the tide frame, and the pond is effectively drained under low water conditions.

In the Eden Landing Ecological Reserve, water levels in the north wetlands remain largely unaffected (Figure 5-31). These wetlands are hydraulically connected to the South Bay via Mount Eden Creek, which experiences only a nominal increase in tidal prism under Alternative C. The southern wetlands are hydraulically connected to the South Bay via North Creek. The tidal prism in North Creek is expected to increase by approximately 380percent due to the tidal breaches under Alternative C (Figure 3-15); therefore the water levels in the southern wetlands experience reductions in tidal amplitude (a decrease in high water levels and an increase in low water levels). The increase in low water levels is fairly similar to the decrease in high water levels (Figure 5-32).

Ponds that are not hydraulically connected to the South Bay under baseline conditions (except by culverts and flap gates) would be connected under Alternative C through tidal breaches to the sloughs. The water levels in the ponds are therefore similar to that of the tidal sloughs. In the Eden Landing and Ravenswood ponds complexes, the pond bottom elevations are relatively high in the tide frame; therefore the ponds are only inundated during high tides. Figure 5-33 shows the water level variability in Pond E6B in the Eden Landing pond complex. This pond only experiences diurnal tidal variability during spring tides, and during neap tides, most of the pond area would be effectively drained. However, marsh channels inside the pond would likely exhibit more tidal variability.

In the Alviso pond complex, pond bottom elevations sit lower in the tide frame and the ponds are therefore exposed to diurnal tidal action throughout the spring-neap tide cycle. Ponds A7 and A8 (Figure 5-34 and Figure 5-35, respectively) provide an example of the tide range expected within the subsided ponds. In this case, the water levels are similar to that seen in Alviso Slough. Unlike Pond E6B and similar ponds with higher bottom elevations, Ponds A7 and A8 do not experience cycles of wetting and drying during the diurnal tidal cycle. Instead, the ponds contain water at all times. The tide range within any specific pond will depend on the location of its hydraulic connection to the Bay and the pond's elevation relative to the tides.

5.2 Tidal Prism

A comparison of the estimates of tidal prism between baseline and Alternative C, year 0, winter conditions is summarized in Table 5-3. A conventional definition of tidal prism is the volume of water exchanged over a complete tidal cycle. However, as discussed in Section 4.2, tidal prism has been estimated as the volume of water crossing a cross-section during a flood tide in order to compare the tidal prism estimates with previous studies.

Changes in tidal prism outside of the project area (i.e. at San Mateo Bridge, Dumbarton Bridge and non-project sloughs), are typically five percent or less. Overall, the changes in tidal prism associated with the sloughs within the three pond complexes under winter conditions are similar to those discussed in Section 4.2 for summer conditions.

Figure 5-36 displays the instantaneous modeled flux through San Mateo and Dumbarton Bridge cross-sections under baseline and Alternative C, year 0, winter conditions. At the San Mateo Bridge cross-section, little difference is evident. However, at the Dumbarton Bridge cross-section, the modeled flux decreases slightly under Alternative C conditions. This is consistent with the tidal prism estimates presented in Table 5-3. At a cross-section through Channel Marker 17, the modeled flux is slightly larger under Alternative C conditions when compared to baseline conditions (Figure 5-37). Further south at Calaveras Point, the modeled flux under Alternative C is noticeably larger than under baseline conditions, which is consistent with the 26 percent increase in tidal prism predicted in Table 5-3.

The tidal prism associated with the sloughs in the three pond complexes is predicted to increase. The increase is dependent on the volume of the tidally-restored ponds breached to particular slough and how accurately a slough is represented in the model. For example, the tidal prism in the ACFCC is predicted to increase by approximately 88 percent. In contrast, the tidal prism in Old Alameda Creek is predicted to increase by approximately 15 percent. As discussed in Section 4.2, this is likely an underestimate of the actual percentage increase in tidal prism as a result of the SBSP Restoration Project. The baseline tidal prism in Old Alameda Creek from estimated from GIS is 0.32 million cubic meters (Table 3-6), which is an order or magnitude less than the baseline estimate from the model of 1.6 million cubic meters (Table 5-3). However, the increase in tidal prism of 0.2 million cubic meters is likely representative of the added pond volume due to the restoration; therefore the tidal prism in Old Alameda Creek could increase approximately 67 percent (from 0.32 to 0.52 million cubic meters). Figure 5-38 presents the modeled flux through cross-sections near the mouths of the ACFCC and Old Alameda Creek under both baseline and Alternative C, year 0, summer conditions. The modeled flux is predicted to increase in both sloughs, with a larger increase associated with the ACFCC.

Along Coyote Creek, there is a progression of tidal prism changes (Figure 5-39). Near the mouth, at the Power Tower, the predicted increase is approximately ten million cubic meters. Since Coyote Creek is a large channel, this change represents an increase of only 42 percent over baseline conditions even though several large ponds would breach to this channel. Further up Coyote Creek, at the Railroad Bridge and east of the Island Ponds, the tidal prism decreases as a result of restoration. This decrease occurs because flows which reach these transects under baseline conditions are deflected into the newly breached ponds under Alternative C.

Alviso Slough and Guadalupe Slough are represented fairly well in the model, and the modeled flux at the downstream transects increases measurably in both sloughs (Figure 5-40), with an increase in tidal prism of approximately 200 percent predicted by the model (Table 5-3). An increase of approximately 310 percent is predicted for Mountain View Slough, a small slough that would connect two large ponds to the Bay. In addition, the large increase associated with Mountain View Slough is caused in part by a portion of Charleston Slough's existing and potential tidal prism being routed through the upstream breach to Pond A1 on Charleston Slough, through Pond A1, and into Mountain View Slough. Mountain View Slough is among those sloughs that are oversized in the model; therefore the actual percent increase in tidal prism may be larger; however, the baseline tidal prism and the Alternative C tidal prism are likely smaller than presented in Table 5-3. The same can be said for Charleston Slough and Stevens Creek. These sloughs have relatively little flow under baseline summer conditions, and the modeled flux at the downstream transects increases markedly under Alternative C, year 0, summer conditions (Figure 5-41 and Figure 5-42).

The model predicts a tidal prism increase of approximately 240 percent for Ravenswood Slough in the Ravenswood pond complex (Figure 5-42). Under baseline conditions, Ravenswood Slough's tidal prism is among the smallest of all the cross-section presented in Table 5-3. Hence, with the addition of nearly the entire complex's pond area to the slough's drainage area, the large increase is expected. Ravenswood Slough is also among those sloughs that are oversized in the model, as discussed in Section 2.3.5; therefore, the actual percent increase in tidal prism may be larger, while the tidal prism values are likely smaller.

The tidal prism within each slough may be larger than presented in Table 5-3 after sloughs scour and deepen and before pond sedimentation raises pond bottom elevations. Due to the subsided nature of the ponds within the Alviso pond complex, this potential increase in tidal prism would be greatest in the Alviso pond complex sloughs.

Table 5-3. Comparison of Tidal Prism between Baseline and Alternative C, Year 0, Winter

Transect location	Tidal prism (millions of cubic meters)		
	Baseline winter	**Alternative C year 0, winter**	**% change baseline to Alt. C**
South Bay			
San Mateo Bridge	270	270	-2.6%
Dumbarton Bridge	74	72	-3.0%
Eden Landing pond complex			
ACFCC	1.4	2.7	88%
Old Alameda Creek	1.6	1.8	15%
Mount Eden Creek	0.75	1.0	37%
Ravenswood pond complex			
Ravenswood Slough	0.58	2.0	240%
Alviso pond complex			
Calaveras Point	15	19	26%
Coyote Creek at Power Tower	7.3	10	42%
Coyote Creek at RR Bridge	2.5	1.7	-30%
Coyote Creek east of Island Ponds	0.51	0.38	-26%
Charleston Slough	0.65	1.2	77%
Mountain View Slough	0.24	0.98	310%
Stevens Creek	0.13	0.30	120%
Guadalupe Slough	1.1	3.3	190%
Alviso Slough	1.1	3.3	200%
Artesian Slough	0.50	0.64	27%
Mud Slough	0.86	0.91	5.9%
Non-project Sloughs			
Corkscrew Slough	3.6	3.6	-1.1%
Redwood Creek	17	16	-2.8%
Westpoint Slough	3.1	3.0	-1.3%
Mowry Slough	0.49	0.46	-6.3%
Plummer Slough	0.34	0.33	-2.8%
Newark Slough	0.98	0.95	-3.1%

5.3 Salinity

This section presents the model results with respect to salinity in the South Bay and the tidal sloughs under Alternative C, year 0, winter conditions. The model predictions are compared to baseline winter predictions in order to assess the impact of opening 90 percent of the ponds to tidal action. The SBSP Restoration Project has the potential to alter the salinity regimes within the South Bay, as presented in the sections below.

Modeled salinity within the South Bay is highly dependent on the initial salinity condition, particularly in the summer when residence times in the South Bay are at their longest. Residence times decrease in the winter due to the influence of higher tributary inflows (Walters and others 1985). As discussed in Section 3.2.2, the initial salinity prescribed within the ponds was set by the salinity in the neighboring tidal sloughs, which likely underestimates salinity levels within the ponds at the time of breaching. This underestimation is most pronounced in the Alviso pond complex where salinities are lowest due to freshwater tributary inflows and the WWTP discharges.

Unlike the simulation for Alternative C under summer conditions (Section 4.3), equilibrium conditions with respect to salinity were met within the tidal sloughs and the far South Bay during the winter analysis period. The high freshwater tributary inflows lowered the residence time in the tidal sloughs, allowing equilibrium conditions to be met fairly rapidly. The analysis period includes both increased tributary freshwater inflows and a high flow event occurring in late February.

5.3.1 South Bay

Under Alternative C, immediately after restoring 90 percent of the ponds to tidal action, little change is seen with respect to salinity north of the Dumbarton Bridge (Table 5-4). Positive values in Table 5-4 represent an increase in salinities relative to the baseline, and negative values represent a decrease in salinities relative to baseline conditions. At the San Mateo and Dumbarton Bridges, there is no significant difference in salinity when compared with baseline conditions (Figure 5-43 and Figure 5-44, respectively).

At Channel Marker 17 (Figure 5-45), little change in salinity is observed at high water levels; however, at higher low water, salinities are 0 – 5 ppt higher than baseline conditions, and at LLW, salinities are 5 – 10 ppt higher. The salinity changes are correlated with the changes in water levels and the increase in tidal prism and mixing observed at this station, with the largest changes occurring at LLW.

Figure 5-46 displays the salinities in the South Bay during spring conditions at HHW, representing peak salinity conditions during the analysis period. As can be seen, little difference in peak South Bay salinities occurs under winter conditions with respect to Alternative C. The largest changes in salinity are confined to the tidal sloughs. Figure 5-47 displays South Bay salinities at LLW during spring tide conditions. At low water, the observed differences are higher downstream of the tidal sloughs under Alternative C, year 0, winter conditions.

Table 5-4. South Bay Salinity Differences under Alt C, Year 0, Winter
(Salinity differences in ppt. Feb 27 = neap tide, Mar 12 = spring tide.)

Station Name	Feb 27 LLW	Feb 27 HHW	Mar 12 LLW	Mar 12 HHW
San Mateo Bridge, Figure 5-43	-0.1	-0.0	-0.0	-0.0
Dumbarton Bridge, Figure 5-44	-0.3	-0.1	-0.2	-0.0
Channel Marker 17, Figure 5-45	4.1	2.0	3.8	0.3

5.3.2 Tidal Sloughs

Within the tidal sloughs, the changes to salinity levels with respect to baseline conditions show similar trends to the changes in water levels. Table 5-5 shows the salinity difference under Alternative C for neap and spring tide winter conditions. Positive values represent an increase in salinities relative to the baseline, and negative values represent a decrease in salinities relative to baseline conditions.

In the Eden Landing pond complex, salinities downstream in the ACFCC increase relative to baseline winter conditions, with the most significant changes occurring at low water levels when salinities are approximately 10 ppt higher than baseline conditions (Figure 5-48). During the moderate storm event when freshwater tributary inflows increase and depress salinities within the slough beginning February 24, the decrease in slough salinities is not as pronounced as observed in the baseline simulation. Under baseline simulation, the entire downstream section of the ACFCC becomes fresh. Under Alternative C, the increased tidal exchange and mixing between the sloughs and the South Bay, coupled with the volume of higher salinity water from the tidally-restored ponds, allows a diurnal salinity signal to remain during the storm event. Salinities fluctuate between 0 and 10 ppt during this period under Alternative C conditions. Upstream in the ACFCC, there is no change in salinities with respect to baseline conditions for the duration of the analysis period as this station is entirely fresh in response to winter tributary inflows (Figure 5-49).

In Old Alameda Creek, salinities are depressed relative to baseline conditions both downstream and upstream under Alternative C (Figure 5-50 and Figure 5-51, respectively). This decrease in salinities is due to freshwater inflows from the ACFCC flowing through the ponds and into Old Alameda Creek. This dynamic can be seen on Figure 5-52 and Figure 5-53 which depict salinities within the Eden Landing pond complex during spring tide at HHW and LLW. This flow path can be prevented during the project-level design phase if desired. This dynamic was not observed during summer conditions (Section 4), therefore it might only occur under storm conditions when flows in the ACFCC are high.

Within the tidal sloughs in the Alviso pond complex, the salinity response is similar to that observed in the ACFCC. Salinities at high water levels experience only minor changes on the order of 1 ppt at the downstream stations near the Bay. At the upstream stations, salinities are largely 0 ppt under baseline conditions due to freshwater tributary inflows. Under Alternative C, increased tidal exchange and mixing in the tidal sloughs and the contribution of higher salinity water from the tidally-restored ponds, pushes the salinity gradient upstream, increasing upstream salinities and providing for a moderate diurnal salinity signal. Figure 5-61 and Figure 5-63 provide an example of this effect in Alviso Slough and Guadalupe South, respectively.

During the moderate flow event beginning February 24, salinities under baseline conditions trend towards zero at low water at the downstream stations in Coyote Creek (Figure 5-54 and Figure 5-55), Mud Slough (Figure 5-58), Alviso Slough (Figure 5-60), and Guadalupe Slough (Figure 5-62). Under Alternative C, salinities are not depressed as significantly due to the increased tidal exchange and mixing. Therefore, the tidally-restored ponds help keep slough salinities high during a moderate storm event, thus reducing salinity variability occurring in response to temporarily high freshwater tributary inflows. At the upstream stations, the effect of the moderate storm can be seen as salinities decrease during the event (e.g., from 10 ppt on Feb 24 upstream in Guadalupe Slough to 4 ppt on Feb 28, Figure 5-63), and slowly increase following the event. Similar trends are seen in Coyote Creek, Alviso Slough, Stevens Creek, Mountain View Slough and Charleston Slough. The magnitude of the response depends on the increase in tidal prism relative to baseline conditions and the magnitude of the freshwater tributary inflows.

Figure 5-71 and Figure 5-72 depict salinities within the Alviso pond complex under Alternative C and baseline conditions during spring tide at both HHW and LLW, respectively. The greatest salinity differences occur within the tidal sloughs in the vicinity of the pond breaches at HHW, and in the downstream reaches of the sloughs and within the subtidal channels in the far South Bay at LLW.

Salinities downstream in Ravenswood Slough in the Ravenswood pond complex (Figure 5-73) are similar under both baseline and Alternative C conditions. At the upstream station (Figure 5-74), the salinity trend is similar to that observed in the Eden landing and Alviso pond complexes, with similar high water salinities when compared with baseline conditions, increased low water salinities, and a reduction in the upstream response to the moderate storm event beginning on February 24.

Figure 5-75 and Figure 5-76 depict salinities within the Ravenswood pond complex under Alternative C and baseline conditions during spring tide at both HHW and LLW, respectively. The greatest salinity differences occur within the tidal sloughs in the vicinity of the pond breaches at HHW, and in the downstream reaches of the sloughs and within the subtidal channels in the far South Bay at LLW.

Table 5-5. Tidal Slough Salinity Differences under Alt C, Year 0, Winter

(Salinity differences in ppt. June 13 = neap tide, June 22 = spring tide.)

Station Name	**Feb 27 LLW**	**Feb 27 HHW**	**Mar 12 LLW**	**Mar 12 HHW**
Eden Landing pond complex				
ACFCC Downstream, Figure 5-48	0.4	9.7	11.4	0.8
ACFCC Upstream, Figure 5-49	0.0	0.0	0.0	0.0
Old Alameda Creek Downstream, Figure 5-50	-5.0	-3.7	-2.7	-0.8
Old Alameda Creek Upstream, Figure 5-51	-7.7	-7.7	-4.2	-4.0
Alviso pond complex				
Coyote Creek Power Tower, Figure 5-54	4.4	4.4	4.1	0.6
Coyote Creek Railroad Bridge, Figure 5-55	1.5	5.9	2.4	0.8
Coyote Creek/Island Ponds , Figure 5-56	0.1	2.6	2.6	3.7
Coyote Creek Upstream, Figure 5-57	0.2	0.2	1.8	1.9
Mud Slough Downstream, Figure 5-58	3.7	6.8	4.8	3.6
Mud Slough Upstream, Figure 5-59	2.0	1.2	2.1	1.5
Alviso Slough Downstream, Figure 5-60	7.3	8.1	8.8	0.9
Alviso Slough Upstream, Figure 5-61	0.0	0.0	2.1	2.4
Guadalupe Slough Downstream, Figure 5-62	11.8	7.1	8.9	1.0
Guadalupe Slough Upstream, Figure 5-63	3.5	4.1	8.2	8.7
Moffett Channel, Figure 5-64	3.0	3.3	7.0	7.5
Stevens Creek Downstream, Figure 5-65	10.9	6.9	4.5	0.8
Stevens Creek Upstream, Figure 5-66	0.1	2.0	3.9	1.0
Mountain View Slough Downstream, Figure 5-67	12.3	8.4	4.2	1.0
Mountain View Slough Upstream, Figure 5-68	5.8	8.6	8.0	2.8
Charleston Slough Downstream, Figure 5-69	5.9	2.7	0.3	0.2
Charleston Slough Upstream, Figure 5-70	4.2	3.3	0.9	0.1
Ravenswood pond complex				
Ravenswood Slough Downstream, Figure 5-73	-0.5	-0.3	0.1	0.3
Ravenswood Slough Upstream, Figure 5-74	10.1	4.4	3.2	0.3

5.4 Circulation

As with summer conditions, potential changes to South Bay circulation can be evaluated by examining current velocities at specific locations within the Bay and tidal sloughs, and by examining general changes to South Bay residual circulation. The most important factor influencing circulation patterns in South Bay is bathymetry (Cheng and Gartner 1985). At year 0, the only bathymetric change associated with the simulation is hydraulically connecting the ponds to the Bay and re-introducing tidal action. This, in itself, represents a large-scale bathymetric change.

5.4.1 Current Velocity

South Bay

In the South Bay, modeled velocities at the San Mateo and Dumbarton Bridges exhibit little change relative to baseline conditions. Table 5-6 shows the peak modeled velocity magnitudes at the bridge and Channel Marker 17 stations under baseline and Alternative C conditions. Positive values indicate a higher modeled velocity magnitude under Alternative C, and negative values indicate a decrease in current velocity magnitude under Alternative C.

At the San Mateo Bridge (Figure 5-77), velocity magnitudes are slightly higher under Alternative C relative to baseline conditions, although the difference is relatively minor (approximately 2 cm/s). At the Dumbarton Bridge (Figure 5-78), velocity magnitudes decrease slightly relative to baseline conditions. This decrease is due in part to the undersized nature of the tidal sloughs and the potentially undersized nature of the main South Bay channel in the far South Bay which has experienced significant infilling in recent years (Jaffe and Foxgrover 2006b). The undersized channels restrict tidal exchange between the ponds and the northern reaches of the Bay.

In the far South Bay at Channel Marker 17 (Figure 5-79), velocity magnitude increases are more pronounced relative to baseline conditions due to the close proximity of the Alviso pond complex and the location of the station in the main South Bay channel. The peak modeled baseline velocity magnitude at Channel Marker 17 is 109 cm/s, compared with only 67 cm/s under summer conditions, owing to the moderate storm event and the increase in tributary inflows. Under Alternative C, the peak modeled velocity magnitude is 122 cm/s under winter conditions, compared with 119 cm/s under summer conditions. Although the peak velocities are similar under winter and summer conditions, the relative increase over baseline conditions is smaller under winter conditions. Under summer conditions, the velocity magnitude increases are strongest on ebb tides. Under winter conditions, the high tributary inflows contribute to increased winter baseline ebb velocities, therefore the additional effect of increasing the tidal prism is not as significant.

Figure 5-80 and Figure 5-81 depict velocity magnitudes within the South Bay under peak flood and peak ebb conditions under baseline and Alternative C conditions, as well as the difference between the two model predictions. As with summer conditions, the difference is strongest under spring ebb conditions near the mouths of the tidal sloughs and in the main South Bay channel. The differences under spring flood conditions are primarily seen near the mouths of the tidal sloughs.

Table 5-6. South Bay Peak Velocity Magnitude Comparisons: Alternative C, Winter, Year 0 vs. Baseline, Winter

(All velocities in cm/s)

Station Name	Baseline	Alt C	Difference
San Mateo Bridge, Figure 5-77	104	106	2
Dumbarton Bridge, Figure 5-78	35	32	-3
Channel Marker 17, Figure 5-79	109	122	13

Tidal Sloughs

In the South Bay, modeled velocities within the tidal sloughs experience significant changes in response to the restoration. The changes observed under winter conditions are similar to those seen under summer conditions described in Section 4.4.1. The majority of the tidal sloughs exhibit a flood-ebb asymmetry in the velocity increases due to the undersized nature of the sloughs, with a larger increase in modeled velocities observed on ebb tide. This asymmetry is expected to dissipate as the sloughs widen and deepen in response to the increased tidal prism. Table 5-7 shows the peak velocity magnitudes at the downstream stations in the tidal sloughs under baseline and Alternative C conditions. Positive values indicate a higher modeled velocity under Alternative C, and negative values indicate a decrease in current velocity under Alternative C.

In the Eden Landing pond complex, velocity magnitudes in the ACFCC increase significantly in response to the increased tidal prism, with velocity magnitudes increasing by a factor of 2 to 3 on strong ebb tides and a factor of two on flood tides (Figure 5-82). This increase is due to the relatively large increase in tidal prism associated with the restored ponds. Old Alameda Creek experiences a greater increase in velocities under winter conditions than observed under summer conditions, with increases throughout the analysis period on the order of 10 – 30 cm/s (Figure 5-83). A portion of this velocity magnitude increase is attributable to flow from the ACFCC being captured by the Eden Landing ponds and re-routed into Old Alameda Creek. This dynamic was not observed during summer conditions when flows were lower in the ACFCC. Figure 5-84 and Figure 5-85 depict the tidal slough velocities within the Eden Landing pond complex at both strong flood and strong ebb, respectively. At strong ebb, the largest differences are seen in the South Bay just beyond the slough mouth. At strong flood, the largest velocity magnitude differences relative to baseline conditions are seen in the downstream reaches of the sloughs. Unlike summer conditions, the differences in peak velocity magnitude are similar under strong ebb and strong flood conditions.

In the Alviso pond complex, velocity magnitudes at the downstream stations increase relative to baseline conditions. The magnitude of the increase is correlated with the associated increase in tidal prism. In Coyote Creek, stations at the Railroad Bridge (Figure 5-87) and at the upstream edge of the Island Ponds (Figure 5-88) are located upstream of the majority of the pond breaches. At these stations, velocity magnitudes decrease relative to baseline conditions due to the large percentage of the flow captured by the downstream ponds. As with summer conditions, velocities are also predicted to decrease in Charleston Slough (Figure 5-95) because the model predicts that a portion of Charleston Slough's existing and potential tidal prism is routed through the upstream breach to Pond A1 on Charleston Slough, through Pond A1, and into Mountain View Slough.

Figure 6-90 and Figure 6-91 depict the tidal slough velocity magnitudes within the Alviso pond complex at both strong flood and strong ebb, respectively. As with the Eden Landing pond complex, the largest differences under strong ebb conditions are seen in the far South Bay just beyond the slough mouth. At strong flood, the largest velocity differences relative to baseline conditions are seen in the downstream reaches of the tidal sloughs.

In Ravenswood Slough, peak velocity magnitudes increase by a factor of two with respect to baseline conditions under both ebb and flood conditions (Figure 5-98). Figure 5-99 and Figure 5-100 depict the tidal slough velocity magnitudes within the Ravenswood pond complex at both strong flood and strong ebb, respectively. As with the other pond complexes, the largest differences under strong ebb conditions are seen in the far South Bay just beyond the slough mouth, and at strong flood, the largest velocity differences relative to baseline conditions are seen in the downstream reach of the slough.

Table 5-7. Tidal Slough Peak Velocity Comparisons: Alternative C, Winter, Year 0 vs. Baseline, Winter
(All velocities in cm/s)

Station Name	**Baseline**	**Alt C**	**Difference**
ACFCC Downstream, Figure 5-82	48	103	56
Old Alameda Creek Downstream, Figure 5-83	55	77	22
Coyote Creek Power Tower, Figure 5-86	78	105	27
Coyote Creek Railroad Bridge, Figure 5-87	82	59	-23
Coyote Creek/Island Ponds, Figure 5-88	40	29	-11
Mud Slough Downstream, Figure 5-89	48	52	4
Alviso Slough Downstream, Figure 5-90	51	133	82
Guadalupe Slough Downstream, Figure 5-91	46	117	71
Moffett Channel , Figure 5-92	4	1	-3
Stevens Creek Downstream, Figure 5-93	53	102	49
Mountain View Slough Downstream, Figure 5-94	50	75	26
Charleston Slough Downstream, Figure 5-95	79	64	-15
Ravenswood Slough Downstream, Figure 5-98	41	87	46

5.4.2 Residual Circulation

The total residual current observed in the South Bay is a product of tidally-driven residual currents, as well as wind-driven and density-driven circulation patterns. Density-driven currents do exist in the South Bay under winter conditions when freshwater tributary inflows are high, and Delta inflows can intrude into the South Bay causing the main South Bay channel to stratify. However, density-driven processes are not well-represented by the 2D depth-averaged model formulation. Wind-driven circulation in the main South Bay channel is also not well-represented in a 2D model, as the wind can drive a surface flow in the direction of the wind, and a return flow in the deep channel. However, wind-driven flows are not as important to the total South Bay residual circulation patterns in the winter period when winds are typically lower.

The residual currents presented here are a product of tidally-driven and wind-driven circulation. In order to compare the potential impact to residual circulation within the South Bay under winter conditions, the velocities at each point in the model were averaged at two hour intervals over two spring-neap tidal cycles, or approximately 29 days (from February 14 to March 14).

Figure 5-101 displays the 29-day residual circulation under winter baseline conditions. In general, the residual circulation pattern is similar to summer conditions. However, there is a stronger net-northward residual current due to the freshwater tributary inflows in the far South Bay.

Figure 5-102 displays the 29-day residual circulation for Alternative C, with 90 percent of the ponds restored to tidal action, and Figure 5-103 displays the difference between the predicted residual circulation under baseline and Alternative C, winter conditions (Alternative C minus baseline). Little to no change in residual circulation is observed north of the San Mateo Bridge, and little change is observed near the Eden Landing pond complex. The increased tidal prism from the Ravenswood pond complex is observed in the residual currents from Ravenswood Slough.

Figure 5-104 displays the 29-day residual circulation under winter baseline conditions for the far South Bay, and Figure 5-105 displays the same under Alternative C, winter conditions, while Figure 5-106 displays the difference. The increased tidal prism associated with each tidal slough in the Alviso pond complex is evident. In general, the largest changes in residual circulation are seen in the far South Bay, as is expected by the comparatively large area of the Alviso pond complex, and the number of deeply subsided ponds which contribute to the increase in tidal prism.

5.5 Bed Shear Stress

Potential impacts to sediment erosion and deposition patterns are inferred based on comparisons of total bed shear stress both before and after tidal restoration, where total bed shear stress is a function of both tidal currents and locally-generated wind-waves. Section 4.5 provides a description of the methodology used to generate and compare the total combined wind-wave- and tidally-induced bed shear stress. As with the summer analysis period, a one day period corresponding with the peak tidal velocities was chosen to calculate the maximum tidally-induced bed shear stress. The one-day period corresponding to the highest wind conditions was chosen was chosen to calculate the maximum combined wind-wave- and tidally-induced bed shear stress. However, winds rarely exceeded 7 m/s for any significant duration within the analysis period, as is typical under winter conditions.

5.5.1 South Bay

As with summer conditions within the South Bay, the largest changes to the tidally-induced bed shear stress are seen in the subtidal channels and in the regions downstream of the tidal sloughs (Figure 5-107). The difference map shown on Figure 5-107 depicts red regions where the erosive potential increases (bed shear stresses are higher under Alternative C relative to baseline conditions), and the areas depicted in blue correspond to regions with a potential for increased deposition. As the critical shear stresses for erosion are not well known within the South Bay, and they vary spatially depending on the sediment characteristics and level of compaction of the substrate, the red and blue areas are for illustrative purposes only and do not predict erosion or deposition under Alternative C.

When the combined wind-wave- and tidally-induced shear stress is considered in the South Bay, additional changes become apparent. MLLW is higher and MHHW is lower under Alternative C (Figure

5-4 and Figure 5-5, respectively). Because wind-wave-driven shear stress is a function of water depth, and the erosive potential decreases with increasing water depth, the reduction in tidal amplitude leads to a slight reduction in the total bed shear stresses in the far South Bay (Figure 5-113). This reduction in total bed shear stress is not apparent along the eastern and western shoals north of the Dumbarton Bridge (Figure 5-112 and Figure 5-114, respectively). The reduction in tidal amplitude could lead to less erosion of the intertidal mudflats and increased erosion of the South Bay shoreline.

In general, the difference between the tidally-induced bed shear stresses and the combined wind-wave- and tidally-induced shear stresses are not as dramatic as under summer conditions due to the lessened influence of the wind under winter conditions. Summer wind conditions in the South Bay are typically more conducive to sediment resuspension and redistribution.

5.5.2 Tidal Sloughs

Within and adjacent to the Eden Landing pond complex (Figure 5-108), the maximum tidally-induced bed shear stress is increased downstream of tidal breaches, corresponding to the increased tidal prism, and decreased upstream of the tidal breaches because a portion of the flow upstream in the tidal slough under baseline conditions is captured within the downstream tidally-restored ponds under restored conditions. Within and adjacent to the Alviso pond complex (Figure 5-109) and the Ravenswood pond complex (Figure 5-110), the dynamic is similar to that observed in the Eden Landing pond complex. Tidally-induced bed shear stresses increase downstream of tidal breaches and decrease upstream of tidal breaches.

The primary effect of the combined wind-wave- and tidally-induced shear stress is evident in the South Bay, rather than in the tidal sloughs, as wind-induced waves require sufficient fetch to develop.

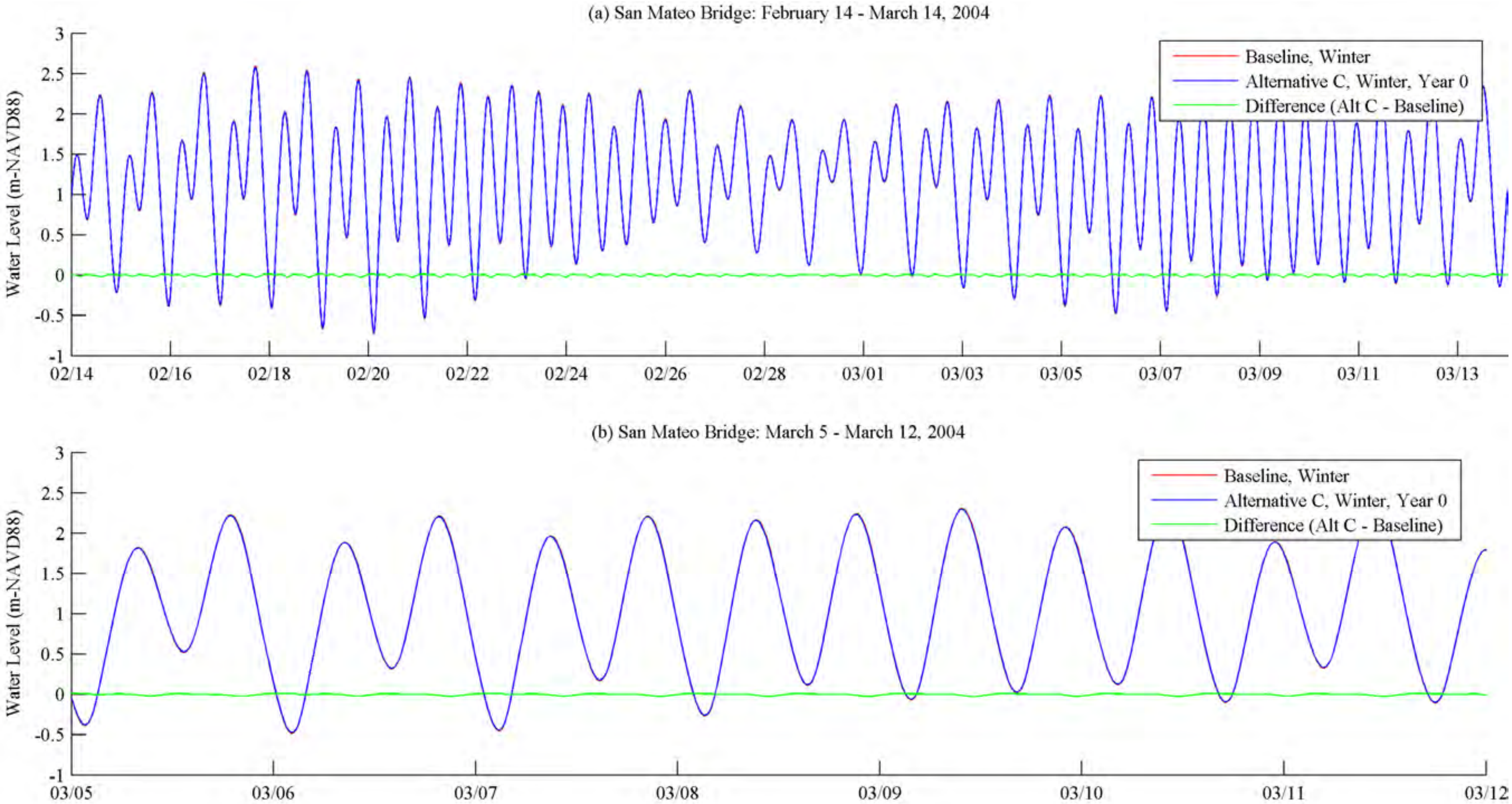

figure 5-1

South Bay Salt Pond Restoration Project

Water Levels, San Mateo Bridge, Alt C, Year 0, Winter

PWA

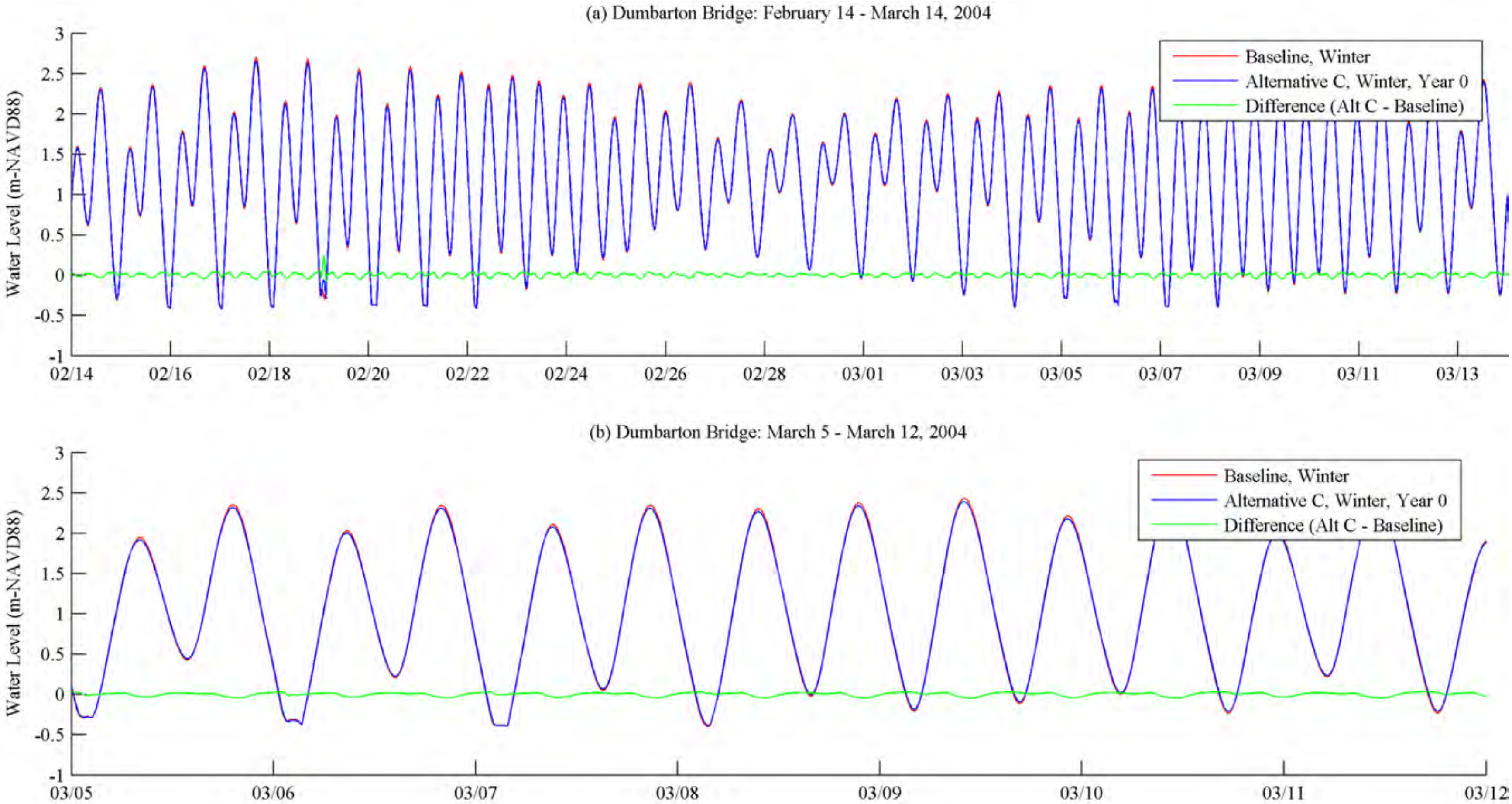

figure 5-2

South Bay Salt Pond Restoration Project

Water Levels, Dumbarton Bridge, Alt C, Year 0, Winter

PWA

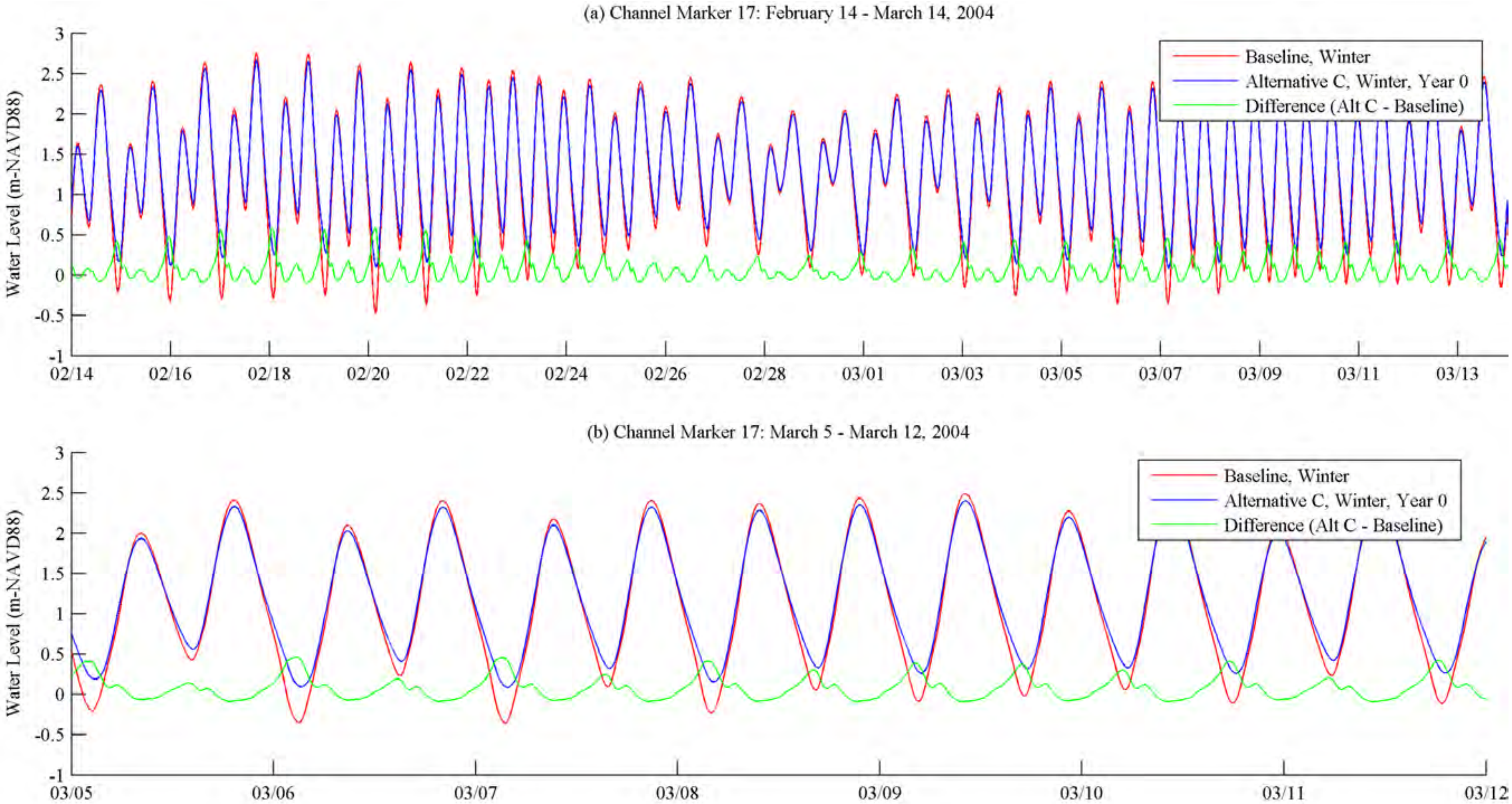

figure 5-3

South Bay Salt Pond Restoration Project

Water Levels, Channel Marker 17, Alt C, Year 0, Winter

PWA

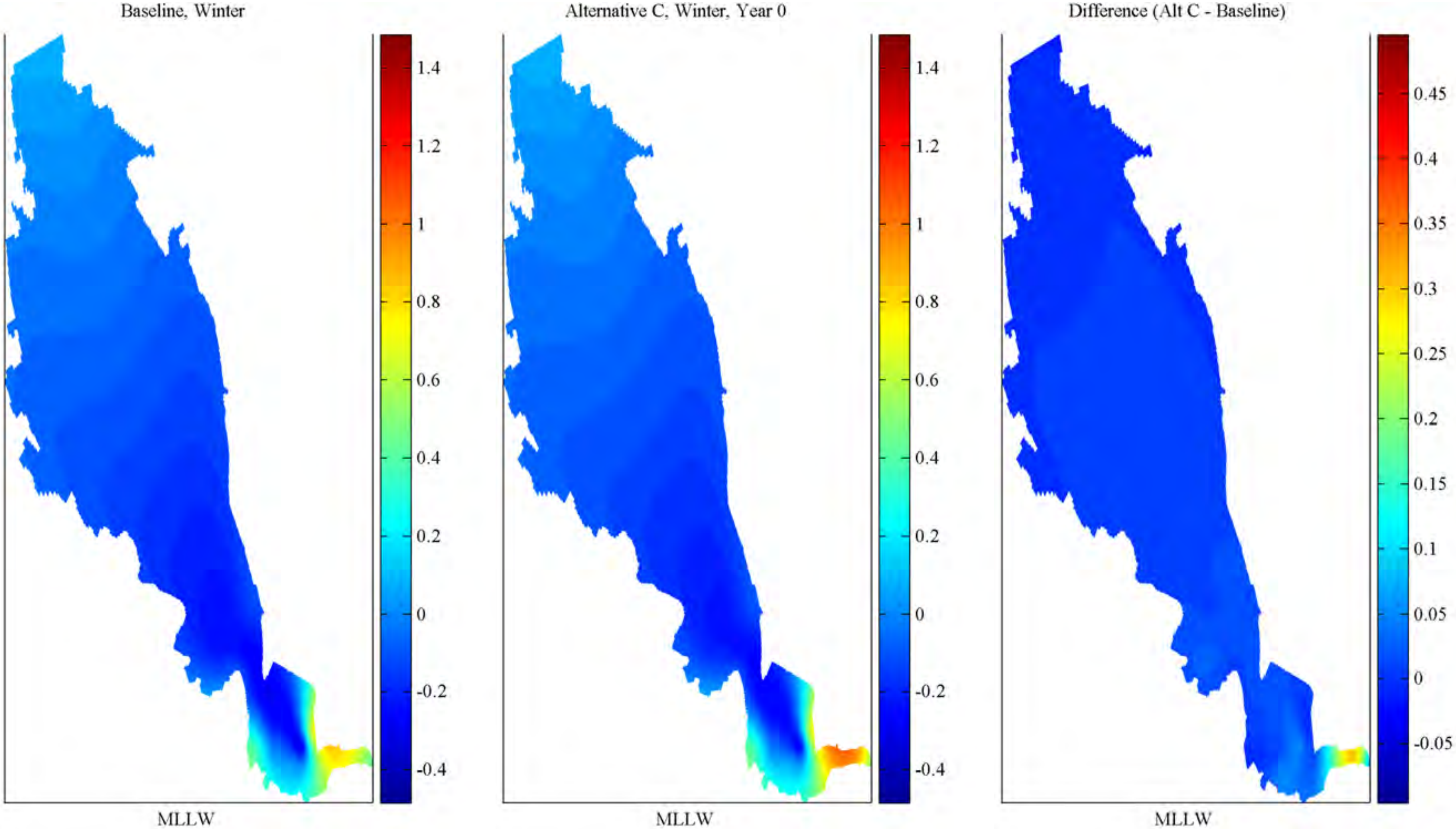

Note: Units shown are m-NAVD88, difference units are m

figure 5-4

South Bay Salt Pond Restoration Project

Changes in MLLW, Alt C, Year 0, Winter

PWA

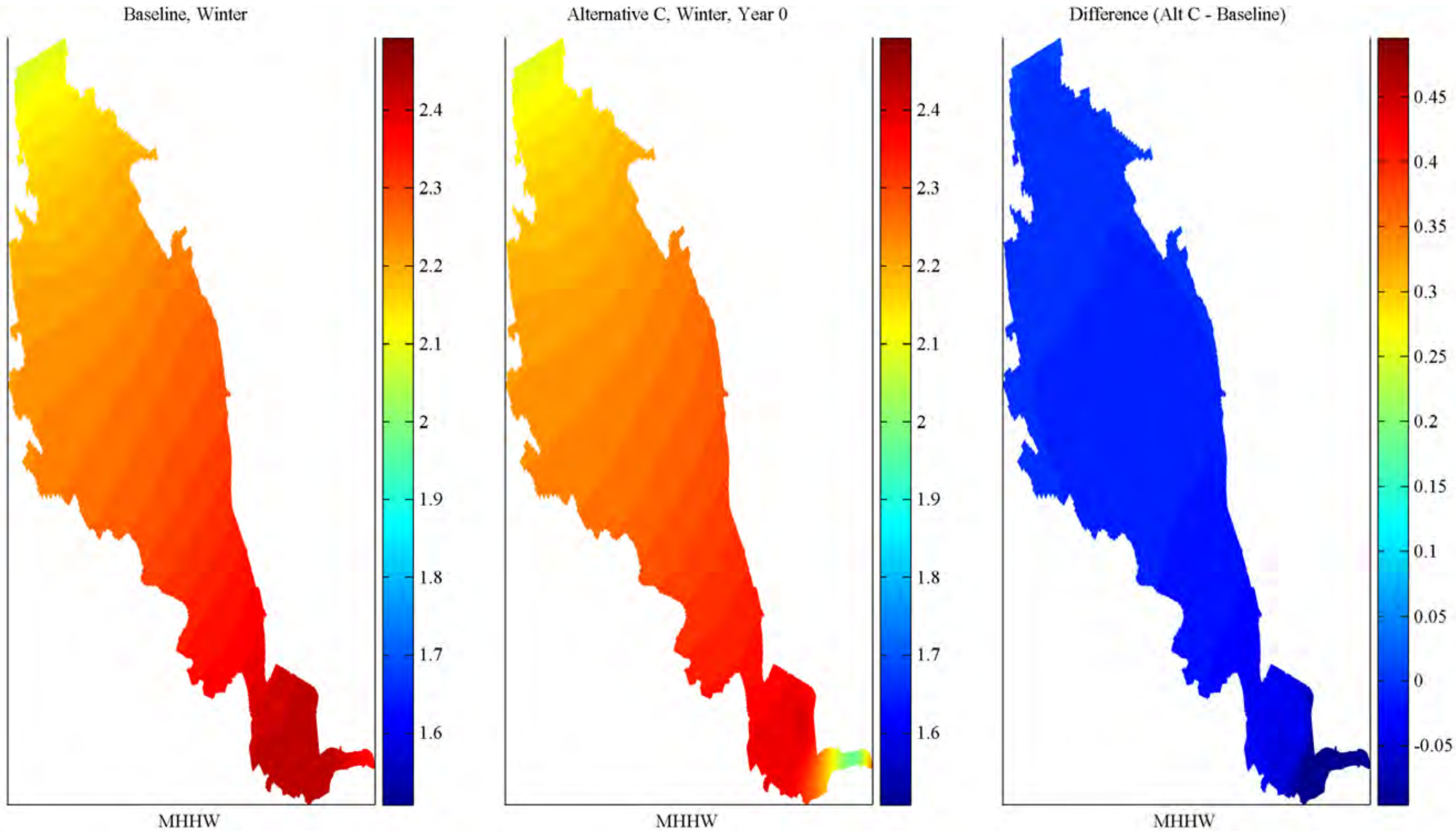

Note: Units shown are m-NAVD88, difference units are m

figure 5-5

South Bay Salt Pond Restoration Project

Changes in MHHW, Alt C, Year 0, Winter

PWA

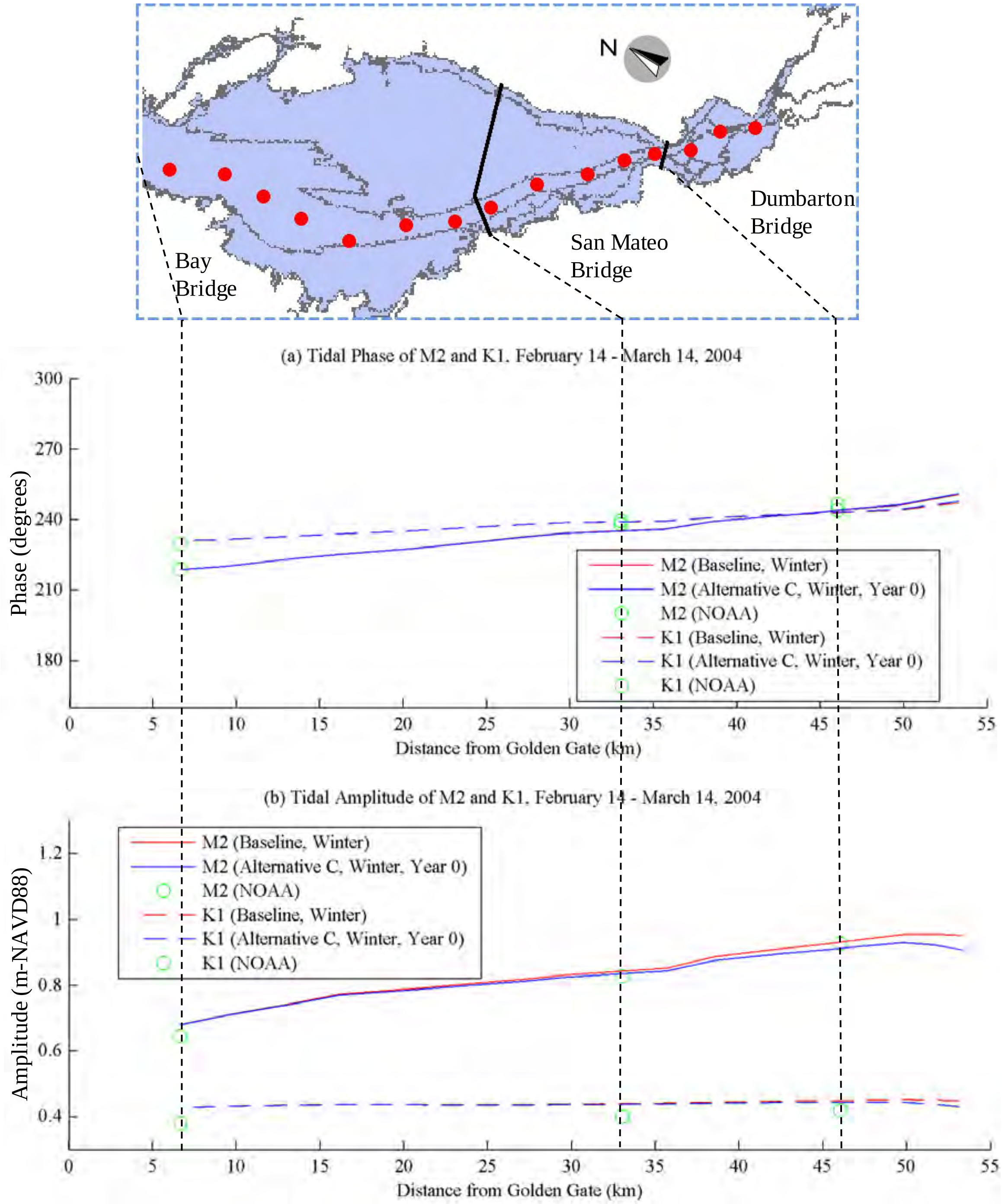

This figure shows the phase and amplitude of the M2 and K1 tidal components, calculated from harmonic analysis of the model. The green data points represent phase and amplitude values calculated by NOAA at the Bay Bridge (Pier 22), San Mateo Bridge, and Dumbarton Bridge.

figure 5-6

South Bay Salt Pond Restoration Project

Changes in Tidal Propagation, Alt C, Year 0, Winter

PWA

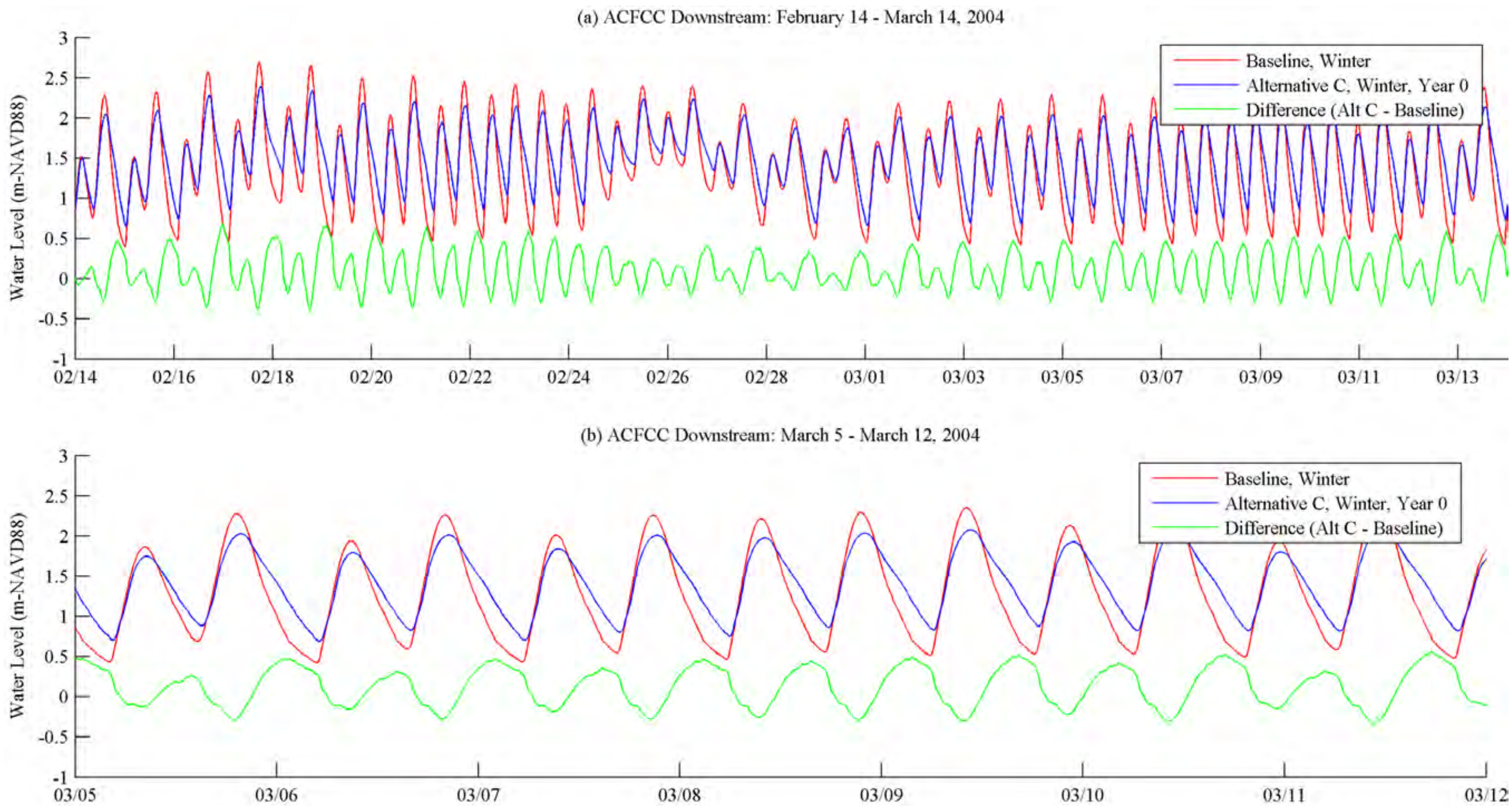

figure 5-7

South Bay Salt Pond Restoration Project

Water Levels, ACFCC Downstream, Alt C, Year 0, Winter

PWA

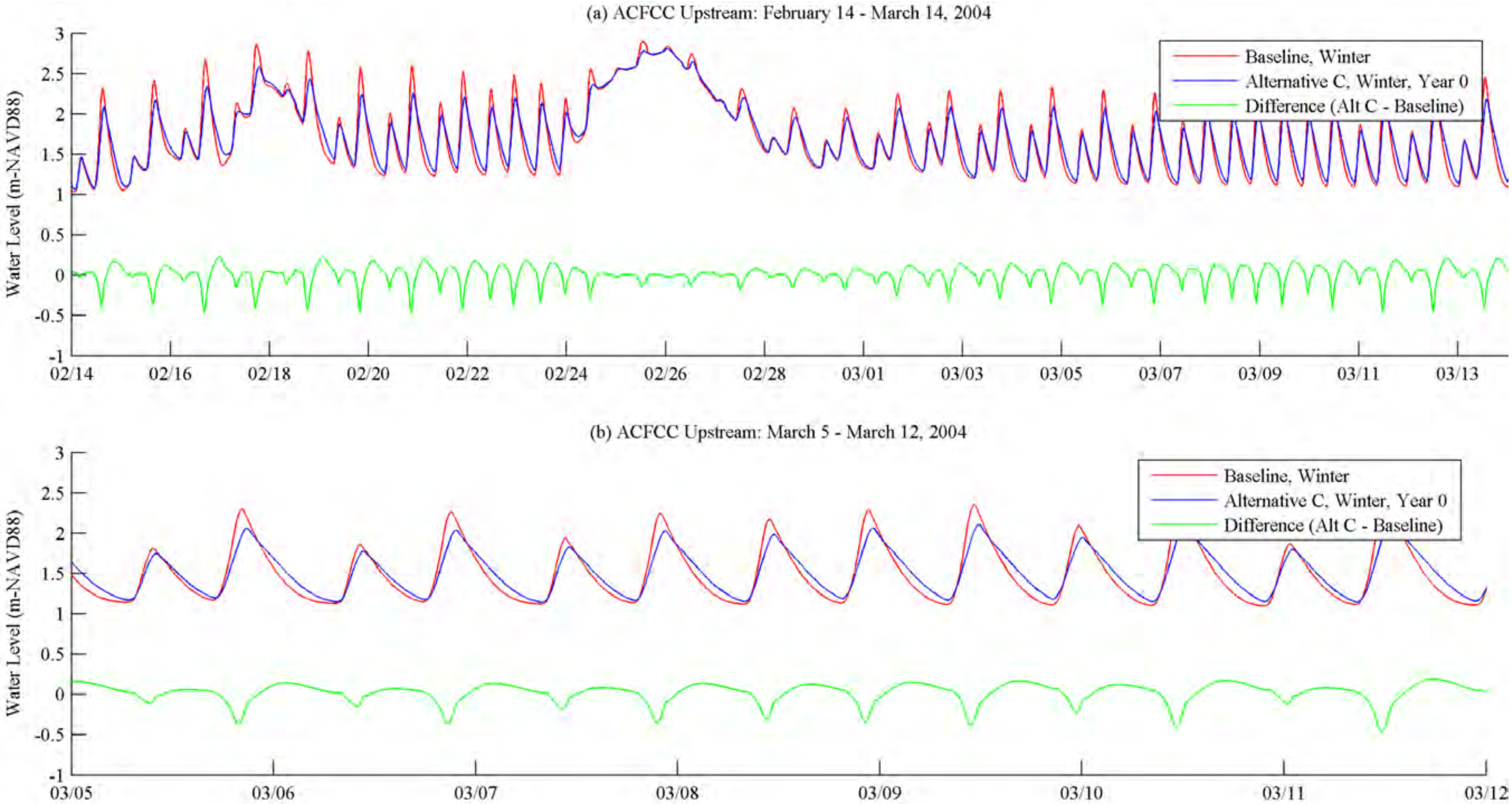

figure 5-8

South Bay Salt Pond Restoration Project

Water Levels, ACFCC Upstream, Alt C, Year 0, Winter

PWA

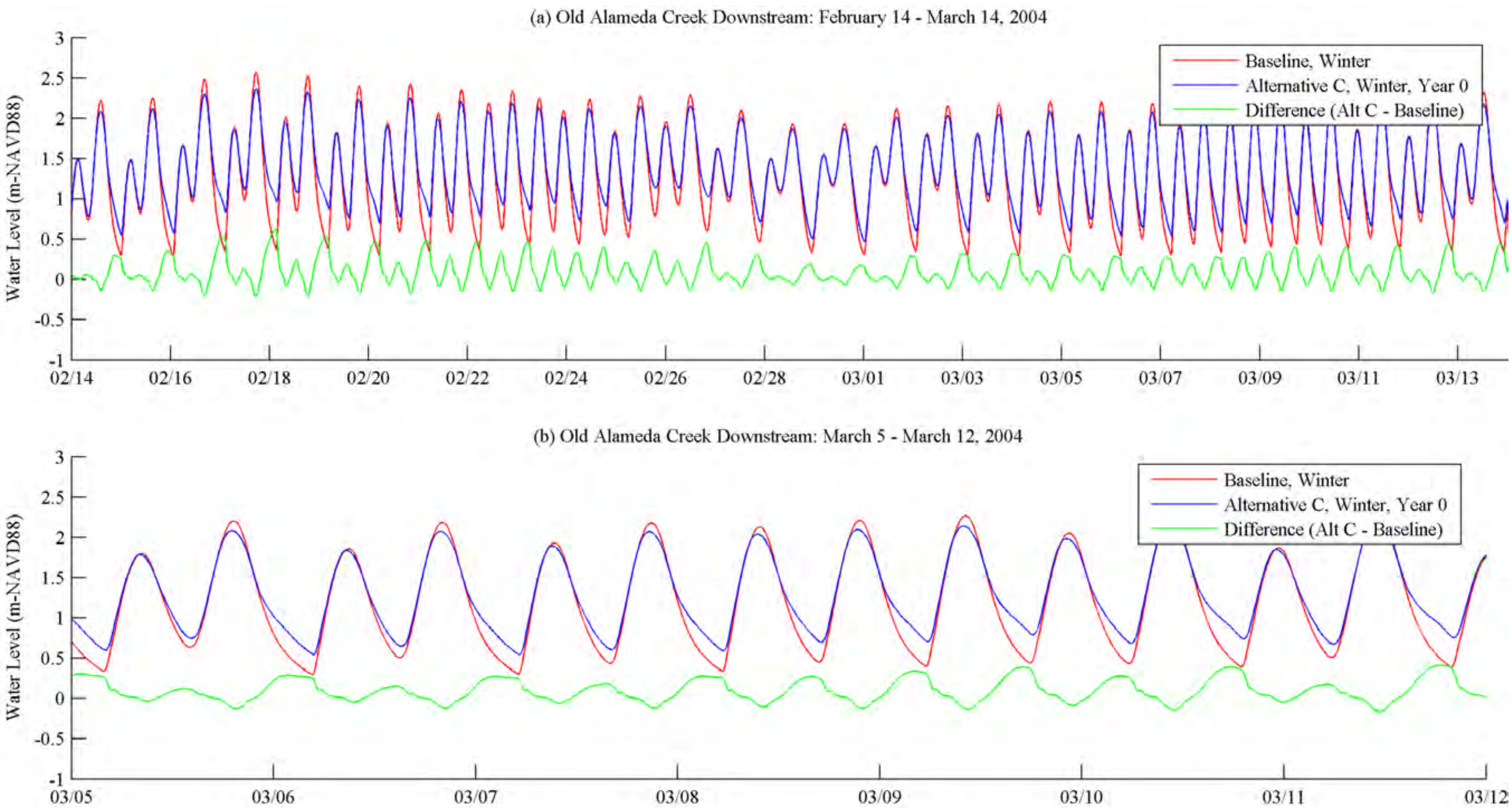

figure 5-9

South Bay Salt Pond Restoration Project

Water Levels, Old Alameda Creek Downstream, Alt C, Year 0, Winter

PWA

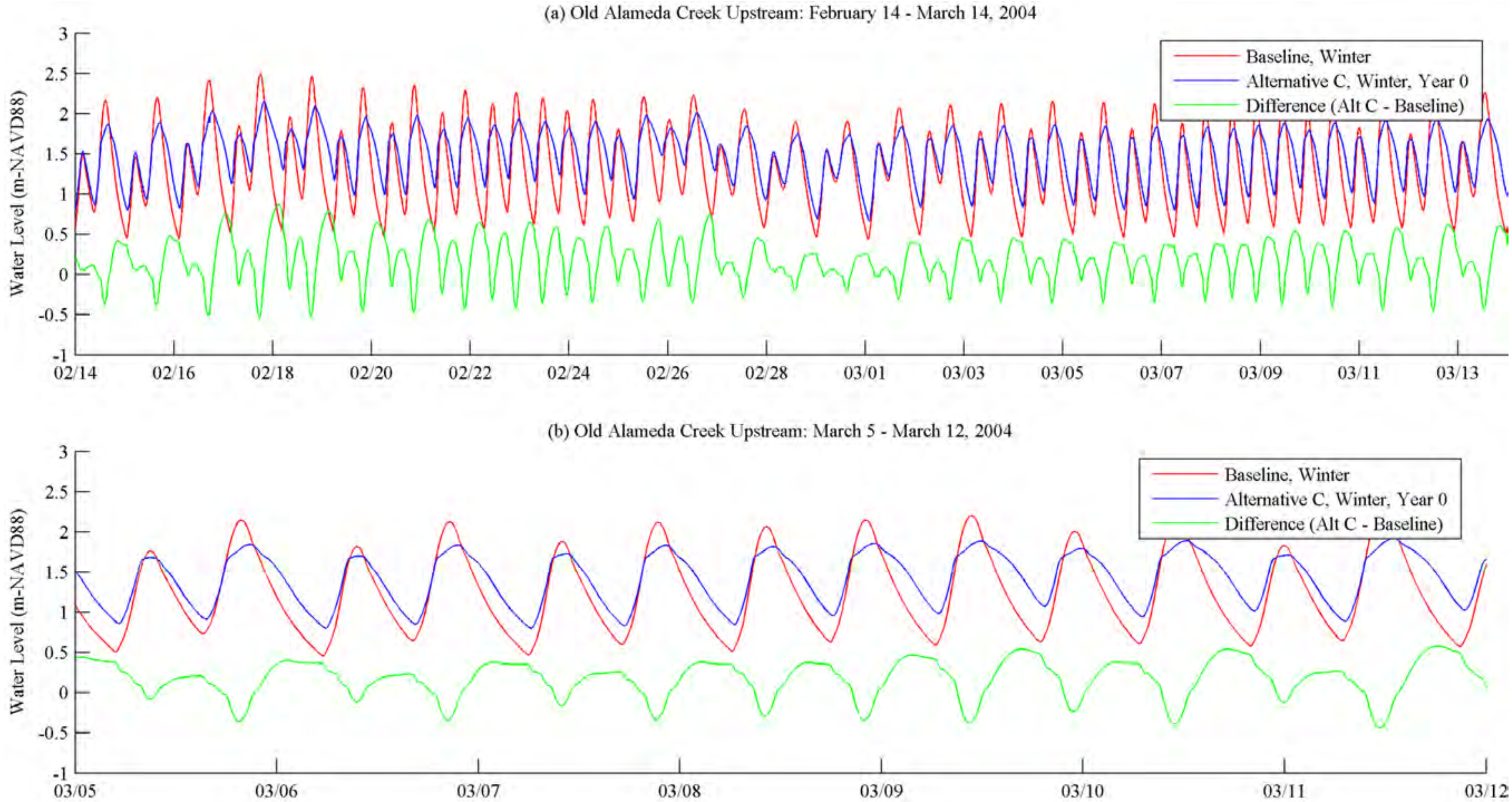

figure 5-10

South Bay Salt Pond Restoration Project

Water Levels, Old Alameda Creek Upstream, Alt C, Year 0, Winter

PWA

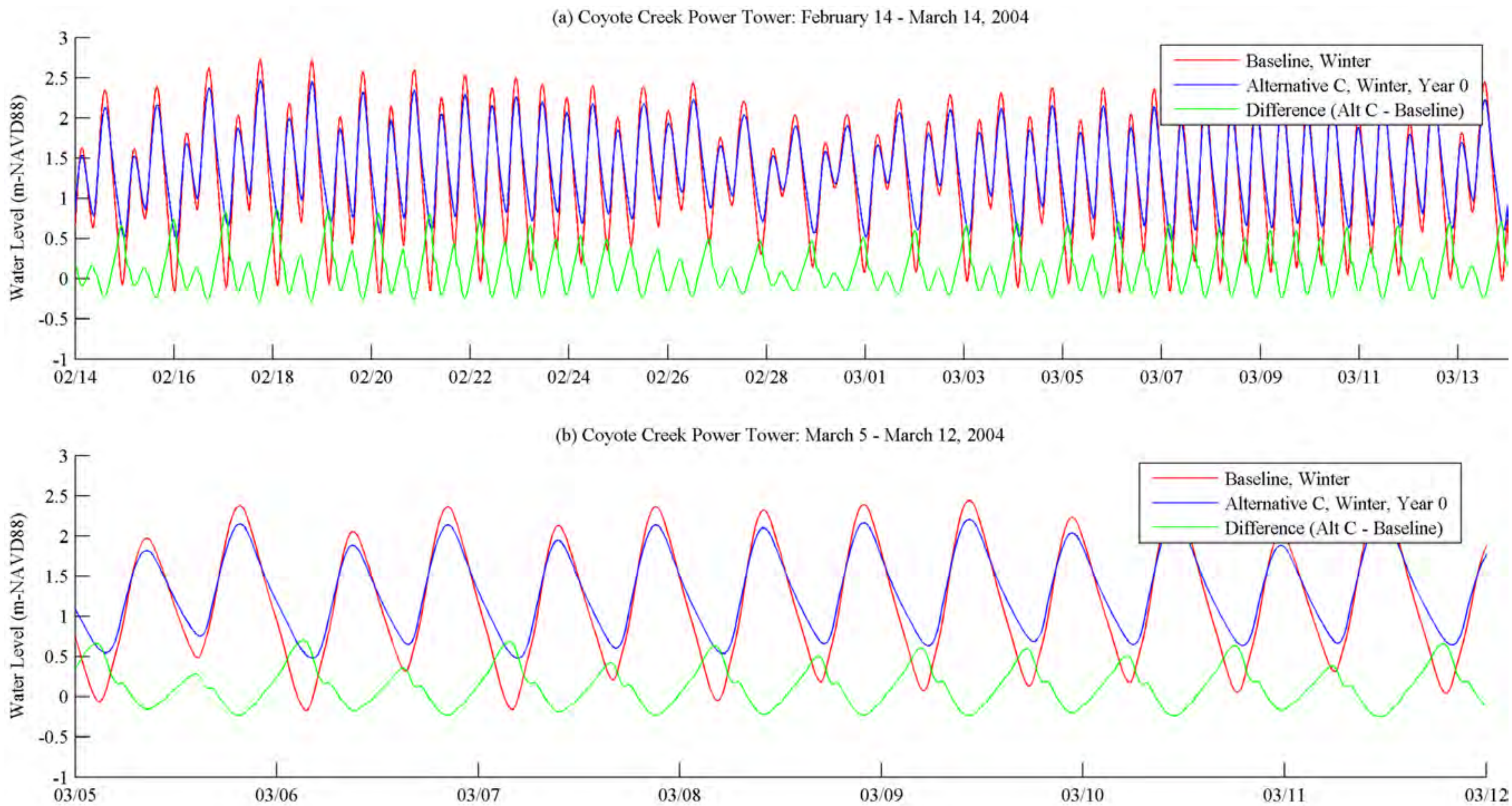

figure *5-11*

South Bay Salt Pond Restoration Project

Water Levels, Coyote Creek Power Tower, Alt C, Year 0, Winter

PWA

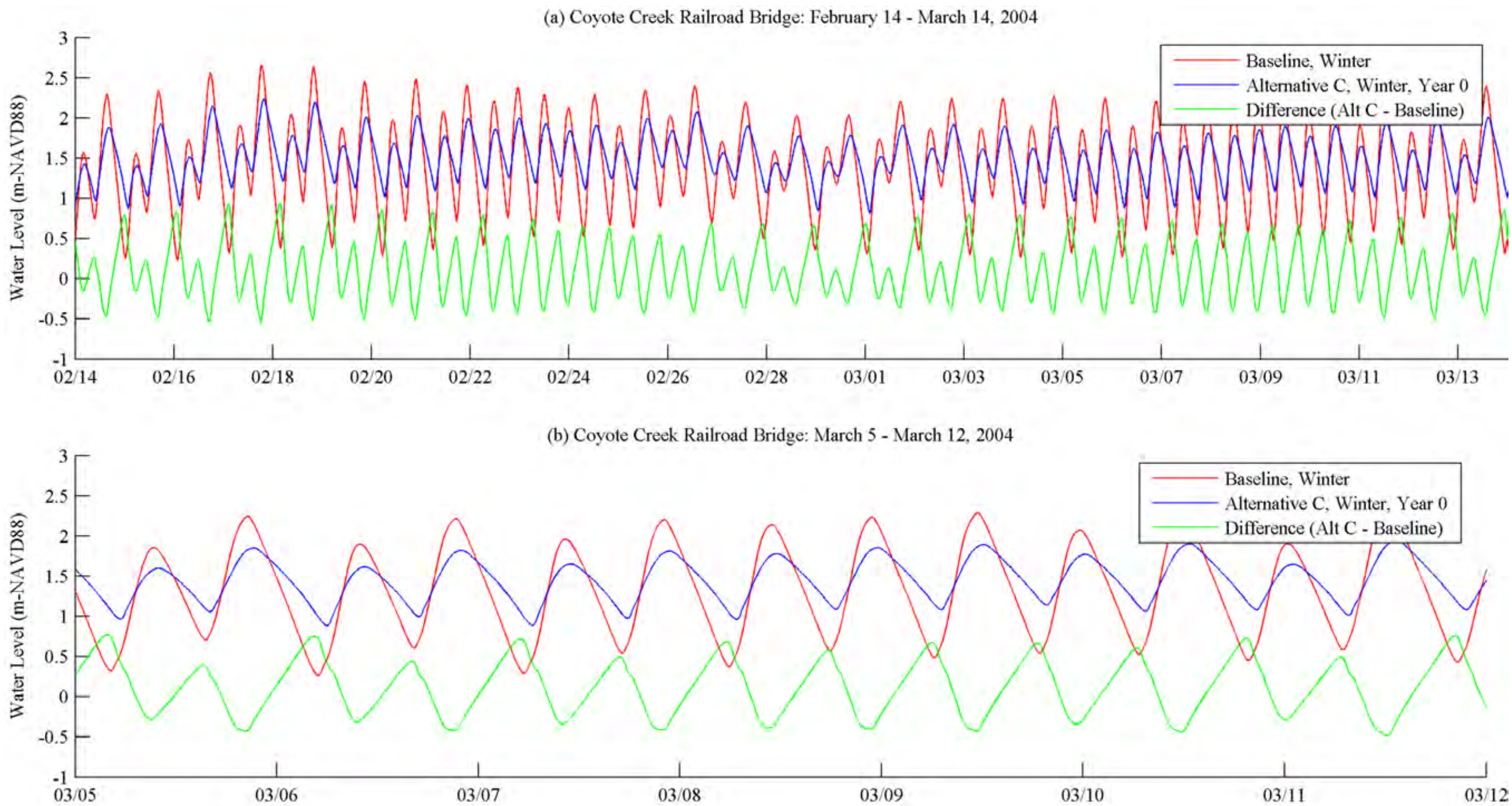

figure 5-12

South Bay Salt Pond Restoration Project

Water Levels, Coyote Creek Railroad Bridge, Alt C, Year 0, Winter

PWA

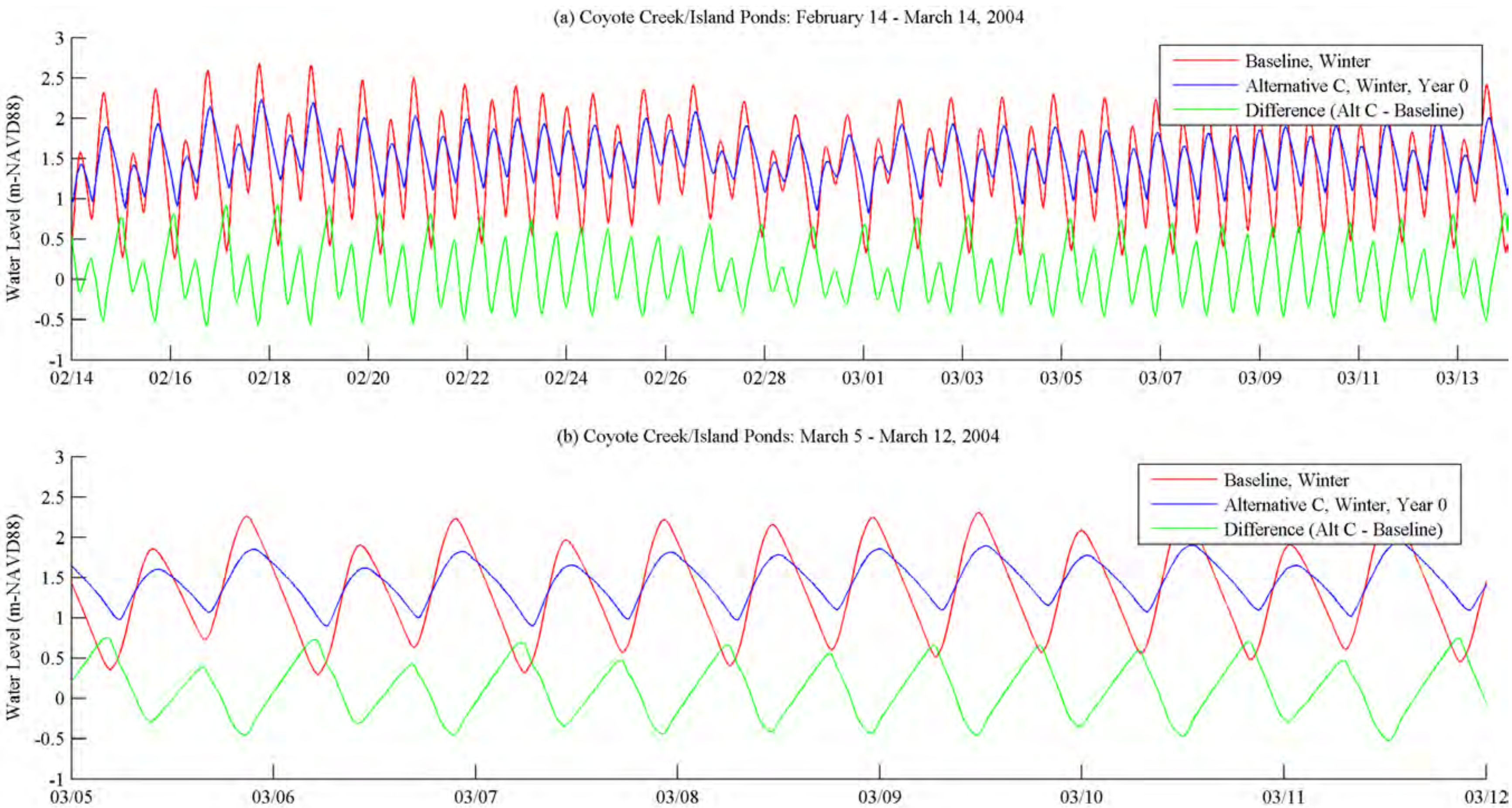

figure 5-13

South Bay Salt Pond Restoration Project

Water Levels, Coyote Creek/Island Ponds, Year 0, Winter

PWA

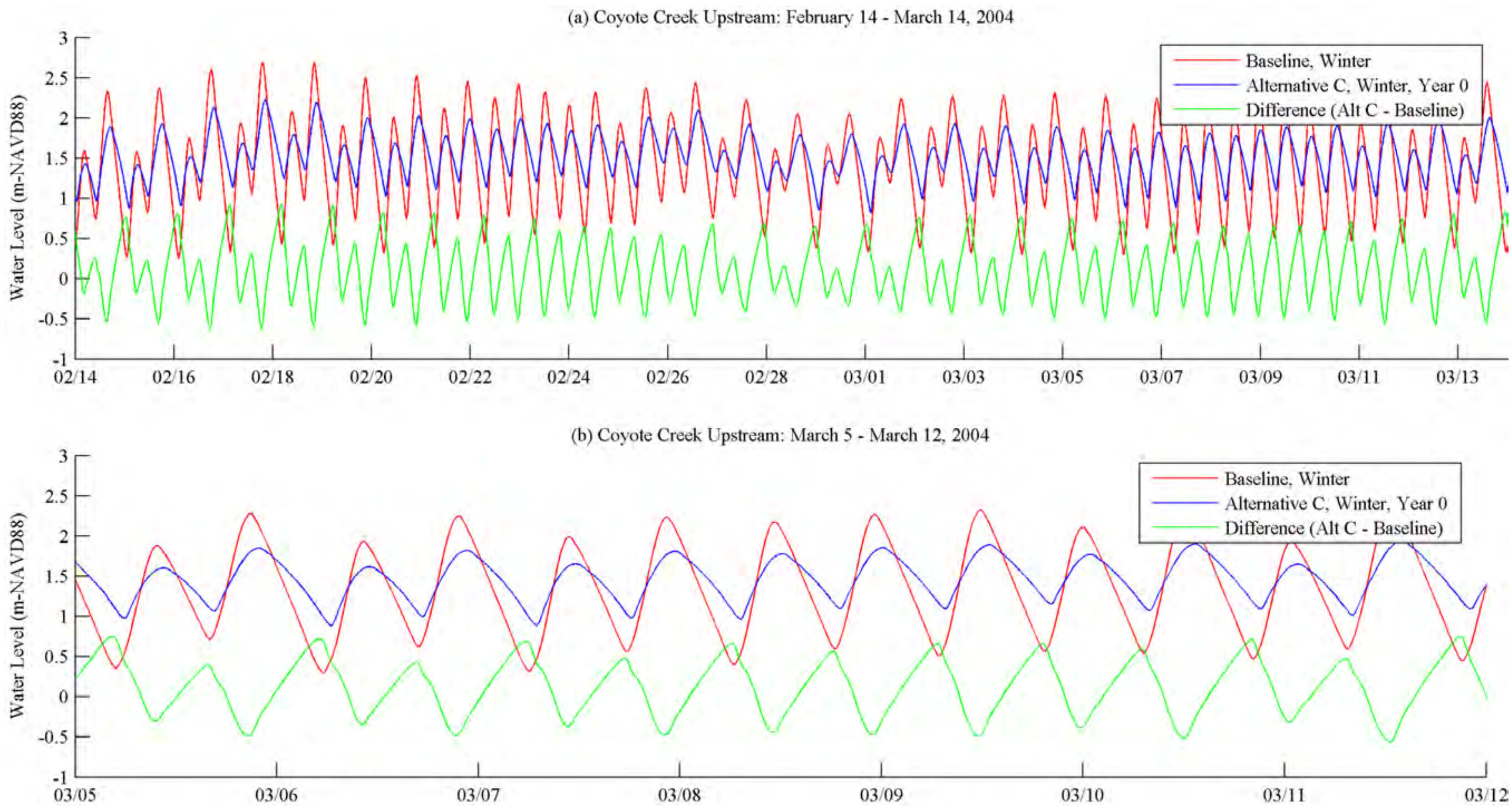

figure 5-14

South Bay Salt Pond Restoration Project

Water Levels, Coyote Creek Upstream, Year 0, Winter

PWA

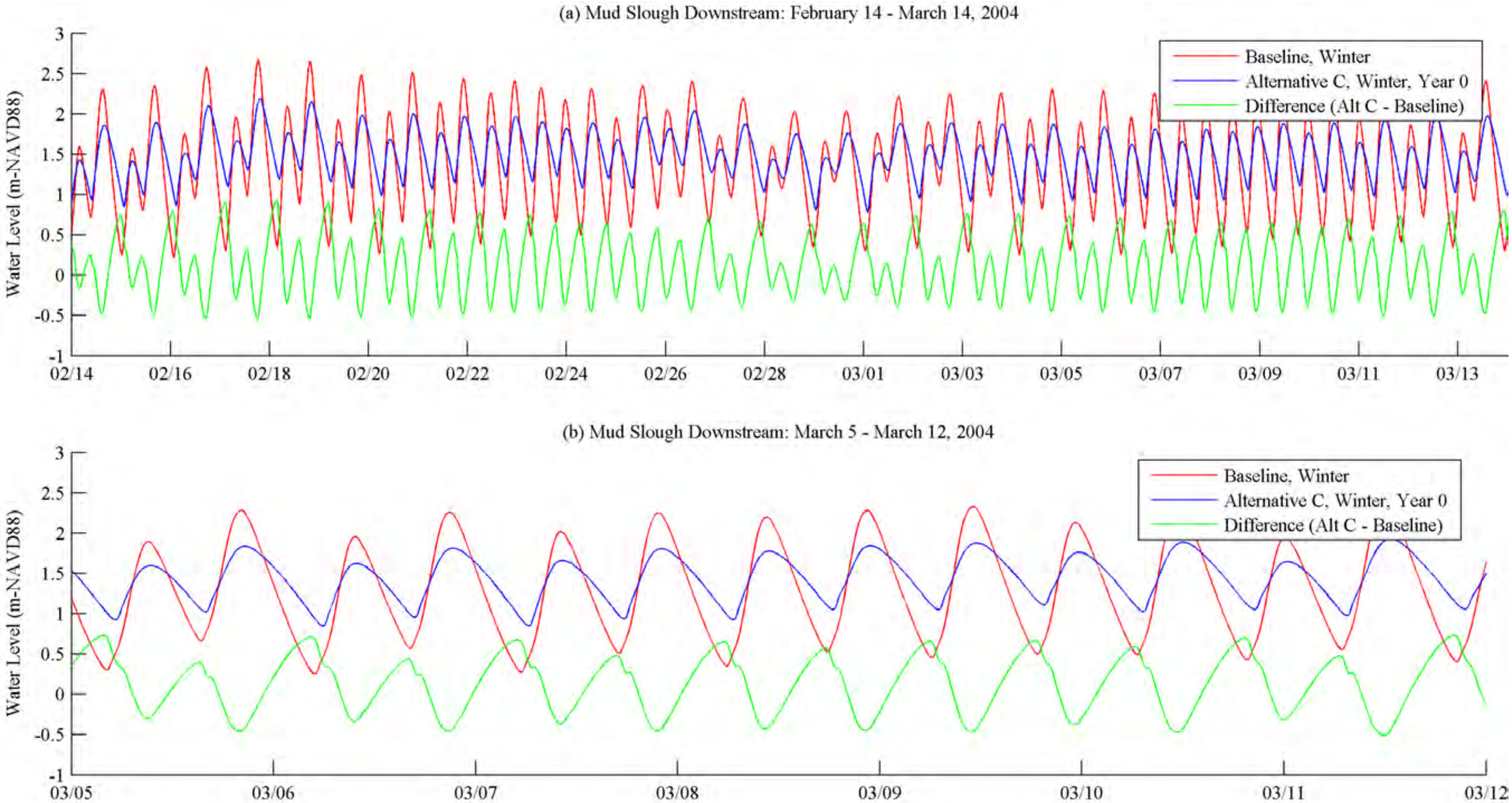

figure 5-15

South Bay Salt Pond Restoration Project

Water Levels, Mud Slough Downstream, Alt C, Year 0, Winter

PWA

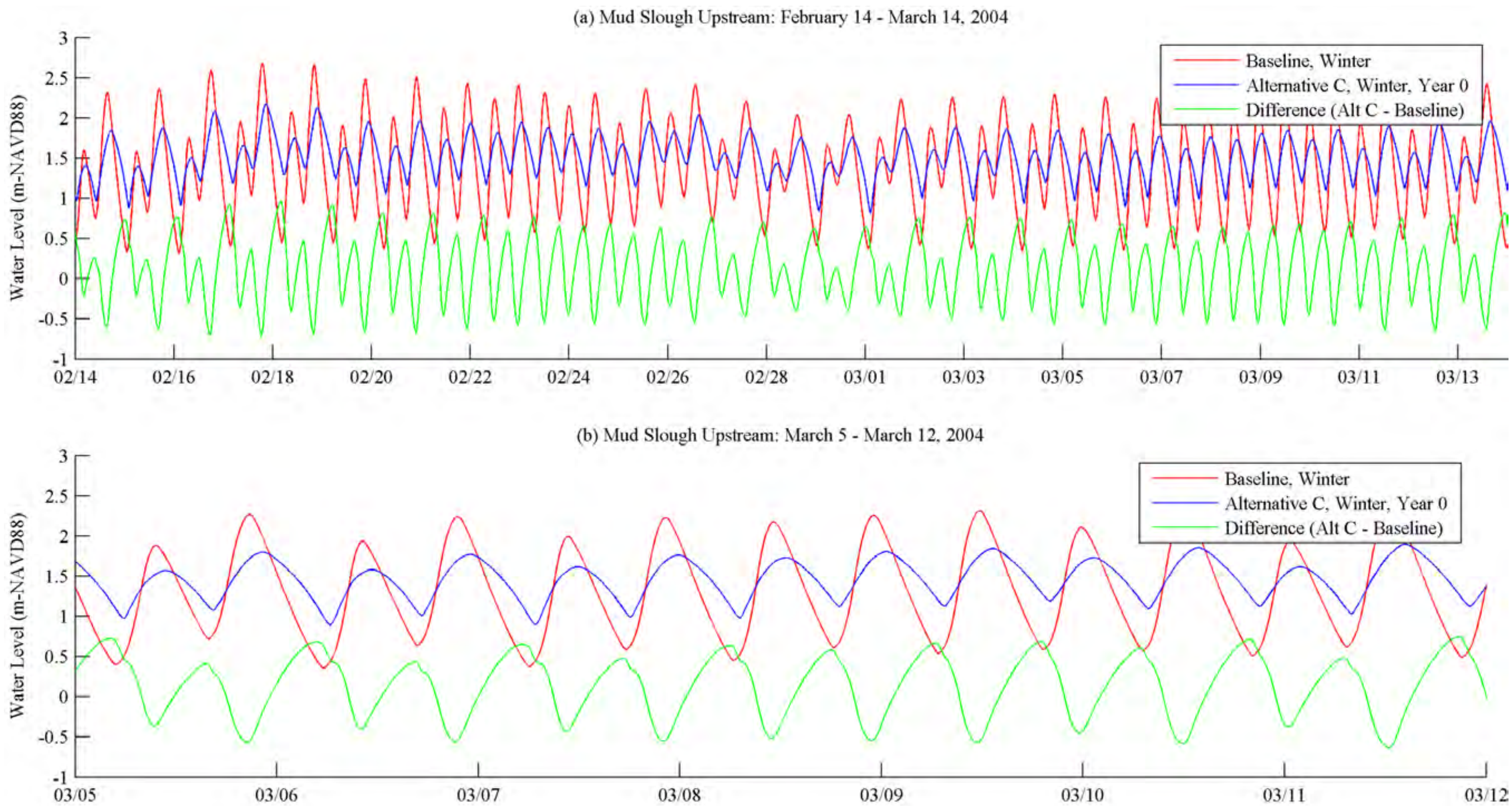

figure 5-16

South Bay Salt Pond Restoration Project

Water Levels, Mud Slough Upstream, Alt C, Year 0, Winter

PWA

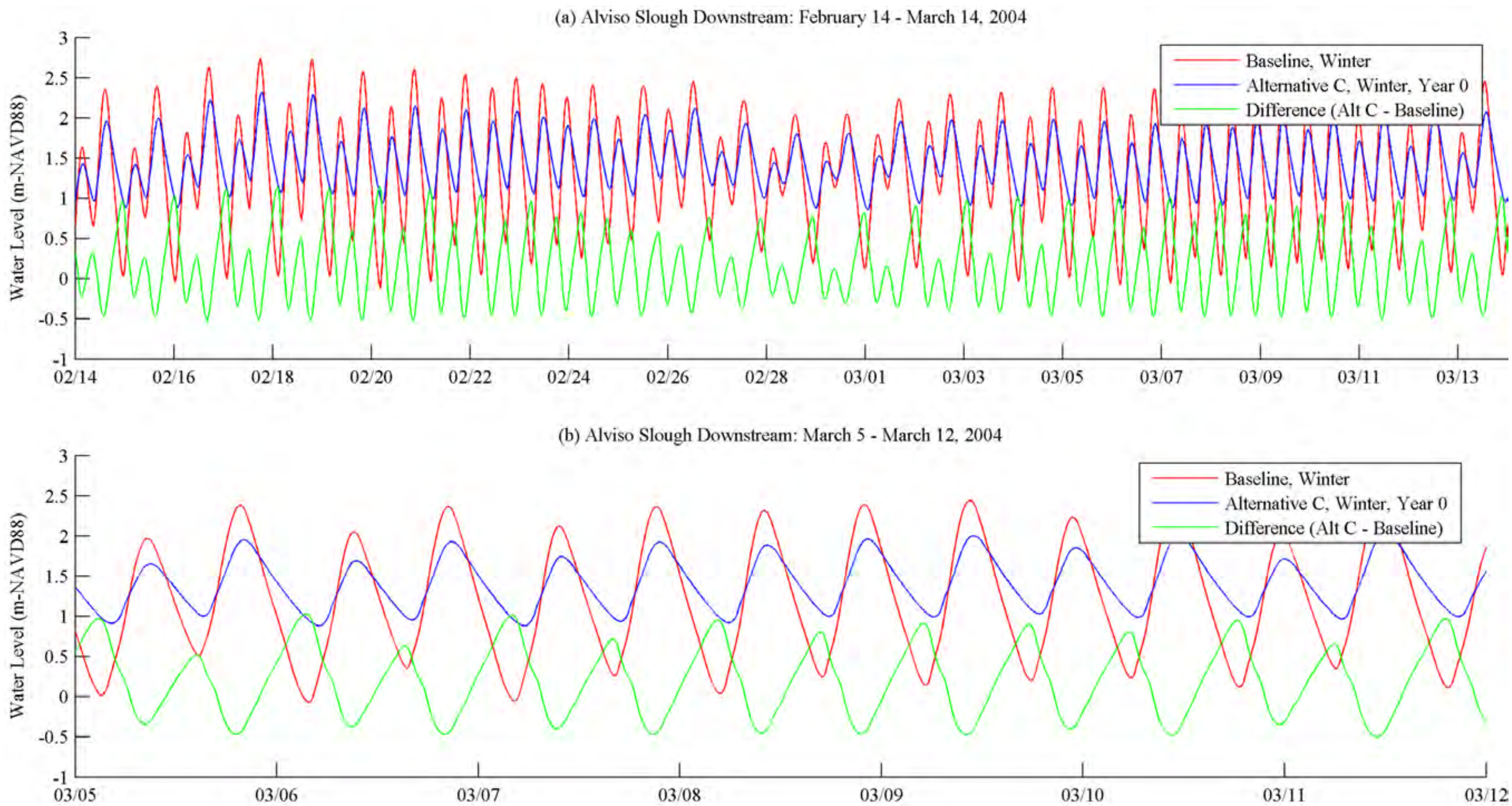

figure 5-17

South Bay Salt Pond Restoration Project

Water Levels, Alviso Slough Downstream, Alt C, Year 0, Winter

PWA

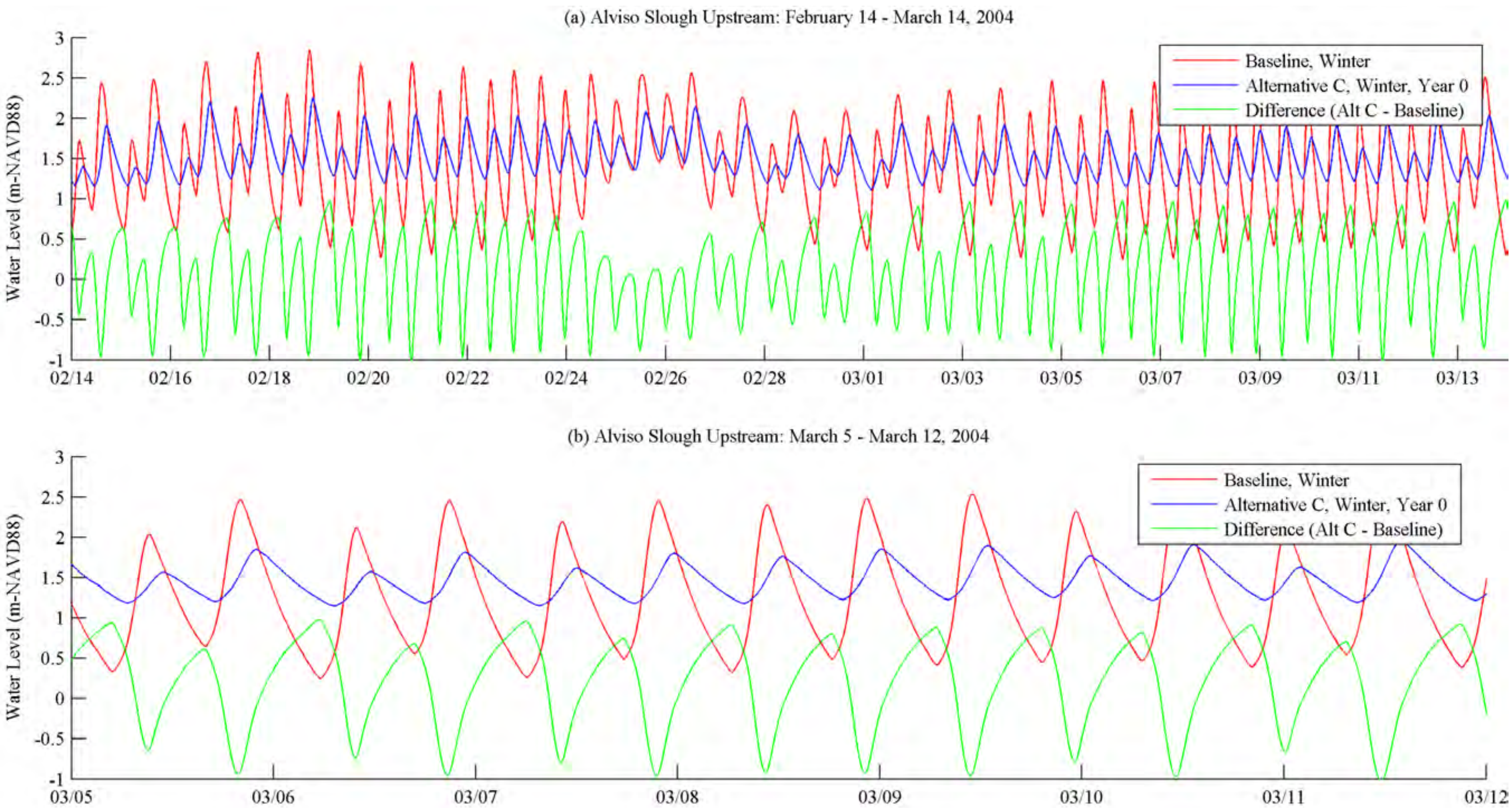

figure 5-18

South Bay Salt Pond Restoration Project

Water Levels, Alviso Slough Upstream, Alt C, Year 0, Winter

PWA

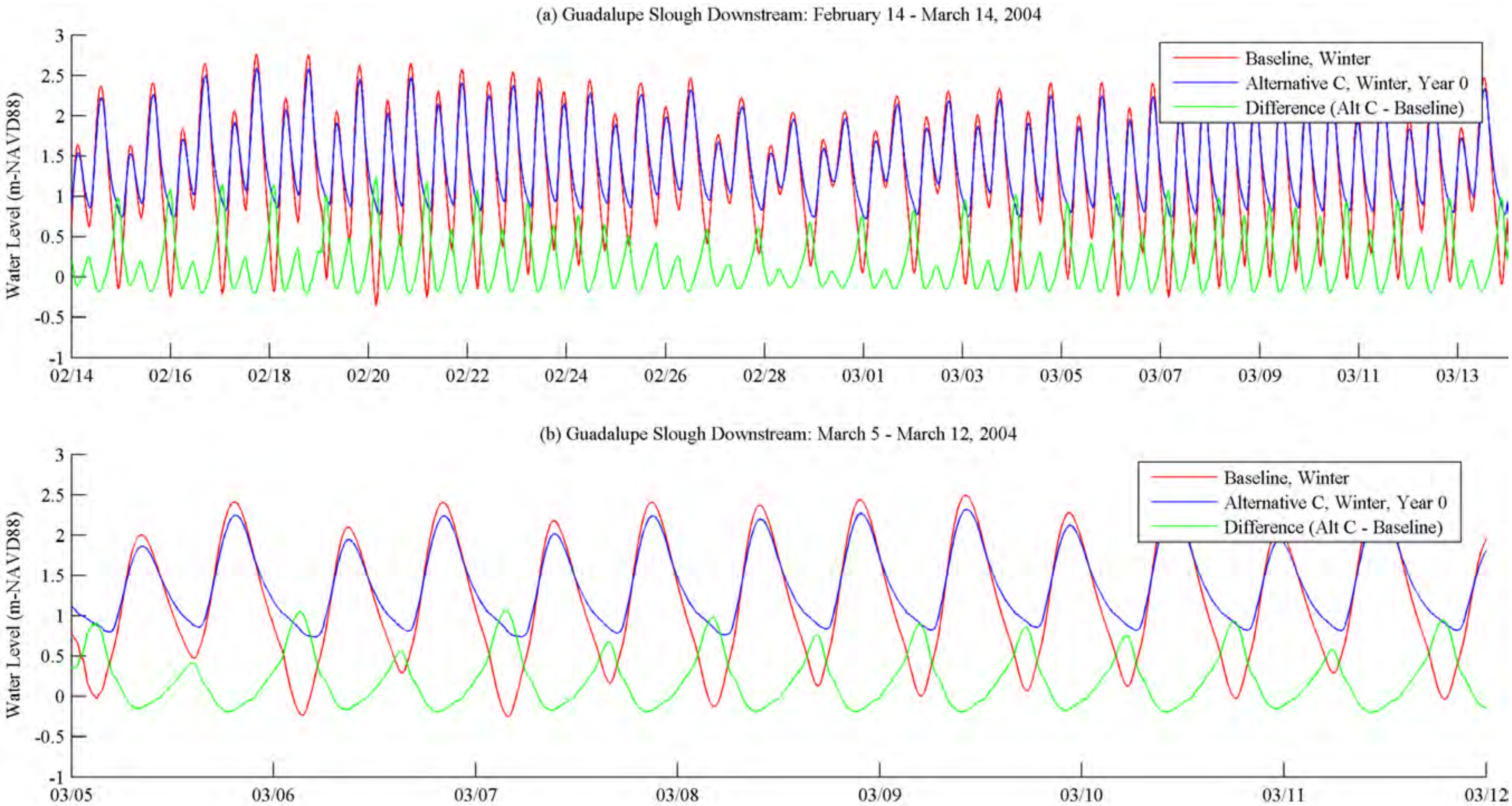

figure 5-19

South Bay Salt Pond Restoration Project

Water Levels, Guadalupe Slough Downstream, Alt C, Year 0, Winter

PWA

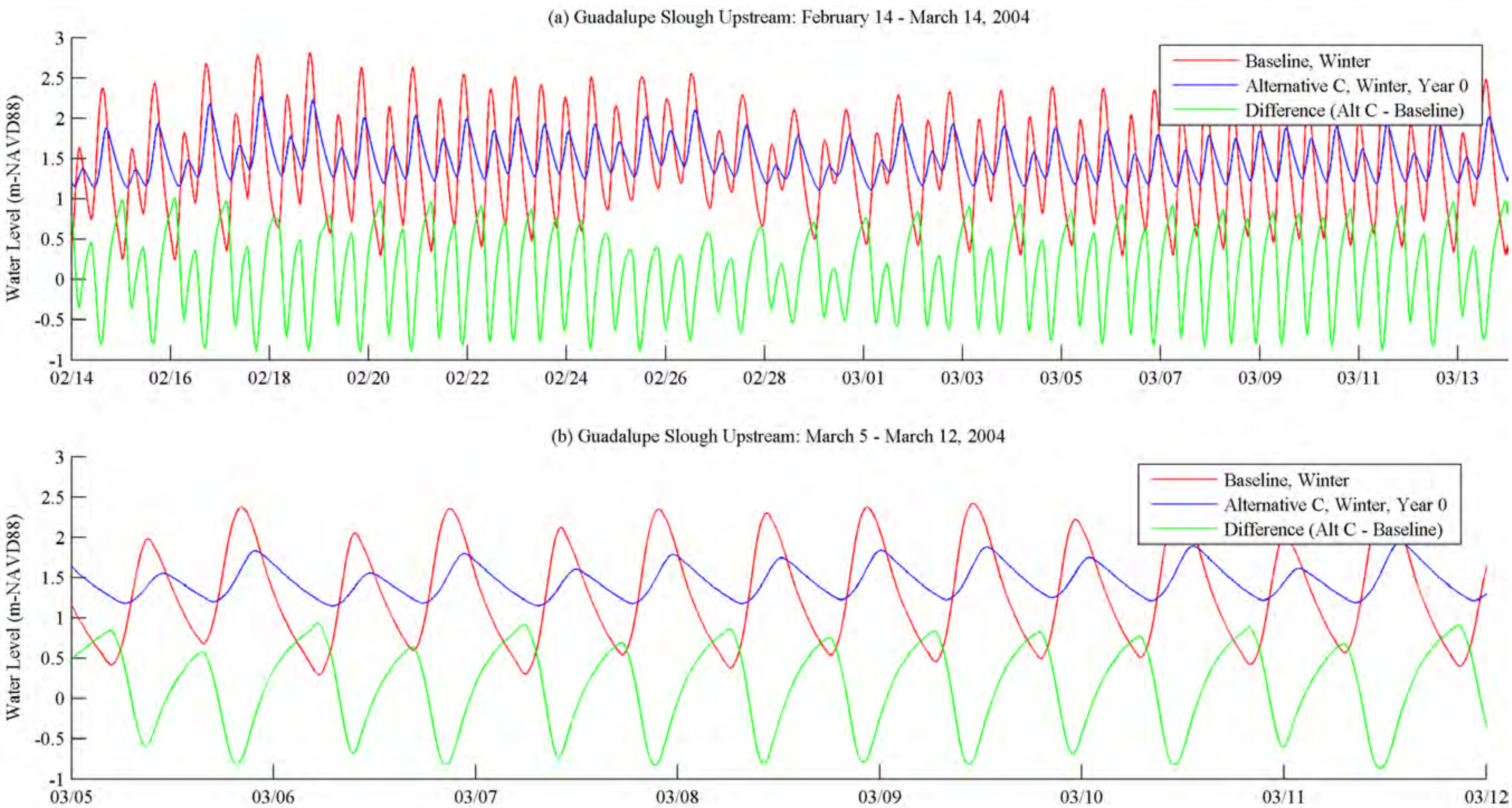

figure 5-20

South Bay Salt Pond Restoration Project

Water Levels, Guadalupe Slough Upstream, Alt C, Year 0, Winter

PWA

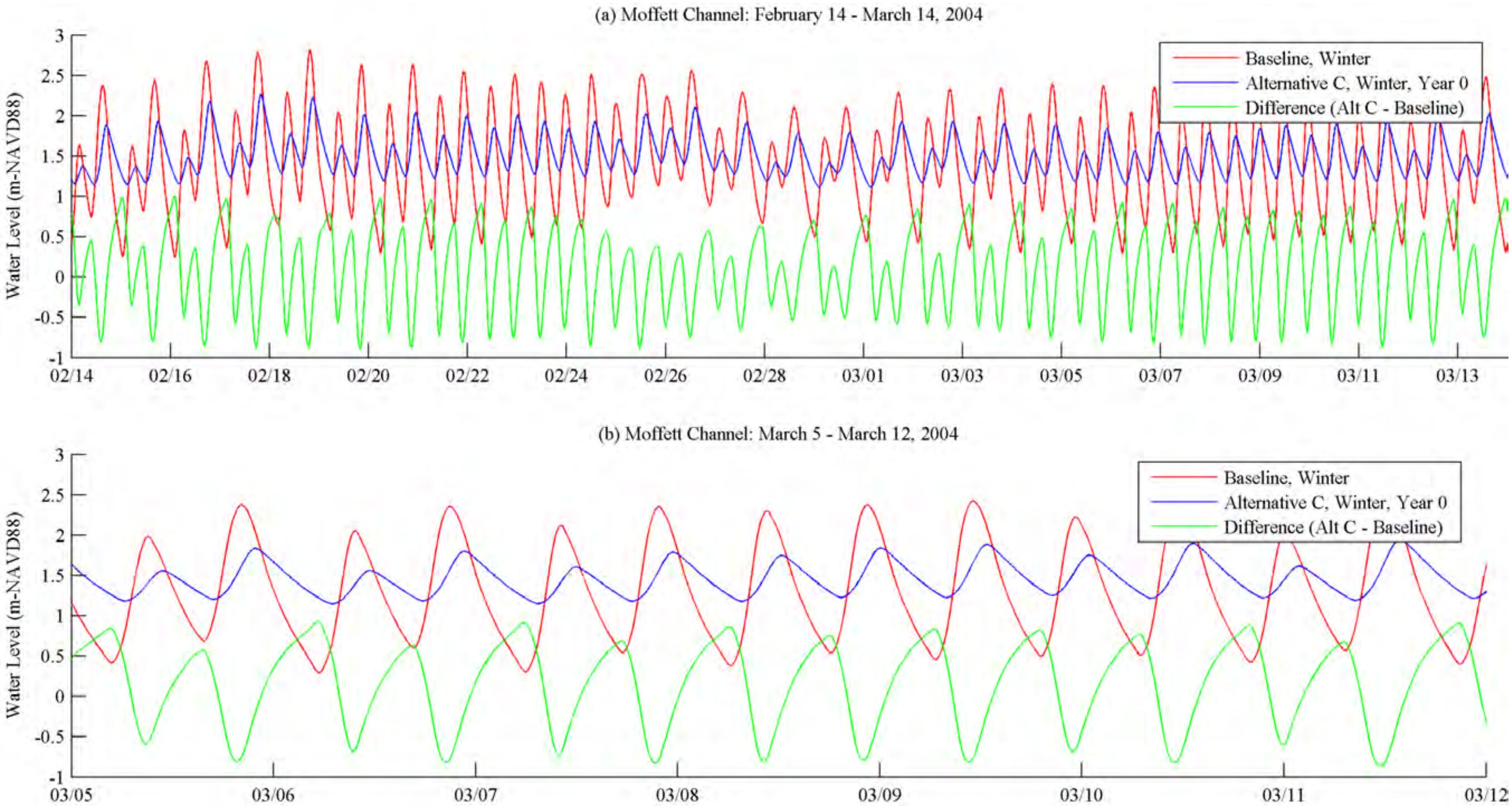

figure 5-21

South Bay Salt Pond Restoration Project

Water Levels, Moffett Channel, Alt C, Year 0, Winter

PWA

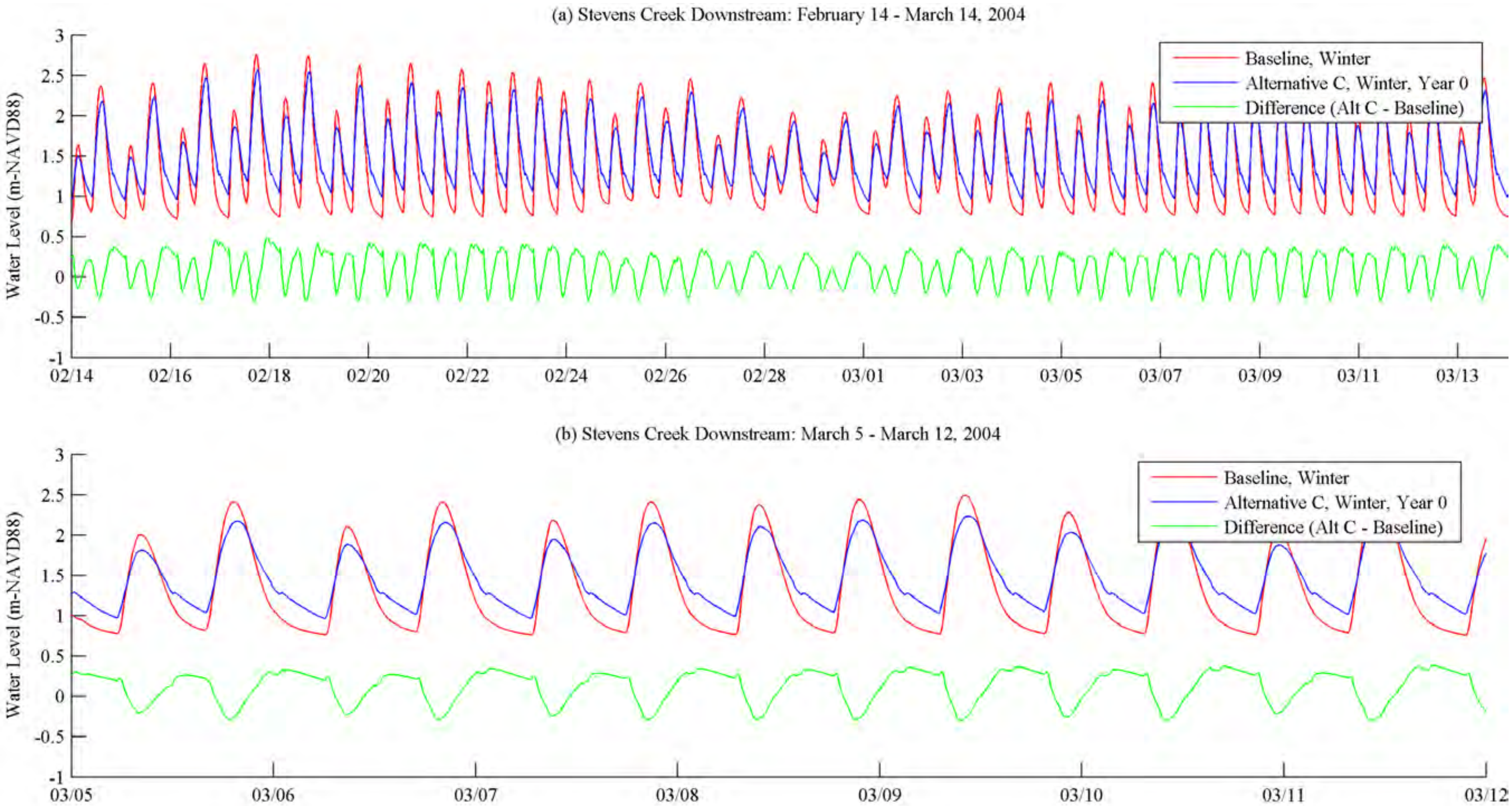

figure *5-22*

South Bay Salt Pond Restoration Project

Water Levels, Steven Creek Downstream, Alt C, Year 0, Winter

PWA

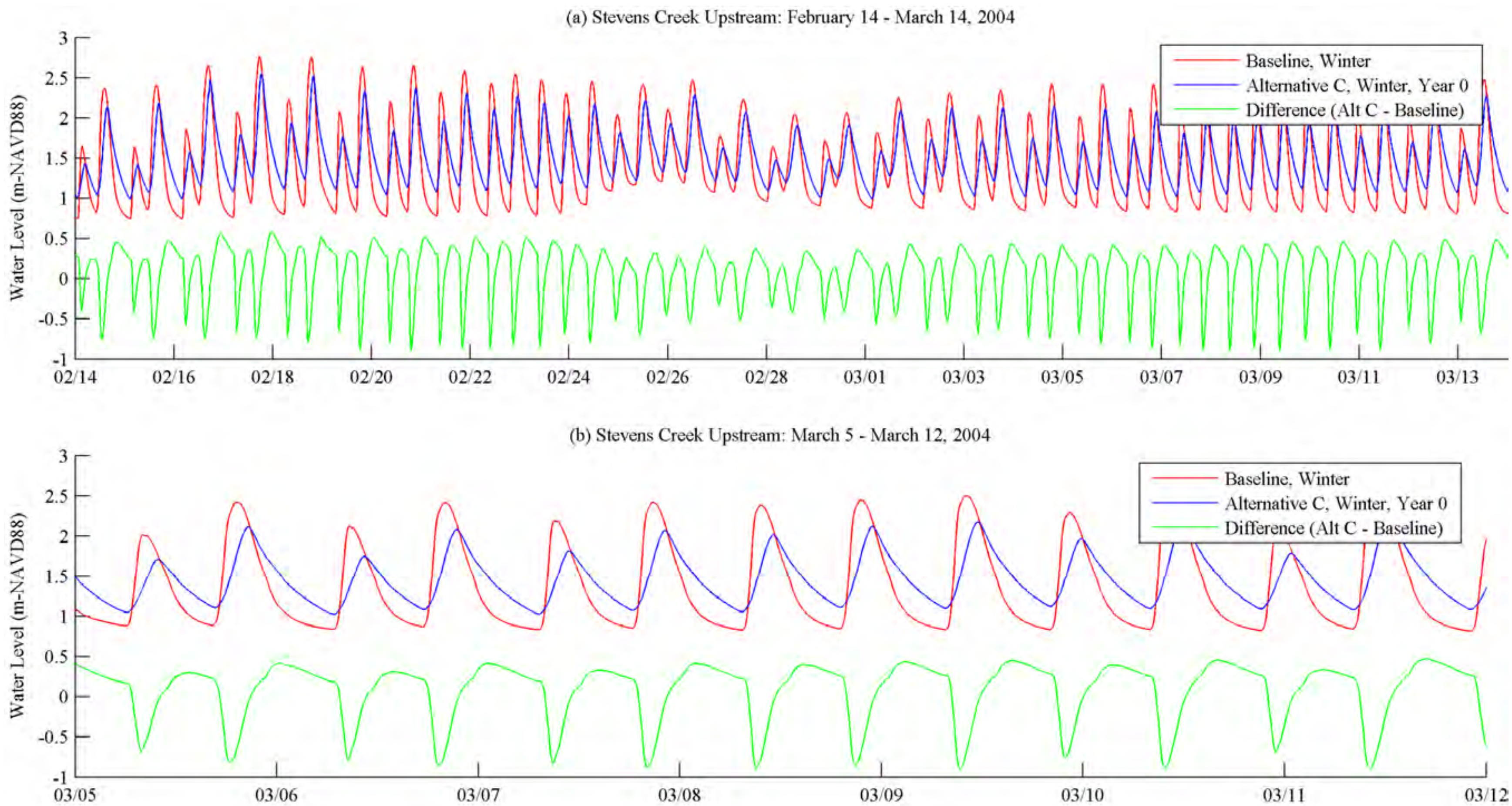

figure 5-23

South Bay Salt Pond Restoration Project

Water Levels, Stevens Creek Upstream, Alt C, Year 0, Winter

PWA

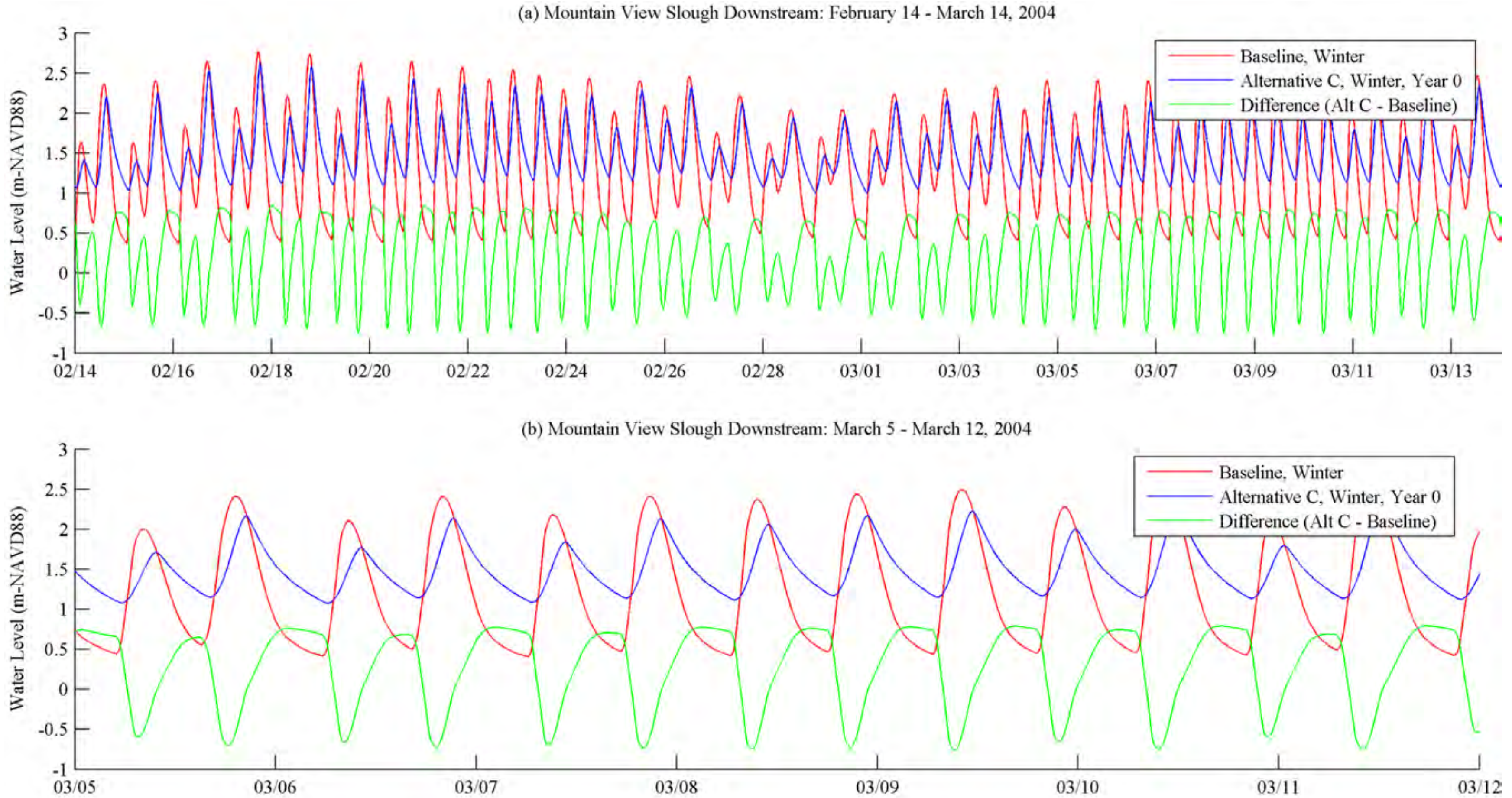

figure 5-24

South Bay Salt Pond Restoration Project

Water Levels, Mountain View Slough Downstream, Alt C, Year 0, Winter

PWA

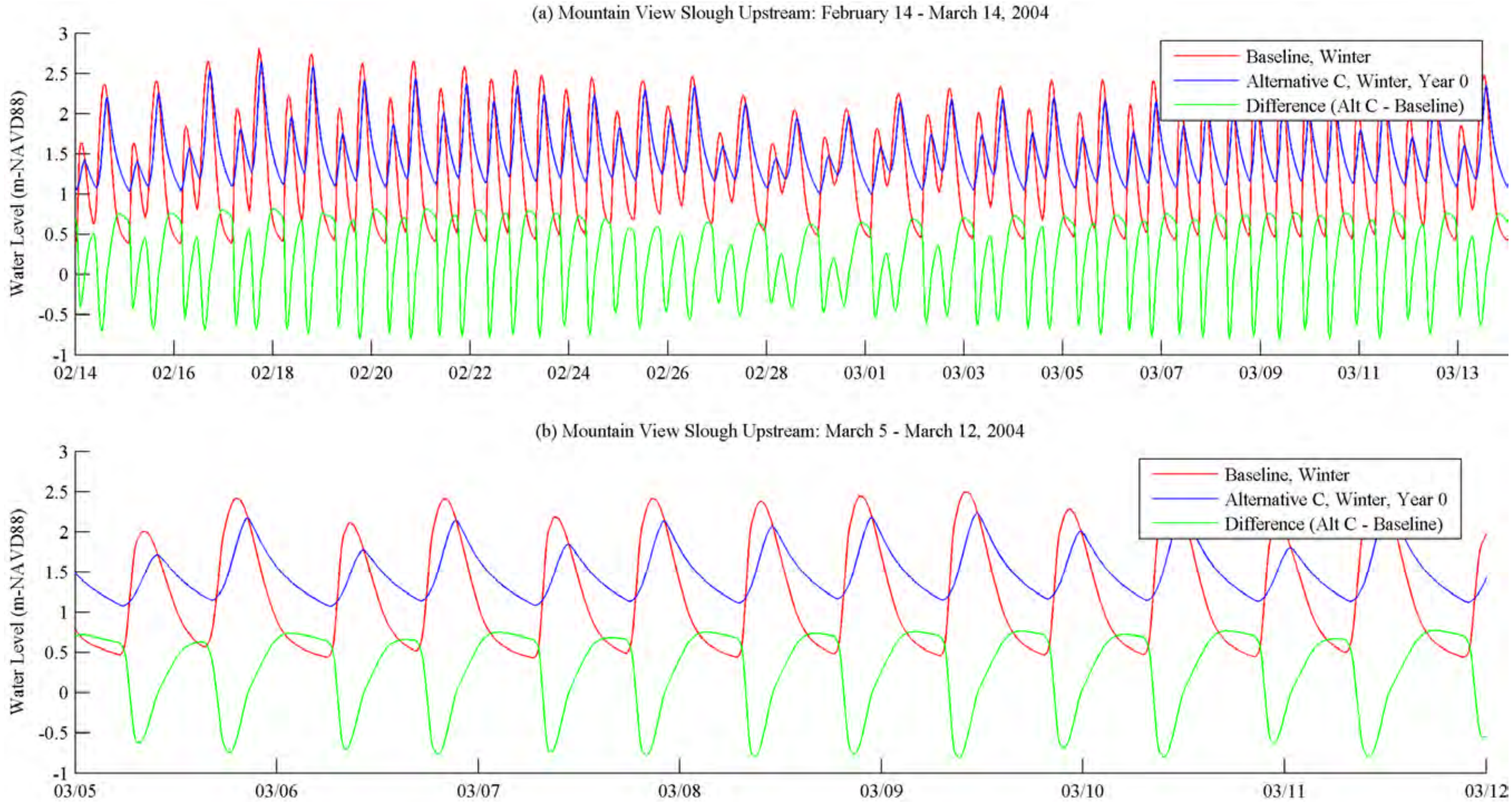

figure 5-25

South Bay Salt Pond Restoration Project

Water Levels, Mountain View Slough Upstream, Alt C, Year 0, Winter

PWA

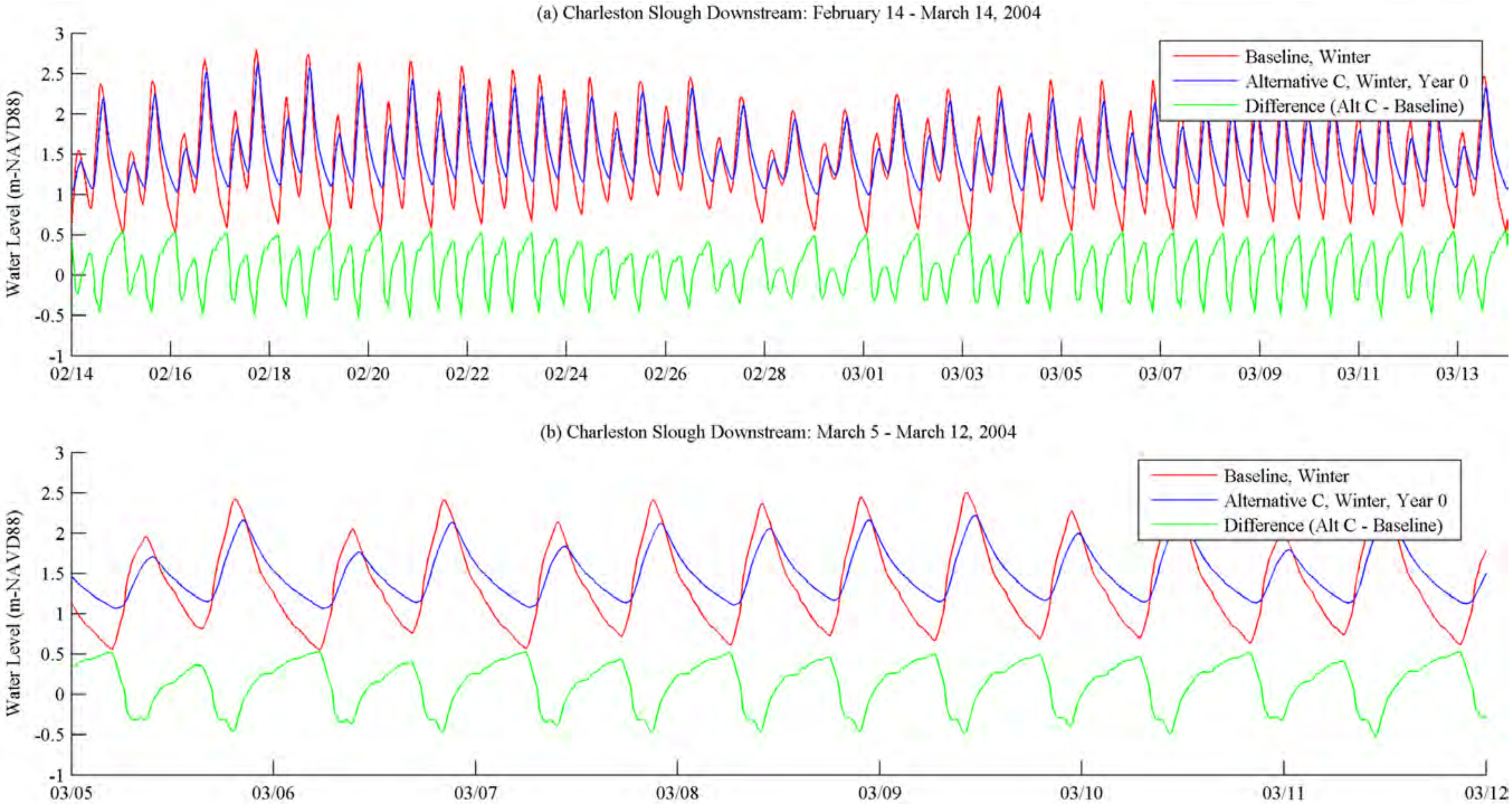

figure 5-26

South Bay Salt Pond Restoration Project

Water Levels, Charleston Slough Downstream, Alt C, Year 0, Winter

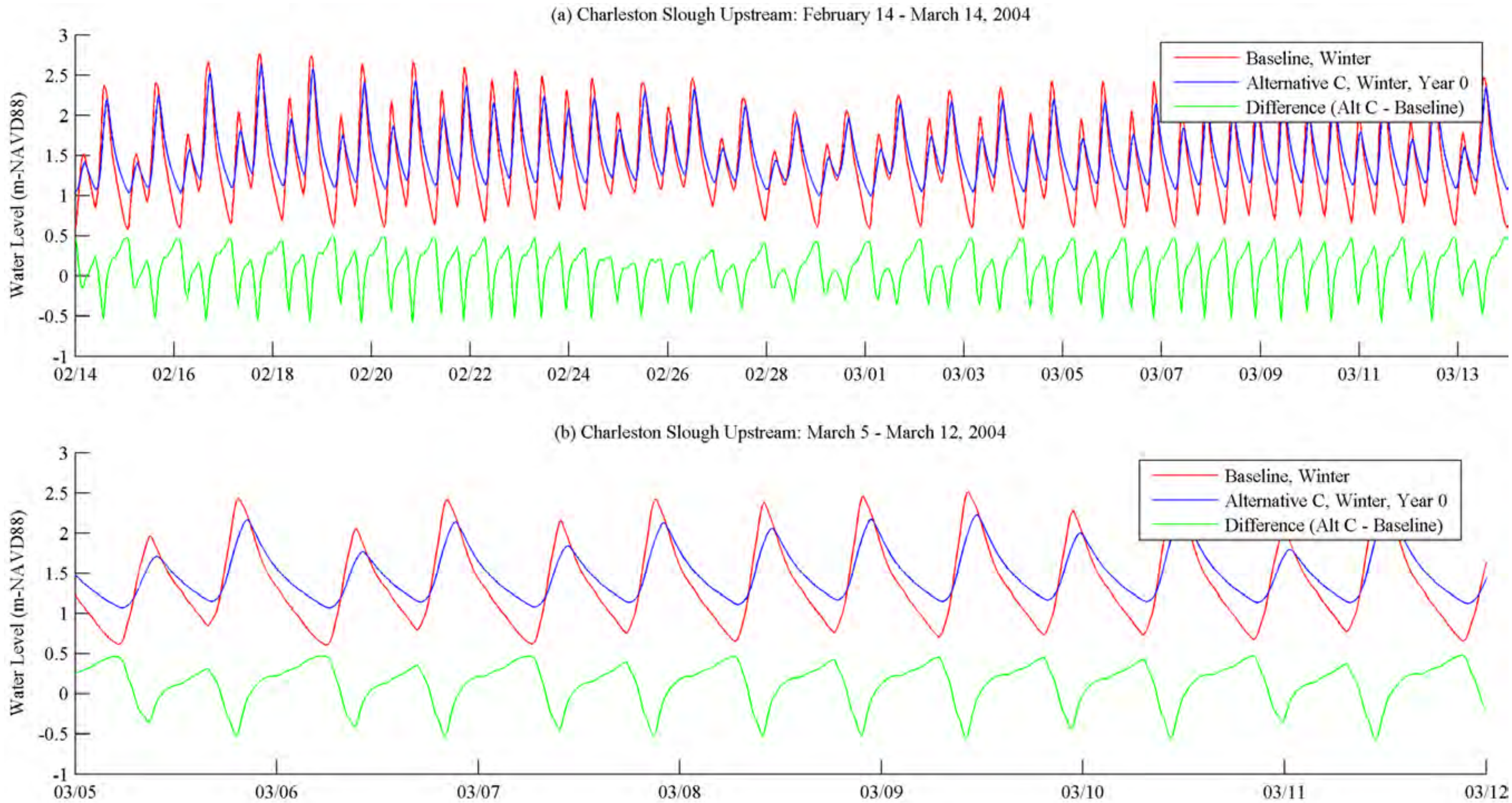

figure 5-27

South Bay Salt Pond Restoration Project

Water Levels, Charleston Slough Upstream, Alt C, Year 0, Winter

PWA

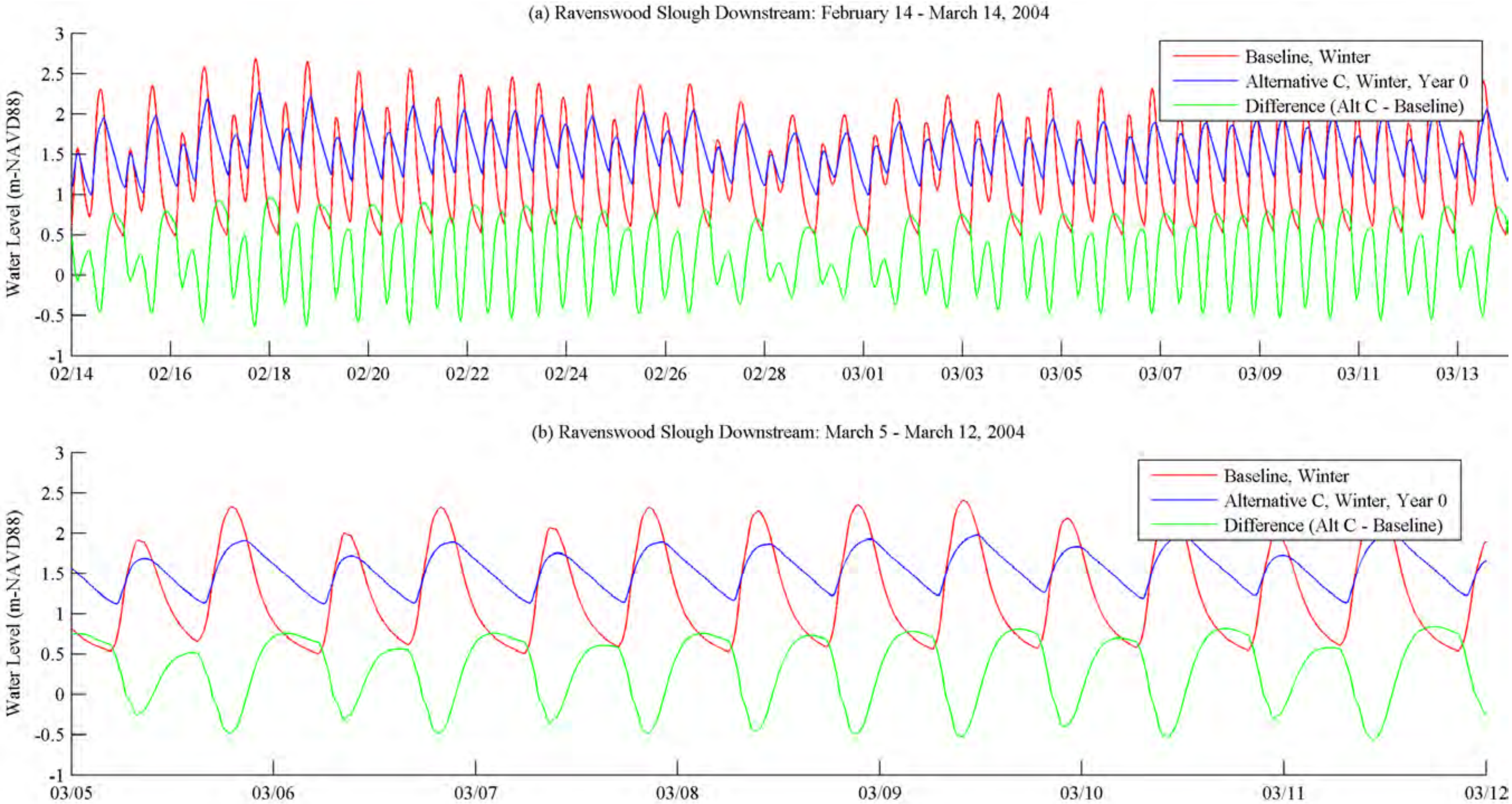

figure *5-28*

South Bay Salt Pond Restoration Project

Water Levels, Ravenswood Slough Downstream, Alt C, Year 0, Winter

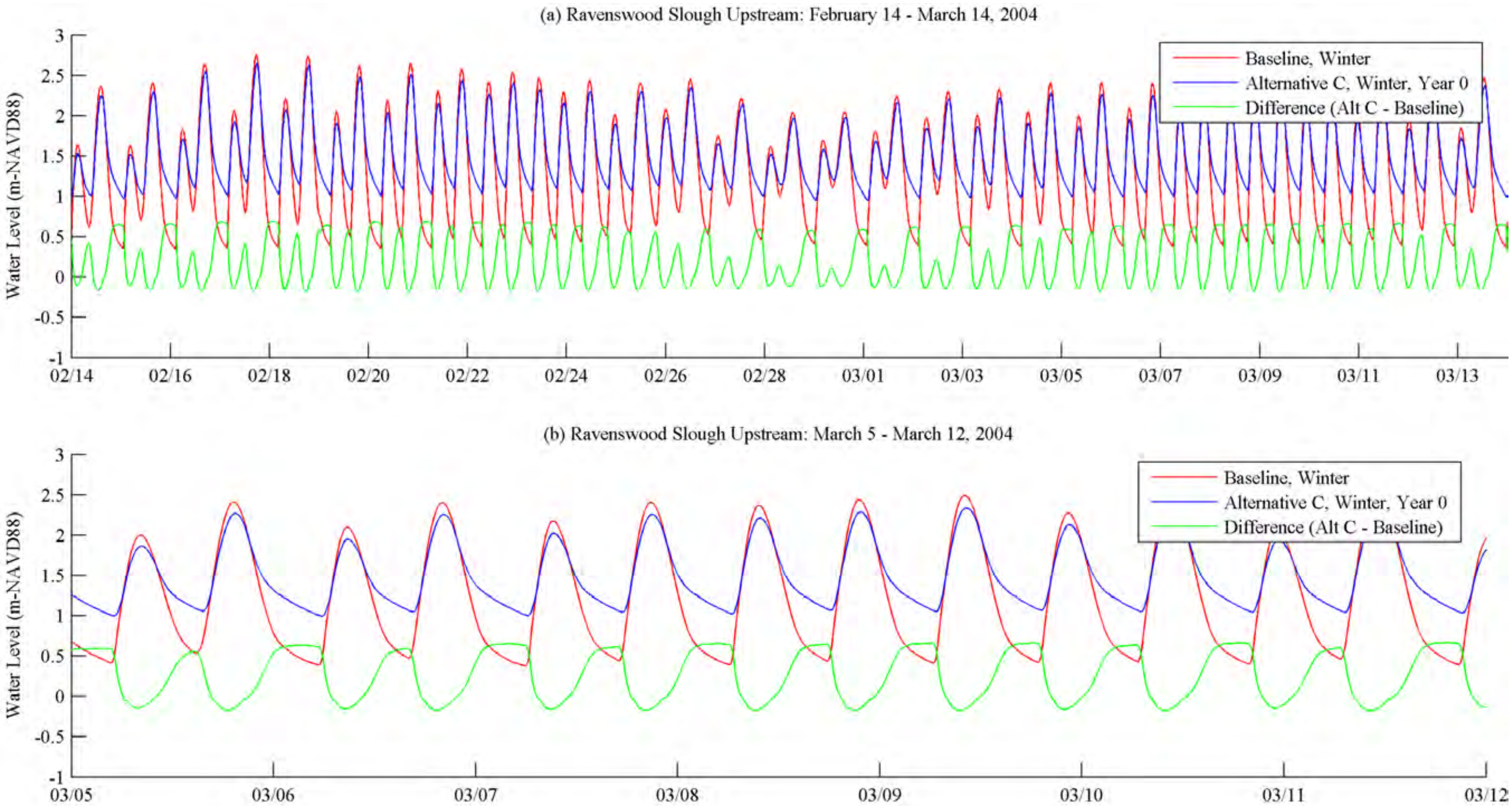

figure 5-29

South Bay Salt Pond Restoration Project

Water Levels, Ravenswood Slough Upstream, Alt C, Year 0, Winter

PWA

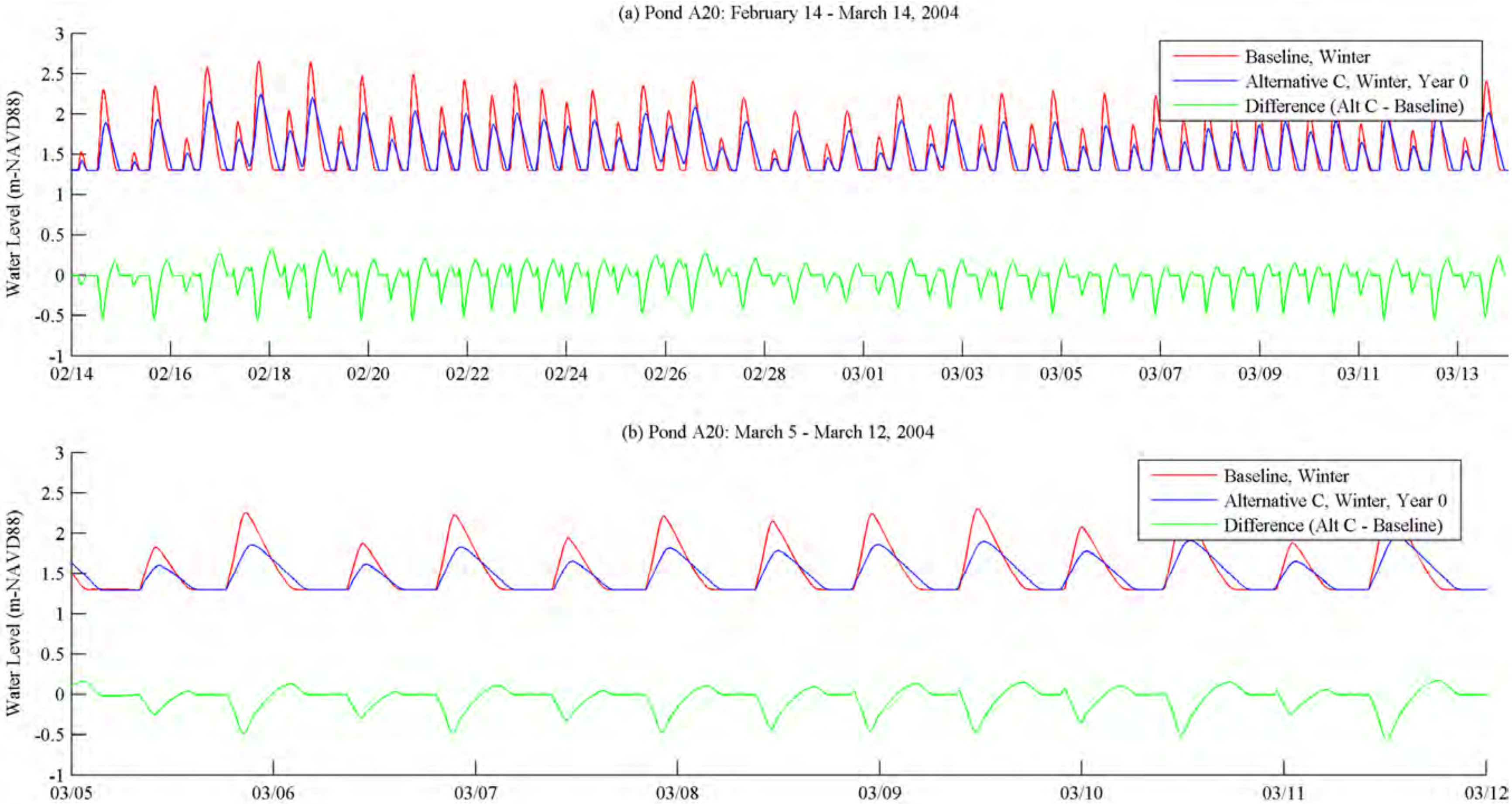

figure 5-30

South Bay Salt Pond Restoration Project

Water Levels, Pond A20, Alt C, Year 0, Winter

PWA

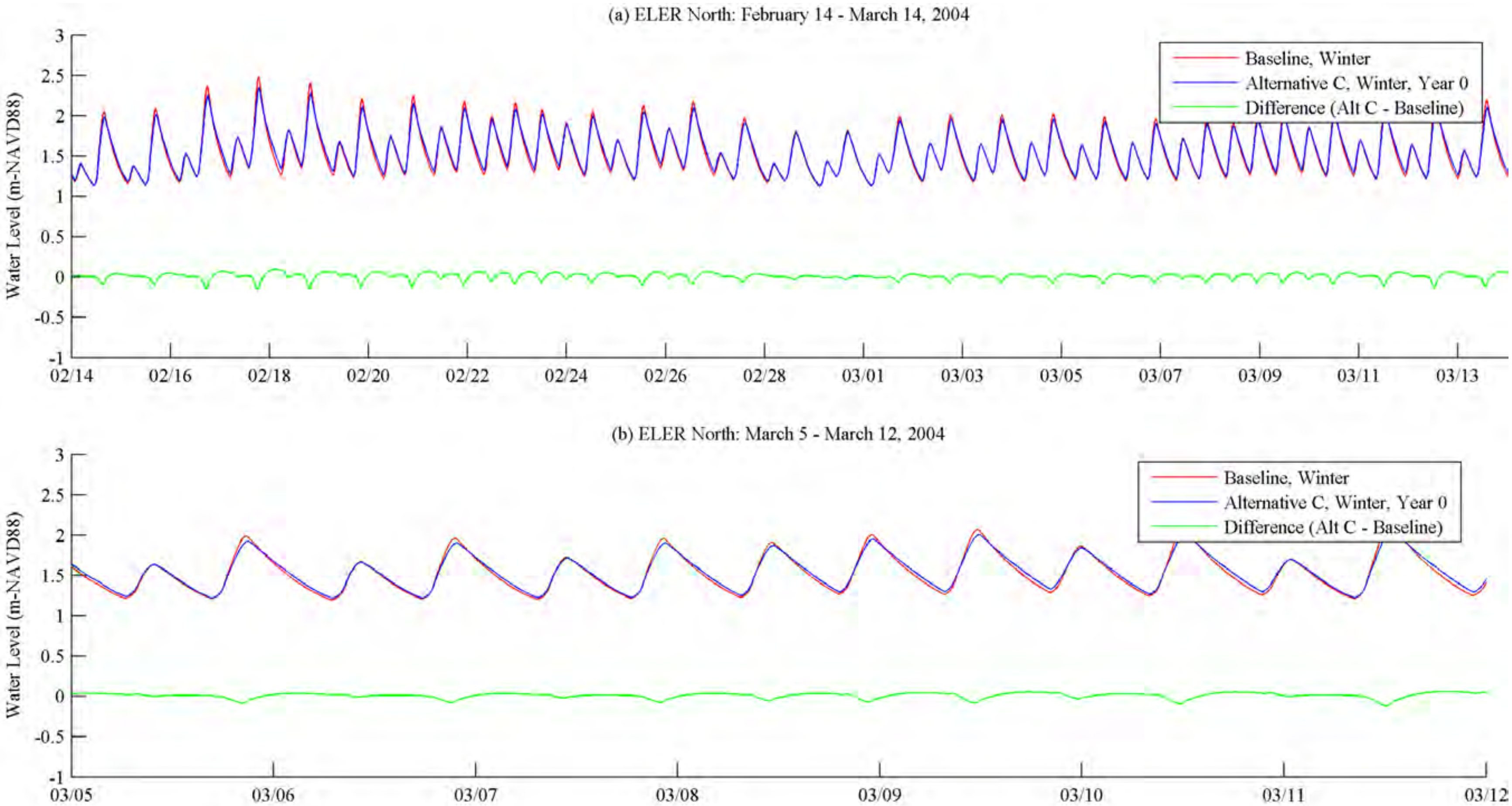

figure 5-31

South Bay Salt Pond Restoration Project

Water Levels, ELER North, Alt C, Year 0, Winter

PWA

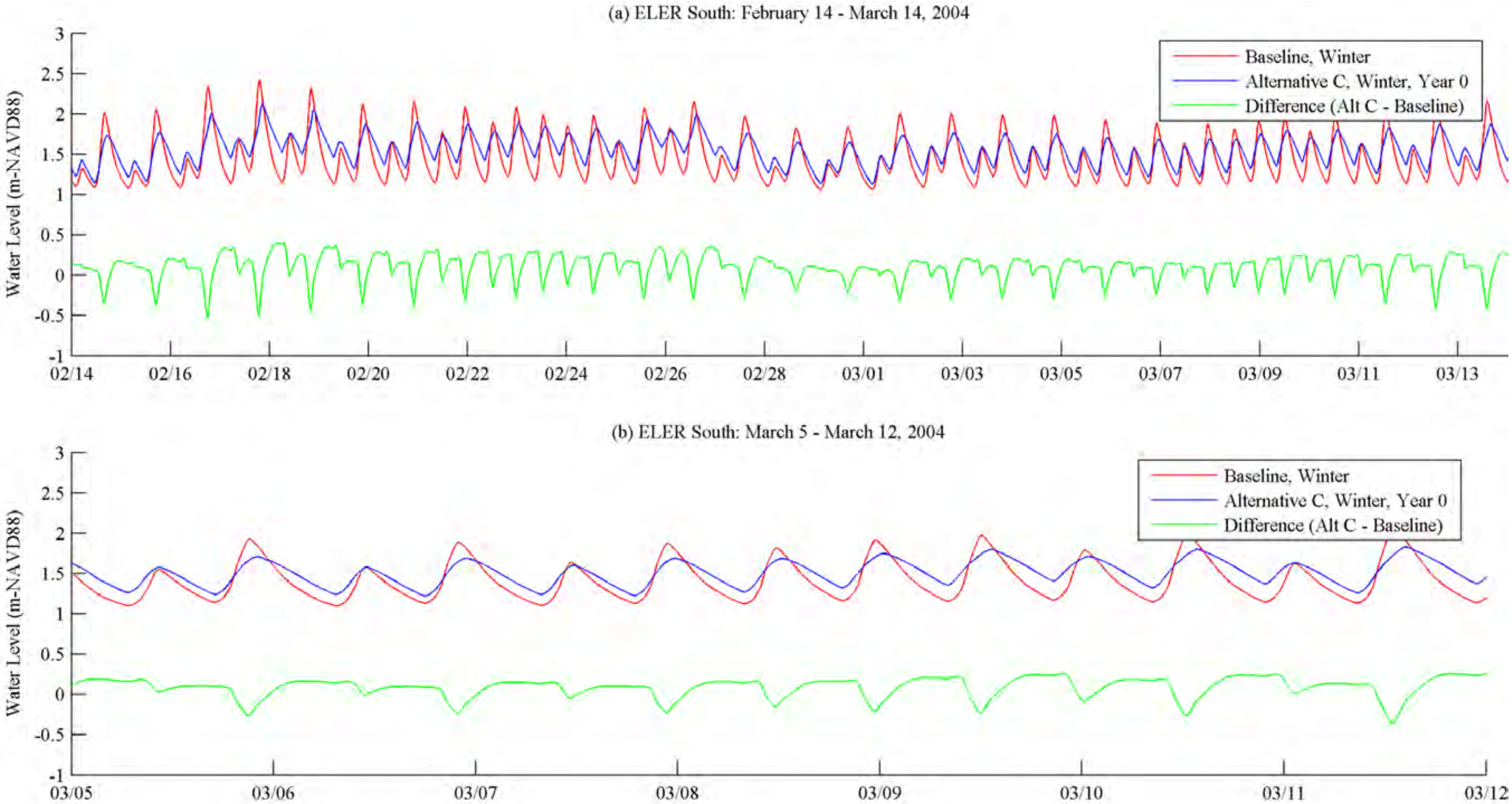

figure 5-32

South Bay Salt Pond Restoration Project

Water Levels, ELER South, Alt C, Year 0, Winter

PWA

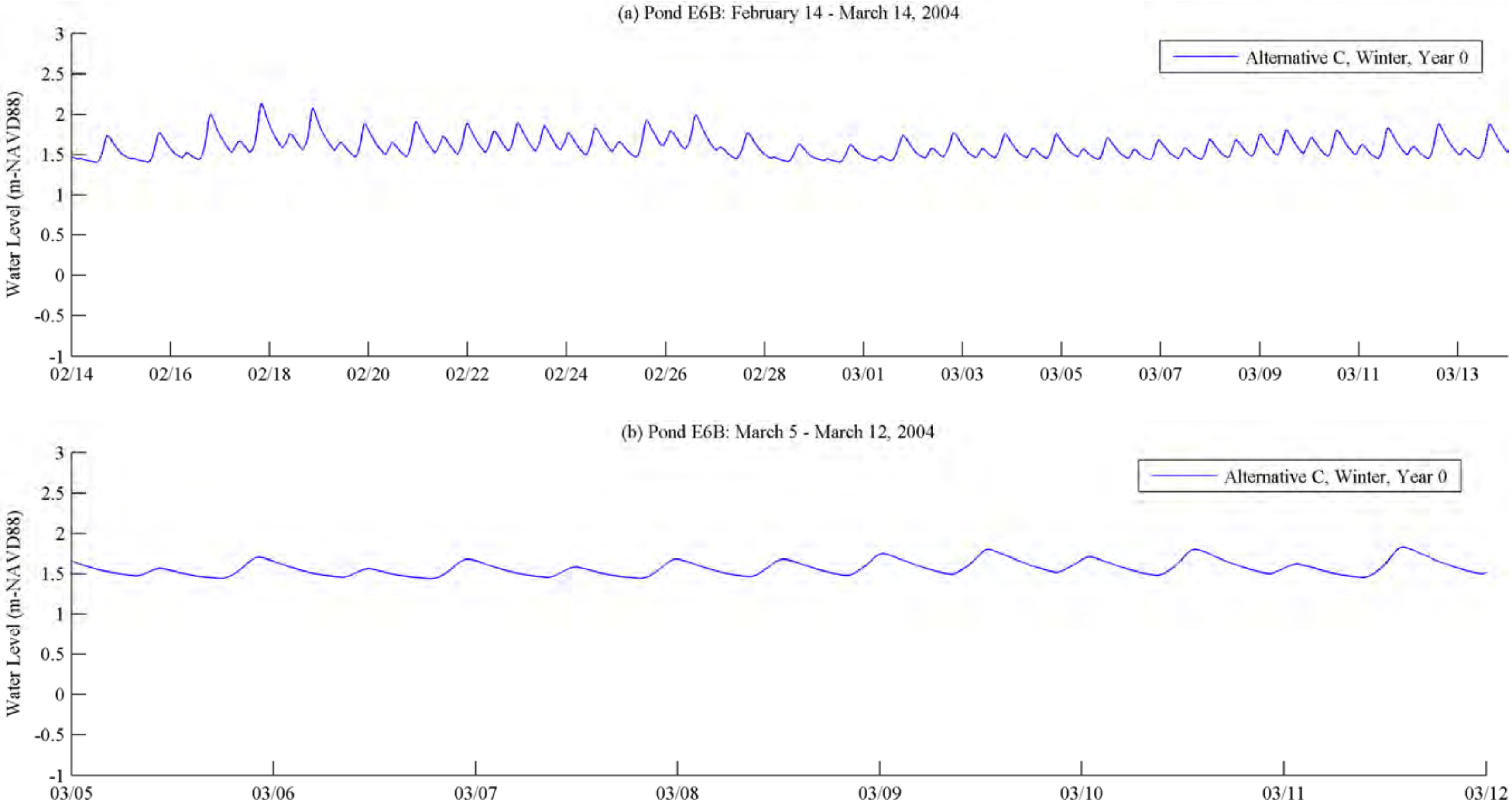

figure 5-33

South Bay Salt Pond Restoration Project

Water Levels, Pond E6B, Alt C, Year 0, Winter

PWA

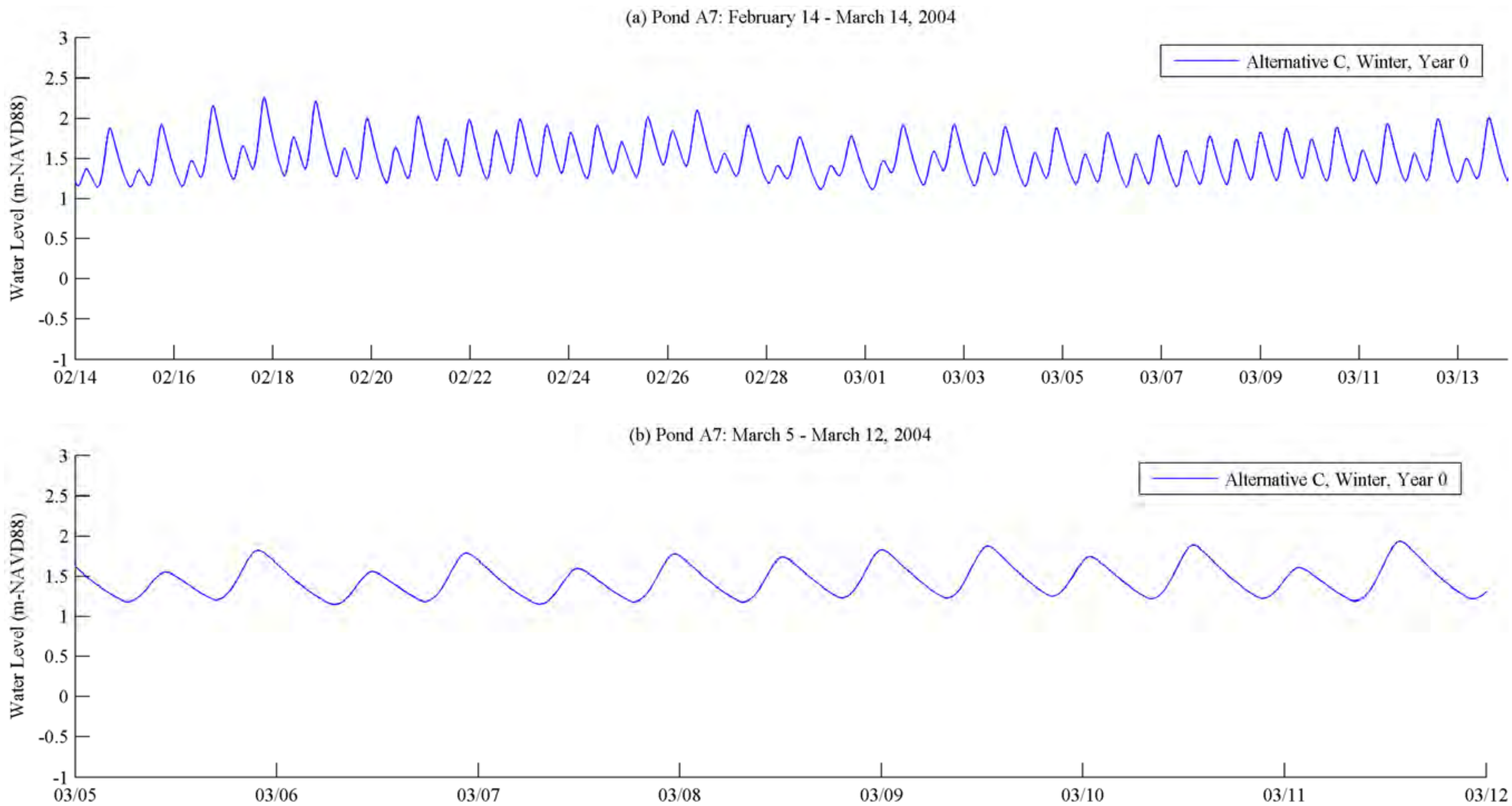

figure 5-34

South Bay Salt Pond Restoration Project

Water Levels, Pond A7, Alt C, Year 0, Winter

PWA

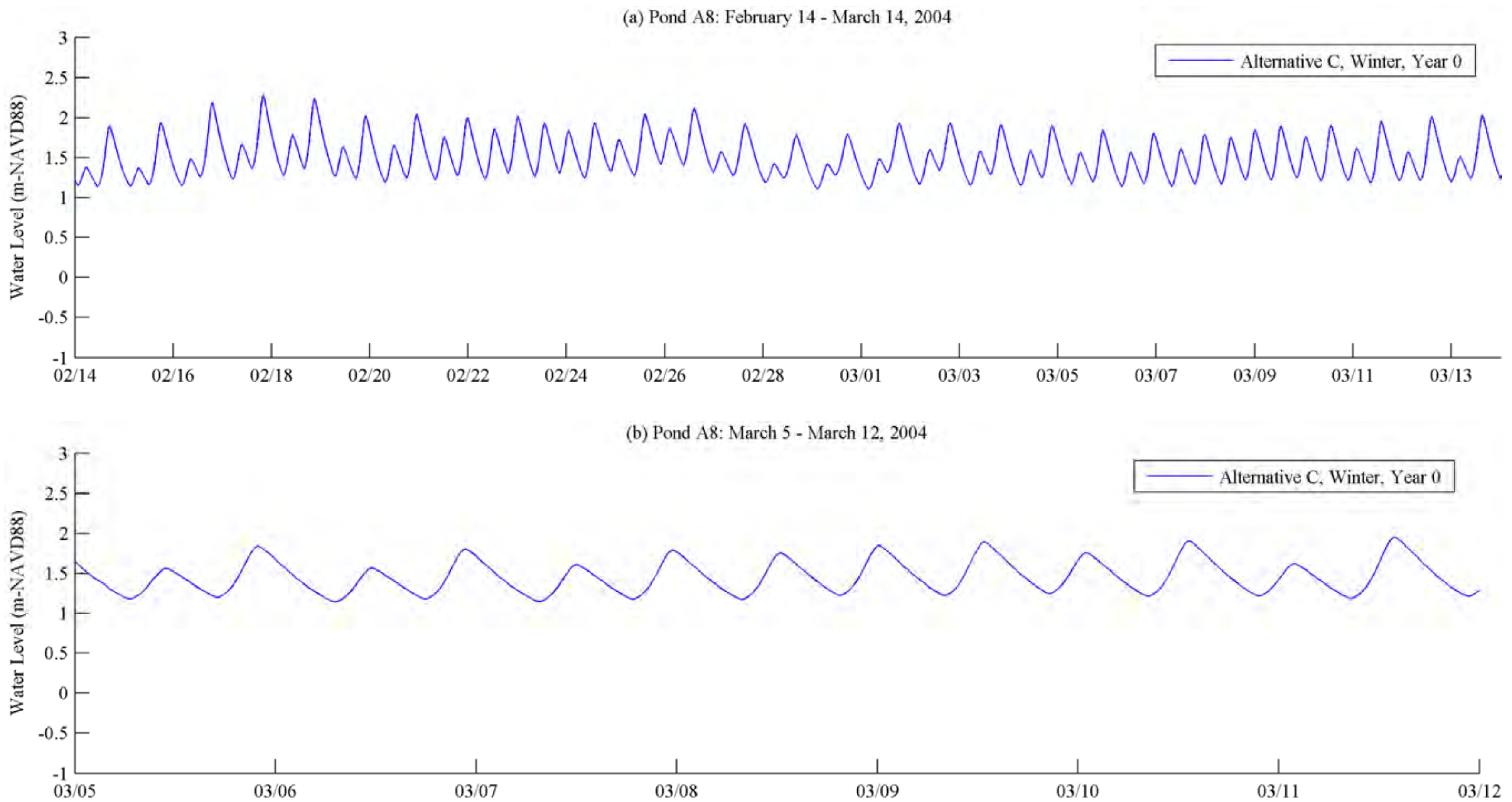

figure *5-35*

South Bay Salt Pond Restoration Project

Water Levels, Pond A8, Alt C, Year 0, Winter

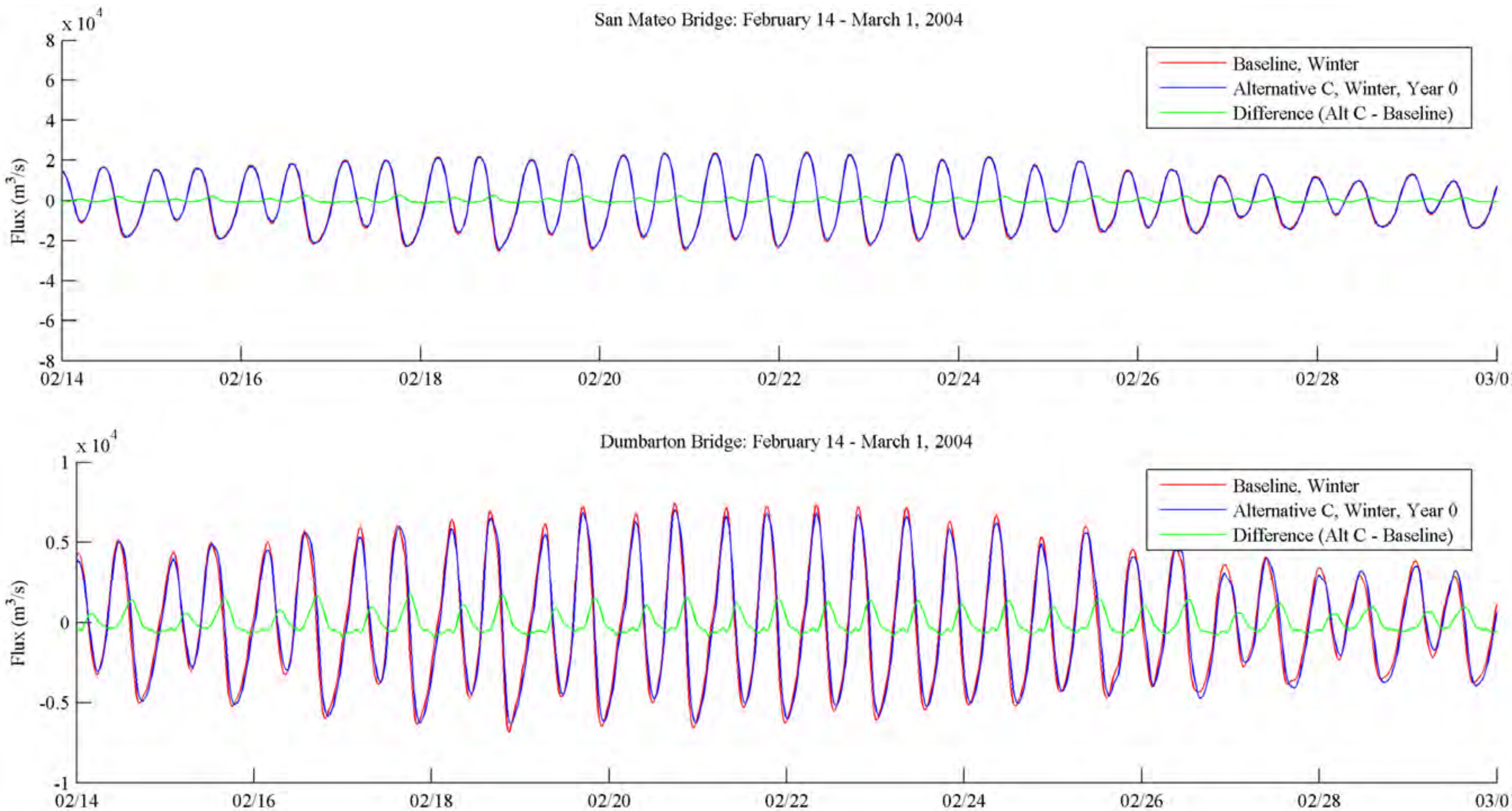

figure 5-36

South Bay Salt Pond Restoration Project

Tidal Prism, San Mateo and Dumbarton Bridges, Alt C, Year 0, Winter

PWA

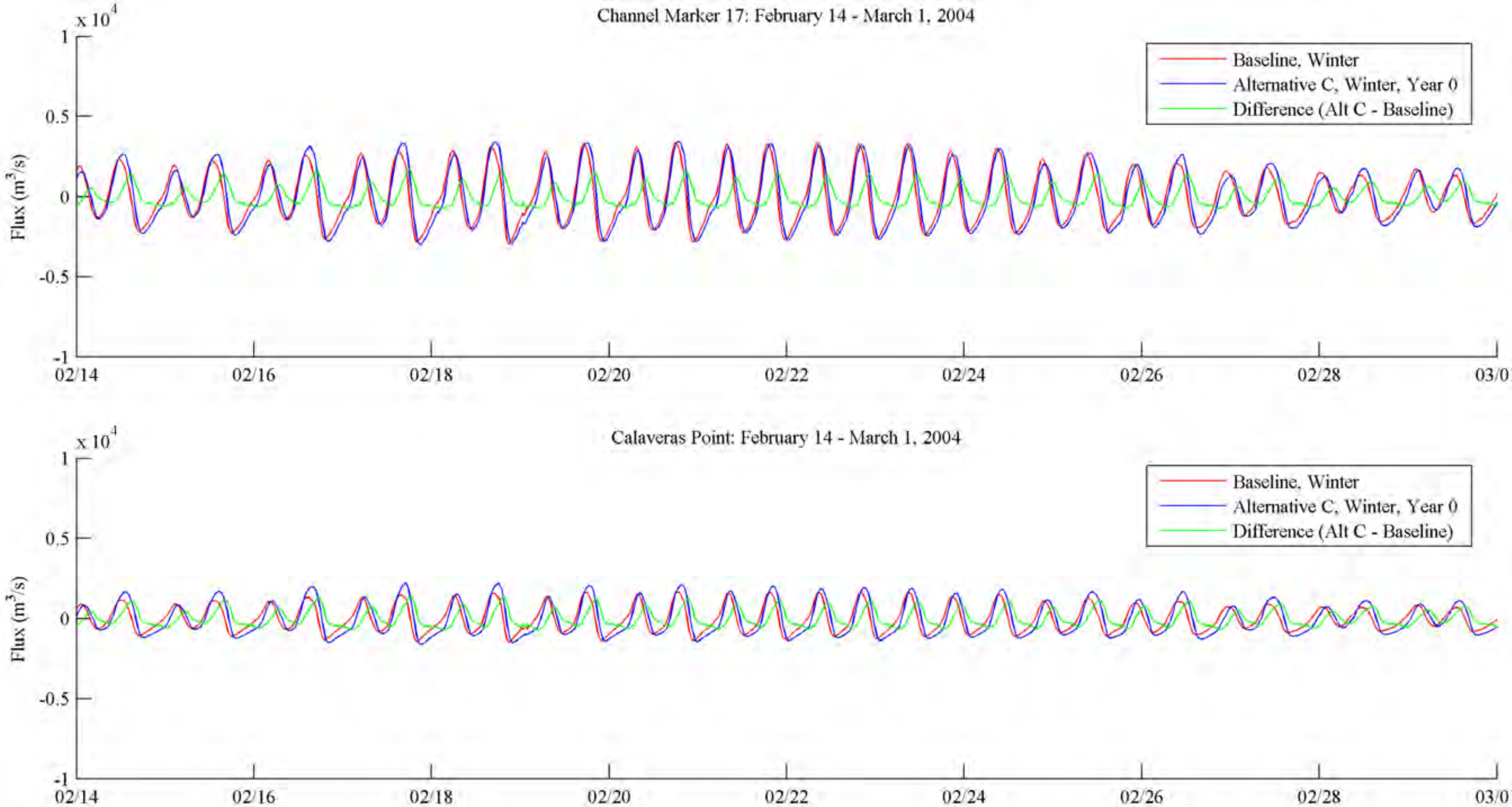

figure 5-37

South Bay Salt Pond Restoration Project

Tidal Prism, Channel Marker 17 and Calaveras Point, Alt C, Year 0, Winter

PWA

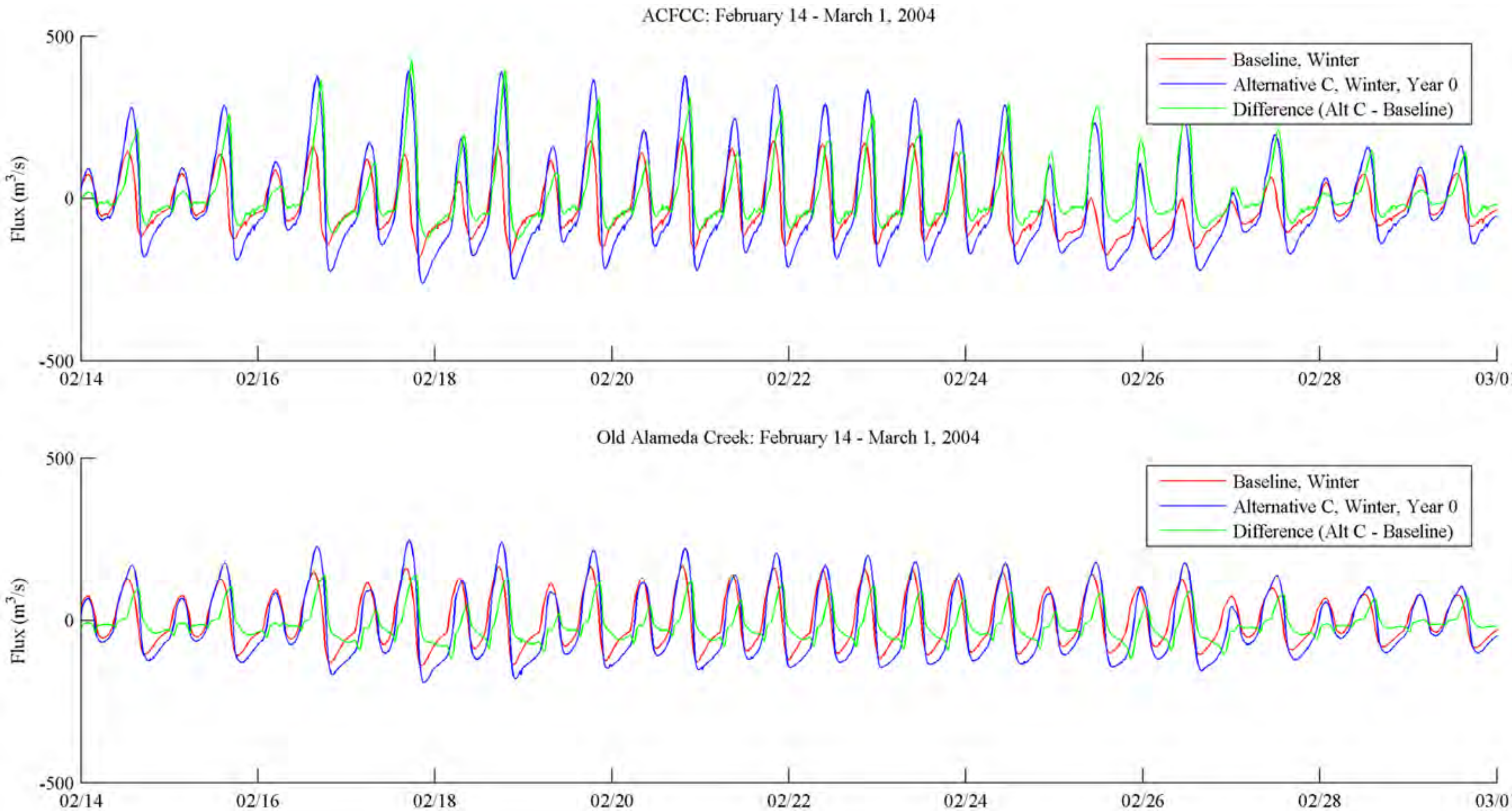

figure 5-38

South Bay Salt Pond Restoration Project

Tidal Prism, ACFCC and Old Alameda Creek, Alt C, Year 0, Winter

PWA

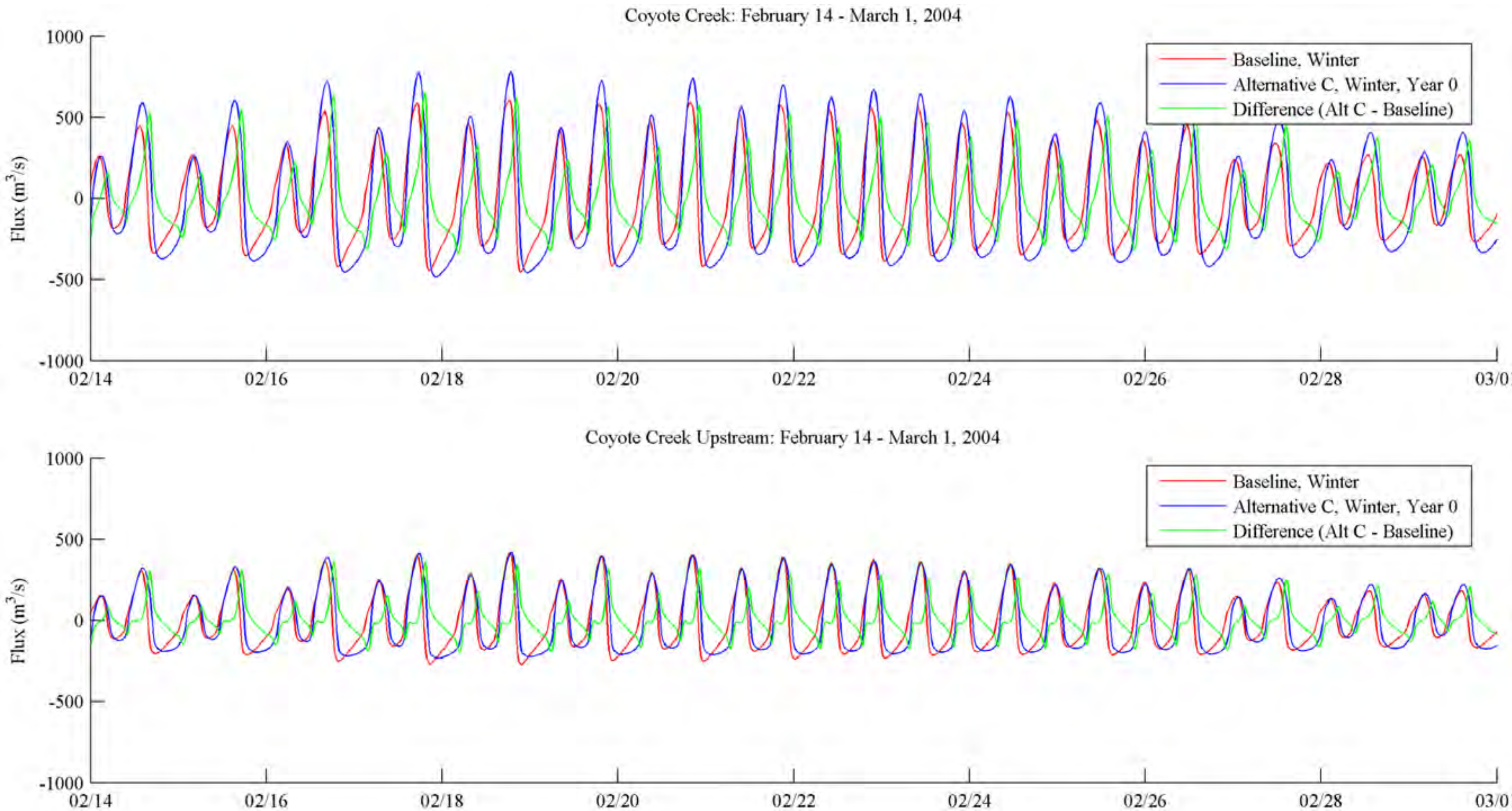

figure 5-39

South Bay Salt Pond Restoration Project

Tidal Prism, Coyote Creek, Alt C, Year 0, Winter

PWA

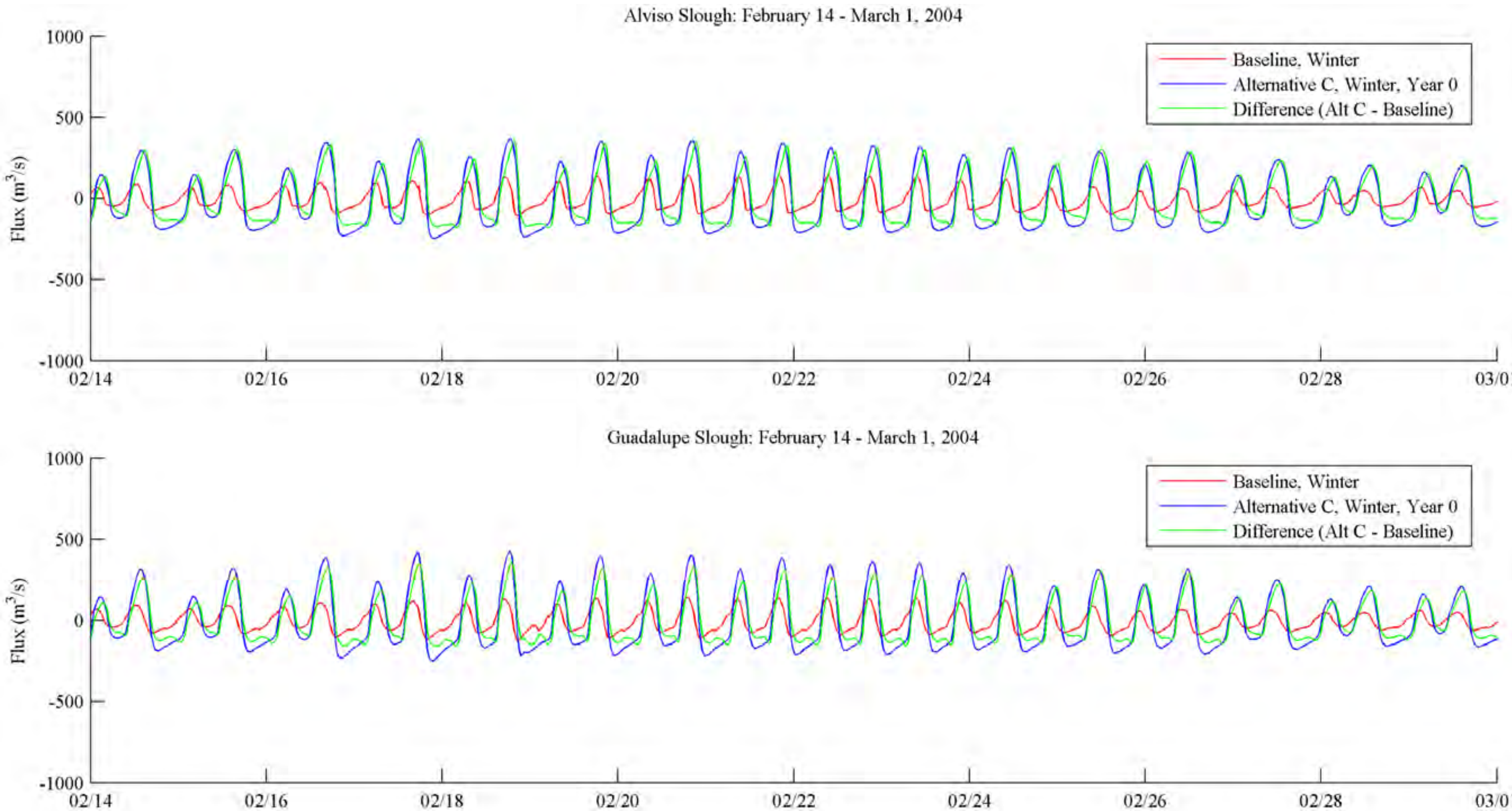

figure *5-40*

South Bay Salt Pond Restoration Project

Tidal Prism, Alviso and Guadalupe Sloughs, Alt C, Year 0, Winter

PWA

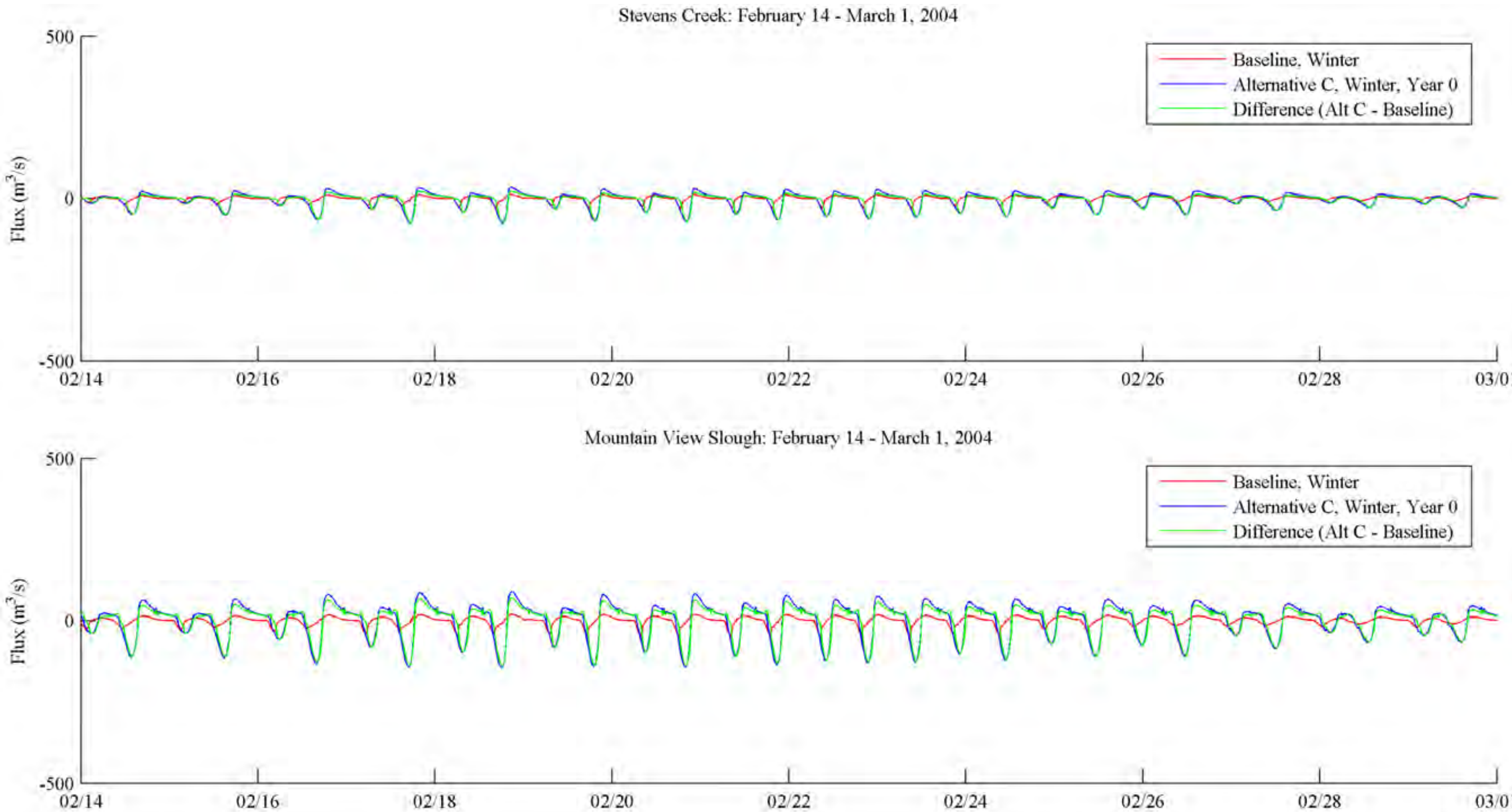

figure 5-41

South Bay Salt Pond Restoration Project

Tidal Prism, Stevens Creek and Mountain View Slough, Alt C, Year 0, Winter

PWA

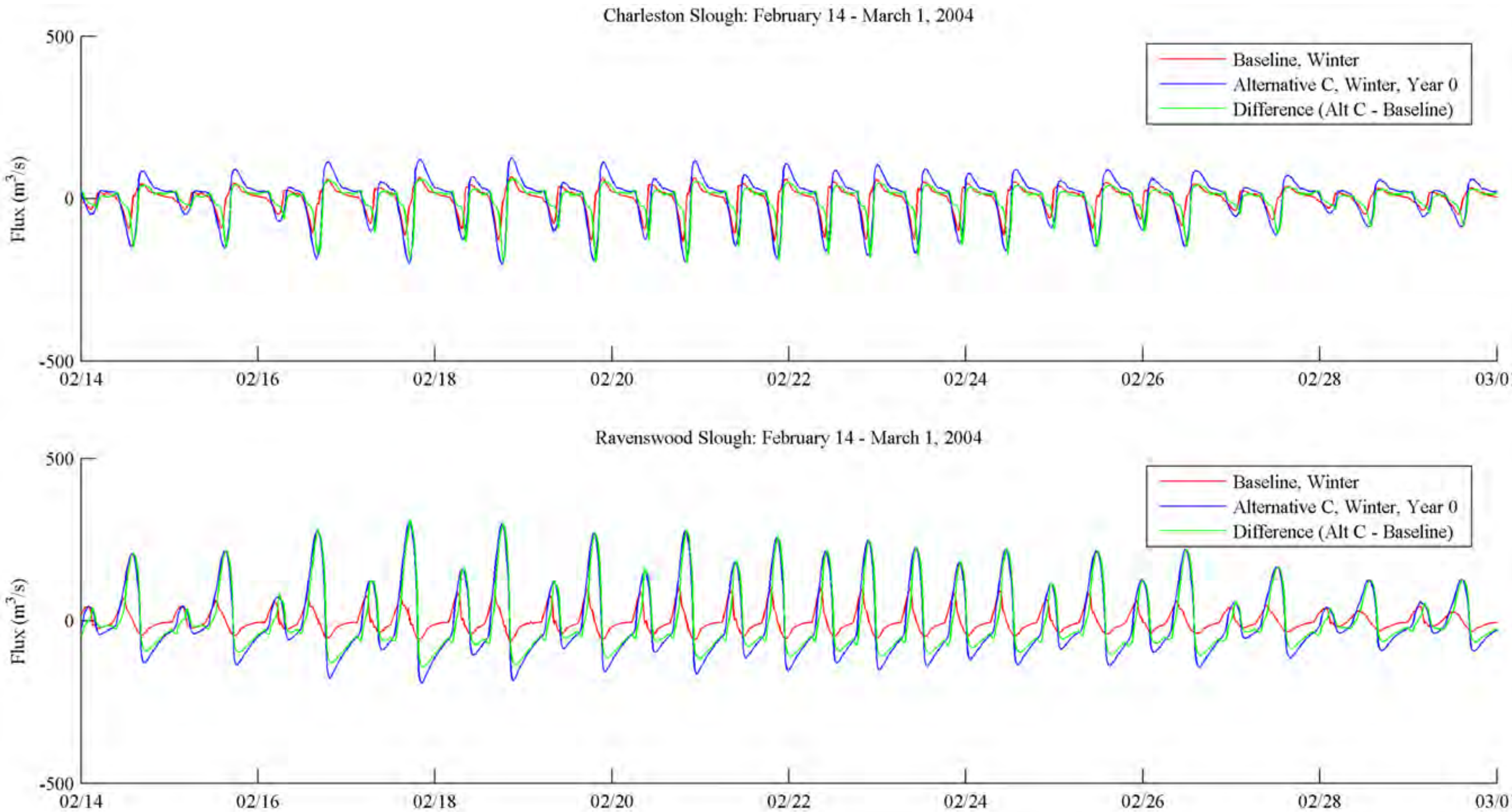

figure 5-42

South Bay Salt Pond Restoration Project

Tidal Prism, Charleston and Ravenswood Sloughs, Alt C, Year 0, Winter

PWA

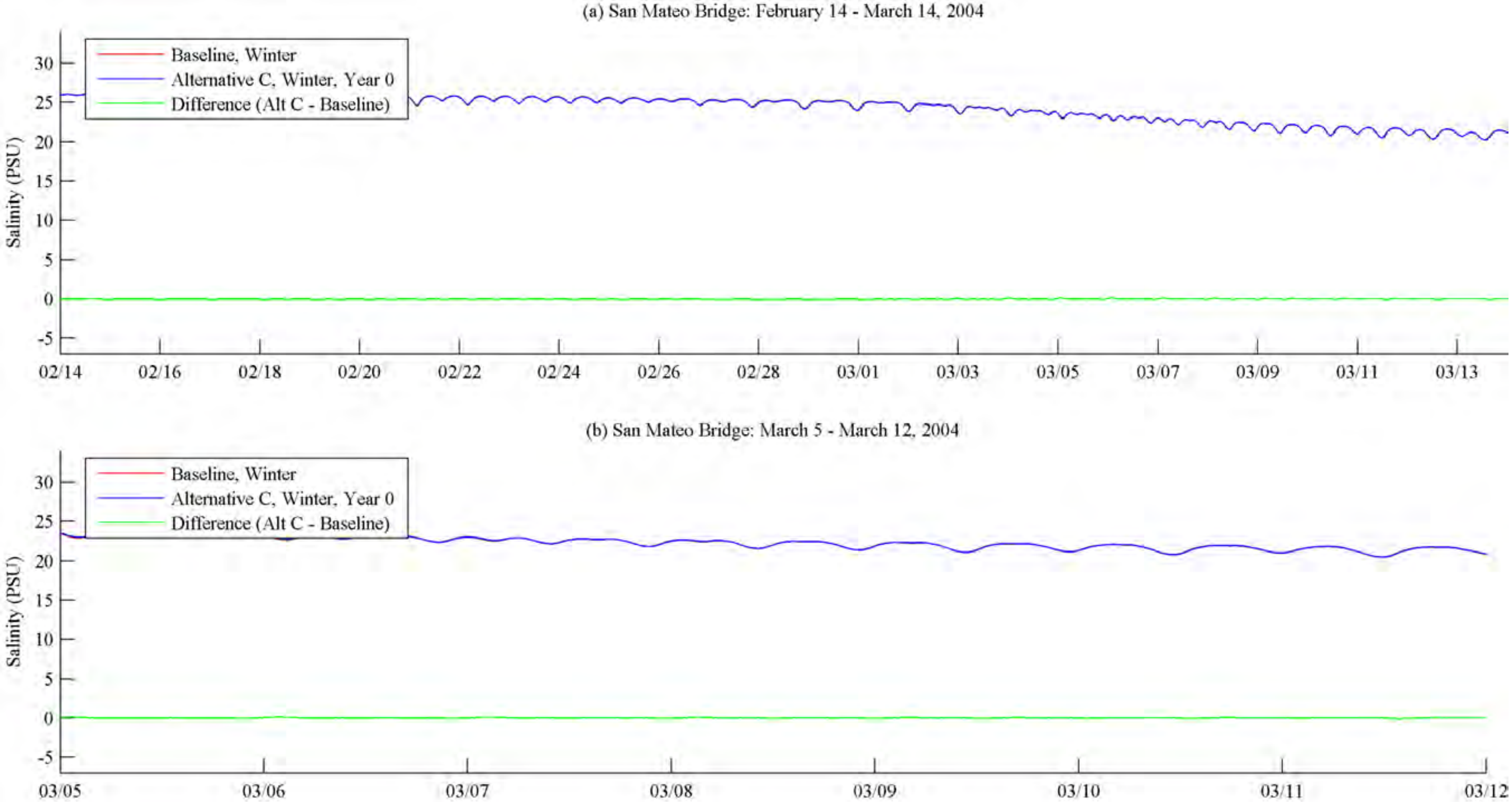

figure 5-43

South Bay Salt Pond Restoration Project

Salinity, San Mateo Bridge, Alt C, Year 0, Winter

PWA

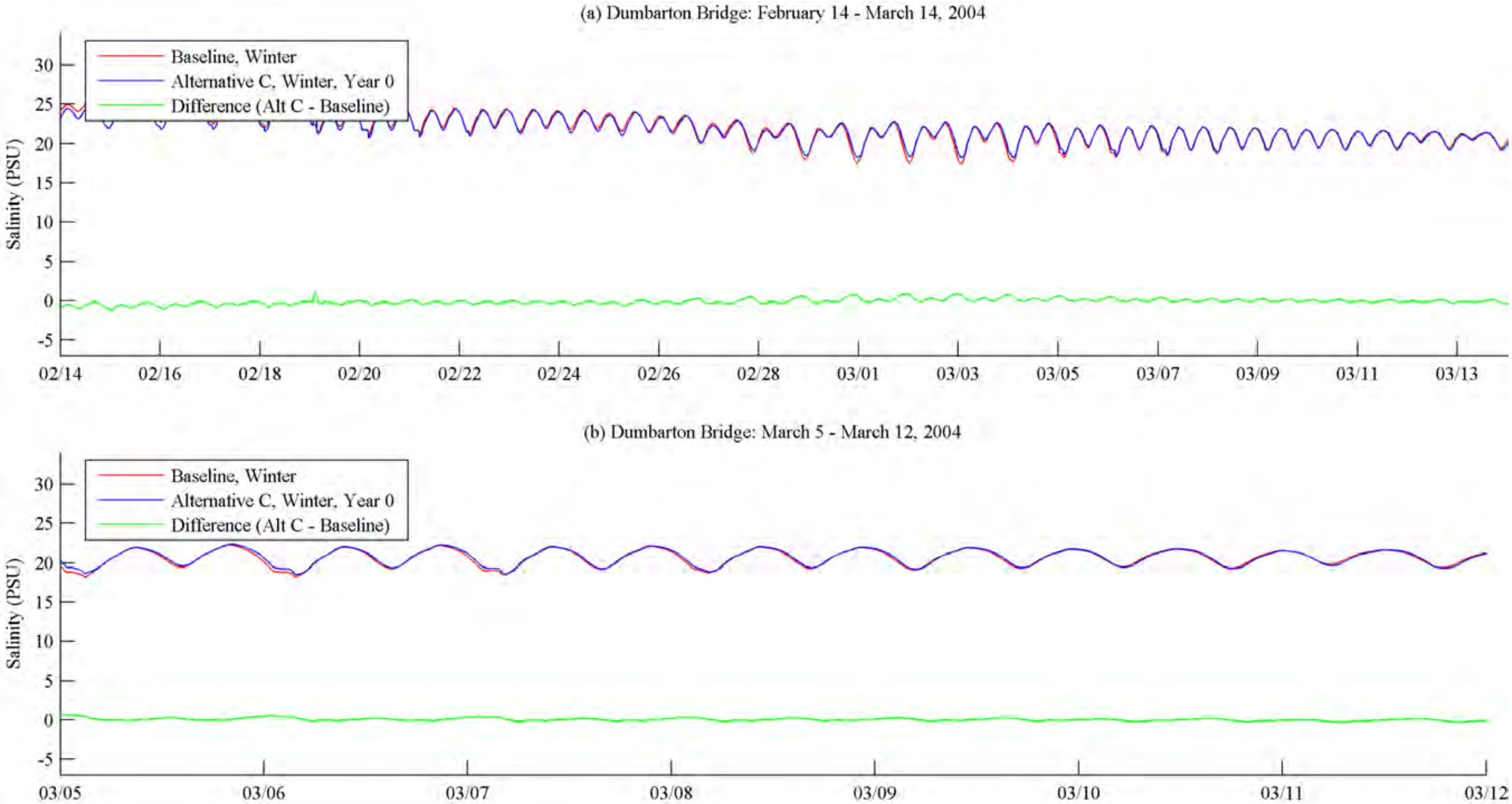

figure *5-44*

South Bay Salt Pond Restoration Project

Salinity, Dumbarton Bridge, Alt C, Year 0, Winter

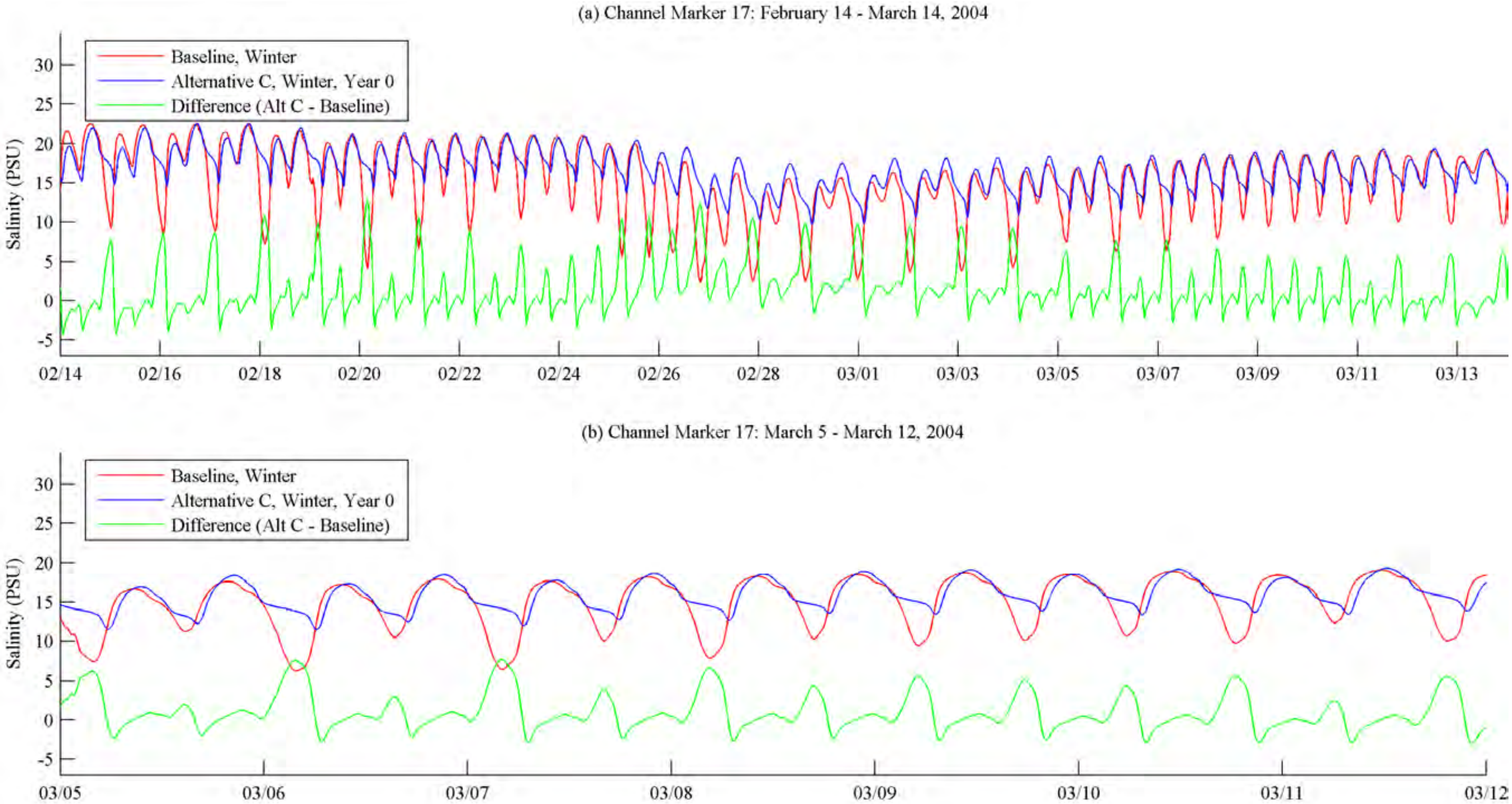

figure 5-45

South Bay Salt Pond Restoration Project

Salinity, Channel Marker 17, Alt C, Year 0, Winter

PWA

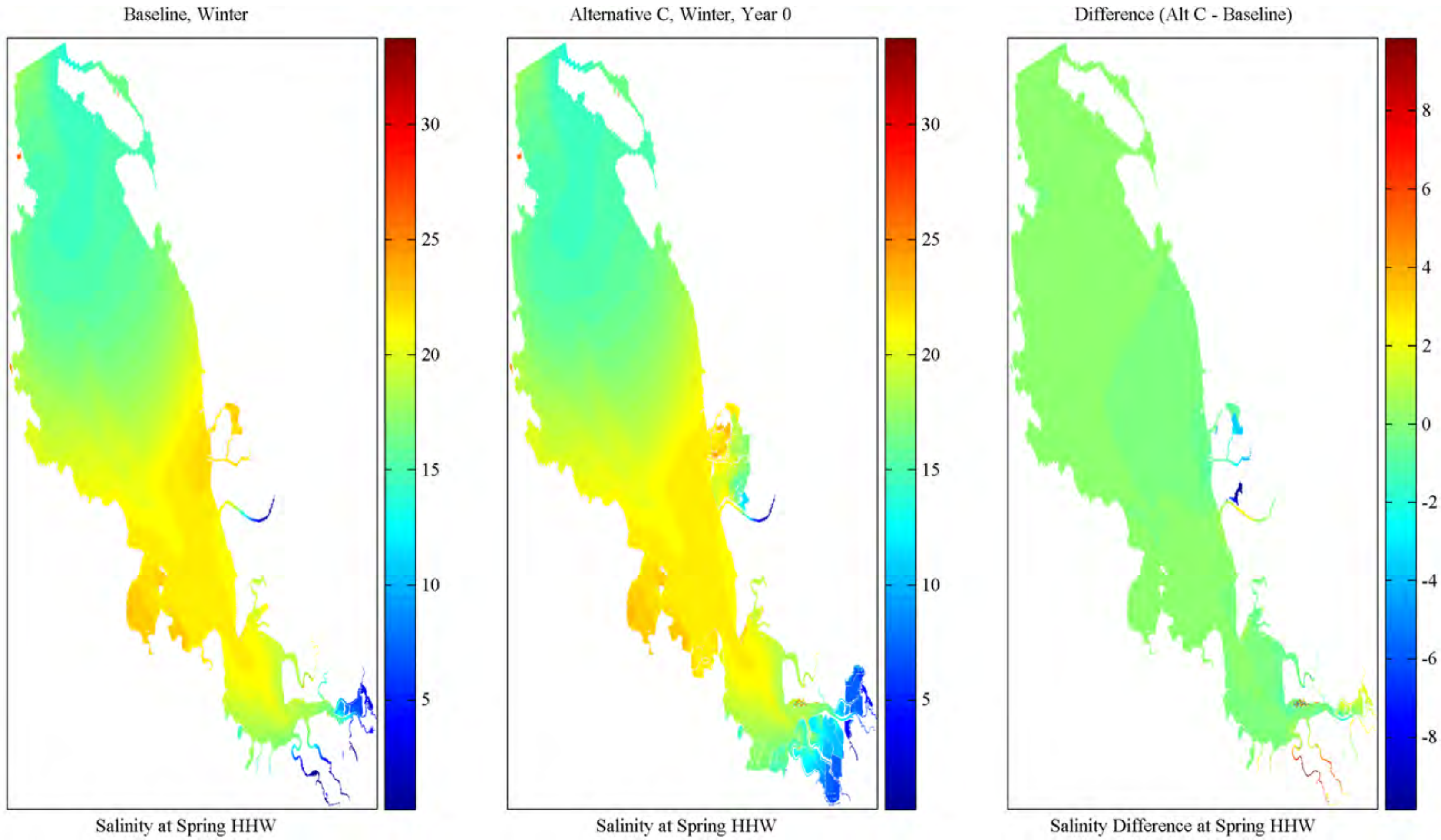

Note: Units shown are PSU

figure *5-46*

South Bay Salt Pond Restoration Project

Salinity at Spring HHW, Alt C, Year 0, Winter

PWA

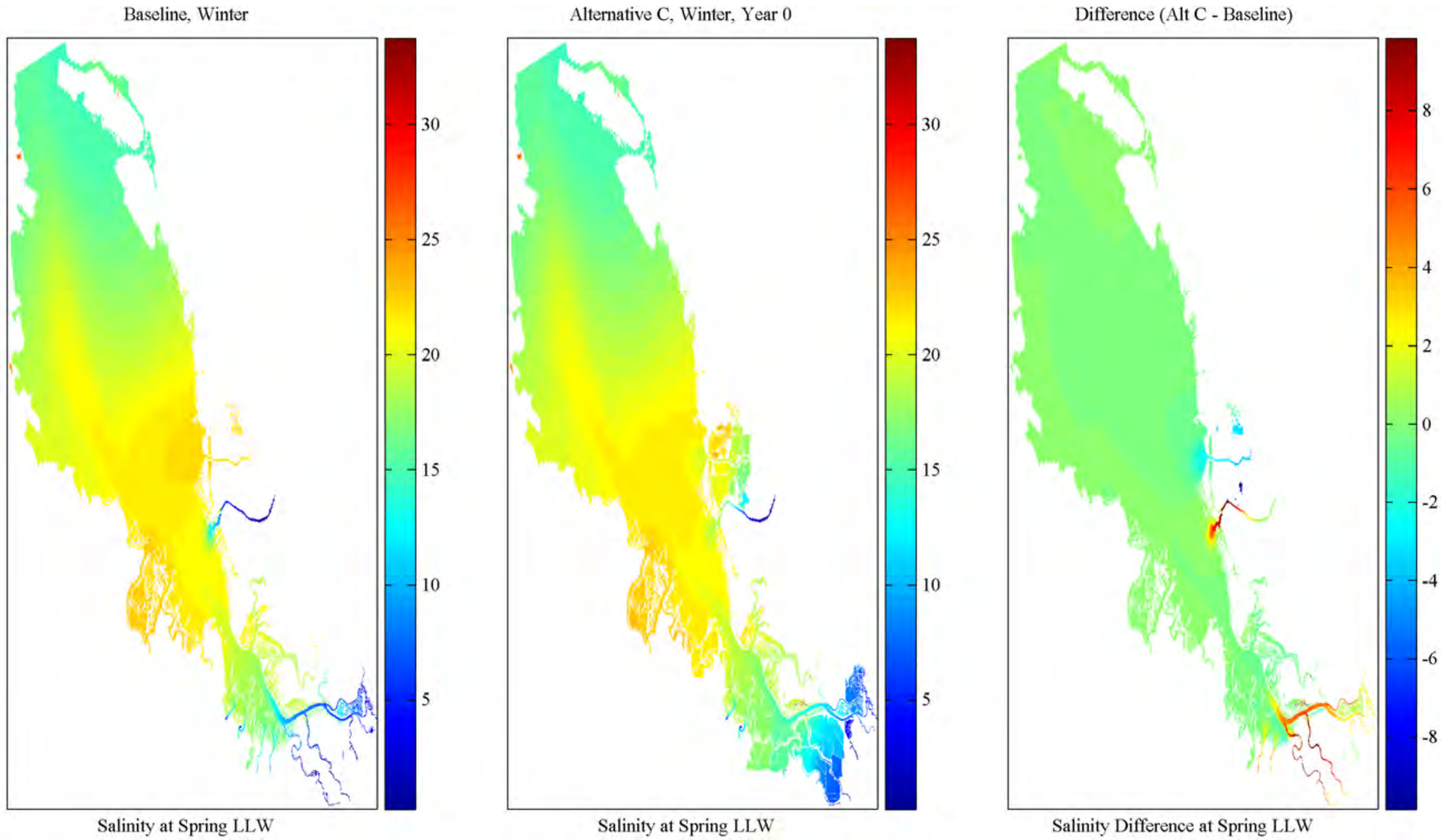

Note: Units shown are PSU

figure 5-47

South Bay Salt Pond Restoration Project

Salinity at Spring LLW, Alt C, Year 0, Winter

PWA

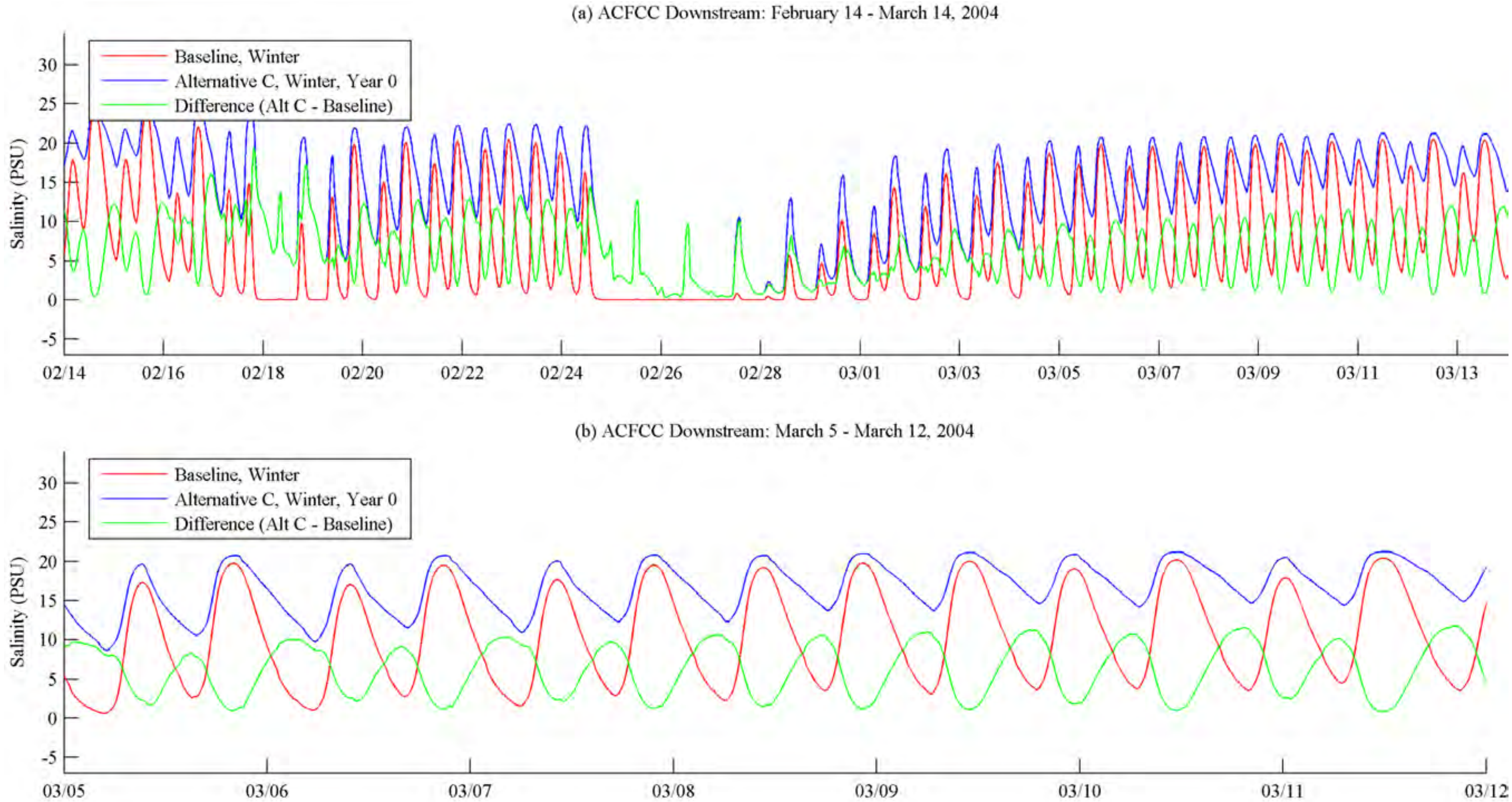

figure *5-48*

South Bay Salt Pond Restoration Project

Salinity, ACFCC Downstream, Alt C, Year 0, Winter

PWA

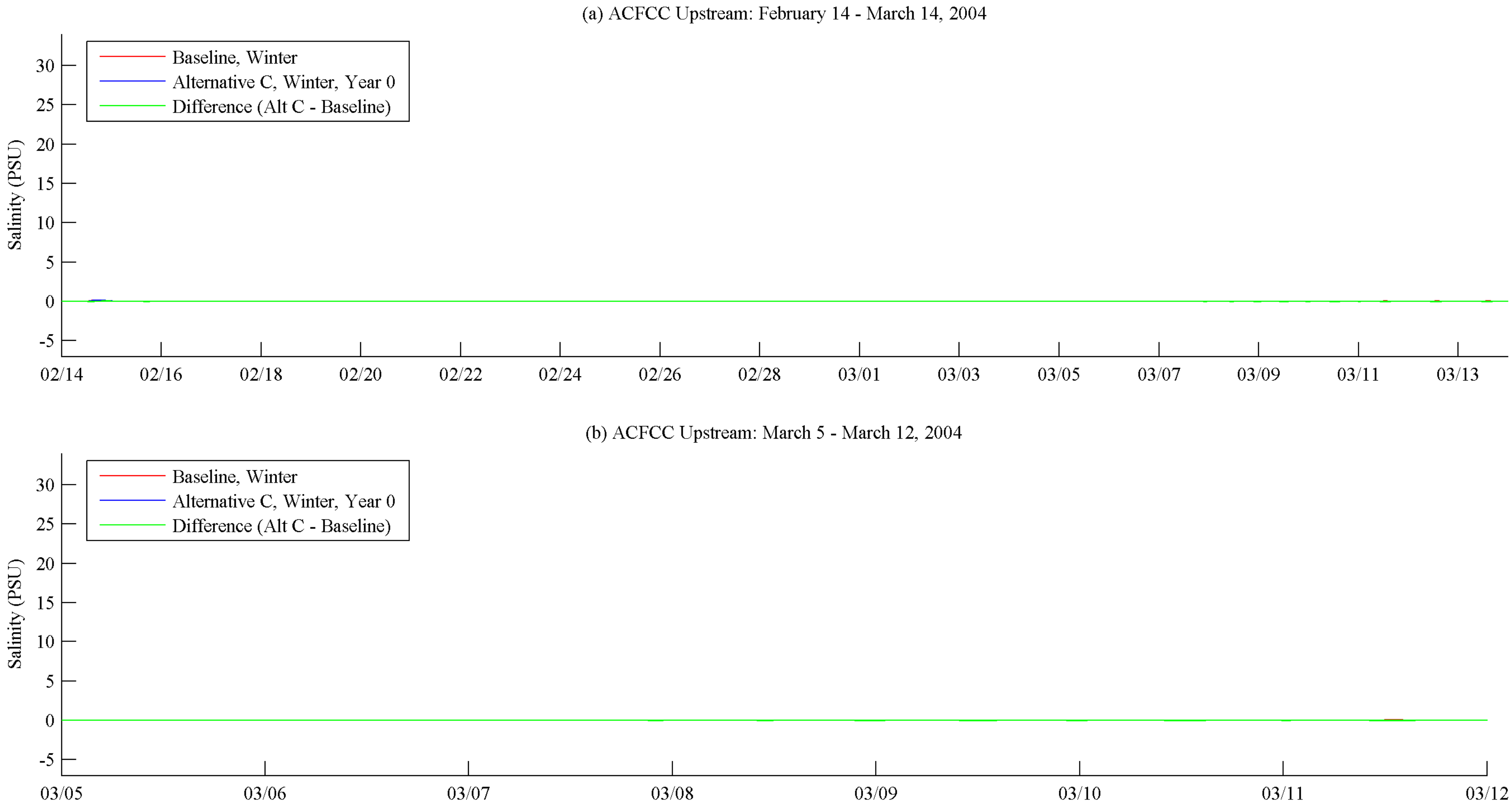

figure 5-49

South Bay Salt Pond Restoration Project

Salinity, ACFCC Upstream, Alt C, Year 0, Winter

PWA

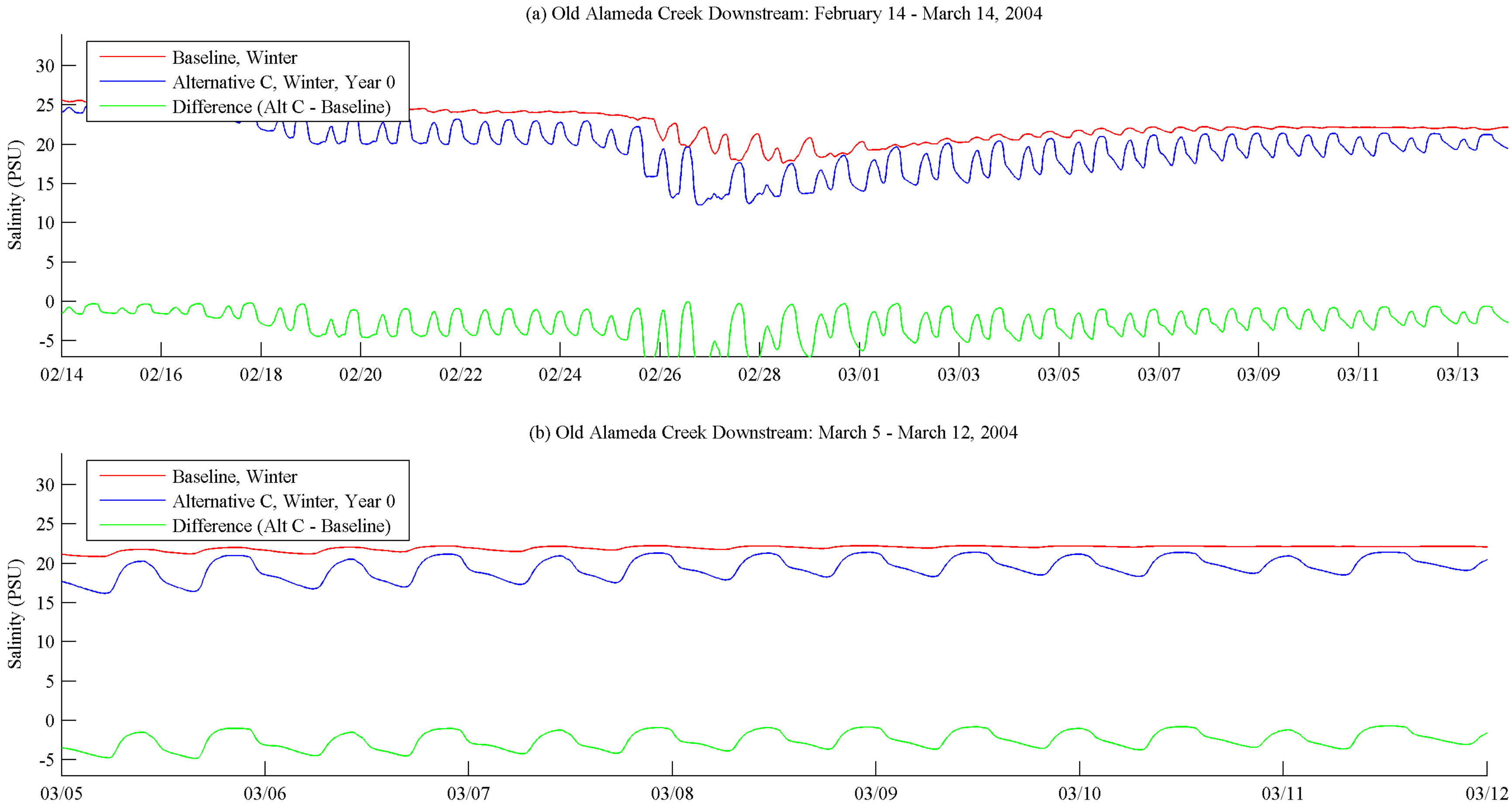

figure 5-50

South Bay Salt Pond Restoration Project

Salinity, Old Alameda Creek Downstream, Alt C, Year 0, Winter

PWA

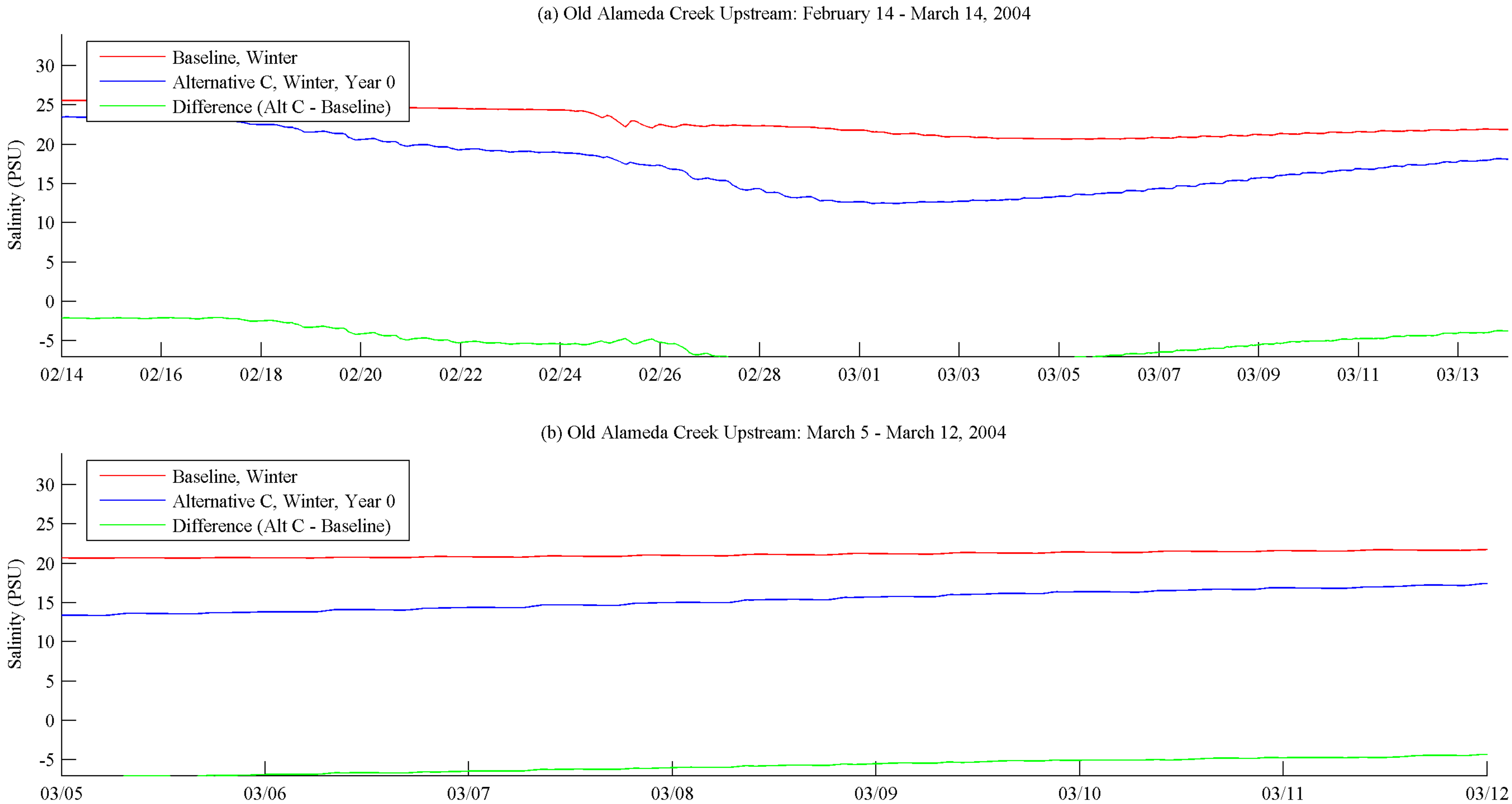

figure 5-51

South Bay Salt Pond Restoration Project

Salinity, Old Alameda Creek Upstream, Alt C, Year 0, Winter

PWA

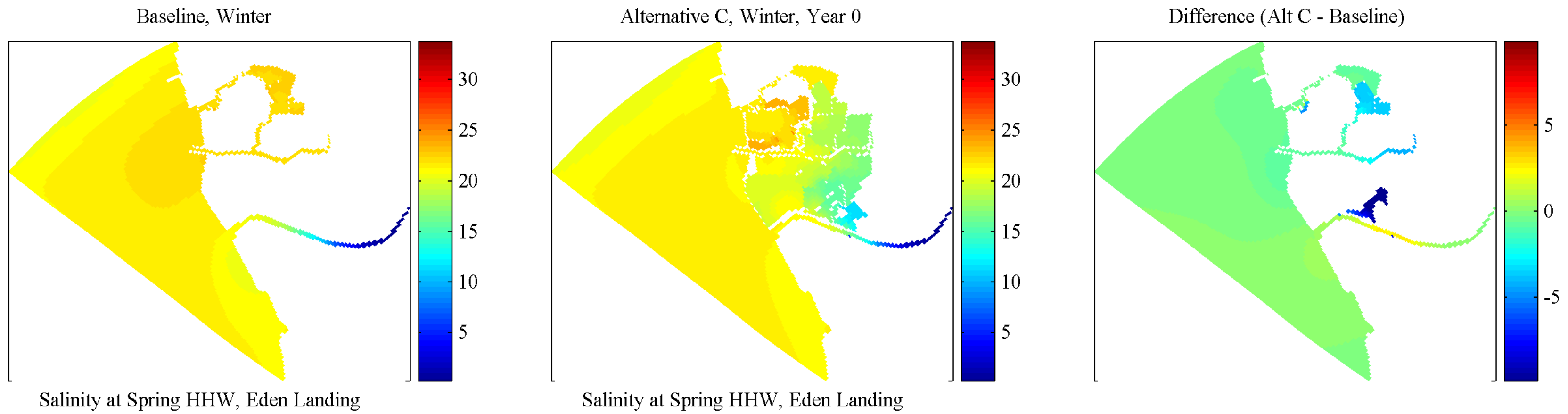

Note: Units shown are PSU

figure 5-52

South Bay Salt Pond Restoration Project

Salinity at Spring HHW, Eden Landing, Alt C, Year 0, Winter

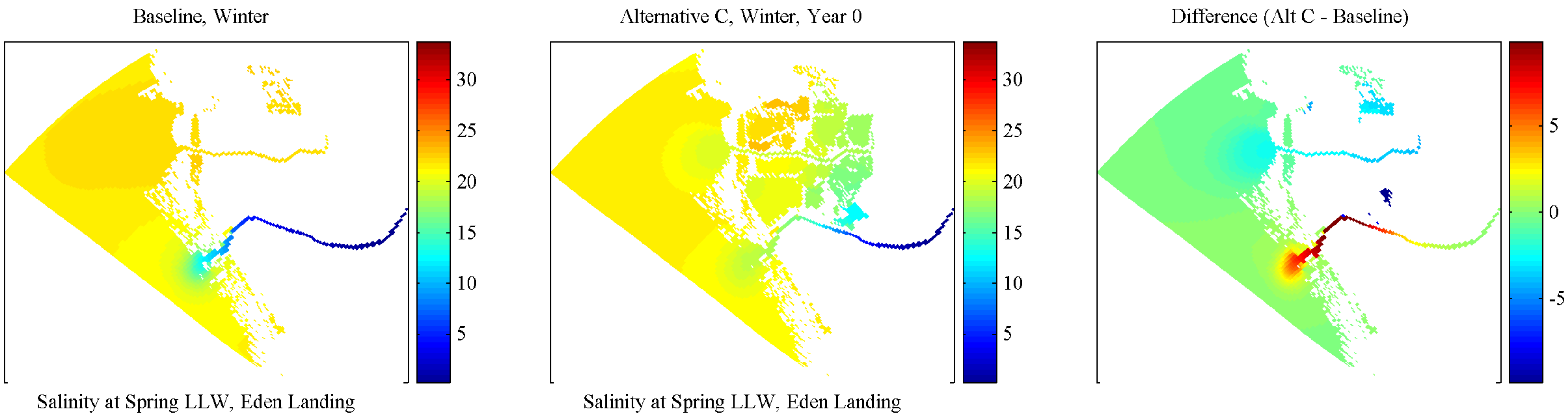

Note: Units shown are PSU

figure 5-53

South Bay Salt Pond Restoration Project

Salinity at Spring LLW, Eden Landing, Alt C, Year 0, Winter

PWA

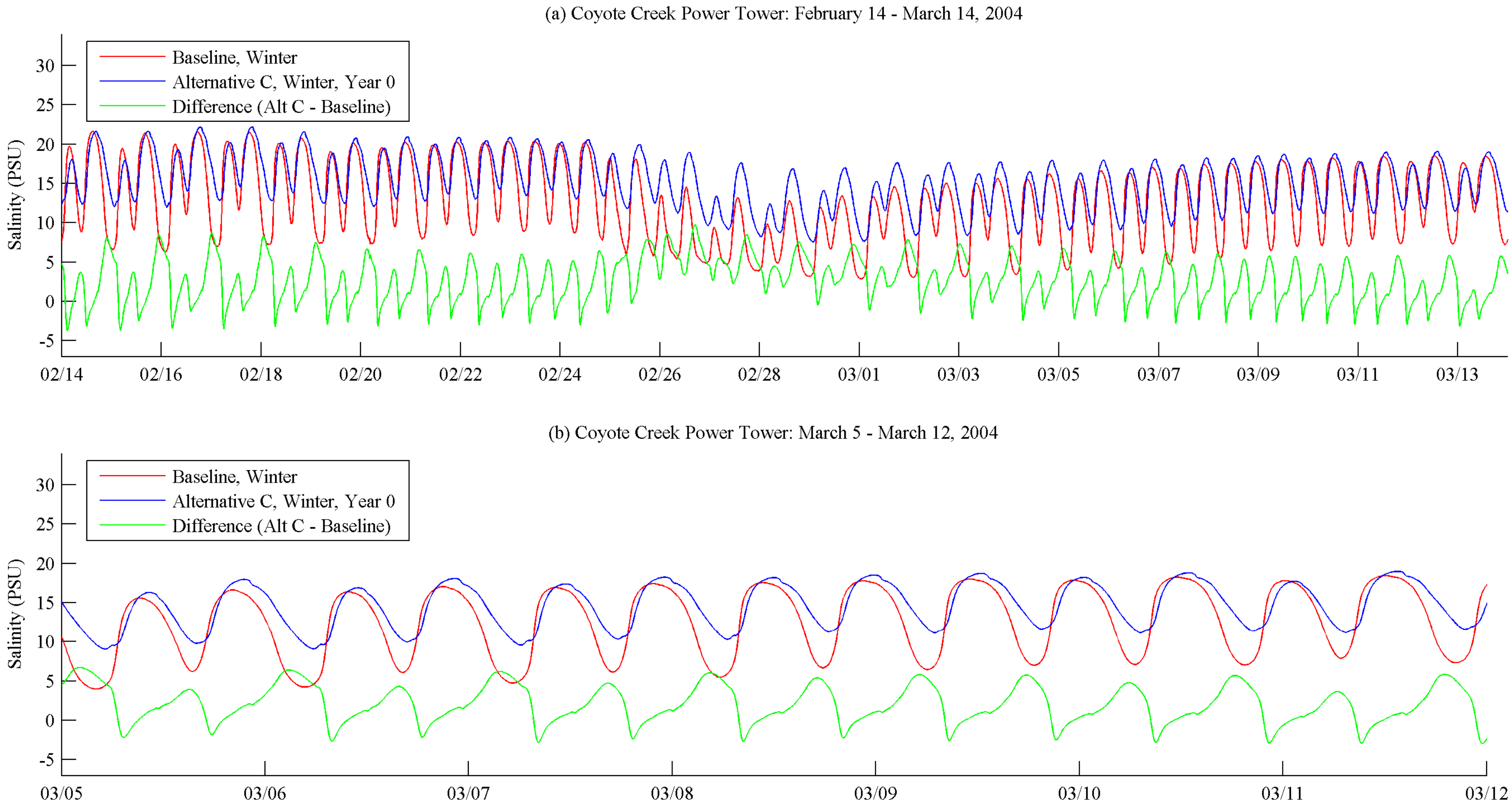

figure 5-54

South Bay Salt Pond Restoration Project

Salinity, Coyote Creek Power Tower, Alt C, Year 0, Winter

PWA

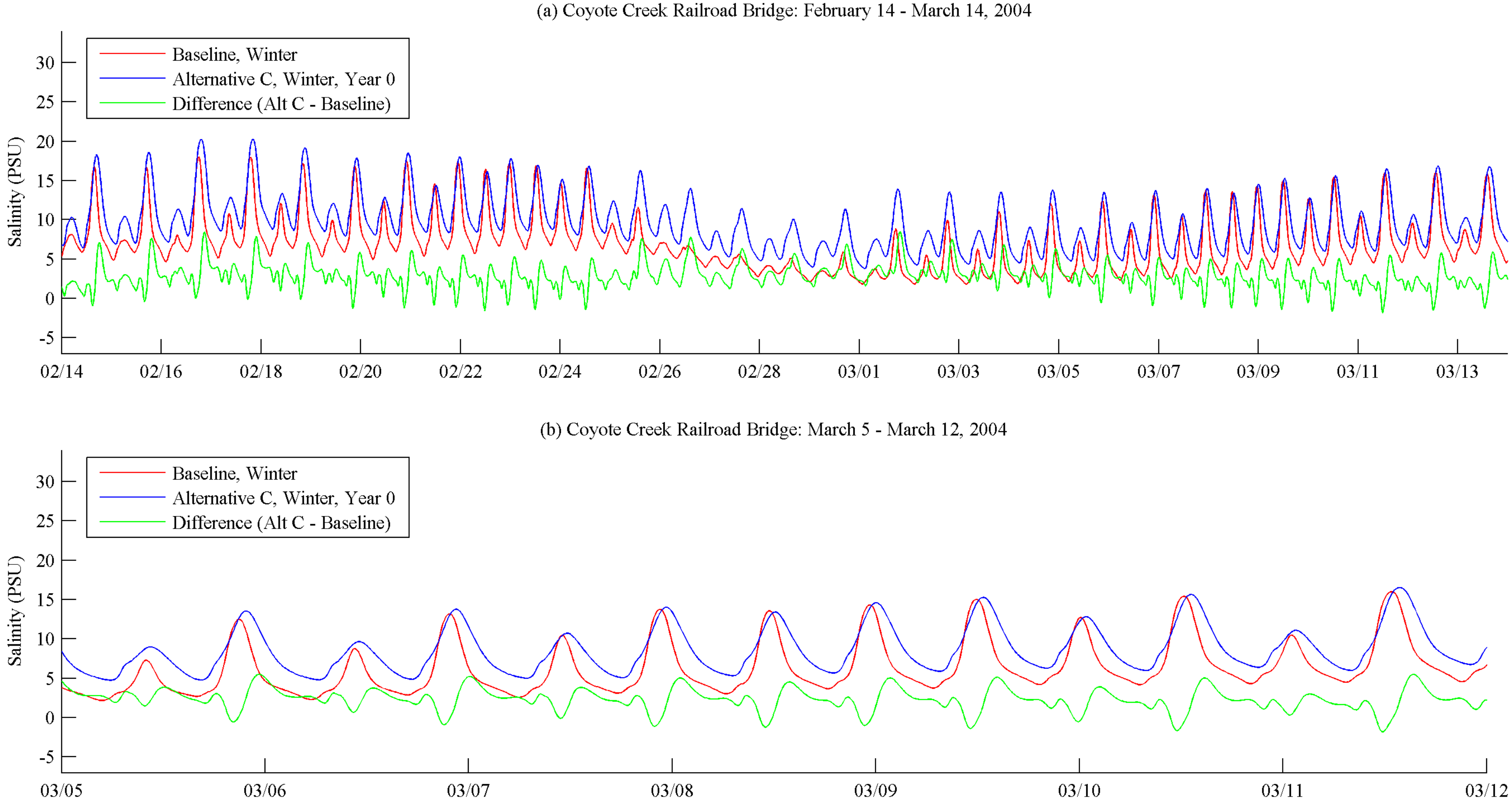

figure 5-55

South Bay Salt Pond Restoration Project

Salinity, Coyote Creek Railroad Bridge, Alt C, Year 0, Winter

PWA

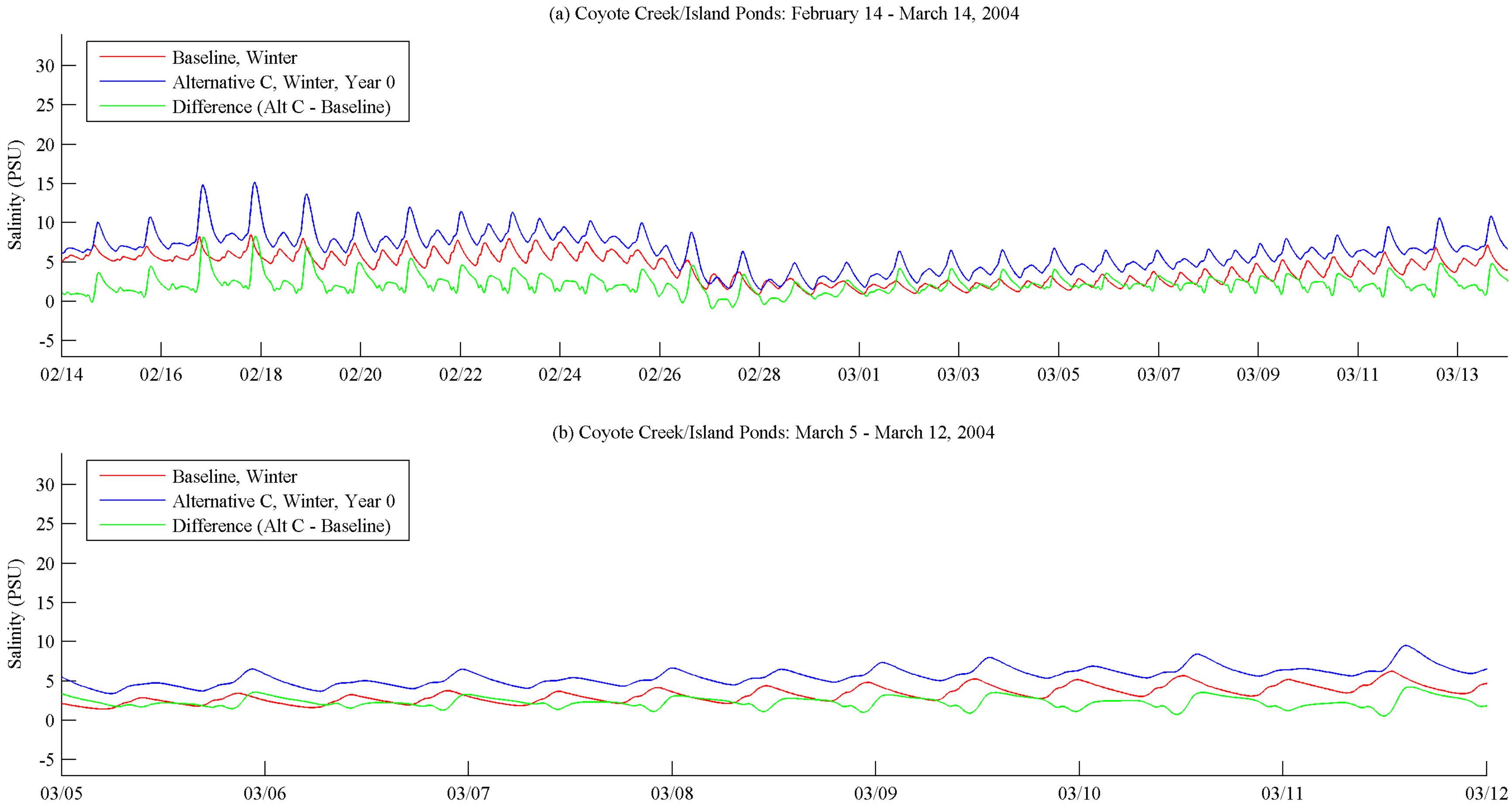

figure 5-56

South Bay Salt Pond Restoration Project

Salinity, Coyote Creek/Island Ponds, Year 0, Winter

PWA

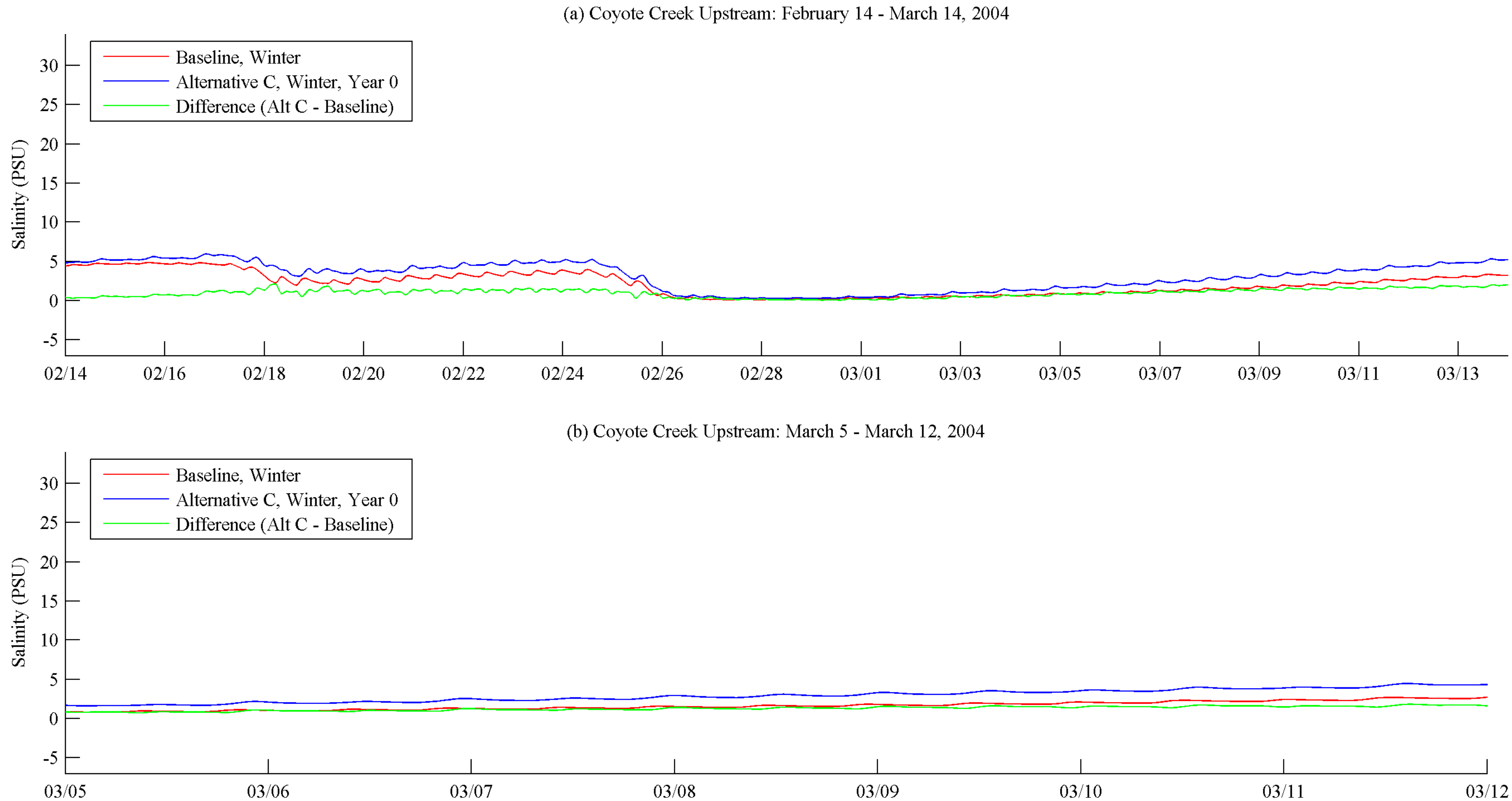

figure 5-57

South Bay Salt Pond Restoration Project

Salinity, Coyote Creek Upstream, Year 0, Winter

PWA

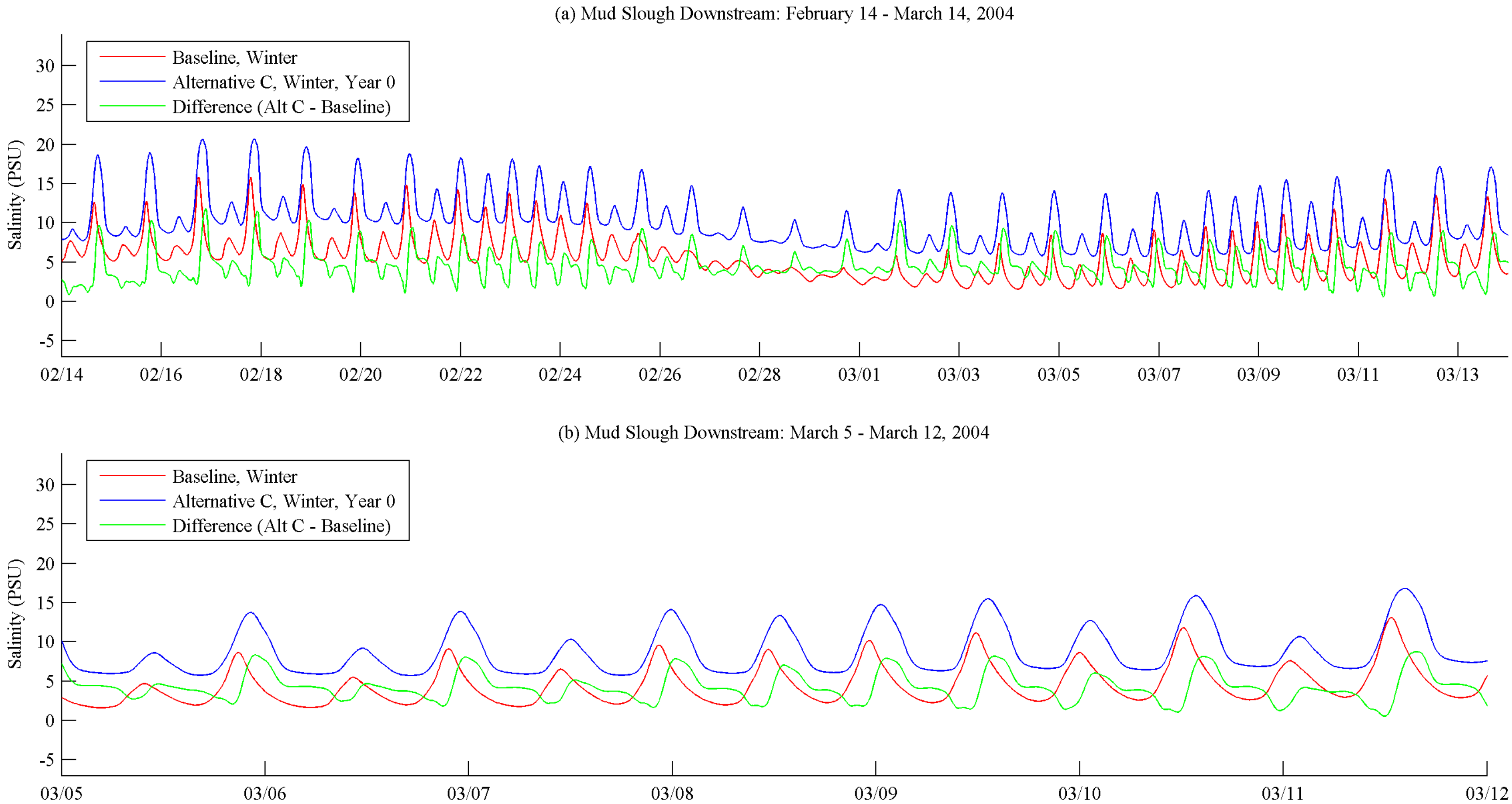

figure 5-58

South Bay Salt Pond Restoration Project

Salinity, Mud Slough Downstream, Alt C, Year 0, Winter

PWA

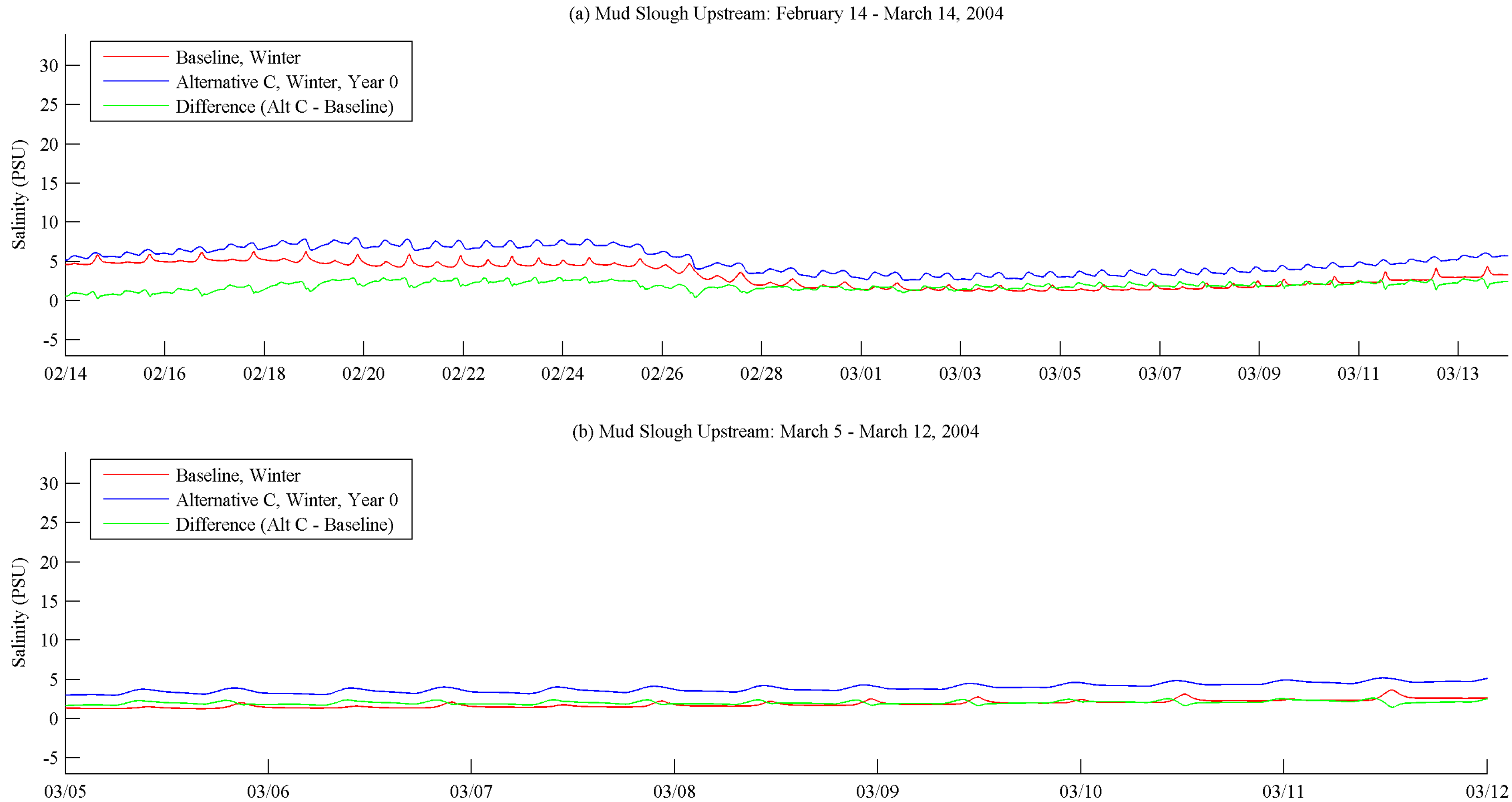

figure 5-59

South Bay Salt Pond Restoration Project

Salinity, Mud Slough Upstream, Alt C, Year 0, Winter

PWA

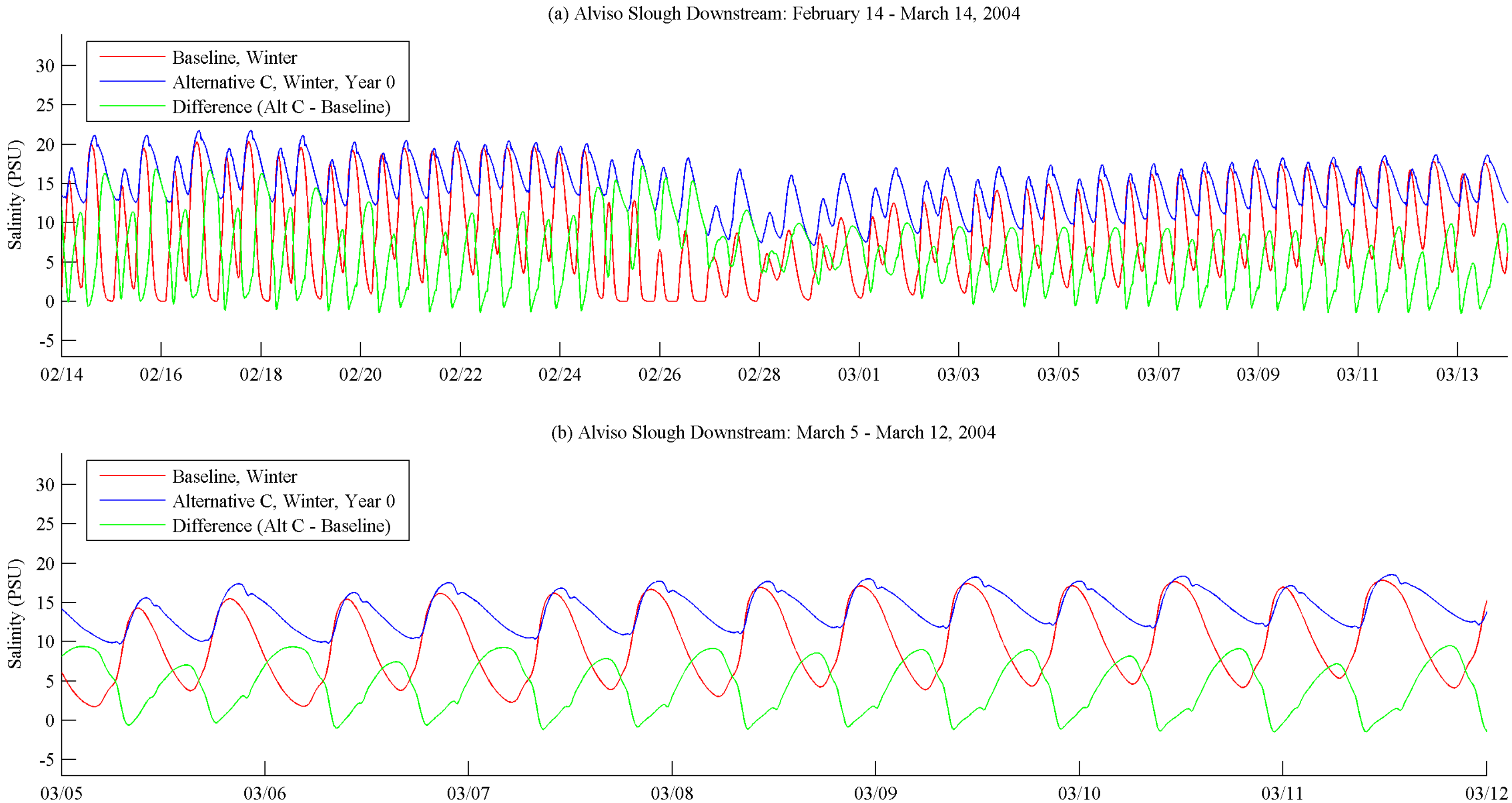

figure 5-60

South Bay Salt Pond Restoration Project

Salinity, Alviso Slough Downstream, Alt C, Year 0, Winter

PWA

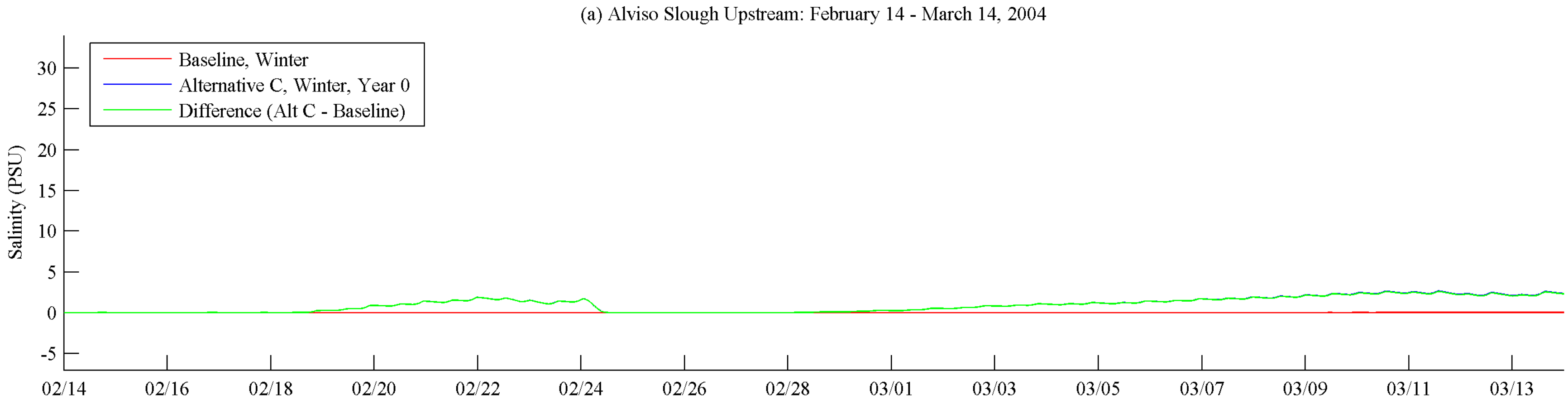

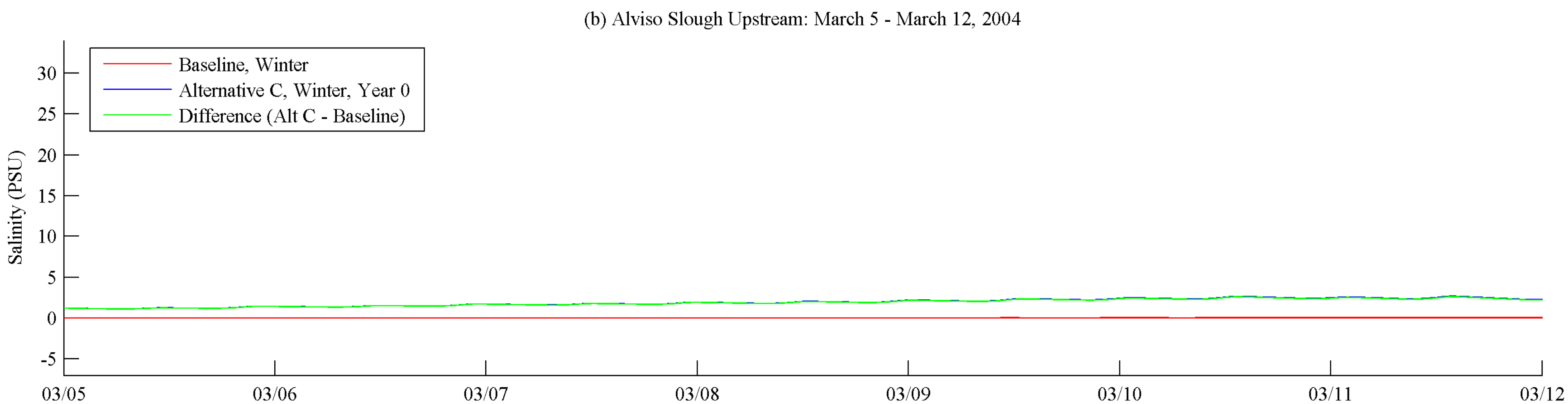

figure 5-61

South Bay Salt Pond Restoration Project

Salinity, Alviso Slough Upstream, Alt C, Year 0, Winter

PWA

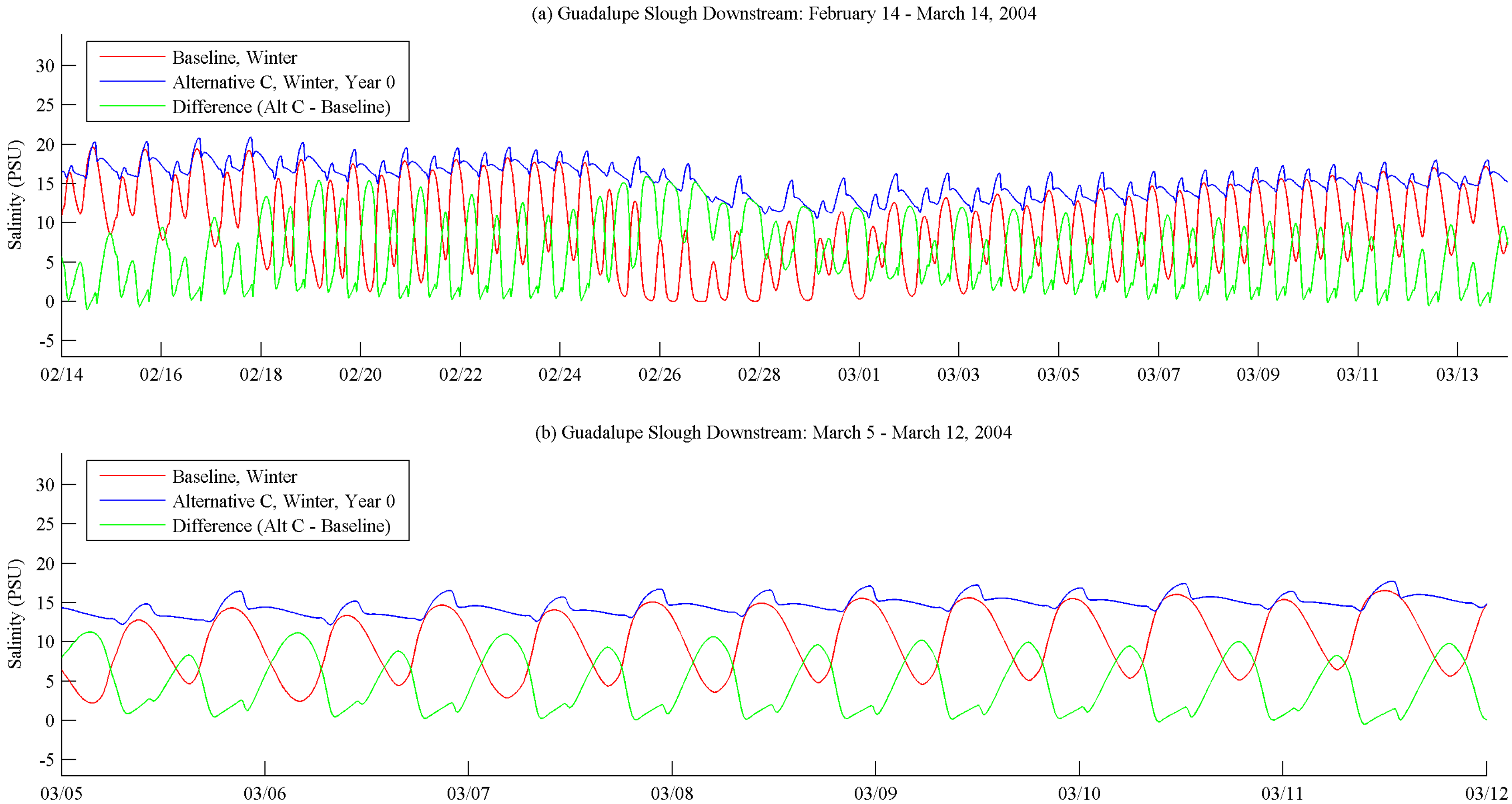

figure 5-62

South Bay Salt Pond Restoration Project

Salinity, Guadalupe Slough Downstream, Alt C, Year 0, Winter

PWA

(a) Guadalupe Slough Upstream: February 14 - March 14, 2004

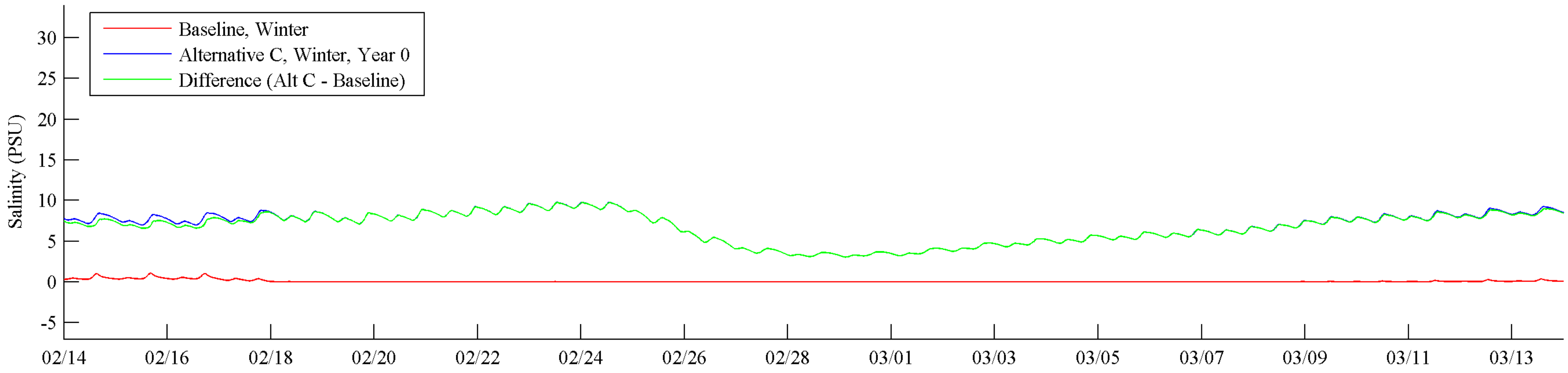

(b) Guadalupe Slough Upstream: March 5 - March 12, 2004

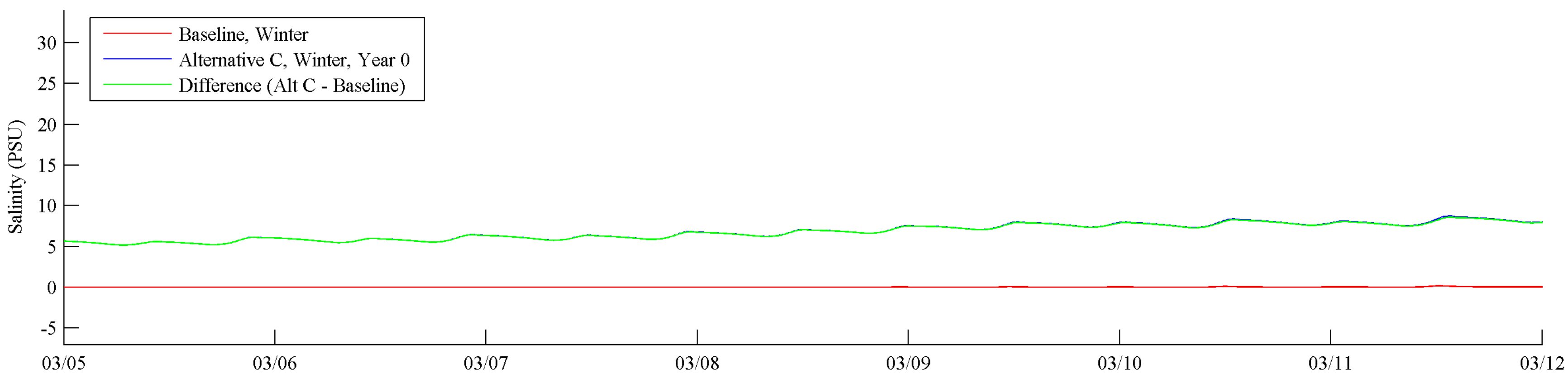

figure 5-63

South Bay Salt Pond Restoration Project

Salinity, Guadalupe Slough Upstream, Alt C, Year 0, Winter

PWA

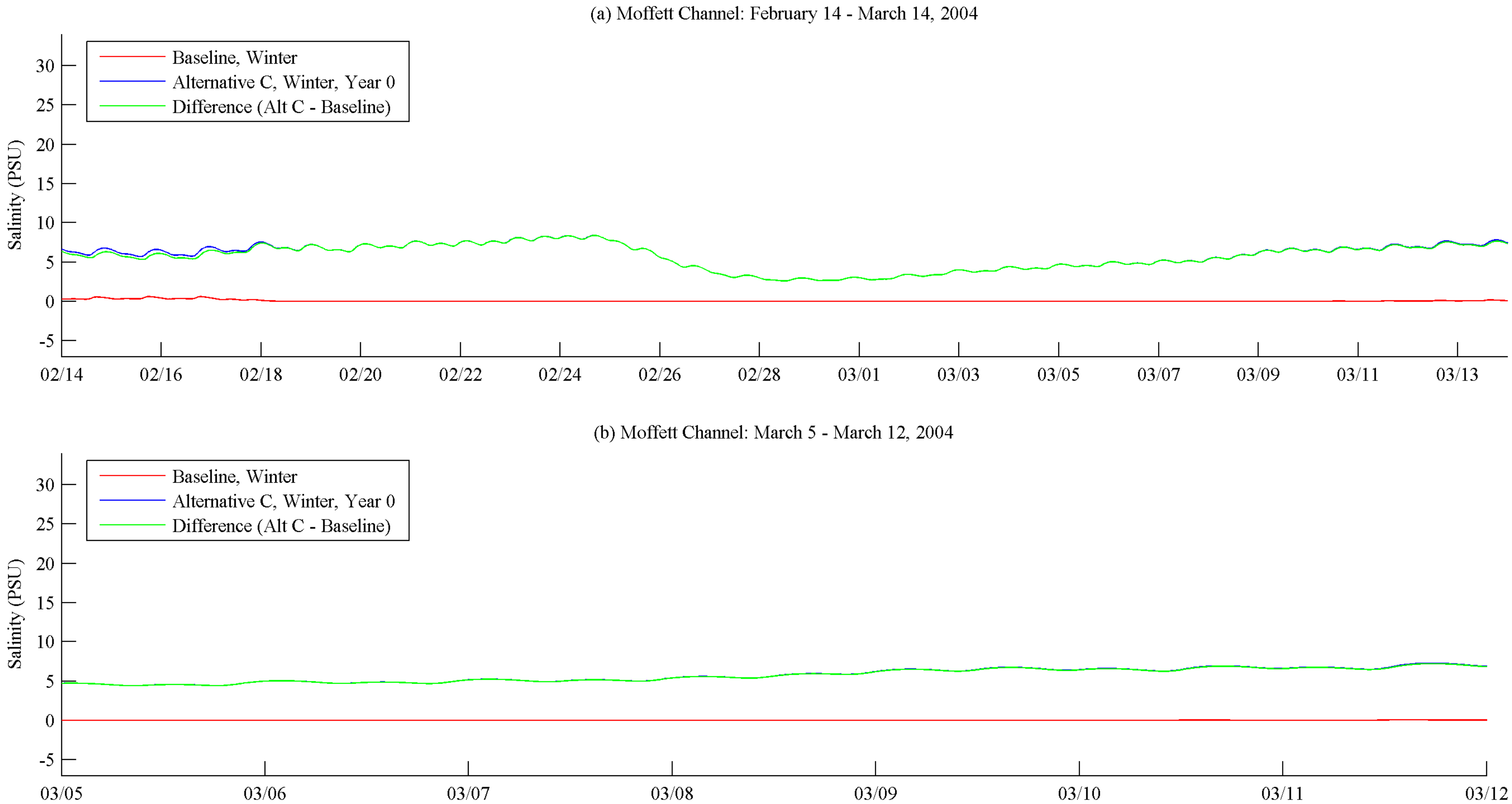

figure 5-64

South Bay Salt Pond Restoration Project

Salinity, Moffett Channel, Alt C, Year 0, Winter

PWA

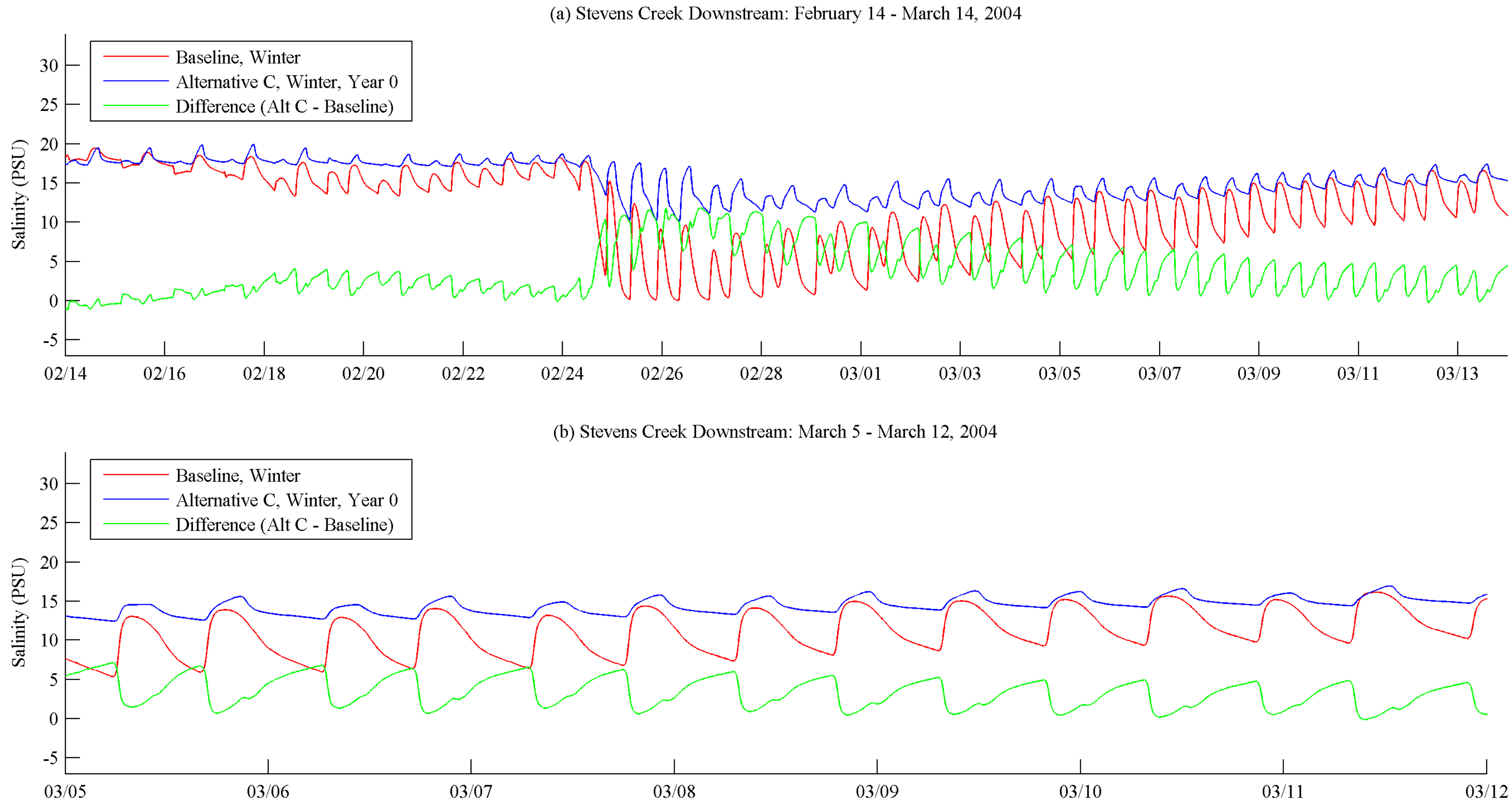

figure 5-65

South Bay Salt Pond Restoration Project

Salinity, Steven Creek Downstream, Alt C, Year 0, Winter

PWA

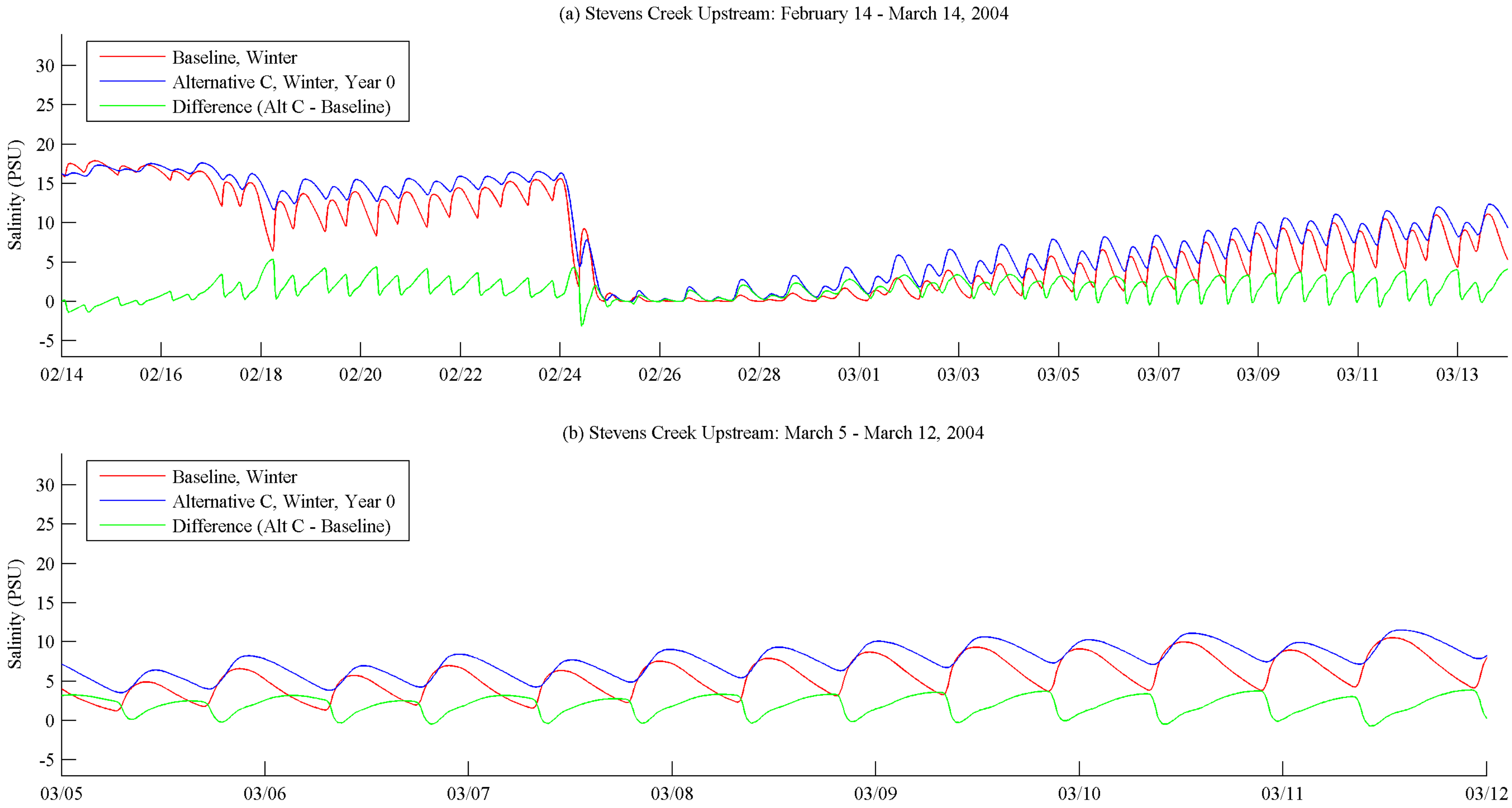

figure 5-66

South Bay Salt Pond Restoration Project

Salinity, Stevens Creek Upstream, Alt C, Year 0, Winter

PWA

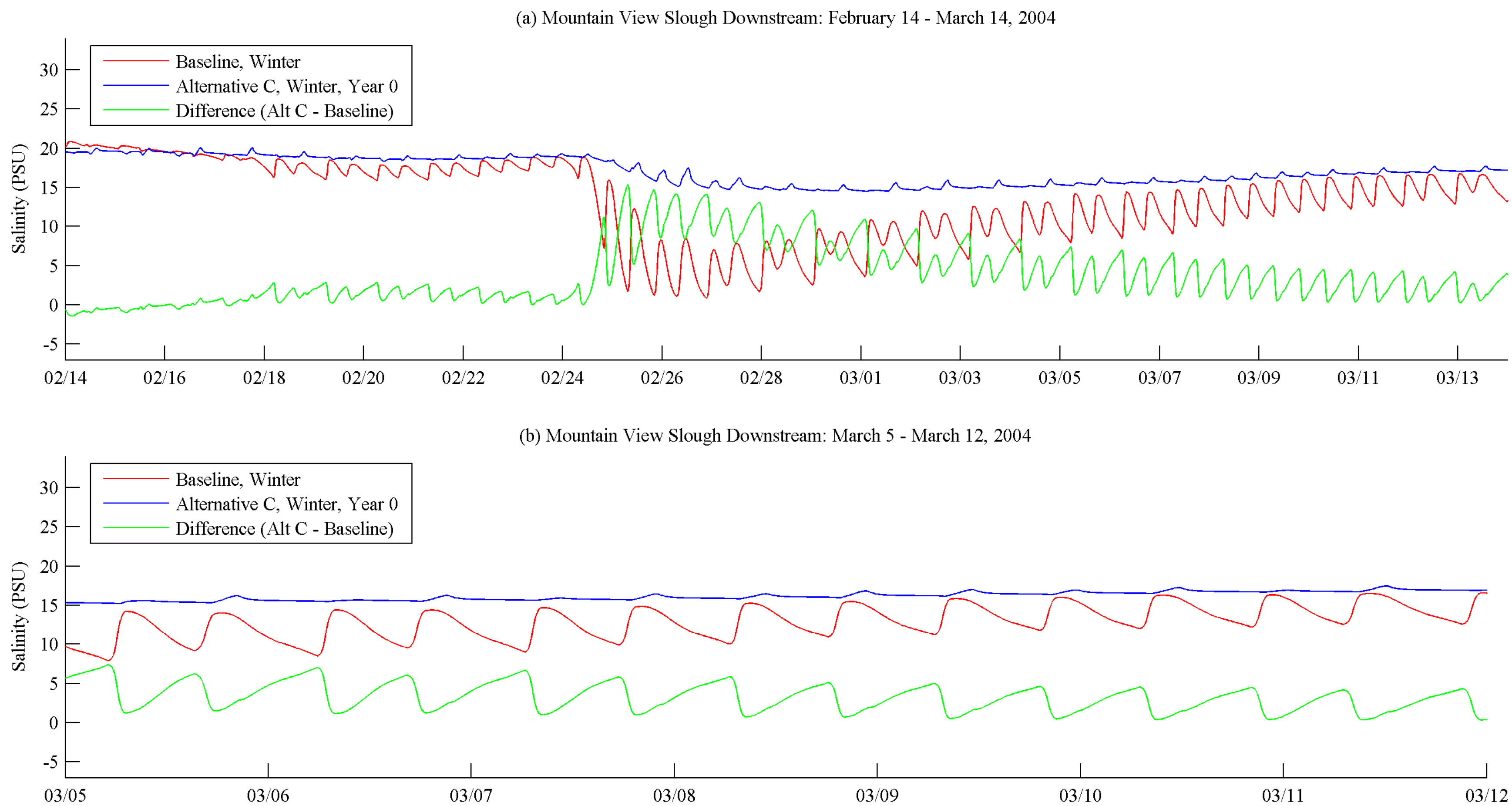

figure 5-67

South Bay Salt Pond Restoration Project

Salinity, Mountain View Slough Downstream, Alt C, Year 0, Winter

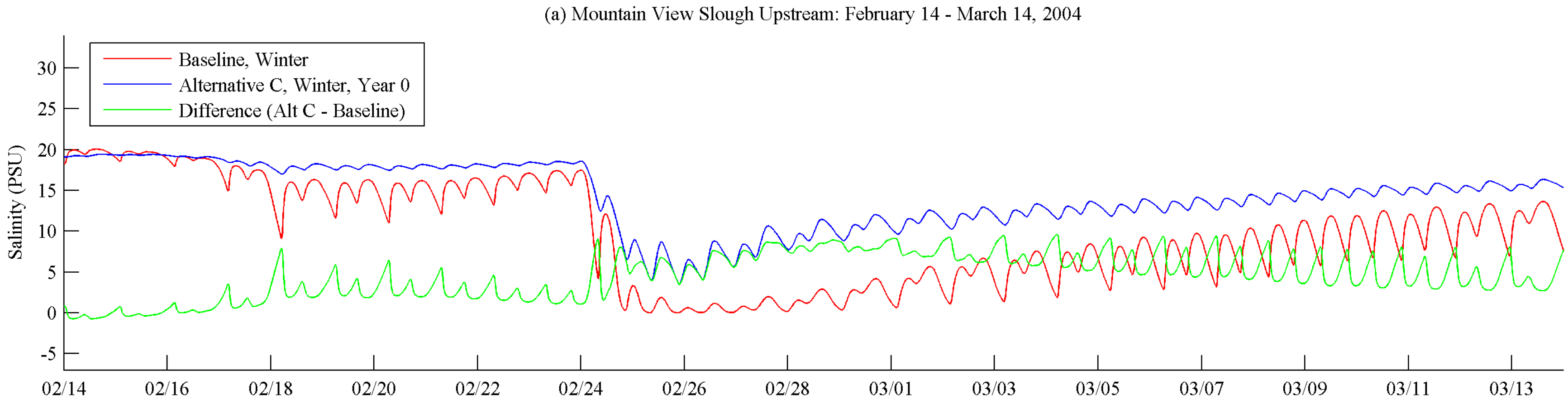

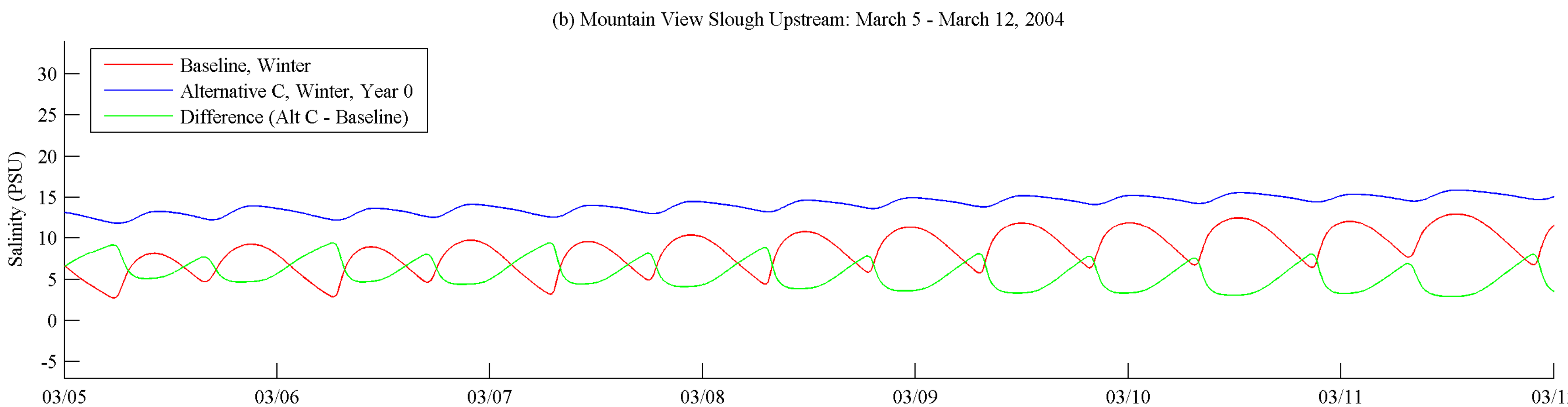

figure 5-68

South Bay Salt Pond Restoration Project

Salinity, Mountain View Slough Upstream, Alt C, Year 0, Winter

PWA

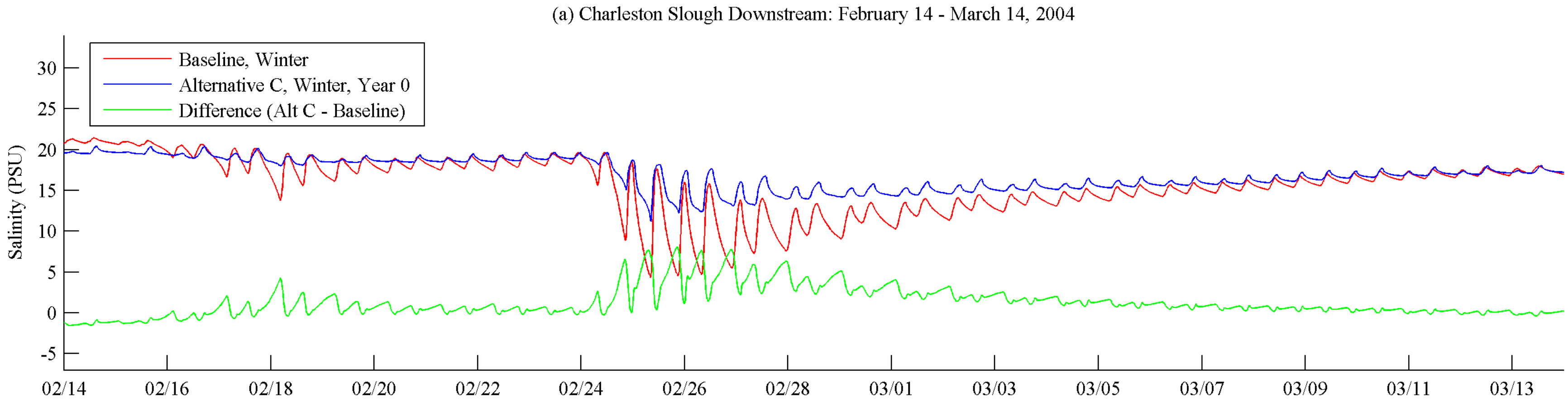

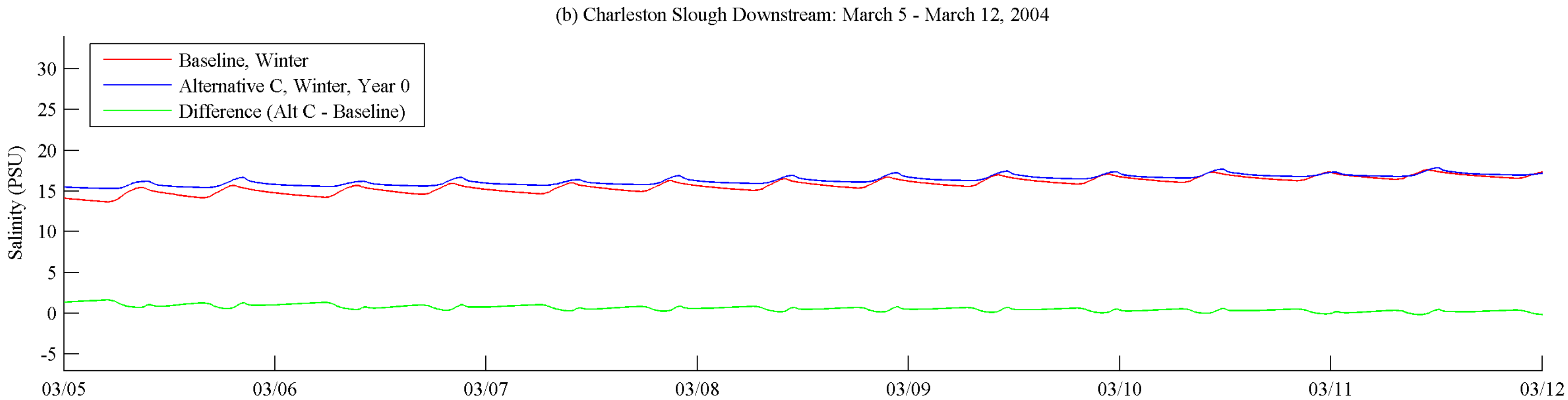

figure 5-69

South Bay Salt Pond Restoration Project

Salinity, Charleston Slough Downstream, Alt C, Year 0, Winter

PWA

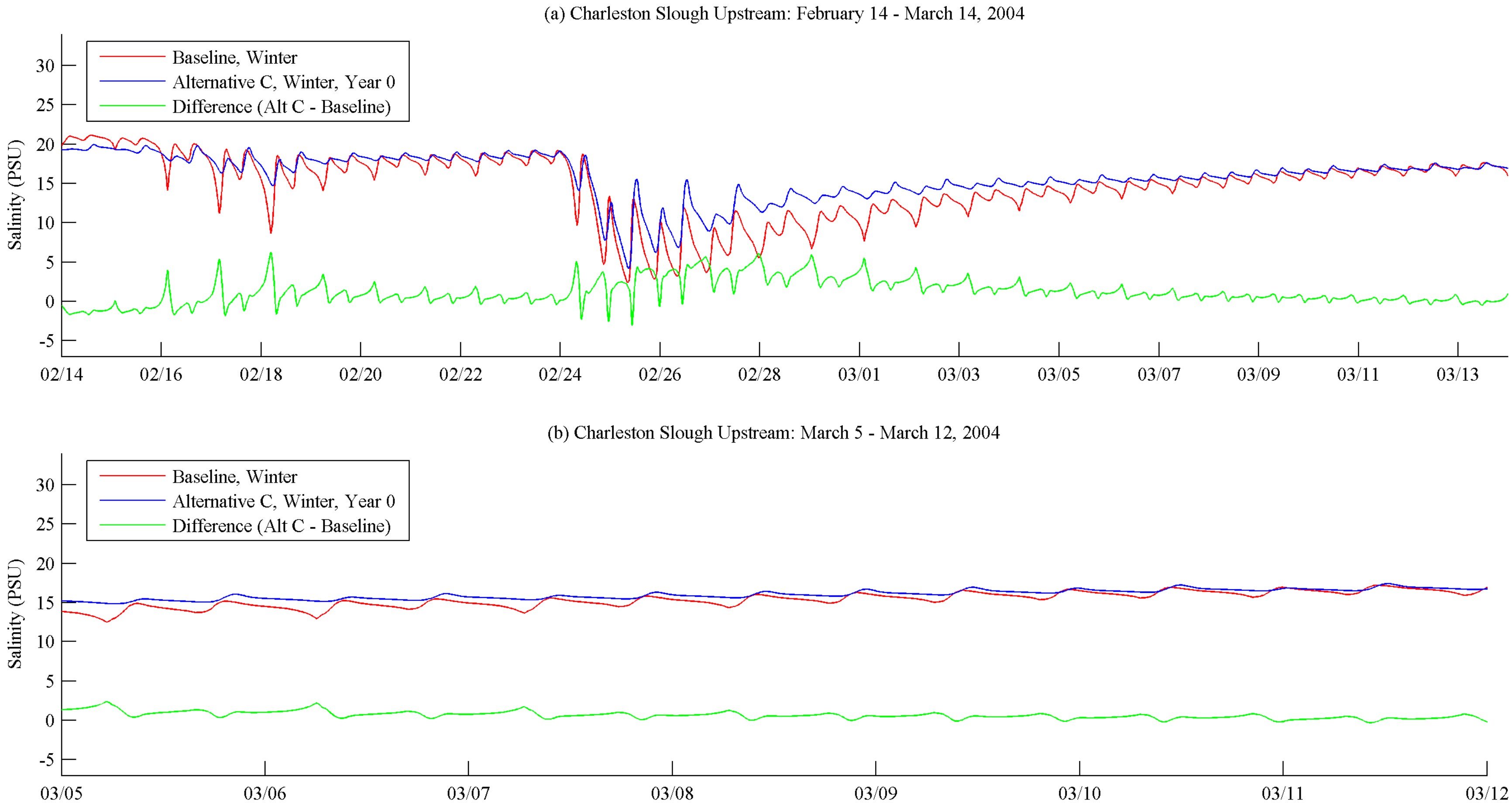

figure 5-70

South Bay Salt Pond Restoration Project

Salinity, Charleston Slough Upstream, Alt C, Year 0, Winter

PWA

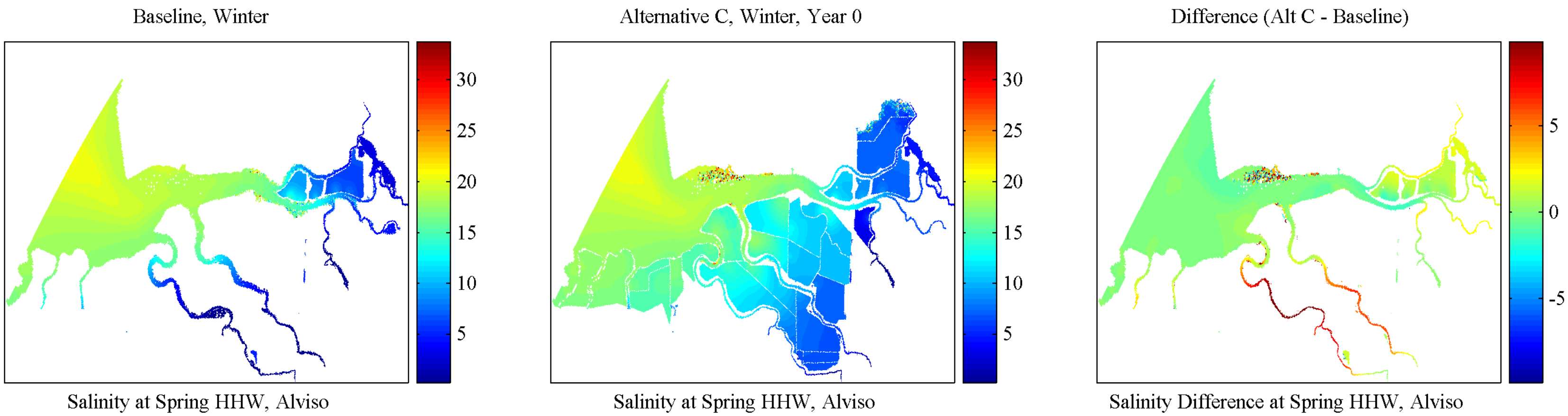

Note: Units shown are PSU

figure 5-71

South Bay Salt Pond Restoration Project

Salinity at Spring HHW, Alt C, Alviso, Year 0, Winter

PWA

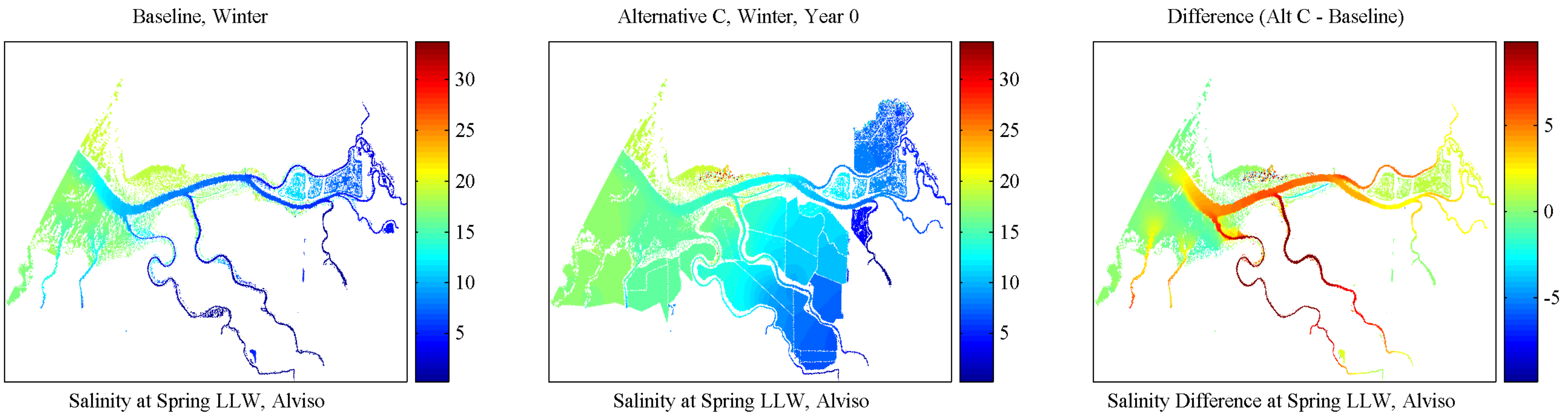

Note: Units shown are PSU

figure 5-72

South Bay Salt Pond Restoration Project

Salinity at Spring LLW, Alt C, Alviso, Year 0, Winter

PWA

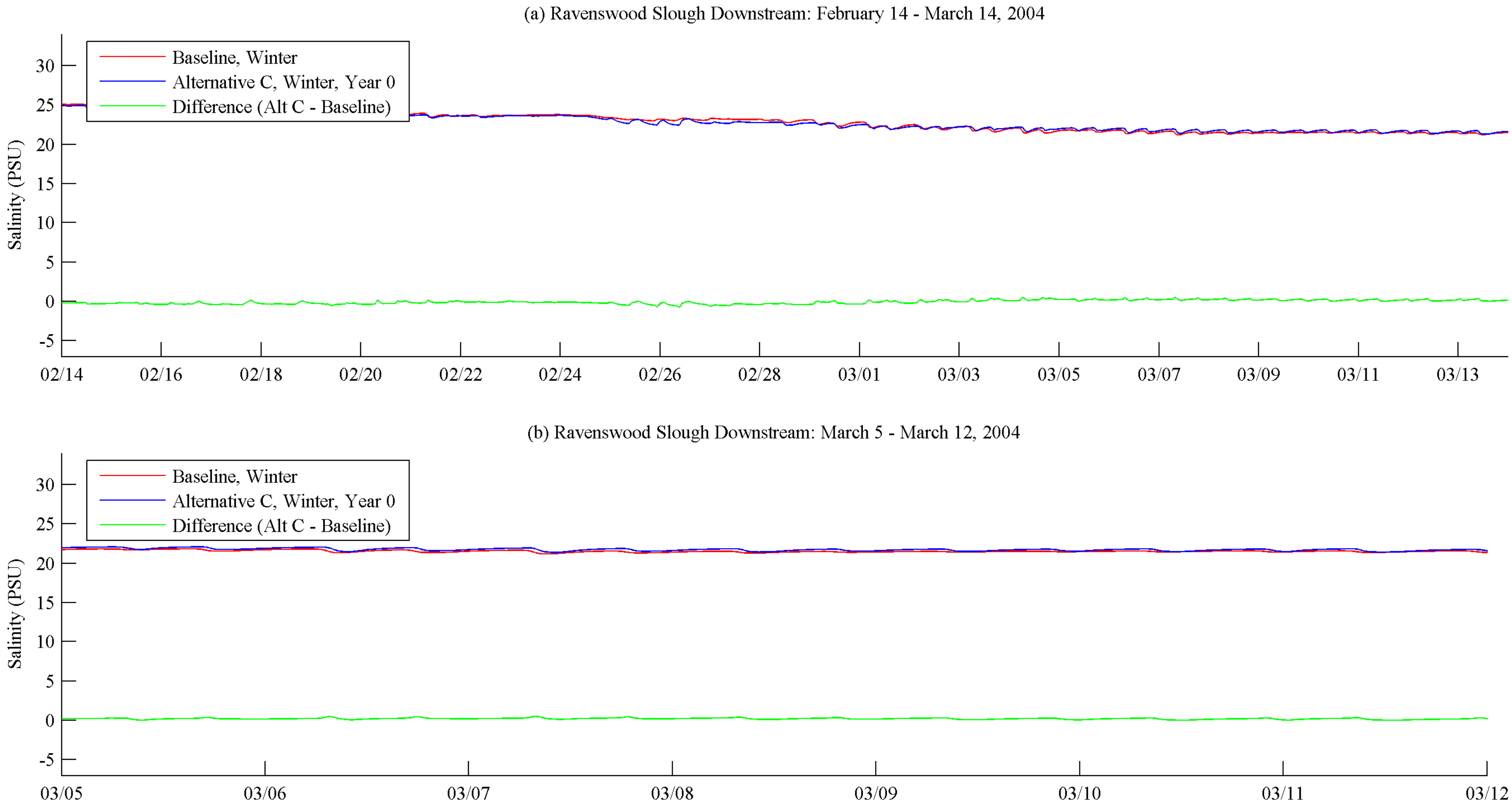

figure 5-73

South Bay Salt Pond Restoration Project

Salinity, Ravenswood Slough Downstream, Ravenswood, Alt C, Year 0, Winter

PWA

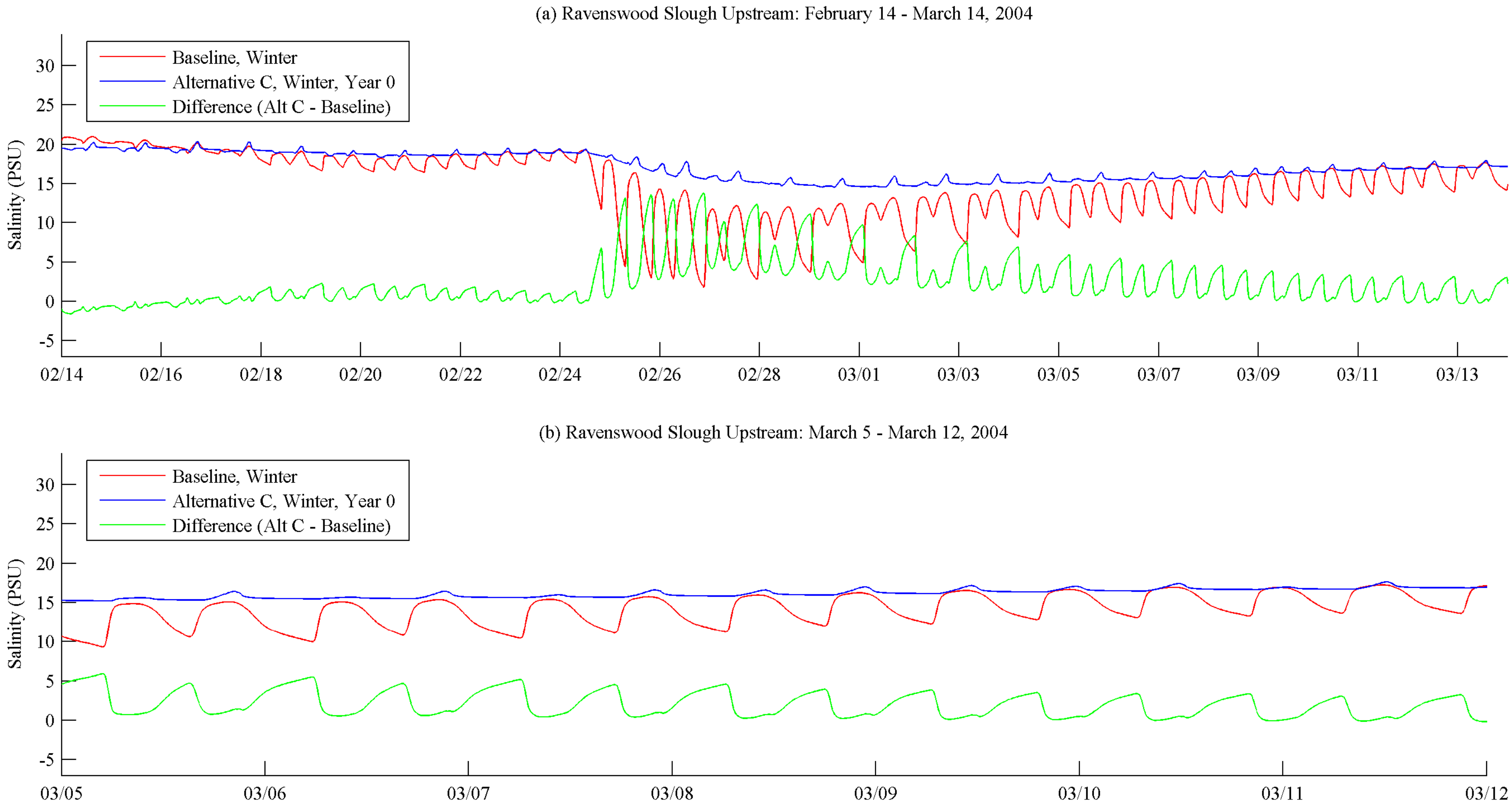

figure 5-74

South Bay Salt Pond Restoration Project

Salinity, Ravenswood Slough Upstream, Ravenswood, Alt C, Year 0, Winter

PWA

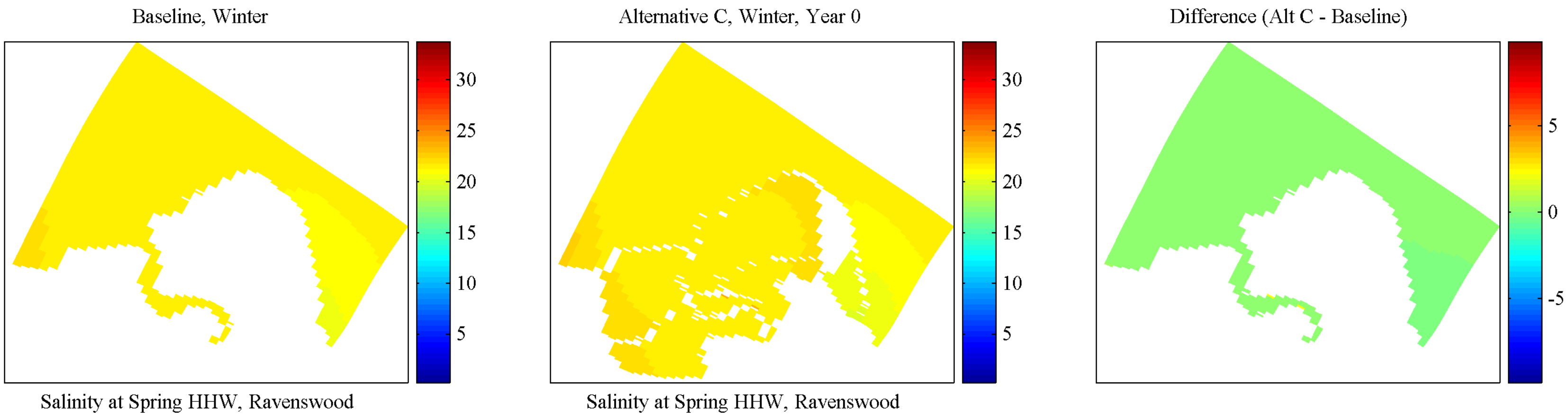

Note: Units shown are PSU

figure 5-75

South Bay Salt Pond Restoration Project

Salinity at Spring HHW, Ravenswood, Alt C, Year 0, Winter

PWA

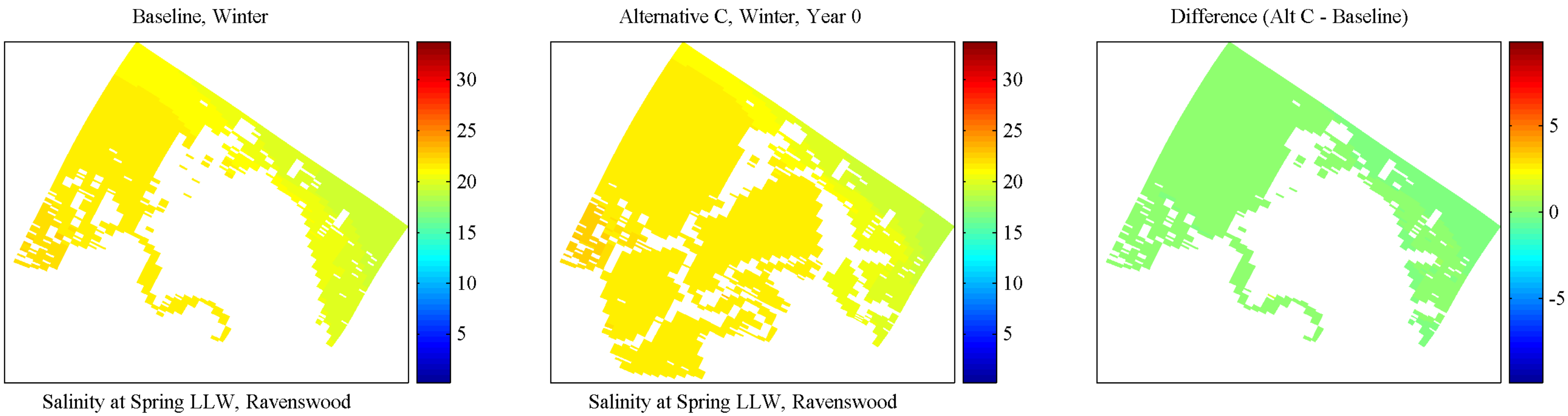

Note: Units shown are PSU

figure 5-76

South Bay Salt Pond Restoration Project

Salinity at Spring LLW, Ravenswood, Alt C, Year 0, Winter

PWA

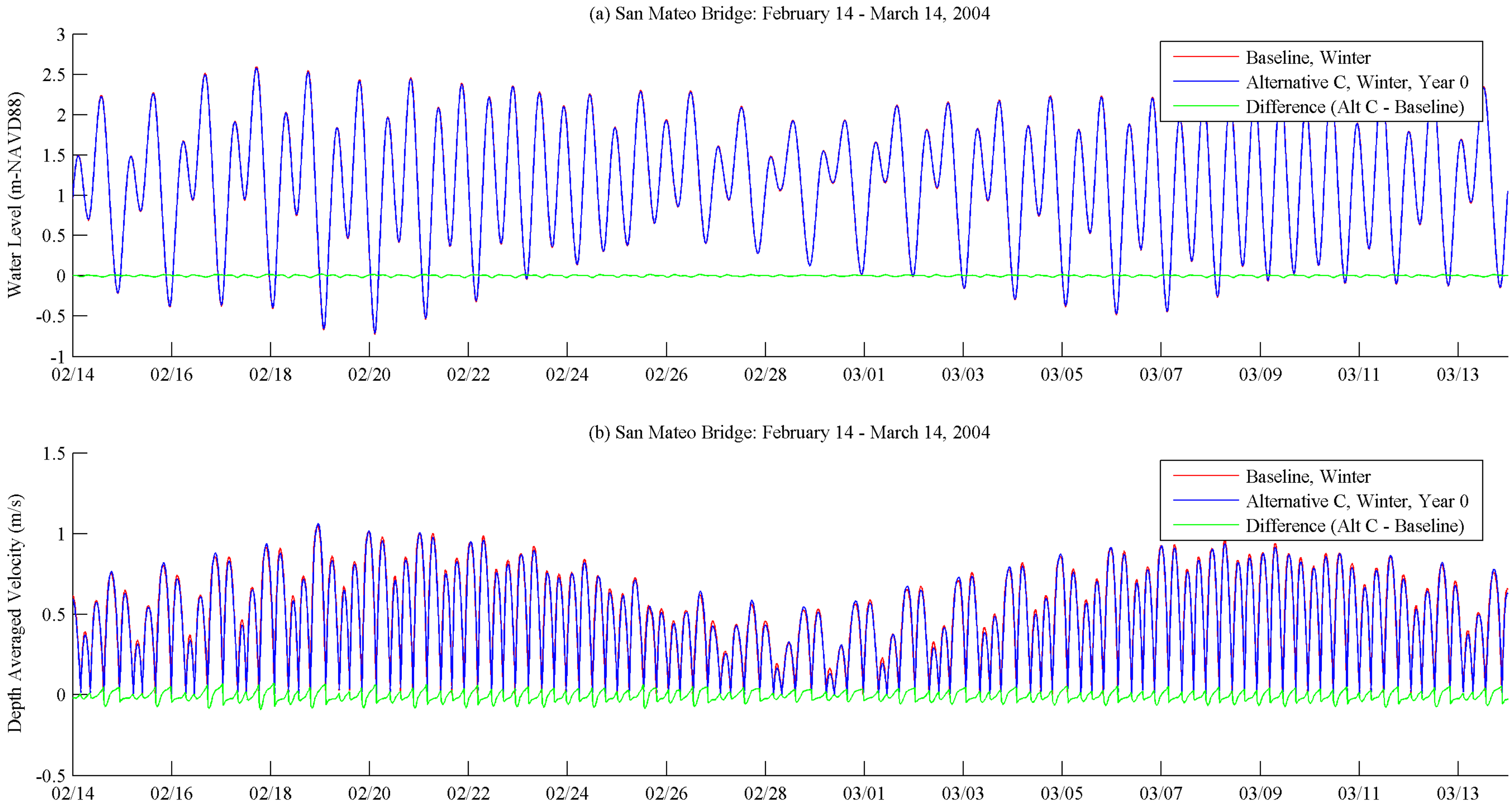

The depth-averaged velocity is calculated as $v = (u^2 + v^2)^{1/2}$, where u and v are the horizontal depth-averaged velocity components.

figure 5-77

South Bay Salt Pond Restoration Project

Velocity, San Mateo Bridge, Alt C, Year 0, Winter

PWA

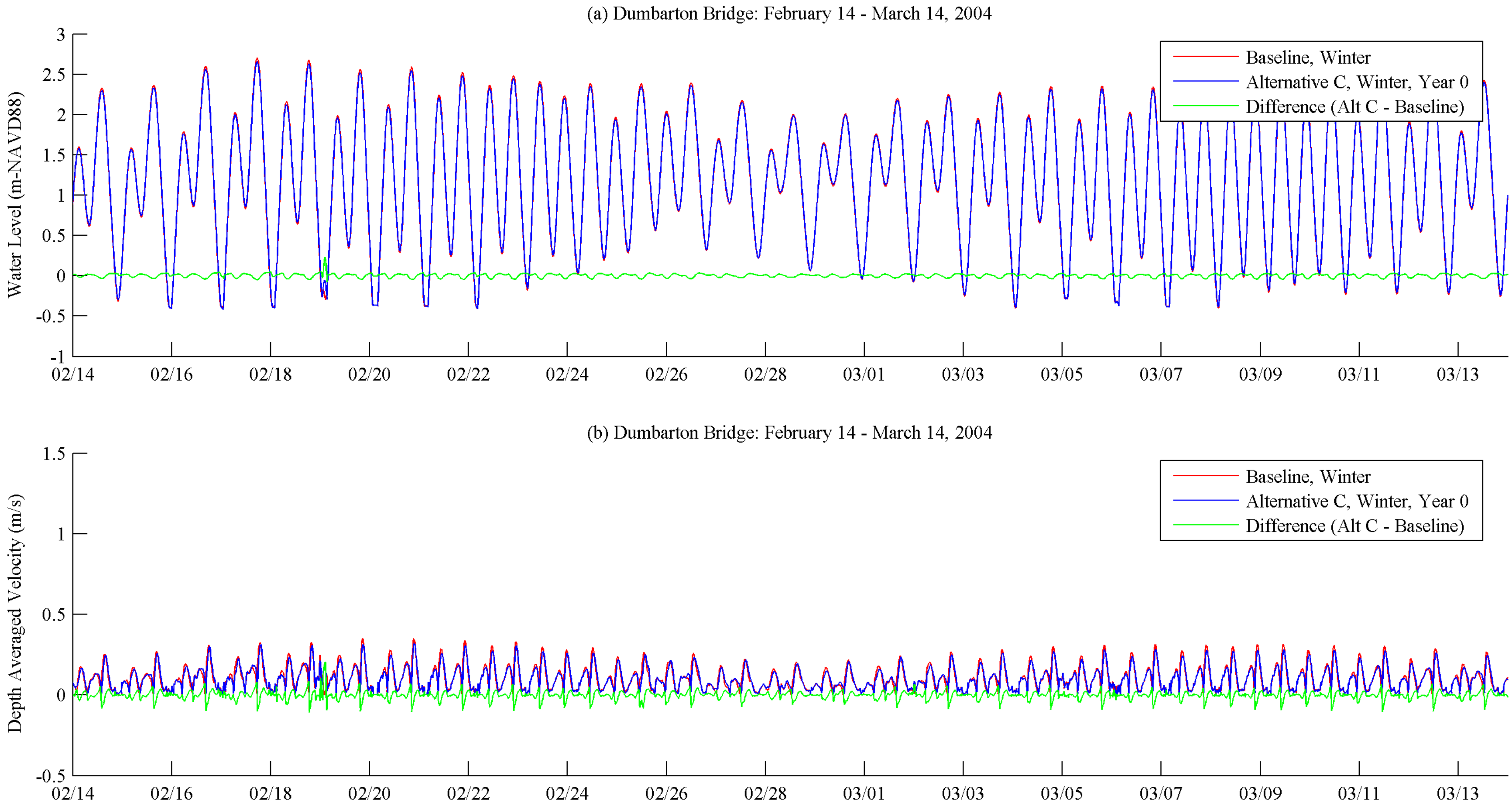

The depth-averaged velocity is calculated as $v = (u^2 + v^2)^{1/2}$, where u and v are the horizontal depth-averaged velocity components.

figure 5-78

South Bay Salt Pond Restoration Project

Velocity, Dumbarton Bridge, Alt C, Year 0, Winter

PWA

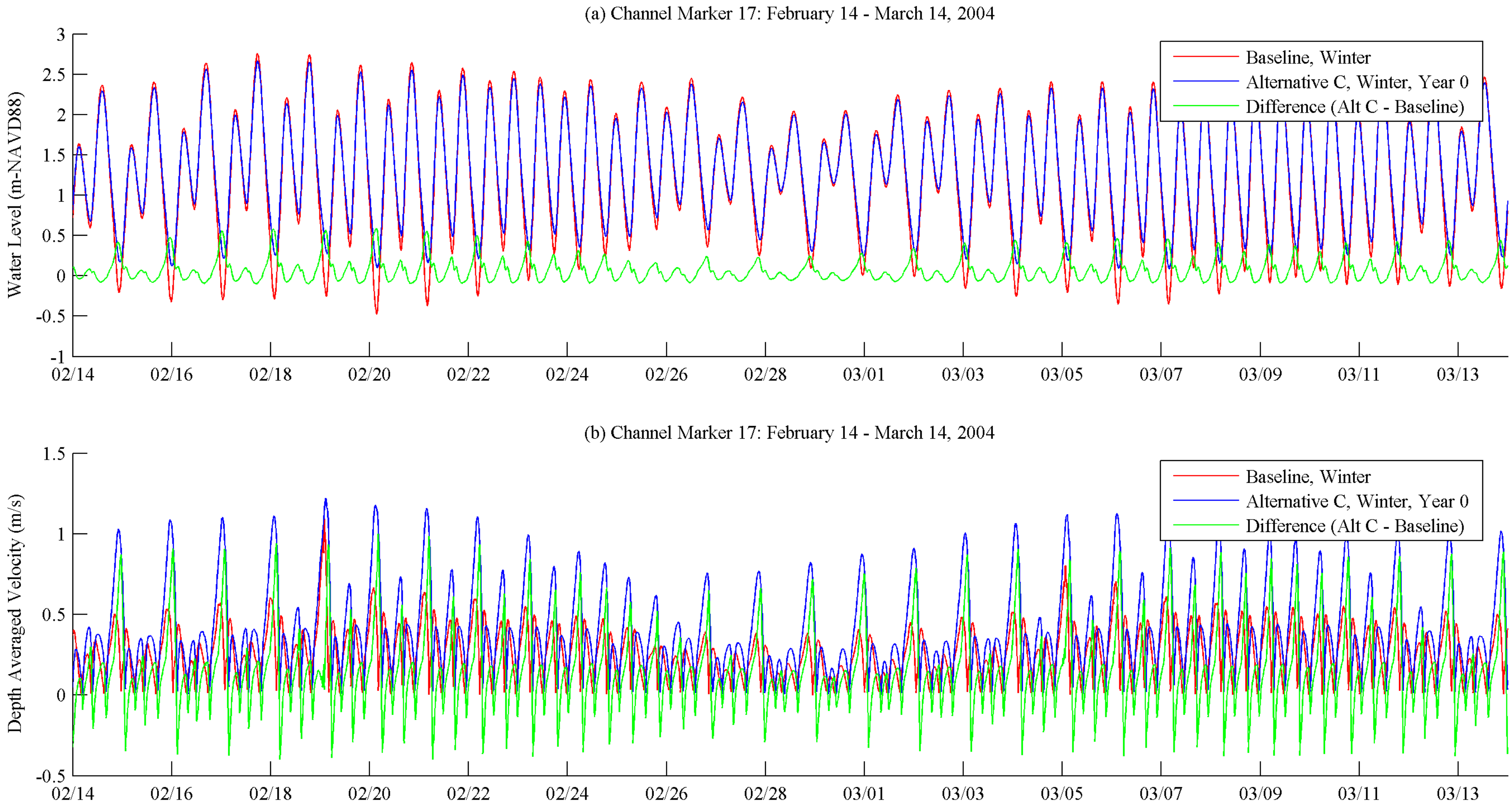

The depth-averaged velocity is calculated as $v = (u^2 + v^2)^{1/2}$, where u and v are the horizontal depth-averaged velocity components.

figure 5-79

South Bay Salt Pond Restoration Project

Velocity, Channel Marker 17, Alt C, Year 0, Winter

PWA

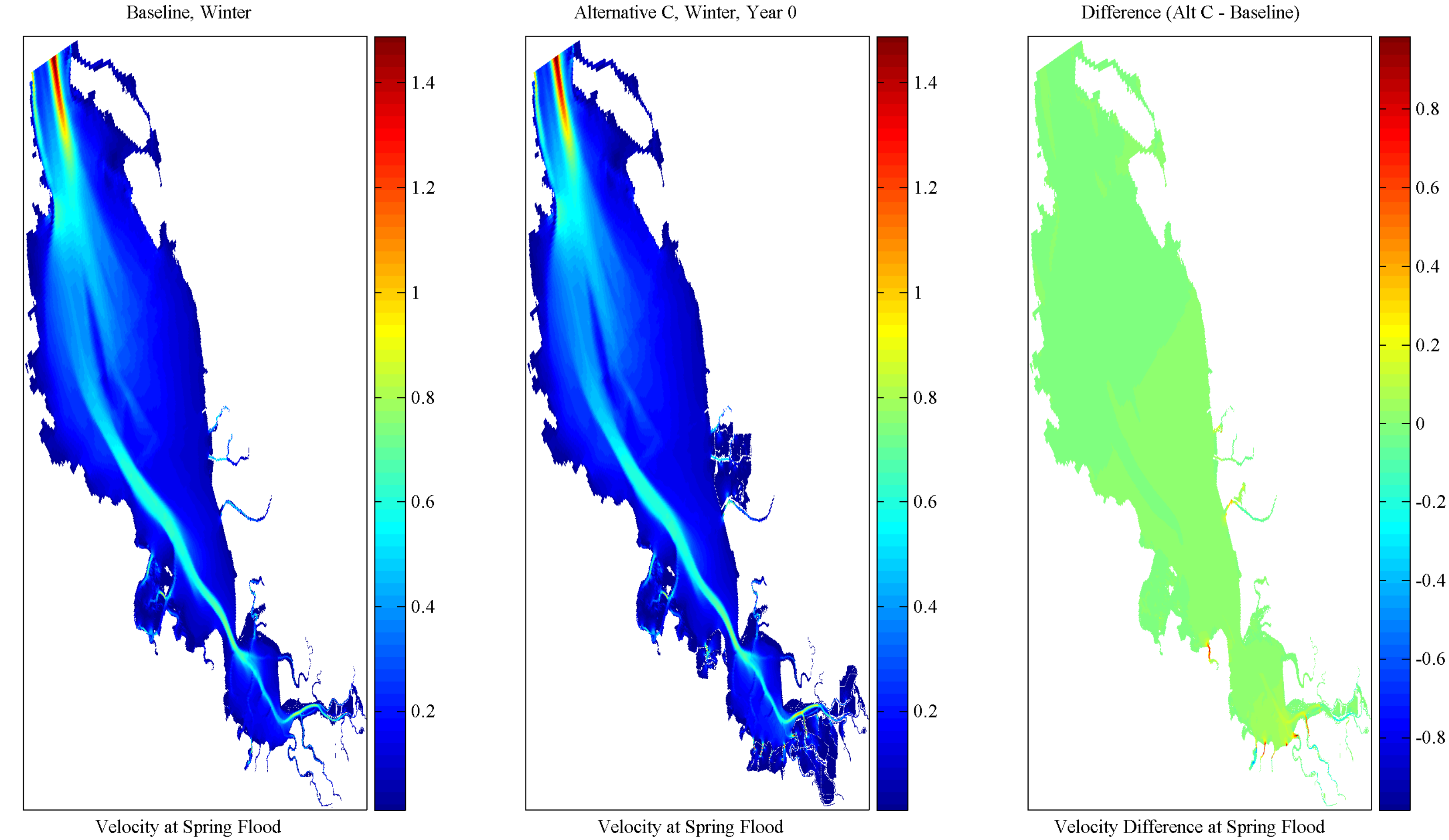

Note: Units shown are m/s

figure 5-80

South Bay Salt Pond Restoration Project

Velocity at Spring Flood, Alt C, Year 0, Winter

PWA

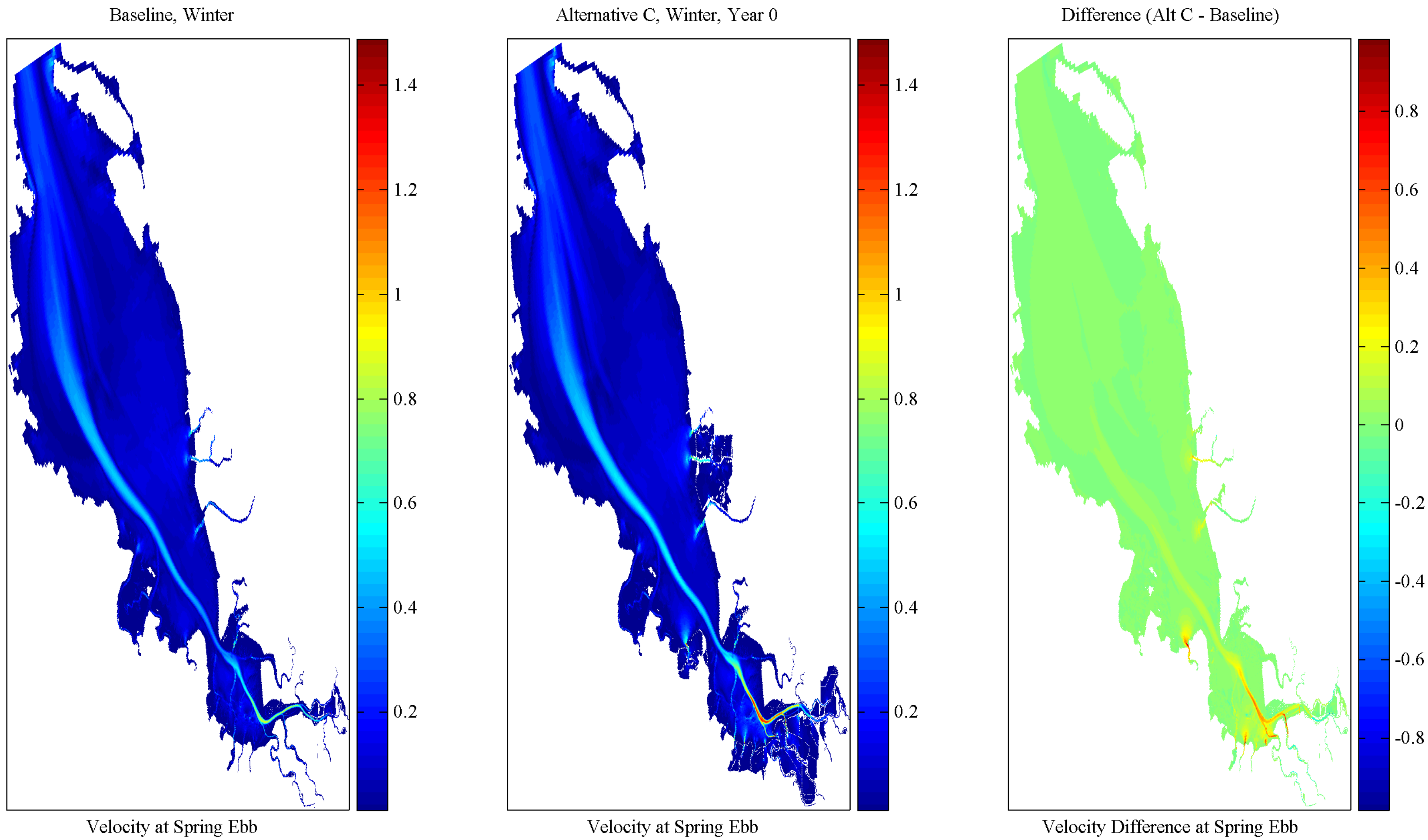

Note: Units shown are m/s

figure *5-81*

South Bay Salt Pond Restoration Project

Velocity at Spring Ebb, Alt C, Year 0, Winter

PWA

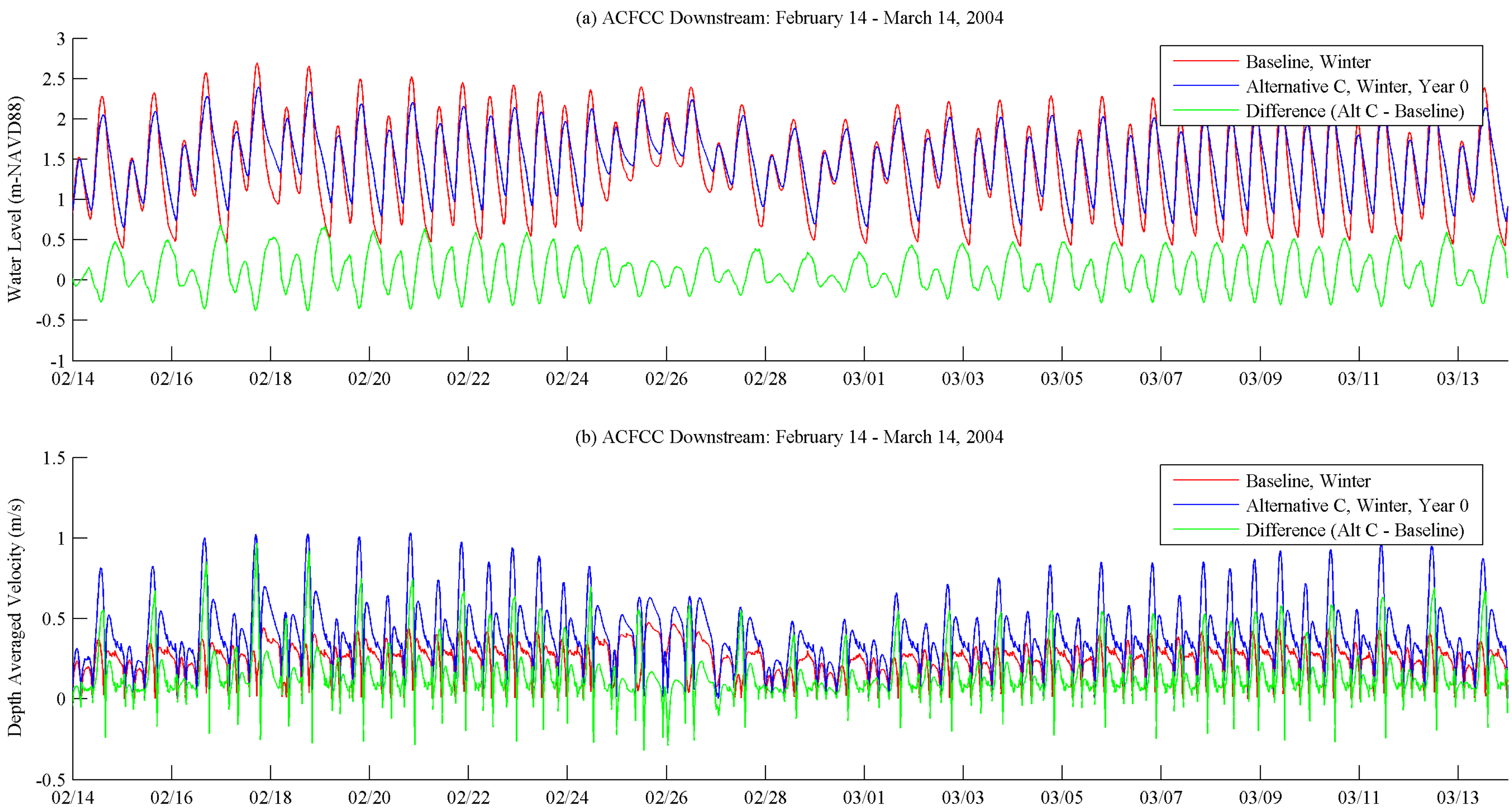

The depth-averaged velocity is calculated as $v = (u^2 + v^2)^{1/2}$, where u and v are the horizontal depth-averaged velocity components.

figure 5-82

South Bay Salt Pond Restoration Project

Velocity, ACFCC Downstream, Alt C, Year 0, Winter

PWA

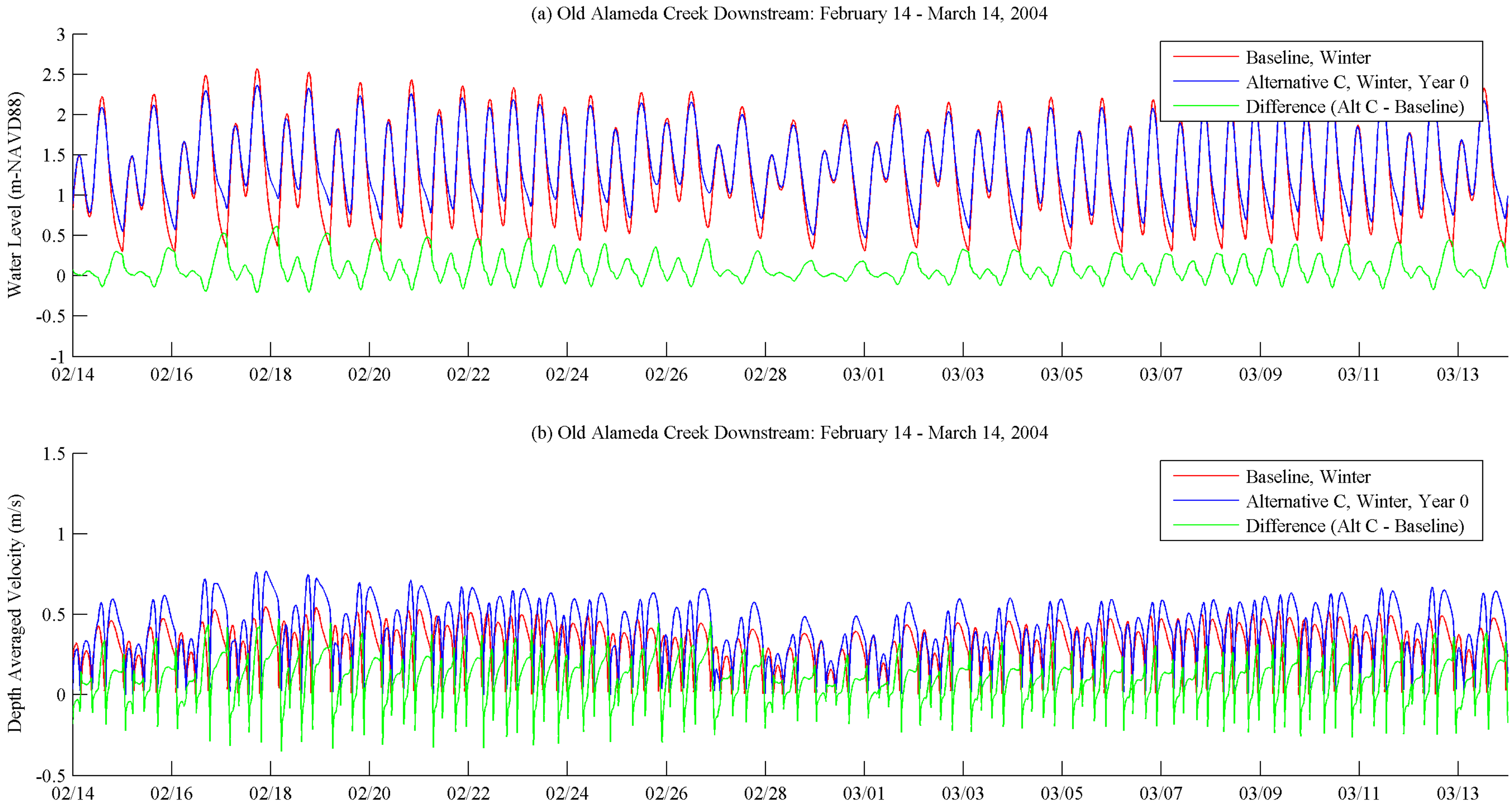

The depth-averaged velocity is calculated as $v = (u^2 + v^2)^{1/2}$, where u and v are the horizontal depth-averaged velocity components.

figure 5-83

South Bay Salt Pond Restoration Project

Velocity, Old Alameda Creek Downstream, Alt C, Year 0, Winter

PWA

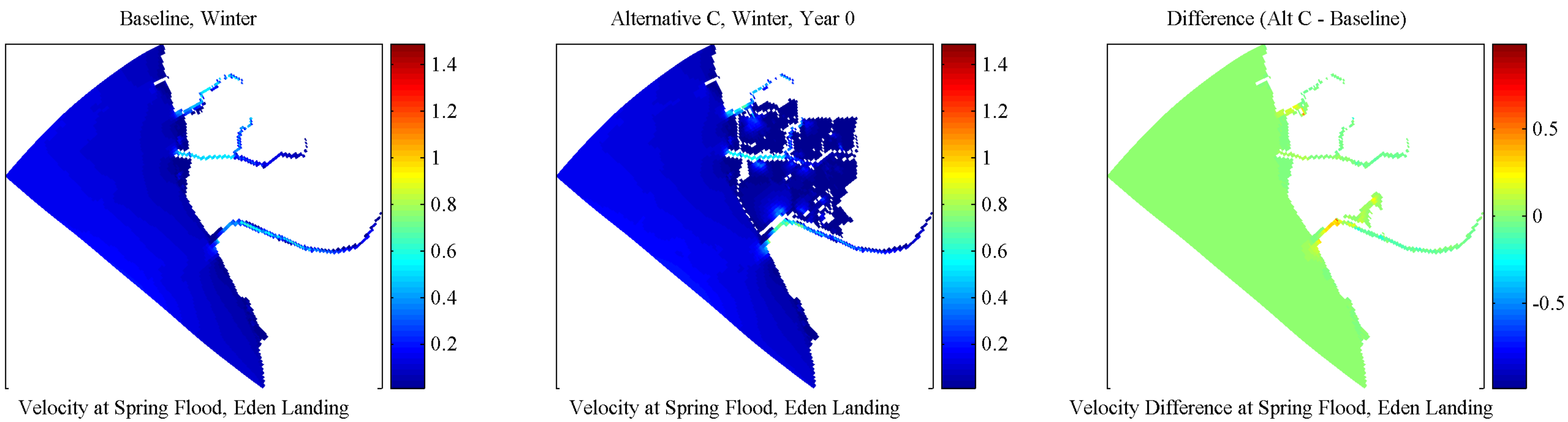

Note: Units shown are m/s

figure *5-84*

South Bay Salt Pond Restoration Project

Velocity at Spring Flood, Eden Landing, Alt C, Year 0, Winter

PWA

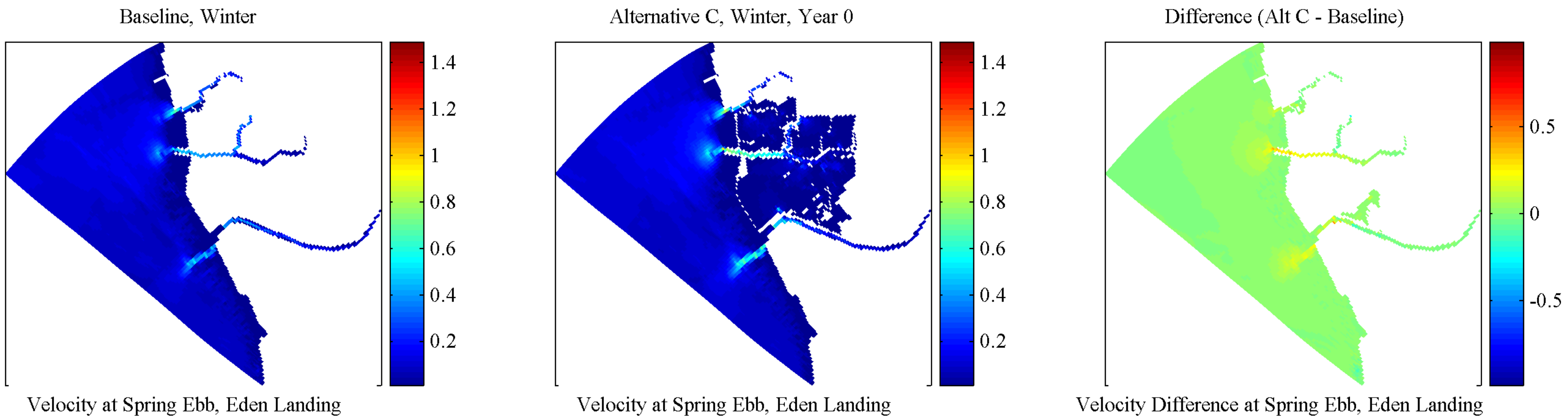

Note: Units shown are m/s

figure 5-85

South Bay Salt Pond Restoration Project

Velocity at Spring Ebb, Eden Landing, Alt C, Year 0, Winter

PWA

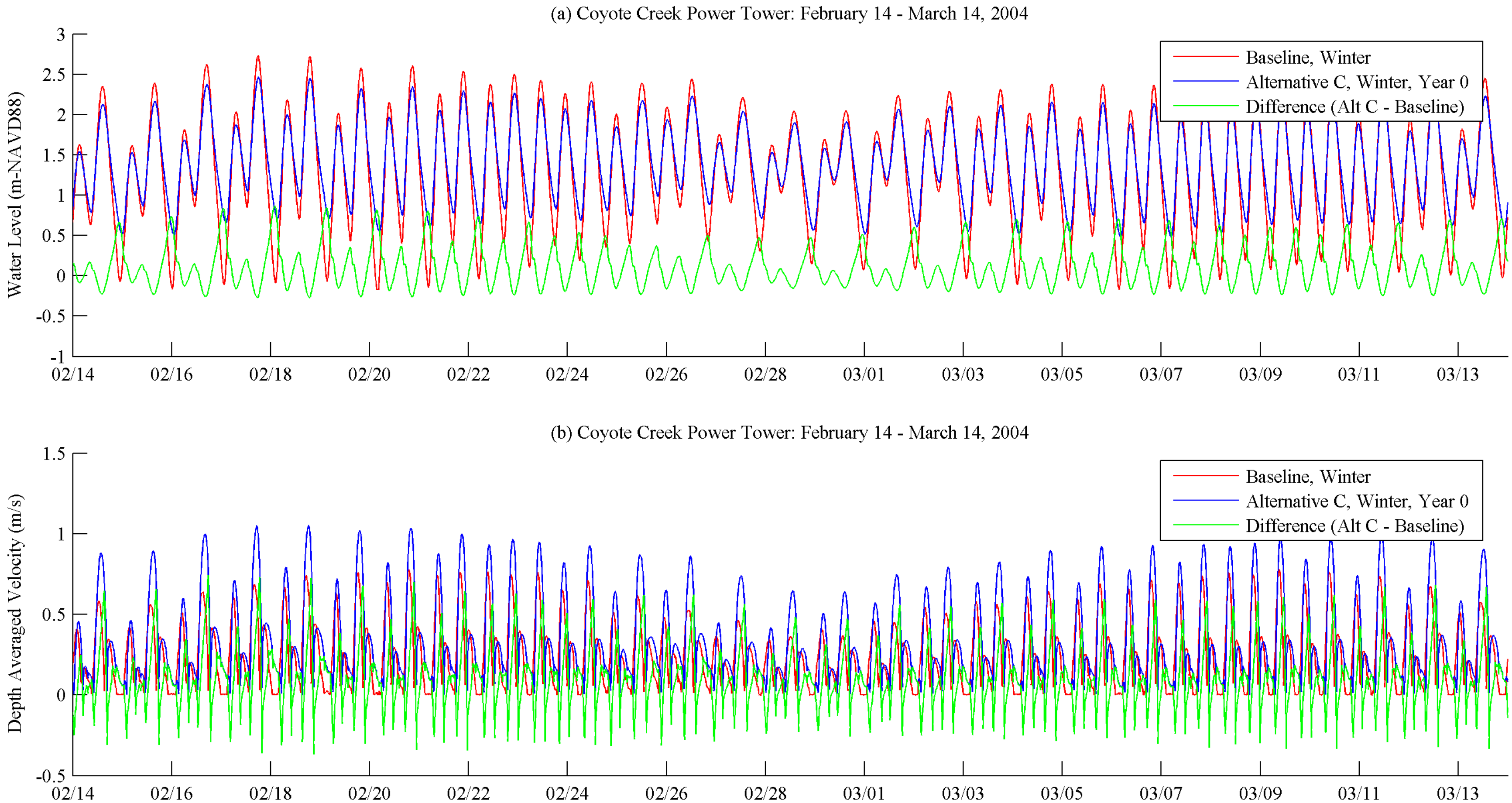

The depth-averaged velocity is calculated as $v = (u^2 + v^2)^{1/2}$, where u and v are the horizontal depth-averaged velocity components.

figure 5-86

South Bay Salt Pond Restoration Project

Velocity, Coyote Creek Power Tower, Alt C, Year 0, Winter

PWA

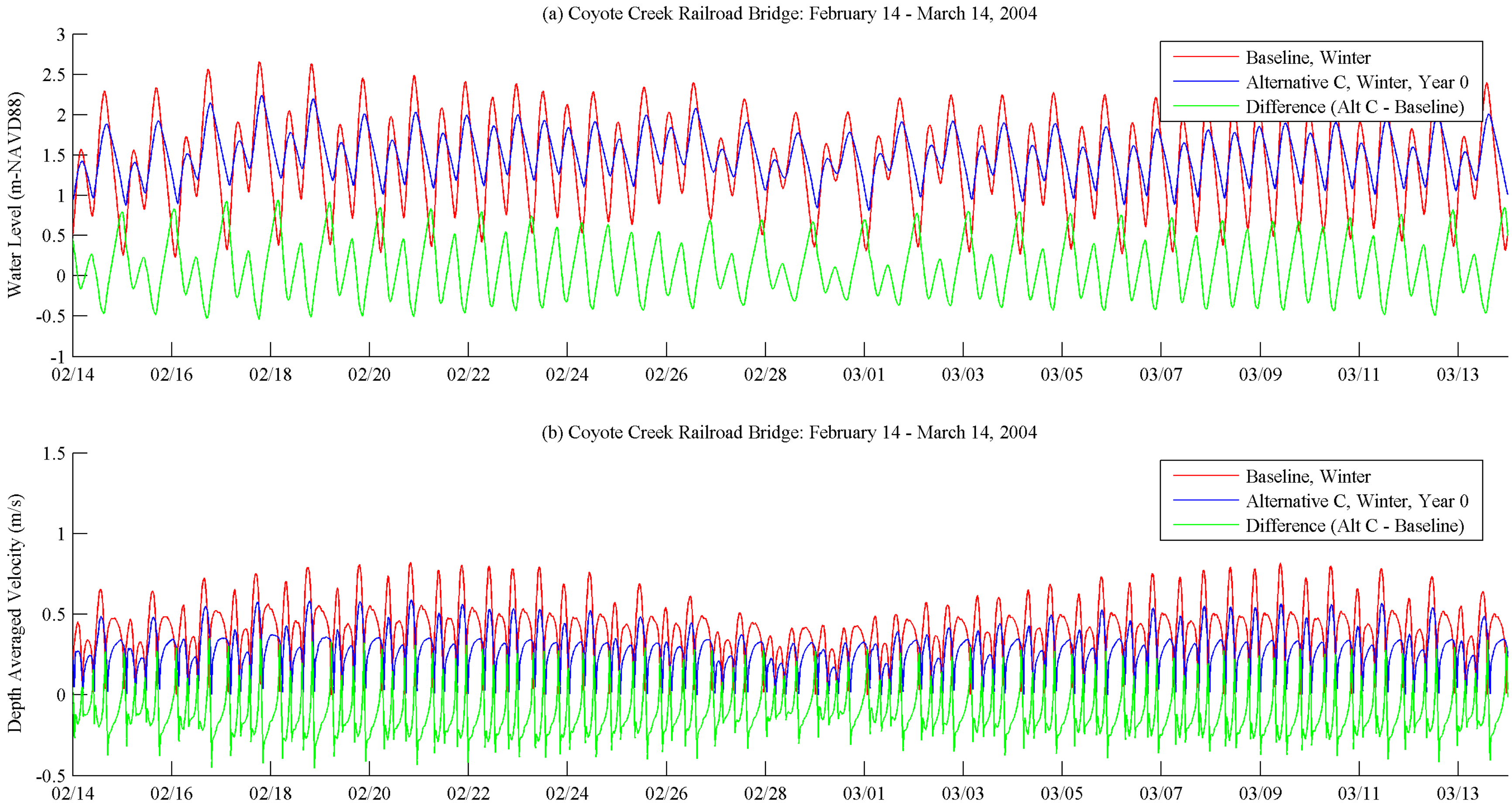

The depth-averaged velocity is calculated as $v = (u^2 + v^2)^{1/2}$, where u and v are the horizontal depth-averaged velocity components.

figure 5-87

South Bay Salt Pond Restoration Project

Velocity, Coyote Creek Railroad Bridge, Alt C, Year 0, Winter

PWA

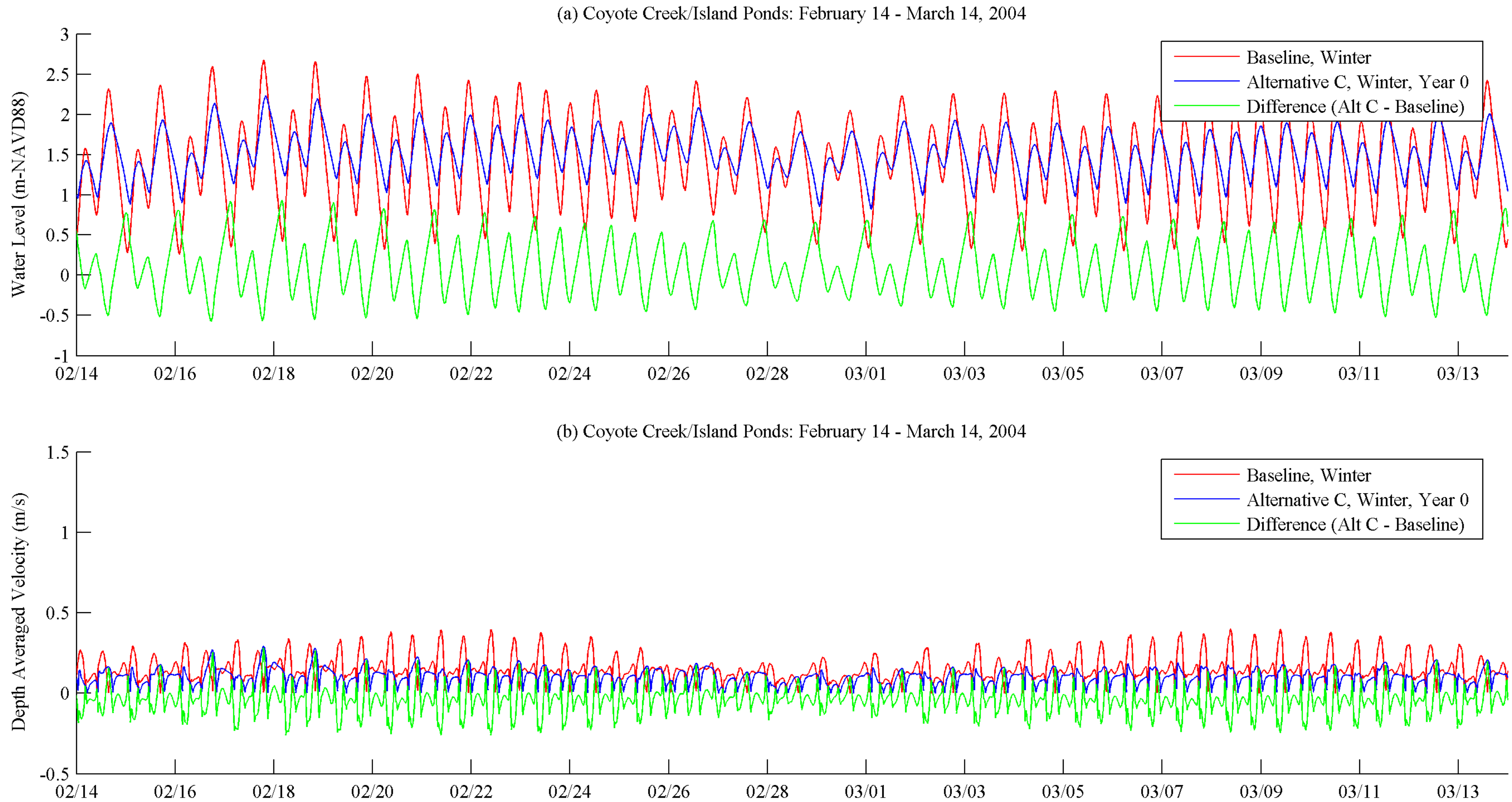

The depth-averaged velocity is calculated as $v = (u^2 + v^2)^{1/2}$, where u and v are the horizontal depth-averaged velocity components.

figure 5-88

South Bay Salt Pond Restoration Project

Velocity, Coyote Creek/Island Ponds, Year 0, Winter

PWA

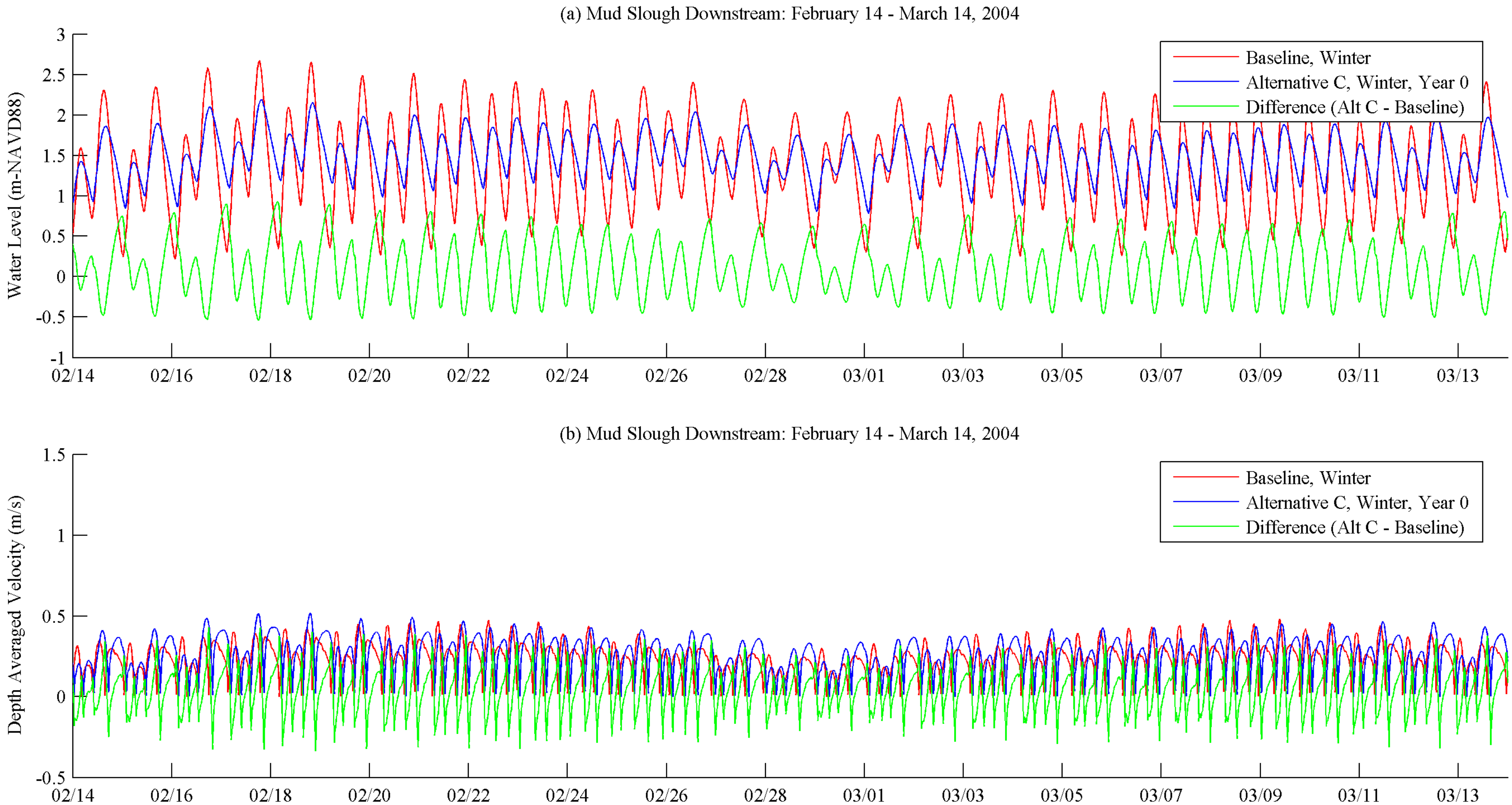

The depth-averaged velocity is calculated as $v = (u^2 + v^2)^{1/2}$, where u and v are the horizontal depth-averaged velocity components.

figure 5-89

South Bay Salt Pond Restoration Project

Velocity, Coyote Creek/Island Ponds, Year 0, Winter

PWA

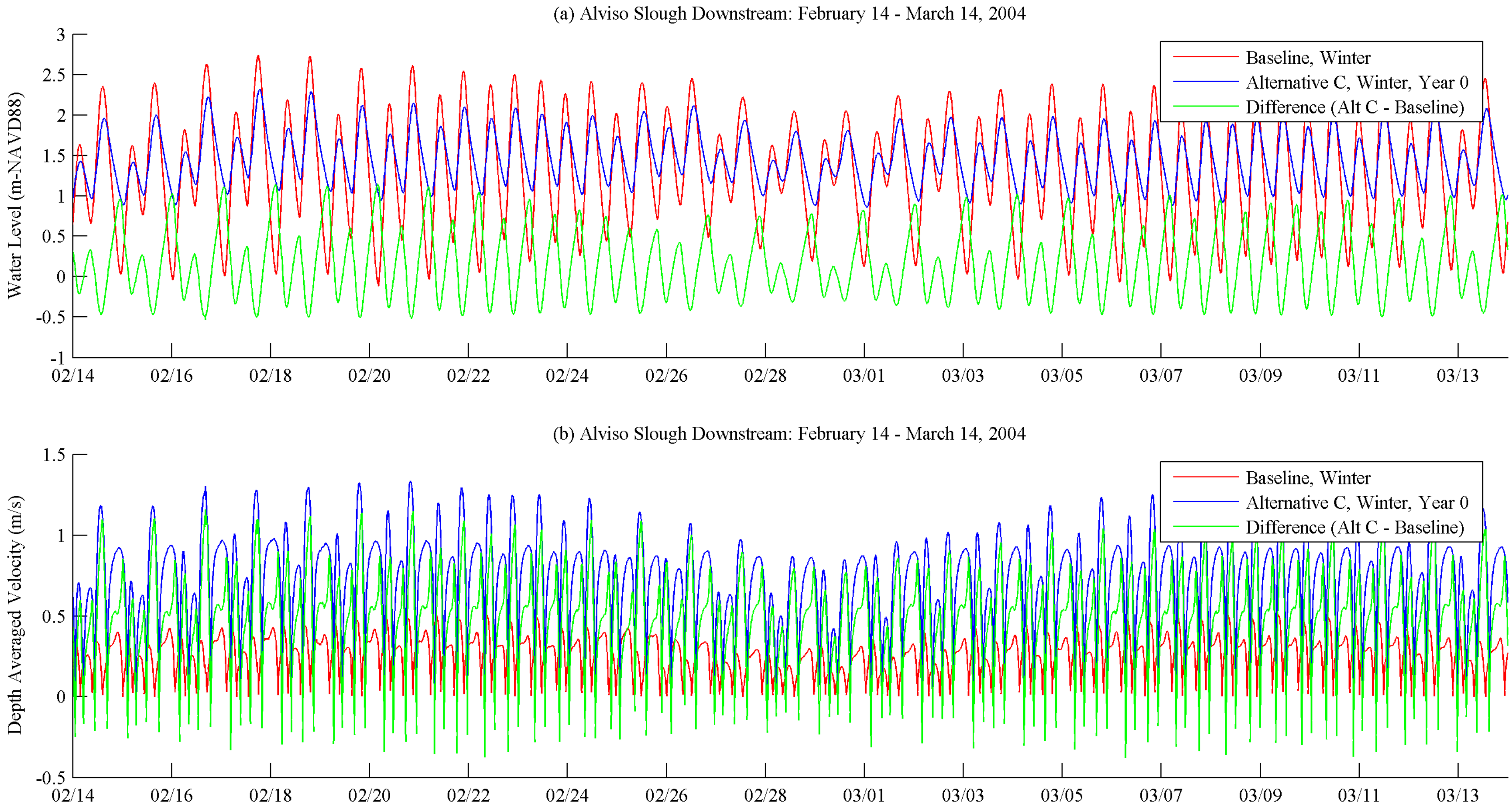

The depth-averaged velocity is calculated as $v = (u^2 + v^2)^{1/2}$, where u and v are the horizontal depth-averaged velocity components.

figure 5-90

South Bay Salt Pond Restoration Project

Velocity, Alviso Slough Downstream, Alt C, Year 0, Winter

PWA

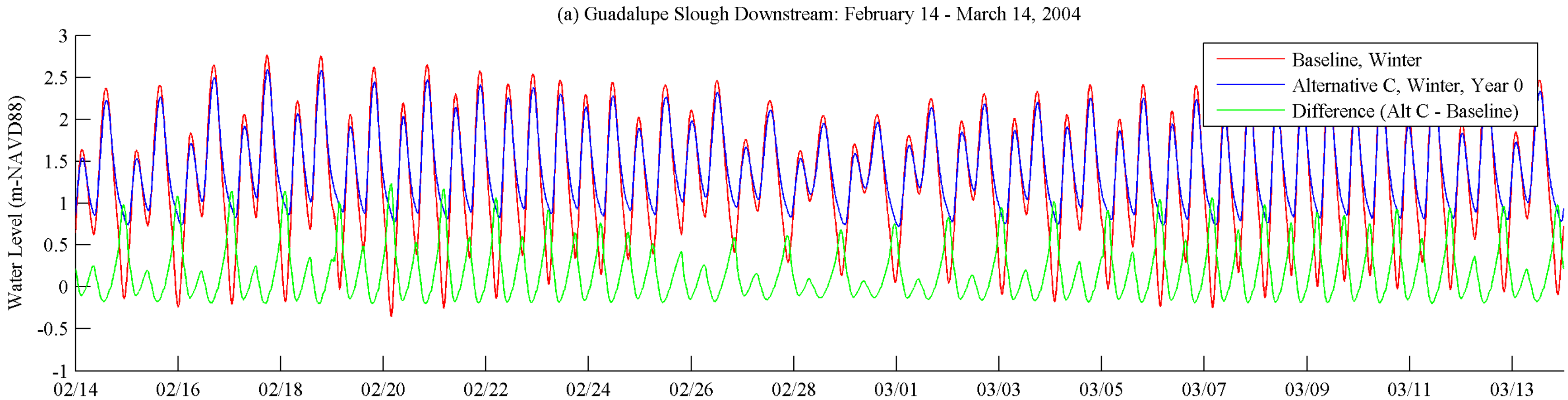

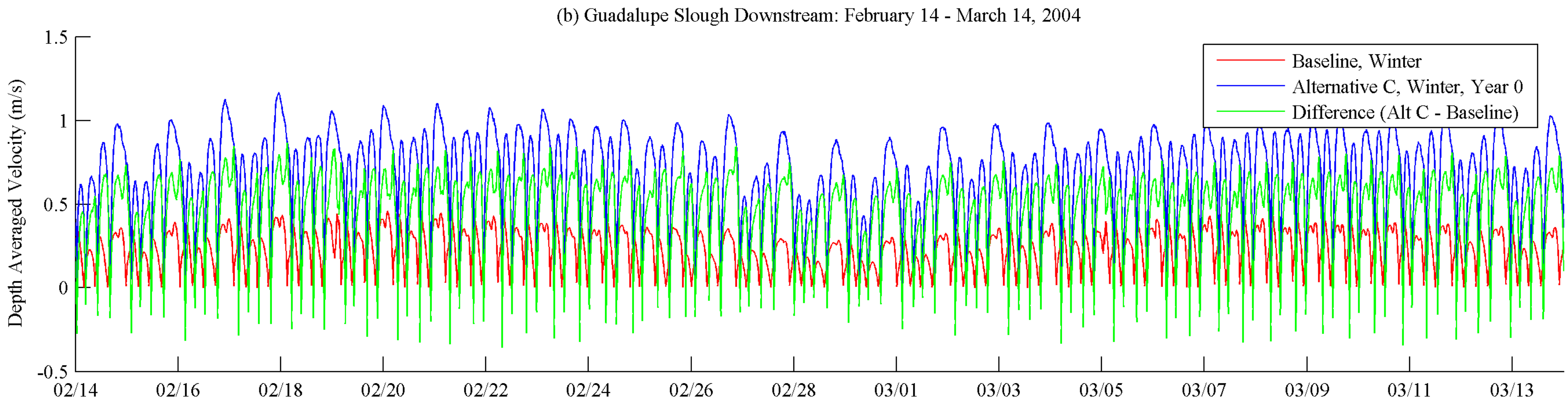

The depth-averaged velocity is calculated as $v = (u^2 + v^2)^{1/2}$, where u and v are the horizontal depth-averaged velocity components.

figure 5-91

South Bay Salt Pond Restoration Project

Velocity, Guadalupe Slough Downstream, Alt C, Year 0, Winter

PWA

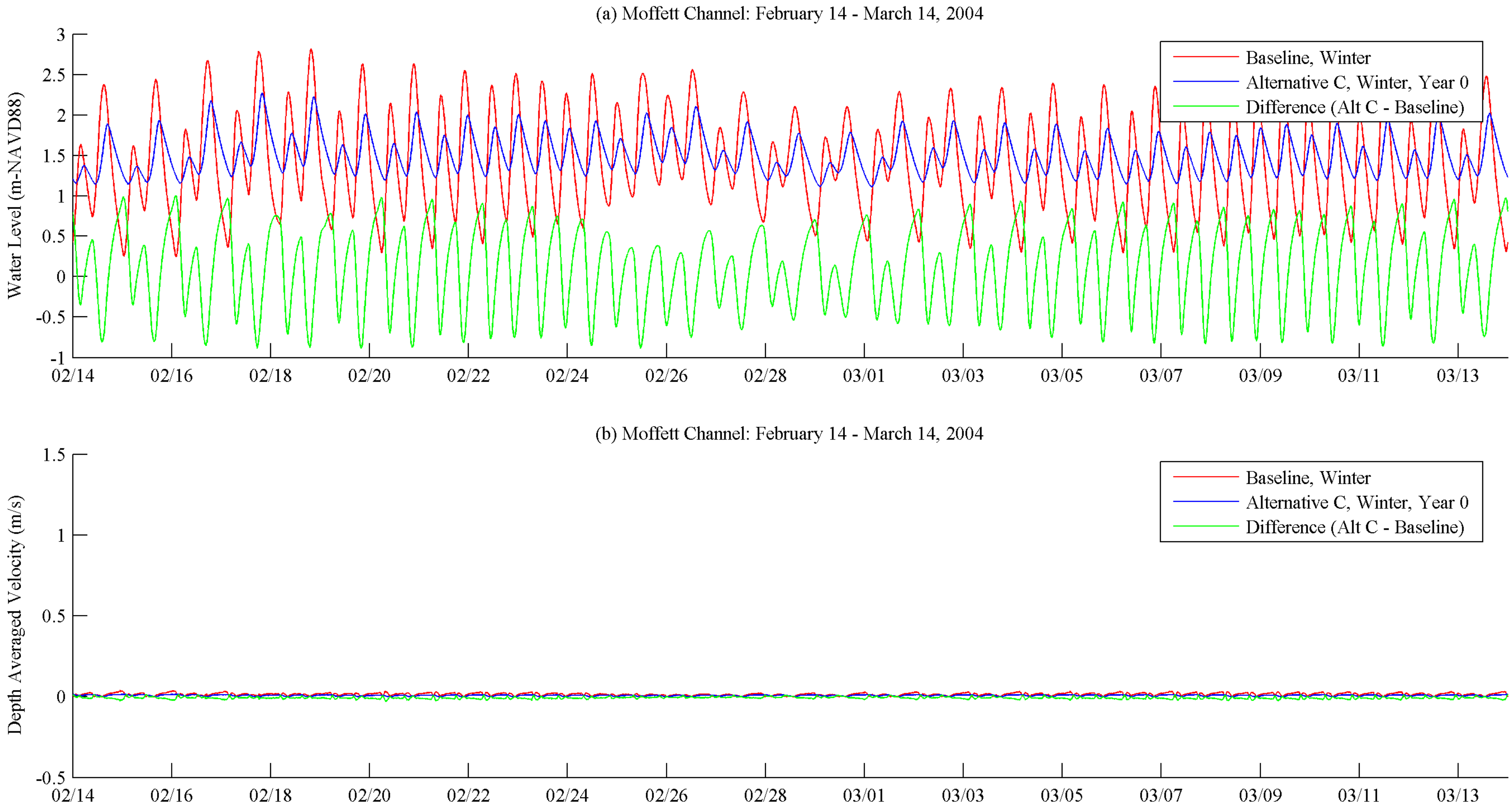

The depth-averaged velocity is calculated as $v = (u^2 + v^2)^{1/2}$, where u and v are the horizontal depth-averaged velocity components.

figure 5-92

South Bay Salt Pond Restoration Project

Velocity, Moffett Channel, Alt C, Year 0, Winter

PWA

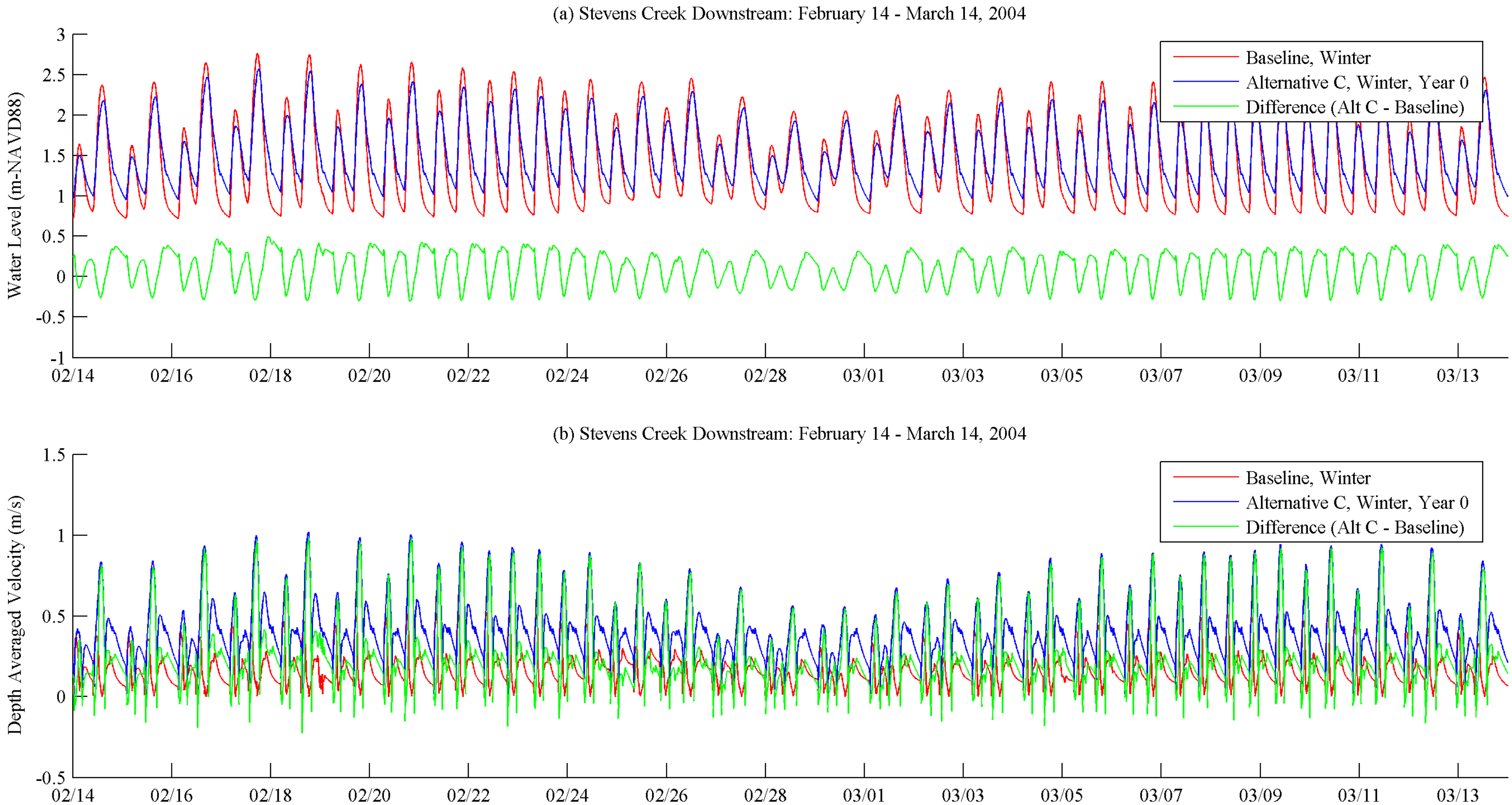

The depth-averaged velocity is calculated as $v = (u^2 + v^2)^{1/2}$, where u and v are the horizontal depth-averaged velocity components.

figure 5-93

South Bay Salt Pond Restoration Project

Velocity, Steven Creek Downstream, Alt C, Year 0, Winter

PWA

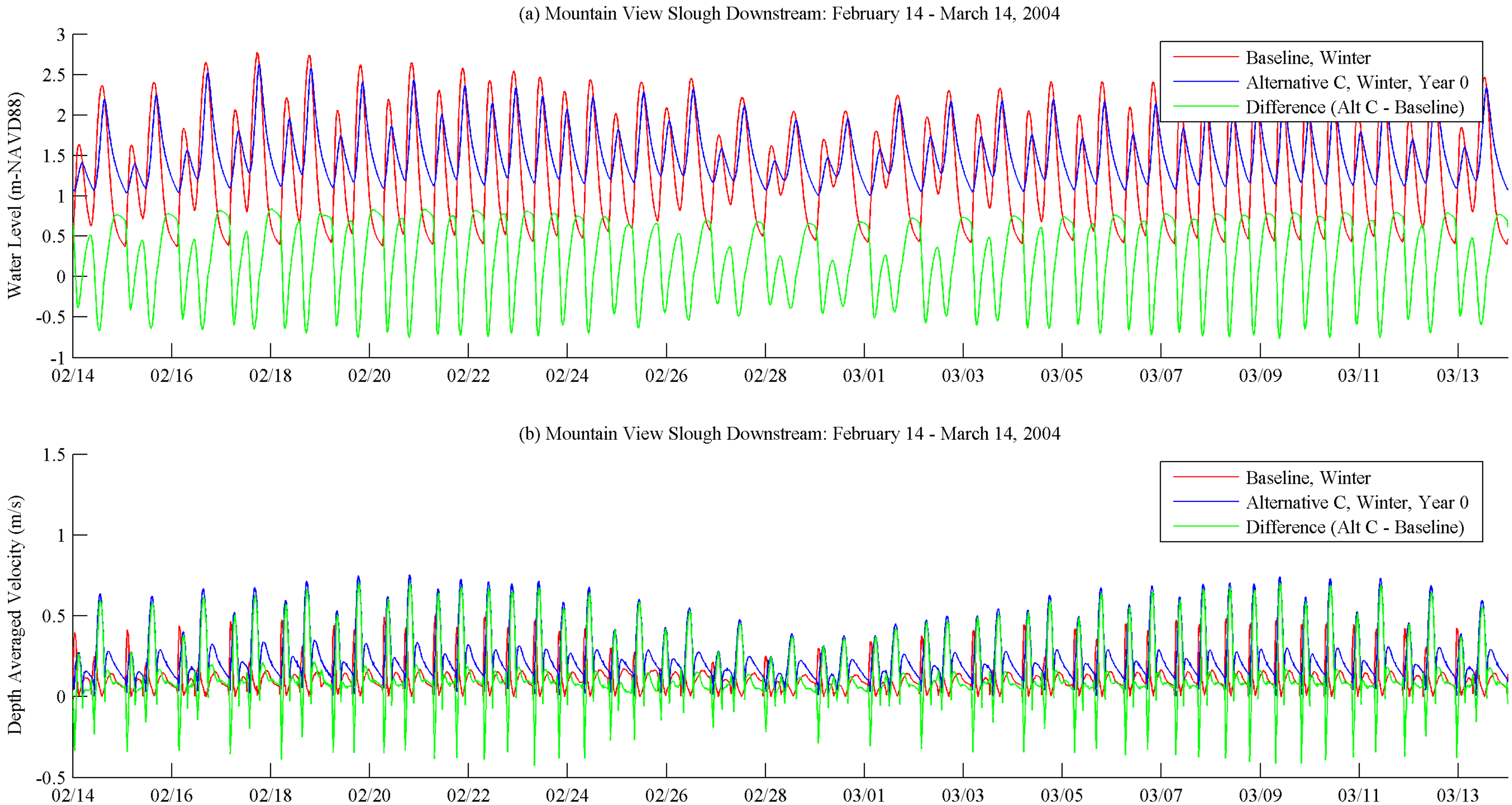

The depth-averaged velocity is calculated as $v = (u^2 + v^2)^{1/2}$, where u and v are the horizontal depth-averaged velocity components.

figure *5-94*

South Bay Salt Pond Restoration Project

Velocity, Mountain View Slough Downstream, Alt C, Year 0, Winter

PWA

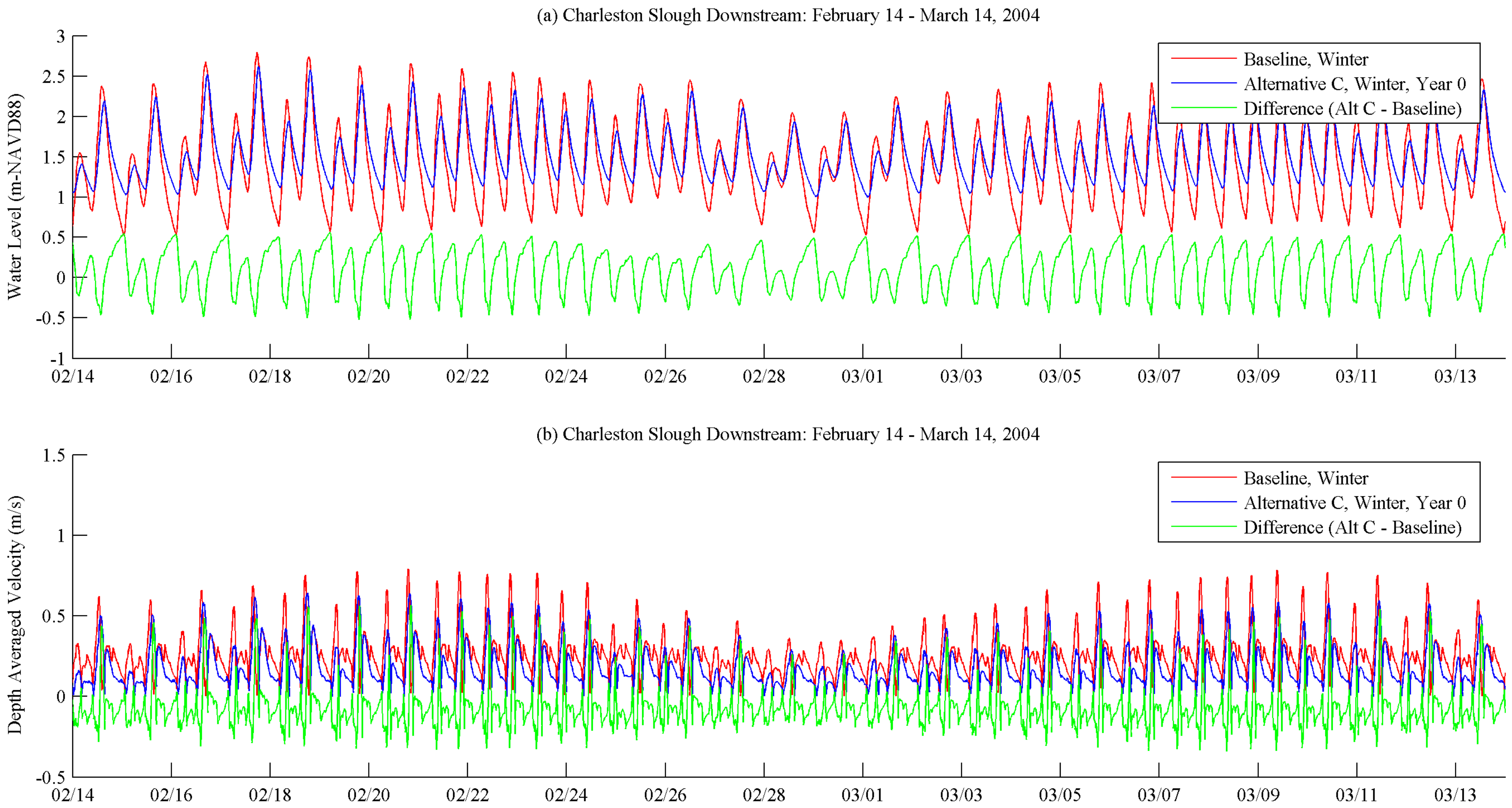

The depth-averaged velocity is calculated as $v = (u^2 + v^2)^{1/2}$, where u and v are the horizontal depth-averaged velocity components.

figure 5-95

South Bay Salt Pond Restoration Project

Velocity, Charleston Slough Downstream, Alt C, Year 0, Winter

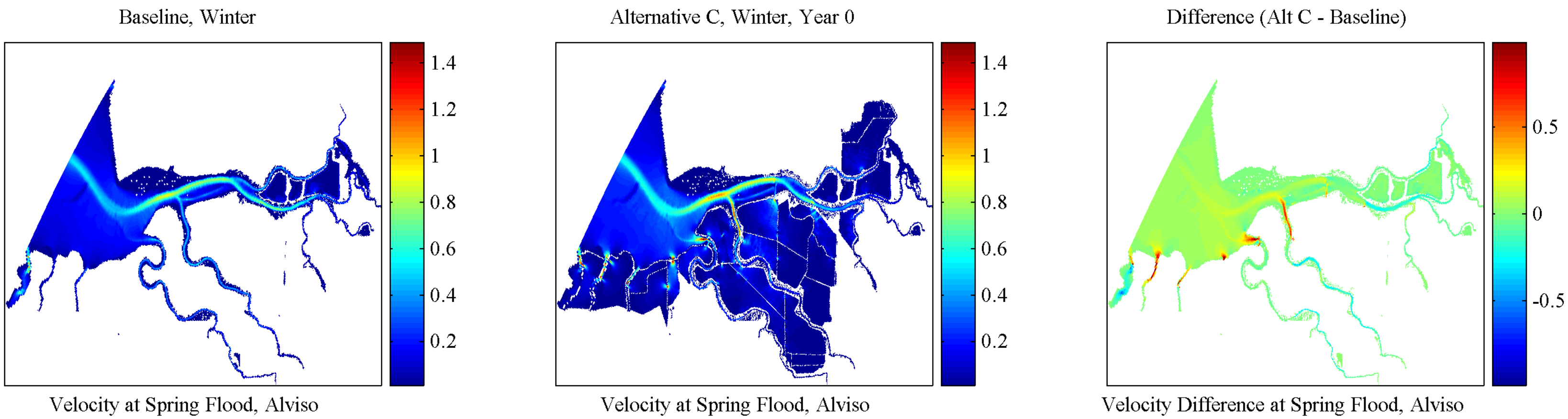

Note: Units shown are m/s

figure 5-96

South Bay Salt Pond Restoration Project

Velocity at Spring Flood, Alviso, Alt C, Year 0, Winter

PWA

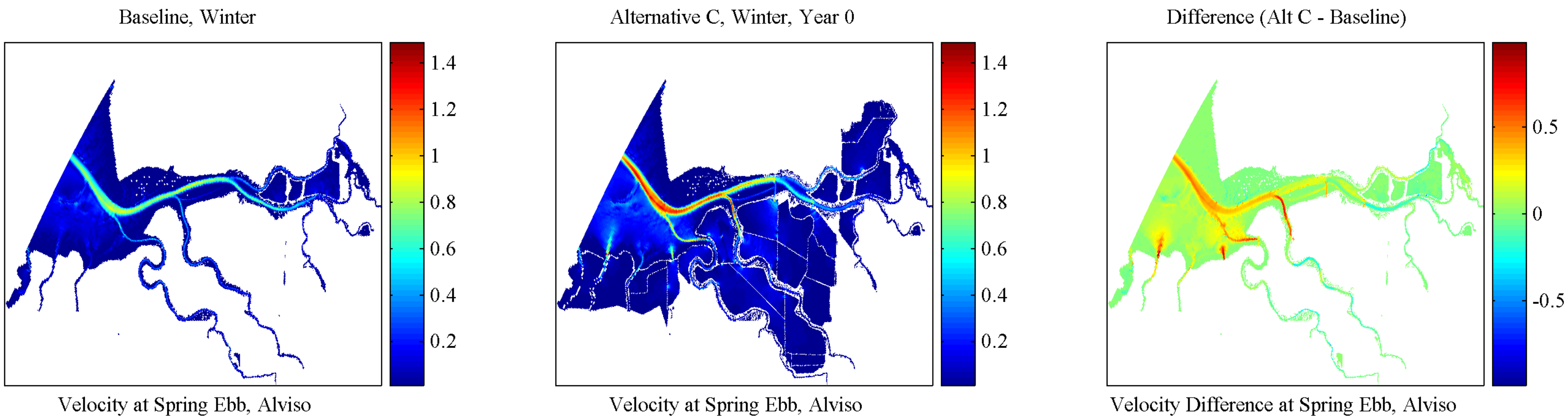

Note: Units shown are m/s

figure *5-97*

South Bay Salt Pond Restoration Project

Velocity at Spring Ebb, Alviso, Alt C, Year 0, Winter

PWA

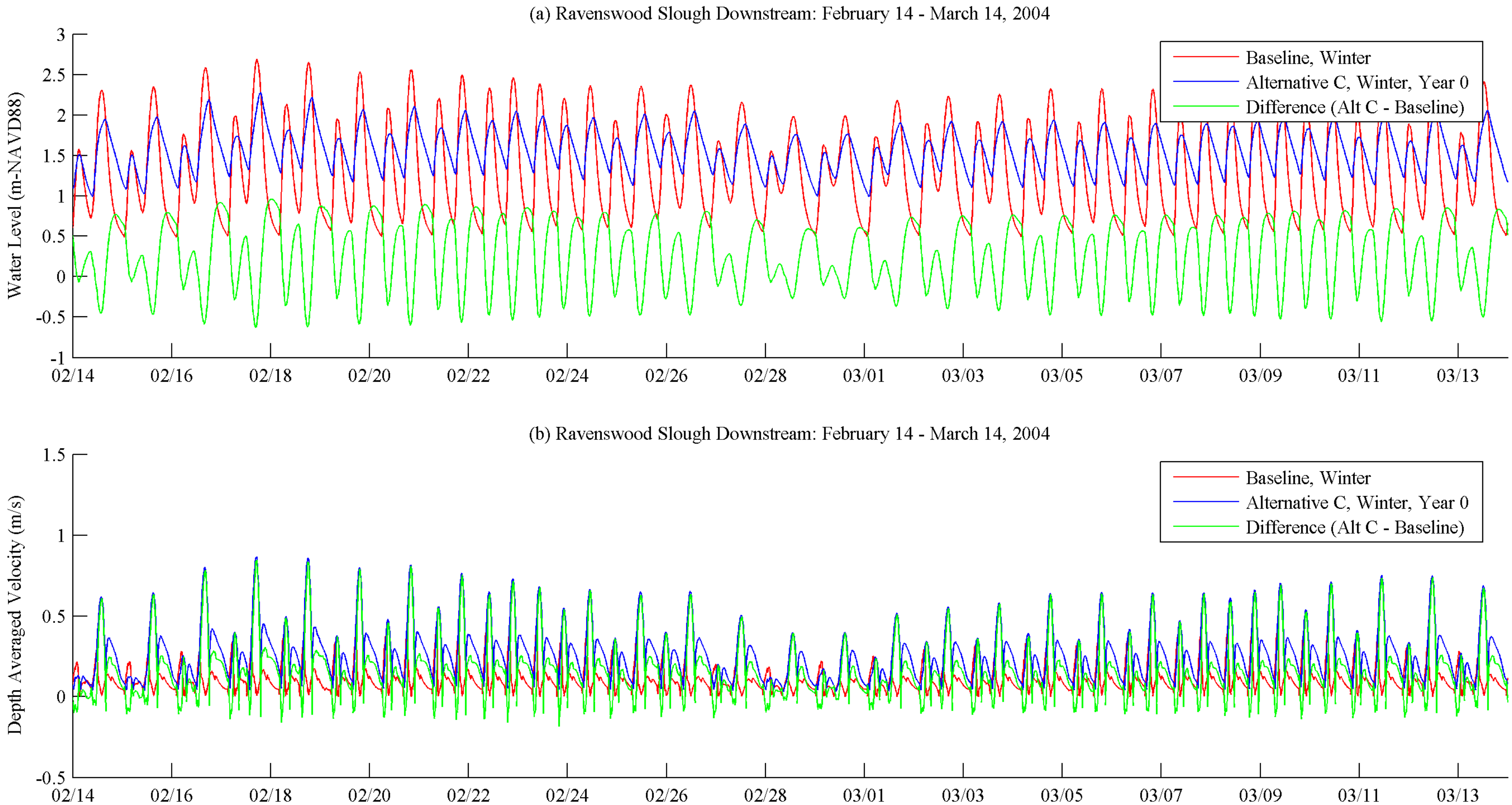

The depth-averaged velocity is calculated as $v = (u^2 + v^2)^{1/2}$, where u and v are the horizontal depth-averaged velocity components.

figure 5-98

South Bay Salt Pond Restoration Project

Velocity, Ravenswood Slough Downstream, Alt C, Year 0, Winter

PWA

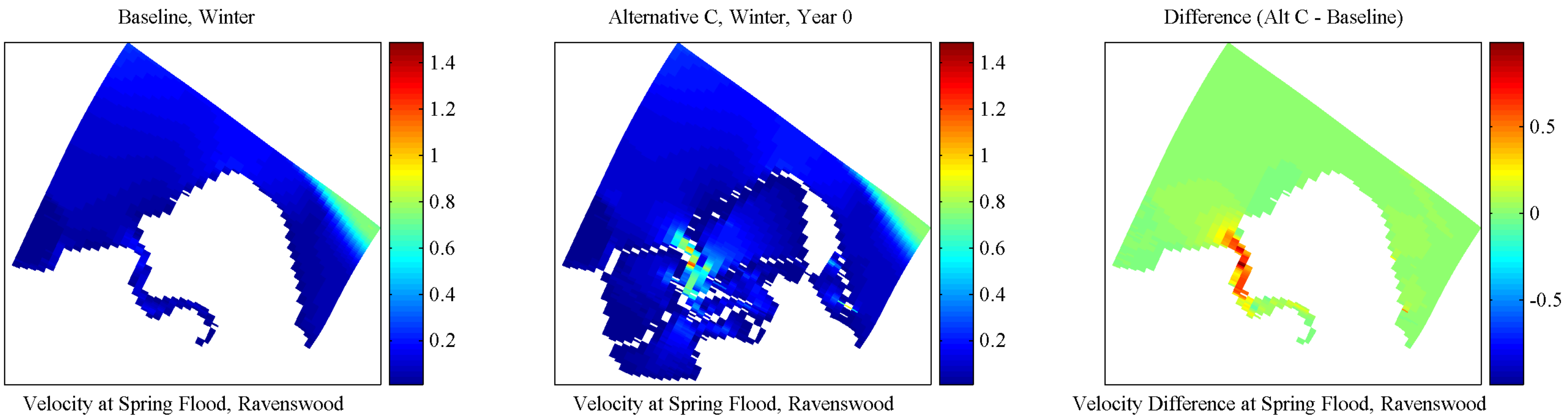

Note: Units shown are m/s

figure *5-99*

South Bay Salt Pond Restoration Project

Velocity at Spring Flood, Ravenswood, Alt C, Year 0, Winter

PWA

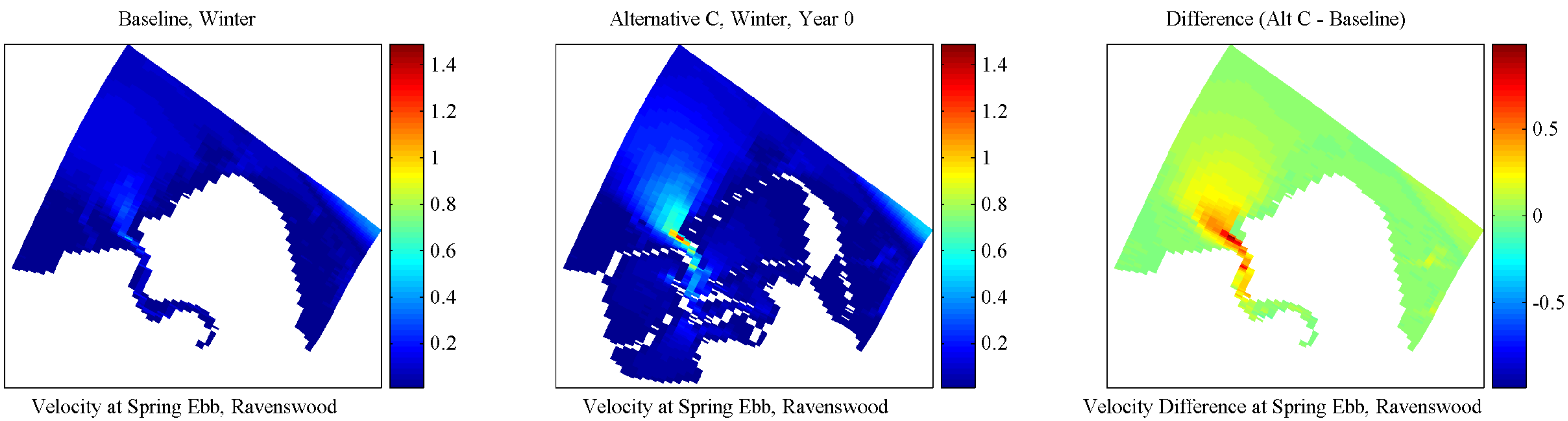

Note: Units shown are m/s

figure 5-100

South Bay Salt Pond Restoration Project

Velocity at Spring Ebb, Ravenswood, Alt C, Year 0, Winter

PWA

Baseline, Winter

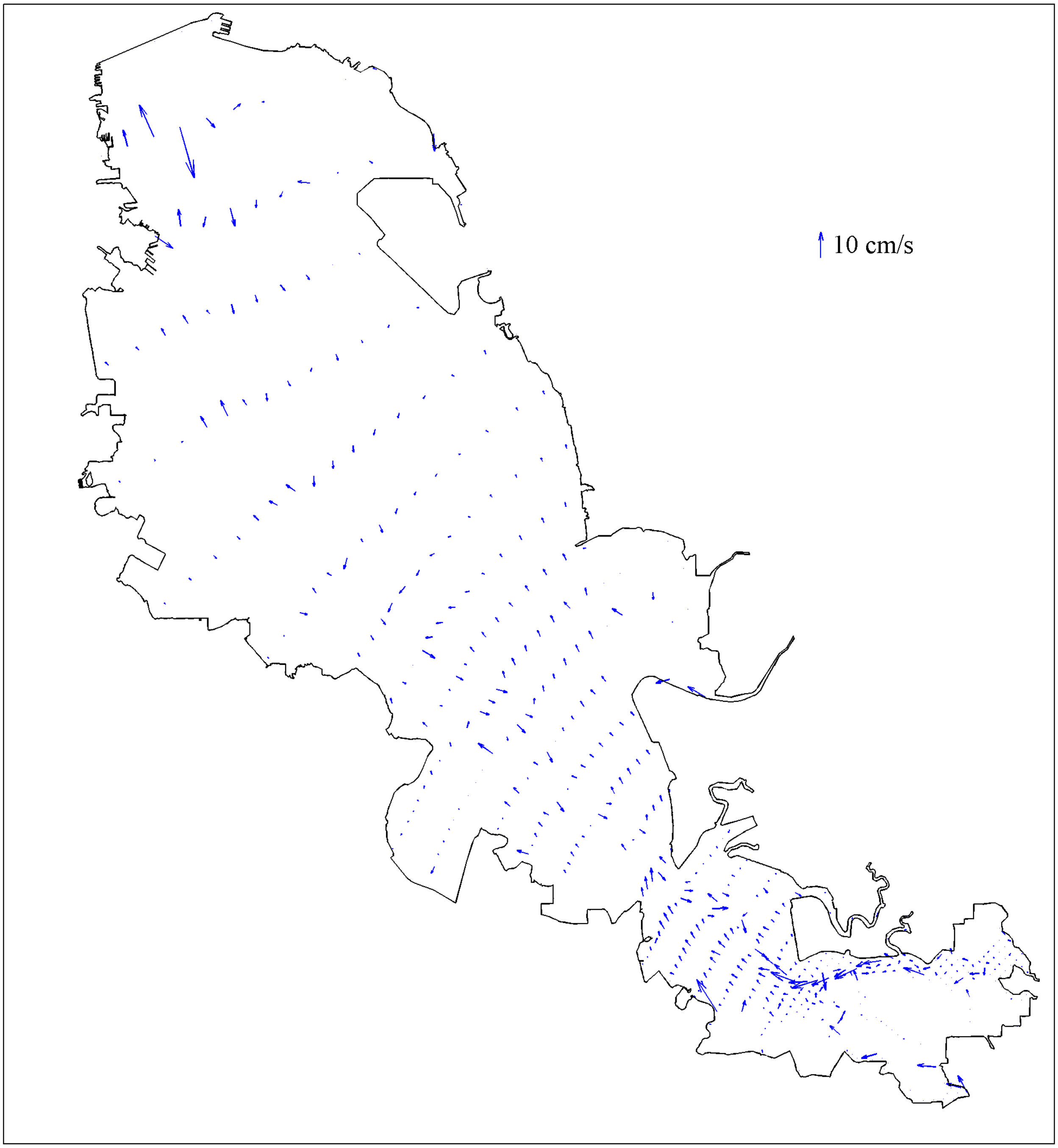

South Bay Residual Circulation (cm/s)

figure 5-101

South Bay Salt Pond Restoration Project

South Bay Residual Circulation, Baseline, Winter

PWA

Alternative C, Winter, Year 0

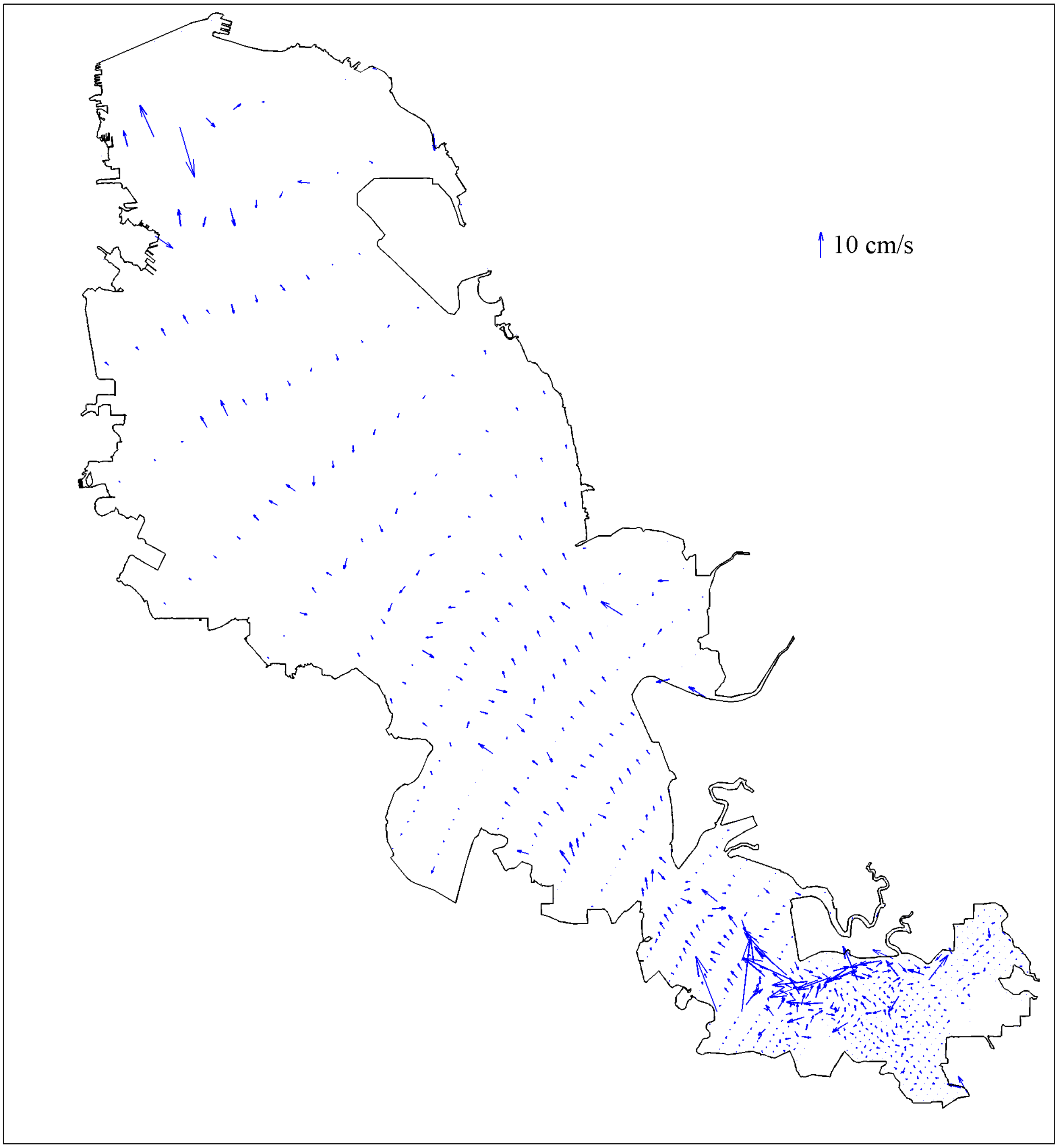

South Bay Residual Circulation (cm/s)

figure 5-102

South Bay Salt Pond Restoration Project

South Bay Residual Circulation, Alt C, Year 0, Winter

PWA

Difference (Alt C - Baseline)

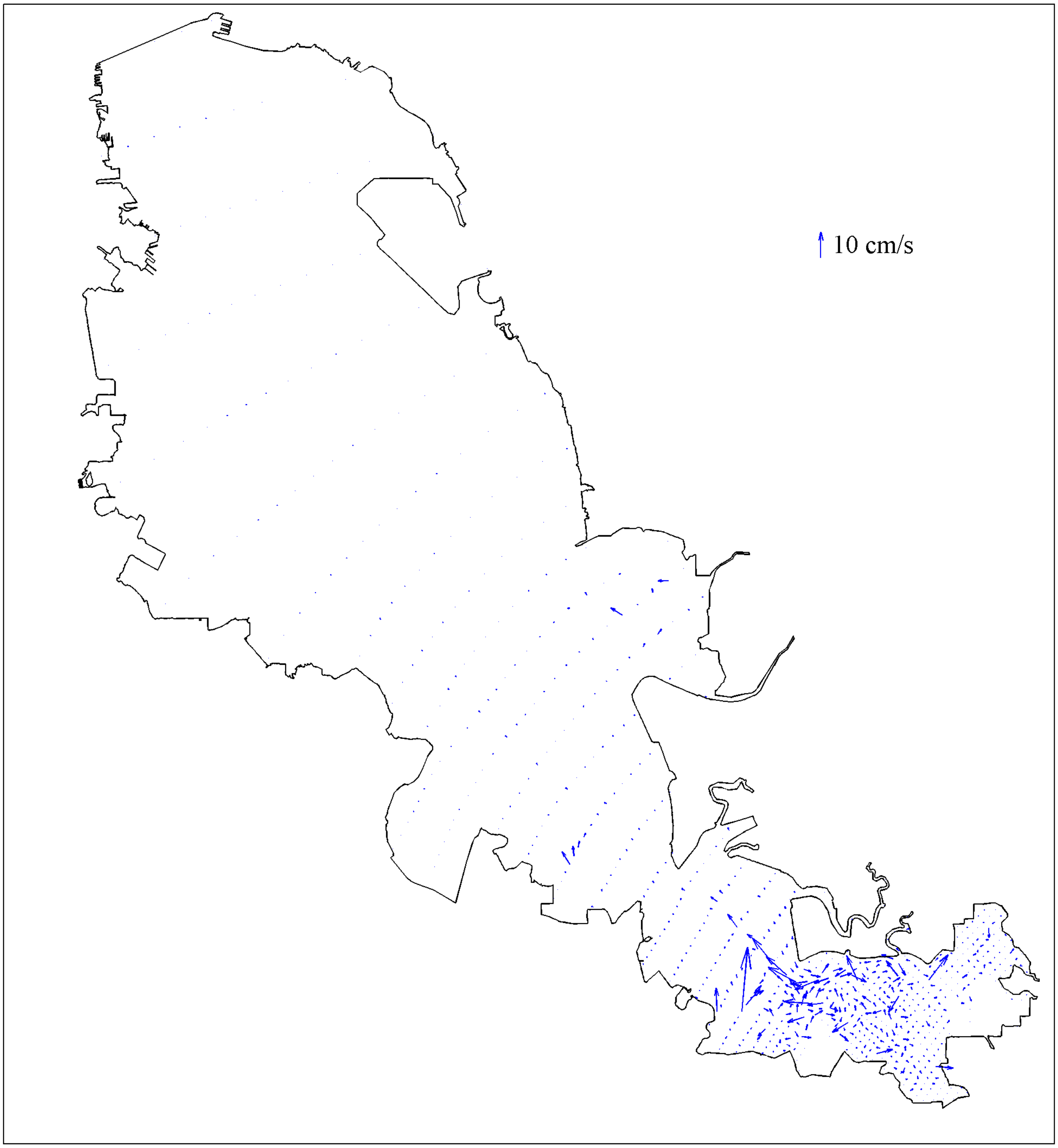

South Bay Residual Circulation Difference (cm/s)

figure 5-103

South Bay Salt Pond Restoration Project

South Bay Residual Circulation, Difference, Year 0, Winter

PWA

Baseline, Winter

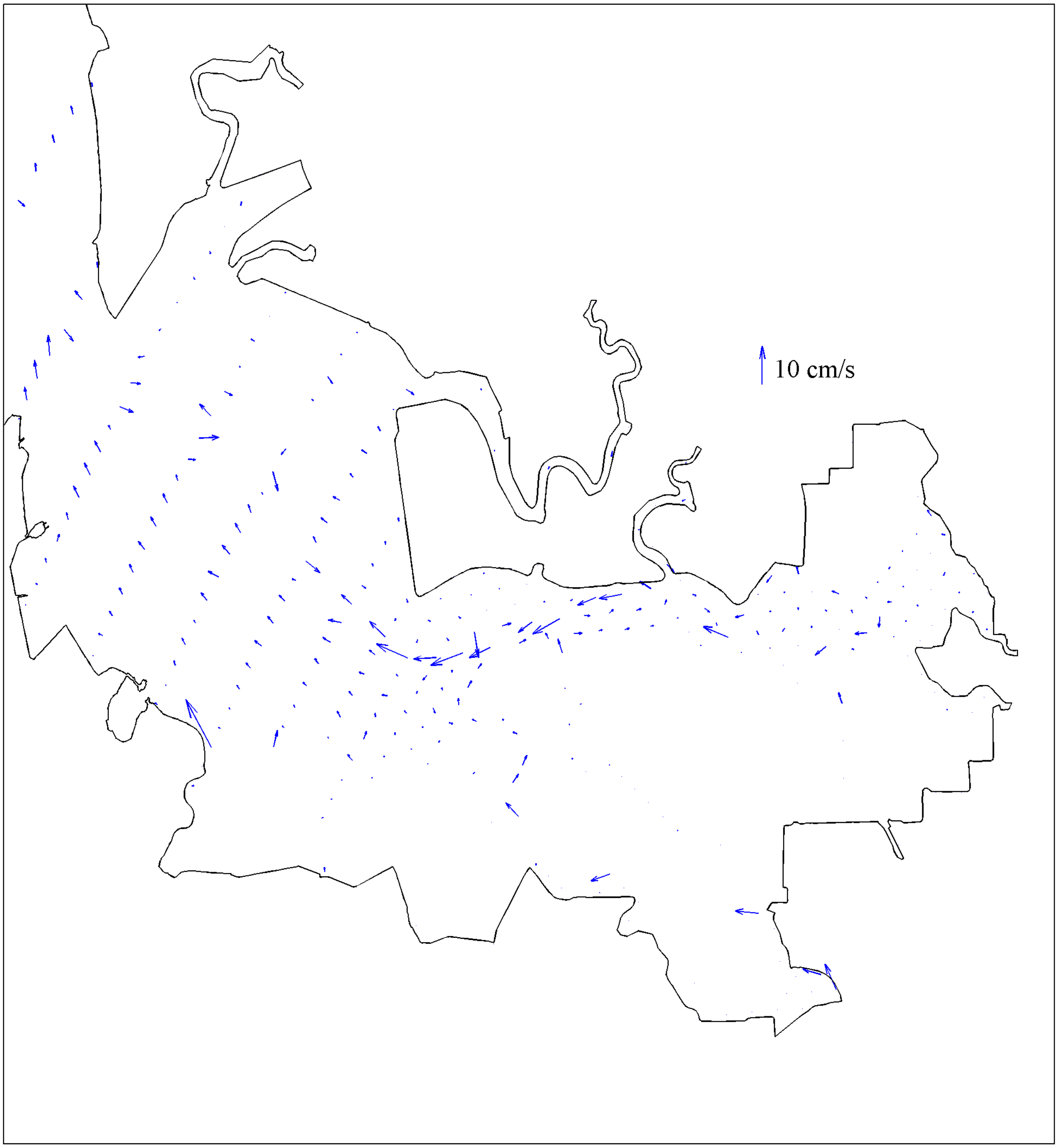

Far South Bay Residual Circulation (cm/s)

figure 5-104

South Bay Salt Pond Restoration Project

Far South Bay Residual Circulation, Baseline, Winter

PWA

Alternative C, Winter, Year 0

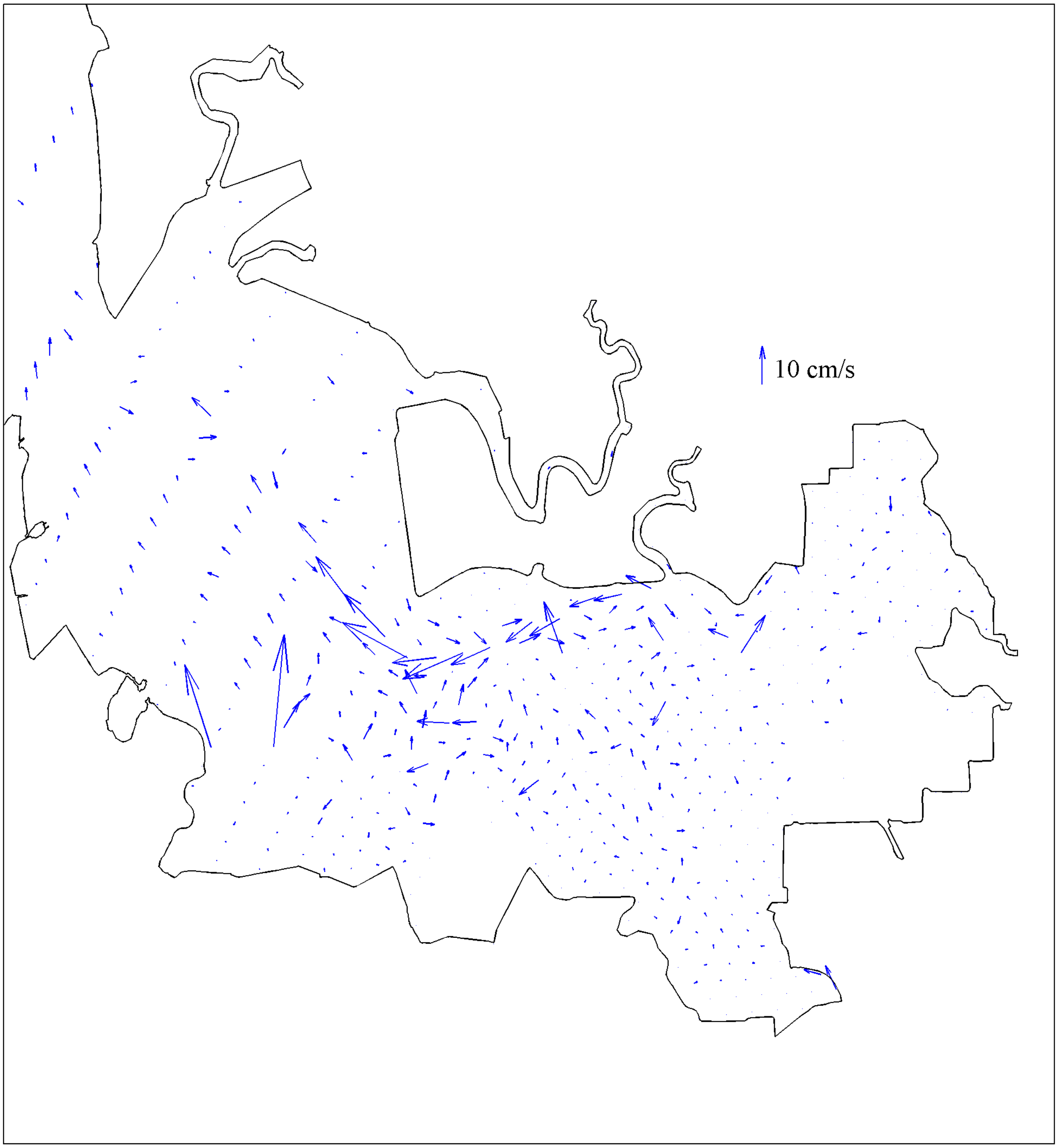

Far South Bay Residual Circulation (cm/s)

figure 5-105

South Bay Salt Pond Restoration Project

Far South Bay Residual Circulation, Alt C, Year 0, Winter

PWA

Difference (Alt C - Baseline)

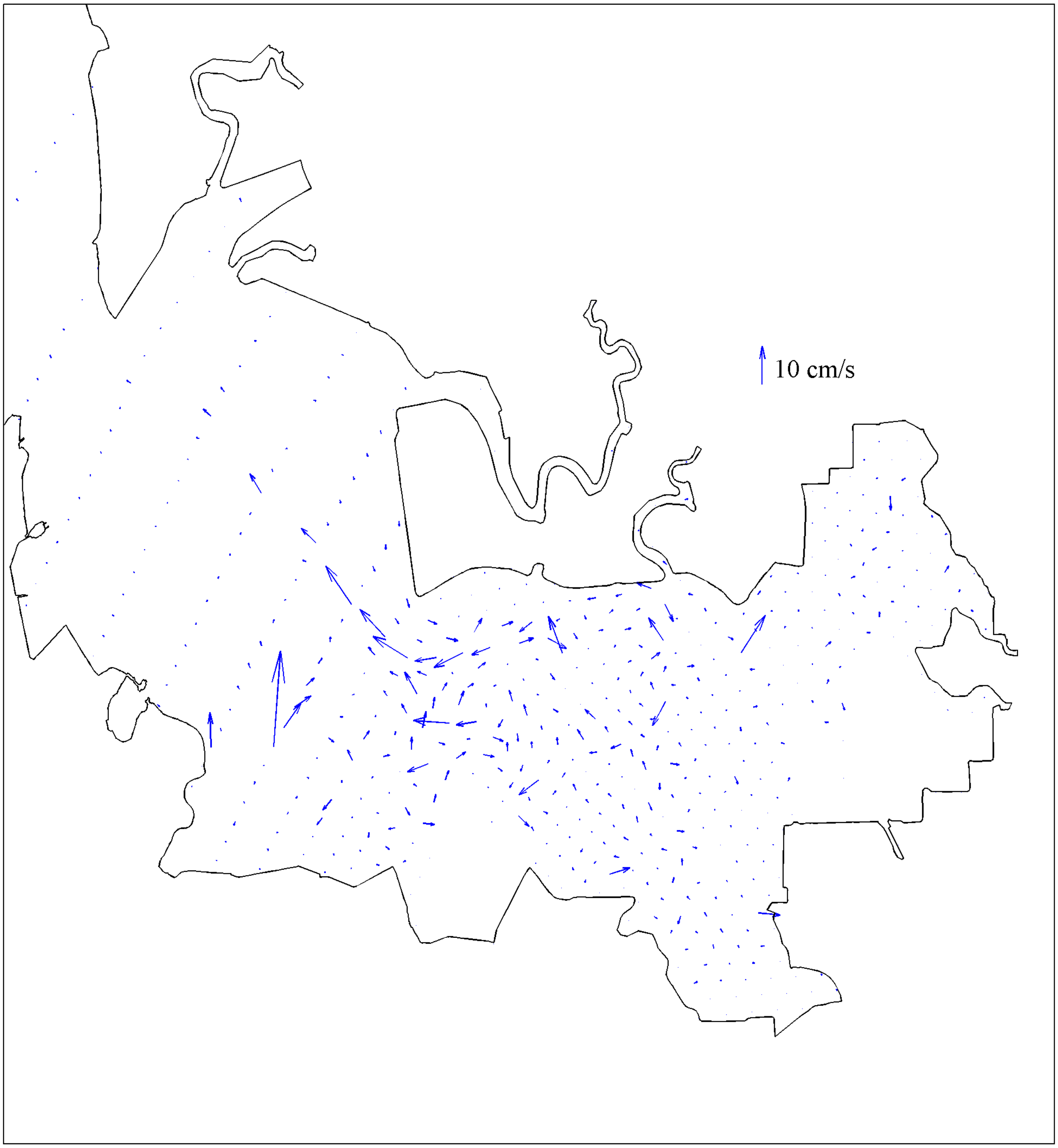

Far South Bay Residual Circulation Difference (cm/s)

figure 5-106

South Bay Salt Pond Restoration Project

Far South Bay Residual Circulation, Difference, Year 0, Winter

PWA

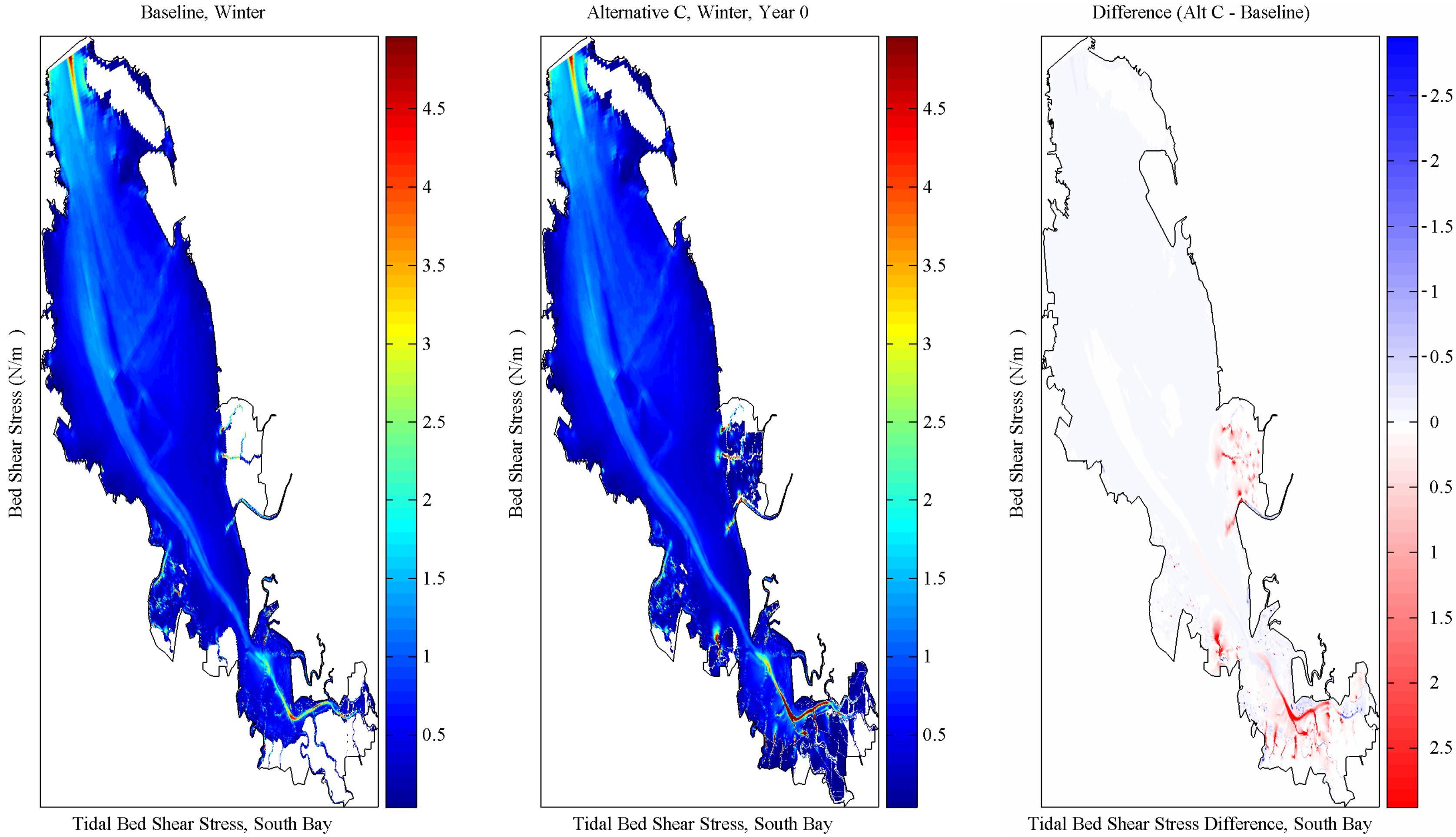

figure 5-107

South Bay Salt Pond Restoration Project

Tidal Bed Shear Stress, South Bay, Alt C, Year 0, Winter

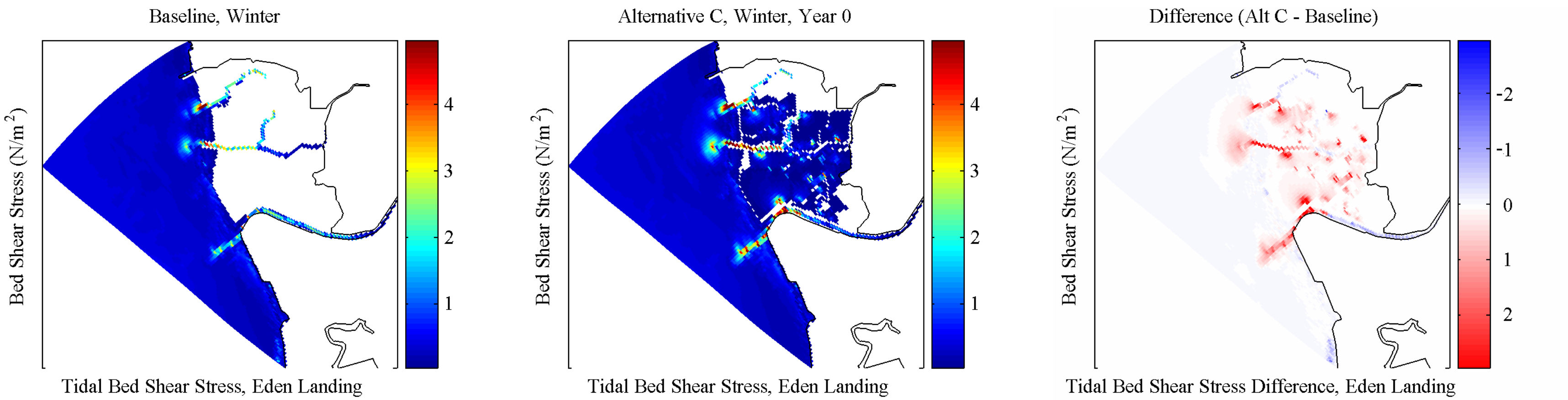

figure 5-108

South Bay Salt Pond Restoration Project

Tidal Bed Shear Stress, Eden Landing, Alt C, Year 0, Winter

PWA

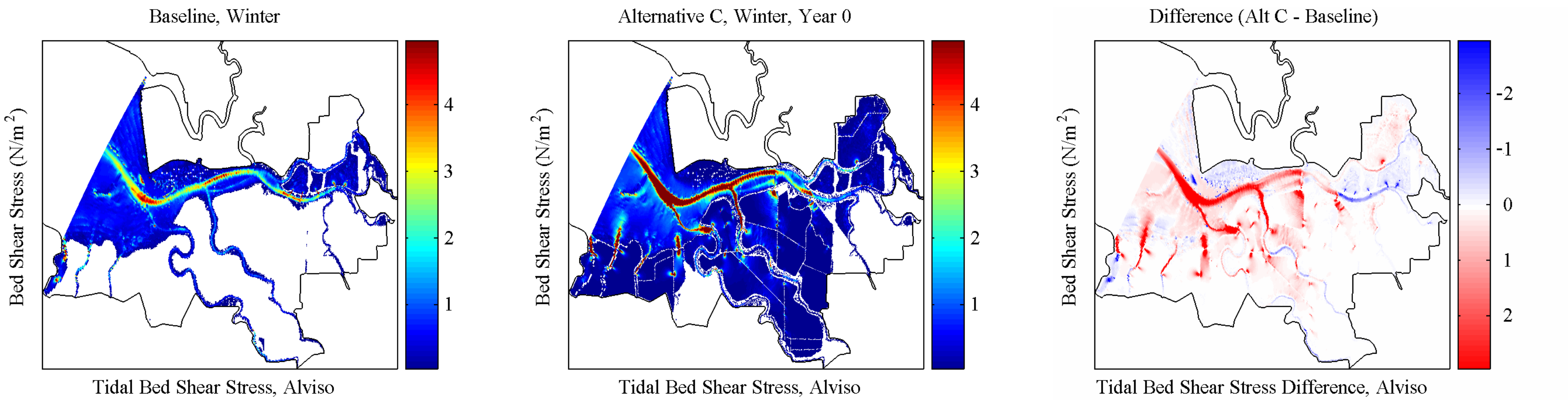

figure 5-109

South Bay Salt Pond Restoration Project

Tidal Bed Shear Stress, Alviso, Alt C, Year 0, Winter

PWA

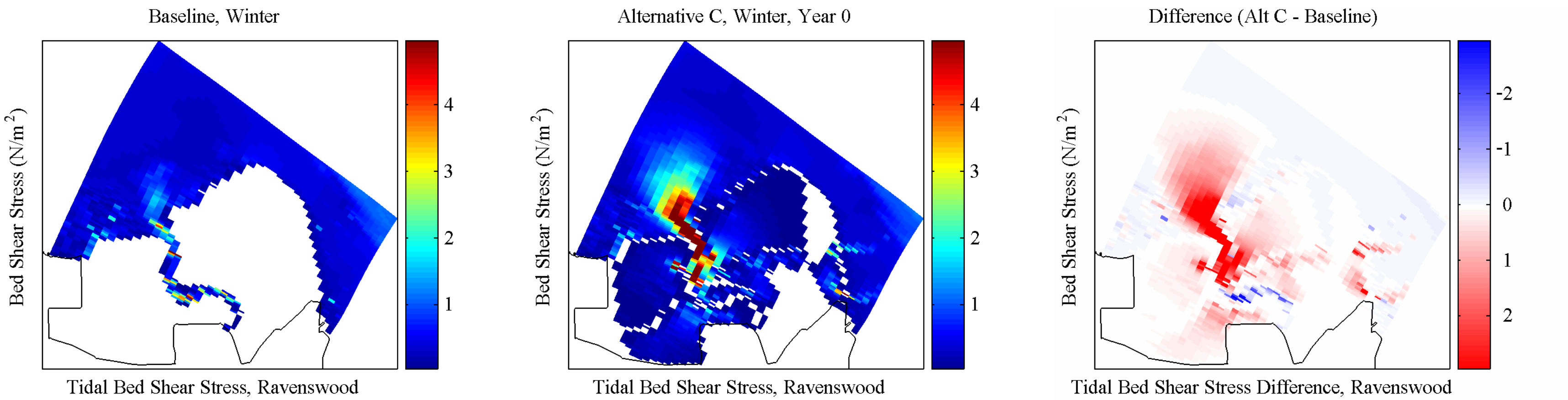

figure 5-110

South Bay Salt Pond Restoration Project

Tidal Bed Shear Stress, Ravenswood, Alt C, Year 0, Winter

PWA

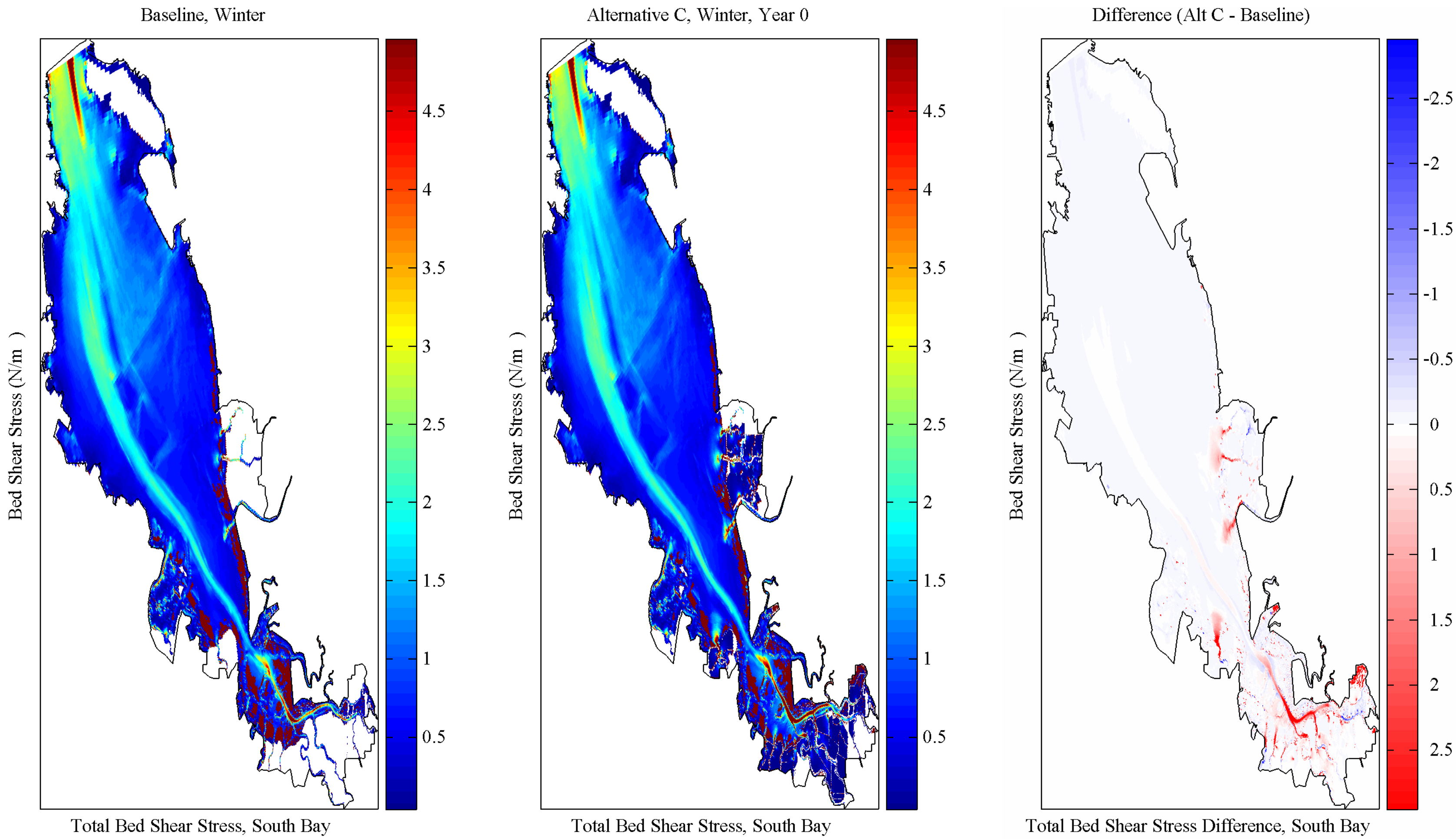

figure 5-111

South Bay Salt Pond Restoration Project

Total Bed Shear Stress, South Bay, Alt C, Year 0, Winter

PWA

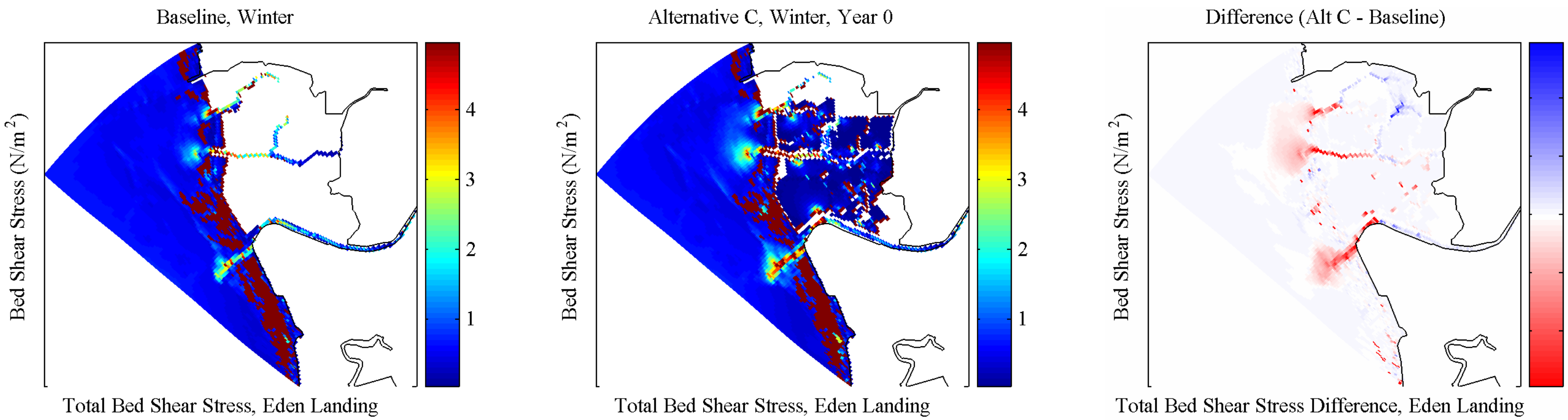

figure 5-112

South Bay Salt Pond Restoration Project

Total Bed Shear Stress, Eden Landing, Alt C, Year 0, Winter

PWA

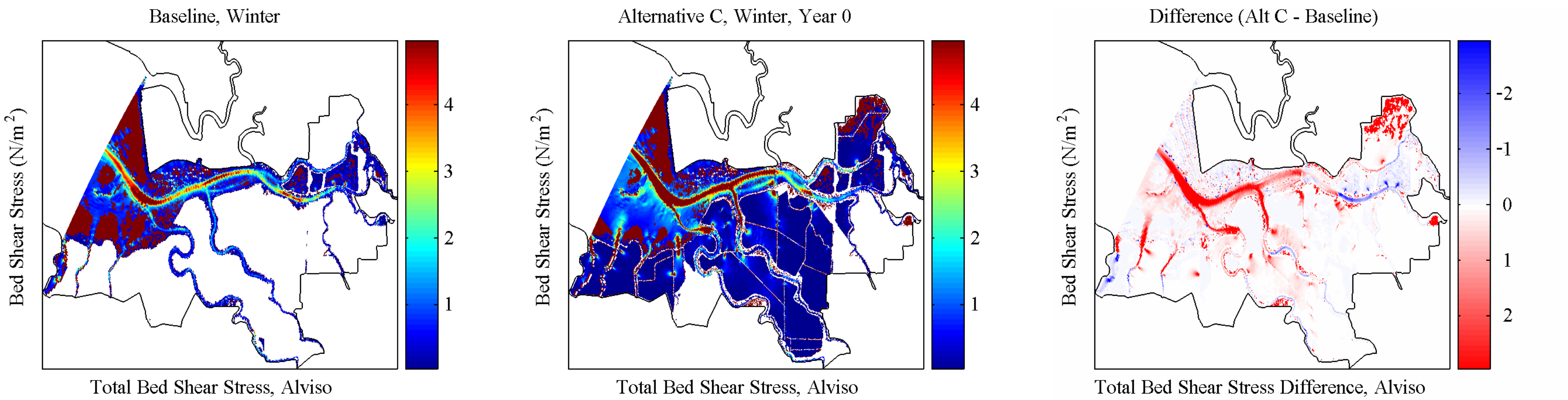

figure 5-113

South Bay Salt Pond Restoration Project

Total Bed Shear Stress, Alviso, Alt C, Year 0, Winter

PWA

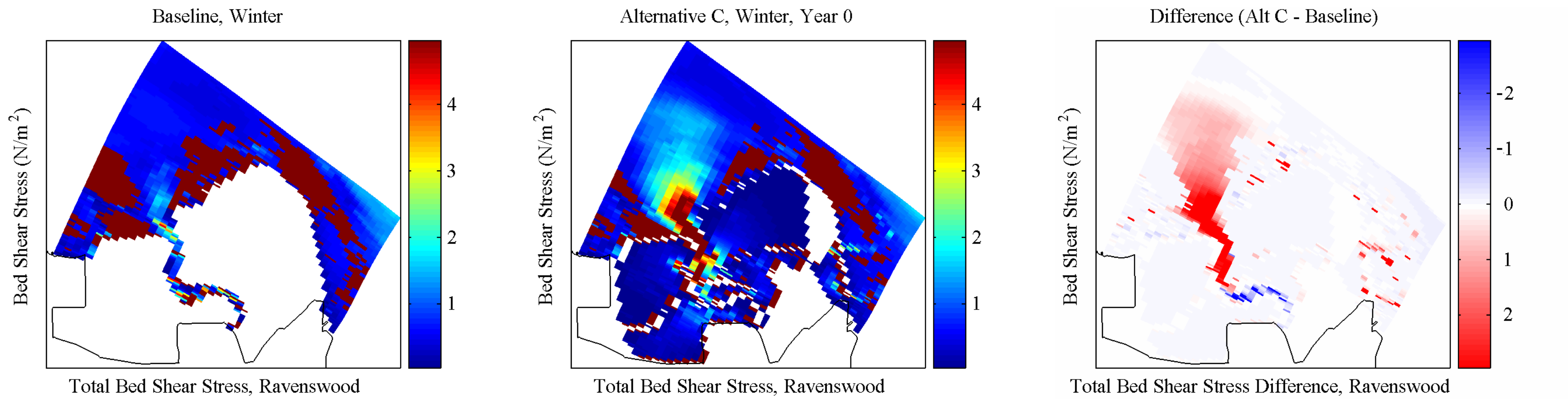

figure *5-114*

South Bay Salt Pond Restoration Project

Total Bed Shear Stress, Ravenswood, Alt C, Year 0, Winter

PWA

6. ALTERNATIVE A, YEAR 50, SUMMER CONDITIONS

This section presents the results of the Alternative A, year 50, simulation under summer conditions, including a comparison with baseline summer conditions. The year 50 simulation includes large-scale bathymetric change in response to unplanned levee failures, tidal conversions occurring throughout the 50-year horizon, and sea-level rise, as described in Section 3.3. The analysis presented utilizes the same approach presented in Section 4 for ease of comparison between simulations. The model predictions are analyzed using time series at stations throughout the South Bay. Figure 4-1 through Figure 4-4 show the station locations for the South Bay and three pond complexes. The model predictions are also analyzed at specific snapshots in time for the entire South Bay and the pond complexes. Figure 4-5 shows where in the analysis period the snapshots were taken with respect to the spring-neap tidal cycle. The sections below present the results with respect to water levels, tidal prism, salinity, circulation, and bed shear stress.

6.1 Water Levels

This section presents the model results with respect to water levels in the South Bay, the tidal sloughs, and the ponds under Alternative A, year 50, summer conditions. The model predictions are compared to baseline summer predictions in order to assess the long-term impacts associated with the No Action Alternative.

6.1.1 South Bay

Table 6-1 shows the water surface elevation and phase difference for the South Bay under Alternative A, long-term, summer conditions. Positive values in Table 6-1 represent an increase in water surface elevation when compared with baseline conditions, and negative values represent a decrease in water surface elevation. Positive phase values correspond to a slower arrival time under Alternative A, long-term conditions, or a phase lag when compared with baseline conditions, whereas negative values represent that modeled water levels under Alternative A are leading baseline conditions.

In the South Bay, the modeled water levels at the San Mateo Bridge increase on all phases of the daily tidal cycle relative to baseline conditions, and the increase is largely representative of the modeled rate of seal-level rise of 15 cm over 50 years (Figure 6-1). At the Dumbarton Bridge (Figure 6-2), the water level increase under Alternative A, year 50 conditions is approximately equal to sea-level rise throughout the analysis period with the exception of LLW during spring tide. Water levels decrease by approximately 25 to 30 cm at LLW during spring tide conditions. The Dumbarton Bridge station is located on the eastern edge of the main South Bay channel, and this station is completely dry at approximately -0.4 m NAVD88 under baseline conditions. At year 50, scour is predicted to occur along the edges of the main South Bay channel to a depth of approximately 6 feet below MLLW (PWA 2006b), therefore the water level at LLW would no longer be constrained by the bed elevation.

At Channel Marker 17 (Figure 6-3), located near the mouth of Coyote Creek, water levels increase on all phases of the tide. The increases at HHW are largely associated with sea-level rise, however, the unplanned tidal conversions under Alternative A temper the water level increase. In other words, the increase in HHW could be larger in the absence of the unplanned tidal conversions. LLW increases by approximately 20 cm under neap tide and 25 cm under spring tide conditions in response to sea-level rise, mudflat accretion in the far South Bay (see Section 3.3.3), and to a lesser extent, the small increase in tidal prism associated with the unplanned tidal conversions in the Alviso pond complex.

The long-term trend in increased water levels leads to an increase in the MLLW and MHHW tidal datums. Figure 6-4 depicts the change in MLLW at year 50. The increase in MLLW is most pronounced in the far South Bay; however, the increase is on-the-order of sea-level rise north of the Dumbarton Bridge. With respect to MHHW (Figure 6-5), the smallest increases occur in the far South Bay, and as a whole, the increase in MHHW is approximately 10 – 15 cm throughout the South Bay.

Harmonic analysis was performed on water levels at several stations along the main South Bay channel, and the computed phase and amplitudes of the M_2 and K_1 tidal constituents for baseline and Alternative A, year 50 conditions are compared in order to assess how the alternative is affecting tidal propagation within the South Bay (Figure 6-6). Figure 6-6a presents the computed phase of the M_2 and K_1 tidal constituents, and little difference is observed in the South Bay between Alternative A, year 50 and baseline conditions. Figure 6-6b presents the computed amplitude of the M_2 and K_1 tidal constituents, and again, little difference is observed.

Table 6-1. South Bay Tidal Water Surface Elevation and Phase Differences under Alt A, Year 50, Summer

(Water surface elevation differences in cm, phase differences in minutes. June 13 = neap tide, June 22 = spring tide.)

Station Name	**June 13 LLW**		**June 13 HHW**		**June 22 LLW**		**June 22 HHW**	
	WSE	**Phase**	**WSE**	**Phase**	**WSE**	**Phase**	**WSE**	**Phase**
San Mateo Bridge, Figure 6-1	15	0	13	0	17	0	15	0
Dumbarton Bridge, Figure 6-2	16	0	12	-10	-27	-40	14	0
Channel Marker 17, Figure 6-3	19	0	12	10	25	10	10	0

6.1.2 Tidal Sloughs

Under Alternative A, approximately 35 percent of the SBSP Restoration Project Area is assumed to convert to tidal action in an unplanned manner in response to levee failures and erosion occurring over the 50-year horizon. The ponds assumed to convert to tidal marsh are shown in Figure 3-18, Figure 3-19 and Figure 3-20 for each pond complex, with the majority of the tidally-converting ponds located in the Eden Landing pond complex. In response to the increase in tidal prism associated with this conversion, the tidal sloughs are expected to scour and deepen as they approach equilibrium conditions, potentially removing the tidal damping effect seen under the Alternative C, year 0 simulations in the absence of channel scour (Section 4). Table 3-5 presents the predicted increase in channel depth for ACFCC, Old Alameda Creek, Alviso Slough and Guadalupe Slough. The remaining sloughs are assumed to retain their existing bathymetry. As discussed in Section 2.3.5, some of the sloughs, particularly those in the Eden Landing and Ravenswood pond complex, are modeled with larger than actual channel widths due to limitations with respect to the grid resolution; therefore, the model results for these sloughs may underestimate the potential long-term changes in water levels.

Table 6-2 presents the water surface elevation and phase difference under Alternative A at both upstream and downstream stations in each tidal slough. Positive water surface elevation values in Table 6-2 represent an increase in water surface elevation when compared with baseline conditions, and negative values represent a decrease in water surface elevation. Positive phase values correspond to a slower arrival time under Alternative A, or a phase lag when compared with baseline conditions, whereas negative values represent that modeled water levels under Alternative A, long-term conditions are leading baseline conditions.

Water levels downstream in ACFCC change in response to the predicted slough scour and sea-level rise (Figure 6-7). The increase in high water levels appears to be on-the-order of sea-level rise. At LLW, water levels decrease nearly 80 cm on spring tides, with smaller decreases occurring on neap tides. This decrease is associated with the 1.2 to 1.4 m of slough scour predicted to occur. The magnitude of the water level changes at LLW could be associated with an over-prediction of potential channel scour. Upstream, no channel scour is predicted because the upstream levees are assumed to be maintained for flood control. The trend in water levels changes is similar to that observed at the downstream station, although the associated amplitude changes are larger and more symmetric across spring and neap tides (Figure 6-8). Water level changes are similar in Old Alameda Creek, although the relative changes are smaller owing to the smaller increase in tidal prism (Figure 6-9).

In Alviso Slough and Guadalupe Slough, water levels increase on all phases of the tidal cycle, and the increases are roughly on the order of sea-level rise (Figure 6-17 and Figure 6-19, respectively). The effect of the increased tidal prism resulting from unplanned upstream tidal conversions is minimal as only Ponds A5, A6 and A7 are assumed to convert to tidal action, and the equilibrium predictions of channel scour appear to properly account for the increased tidal prism.

The remaining sloughs within the SBSP Restoration Project Area, including Ravenswood Slough in the Ravenswood pond complex and the remaining sloughs within the Alviso pond complex experience water level changes that are largely attributable to sea-level rise, with increases at LLW roughly twice those at HHW. One exception is Coyote Creek, which continues to accrete sediment over the 50-year horizon. This decrease in tidal prism is associated with minor decreases in LLW during spring tides.

Phasing changes are relatively small (on the order of 10 to 30 minutes) throughout the SBSP Restoration Project Area. The largest changes are observed in the ACFCC where Alternative A at year 50 leads baseline conditions by more than 60 minutes at LLW. As with the water level changes, this may be attributable to an over-prediction of channel scour relative to the increased upstream tidal prism.

Table 6-2. Tidal Slough Water Surface Elevation and Phase Differences under Alt A, Year 50, Summer
(Water surface elevation differences in cm, phase differences in minutes. June 13 = neap tide, June 22 = spring tide.)

Station Name	June 13 LLW		June 13 HHW		June 22 LLW		June 22 HHW	
	WSE	Phase	WSE	Phase	WSE	Phase	WSE	Phase
Eden Landing pond complex								
ACFCC Downstream, Figure 6-7	-28	-100	16	-10	-77	-80	17	0
ACFCC Upstream, Figure 6-8	-58	-50	35	-90	-60	-160	23	-60
Old Alameda Creek Downstream, Figure 6-9	-12	-70	14	0	-36	-40	13	0
Old Alameda Creek Upstream, Figure 6-10	30	40	18	10	17	30	13	40
Alviso pond complex								
Coyote Creek Power Tower, Figure 6-11	24	-20	13	10	34	-30	14	0
Coyote Creek Railroad Bridge, Figure 6-12	10	-10	25	-20	-8	-20	26	-20
Coyote Creek/Island Ponds , Figure 6-13	8	-20	26	-20	-10	-30	28	-30
Coyote Creek Upstream, Figure 6-14	8	-20	26	-20	-10	-40	28	-40
Mud Slough Downstream, Figure 6-15	13	0	21	0	-1	-10	24	-20
Mud Slough Upstream, Figure 6-16	11	-10	24	-10	-1	-20	28	-30
Alviso Slough Downstream, Figure 6-17	20	0	12	0	19	10	11	10
Alviso Slough Upstream, Figure 6-18	23	10	2	30	30	20	2	50
Guadalupe Slough Downstream, Figure 6-19	22	10	12	0	31	20	13	0
Guadalupe Slough Upstream, Figure 6-20	36	30	1	70	44	40	-7	20
Moffett Channel, Figure 6-21	36	30	1	70	45	40	-6	40
Stevens Creek Downstream, Figure 6-22	28	10	12	10	27	10	13	-10
Stevens Creek Upstream, Figure 6-23	23	-30	12	10	24	-10	14	10
Mountain View Slough Downstream, Figure 6-24	19	10	13	0	20	0	14	-10
Mountain View Slough Upstream, Figure 6-25	17	-10	13	0	18	0	14	-10
Charleston Slough Downstream, Figure 6-26	-3	-30	17	-20	-7	-20	14	10
Charleston Slough Upstream, Figure 6-27	-4	20	17	-20	-5	0	14	0
Ravenswood pond complex								
Ravenswood Slough Downstream, Figure 6-28	-16	60	12	-10	-21	-40	14	-10
Ravenswood Slough Upstream, Figure 6-29	21	10	13	0	22	0	14	-10

6.2 Tidal Prism

A comparison of the estimates of modeled tidal prism between baseline conditions and Alternative A, year 50 with summer boundary conditions is summarized in Table 6-3. As discussed in Section 4.2, tidal prism has been estimated as the volume of water crossing a cross-section during a flood tide for the basis of comparing tidal prism estimates with previous studies. Overall, the unplanned levee breaches and sea-level rise combine to alter the tidal prism across many of the South Bay cross-sections. Although the exact location of the levee breaches is impossible to predict, this comparison between baseline and

Alternative A, long-term conditions provides an indication of the magnitude of tidal prism changes regardless of the specific breach locations.

The cross-sections at the San Mateo and Dumbarton Bridges exhibit small changes in tidal prism. At the San Mateo Bridge, a four percent increase in tidal prism is predicted and is largely in response to sea-level rise and the mudflat erosion predicted north of the Dumbarton Bridge (see Section 3.3.3). At the Dumbarton Bridge, a five percent decrease in tidal prism is predicted under Alternative A, long-term conditions. This decrease in tidal prism is likely largely associated with the continuing trend of mudflat accretion predicted to occur in the far South Bay (PWA 2006b). Figure 6-30 presents the modeled flux of water across both bridge cross-sections under baseline and Alternative A, long-term conditions, and the relative increase and decrease in tidal prism are evident. In the far South Bay, slight decreases in the modeled flux of water across cross-sections near Channel Marker 17 and Calaveras Point are predicted to occur under Alternative A, long-term conditions (Figure 6-31).

Sloughs in the Eden Landing pond complex have the largest predicted changes in tidal prism under Alternative A, long-term conditions. The magnitude of the changes ranges from 80 percent in the ACFCC to 360 percent in Mount Eden Creek. The tidal prism increases are consistent with the assumption that this complex would have the largest extent of unplanned breaches due to levee erosion and failures. Along Mount Eden Creek, the large increase in tidal prism is associated with several factors. First, Ponds E12 and E13 are assumed to convert to tidal marsh in an unplanned manner and breach to Mount Eden Creek. In response to this tidal conversion, the slough is expected to scour, as discussed Section 3.3.2. In addition, mudflat erosion is predicted to occur adjacent to the Eden Landing pond complex. This large-scale geomorphic change enables better tidal propagation into the Eden Landing Complex, thereby increasing tidal prism. A final factor which contributes to the tidal prism increase is an artifact of the model's grid cell sizing in this region. As discussed in Section 2.3.5, the grid resolution limitations cause the sloughs to be represented in the model at a larger than actual width. All of these factors together account for the large increase in tidal prism observed in Mount Eden Creek. Lesser tidal prism increases are predicted for Old Alameda Creek and the ACFCC. Figure 6-32 presents the modeled flux of water near the mouth of Old Alameda Creek and the ACFCC; the relative increases in tidal prism are evident.

Along Coyote Creek, the tidal prism changes are influenced by the bathymetric changes that occur to the adjacent ponds. Nearly the same tidal prism enters the mouth of Coyote Creek at the Power Tower in year 50 as in year 0 (Figure 6-33). However, because of the unplanned tidal conversions, a greater portion of this tidal prism is drawn into Alviso Slough than under baseline conditions. The reduced tidal prism remaining in the main stem of Coyote Creek registers as decreased tidal prism at the Railroad Bridge (Table 6-3). However, further upstream from the Railroad Bridge, east of the Island Ponds and in the creek's tributary, Artesian Slough, tidal prism is predicted to increase. This increase occurs because the Island Ponds are assumed to develop into mature marsh by year 50, thus reducing the tidal prism introduced by the ponds under baseline conditions. Therefore, more water is available for propagation up Coyote Creek east of the ponds and into Artesian Slough.

Within the Alviso pond complex, the only ponds which are assumed to undergo unplanned tidal conversions are Ponds A5, A6 and A7 between Guadalupe and Alviso Slough. As a result of these tidal conversions, the tidal prism in these two sloughs is predicted to increase approximately 30 – 50 percent. Figure 6-34 presents the modeled flux of near the mouth of both sloughs, and the relative increases in tidal prism are evident. The smaller sloughs in the Alviso pond complex, such as Stevens Creek, Charleston Slough and Mountain View Slough exhibit minimal change in tidal prism in the absence of any ponds breached along their length (see Figure 6-35 and Figure 6-36). The decrease in tidal prism associated with these sloughs is likely a function of the reduced tidal range and mudflat accretion predicted in the far South Bay.

Ravenswood Slough in the Ravenswood pond complex exhibits a modest increase of tidal prism on the order of 20 percent (Figure 6-36). This is likely a result of the large-scale mudflat erosion predicted to occur between the San Mateo and Dumbarton Bridges (PWA 2006b), as well as the assumed rate of sea-level rise. A similar dynamic is likely associated with the non-project sloughs north of Dumbarton Bridge (Corkscrew Slough, Redwood Slough and Westpoint Slough).

Table 6-3. Comparison of Tidal Prism between Baseline and Alternative A, year 50, summer

Transect Location	Tidal Prism (millions of cubic meters)		
	Baseline summer	**Alternative A year 50, summer**	**% change baseline to yr 50**
South Bay			
San Mateo Bridge	270	280	3.9%
Dumbarton Bridge	71	68	-5.2%
Eden Landing pond complex			
ACFCC	1.4	2.6	84%
Old Alameda Creek	1.4	3.5	150%
Mount Eden Creek	0.58	2.7	360%
Ravenswood pond complex			
Ravenswood Slough	0.53	0.64	19%
Alviso pond complex			
Calaveras Point	14	14	-1.2%
Coyote Creek at Power Tower	6.8	6.9	1.2%
Coyote Creek at RR Bridge	2.2	1.8	-17%
Coyote Creek east of Island Ponds	0.53	0.73	39%
Charleston Slough	0.55	0.51	-6.2%
Mountain View Slough	0.21	0.21	-3.0%
Stevens Creek	0.11	0.10	-11%
Guadalupe Slough	1.1	1.5	33%
Alviso Slough	1.1	1.7	50%
Artesian Slough	0.48	0.54	12%
Mud Slough	0.79	0.78	-1.4%
Non-project Sloughs			
Corkscrew Slough	3.4	3.9	12%
Redwood Creek	16	18	14%
Westpoint Slough	2.9	3.3	14%
Mowry Slough	0.41	0.43	5.3%
Plummer Slough	0.32	0.31	-3.2%
Newark Slough	0.86	0.92	6.6%

6.3 Salinity

This section presents the model results with respect to salinity in the South Bay and the tidal sloughs under Alternative A, year 50, summer conditions. The model predictions are compared to baseline summer predictions in order to assess the long-term impact of unplanned tidal conversion occurring under the No Action Alternative on the South Bay and the tidal sloughs, as presented below.

6.3.1 South Bay

Under Alternative A, long-term conditions, little change is observed with respect to salinity within the South Bay (Table 6-4). Positive values in Table 6-4 represent an increase in salinities relative to the baseline, and negative values represent a decrease in salinities relative to baseline conditions. At the San Mateo and Dumbarton Bridges, there is no significant difference in salinity when compared with baseline conditions (Figure 6-37 and Figure 6-38, respectively). Slightly higher salinity differences are observed at Channel Marker 17 (Figure 6-39), with salinity increases on the order of 0 – 2 ppt the observed at LLW.

Figure 6-40 displays the salinities in the South Bay during spring conditions at HHW, representing peak salinity conditions during the analysis period. As can be seen, little difference in peak South Bay salinities occurs under summer conditions with respect to long-term Alternative A conditions. The largest changes in salinity are confined to the tidal sloughs. Figure 6-41 displays South Bay salinities at LLW during spring tide conditions. At low water, the observed differences are greatest downstream of the tidal sloughs and in the subtidal channels in the South Bay.

Table 6-4. South Bay Salinity Differences under Alt A, Year 50, Summer

(Salinity differences in ppt. June 13 = neap tide, June 22 = spring tide.)

Station Name	**June 13 LLW**	**June 13 HHW**	**June 22 LLW**	**June 22 HHW**
San Mateo Bridge, Figure 6-37	0.1	0.0	0.1	0.0
Dumbarton Bridge, Figure 6-38	0.4	0.1	0.2	0.0
Channel Marker 17, Figure 6-39	0.8	0.3	1.7	0.4

6.3.2 Tidal Sloughs

Table 6-5 shows the salinity difference between Alternative A long-term conditions and baseline conditions in the tidal sloughs during neap and spring tide summer conditions. Positive values represent an increase in salinities relative to the baseline, and negative values represent a decrease in salinities relative to baseline conditions.

In the Eden Landing pond complex, salinities increase in the downstream reach of the ACFCC in response to the increased tidal exchange and mixing associated with the deeper channel (Figure 6-42). At high water levels, only a moderate salinity increase of 0 – 2 ppt is observed; however low water salinities increase up to 8 ppt. This increase in downstream salinities shifts the salinity gradient upstream, and salinities at the upstream station in ACFCC are 5 – 10 ppt higher throughout the analysis period (Figure 6-43). Salinities in Old Alameda Creek exhibit little change with respect to baseline salinities (Figure 6-44 and Figure 6-45). Due to the oversized representation of the Old Alameda Creek in the model (see Section 2.3.5), salinity changes in Old Alameda Creek may be underestimated.

Figure 6-46 and Figure 6-47 present the peak salinities in the Eden Landing pond complex during spring HHW and LLW conditions, respectively. As can be seen, the largest salinity changes are observed in the ACFCC and the South Bay directly downstream of the slough mouths.

The most significant change in the Alviso pond complex can be seen in Coyote Creek and Mud Slough. At the Power Tower (Figure 6-48), little change is seen between Alternative A, long-term and baseline conditions. However, at the Railroad Bridge (Figure 6-49), salinities decrease approximately 3 – 5 ppt throughout the analysis period, and the decrease in salinity is slightly higher at the upstream stations at

the eastern end of Pond A19 (Figure 6-50) and near Warm Springs (Figure 6-51). A similar decrease in salinity is observed in Mud Slough (
Figure 6-52 and Figure 6-53). Coyote Creek is assumed to continue accreting sediment over the 50-year horizon (PWA 2006b). This leads to a reduction in the tidal exchange between the upstream reaches of Coyote Creek and the South Bay and reduced velocities along Coyote Creek. This trend leads to an increased residence time in the upper reaches of Coyote Creek, increasing the effect of the City of San Jose's WWTP freshwater discharge on upstream salinities.

In Alviso Slough, Guadalupe Slough and Moffett Channel, salinities increase 1 – 6 ppt in response to the unplanned tidal conversion of Ponds A5, A6 and A7. The remaining slough channels within the SBSP Restoration Project Area exhibit relatively little change with respect to salinities. In general, salinities increase less than 1 ppt throughout the analysis period. This may at least partially be due to the oversized representation of the sloughs in the model, particularly with respect to Stevens Creek, Mountain View and Charleston Sloughs.

Figure 6-65 and Figure 6-66 present the peak salinities in the Alviso pond complex during spring HHW and LLW conditions, respectively. The decreased salinities in Coyote Creek and increased salinities in Alviso Slough, Guadalupe Slough and the Moffett Channel are evident. In the Ravenswood pond complex, all pond levees are assumed to be maintained due to the presence of the PG&E substation, therefore no ponds are converted to tidal action due to levee failure and little salinity differences are observed between long-term, Alternative A and baseline conditions (Figure 6-69 and Figure 6-70).

Table 6-5. Tidal Slough Salinity Differences under Alt A, Year 50, Summer
(Salinity differences in ppt. June 13 = neap tide, June 22 = spring tide.)

Station Name	**June 13 LLW**	**June 13 HHW**	**June 22 LLW**	**June 22 HHW**
Eden Landing pond complex				
ACFCC Downstream, Figure 6-42	6.7	0.9	4.9	0.1
ACFCC Upstream, Figure 6-43	7.6	7.3	10.0	5.0
Old Alameda Creek Downstream, Figure 6-44	0.1	0.0	0.0	0.0
Old Alameda Creek Upstream, Figure 6-45	-0.2	-0.2	-0.2	-0.3
Alviso pond complex				
Coyote Creek Power Tower, Figure 6-48	-0.1	0.5	-1.3	0.5
Coyote Creek Railroad Bridge, Figure 6-49	-3.2	-4.9	-5.3	-3.2
Coyote Creek/Island Ponds , Figure 6-50	-4.4	-4.3	-5.1	-4.9
Coyote Creek Upstream, Figure 6-51	-3.9	-4.1	-4.2	-4.4
Mud Slough Downstream, Figure 6-52	-3.6	-1.4	-4.2	-2.5
Mud Slough Upstream, Figure 6-53	-4.0	-3.9	-4.2	-5.0
Alviso Slough Downstream, Figure 6-54	2.3	0.8	3.4	0.7
Alviso Slough Upstream, Figure 6-55	1.5	1.7	1.8	1.9
Guadalupe Slough Downstream, Figure 6-56	2.0	1.0	3.2	0.9
Guadalupe Slough Upstream, Figure 6-57	4.1	5.6	4.9	6.7
Moffett Channel, Figure 6-58	3.6	4.4	4.4	5.5
Stevens Creek Downstream, Figure 6-59	0.6	0.2	0.9	0.5
Stevens Creek Upstream, Figure 6-60	0.7	0.6	0.9	0.8
Mountain View Slough Downstream, Figure 6-61	0.3	0.3	0.4	0.4
Mountain View Slough Upstream, Figure 6-62	0.4	0.3	0.5	0.4
Charleston Slough Downstream, Figure 6-63	0.4	0.4	0.2	0.1
Charleston Slough Upstream, Figure 6-64	0.0	0.5	-0.4	0.2
Ravenswood pond complex				
Ravenswood Slough Downstream, Figure 6-67	0.1	0.1	0.2	0.1
Ravenswood Slough Upstream, Figure 6-68	0.3	0.3	0.4	0.3

6.4 Circulation

Potential changes to South Bay circulation can be evaluated by examining current velocities at specific locations within the Bay and tidal sloughs, and by examining general changes to South Bay residual circulation. The most important factor influencing circulation patterns in South Bay is bathymetry (Cheng and Gartner 1985). At year 50, significant large-scale bathymetric change is assumed to have occurred under the No Action Alternative. Mudflat accretion is assumed in the far South Bay, mudflat erosion occurs between the San Mateo and Dumbarton Bridges, the unplanned, tidally-converted ponds have developed into mature salt marsh with a corresponding marsh channel network, and the tidal sloughs have scoured in response to the associated increased tidal prism.

6.4.1 Current Velocity

South Bay

In the South Bay, modeled velocities at the San Mateo and Dumbarton Bridges exhibit little change relative to baseline conditions. Table 6-6 shows the peak velocity magnitudes at the bridge and Channel Marker 17 stations under baseline and Alternative A, long-term conditions. Positive values indicate a higher modeled velocity under Alternative A, and negative values indicate a decrease in current velocity under Alternative A.

At the San Mateo and Dumbarton Bridges, velocity magnitudes exhibit little change with respect to baseline conditions (Figure 6-71 and Figure 6-72, respectively). At Channel Marker 17 (Figure 6-73), velocities are increased under Alternative A, long-term conditions. This increase in velocities is due to the sediment accretion on the far South Bay mudflats. The mudflat elevations increased at a rate greater than sea-level rise, which leads to more mudflat area being exposed at LLW and more flow being directed through the subtidal channels on ebb tides.

Figure 6-74 and Figure 6-75 present velocity magnitudes within the South Bay under peak flood and peak ebb conditions under baseline and Alternative A, long-term conditions, as well as the difference between the two model predictions. The differences are minor under spring flood conditions, and the greatest change occurs in the subtidal channels under ebb tide conditions.

Tidal Sloughs

Table 6-7 shows the peak velocity magnitudes at the downstream stations in the tidal sloughs under baseline and Alternative A conditions. Positive values indicate a higher modeled velocity under Alternative A, and negative values indicate a decrease in current velocity under Alternative A. Little change in tidal slough velocities is observed when comparing Alternative A, long-term and baseline conditions. The largest changes are seen downstream in Old Alameda Creek in the Eden Landing pond complex, in Coyote Creek near the Railroad Bridge, and downstream in Alviso Slough in the Alviso pond complex.

The velocity increases in Old Alameda Creek are a result of unplanned tidal conversion of Ponds E8A, E8, E6B and E6A to the north, and Ponds E5, E6, and E7 to the south (Figure 6-77). Figure 6-78 and Figure 6-79 present peak velocity magnitude within the South Bay under flood and ebb conditions under baseline and Alternative A, long-term conditions. On flood, the primary changes are observed within the tidal channels, and on ebb tide, the largest differences are observed downstream of the channel mouths.

Velocities decrease near the Railroad Bridge in Coyote Creek (Figure 6-81) due to the assumption of continuing sediment accretion within Coyote Creek, as discussed in Section 6.3.2. This velocity magnitude decrease is observed at both peak flood (Figure 6-90) and peak ebb conditions (Figure 6-91). Also evident are the increased velocities in the main South Bay subtidal channel and Alviso and Guadalupe Sloughs under both flood and ebb conditions.

No velocity increases are expected or observed within the Ravenswood pond complex as all ponds levees are assumed to be maintained, therefore no unplanned tidal conversions are assumed to occur within the 50-year horizon (Figure 6-93and Figure 6-94).

Table 6-6. South Bay Peak Velocity Magnitude Comparisons: Alt A, Year 50, Summer vs. Baseline, Summer

(All velocities in cm/s)

Station Name	**Baseline**	**Alt A**	**Difference**
San Mateo Bridge, Figure 6-71	102	100	-2
Dumbarton Bridge, Figure 6-72	34	36	2
Channel Marker 17,Figure 6-73	67	81	14

Table 6-7. Tidal Slough Peak Velocity Magnitude Comparisons: Alt A, Year 50, Summer vs. Baseline, Summer

(All velocities in cm/s)

Station Name	**Baseline**	**Alt A**	**Difference**
ACFCC Downstream, Figure 6-76	45	38	-7
Old Alameda Creek Downstream, Figure 6-77	53	80	27
Coyote Creek Power Tower, Figure 6-80	76	78	3
Coyote Creek Railroad Bridge, Figure 6-81	82	68	-14
Coyote Creek/Island Ponds, Figure 6-82	39	46	7
Mud Slough Downstream, Figure 6-83	46	46	0
Alviso Slough Downstream, Figure 6-84	49	72	23
Guadalupe Slough Downstream, Figure 6-85	46	49	3
Moffett Channel , Figure 6-86	5	3	-2
Stevens Creek Downstream, Figure 6-87	51	46	-6
Mountain View Slough Downstream, Figure 6-88	4	49	0
Charleston Slough Downstream, Figure 6-89	77	64	-13
Ravenswood Slough Downstream, Figure 6-92	38	40	2

6.4.2 Residual Circulation

The total residual current observed in the South Bay is a product of tidally-driven residual currents, as well as wind-driven and density-driven circulation patterns. The long-term conditions under Alternative A, including large-scale bathymetric change and sea-level rise, have the potential to alter residual circulation patterns within the South Bay.

Figure 6-95 displays the 29-day residual circulation under summer baseline conditions. Figure 6-96 displays the 29-day residual circulation for long-term, Alternative A conditions, and Figure 6-97 displays the difference between the predicted residual circulation under baseline and Alternative A conditions

(Alternative A, year 50 minus baseline). Little change is observed in the South Bay north of the Dumbarton Bridge.

More noticeable changes are observed in the far South Bay, south of the Dumbarton Bridge. Figure 6-98 displays the 29-day residual circulation under summer baseline conditions for the far South Bay, Figure 6-99 displays the same for long-term, Alternative A conditions, and Figure 6-100 displays the difference. The largest difference in residual circulation pattern is observed in the main South Bay subtidal channel and Coyote Creek. A net-northward residual current is still present under Alternative A, long-term conditions; however, its magnitude has lessened, resulting in an increased residence time in the upper reaches of Coyote Creek, as discussed under Section 6.3.2.

6.5 Bed Shear Stress

Potential impacts to sediment erosion and deposition patterns are inferred based on comparisons of total bed shear stress both before and after tidal restoration, where total bed shear stress is a function of both tidal currents and locally-generated wind-waves. Section 4.5 provides a description of the methodology used to generate and compare the total combined wind-wave- and tidally-induced bed shear stress.

6.5.1 South Bay

The increase in water levels and tidal datums associated with sea-level rise result in minor decreases in tidally-induced bed shear stresses in much of the South Bay (Figure 6-101). The difference map shown on Figure 6-101 depicts red regions where the erosive potential increases (bed shear stresses are higher under Alternative A relative to baseline conditions), and the areas depicted in blue correspond to regions with a potential for increased deposition. As the critical shear stresses for erosion are not well known within the South Bay, and they vary spatially depending on the sediment characteristics and level of compaction of the substrate, the red and blue areas are for illustrative purposes only and do not predict erosion or deposition under Alternative A.

Slight decreases in tidally-induced bed shear stress are observed in the main South Bay channel and the shallow mudflat areas in the far South Bay and on the western and eastern shores, with little change observed in the shallow subtidal areas. Slight increases in tidally-induced bed shear stresses are observed downstream of Alviso Slough and Guadalupe Slough in the far South Bay, and Old Alameda Creek and Mt. Eden in the Eden Landing pond complex.

More significant changes are observed when the combined wind-wave- and tidally-induced bed shear stresses are considered (Figure 6-105). Both MLLW and MHHW are higher under Alternative A, long-term conditions. Because wind-wave-driven bed shear stress is a function of water depth, and the erosive potential decreases with increasing water depth, the overall increase in water levels leads to a reduction in the total bed shear stresses in the shallow areas of the South Bay. This dynamic is primarily seen along the eastern and western shoals north of the Dumbarton Bridge. Within the far South Bay, mudflat accretion was assumed to outpace sea-level rise, therefore mean water depths are actually lower under

Alternative A in the long term when compared with baseline conditions. This leads to an increase in total bed shear stress in the far South Bay and an increase in the erosive potential.

6.5.2 Tidal Sloughs

Within and adjacent to the Eden Landing pond complex (Figure 6-102), the maximum tidally-induced bed shear stress is increased downstream of the unplanned tidal breaches, corresponding to the increased tidal prism, and decreased upstream of the tidal breaches because a portion of the flow upstream in the tidal slough under baseline conditions is captured within the tidally-restored ponds under restored conditions. Within and adjacent to the Alviso pond complex (Figure 6-103), the dynamic is similar to that observed in the Eden Landing pond complex. Tidally-induced bed shear stresses increase downstream of tidal breaches and decrease upstream of tidal breaches. No change is observed within the Ravenswood pond complex because no levee failures are assumed to occur (Figure 6-104).

The primary effect of the combined wind-wave- and tidally-induced shear stress is evident in the South Bay rather than in the tidal sloughs as wind-induced waves require sufficient fetch to develop.

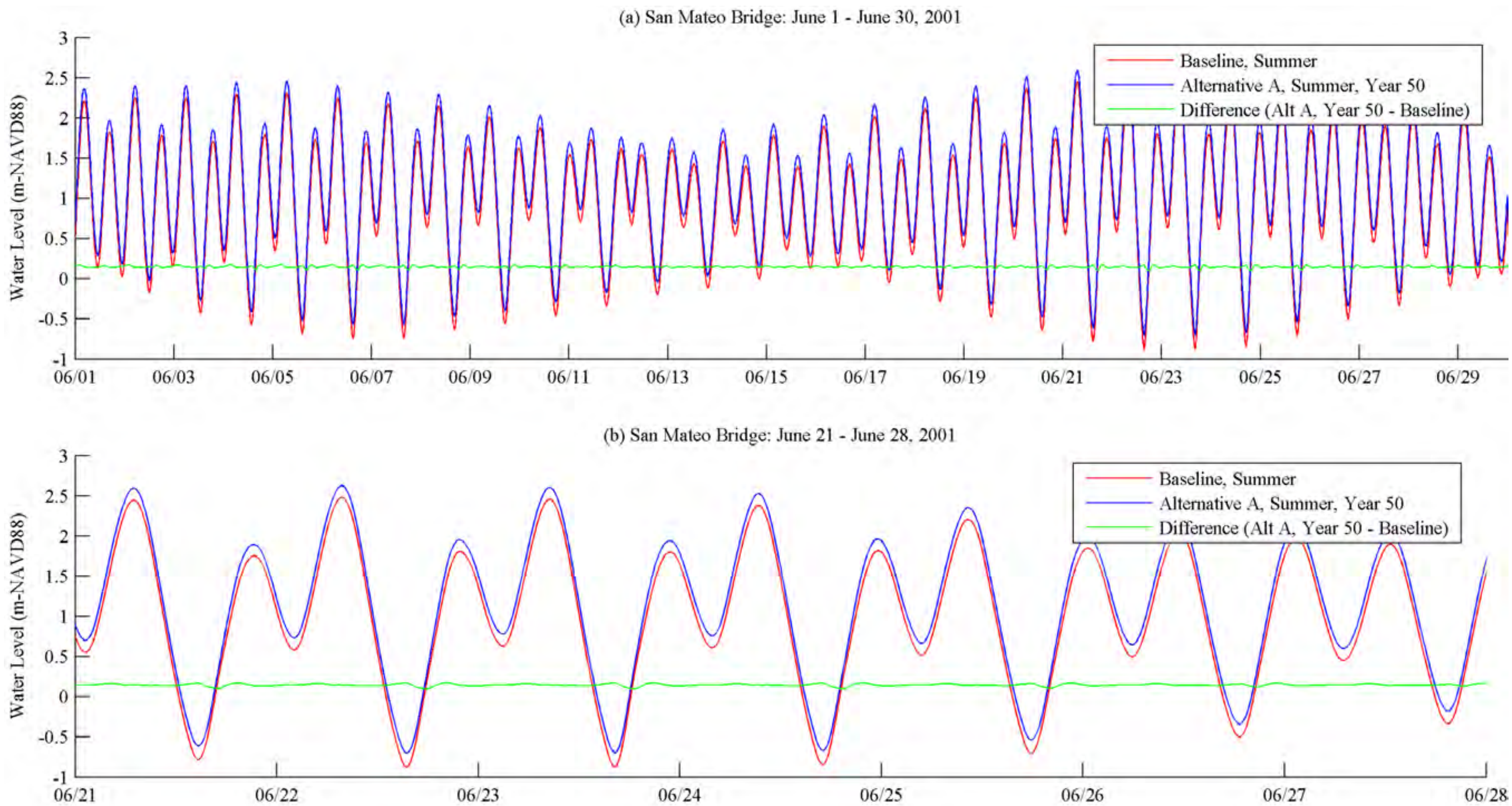

figure 6-1

South Bay Salt Pond Restoration Project

Water Levels, San Mateo Bridge, Alt A, Year 50, Summer

PWA

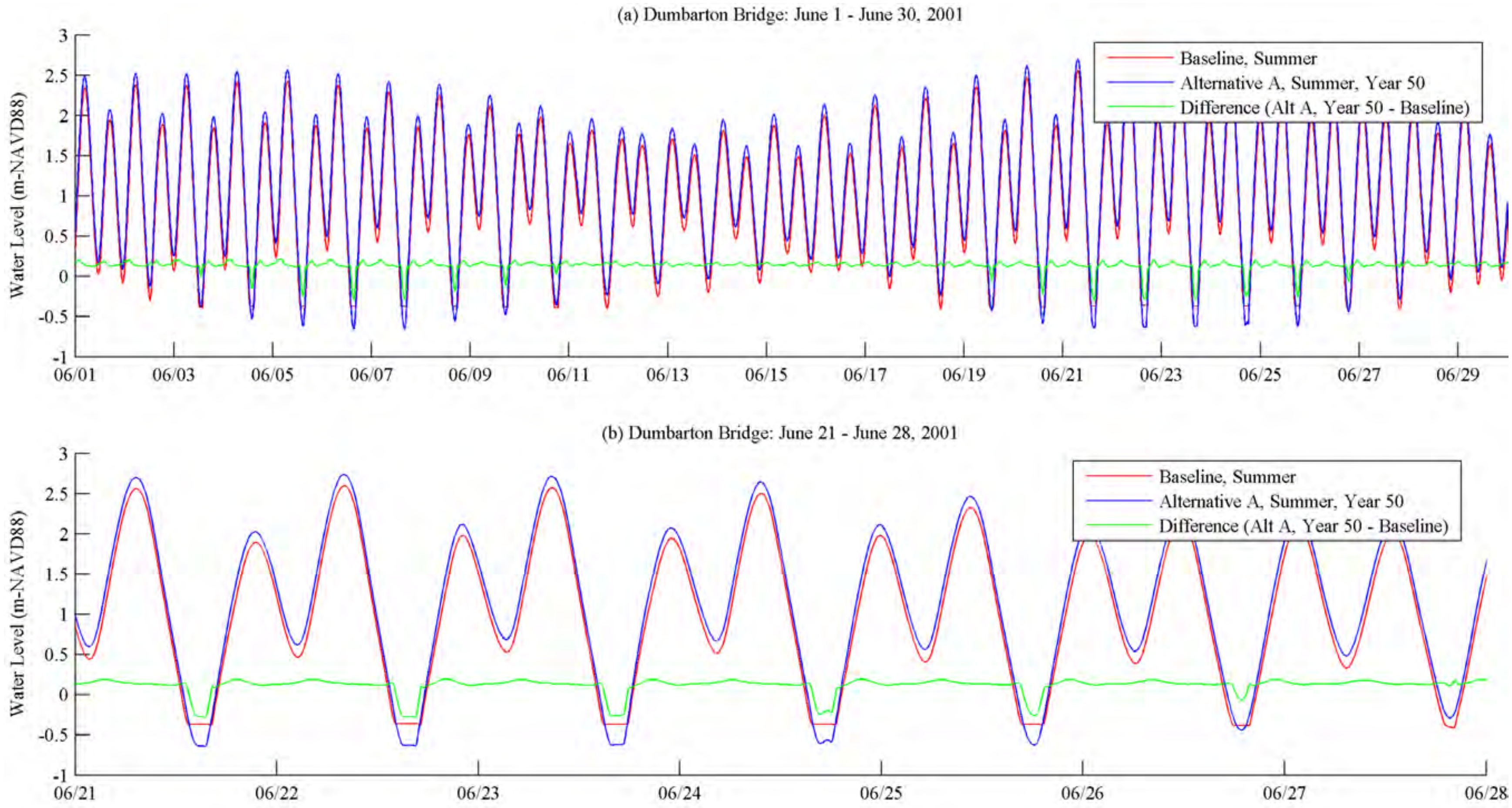

figure 6-2

South Bay Salt Pond Restoration Project

Water Levels, Dumbarton Bridge, Alt A, Year 50, Summer

PWA

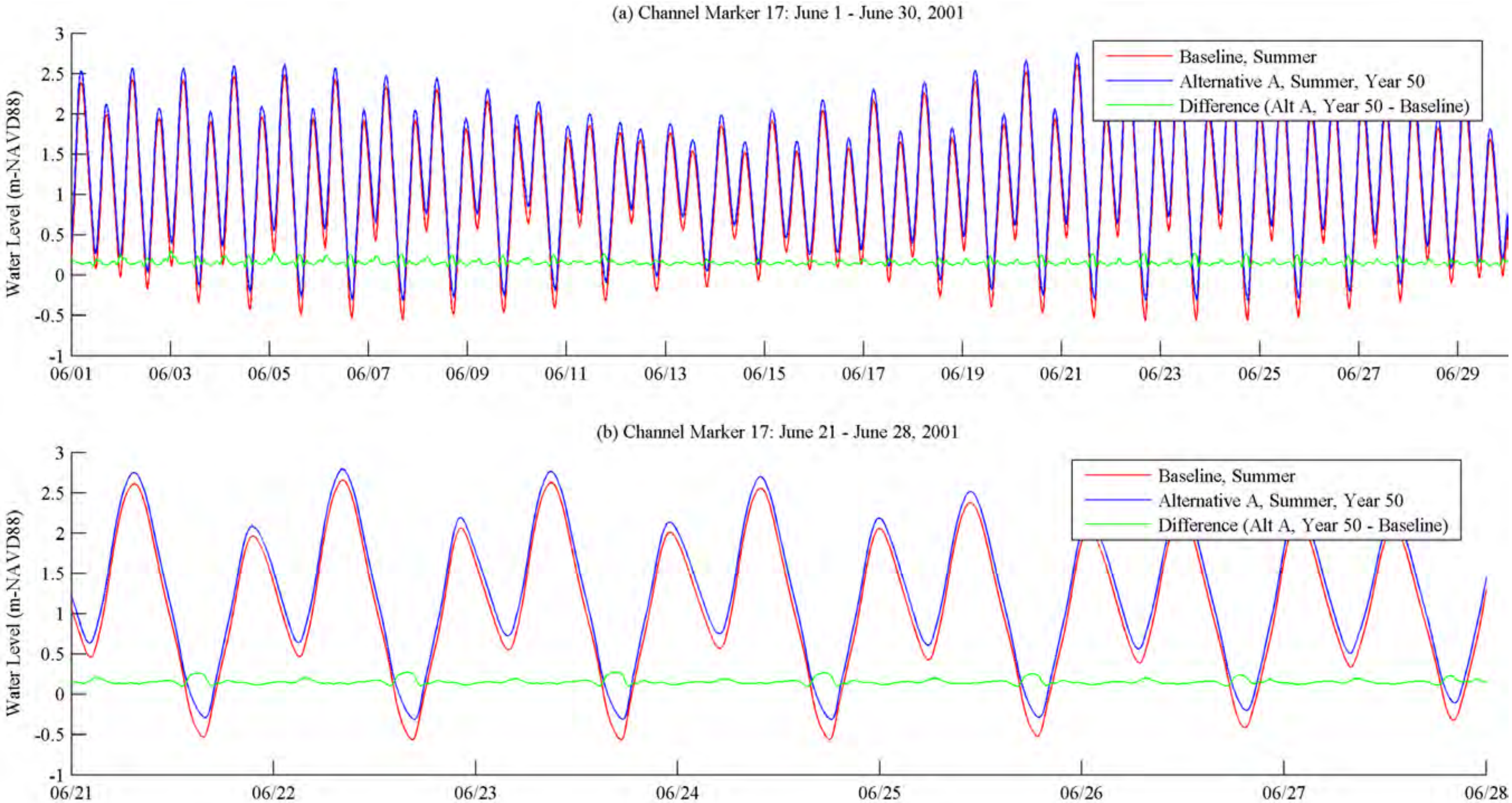

figure 6-3

South Bay Salt Pond Restoration Project

Water Levels, Channel Marker 17, Alt A, Year 50, Summer

PWA

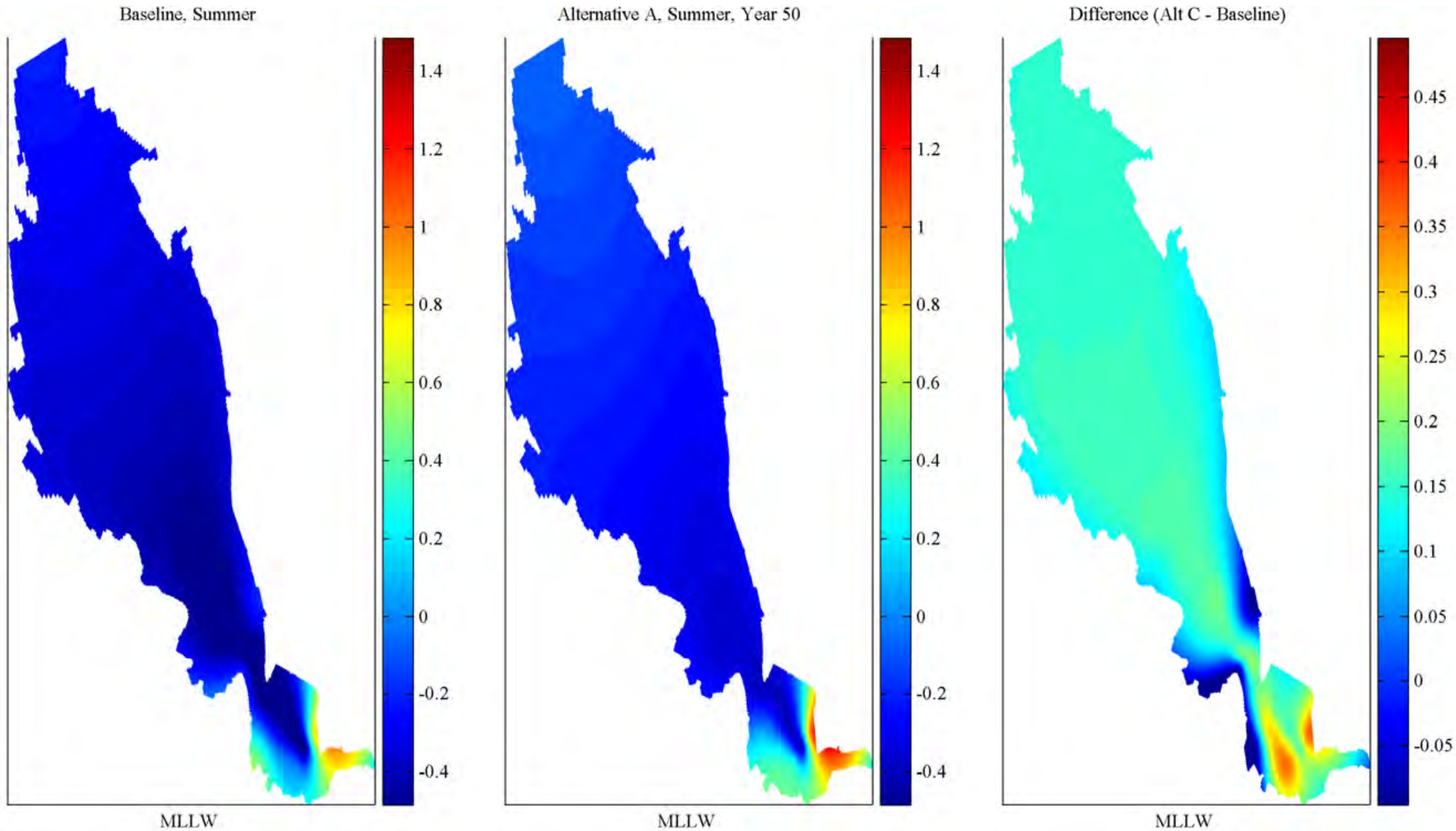

Note: Units shown are m-NAVD88, difference units are m

figure *6-4*

South Bay Salt Pond Restoration Project

Changes in MLLW, Alt A, Year 50, Summer

PWA

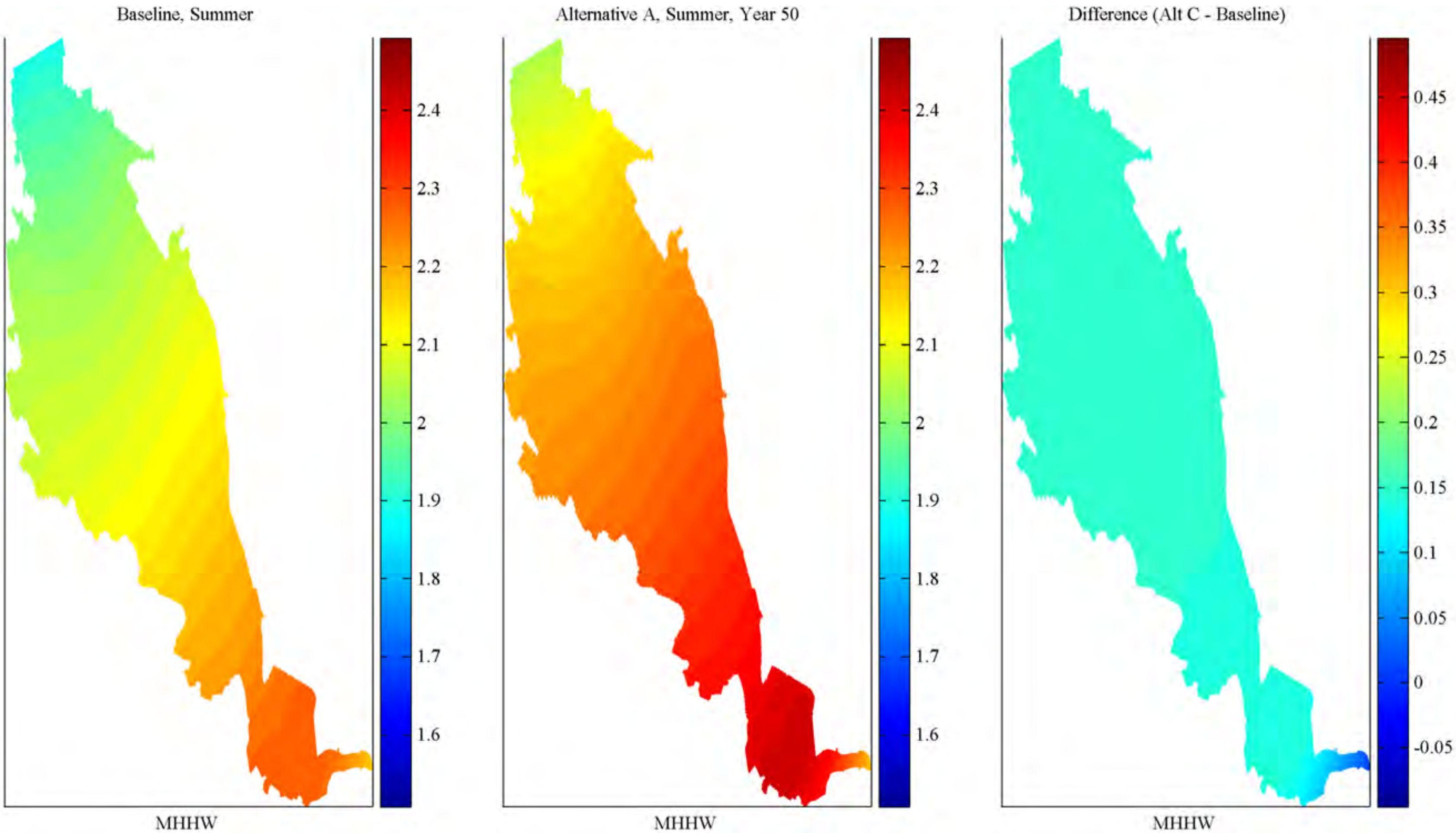

Note: Units shown are m-NAVD88, difference units are m

figure 6-5

South Bay Salt Pond Restoration Project

Changes in MHHW, Alt A, Year 50, Summer

PWA

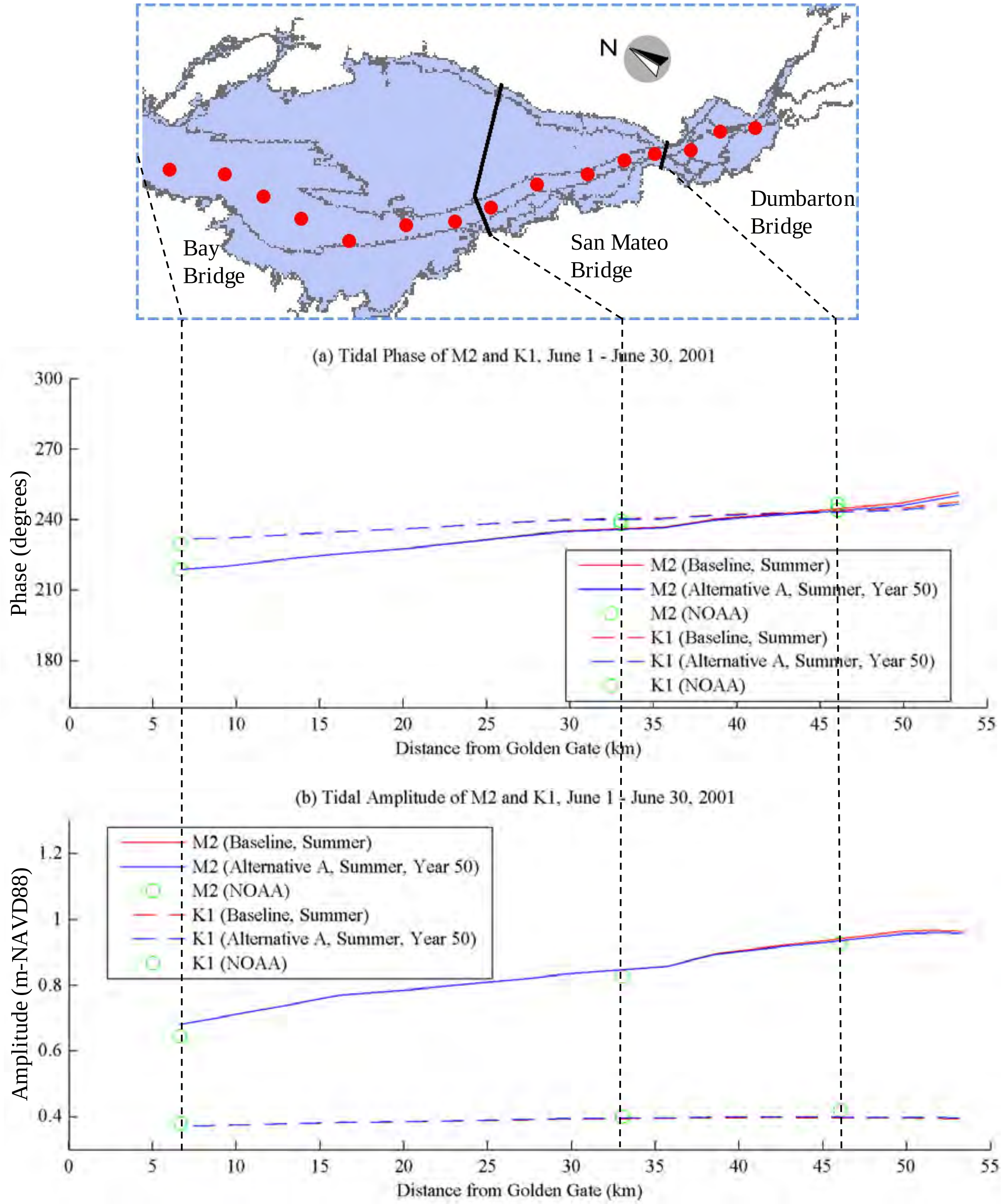

This figure shows the phase and amplitude of the M2 and K1 tidal components, calculated from harmonic analysis of the model. The green data points represent phase and amplitude values calculated by NOAA at the Bay Bridge (Pier 22), San Mateo Bridge, and Dumbarton Bridge.

figure 6-6

South Bay Salt Pond Restoration Project

Changes in Tidal Propagation, Alt C, Year 50, Summer

PWA

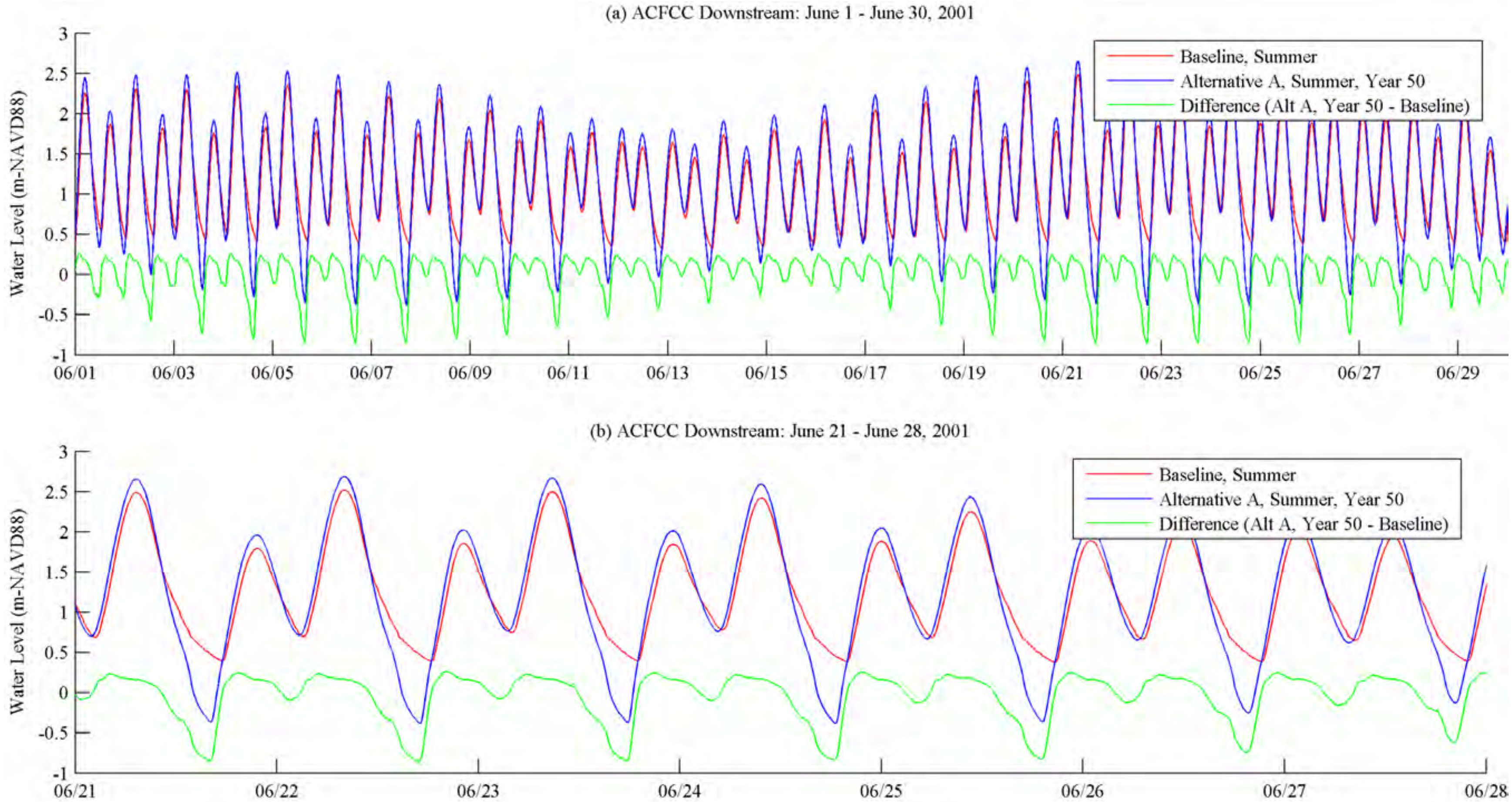

figure 6-7

South Bay Salt Pond Restoration Project

Water Levels, ACFCC Downstream, Alt A, Year 50, Summer

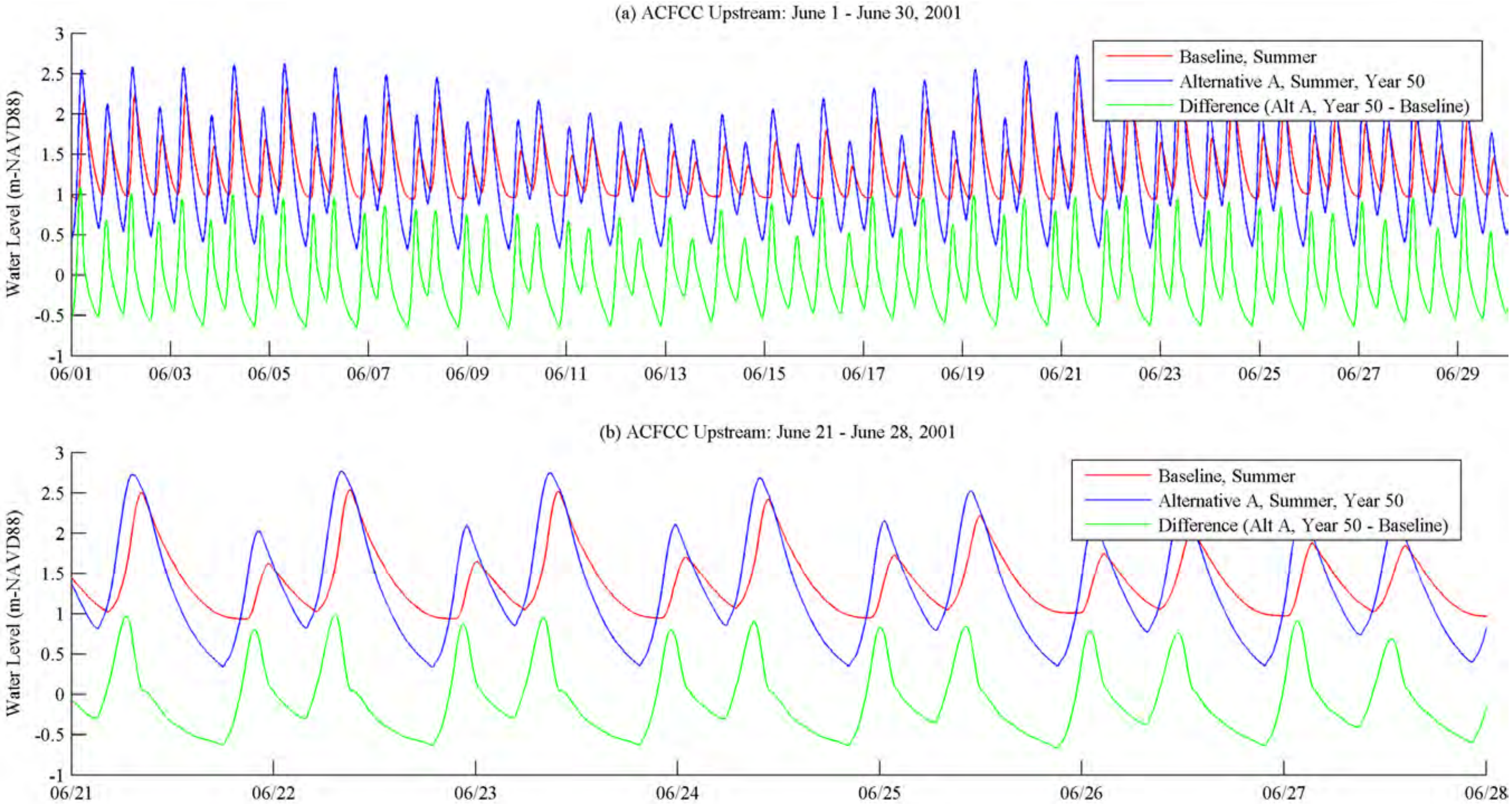

figure 6-8

South Bay Salt Pond Restoration Project

Water Levels, ACFCC Upstream, Alt A, Year 50, Summer

PWA

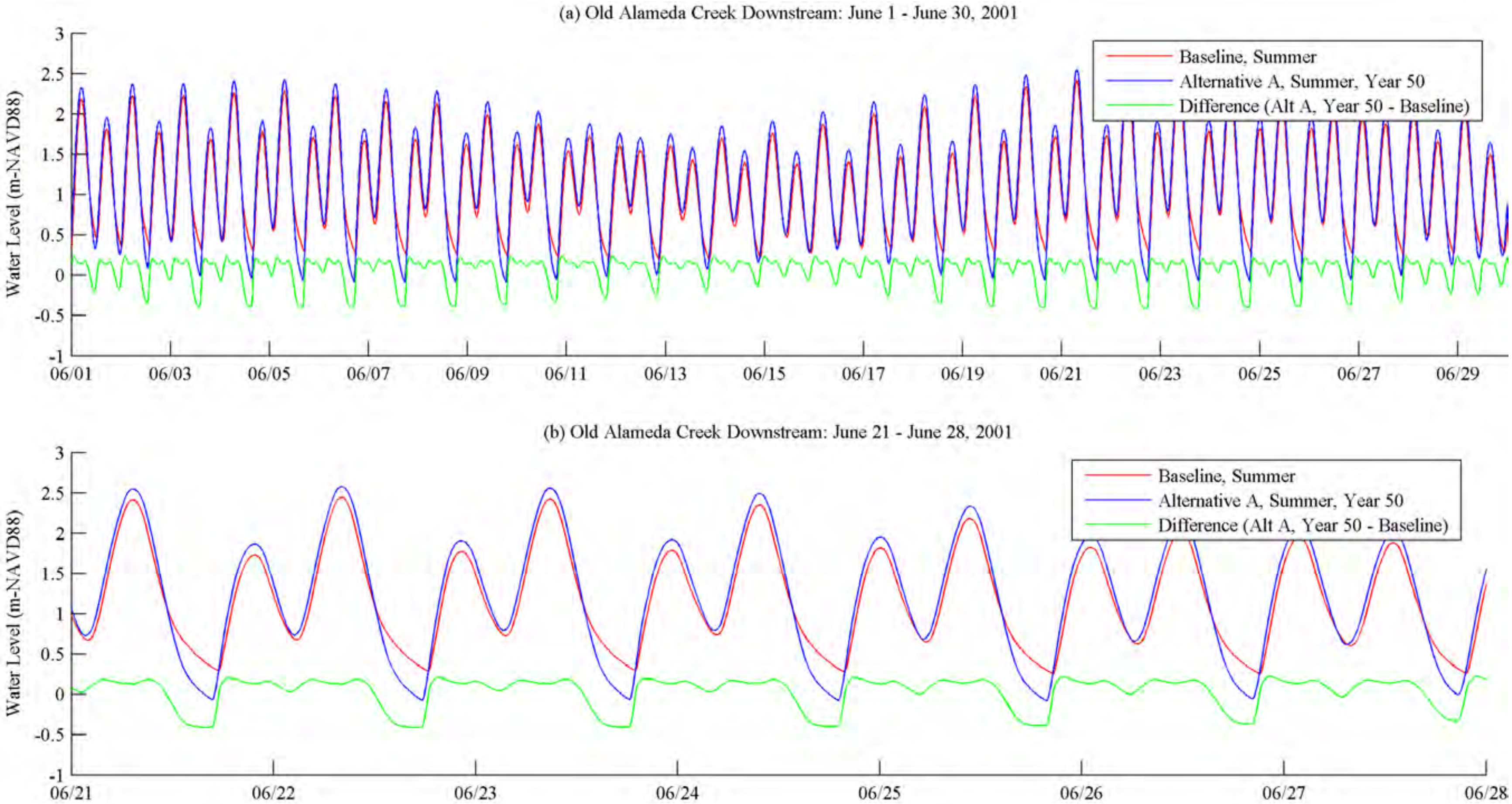

figure 6-9

South Bay Salt Pond Restoration Project

Water Levels, Old Alameda Creek Downstream, Alt A, Year 50, Summer

PWA

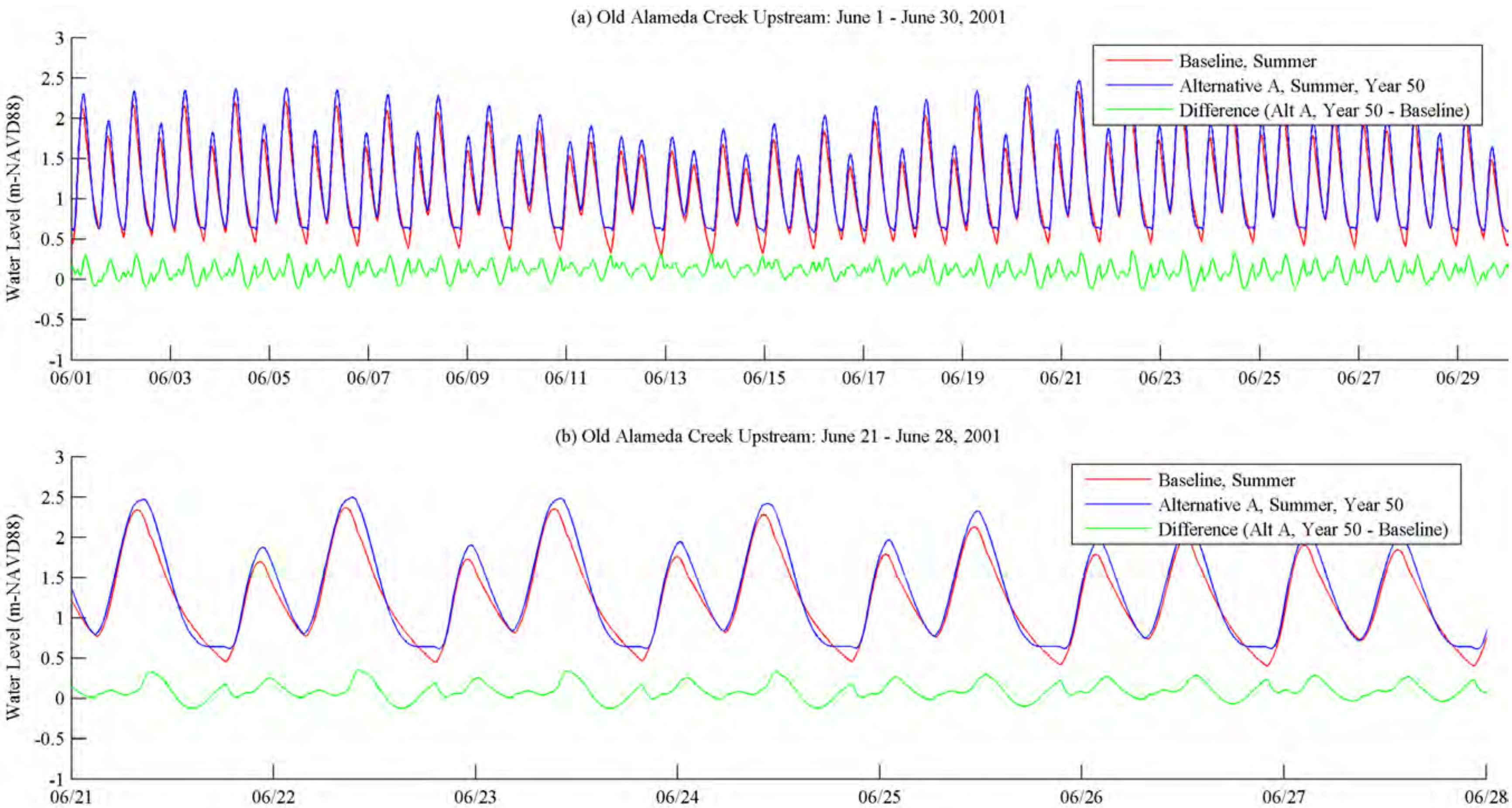

figure *6-10*

South Bay Salt Pond Restoration Project

Water Levels, Old Alameda Creek Upstream, Alt A, Year 50, Summer

PWA

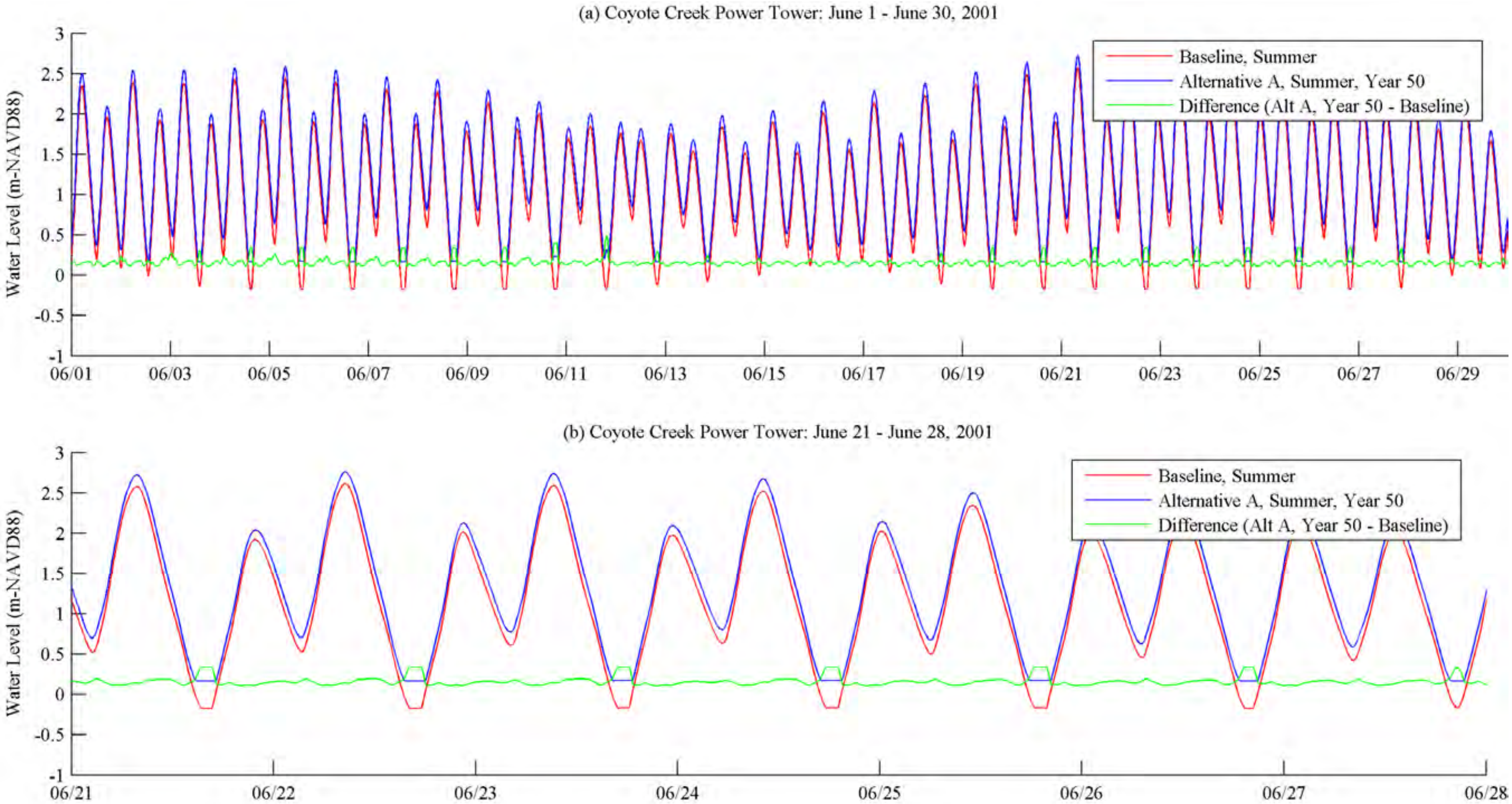

figure 6-11

South Bay Salt Pond Restoration Project

Water Levels, Coyote Creek Power Tower, Alt A, Year 50, Summer

PWA

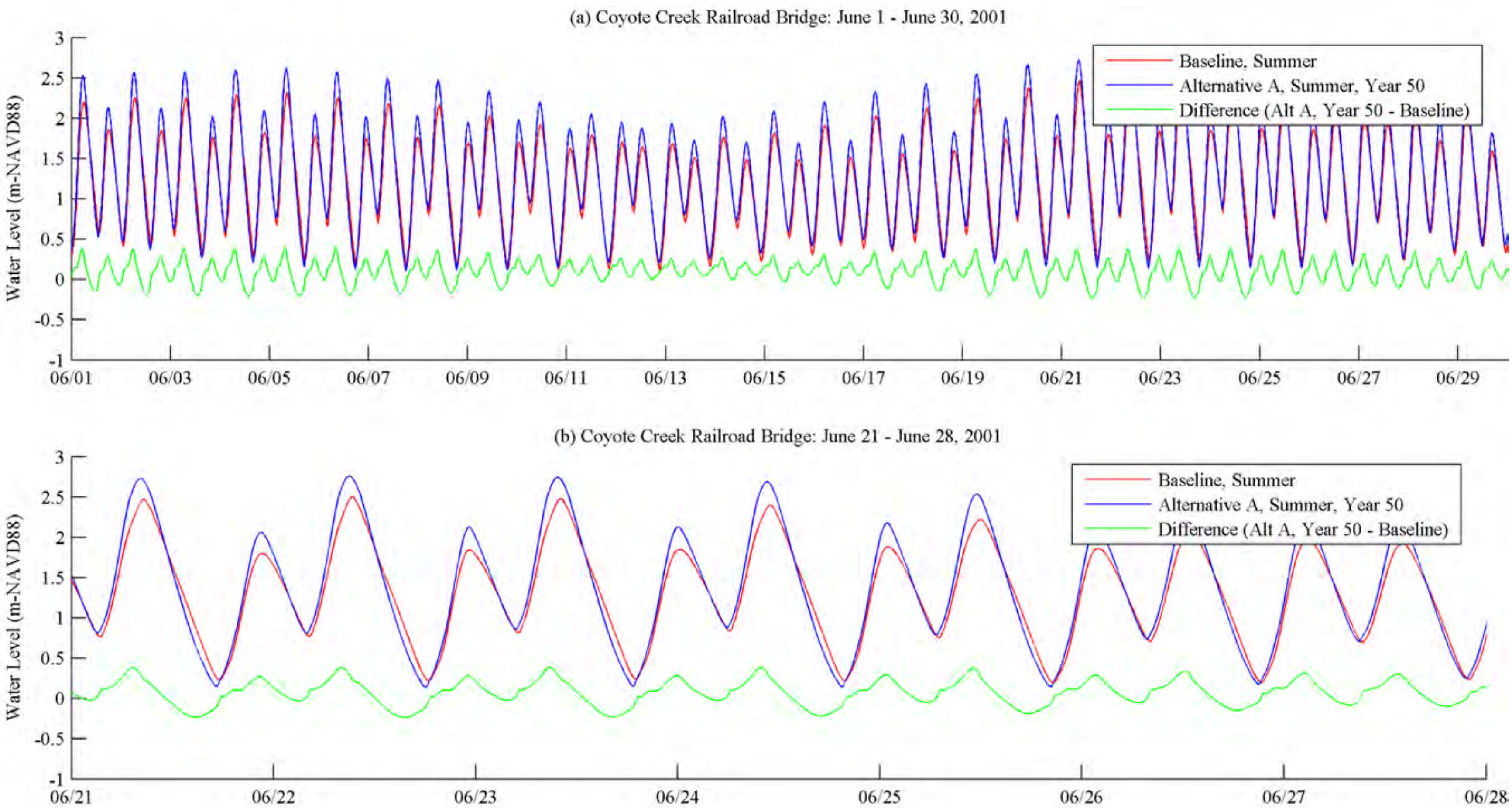

figure 6-12

South Bay Salt Pond Restoration Project

Water Levels, Coyote Creek Railroad Bridge, Alt A, Year 50, Summer

PWA

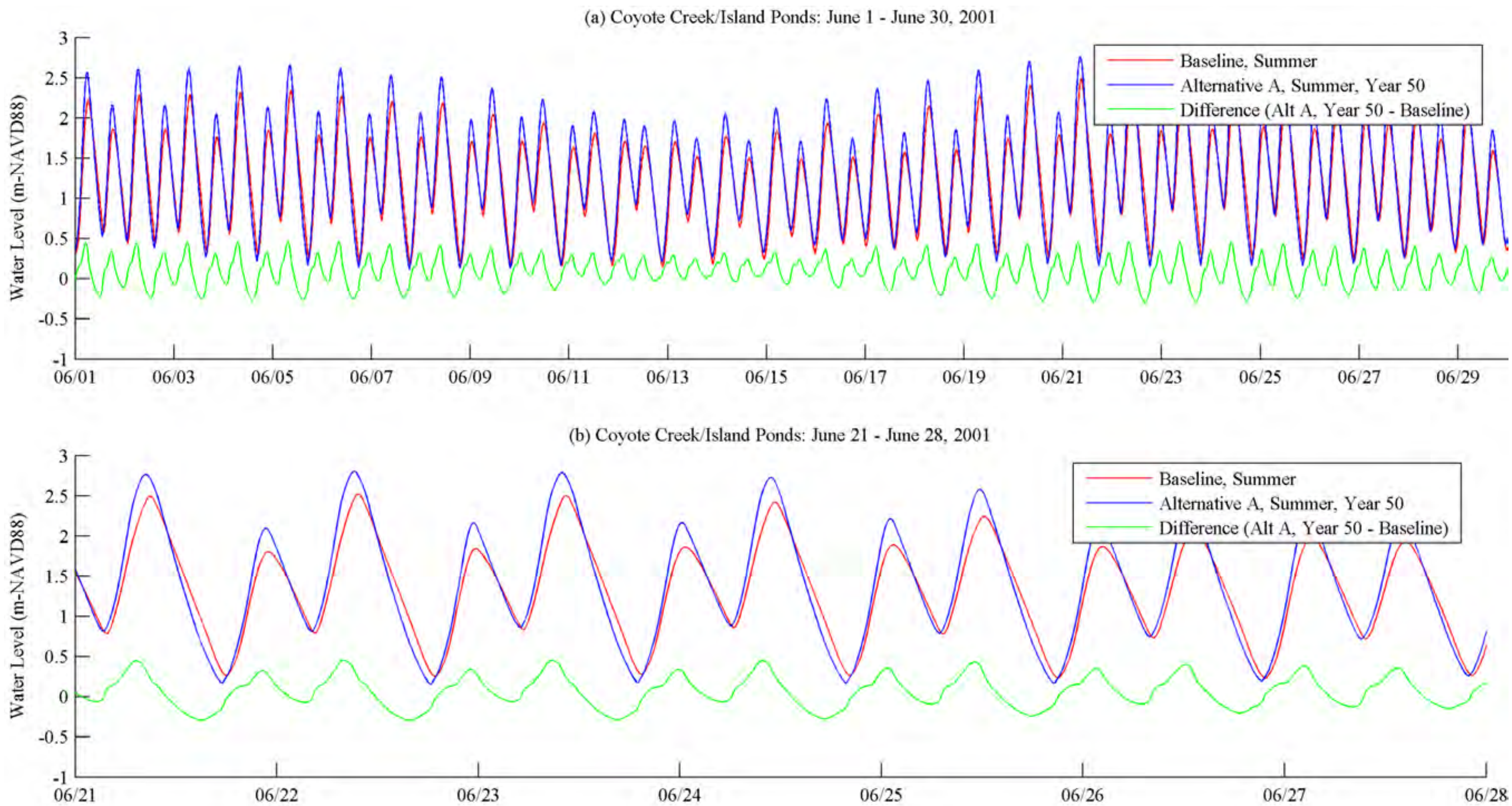

figure 6-13

South Bay Salt Pond Restoration Project

Water Levels, Coyote Creek/Island Ponds, Year 50, Summer

PWA

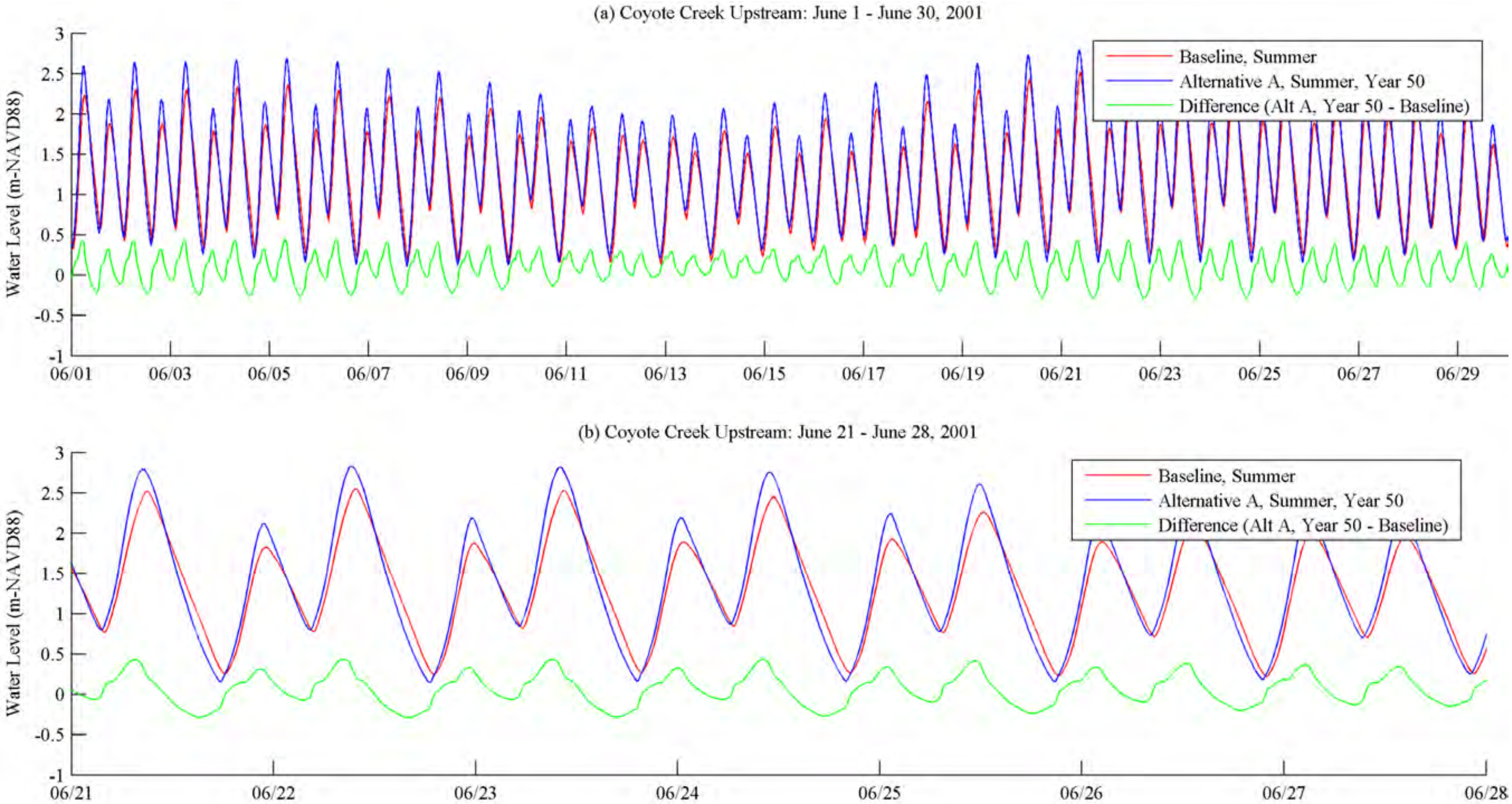

figure 6-14

South Bay Salt Pond Restoration Project

Water Levels, Coyote Creek Upstream, Year 50, Summer

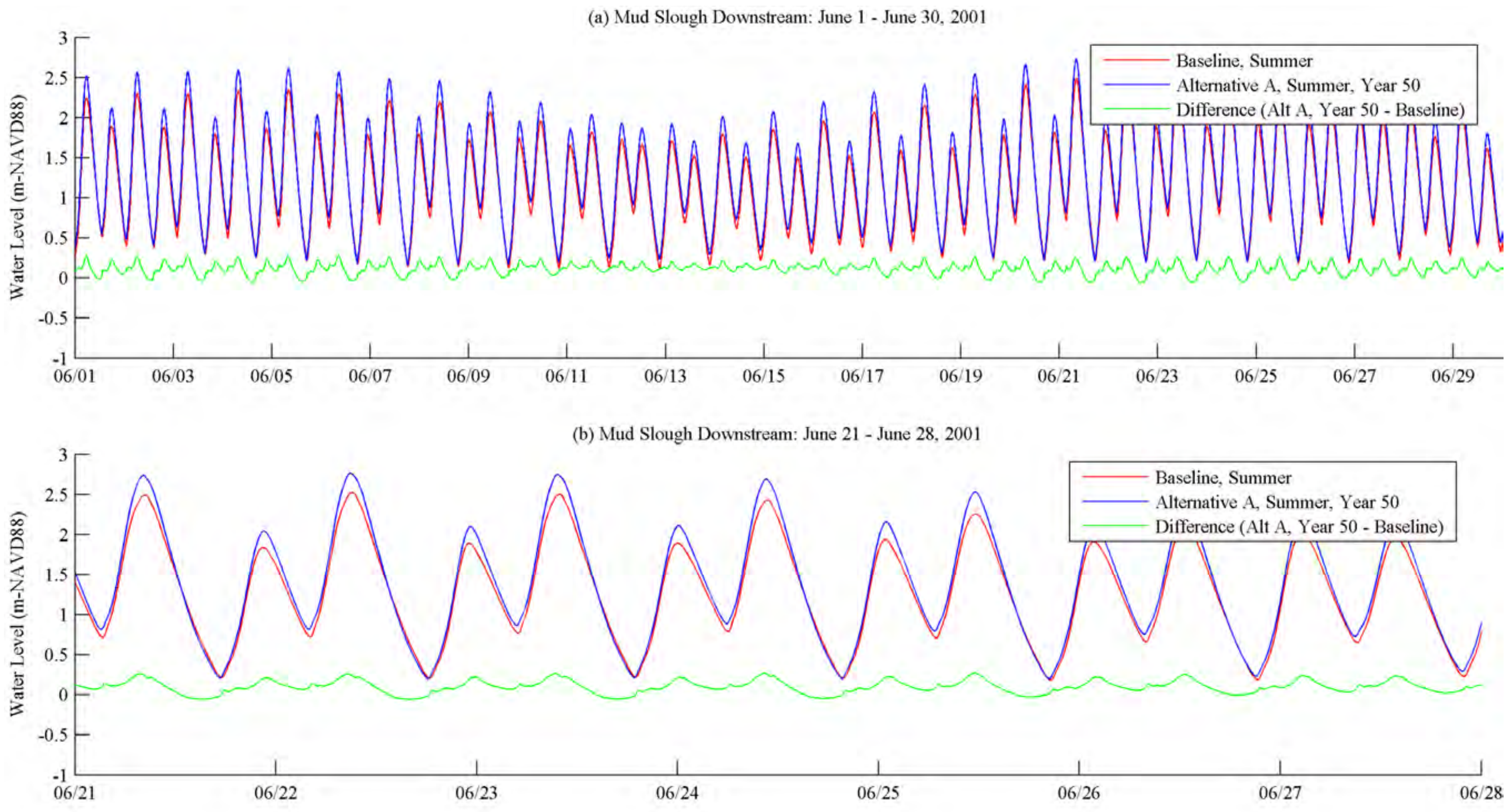

figure *6-15*

South Bay Salt Pond Restoration Project

Water Levels, Mud Slough Downstream, Alt A, Year 50, Summer

PWA

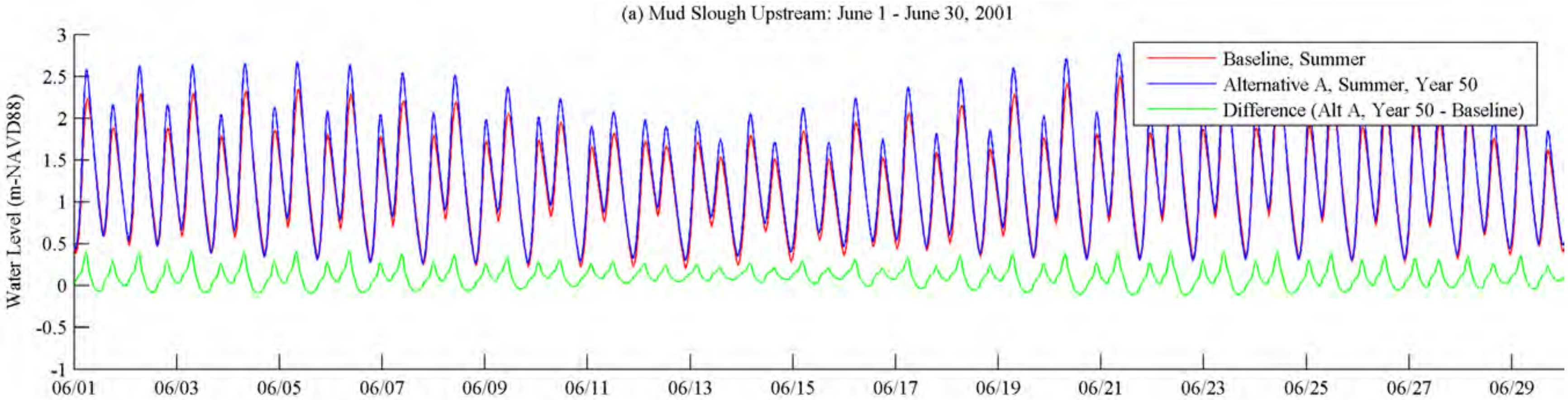

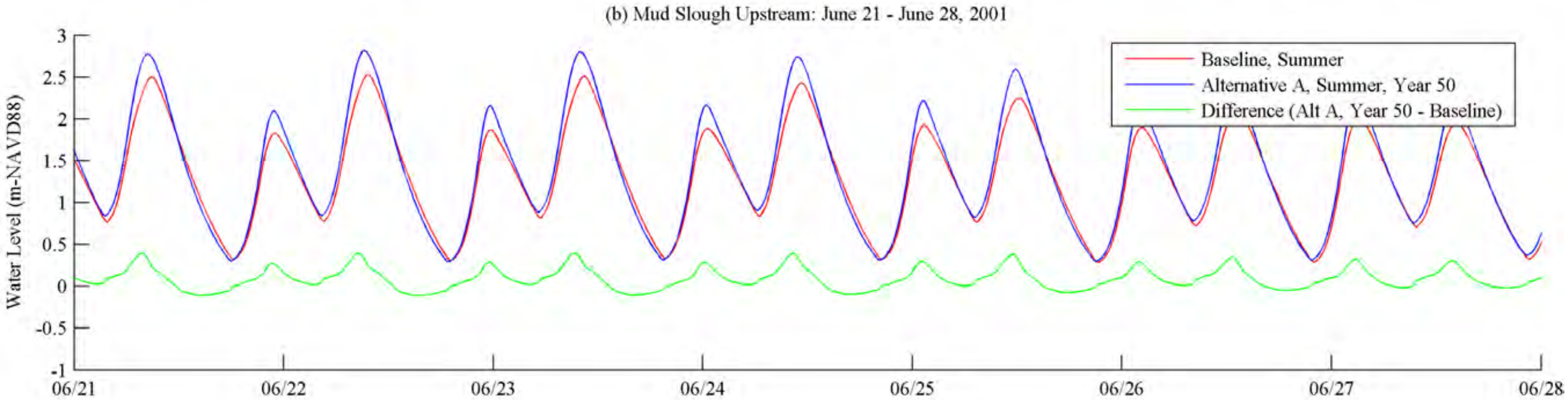

figure 6-16

South Bay Salt Pond Restoration Project

Water Levels, Mud Slough Upstream, Alt A, Year 50, Summer

PWA

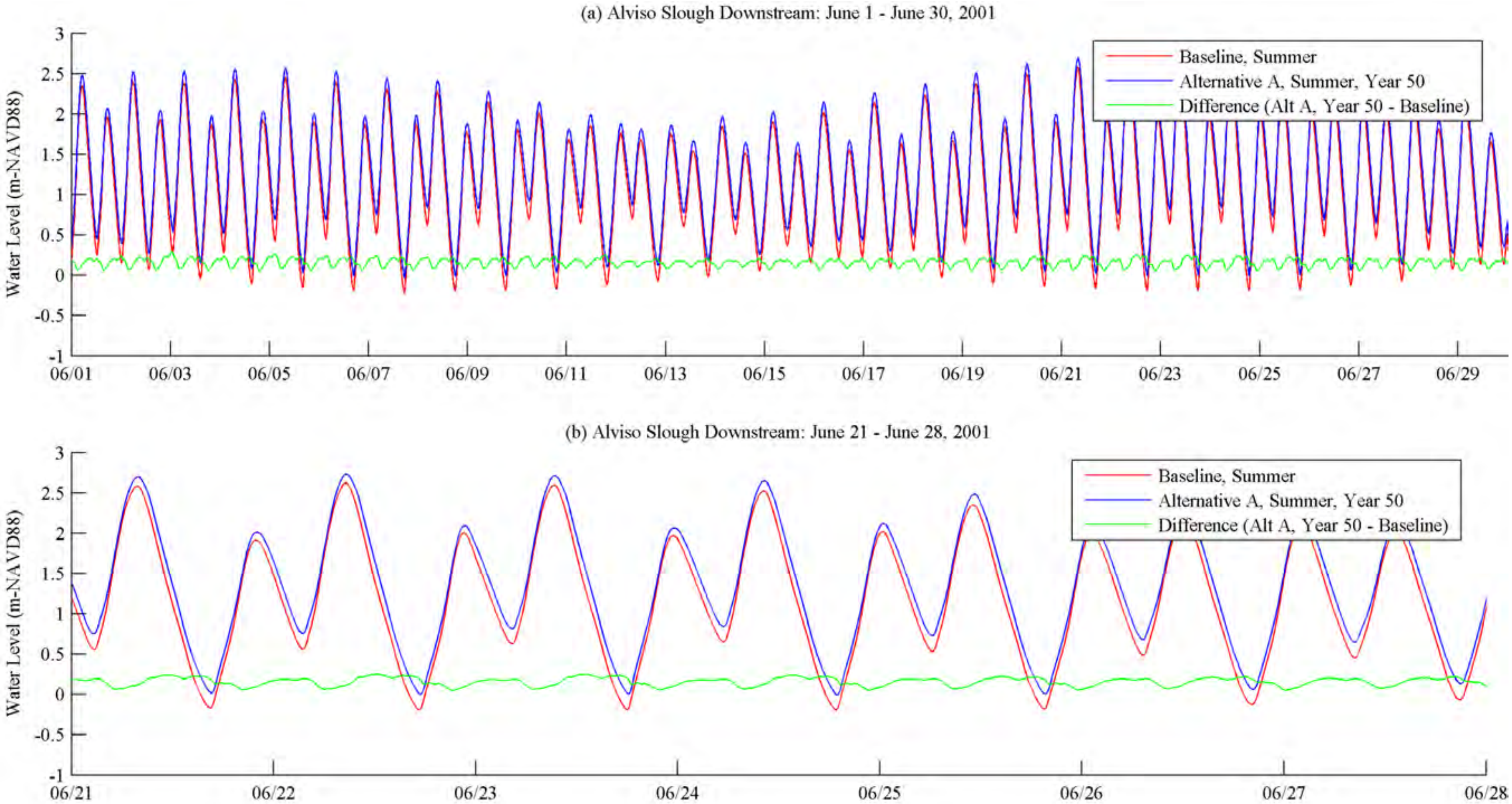

figure 6-17

South Bay Salt Pond Restoration Project

Water Levels, Alviso Slough Downstream, Alt A, Year 50, Summer

PWA

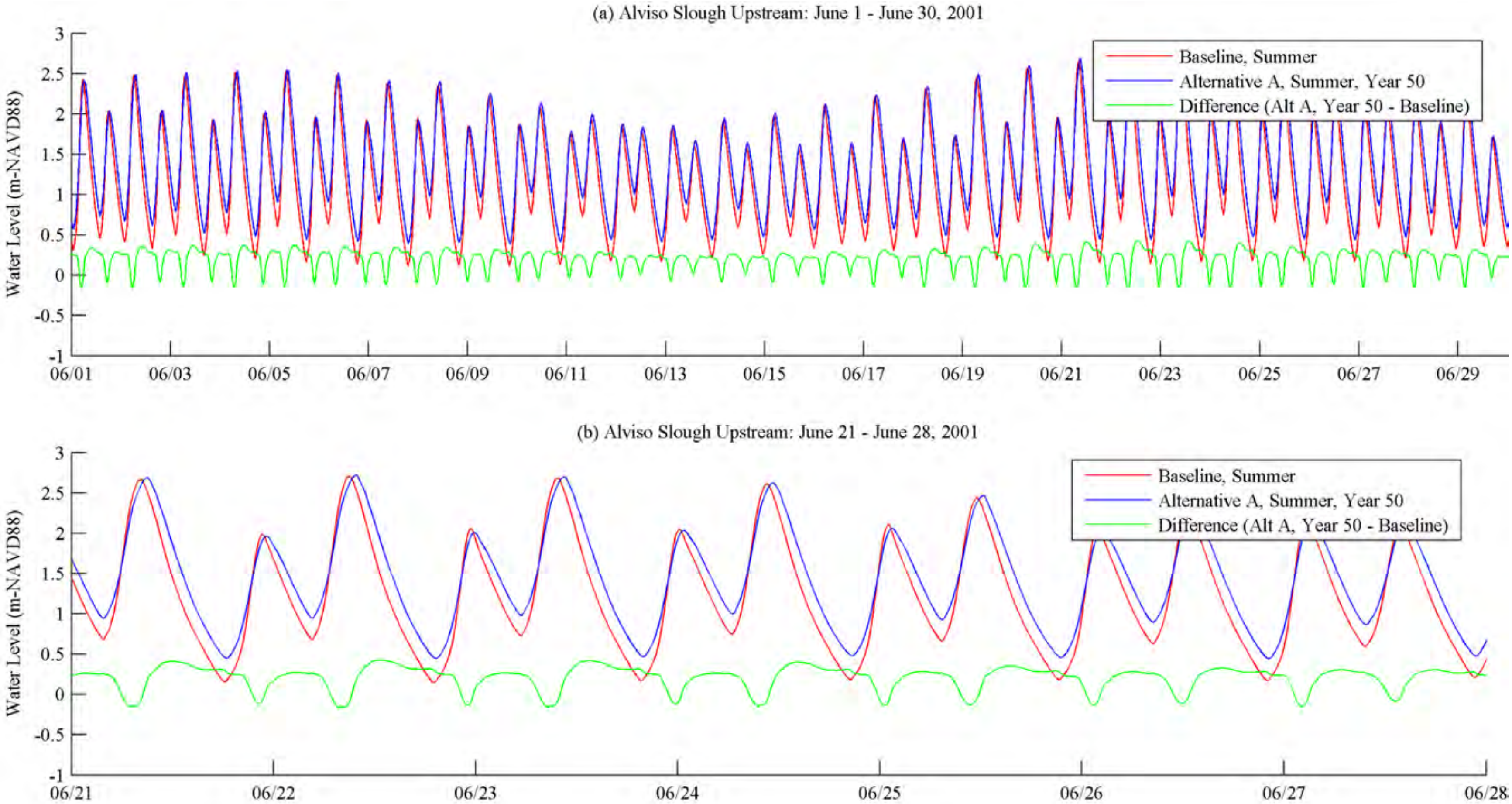

figure *6-18*

South Bay Salt Pond Restoration Project

Water Levels, Alviso Slough Upstream, Alt A, Year 50, Summer

PWA

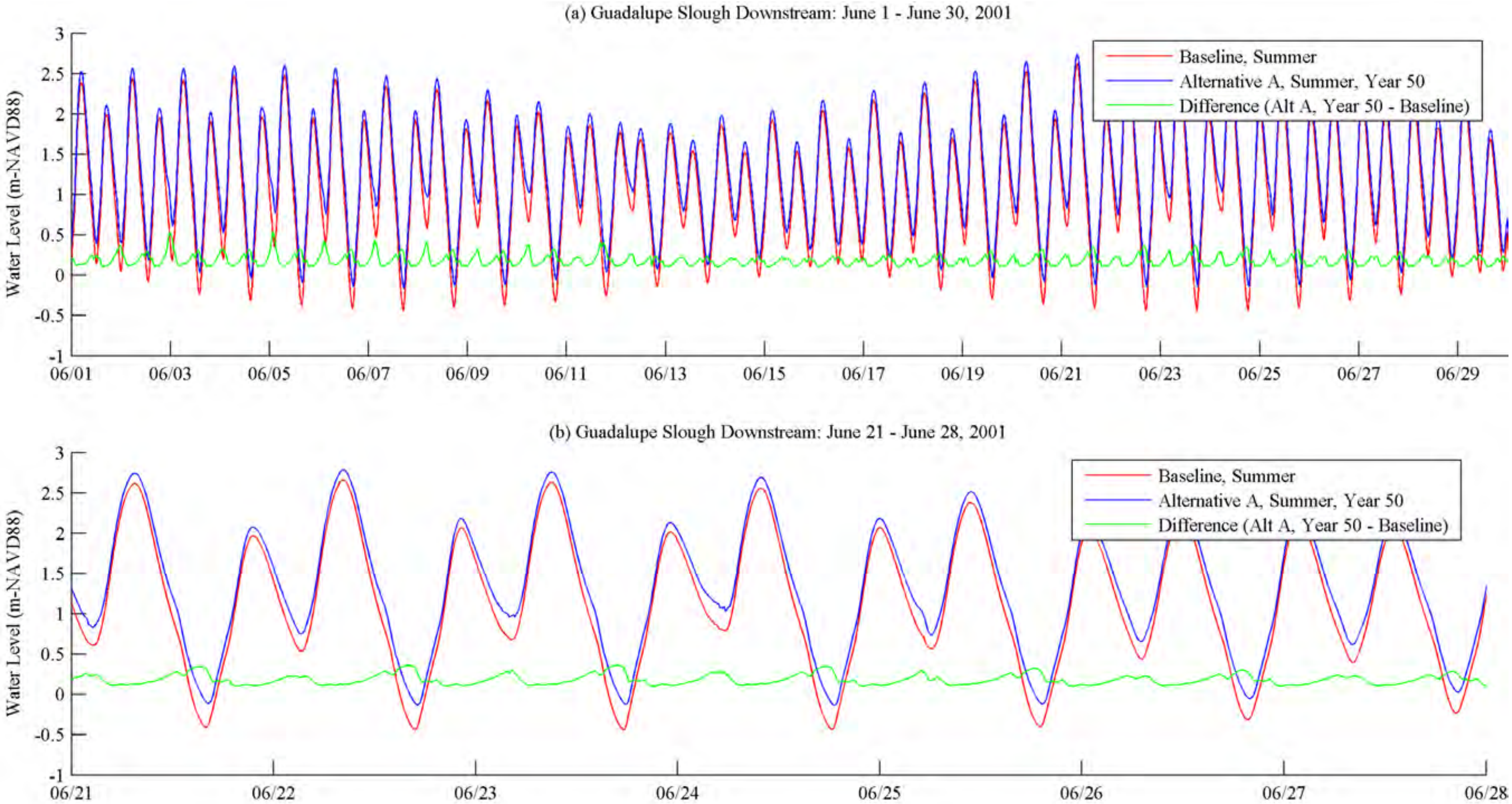

figure 6-19

South Bay Salt Pond Restoration Project

Water Levels, Guadalupe Slough Downstream, Alt A, Year 50, Summer

PWA

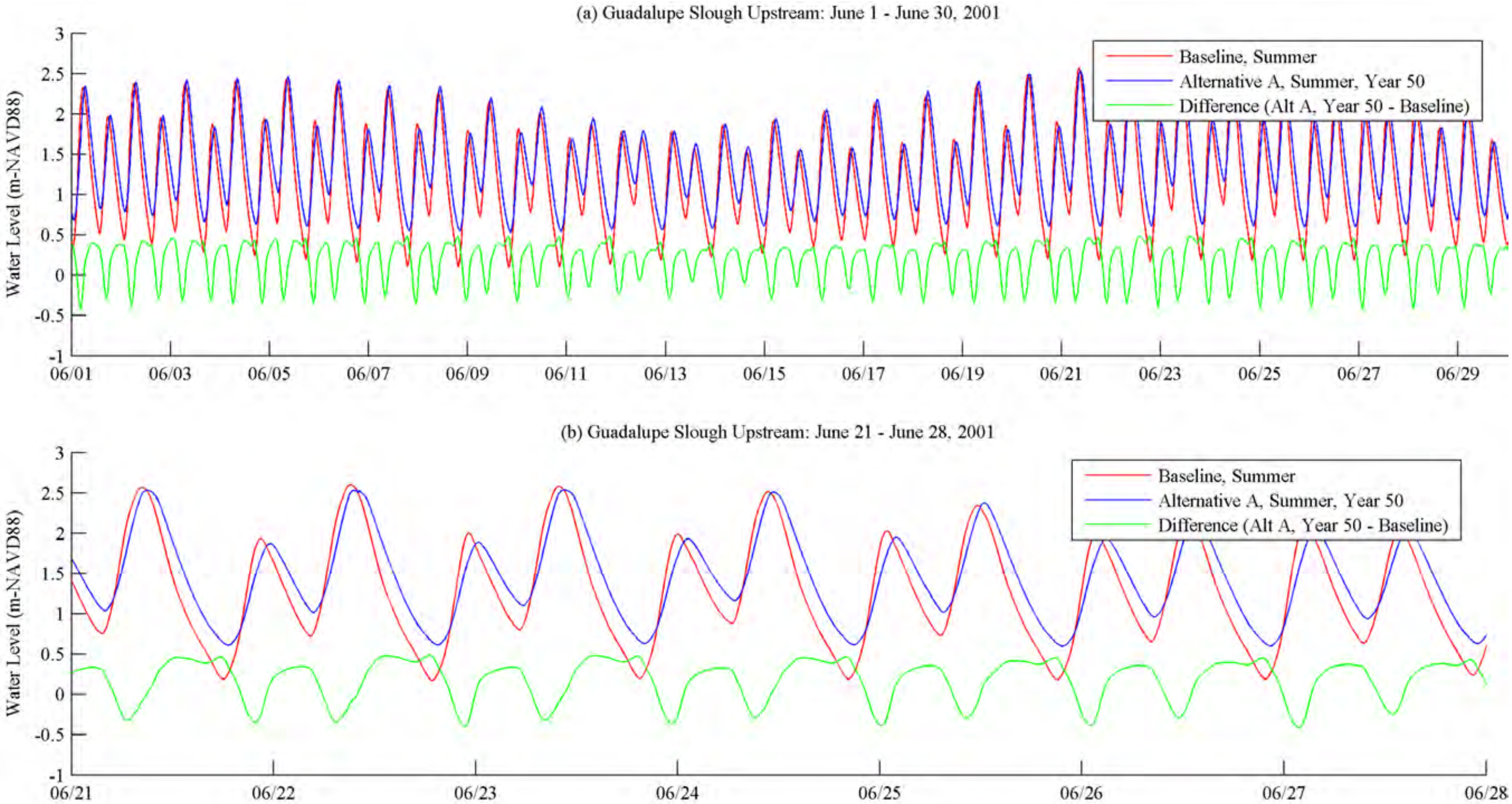

figure 6-20

South Bay Salt Pond Restoration Project

Water Levels, Guadalupe Slough Upstream, Alt A, Year 50, Summer

PWA

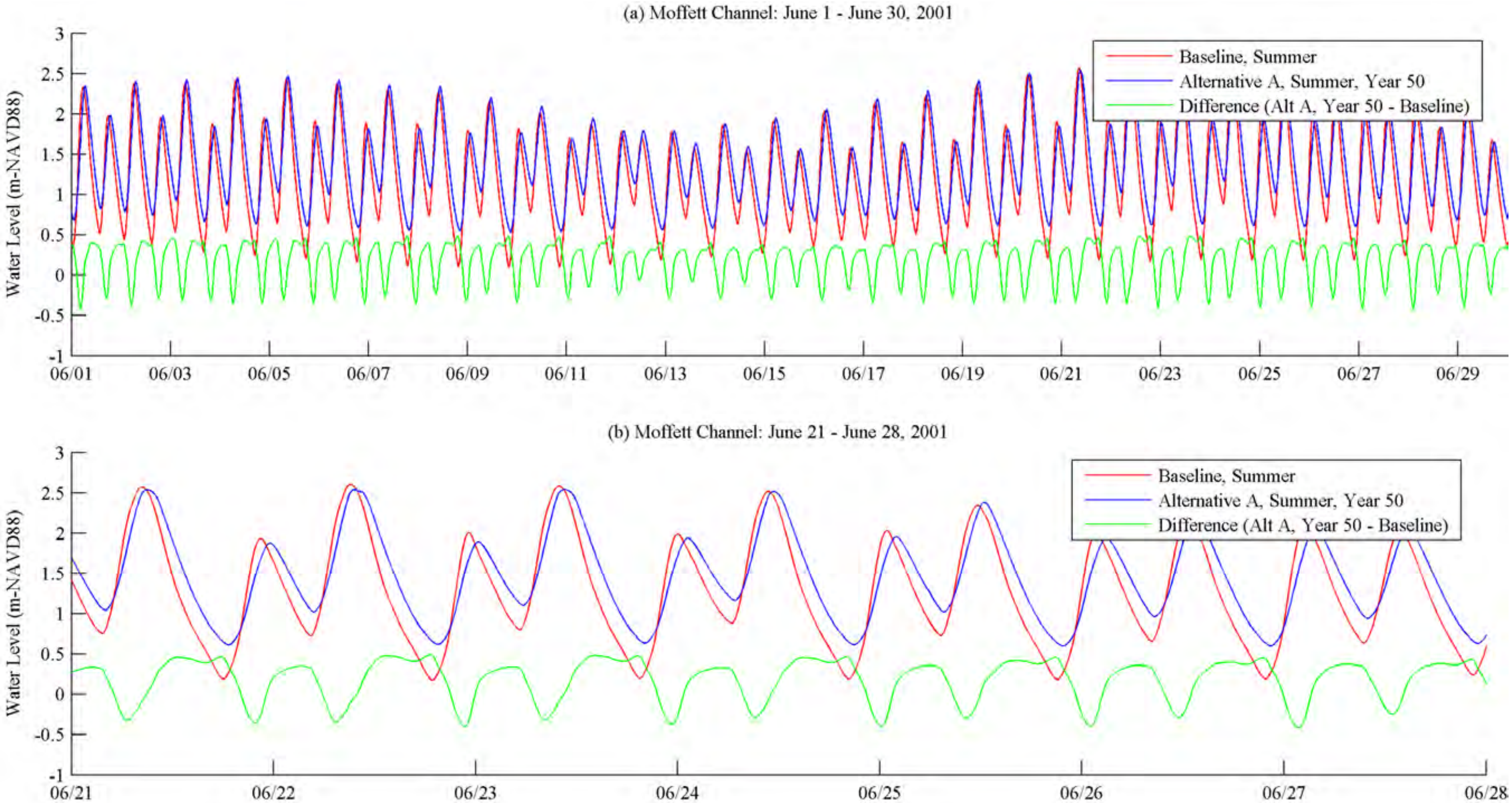

figure 6-21

South Bay Salt Pond Restoration Project

Water Levels, Moffett Channel, Alt A, Year 50, Summer

PWA

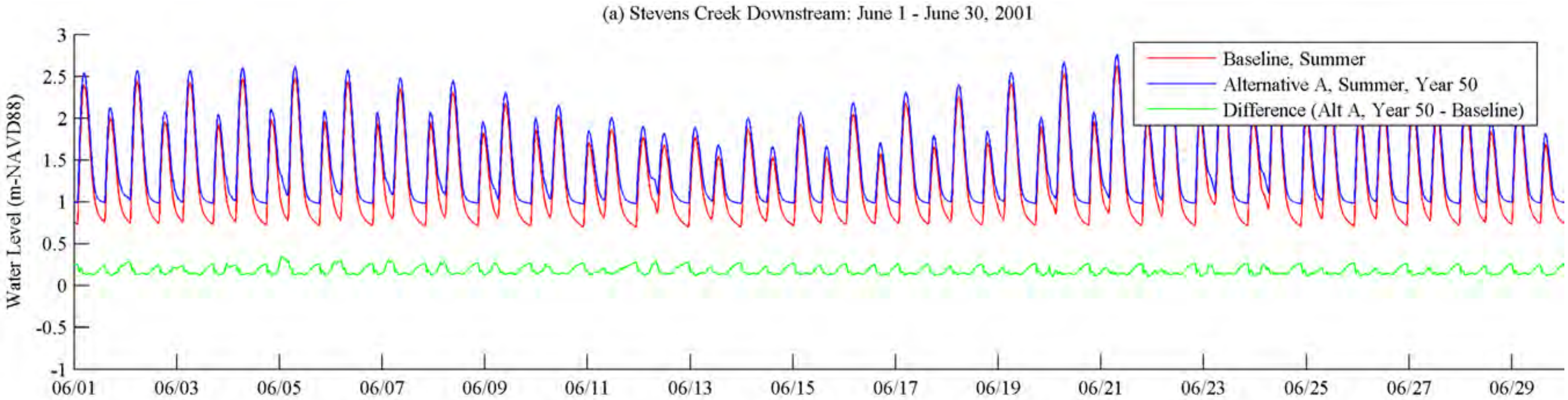

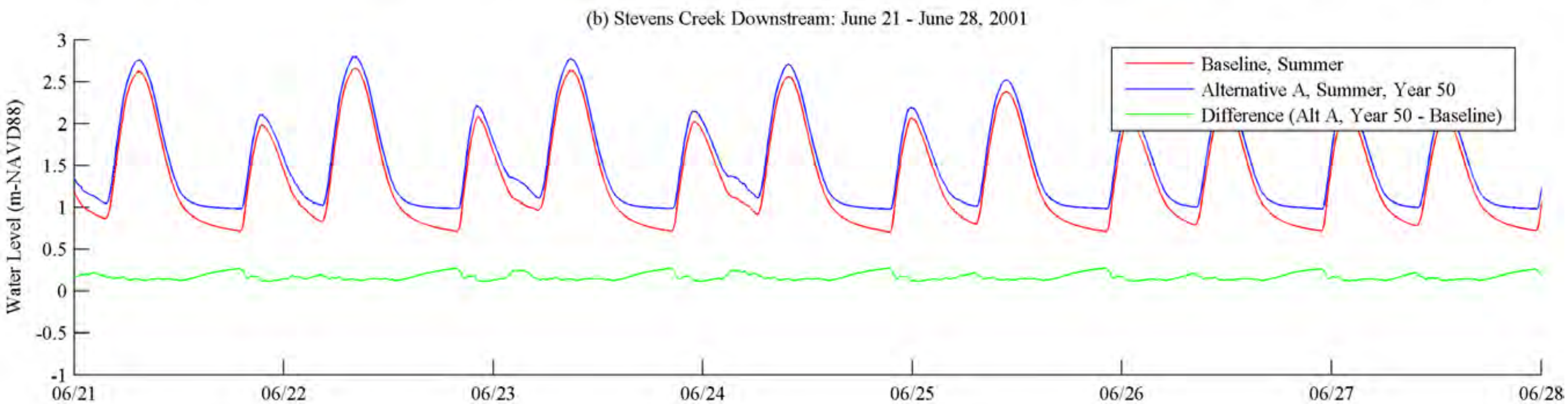

figure 6-22

South Bay Salt Pond Restoration Project

Water Levels, Steven Creek Downstream, Alt A, Year 50, Summer

PWA

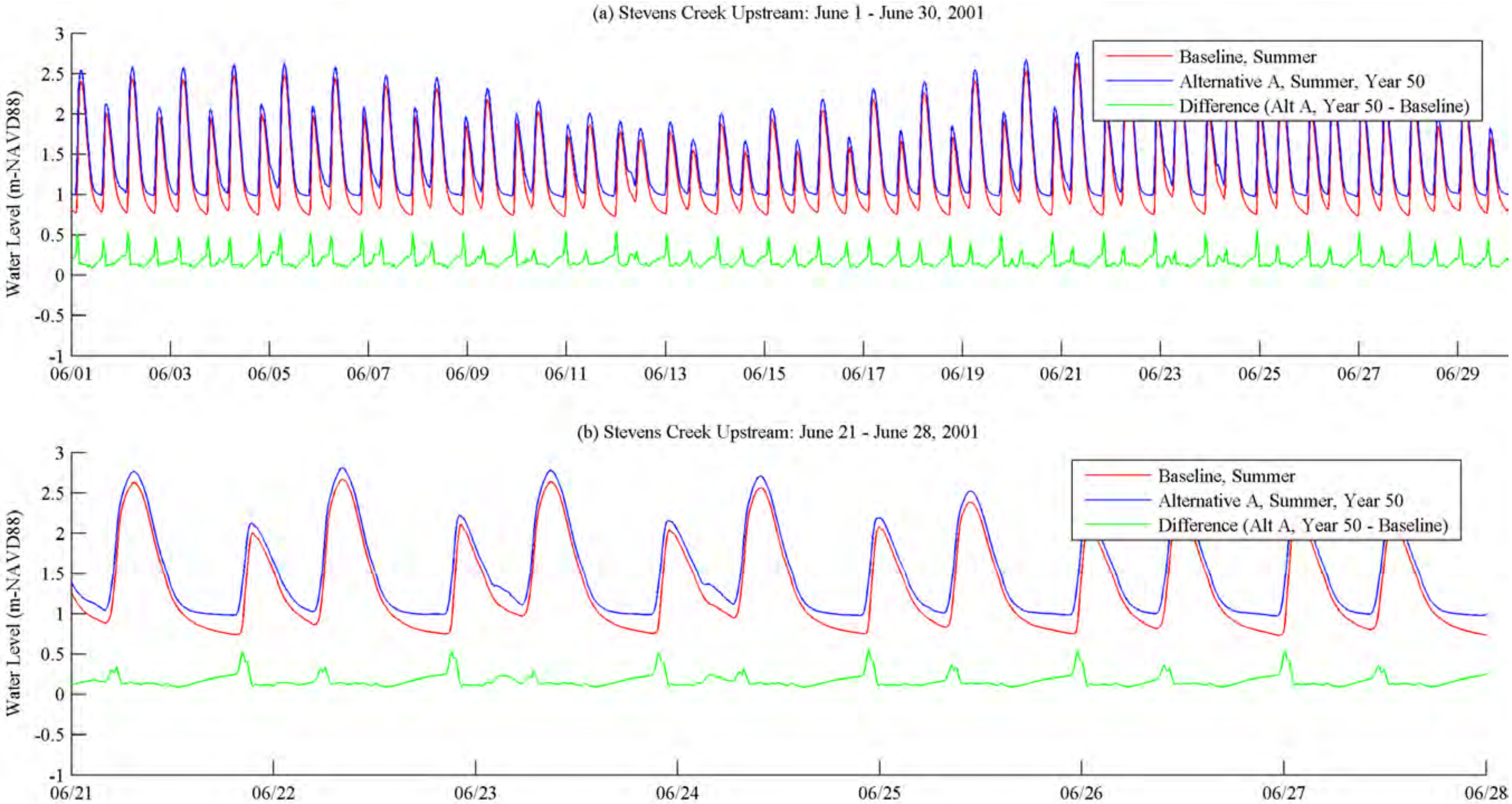

figure 6-23

South Bay Salt Pond Restoration Project

Water Levels, Stevens Creek Upstream, Alt A, Year 50, Summer

PWA

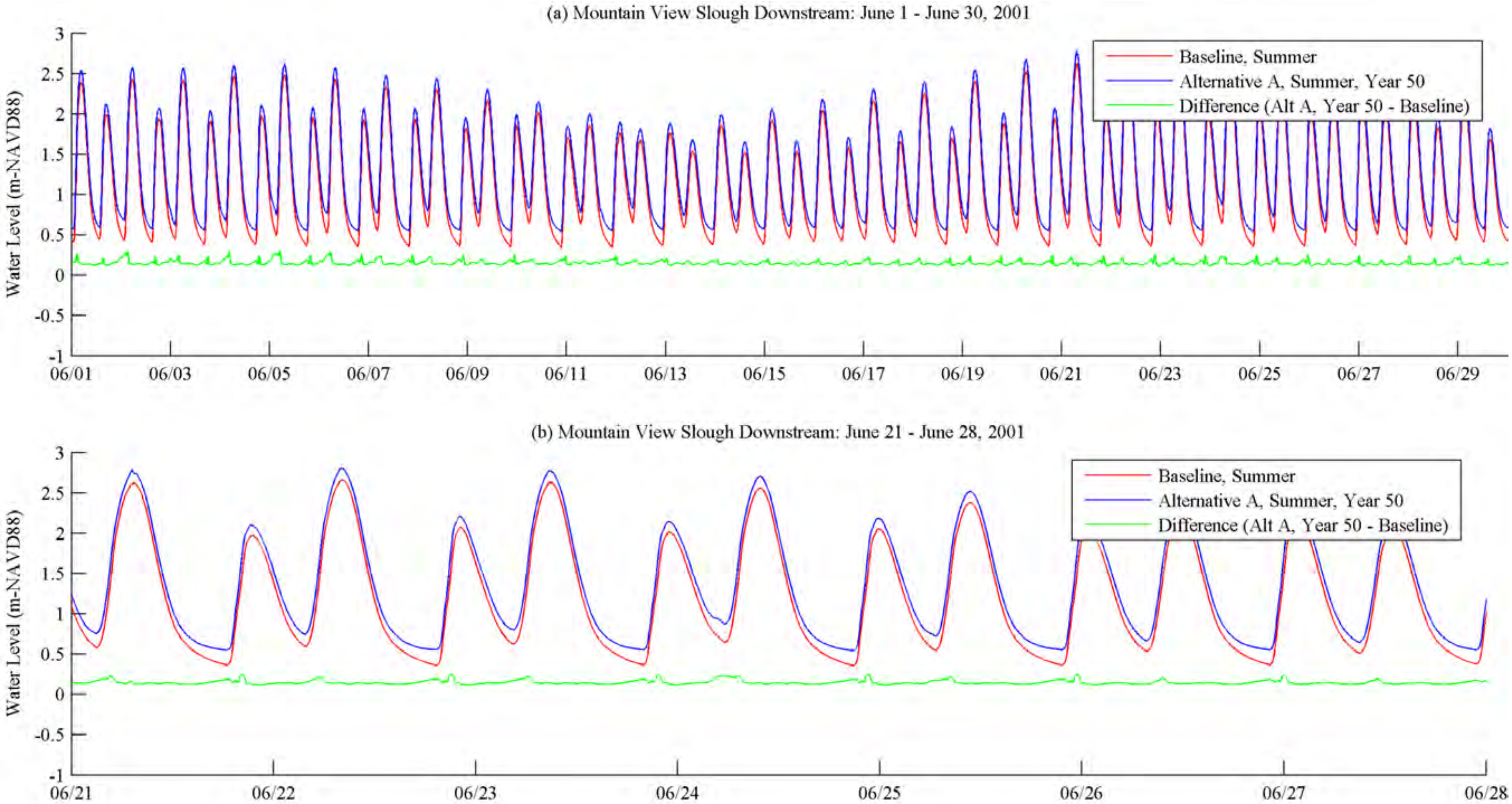

figure *6-24*

South Bay Salt Pond Restoration Project

Water Levels, Mountain View Slough Downstream, Alt A, Year 50, Summer

PWA

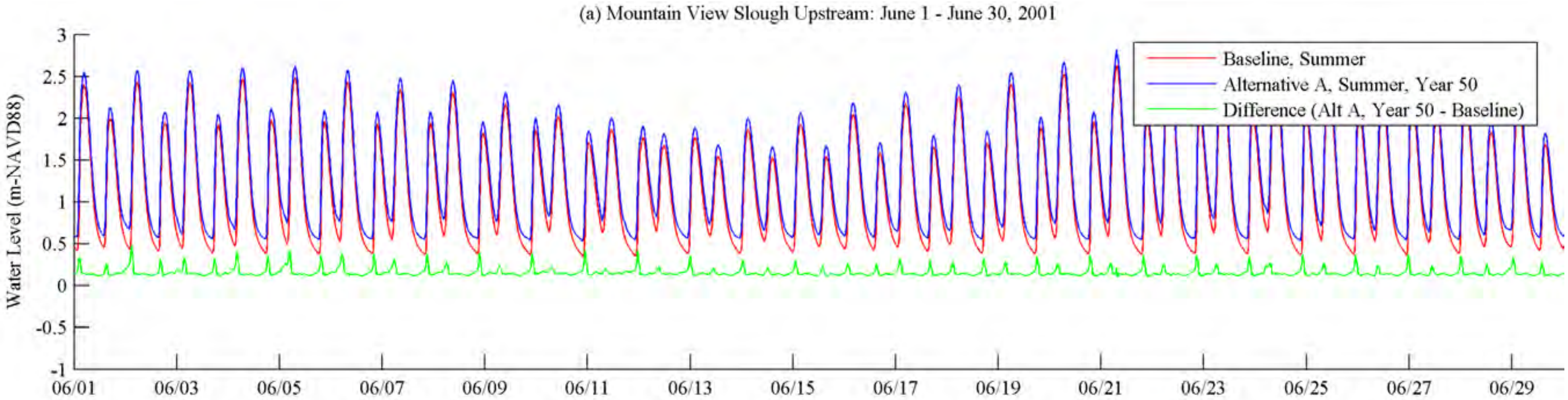

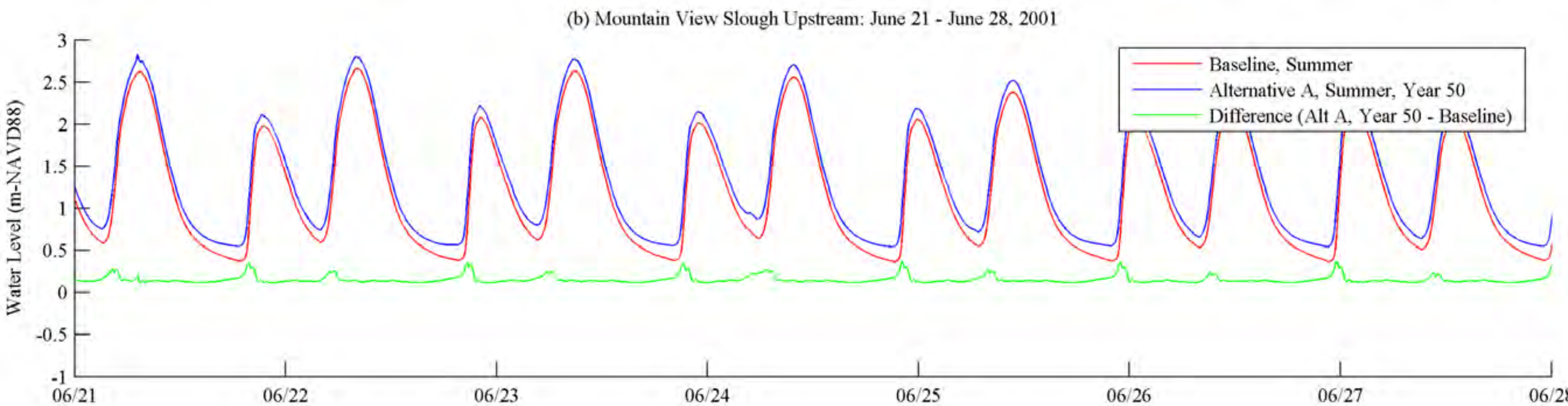

figure 6-25

South Bay Salt Pond Restoration Project

Water Levels, Mountain View Slough Upstream, Alt A, Year 50, Summer

PWA

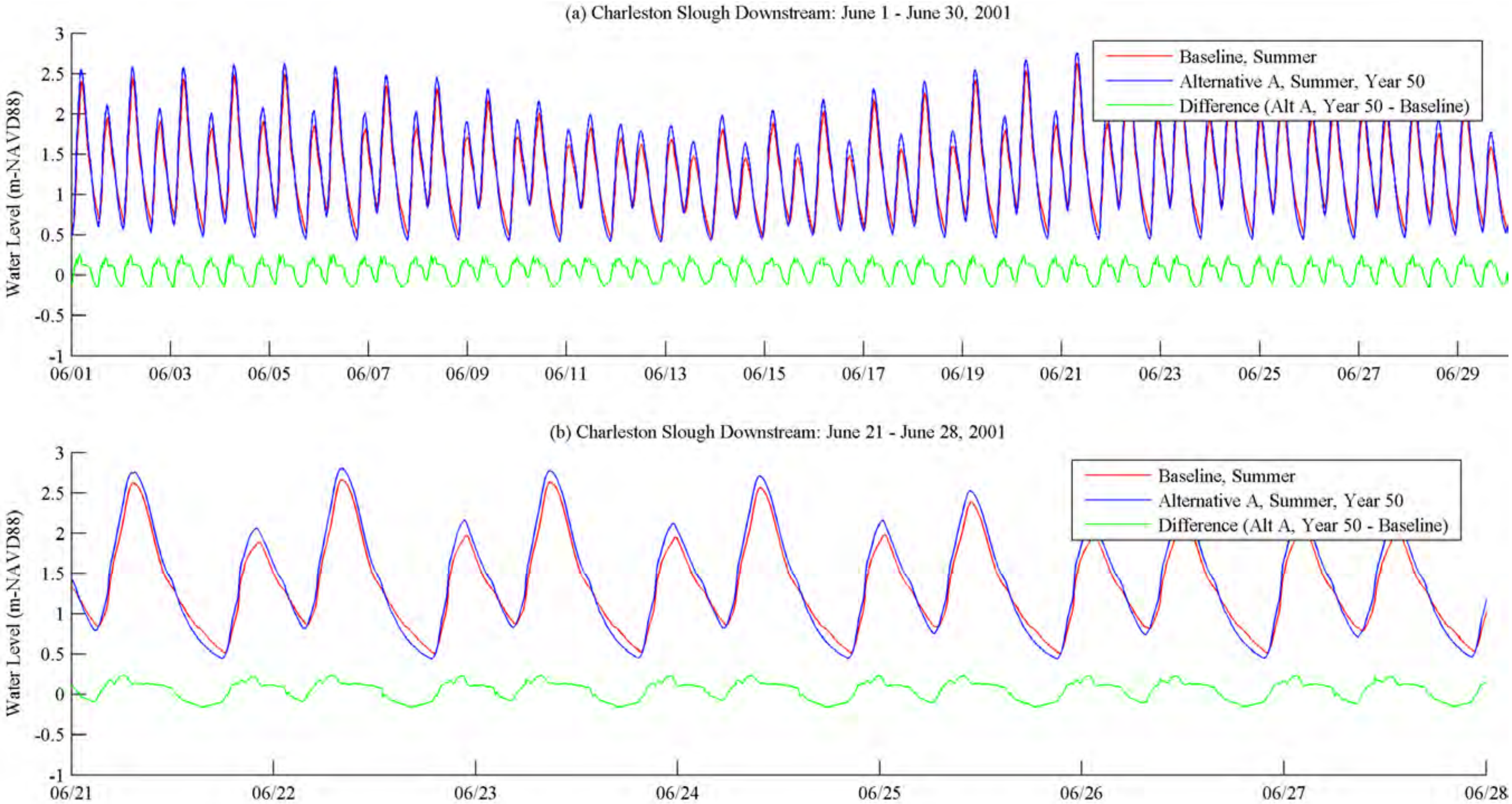

figure 6-26

South Bay Salt Pond Restoration Project

Water Levels, Charleston Slough Downstream, Alt A, Year 50, Summer

PWA

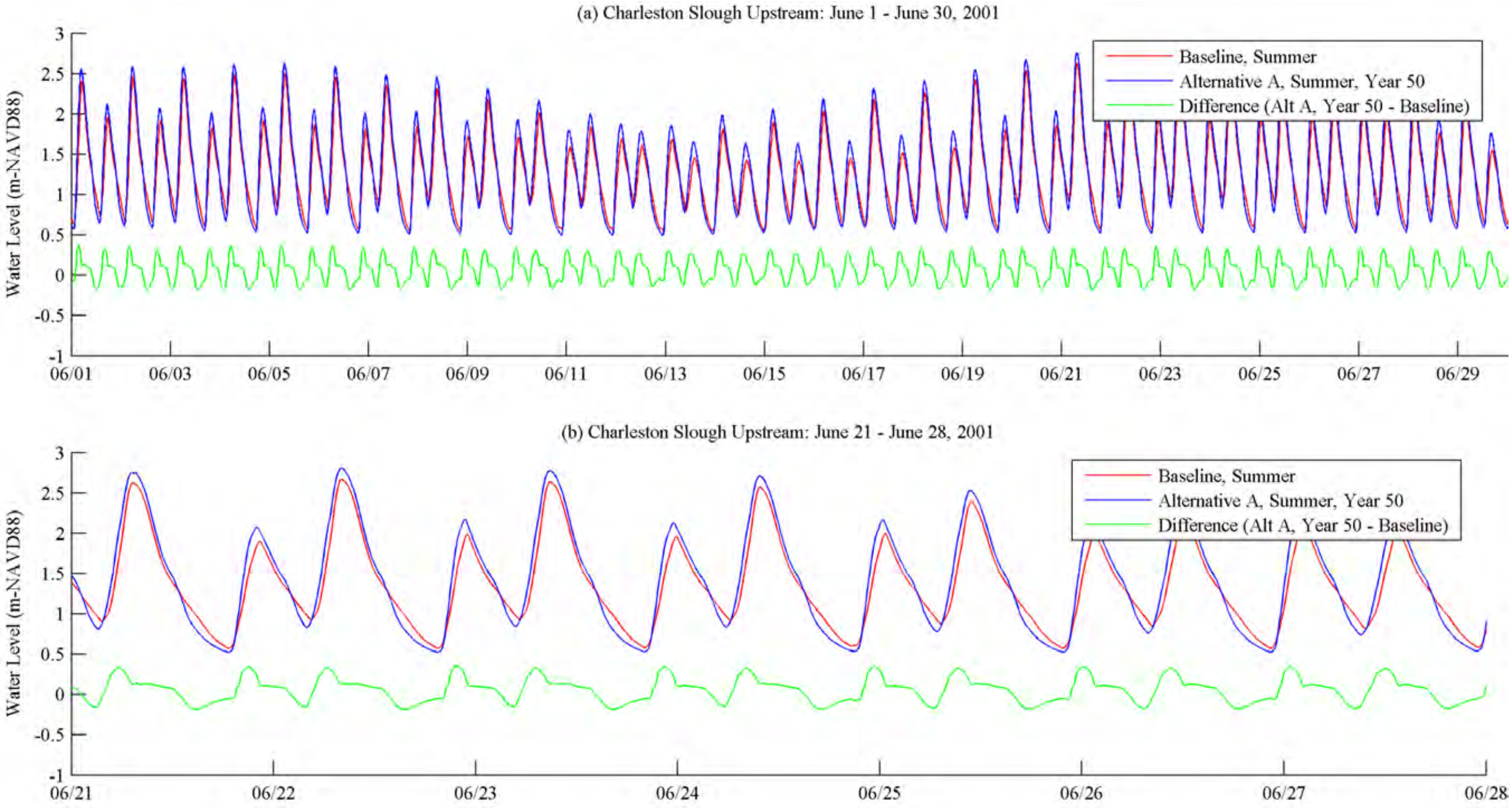

figure 6-27

South Bay Salt Pond Restoration Project

Water Levels, Charleston Slough Upstream, Alt A, Year 50, Summer

PWA

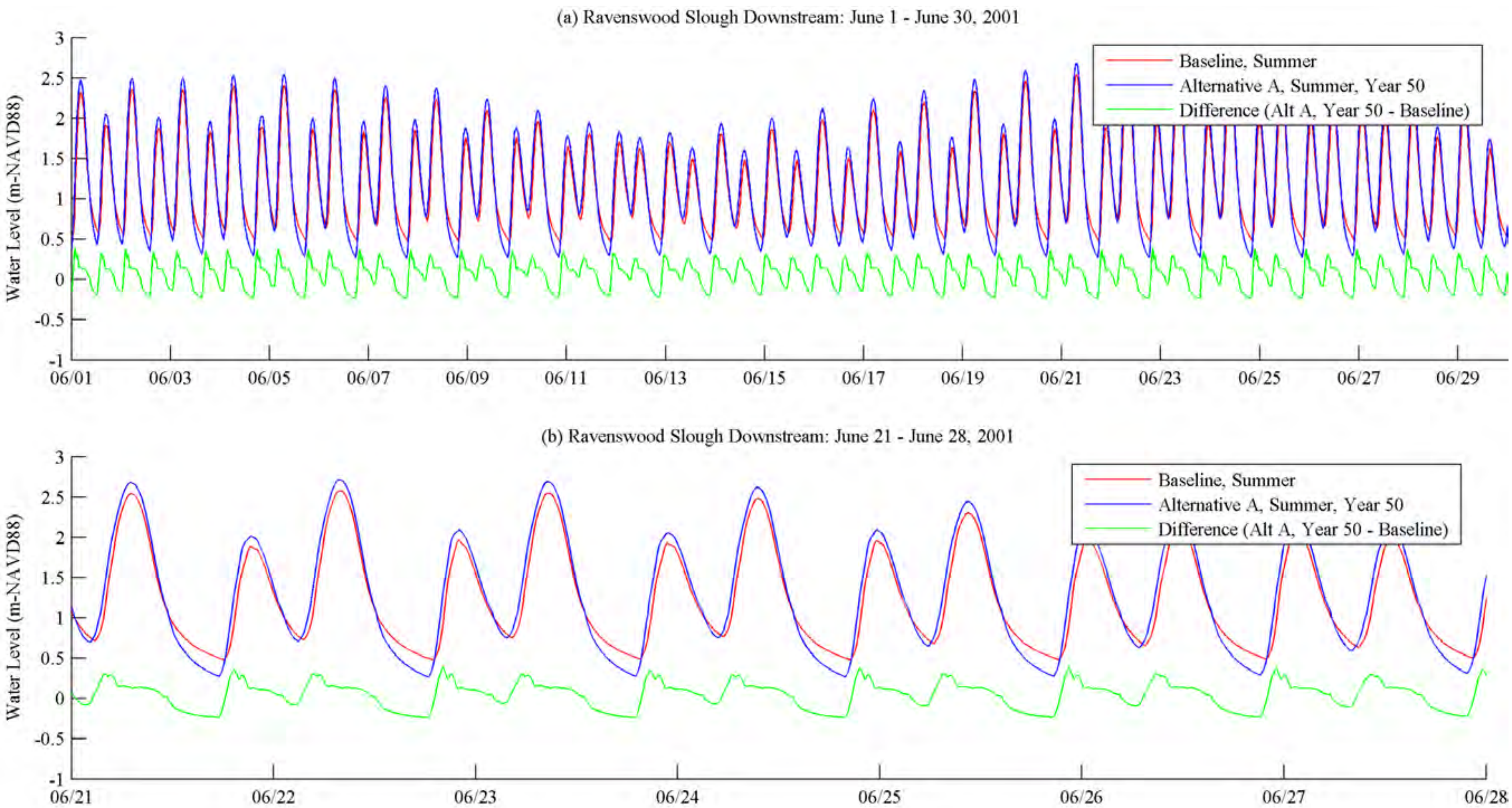

figure 6-28

South Bay Salt Pond Restoration Project

Water Levels, Ravenswood Slough Downstream, Alt A, Year 50, Summer

PWA

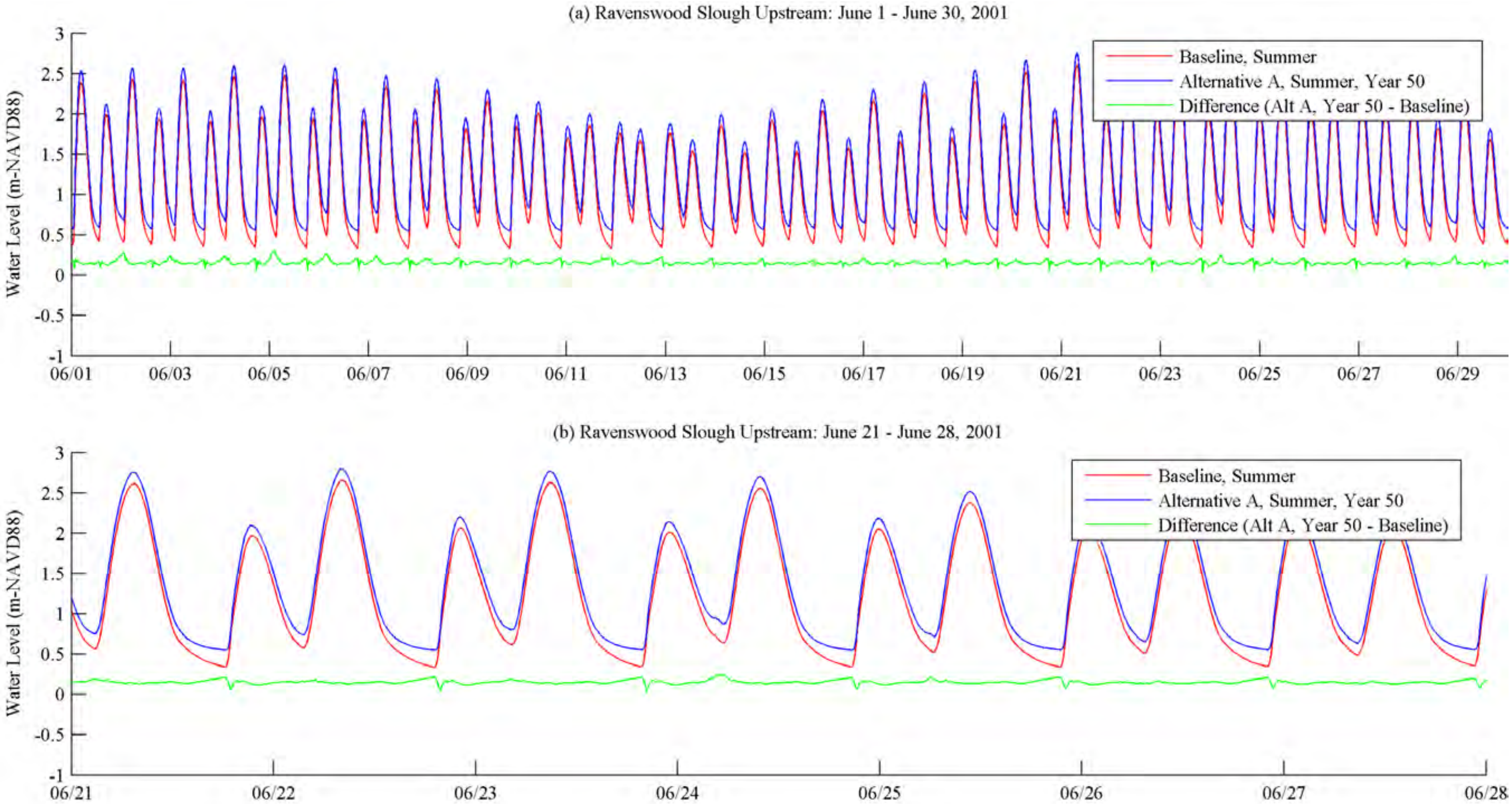

figure 6-29

South Bay Salt Pond Restoration Project

Water Levels, Ravenswood Slough Upstream, Alt A, Year 50, Summer

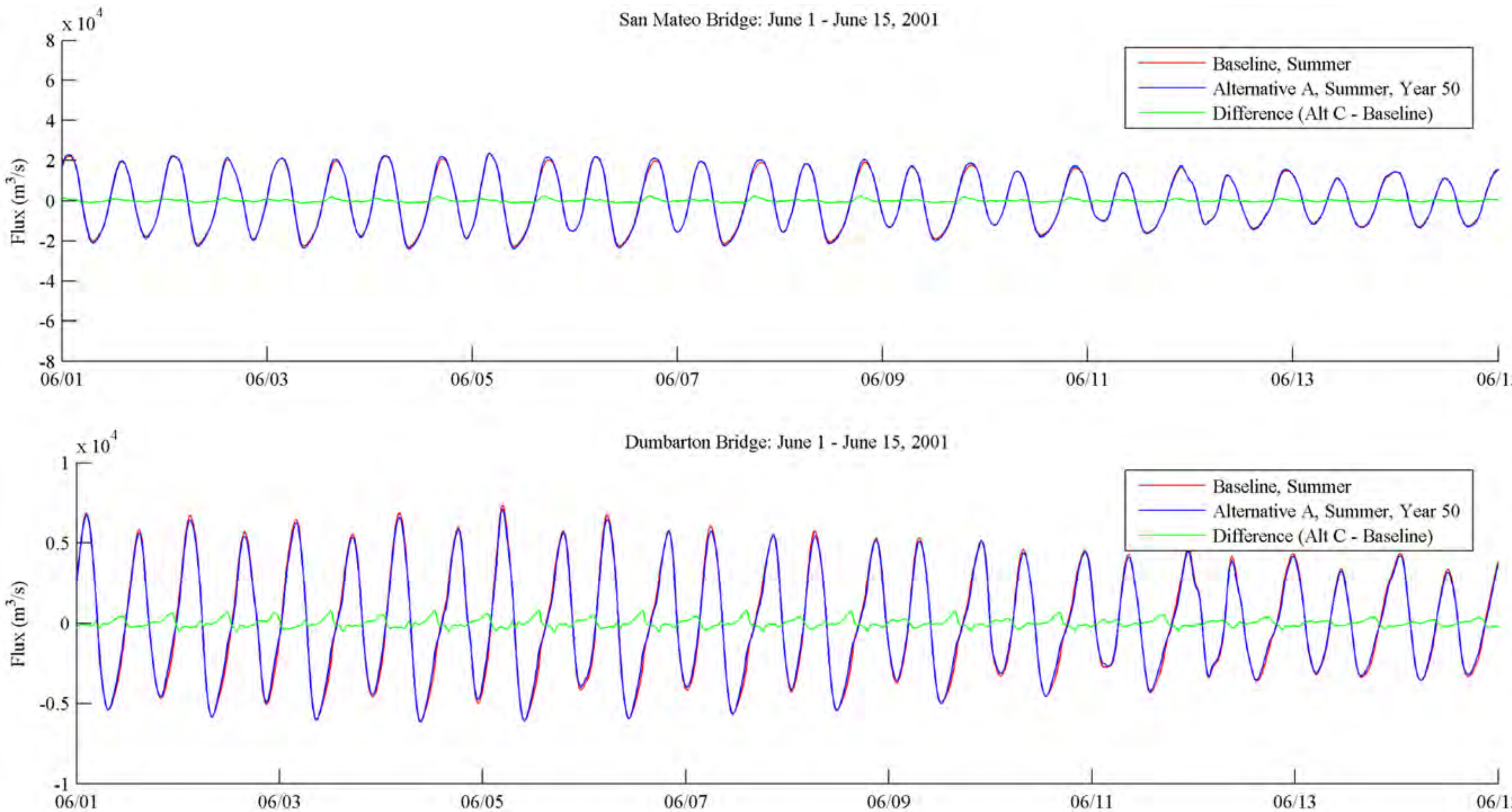

figure 6-30

South Bay Salt Pond Restoration Project

Tidal Prism, San Mateo and Dumbarton Bridges, Alt A, Year 5, Summer

PWA

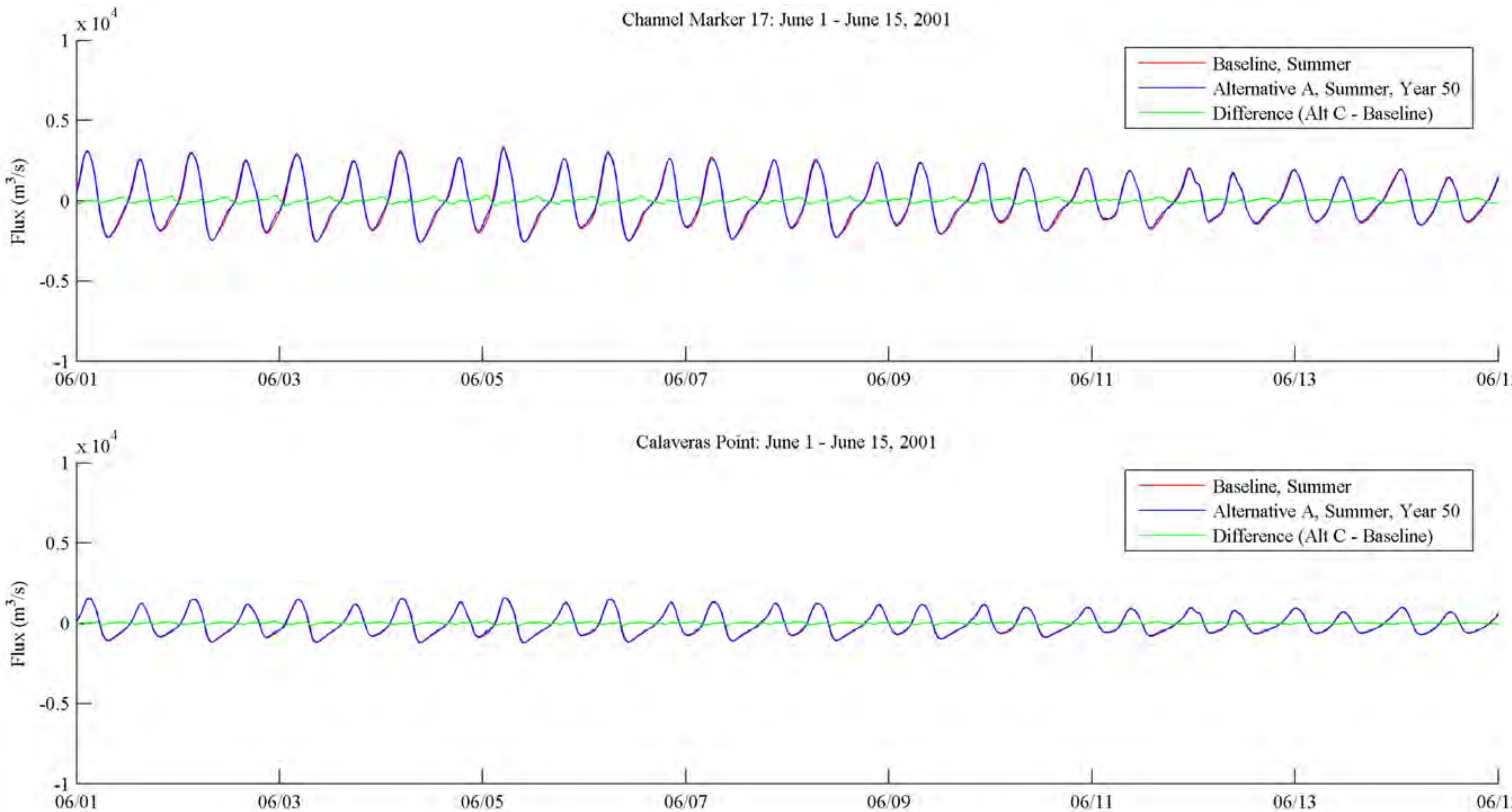

figure 6-31

South Bay Salt Pond Restoration Project

Tidal Prism, Channel Marker 17 and Calaveras Point, Alt A, Year 50, Summer

PWA

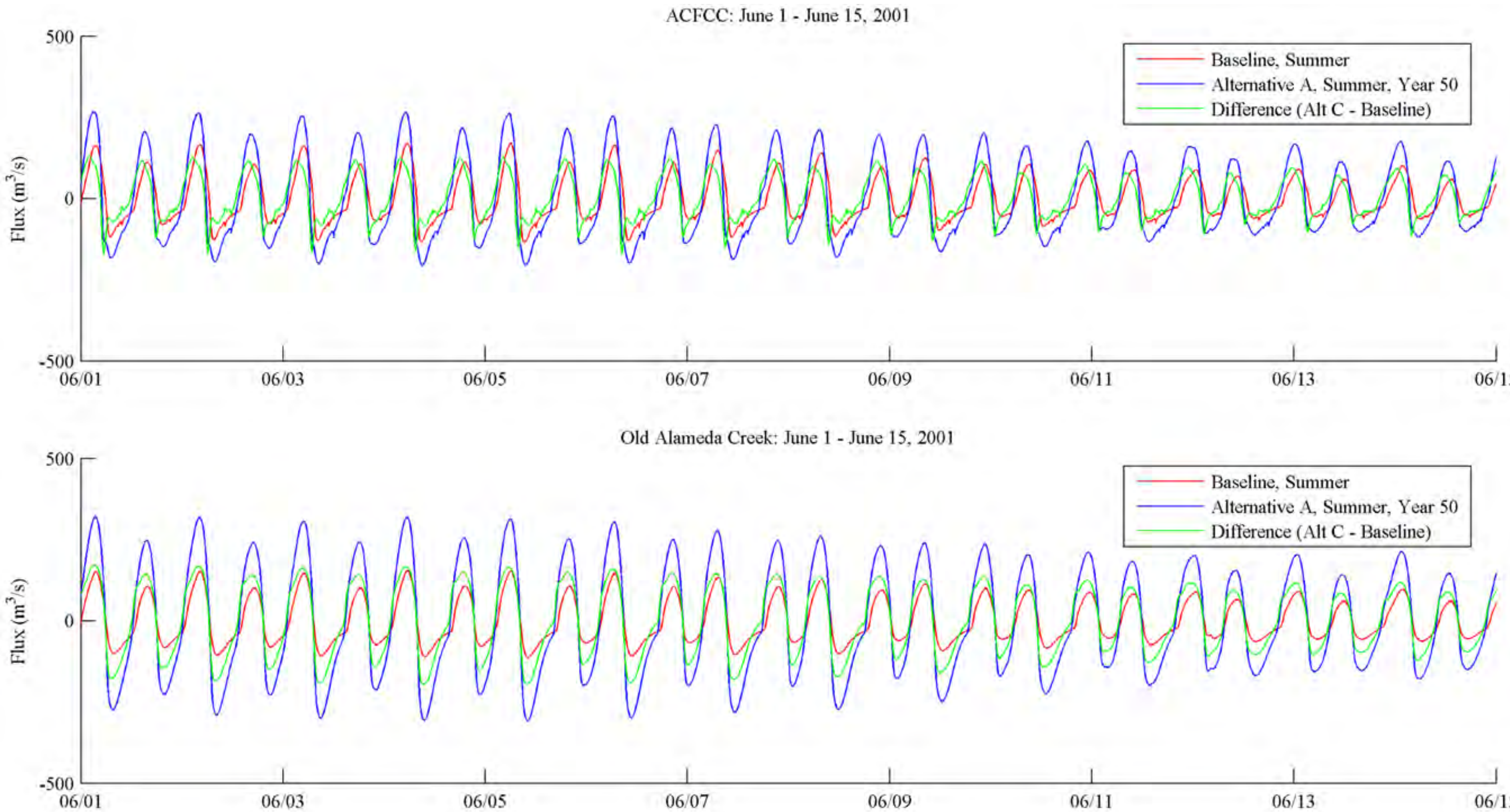

figure *6-32*

South Bay Salt Pond Restoration Project

Tidal Prism, ACFCC and Old Alameda Creek, Alt A, Year 50, Summer

PWA

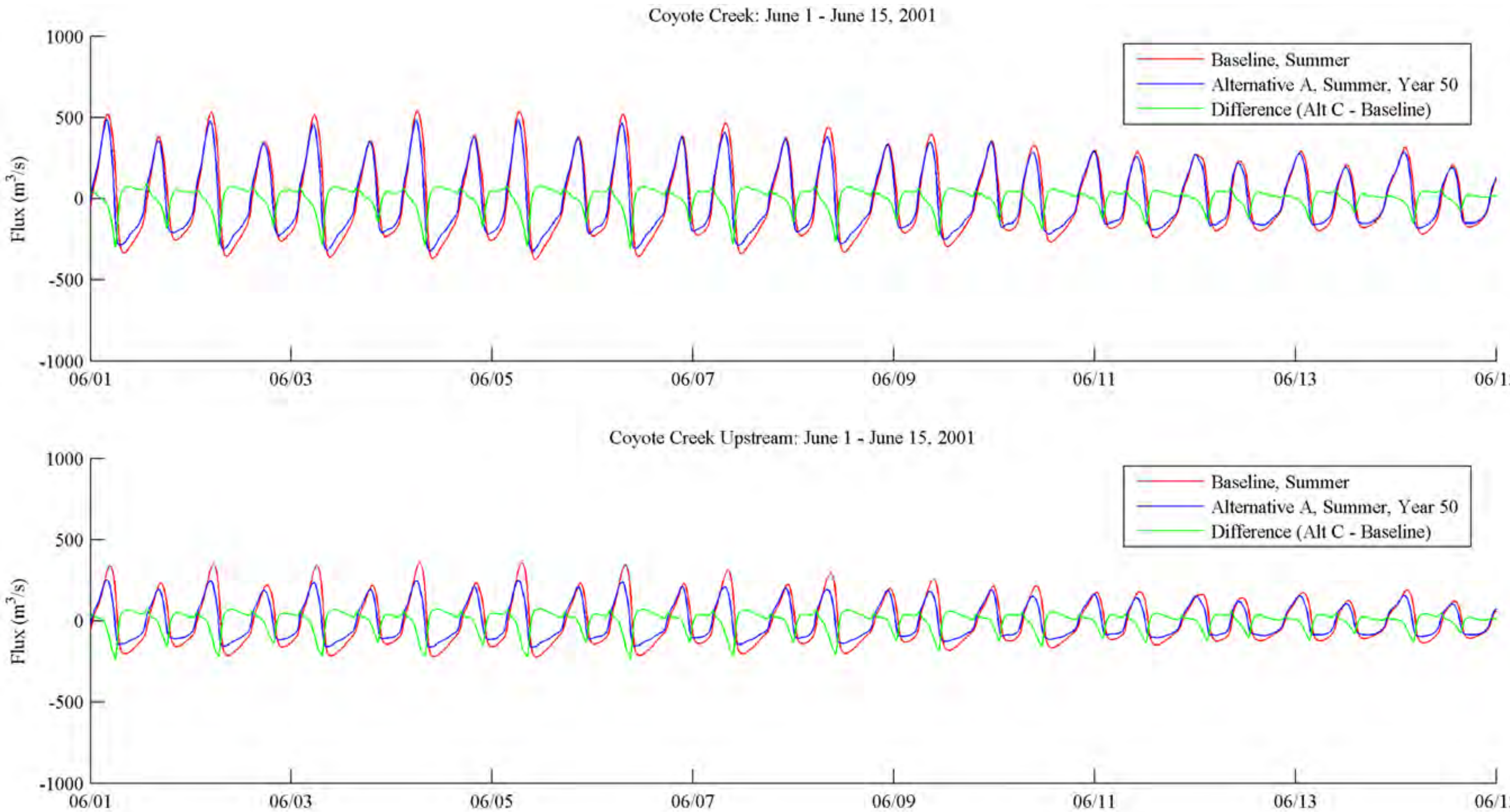

figure 6-33

South Bay Salt Pond Restoration Project

Tidal Prism, Coyote Creek, Alt A, Year 50, Summer

PWA

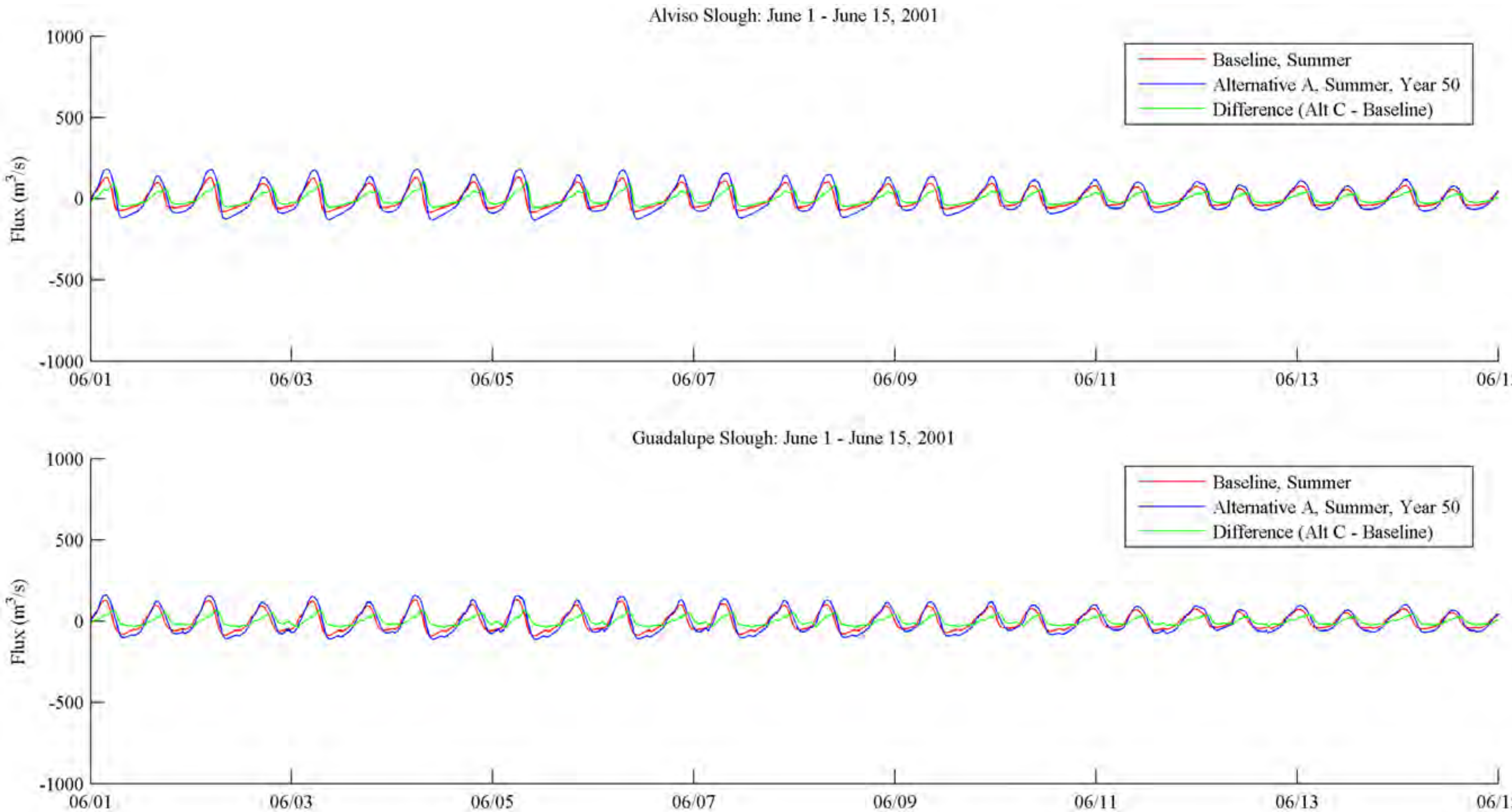

figure *6-34*

South Bay Salt Pond Restoration Project

Tidal Prism, Alviso and Guadalupe Sloughs, Alt A, Year 50, Summer

PWA

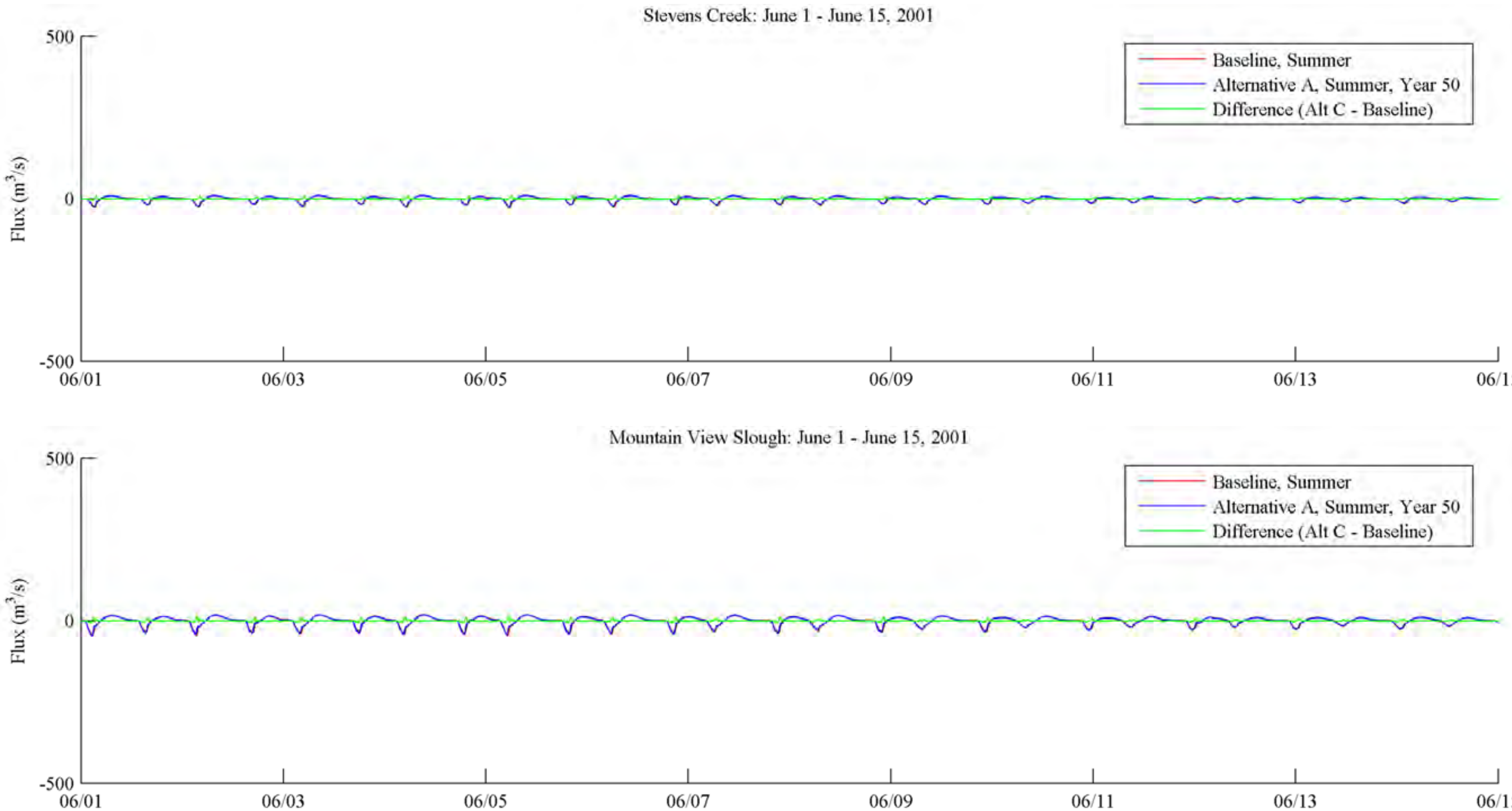

figure 6-35

South Bay Salt Pond Restoration Project

Tidal Prism, Stevens Creek and Mountain View Slough, Alt A, Year 50, Summer

PWA

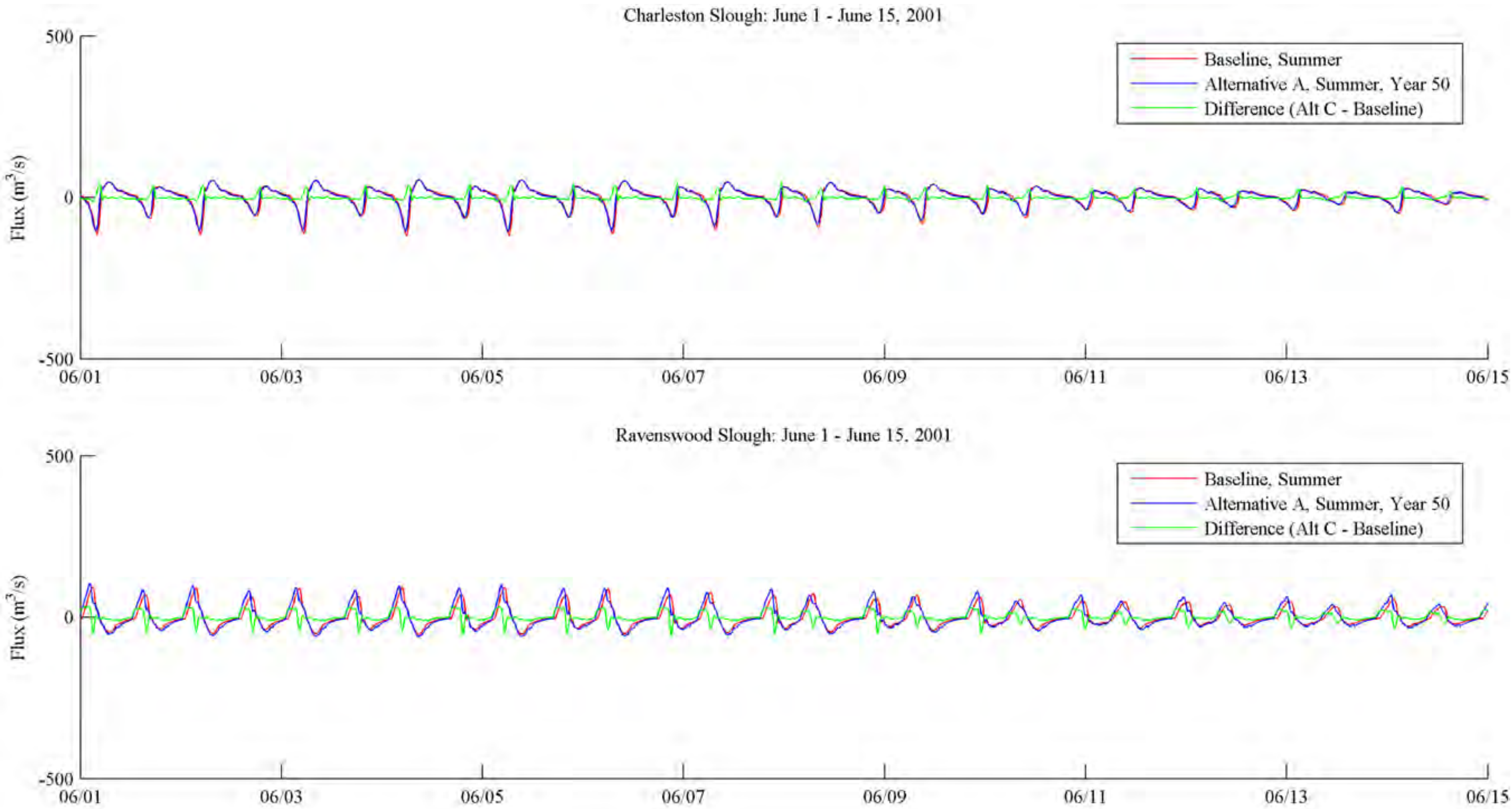

figure *6-36*

South Bay Salt Pond Restoration Project

Tidal Prism, Charleston and Ravenswood Sloughs, Alt A, Year 50, Summer

PWA

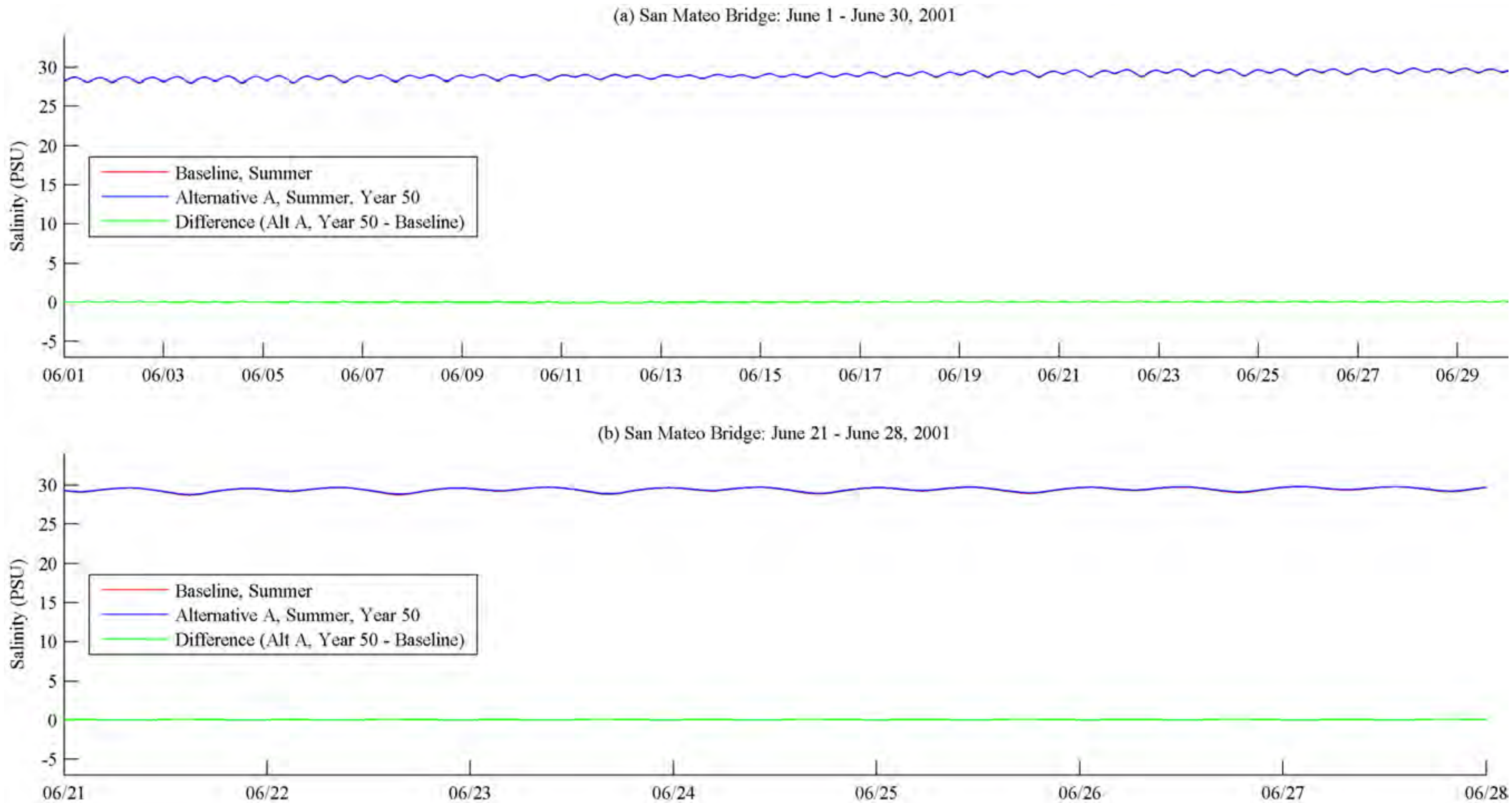

figure *6-37*

South Bay Salt Pond Restoration Project

Salinity, San Mateo Bridge, Alt A, Year 50, Summer

PWA

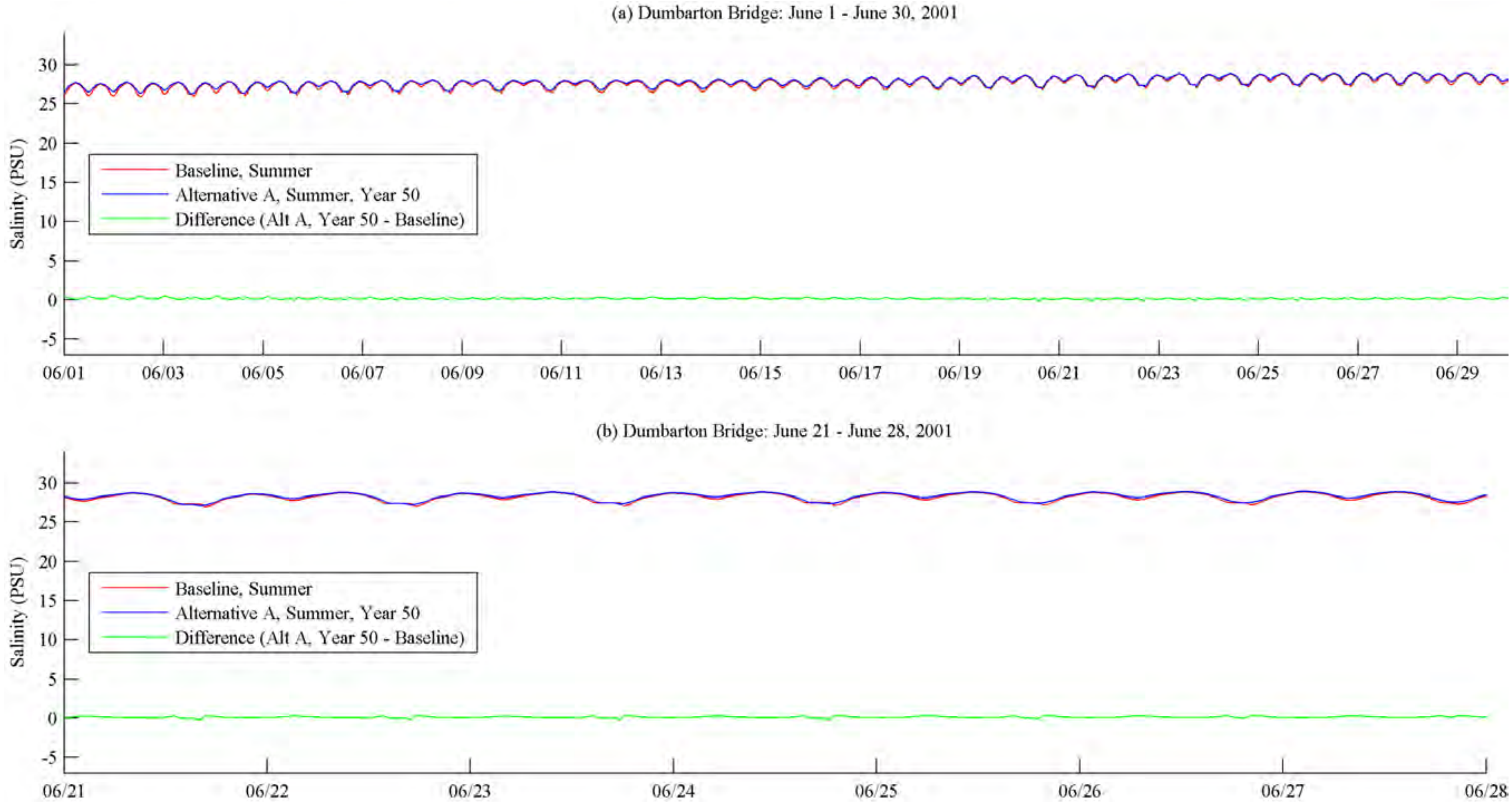

figure *6-38*

South Bay Salt Pond Restoration Project

Salinity, Dumbarton Bridge, Alt A, Year 50, Summer

PWA

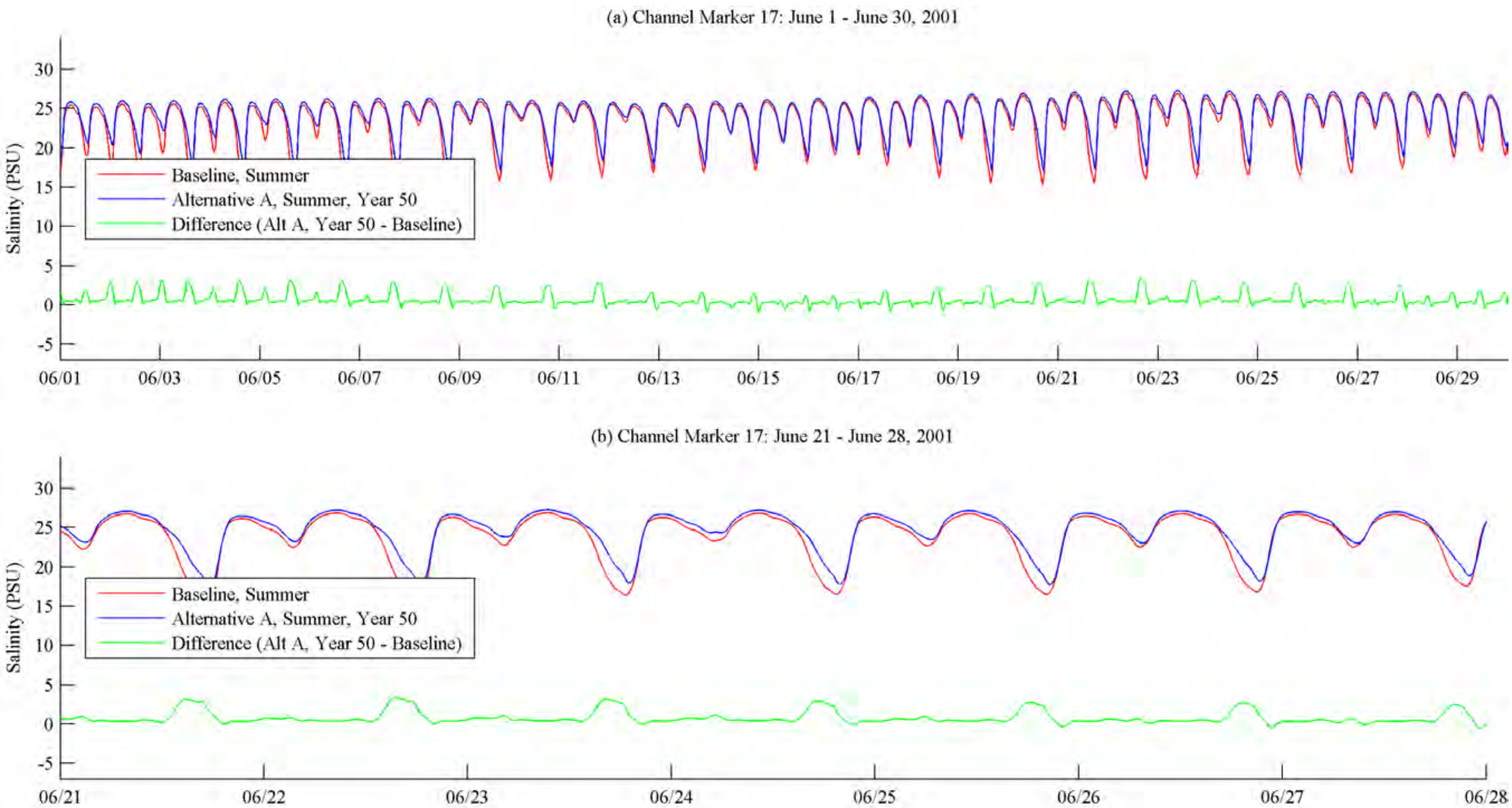

figure 6-39

South Bay Salt Pond Restoration Project

Salinity, Channel Marker 17, Alt A, Year 50, Summer

PWA

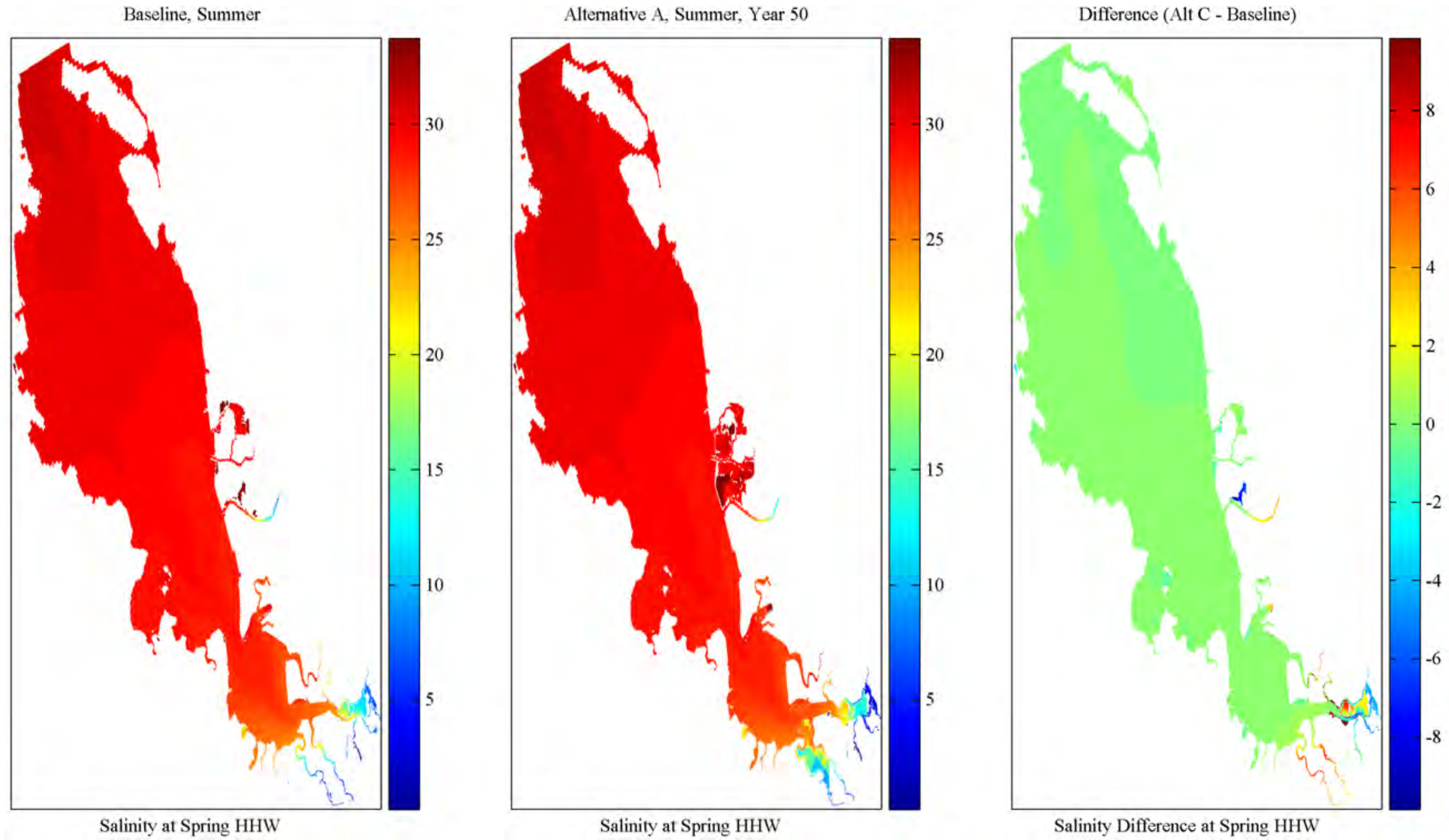

Note: Units shown are PSU

figure *6-40*

South Bay Salt Pond Restoration Project

Salinity at Spring HHW, Alt A, Year 50, Summer

PWA

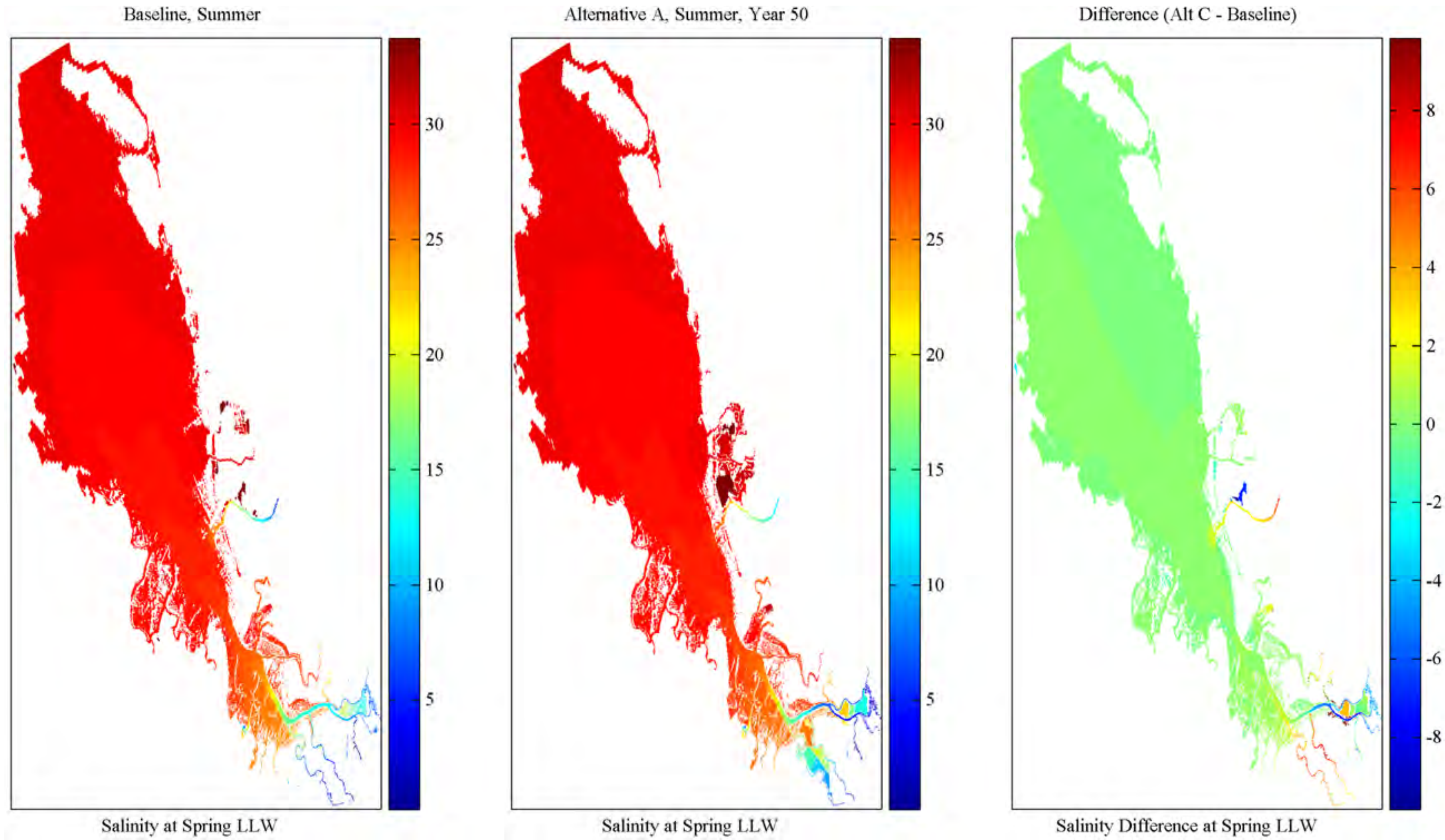

Note: Units shown are PSU

figure *6-41*

South Bay Salt Pond Restoration Project

Salinity at Spring LLW, Alt A, Year 50, Summer

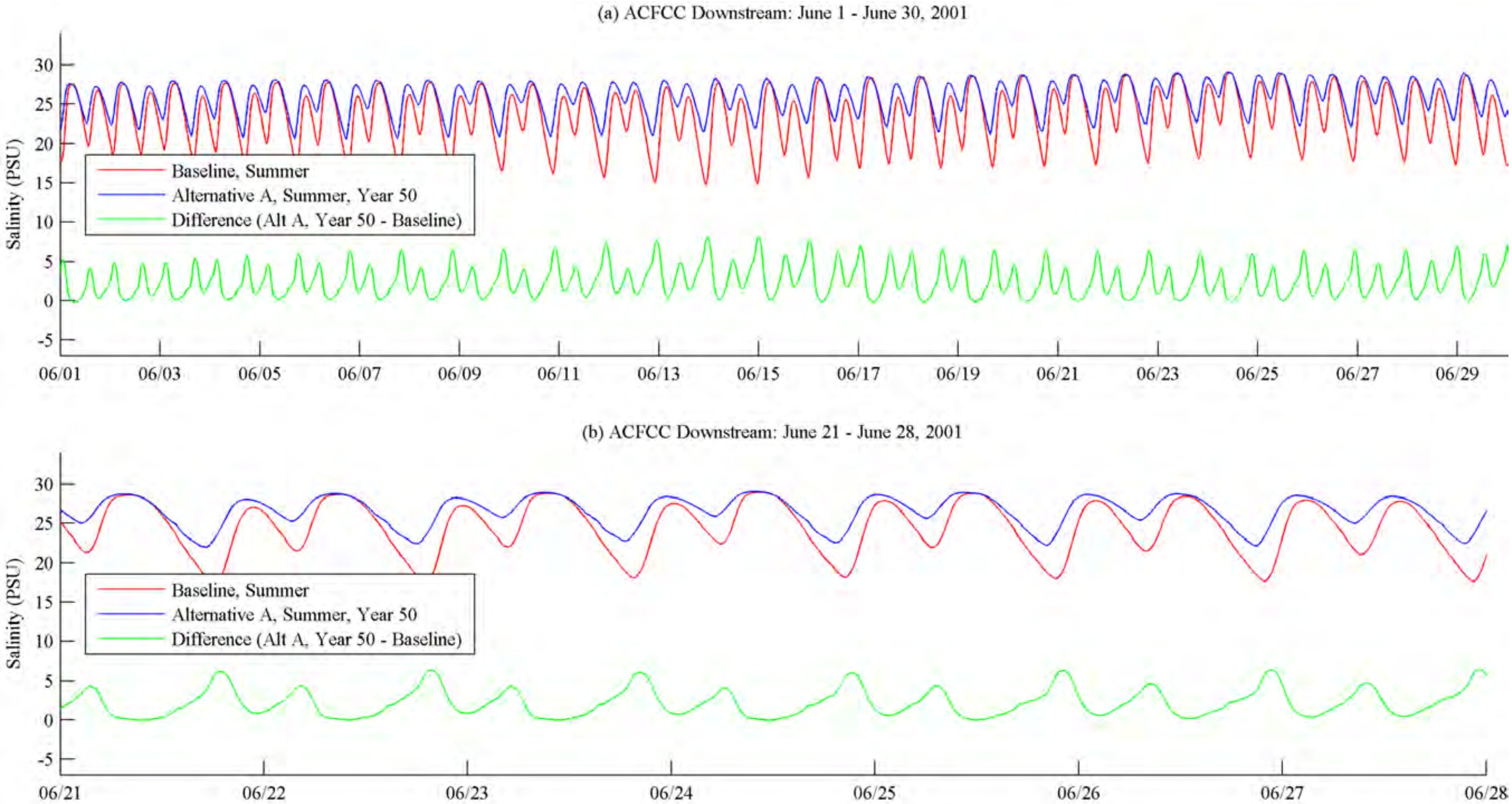

figure *6-42*

South Bay Salt Pond Restoration Project

Salinity, ACFCC Downstream, Alt A, Year 50, Summer

PWA

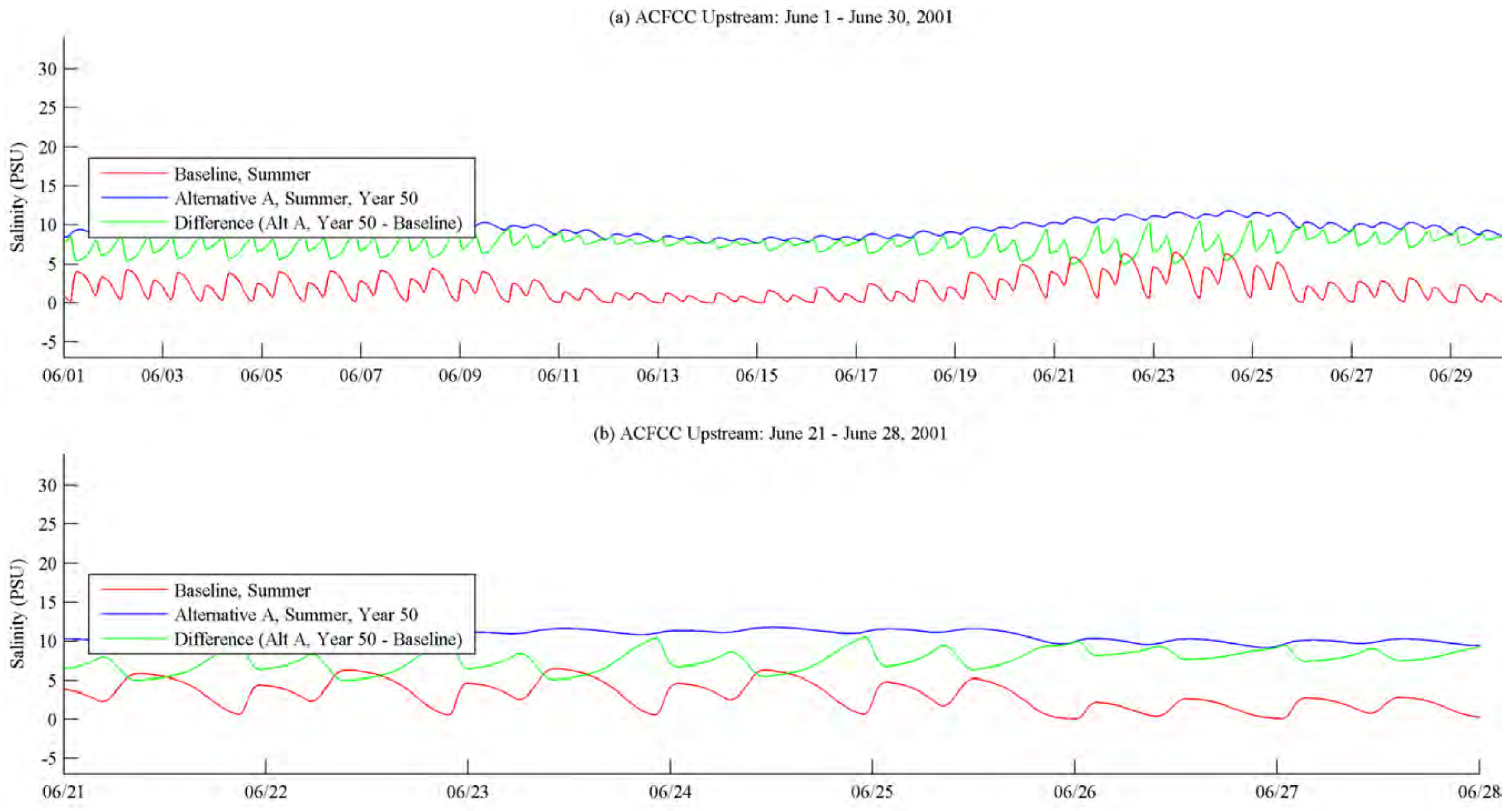

figure *6-43*

South Bay Salt Pond Restoration Project

Salinity, ACFCC Upstream, Alt A, Year 50, Summer

PWA

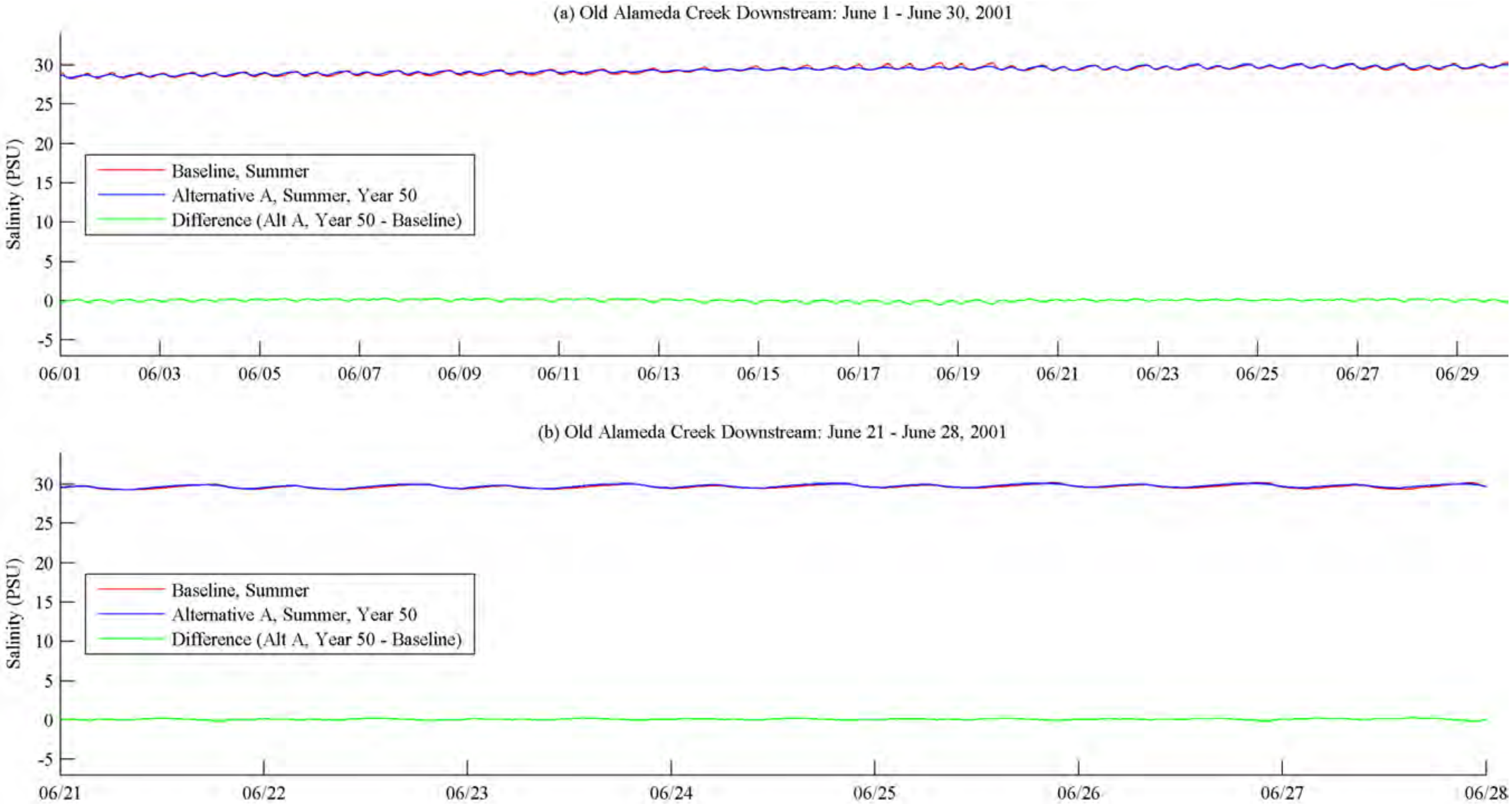

figure 6-44

South Bay Salt Pond Restoration Project

Salinity, Old Alameda Creek Downstream, Alt A, Year 50, Summer

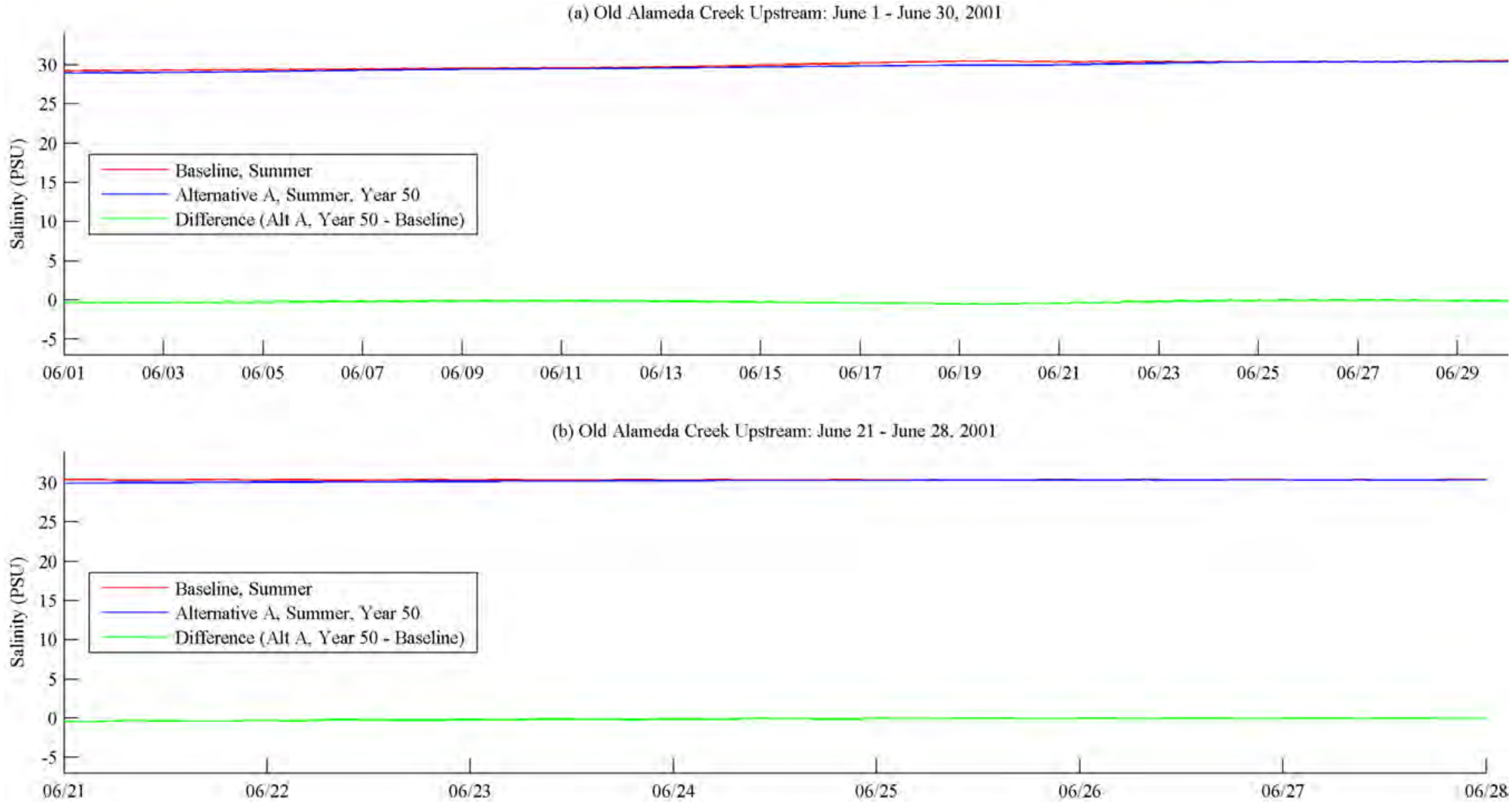

figure 6-45

South Bay Salt Pond Restoration Project

Salinity, Old Alameda Creek Upstream, Alt A, Year 50, Summer

PWA

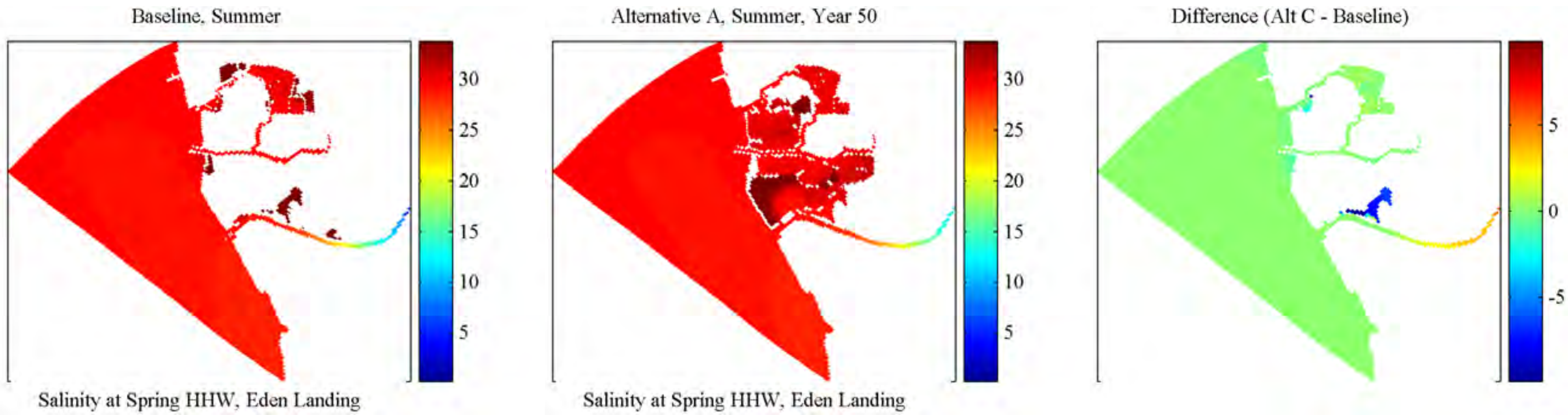

Note: Units shown are PSU

figure 6-46

South Bay Salt Pond Restoration Project

Salinity at Spring HHW, Eden Landing, Alt A, Year 50, Summer

PWA

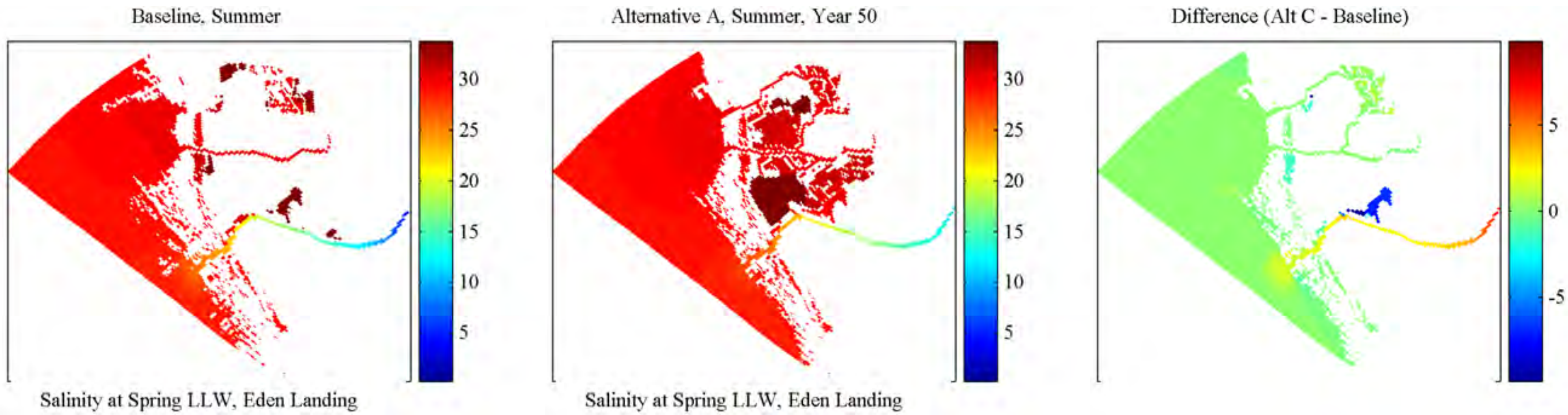

Note: Units shown are PSU

figure *6-47*

South Bay Salt Pond Restoration Project

Salinity at Spring LLW, Eden Landing, Alt A, Year 50, Summer

PWA

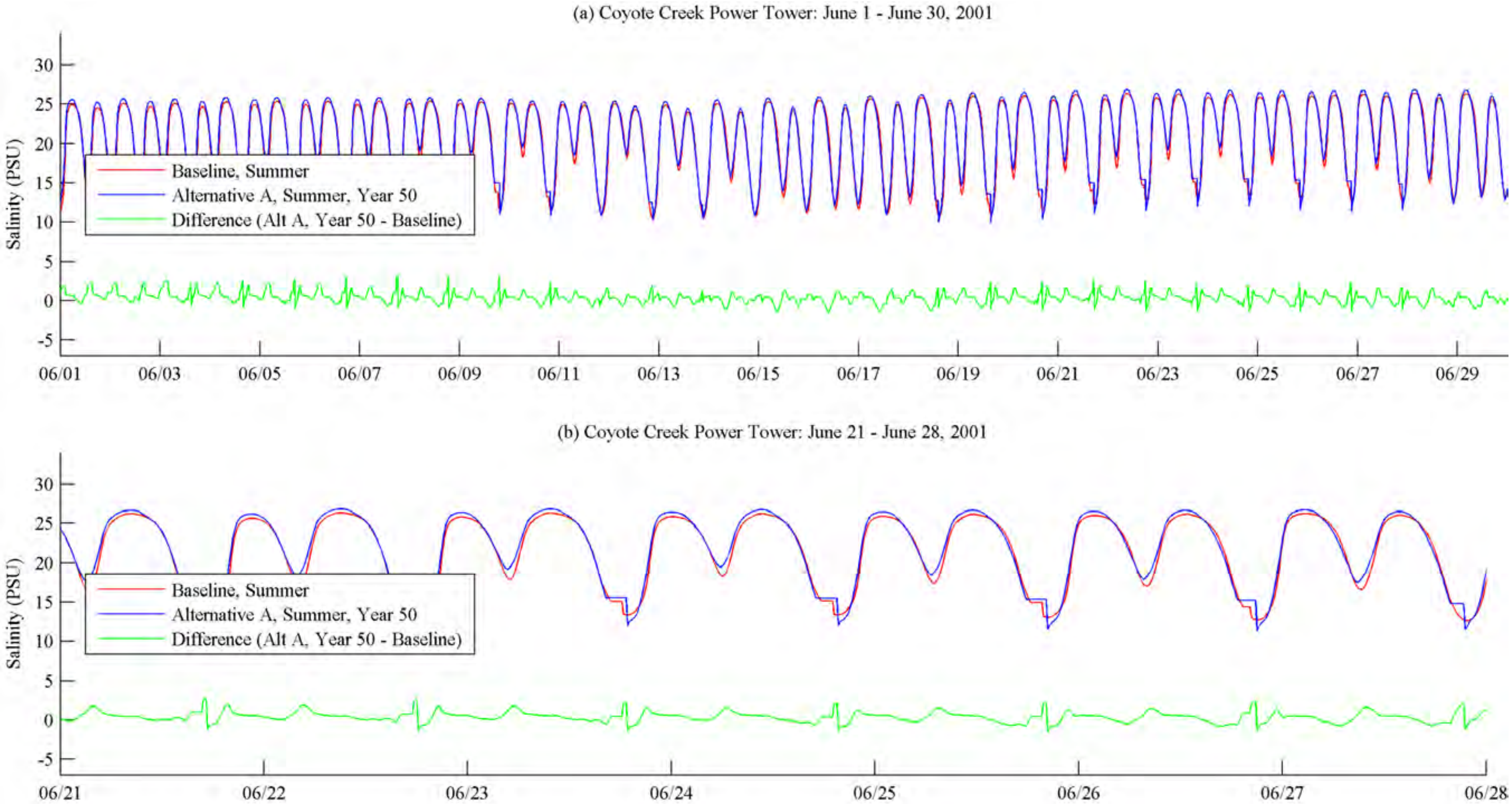

figure 6-48

South Bay Salt Pond Restoration Project

Salinity, Coyote Creek Power Tower, Alt A, Year 50, Summer

PWA

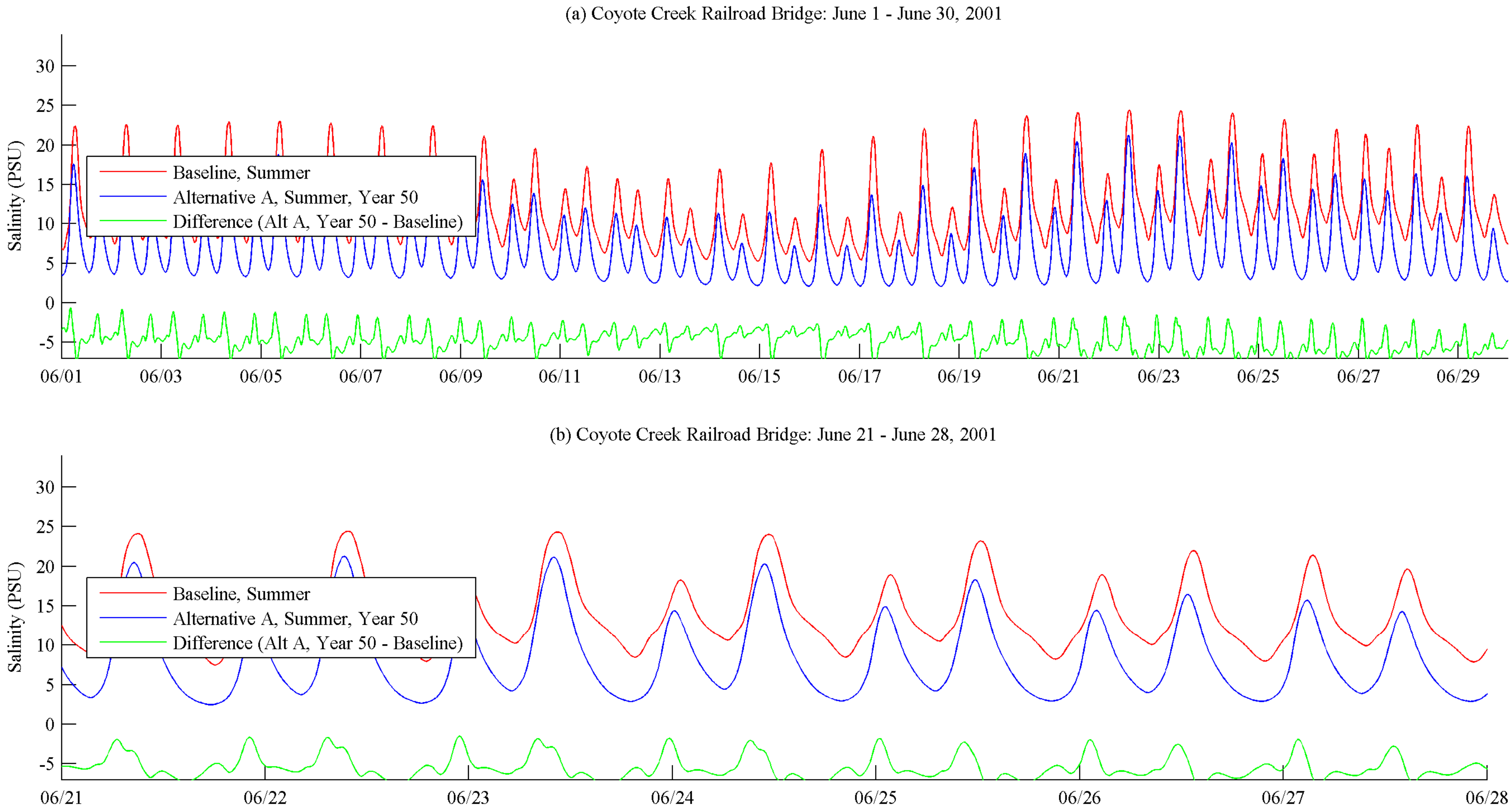

figure *6-49*

South Bay Salt Pond Restoration Project

Salinity, Coyote Creek Railroad Bridge, Alt A, Year 50, Summer

PWA

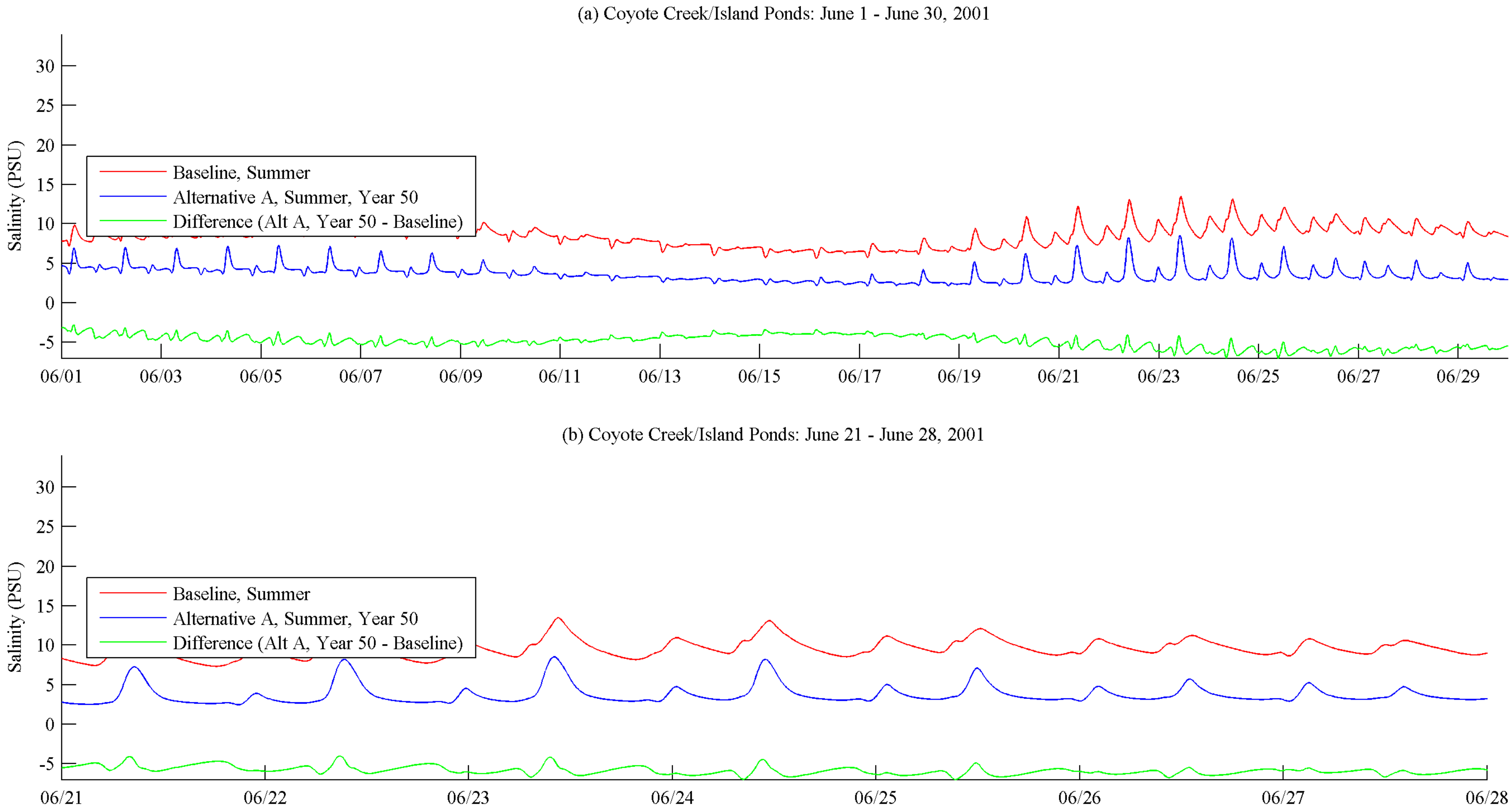

figure 6-50

South Bay Salt Pond Restoration Project

Salinity, Coyote Creek/Island Ponds, Year 50, Summer

PWA

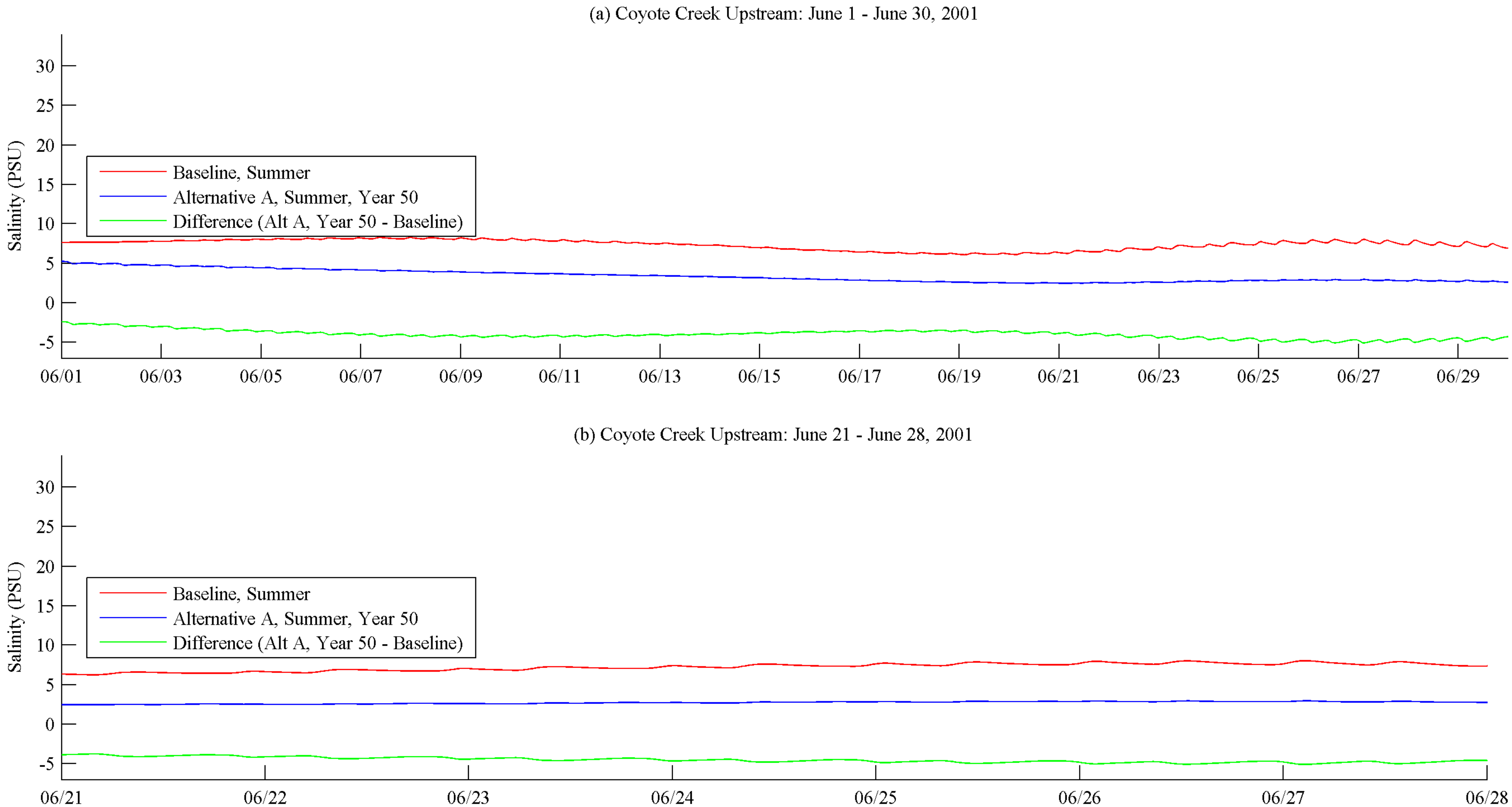

figure 6-51

South Bay Salt Pond Restoration Project

Salinity, Coyote Creek Upstream, Year 50, Summer

PWA

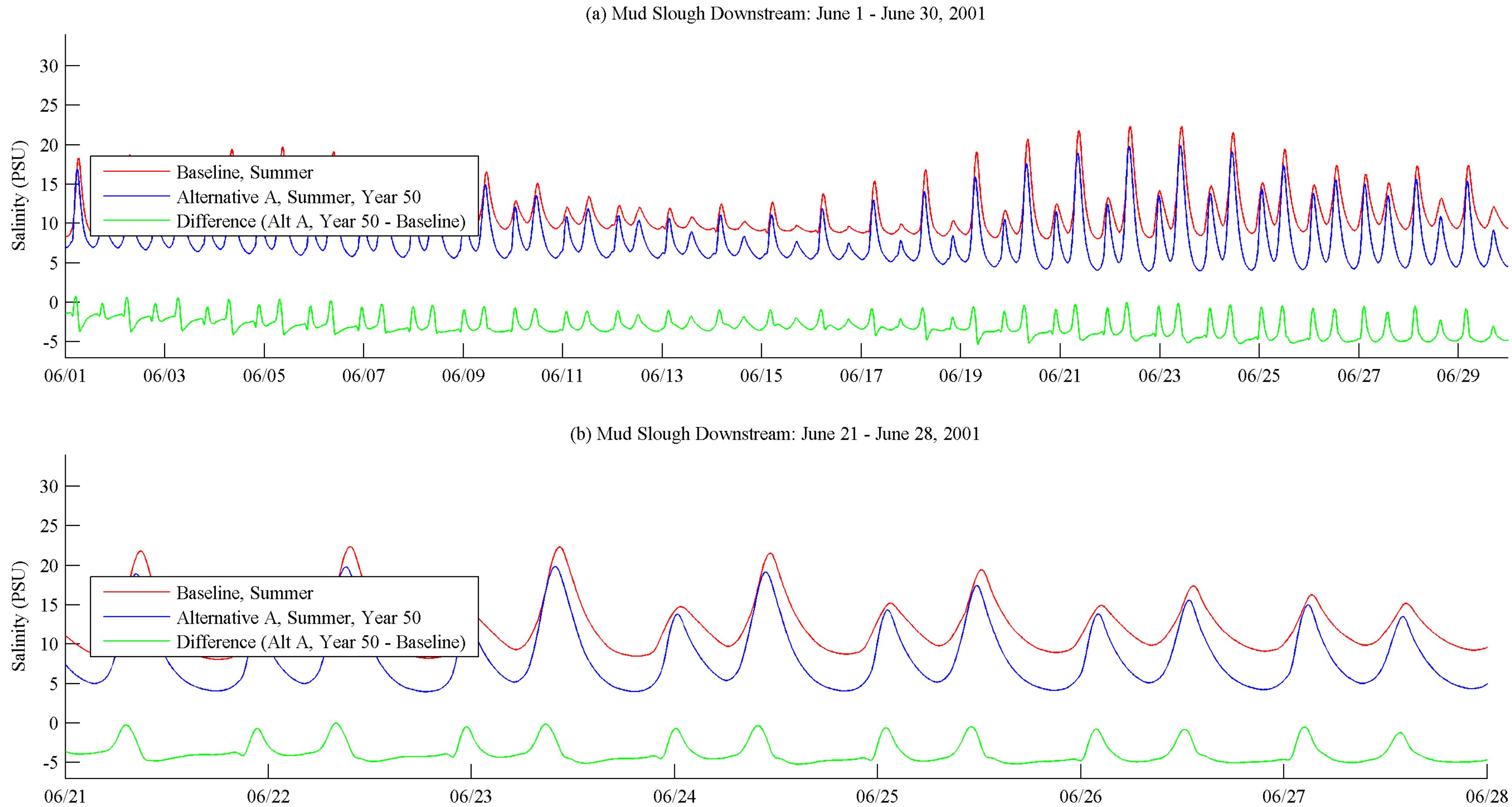

figure 6-52

South Bay Salt Pond Restoration Project

Salinity, Mud Slough Downstream, Alt A, Year 50, Summer

PWA

(a) Mud Slough Upstream: June 1 - June 30, 2001

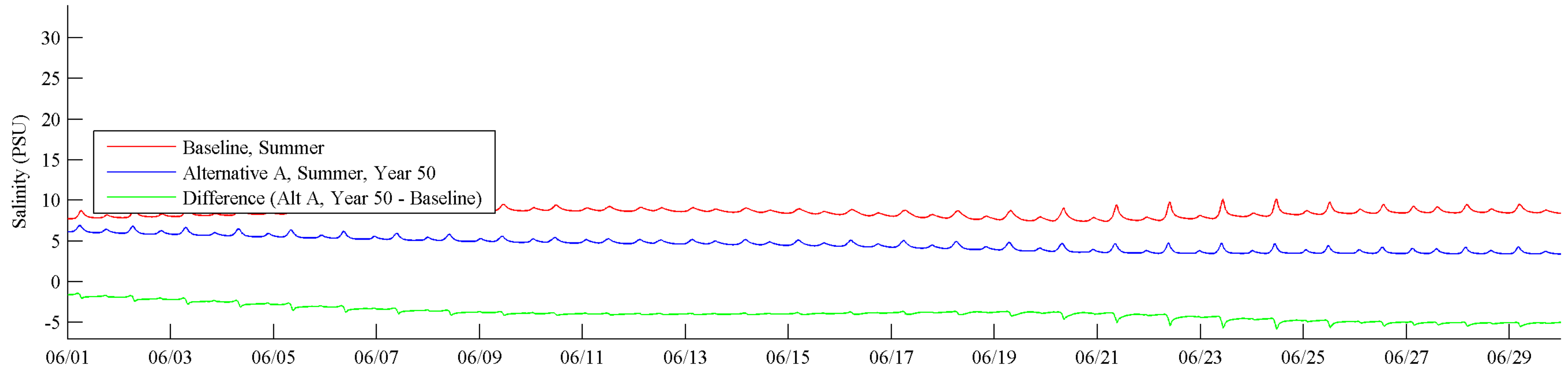

(b) Mud Slough Upstream: June 21 - June 28, 2001

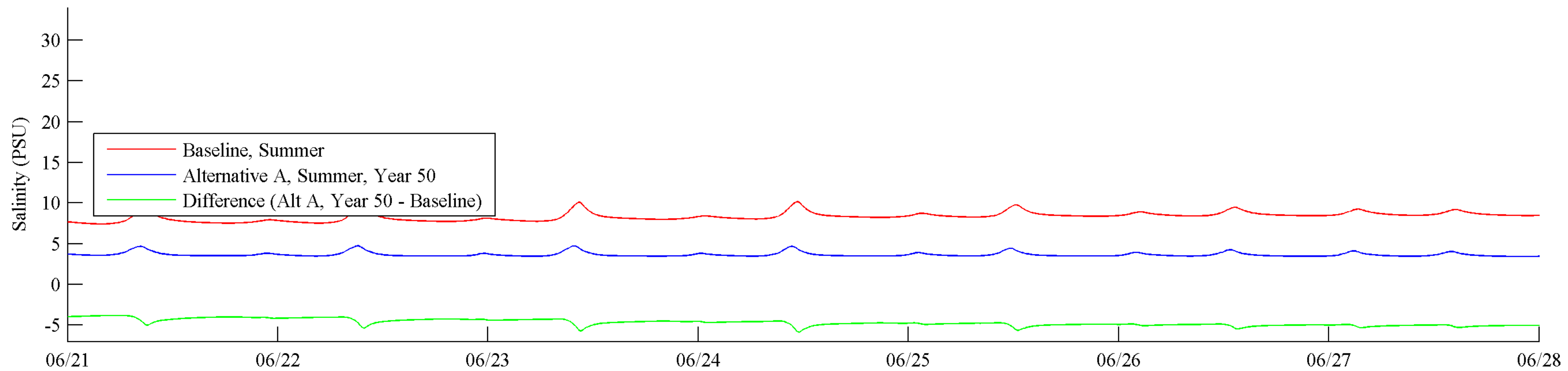

figure 6-53

South Bay Salt Pond Restoration Project

Salinity, Mud Slough Upstream, Alt A, Year 50, Summer

PWA

(a) Alviso Slough Downstream: June 1 - June 30, 2001

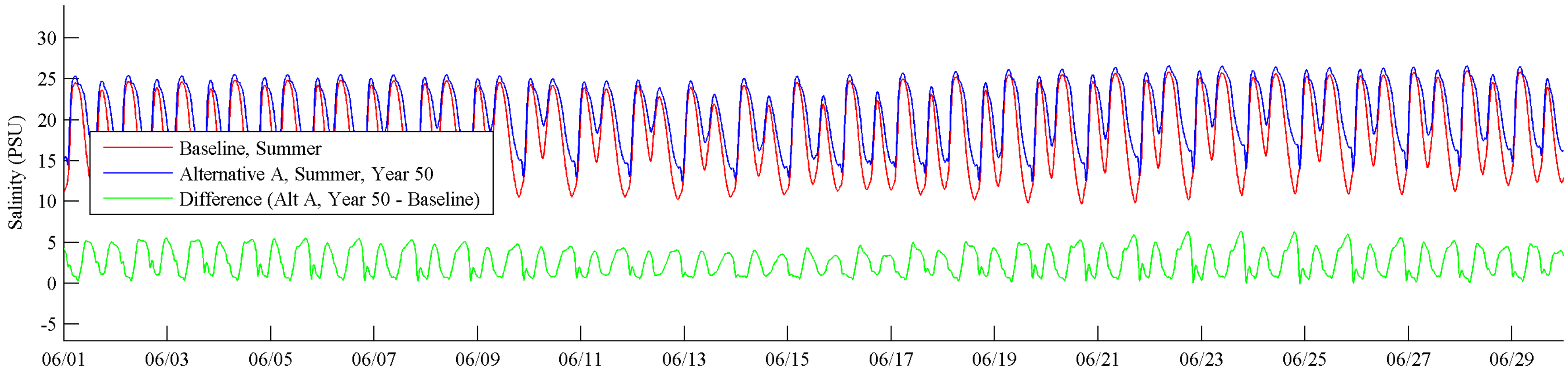

(b) Alviso Slough Downstream: June 21 - June 28, 2001

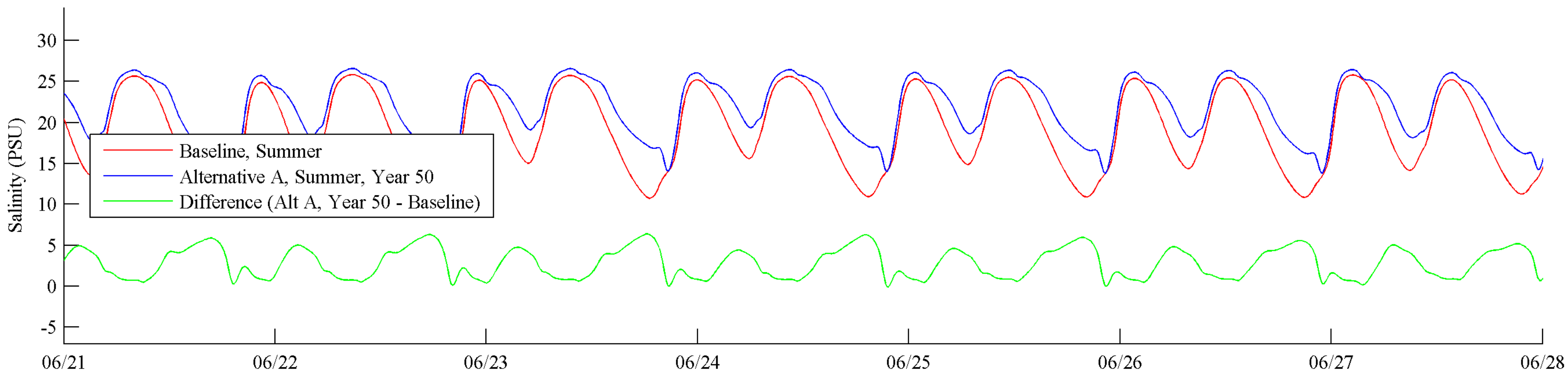

figure 6-54

South Bay Salt Pond Restoration Project

Salinity, Alviso Slough Downstream, Alt A, Year 50, Summer

PWA

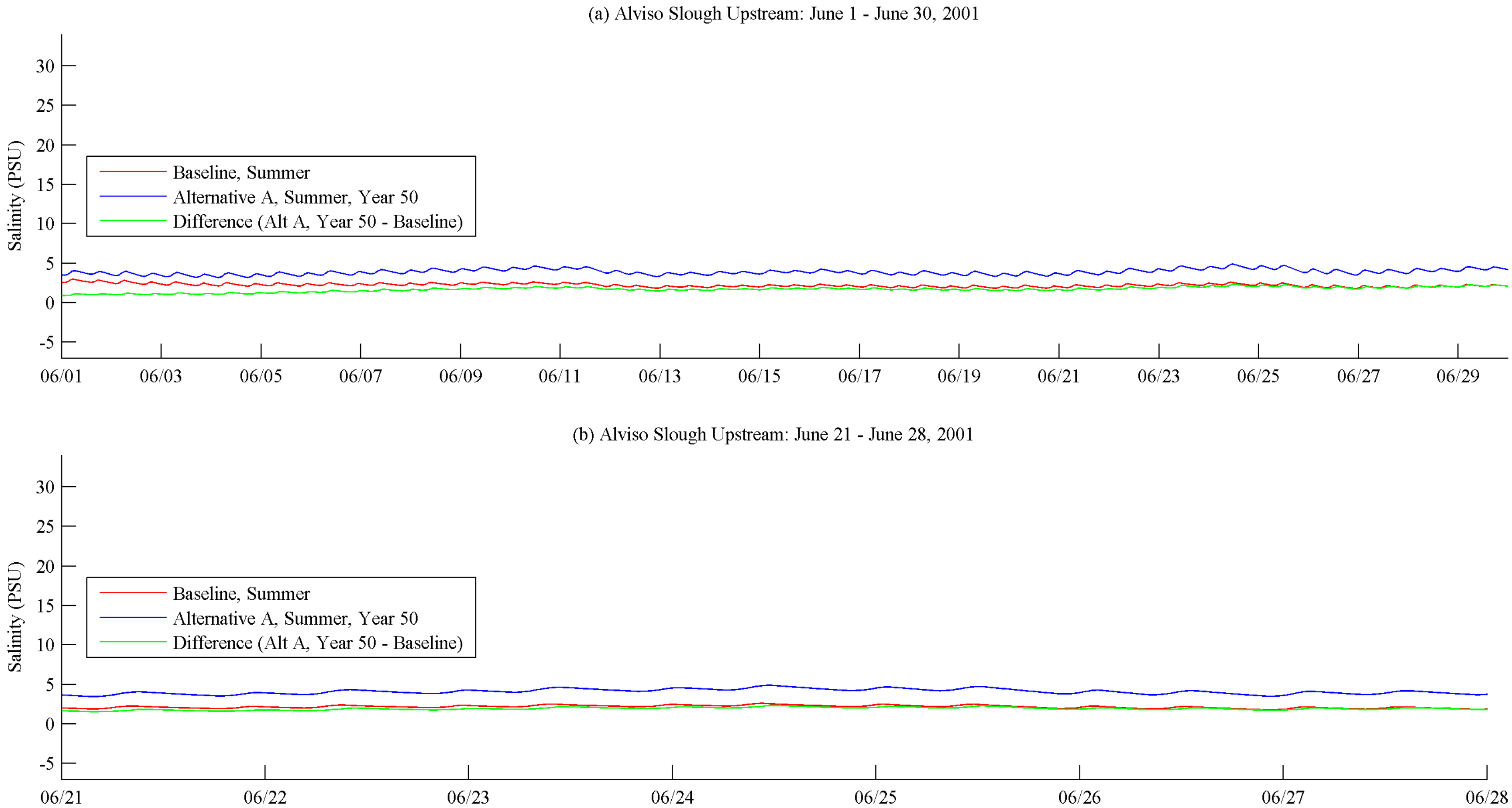

figure 6-55

South Bay Salt Pond Restoration Project

Salinity, Alviso Slough Upstream, Alt A, Year 50, Summer

PWA

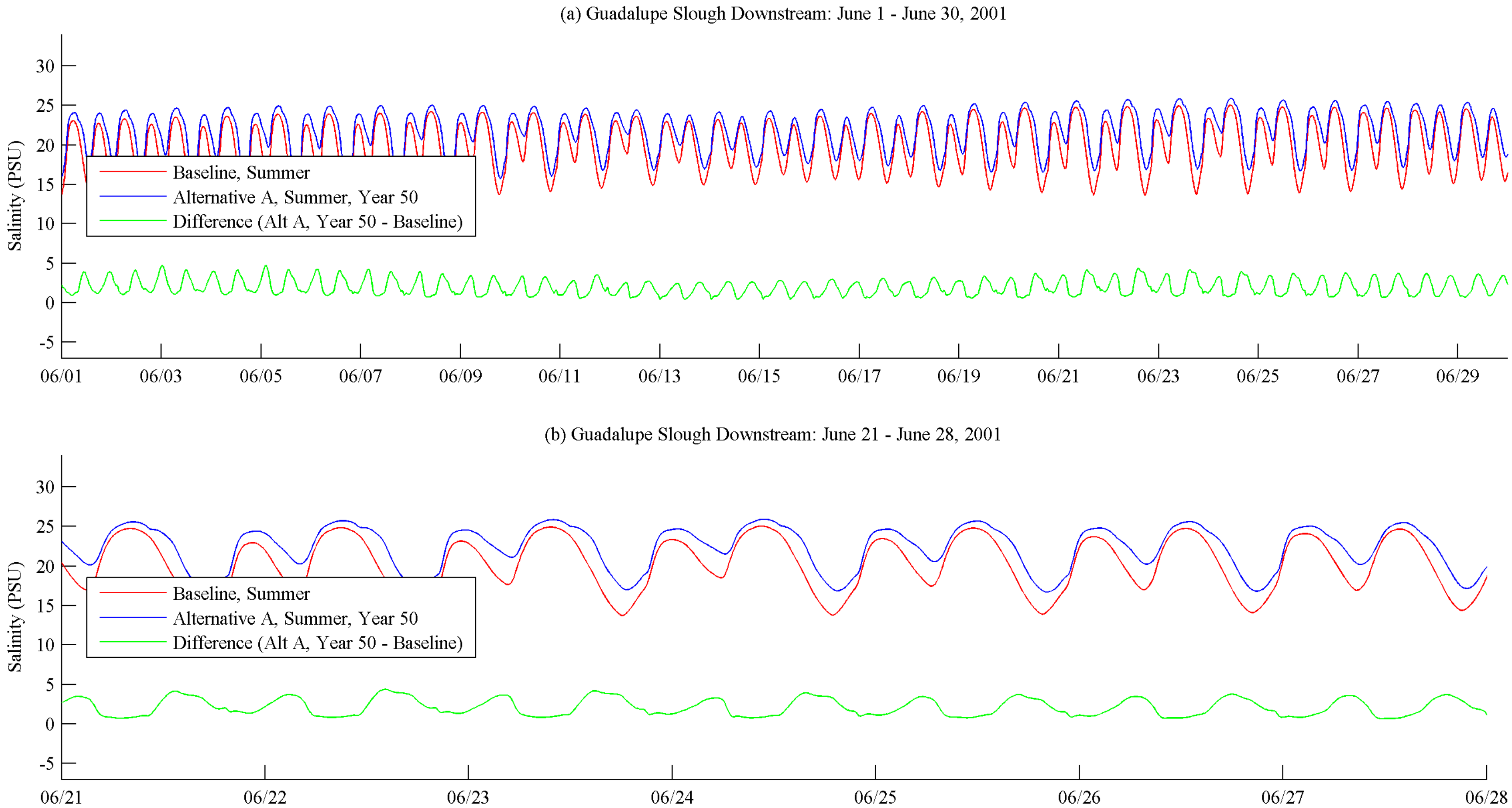

figure 6-56

South Bay Salt Pond Restoration Project

Salinity, Guadalupe Slough Downstream, Alt A, Year 50, Summer

PWA

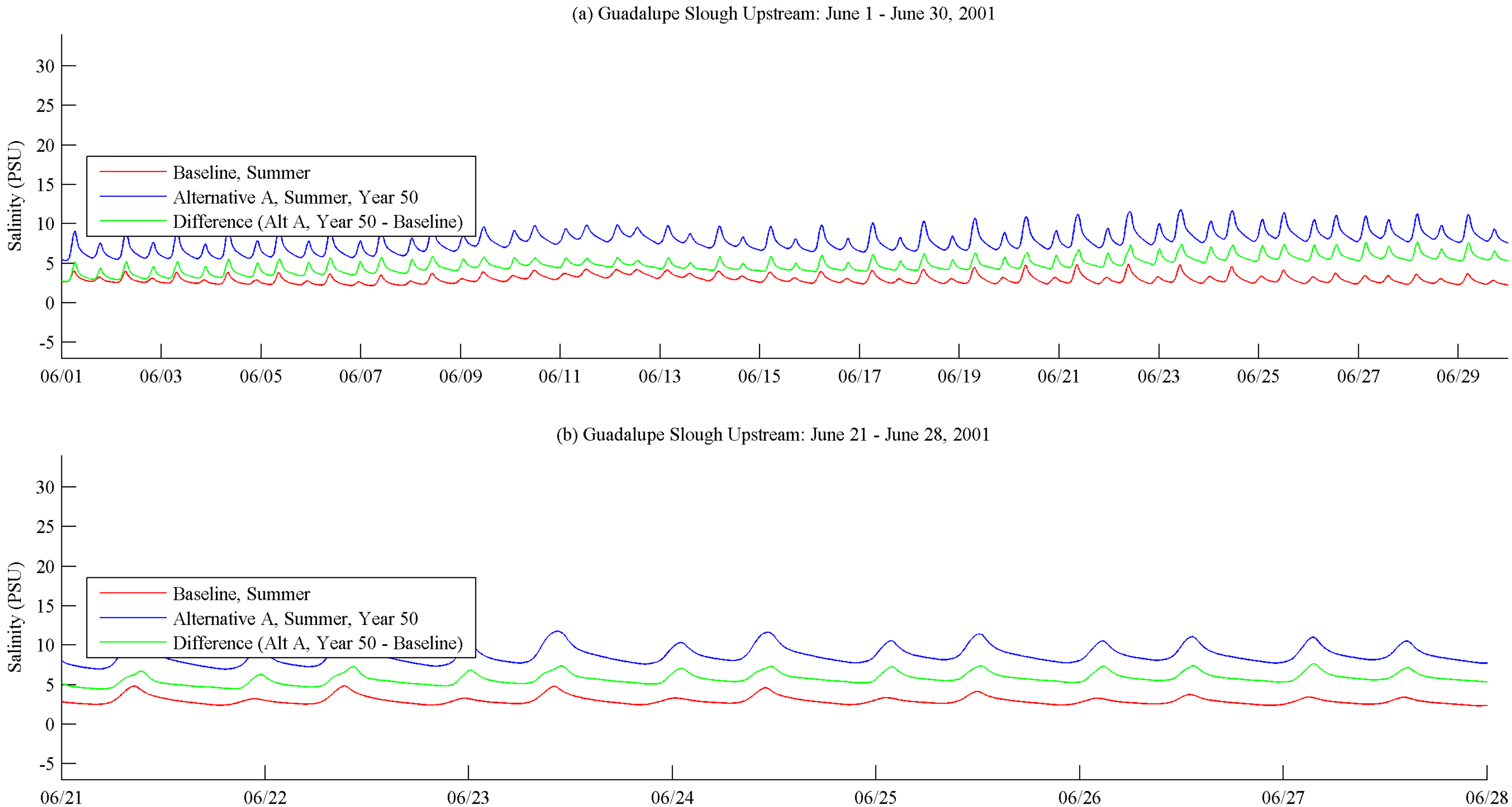

figure 6-57

South Bay Salt Pond Restoration Project

Salinity, Guadalupe Slough Upstream, Alt A, Year 50, Summer

PWA

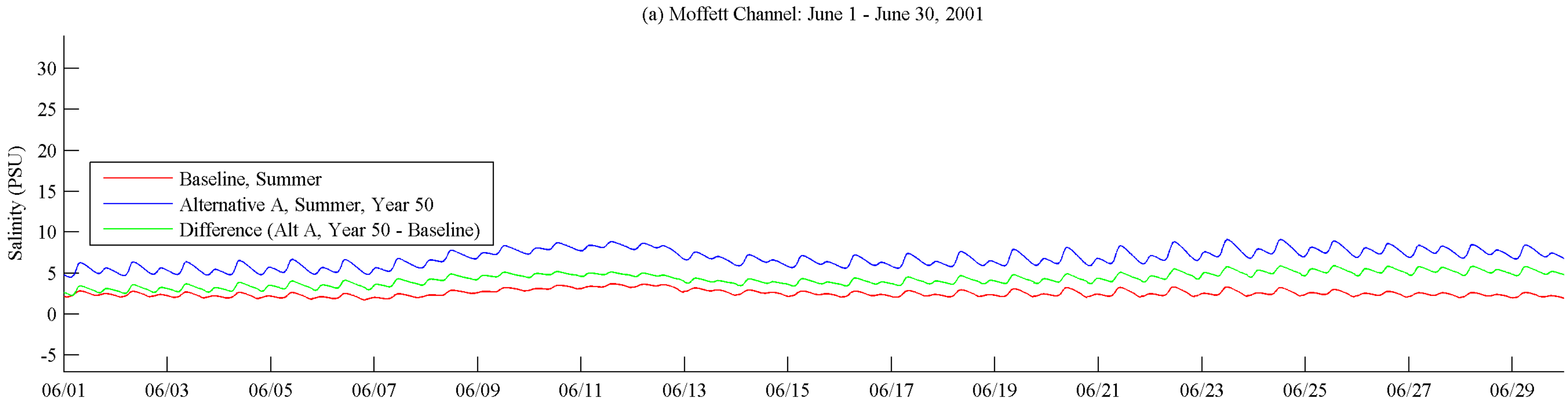

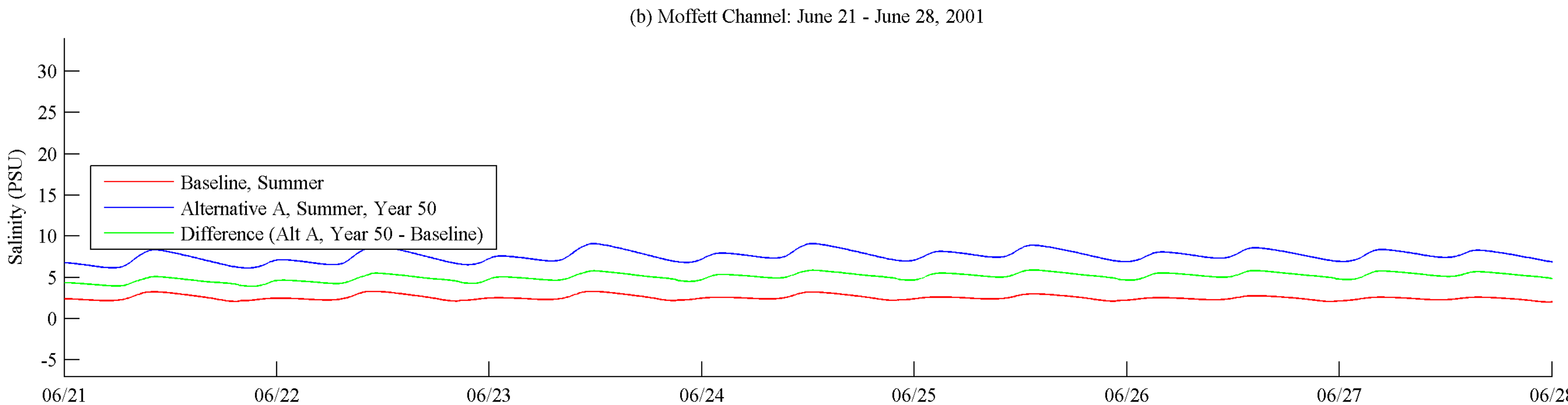

figure 6-58

South Bay Salt Pond Restoration Project

Salinity, Moffett Channel, Alt A, Year 50, Summer

PWA

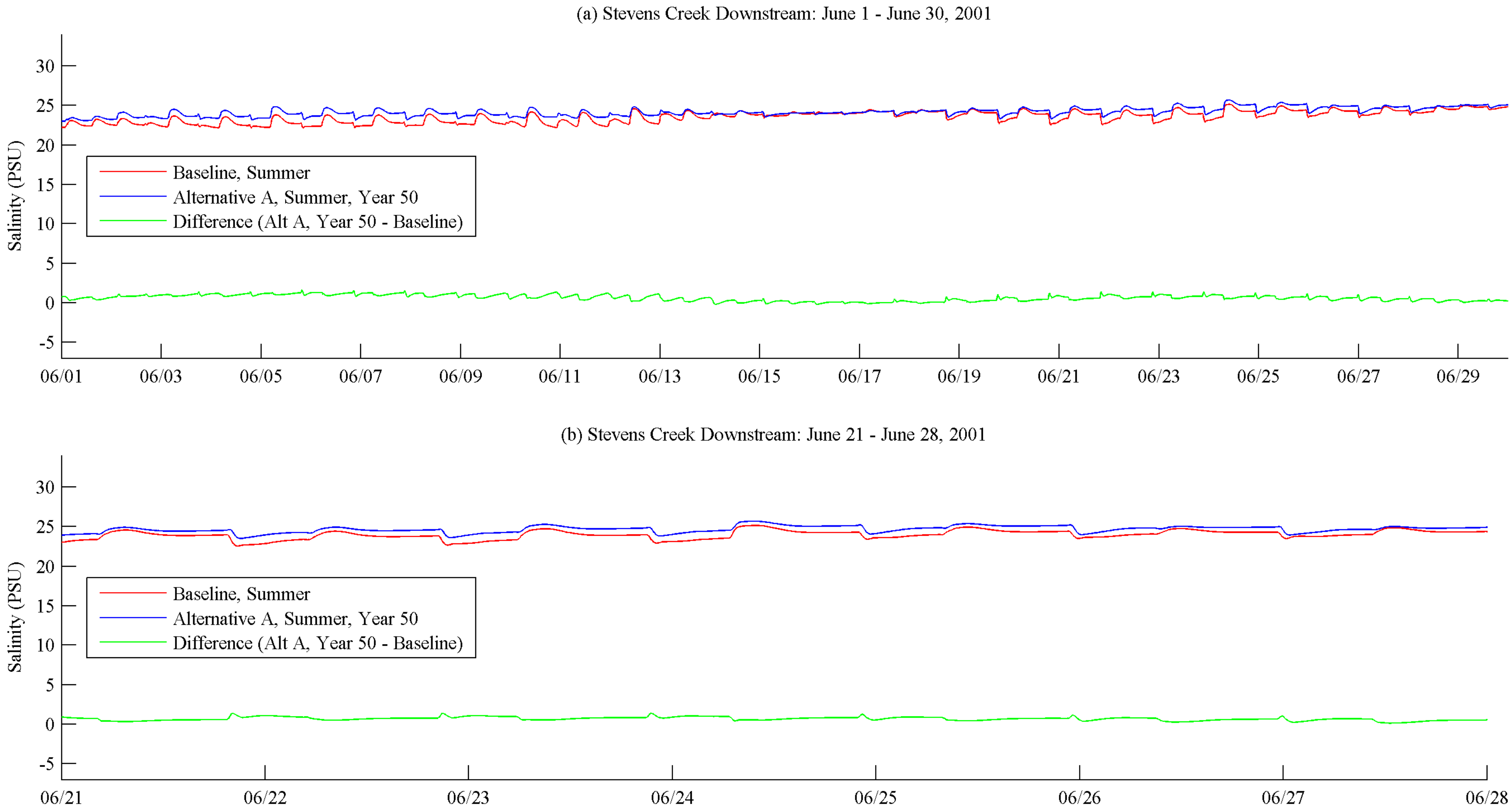

figure 6-59

South Bay Salt Pond Restoration Project

Salinity, Steven Creek Downstream, Alt A, Year 50, Summer

PWA

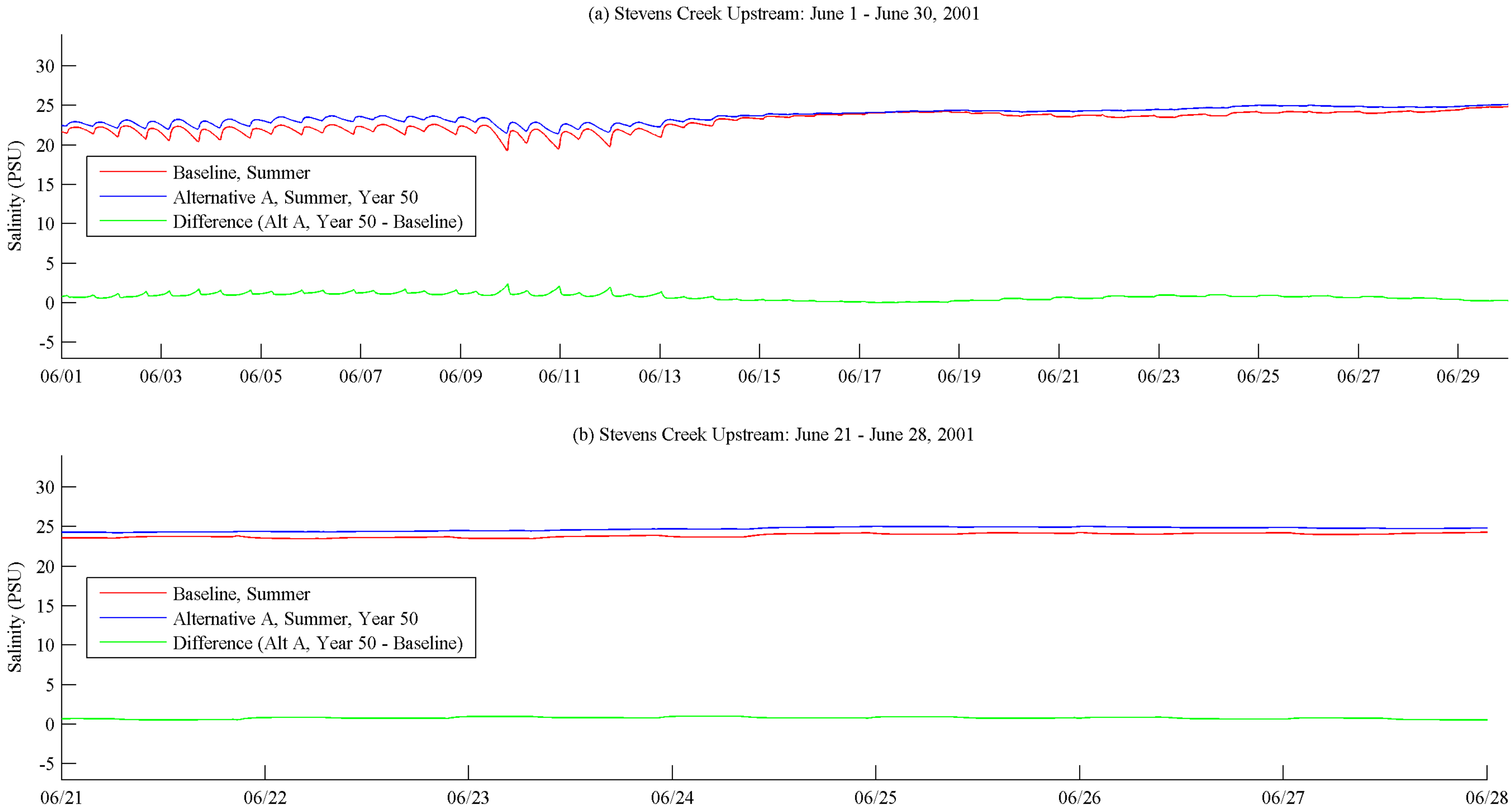

figure *6-60*

South Bay Salt Pond Restoration Project

Salinity, Stevens Creek Upstream, Alt A, Year 50, Summer

PWA

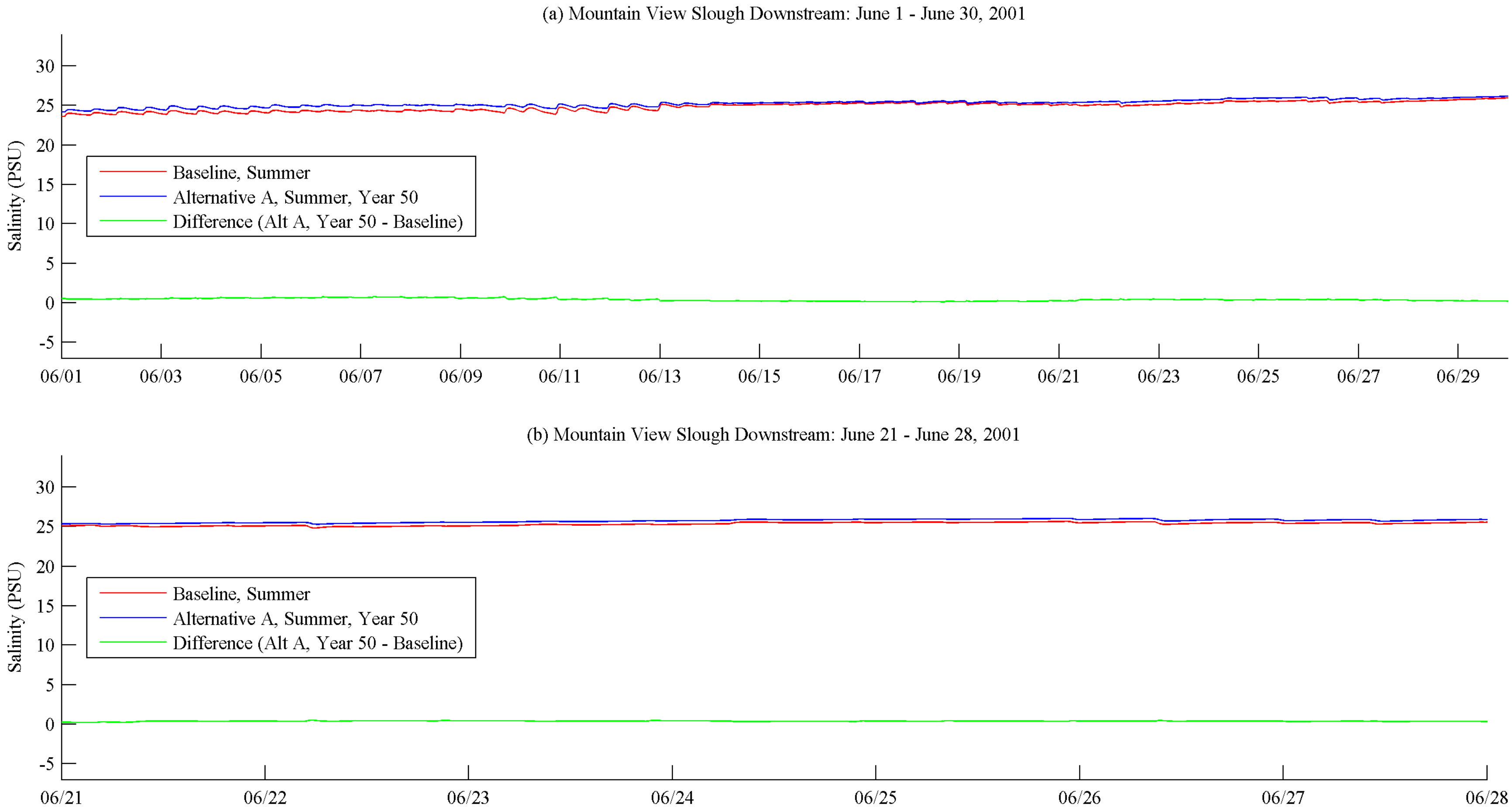

figure 6-61

South Bay Salt Pond Restoration Project

Salinity, Mountain View Slough Downstream, Alt A, Year 50, Summer

PWA

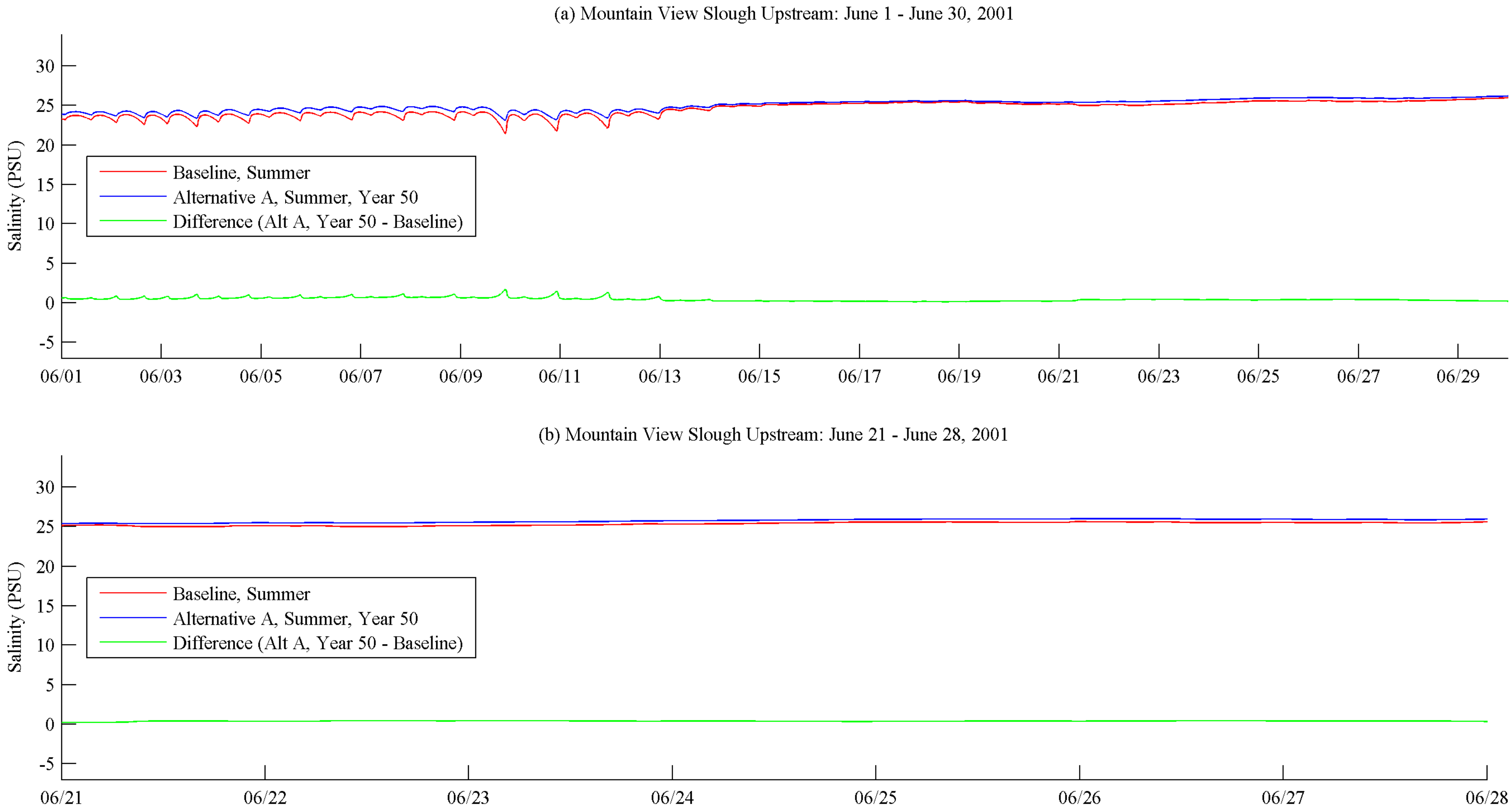

figure 6-62

South Bay Salt Pond Restoration Project

Salinity, Mountain View Slough Upstream, Alt A, Year 50, Summer

PWA

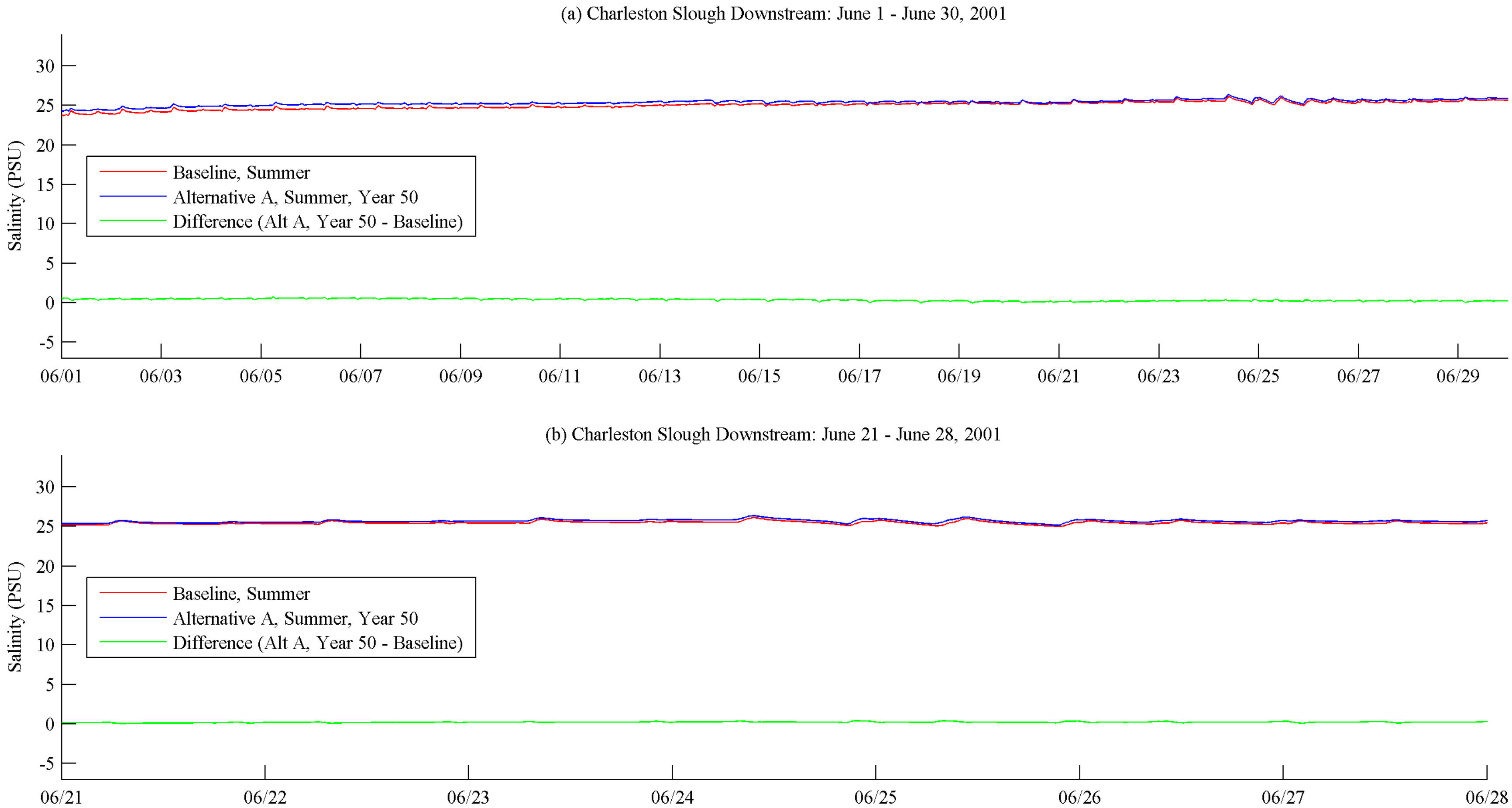

figure 6-63

South Bay Salt Pond Restoration Project

Salinity, Charleston Slough Downstream, Alt A, Year 50, Summer

PWA

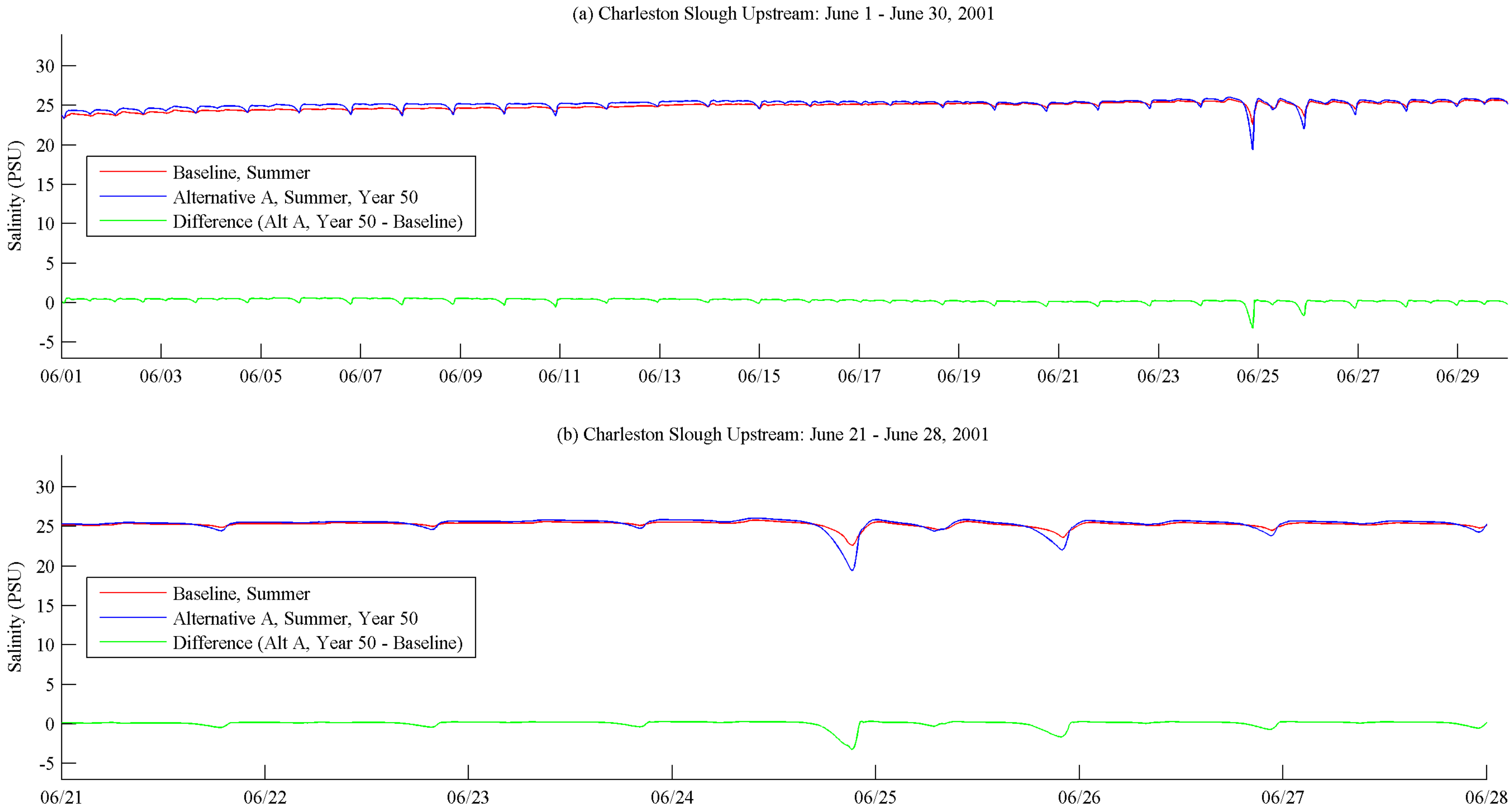

figure 6-64

South Bay Salt Pond Restoration Project

Salinity, Charleston Slough Upstream, Alt A, Year 50, Summer

PWA

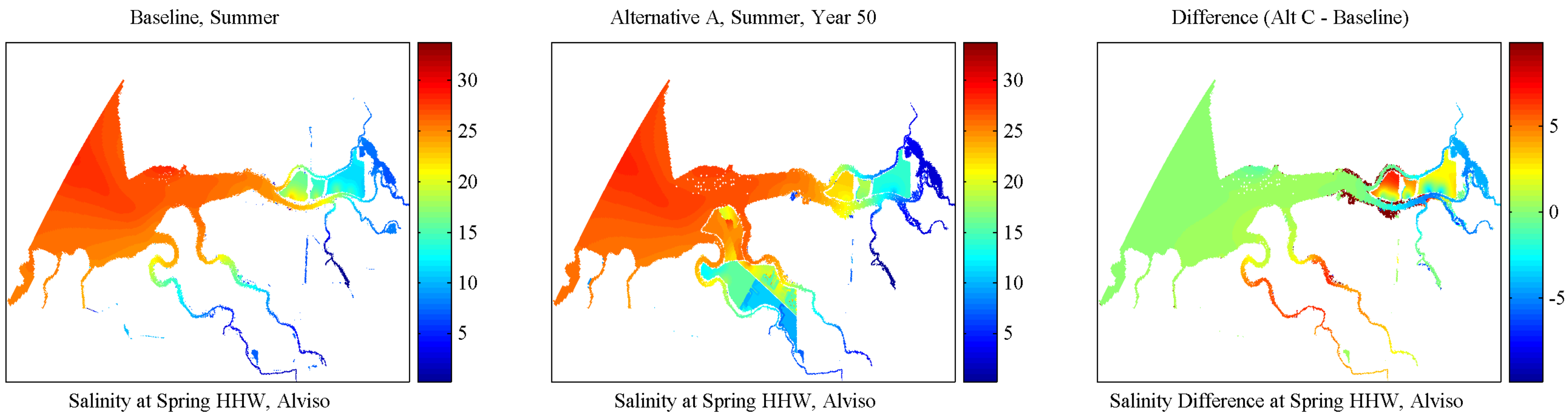

Note: Units shown are PSU

figure *6-65*

South Bay Salt Pond Restoration Project

Salinity at Spring HHW, Alt A, Alviso, Year 50, Summer

PWA

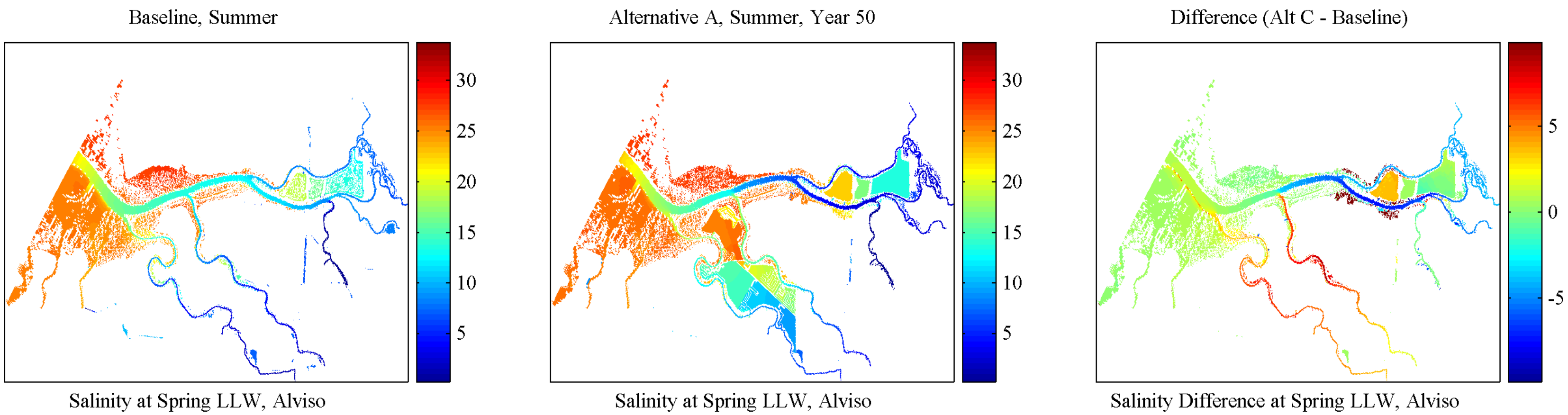

Note: Units shown are PSU

figure 6-66

South Bay Salt Pond Restoration Project

Salinity at Spring LLW, Alt A, Alviso, Year 50, Summer

PWA

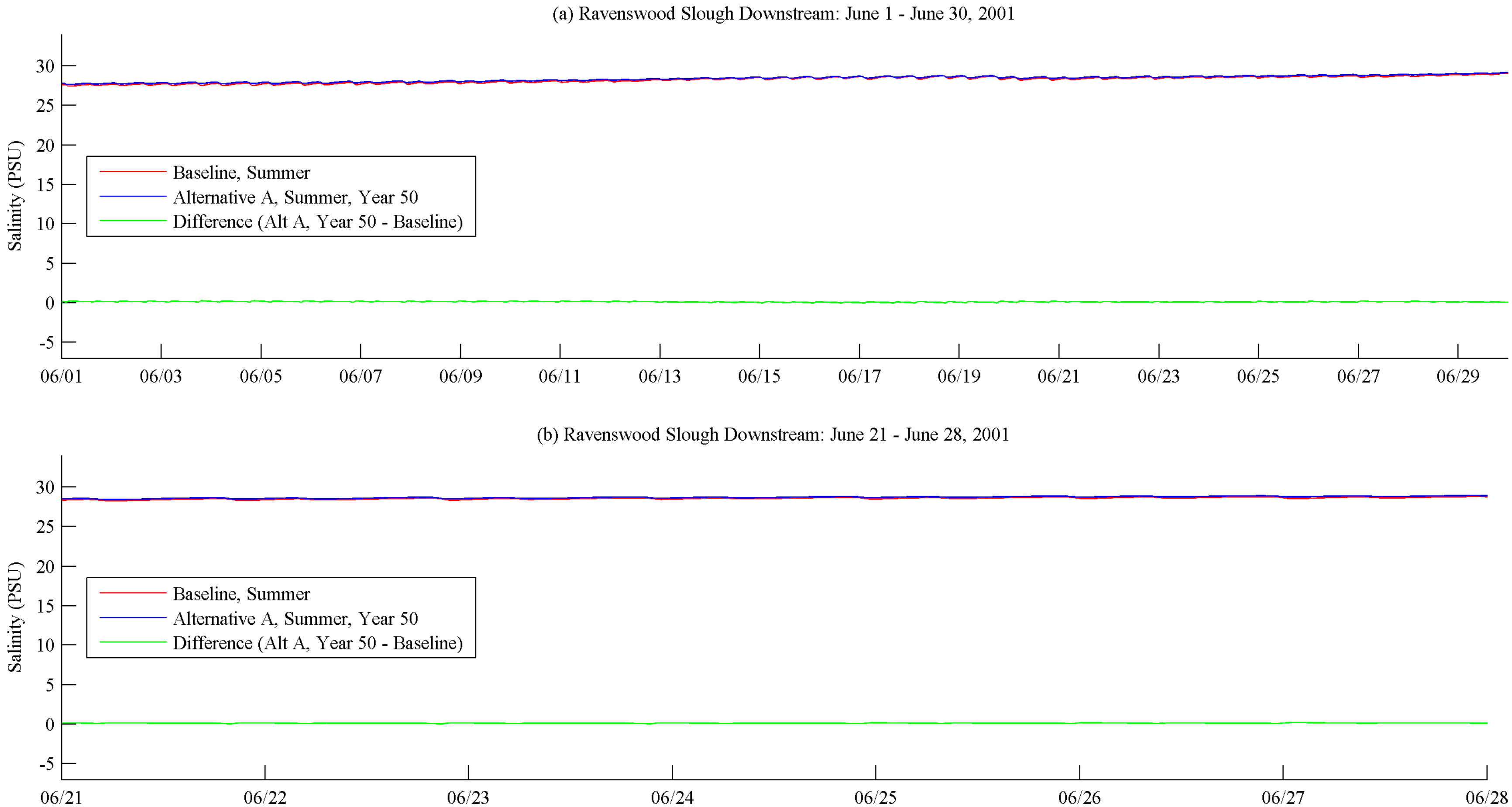

figure 6-67

South Bay Salt Pond Restoration Project

Salinity, Ravenswood Slough Downstream, Ravenswood, Alt A, Year 50, Summer

PWA

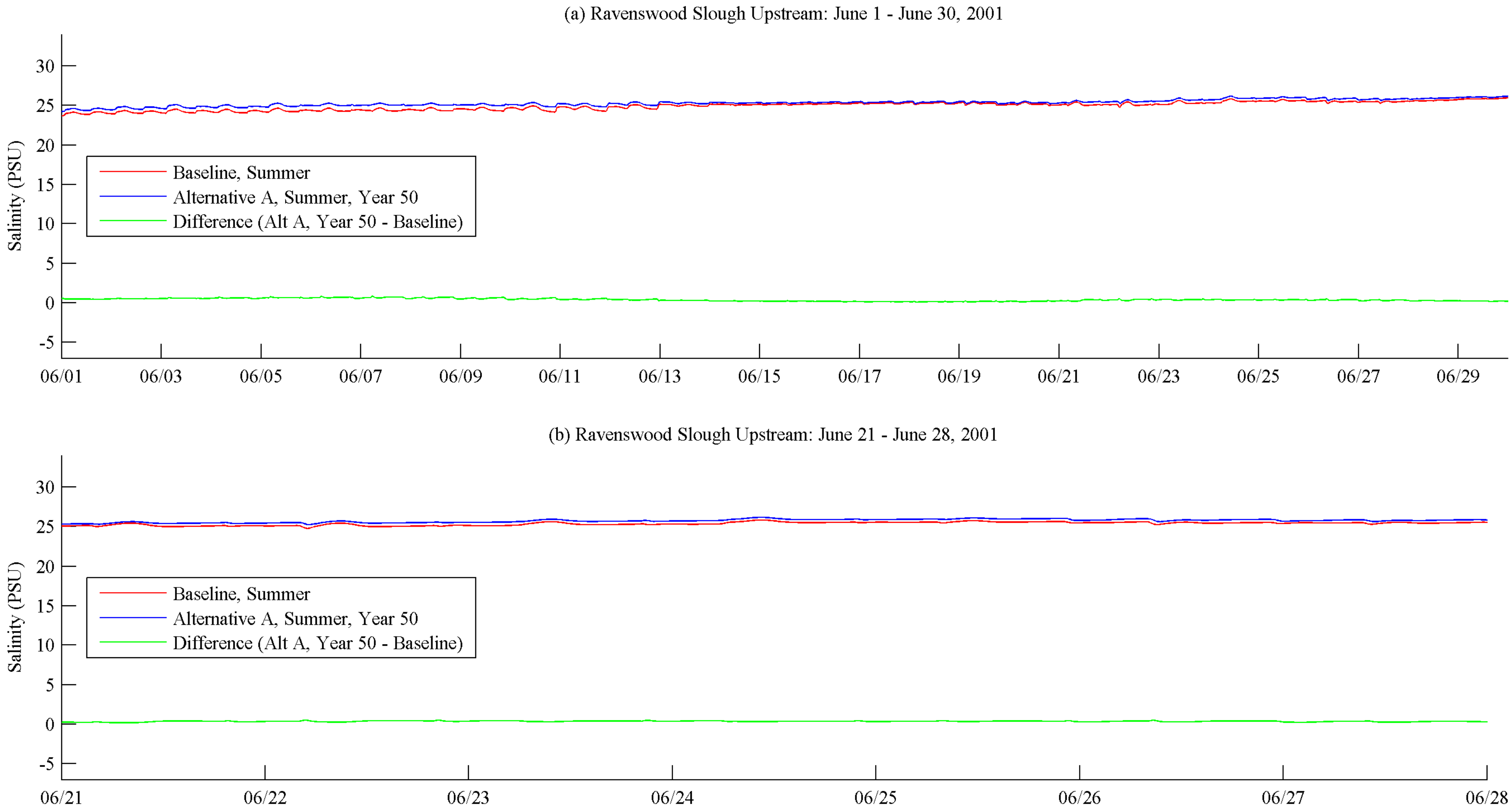

figure 6-68

South Bay Salt Pond Restoration Project

Salinity, Ravenswood Slough Upstream, Ravenswood, Alt A, Year 50, Summer

PWA

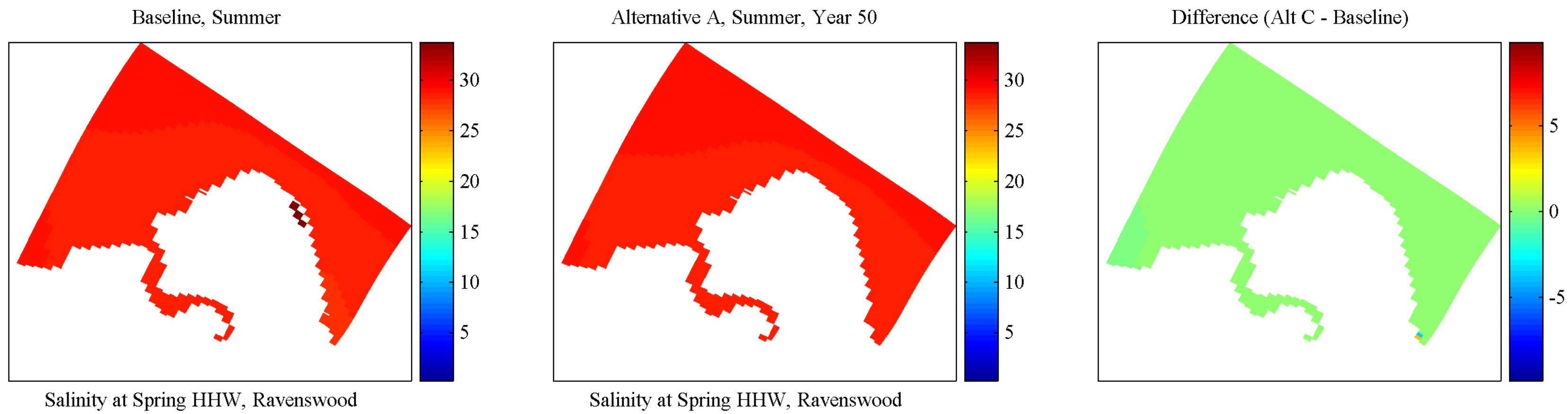

Note: Units shown are PSU

figure *6-69*

South Bay Salt Pond Restoration Project

Salinity at Spring HHW, Ravenswood, Alt A, Year 50, Summer

PWA

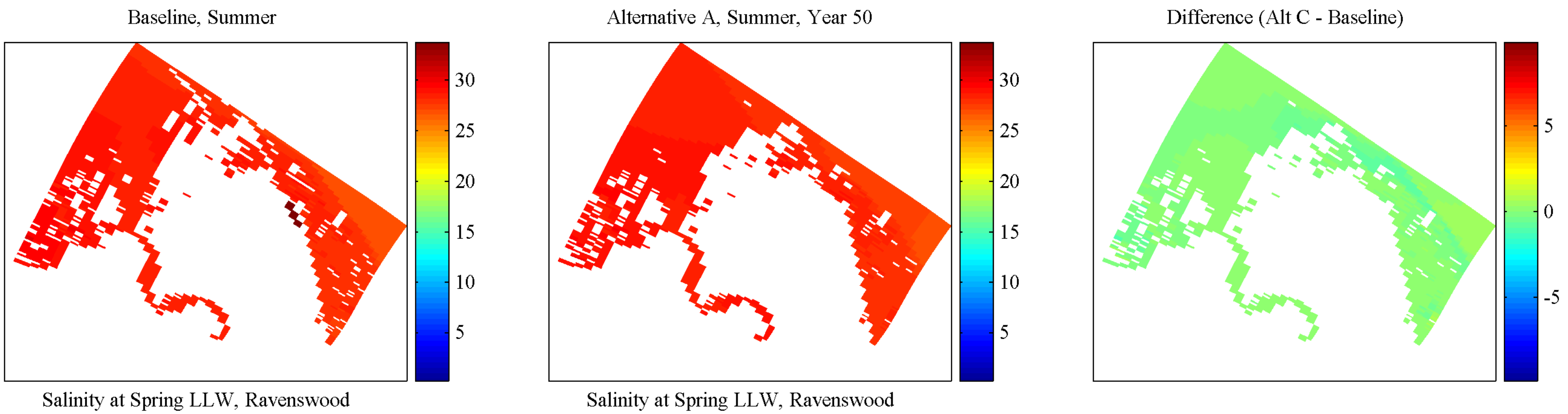

Note: Units shown are PSU

figure 6-70

South Bay Salt Pond Restoration Project

Salinity at Spring LLW, Ravenswood, Alt A, Year 50, Summer

PWA

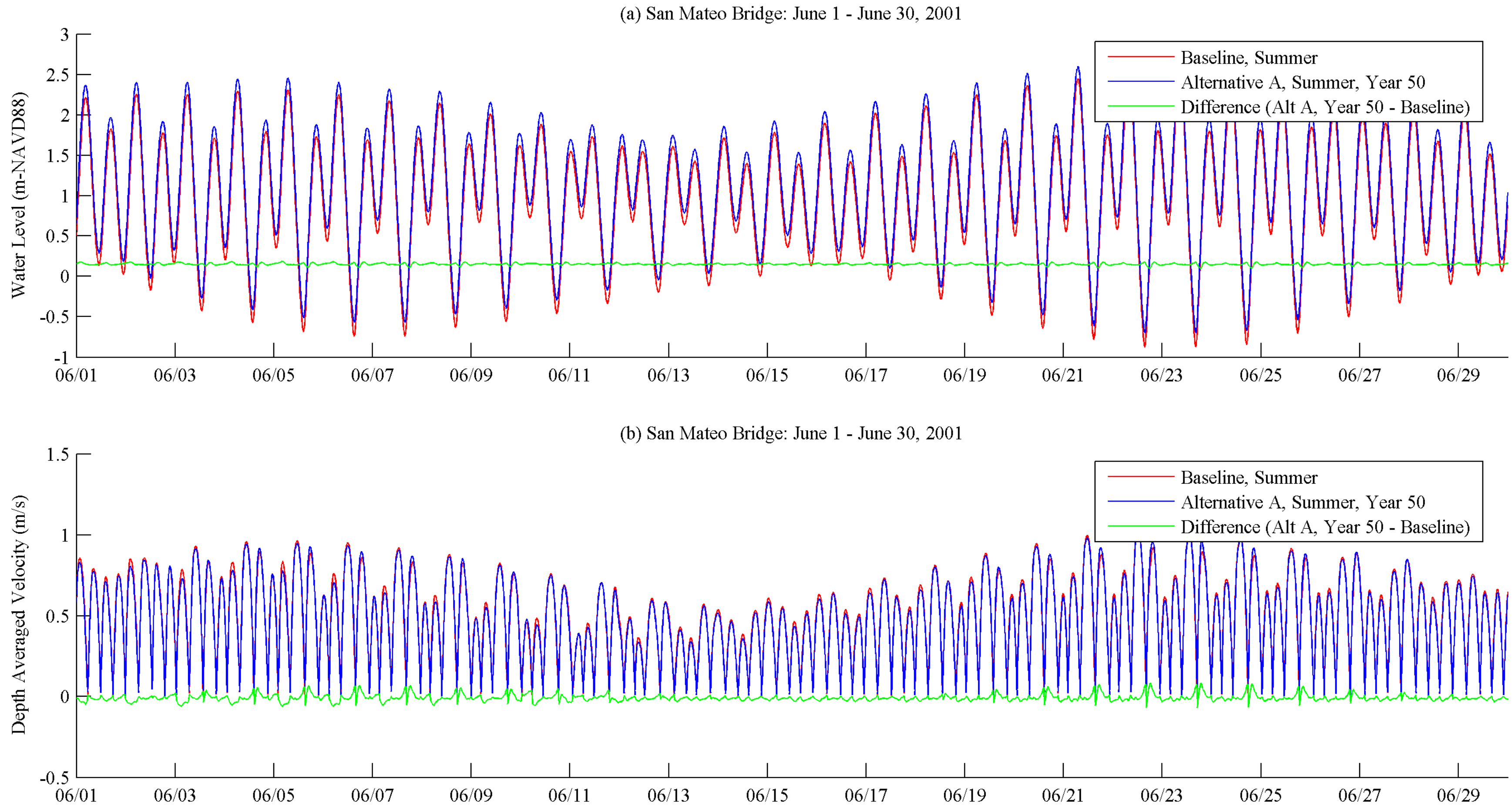

The depth-averaged velocity is calculated as $v = (u^2 + v^2)^{1/2}$, where u and v are the horizontal depth-averaged velocity components.

figure 6-71

South Bay Salt Pond Restoration Project

Velocity, San Mateo Bridge, Alt A, Year 50, Summer

PWA

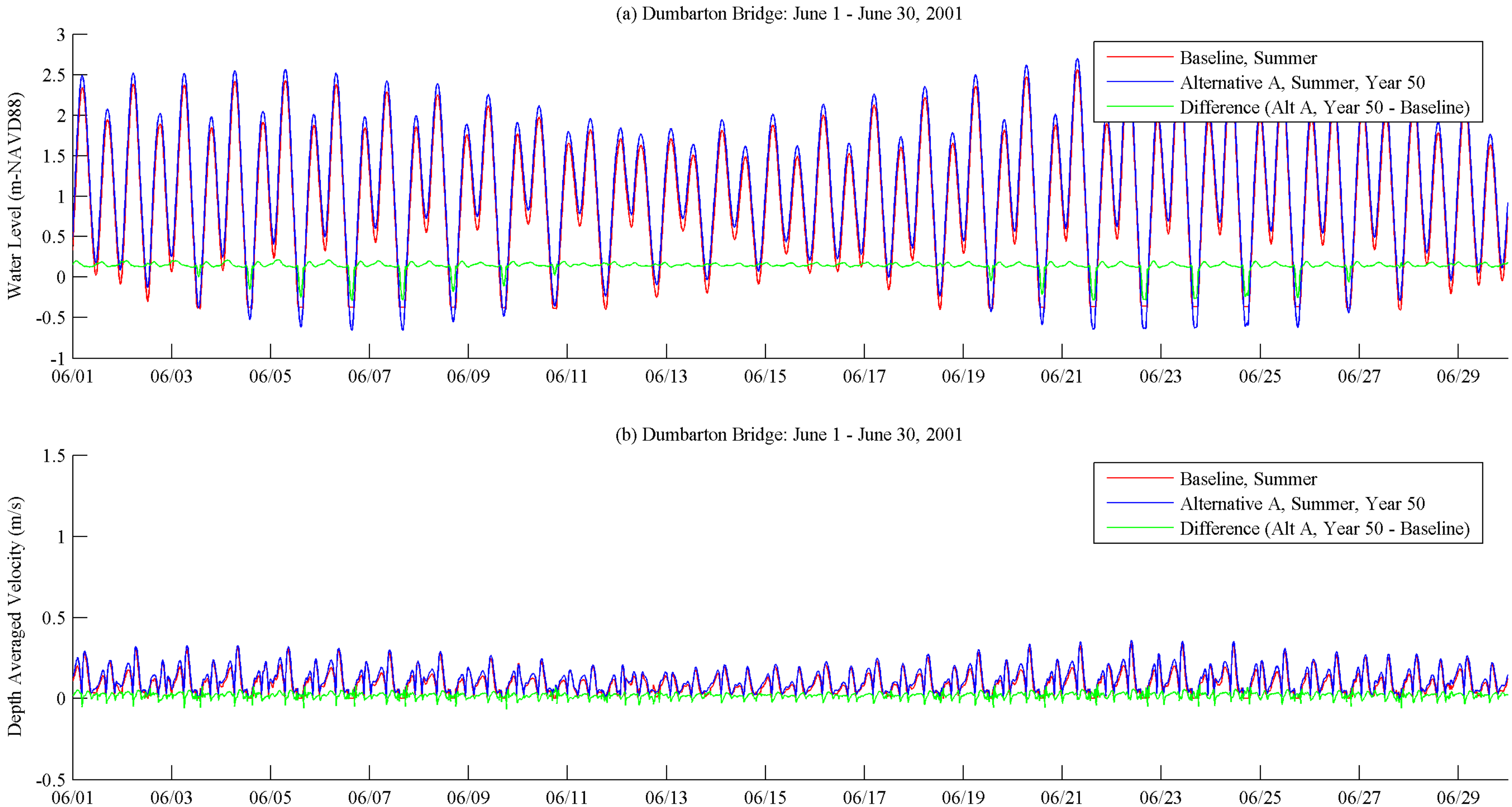

The depth-averaged velocity is calculated as $v = (u^2 + v^2)^{1/2}$, where u and v are the horizontal depth-averaged velocity components.

figure 6-72

South Bay Salt Pond Restoration Project

Velocity, Dumbarton Bridge, Alt A, Year 50, Summer

PWA

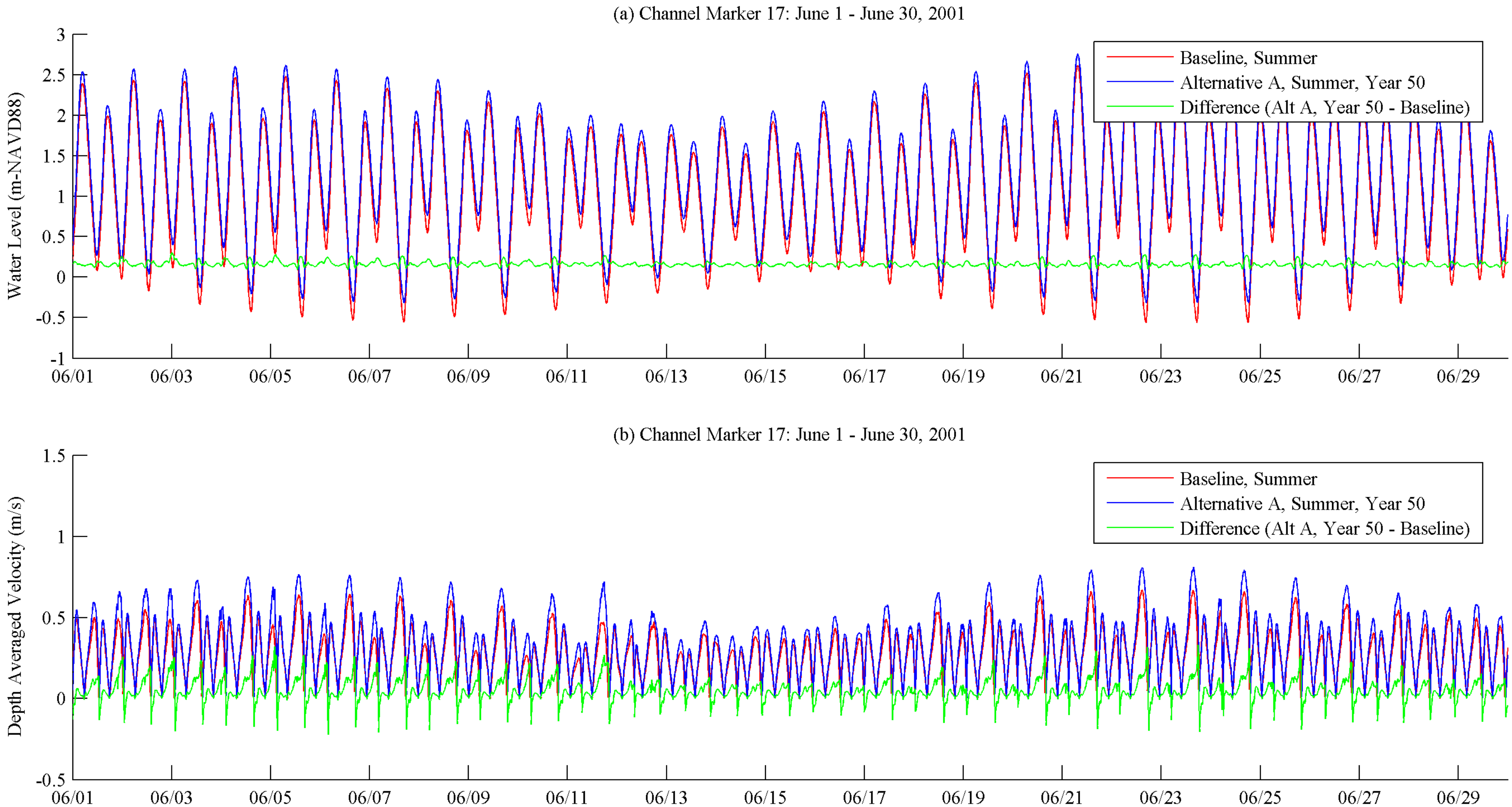

The depth-averaged velocity is calculated as $v = (u^2 + v^2)^{1/2}$, where u and v are the horizontal depth-averaged velocity components.

figure 6-73

South Bay Salt Pond Restoration Project

Velocity, Channel Marker 17, Alt A, Year 50, Summer

PWA

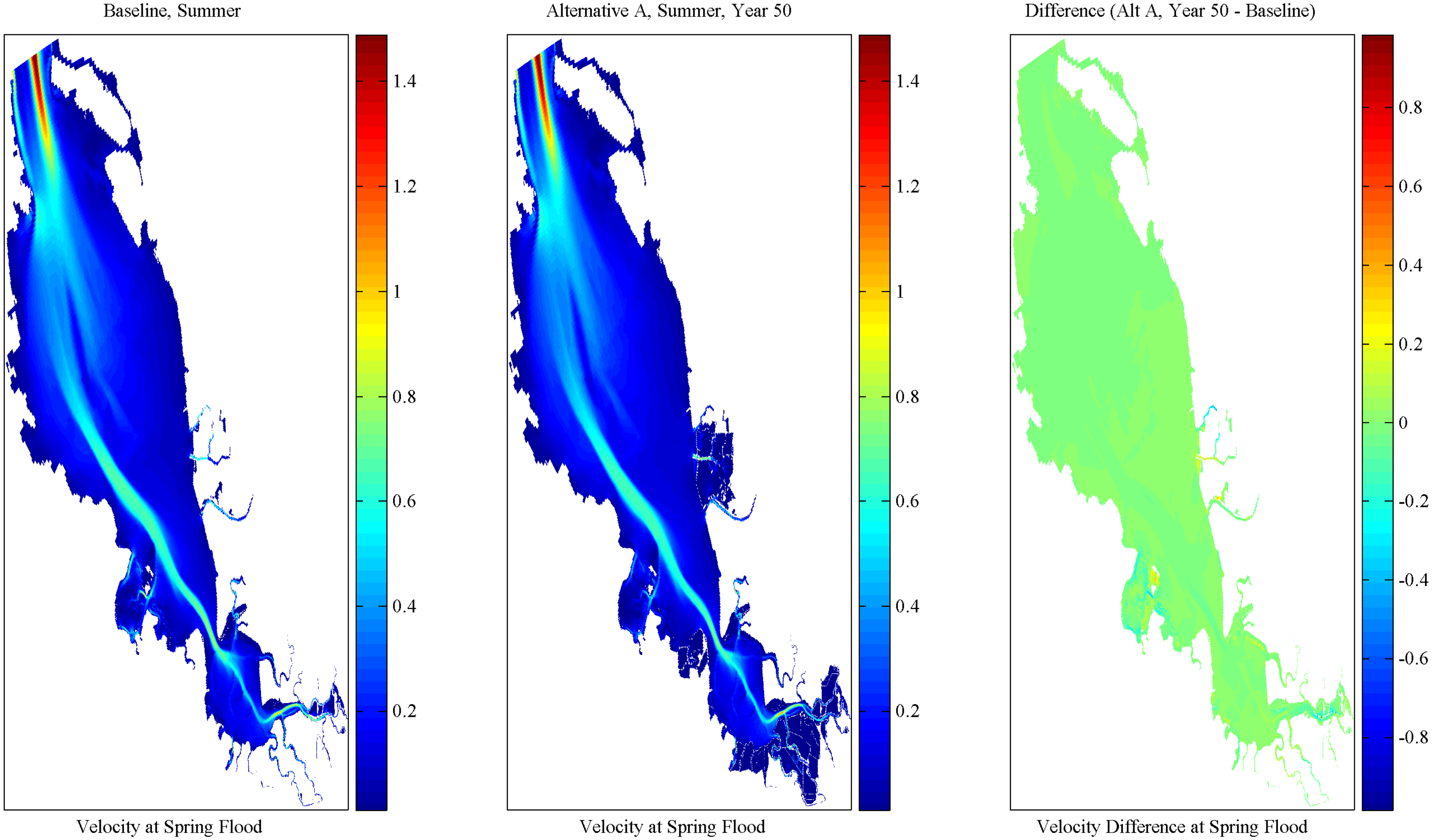

Note: Units shown are m/s

figure *6-74*

South Bay Salt Pond Restoration Project

Velocity at Spring Flood, Alt A, Year 50, Summer

PWA

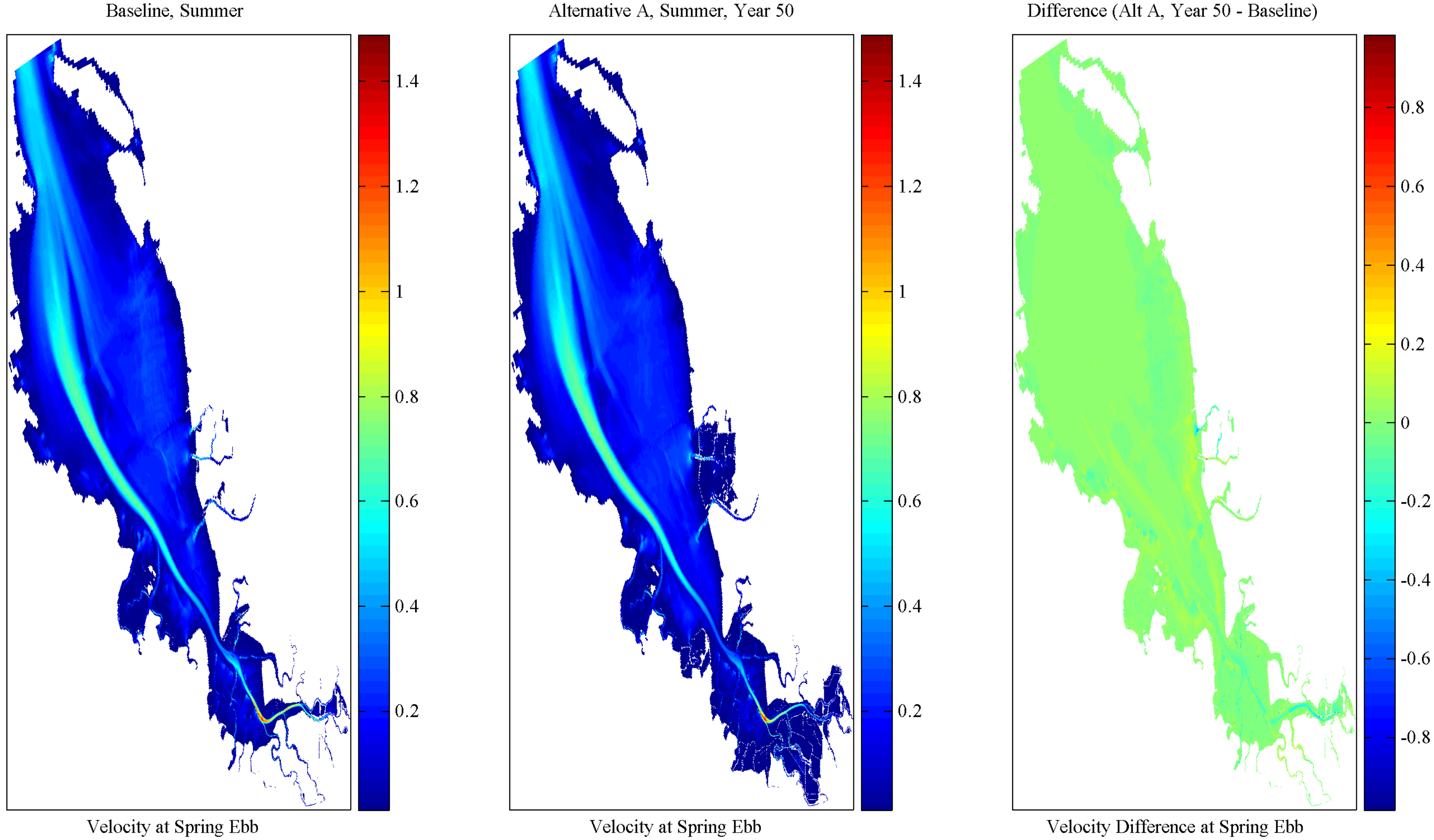

Note: Units shown are m/s

figure 6-75

South Bay Salt Pond Restoration Project

Velocity at Spring Ebb, Alt A, Year 50, Summer

PWA

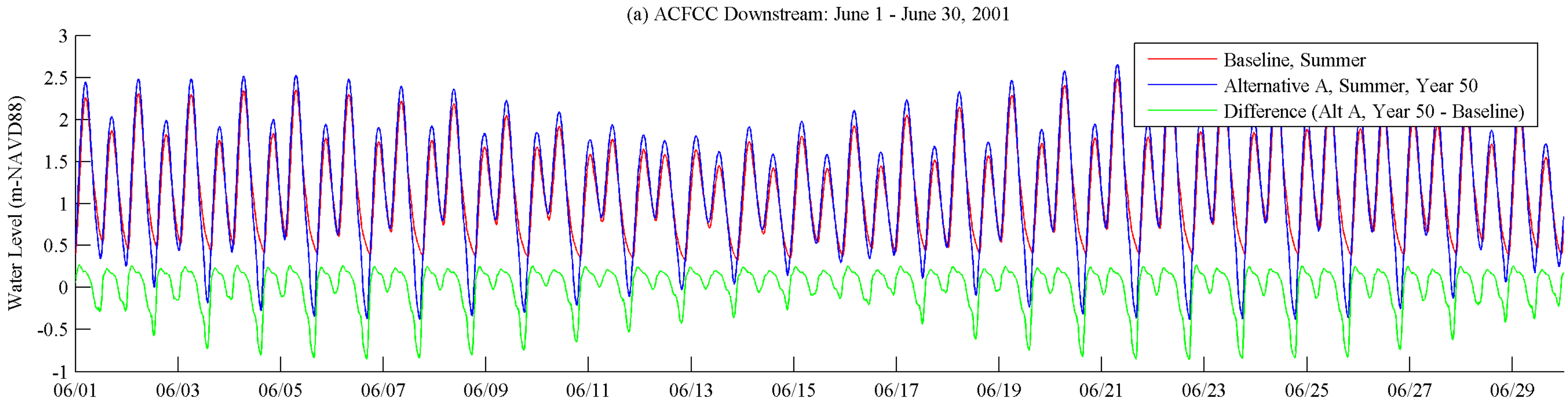

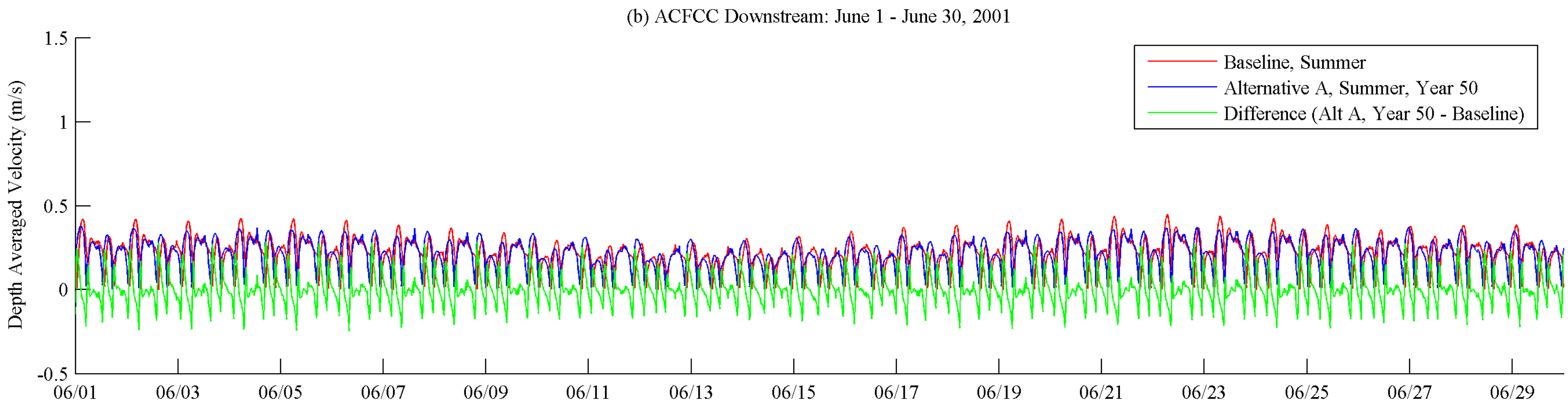

The depth-averaged velocity is calculated as $v = (u^2 + v^2)^{1/2}$, where u and v are the horizontal depth-averaged velocity components.

figure 6-76

South Bay Salt Pond Restoration Project

Velocity, ACFCC Downstream, Alt A, Year 50, Summer

PWA

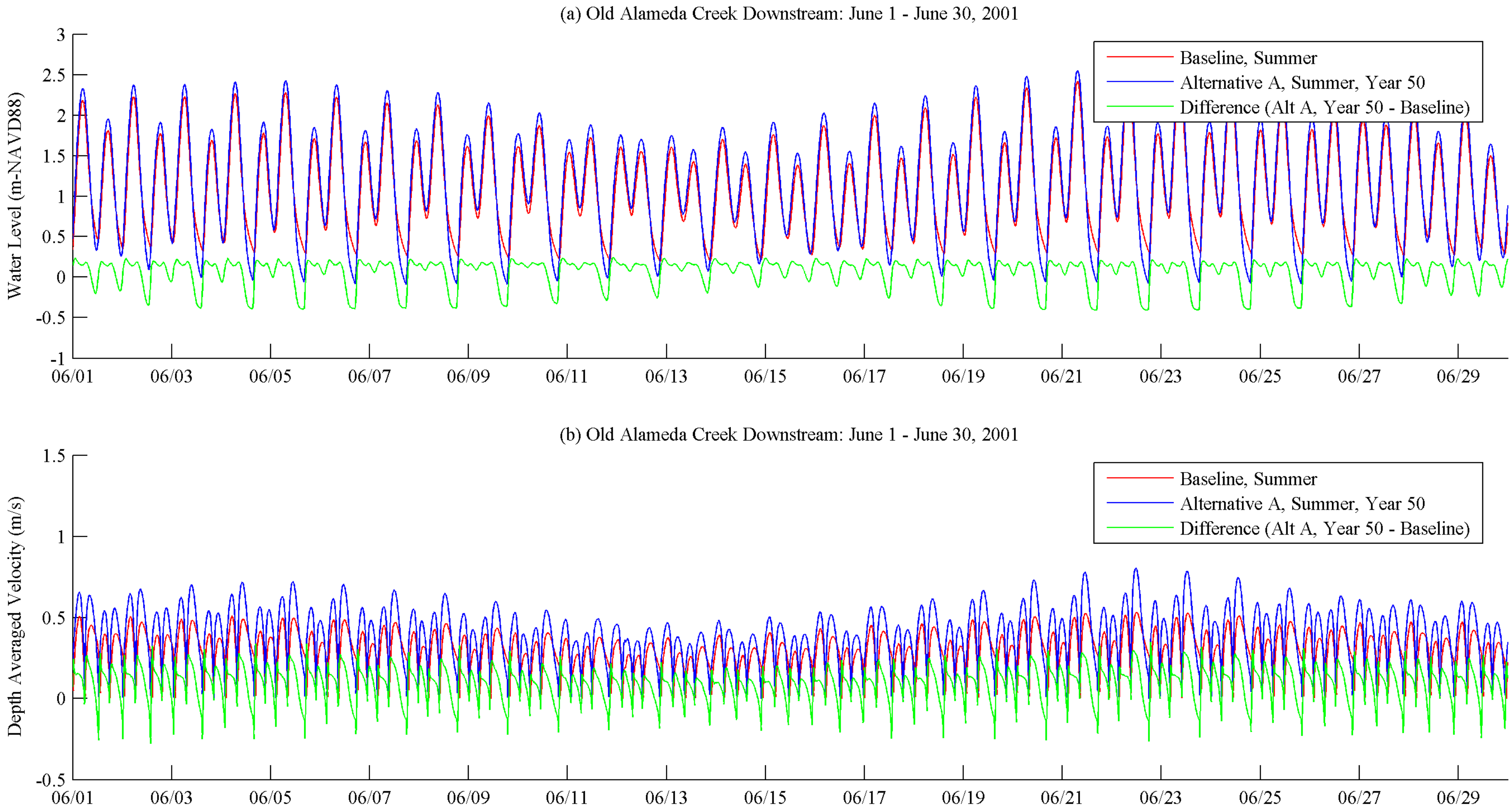

The depth-averaged velocity is calculated as $v = (u^2 + v^2)^{1/2}$, where u and v are the horizontal depth-averaged velocity components.

figure 6-77

South Bay Salt Pond Restoration Project

Velocity, Old Alameda Creek Downstream, Alt A, Year 50, Summer

PWA

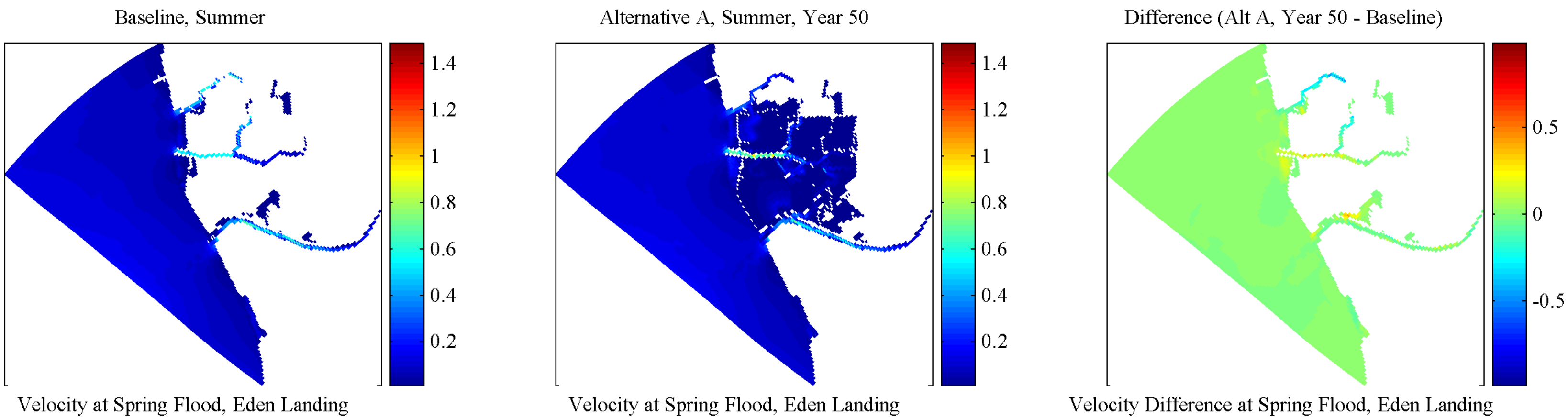

Note: Units shown are m/s

figure 6-78

South Bay Salt Pond Restoration Project

Velocity at Spring Flood, Eden Landing, Alt A, Year 50, Summer

PWA

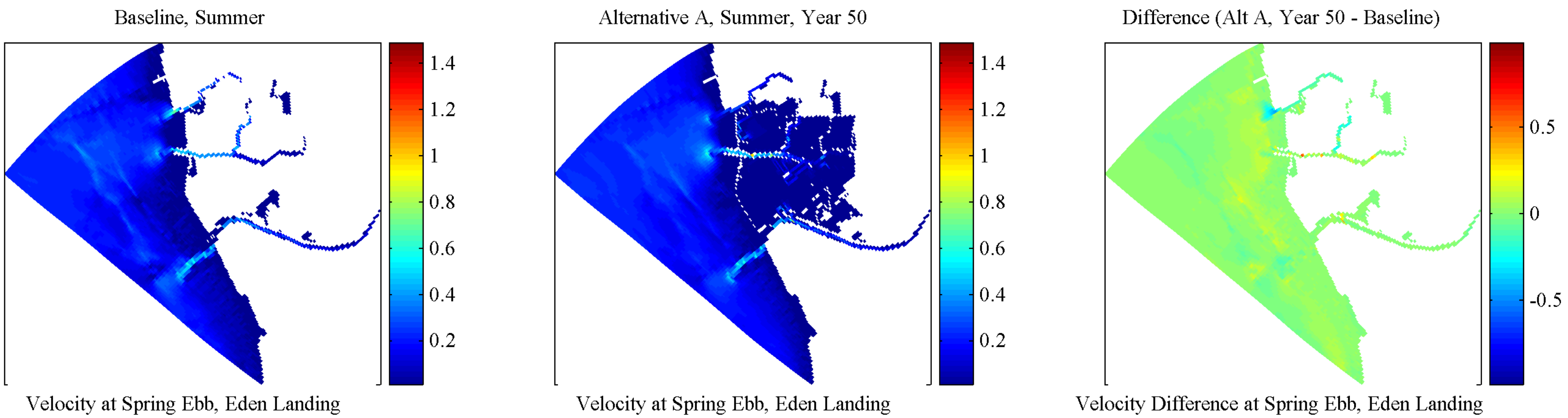

Note: Units shown are m/s

figure 6-79

South Bay Salt Pond Restoration Project

Velocity at Spring Ebb, Eden Landing, Alt A, Year 50, Summer

PWA

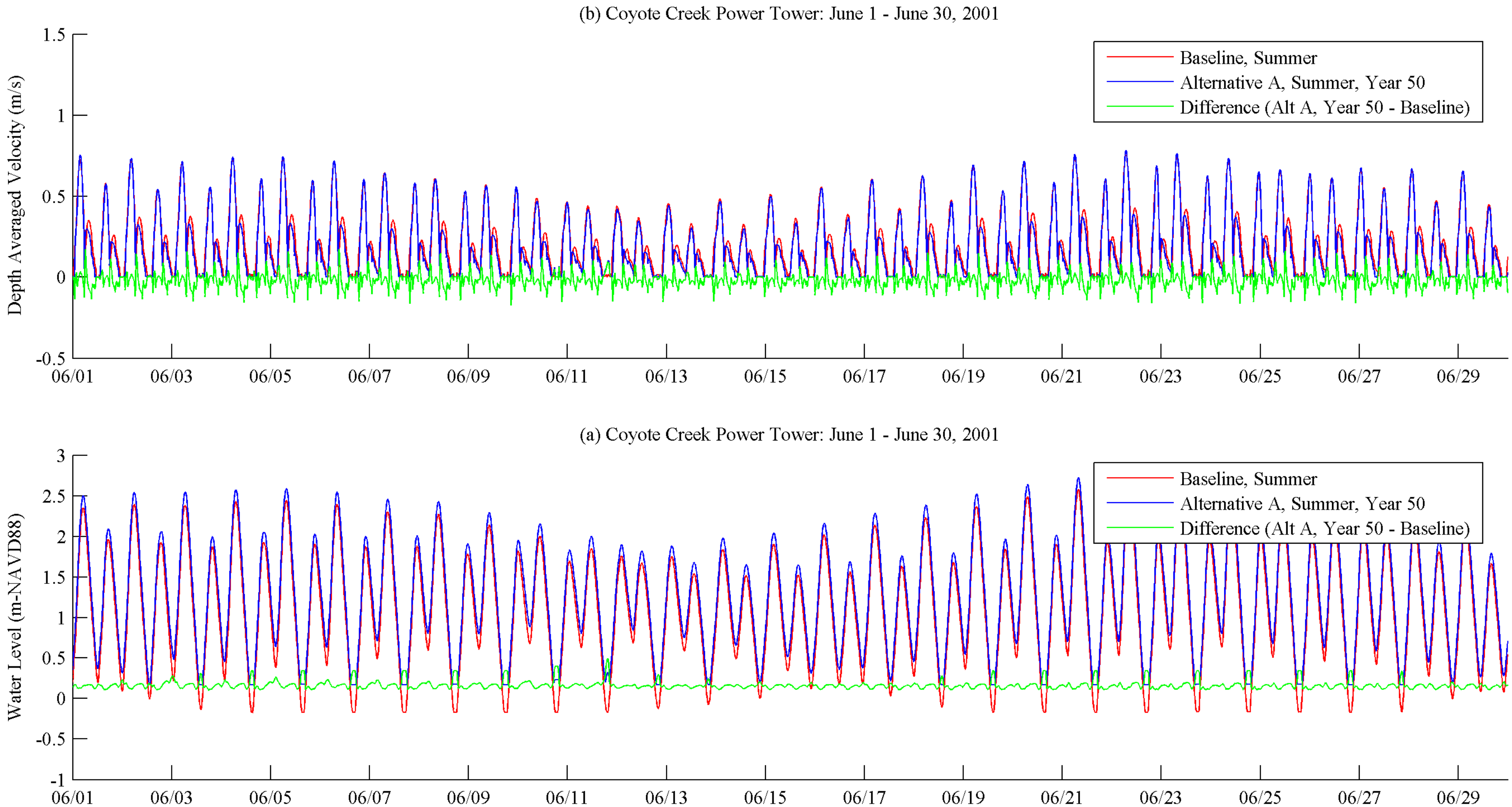

The depth-averaged velocity is calculated as $v = (u^2 + v^2)^{1/2}$, where u and v are the horizontal depth-averaged velocity components.

figure 6-80

South Bay Salt Pond Restoration Project

Velocity, Coyote Creek Power Tower, Alt A, Year 50, Summer

PWA

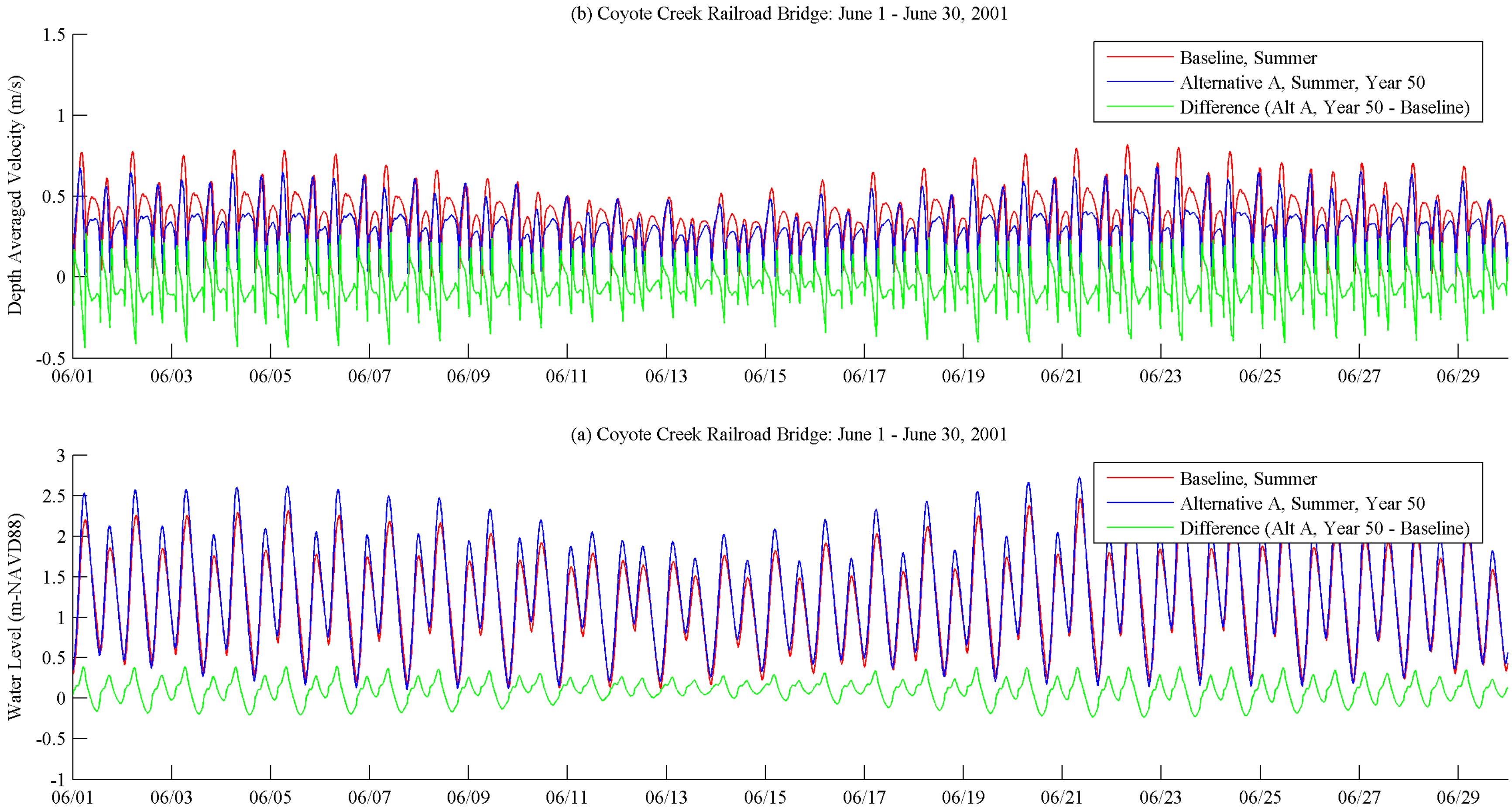

The depth-averaged velocity is calculated as $v = (u^2 + v^2)^{1/2}$, where u and v are the horizontal depth-averaged velocity components.

figure *6-81*

South Bay Salt Pond Restoration Project

Velocity, Coyote Creek Railroad Bridge, Alt A, Year 50, Summer

PWA

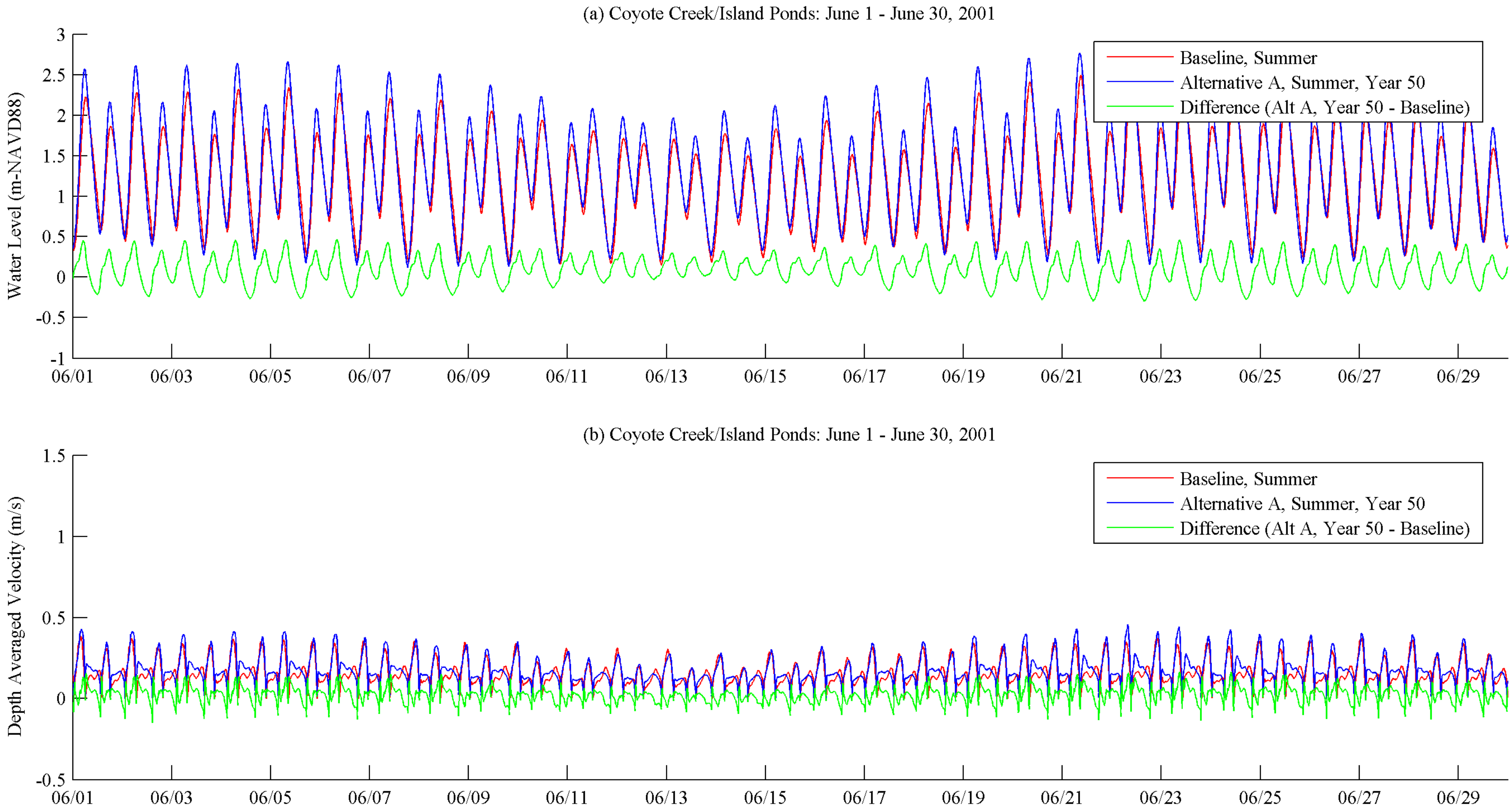

The depth-averaged velocity is calculated as $v = (u^2 + v^2)^{1/2}$, where u and v are the horizontal depth-averaged velocity components.

figure 6-82

South Bay Salt Pond Restoration Project

Velocity, Coyote Creek/Island Ponds, Year 50, Summer

PWA

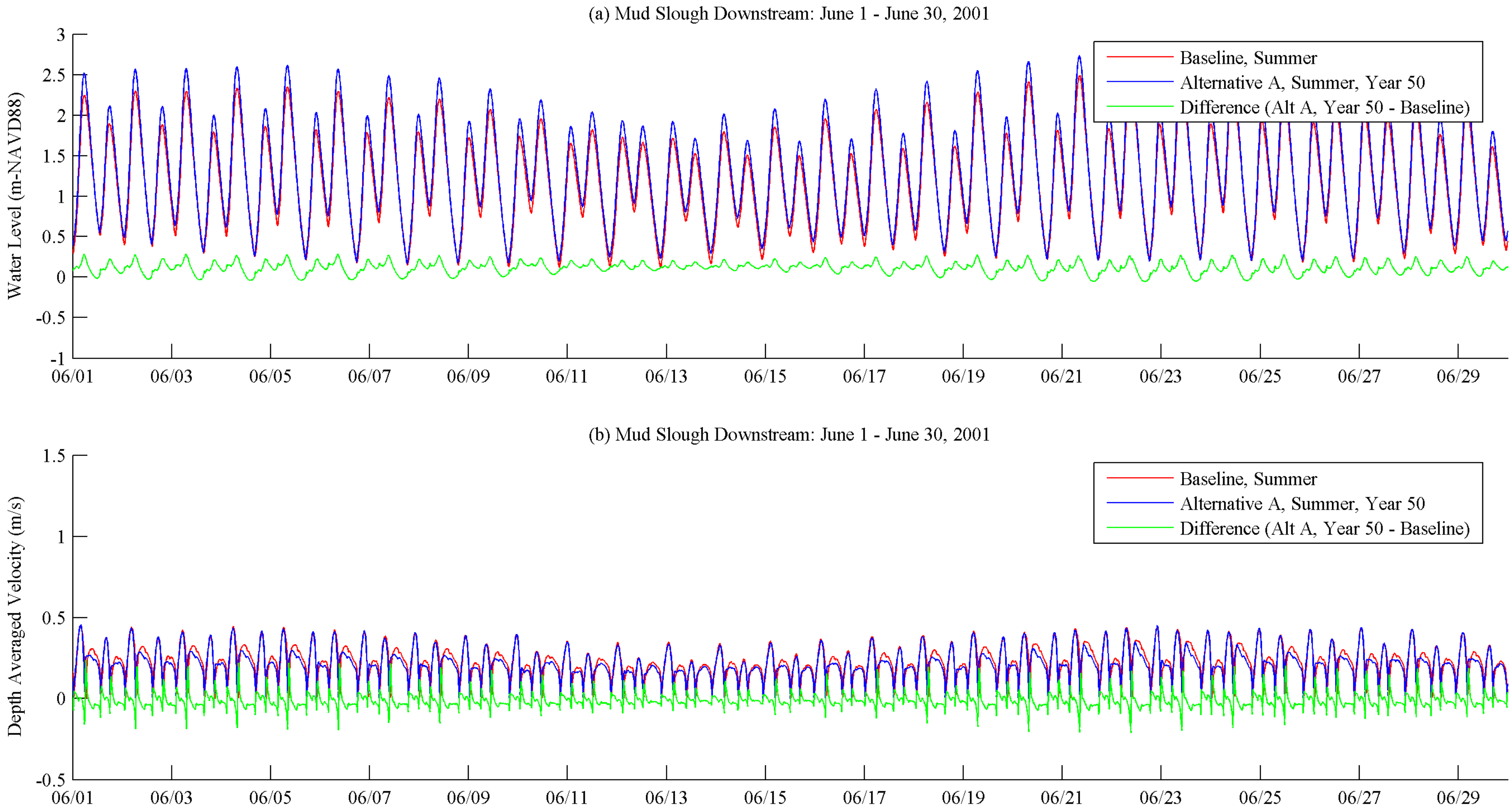

The depth-averaged velocity is calculated as $v = (u^2 + v^2)^{1/2}$, where u and v are the horizontal depth-averaged velocity components.

figure 6-83

South Bay Salt Pond Restoration Project

Velocity, Mud Slough Downstream, Alt A, Year 50, Summer

PWA

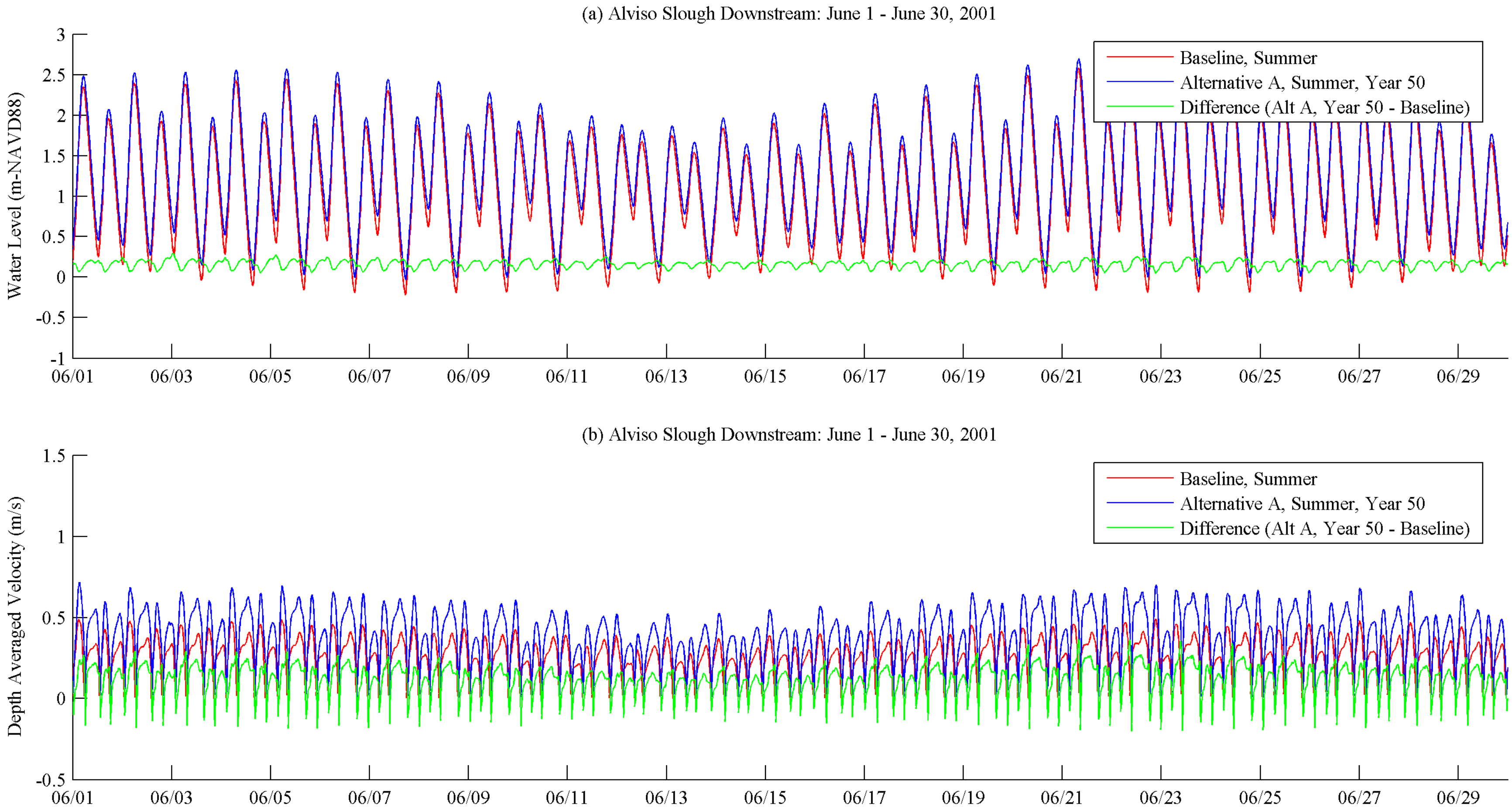

The depth-averaged velocity is calculated as $v = (u^2 + v^2)^{1/2}$, where u and v are the horizontal depth-averaged velocity components.

figure 6-84

South Bay Salt Pond Restoration Project

Velocity, Alviso Slough Downstream, Alt A, Year 50, Summer

PWA

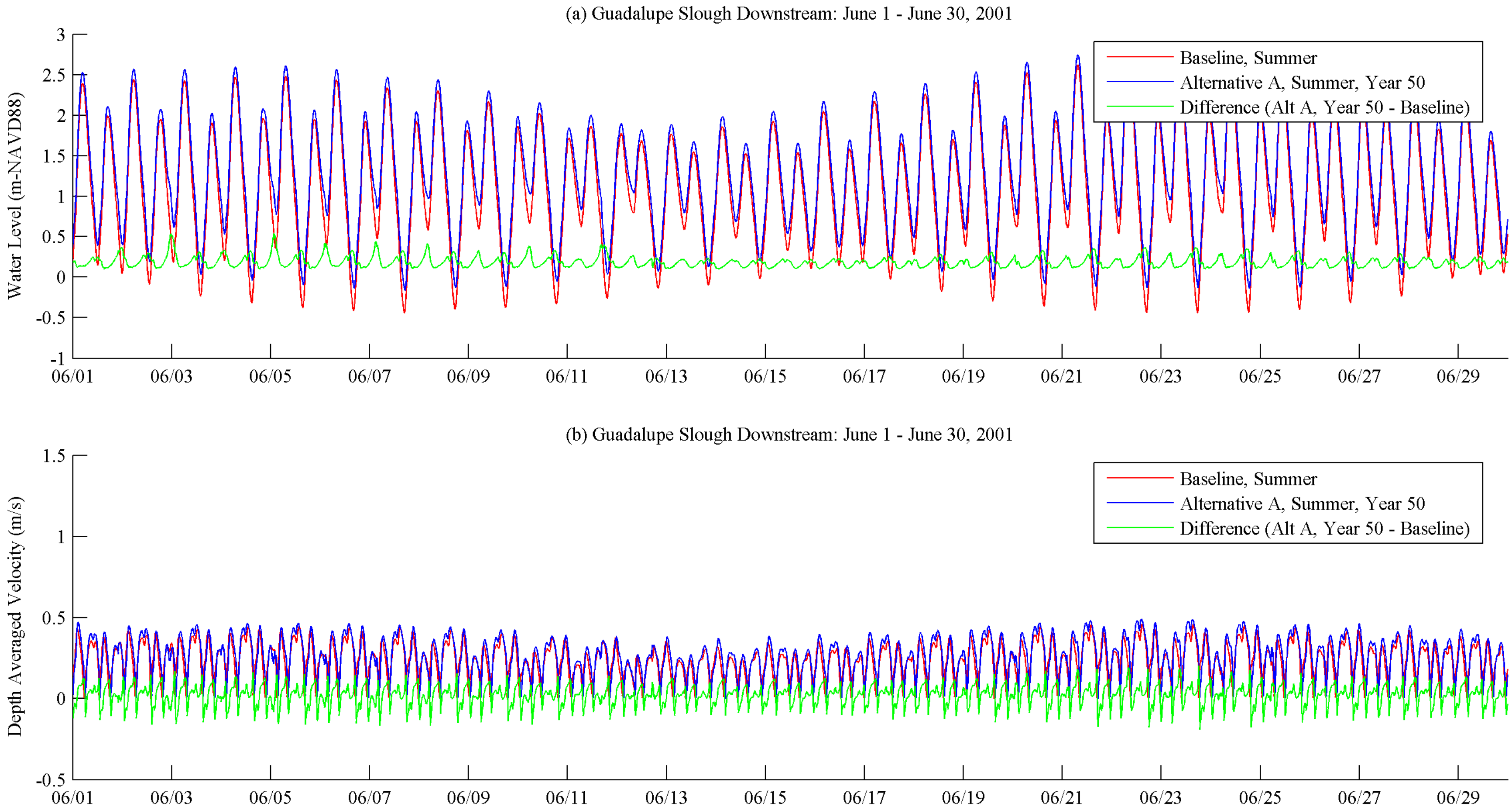

The depth-averaged velocity is calculated as $v = (u^2 + v^2)^{1/2}$, where u and v are the horizontal depth-averaged velocity components.

figure 6-85

South Bay Salt Pond Restoration Project

Velocity, Guadalupe Slough Downstream, Alt A, Year 50, Summer

PWA

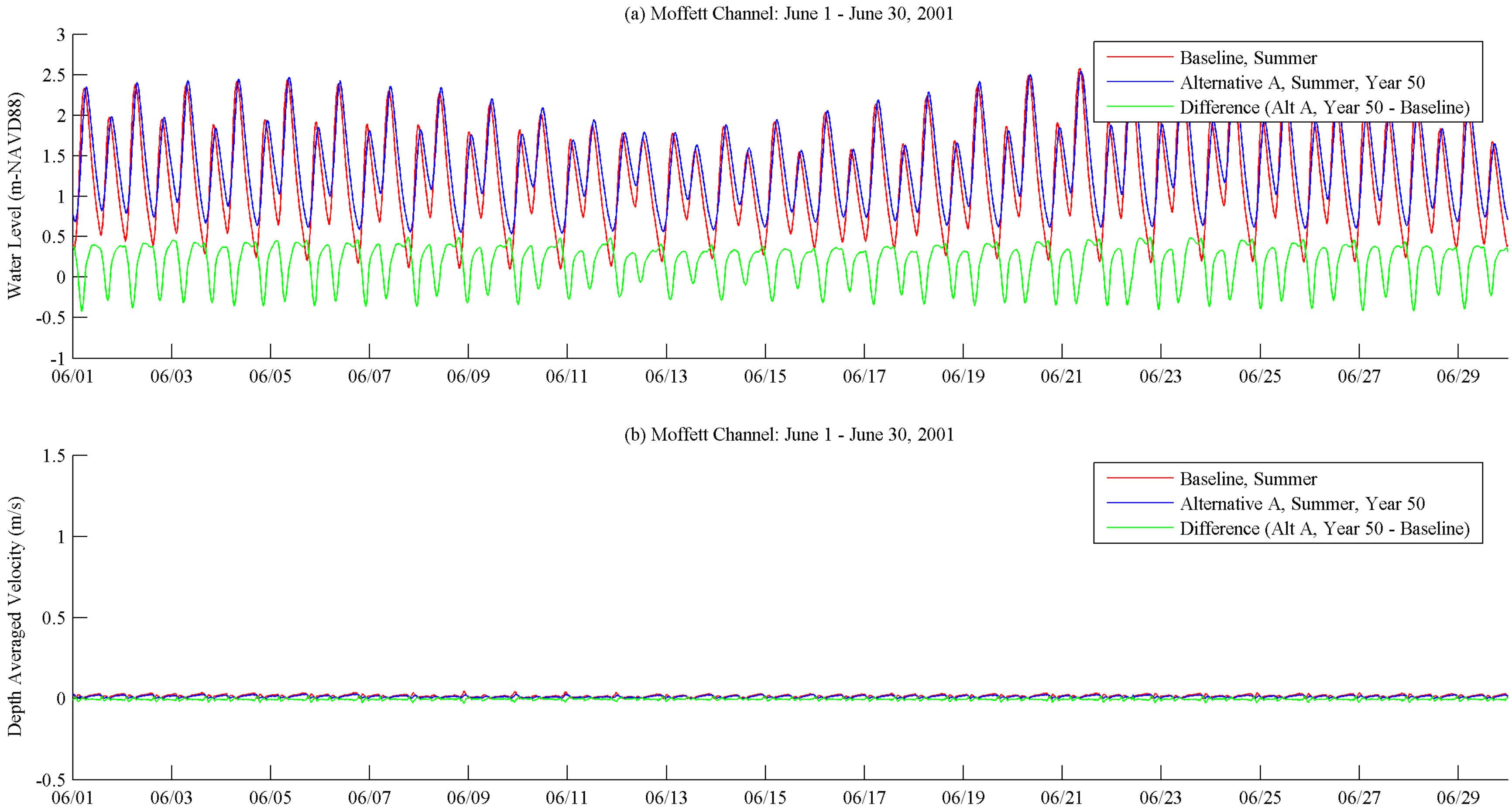

The depth-averaged velocity is calculated as $v = (u^2 + v^2)^{1/2}$, where u and v are the horizontal depth-averaged velocity components.

figure 6-86

South Bay Salt Pond Restoration Project

Velocity, Moffett Channel, Alt A, Year 50, Summer

PWA

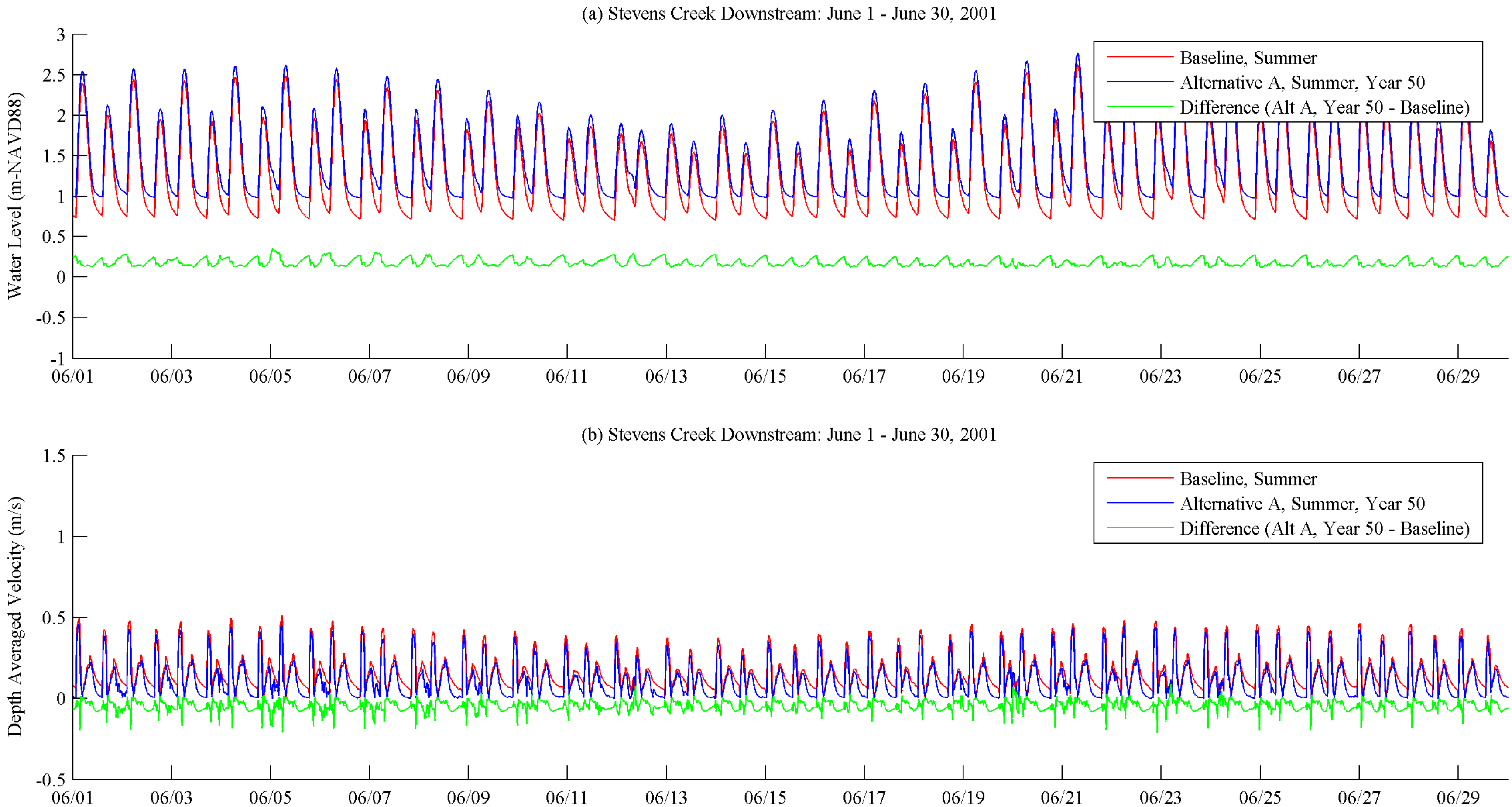

The depth-averaged velocity is calculated as $v = (u^2 + v^2)^{1/2}$, where u and v are the horizontal depth-averaged velocity components.

figure 6-87

South Bay Salt Pond Restoration Project

Velocity, Steven Creek Downstream, Alt A, Year 50, Summer

PWA

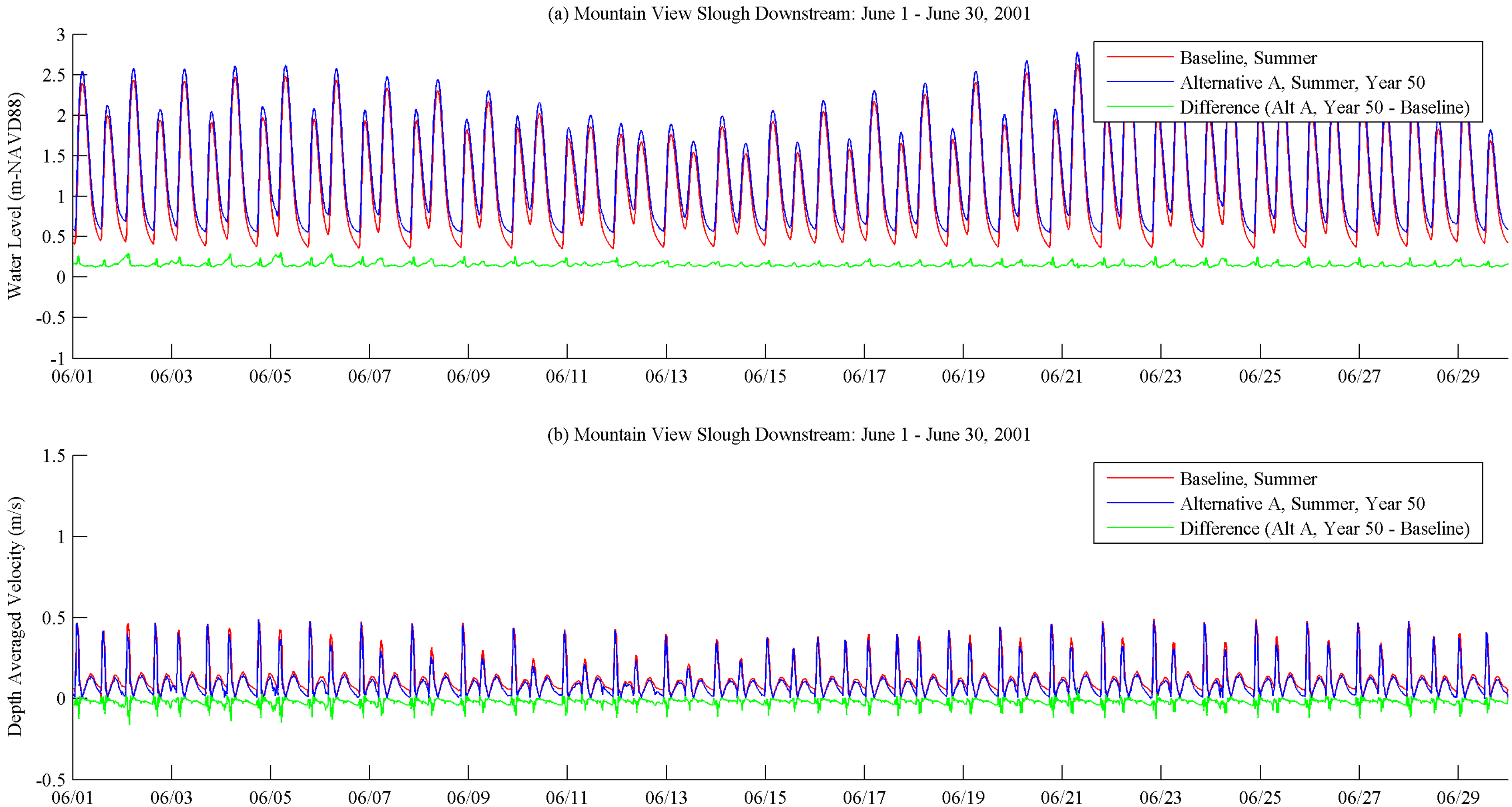

The depth-averaged velocity is calculated as $v = (u^2 + v^2)^{1/2}$, where u and v are the horizontal depth-averaged velocity components.

figure 6-88

South Bay Salt Pond Restoration Project

Velocity, Mountain View Slough Downstream, Alt A, Year 50, Summer

PWA

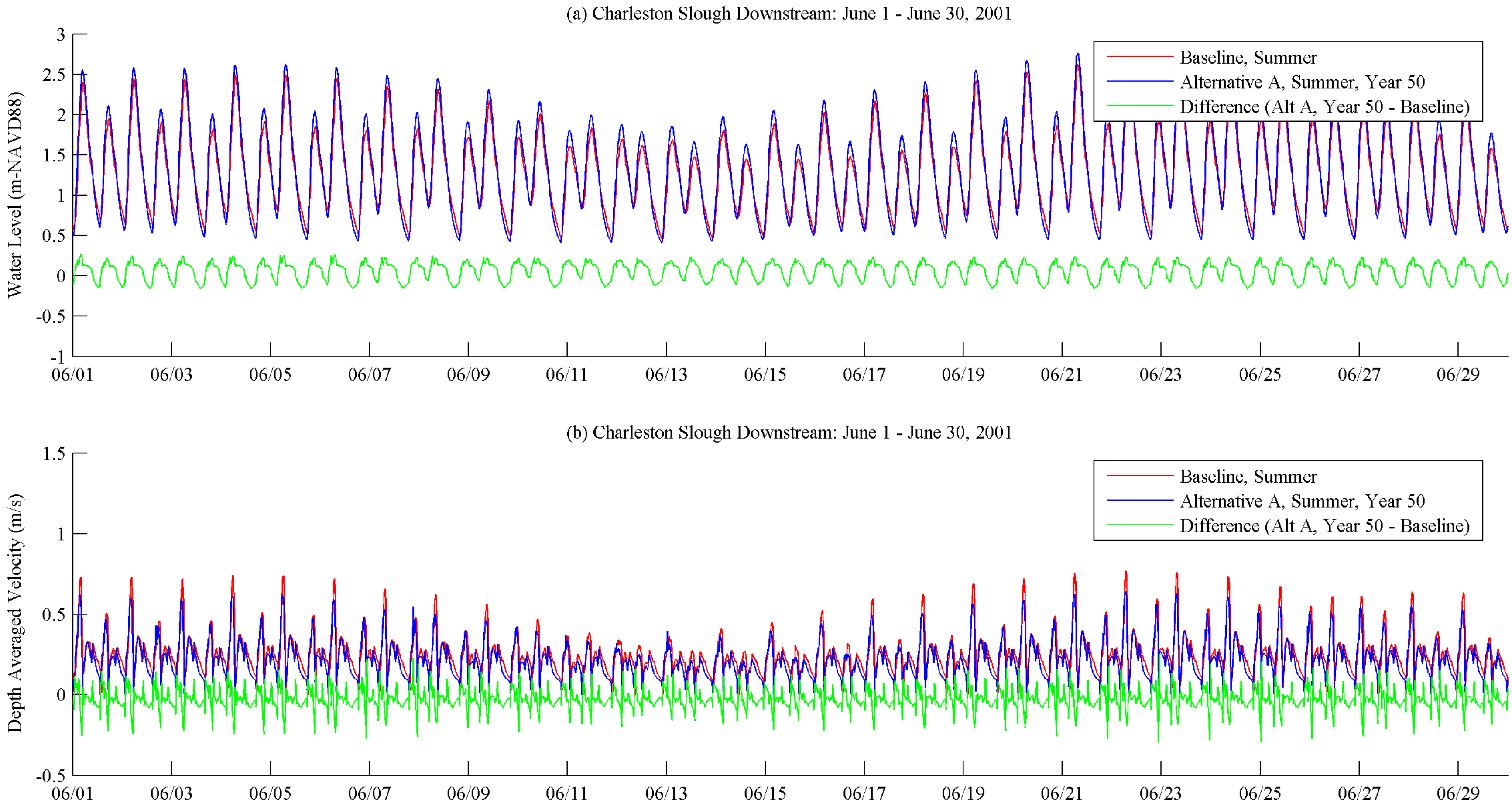

The depth-averaged velocity is calculated as $v = (u^2 + v^2)^{1/2}$, where u and v are the horizontal depth-averaged velocity components.

figure *6-89*

South Bay Salt Pond Restoration Project

Velocity, Charleston Slough Downstream, Alt A, Year 50, Summer

PWA

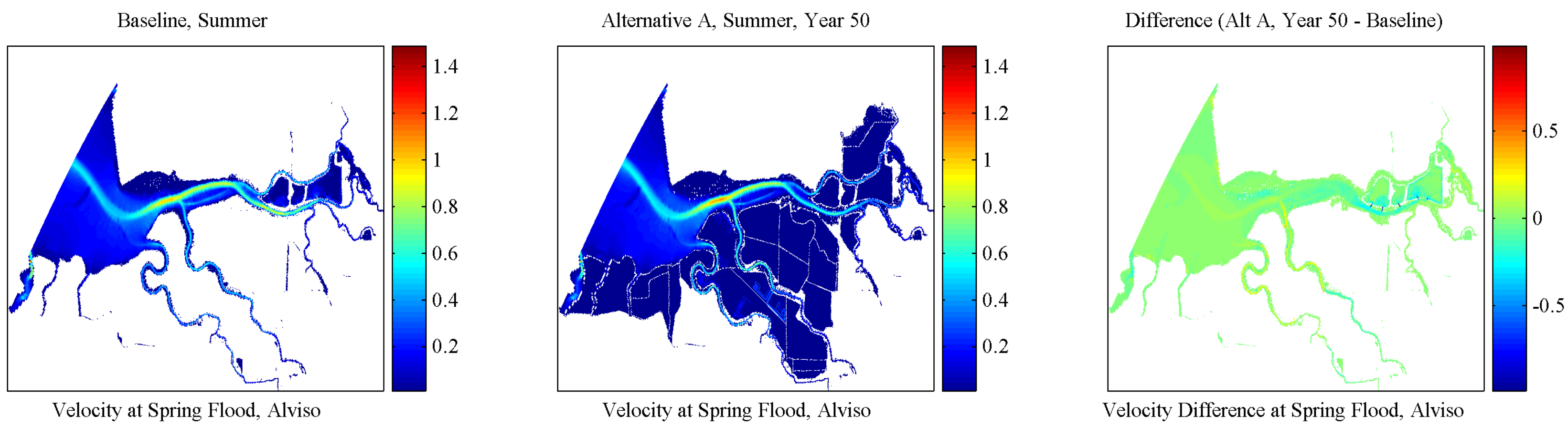

Note: Units shown are m/s

figure *6-90*

South Bay Salt Pond Restoration Project

Velocity at Spring Flood, Alviso, Alt A, Year 50, Summer

PWA

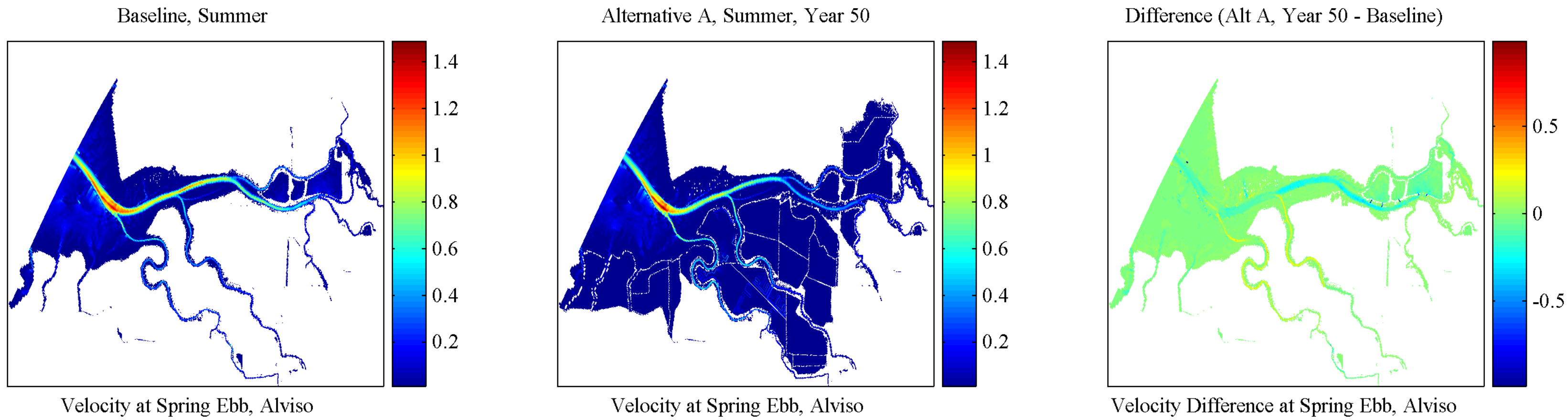

Note: Units shown are m/s

figure 6-91

South Bay Salt Pond Restoration Project

Velocity at Spring Ebb, Alviso, Alt A, Year 50, Summer

PWA

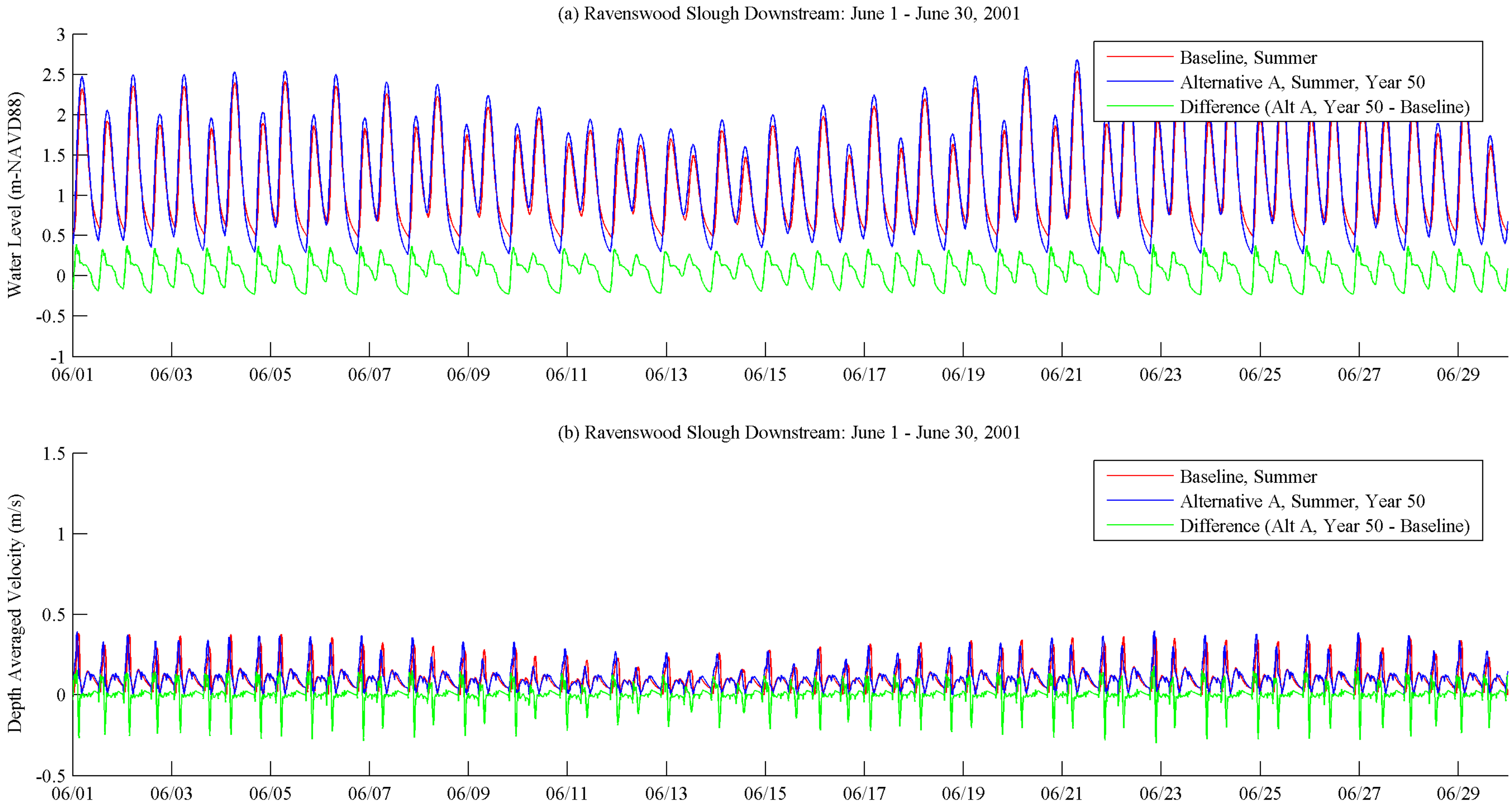

The depth-averaged velocity is calculated as $v = (u^2 + v^2)^{1/2}$, where u and v are the horizontal depth-averaged velocity components.

figure 6-92

South Bay Salt Pond Restoration Project

Velocity, Ravenswood Slough Downstream, Alt A, Year 50, Summer

PWA

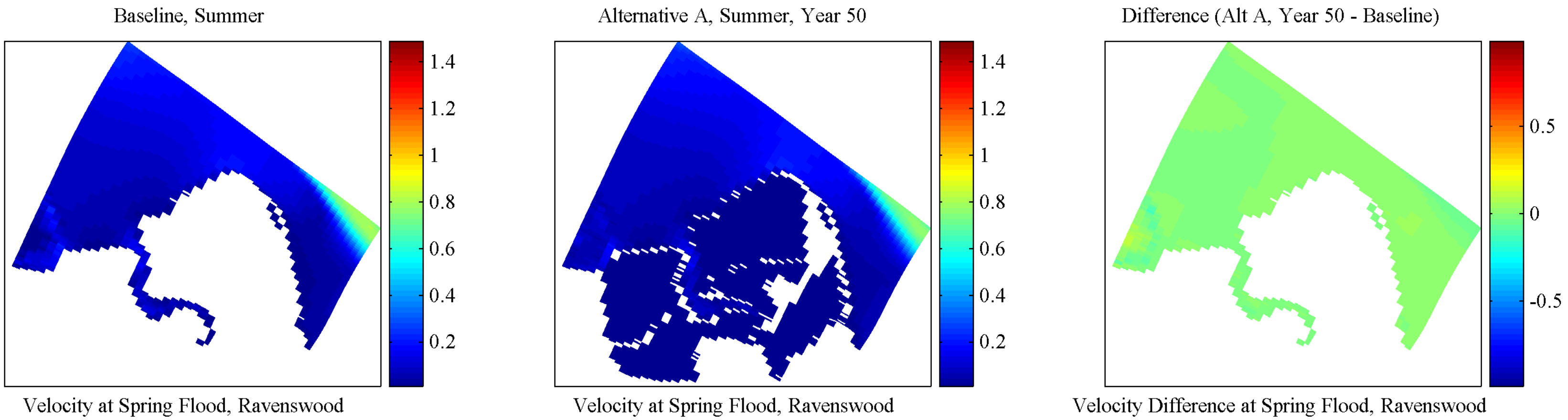

Note: Units shown are m/s

figure 6-93

South Bay Salt Pond Restoration Project

Velocity at Spring Flood, Ravenswood, Alt A, Year 50, Summer

PWA

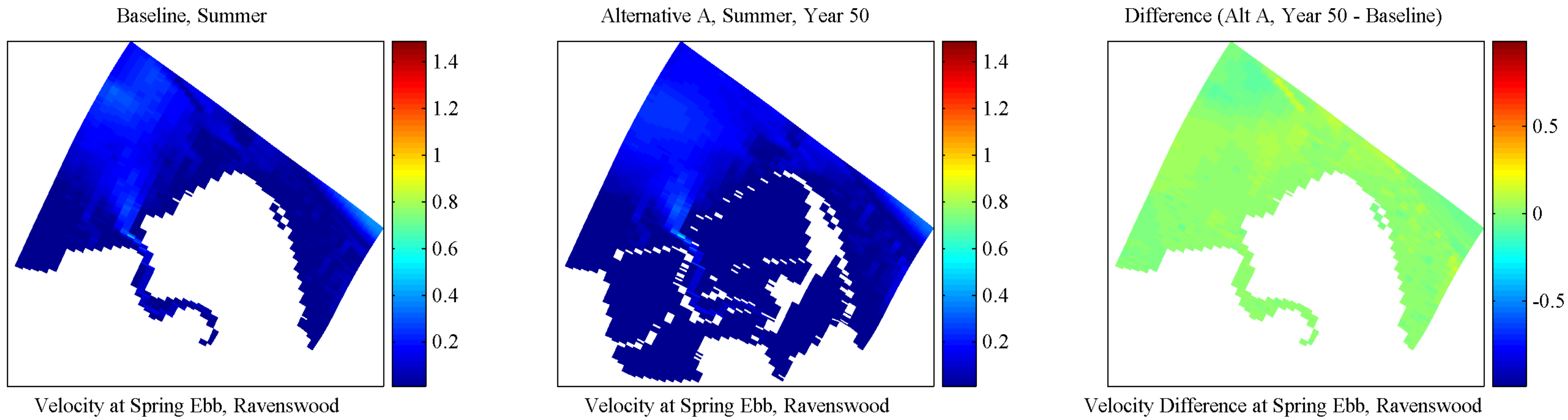

Note: Units shown are m/s

figure *6-94*

South Bay Salt Pond Restoration Project

Velocity at Spring Ebb, Ravenswood, Alt A, Year 50, Summer

PWA

Baseline, Summer

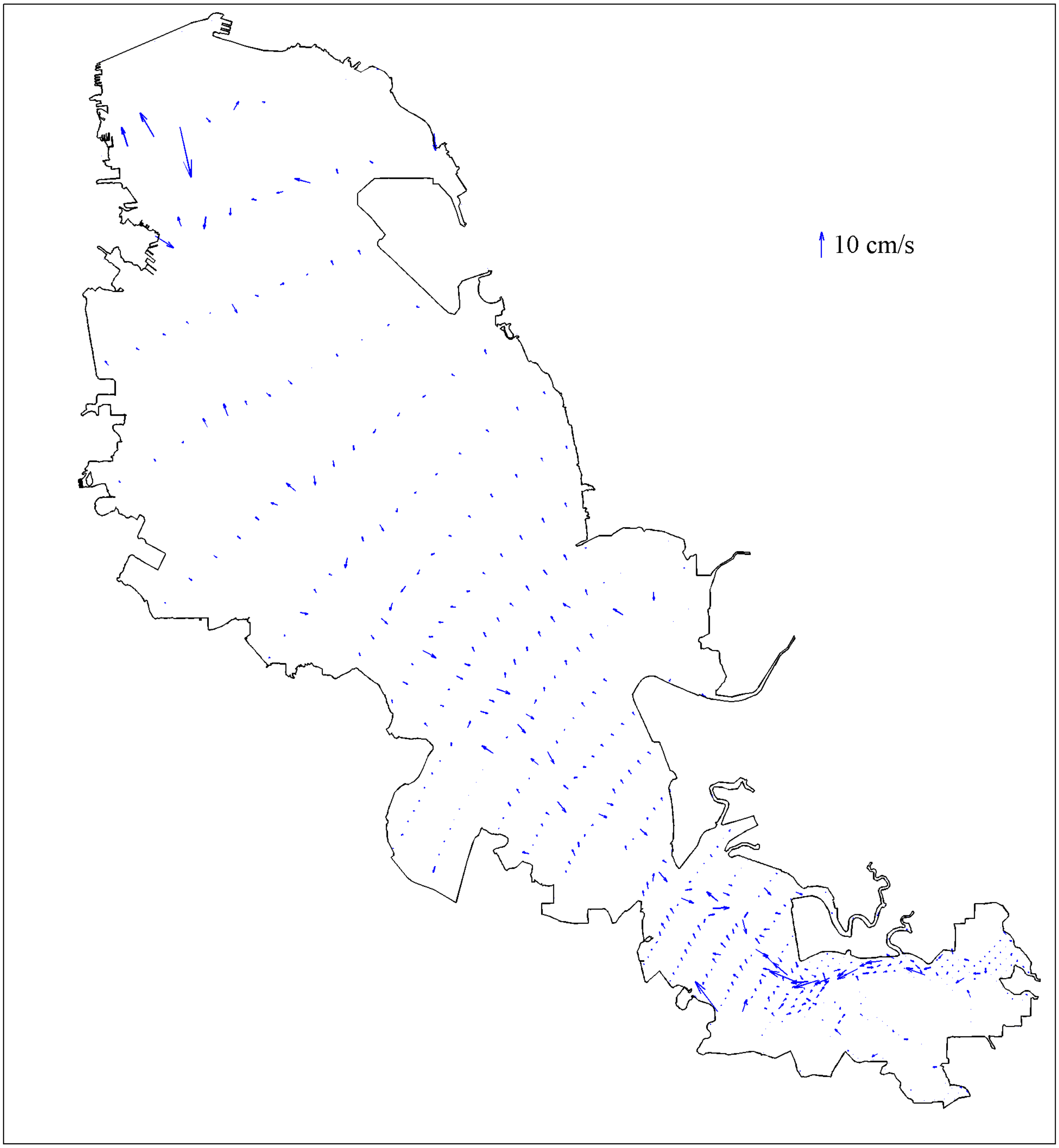

South Bay Residual Circulation (cm/s)

figure 6-95

South Bay Salt Pond Restoration Project

South Bay Residual Circulation, Baseline, Summer

PWA

Alternative A, Summer, Year 50

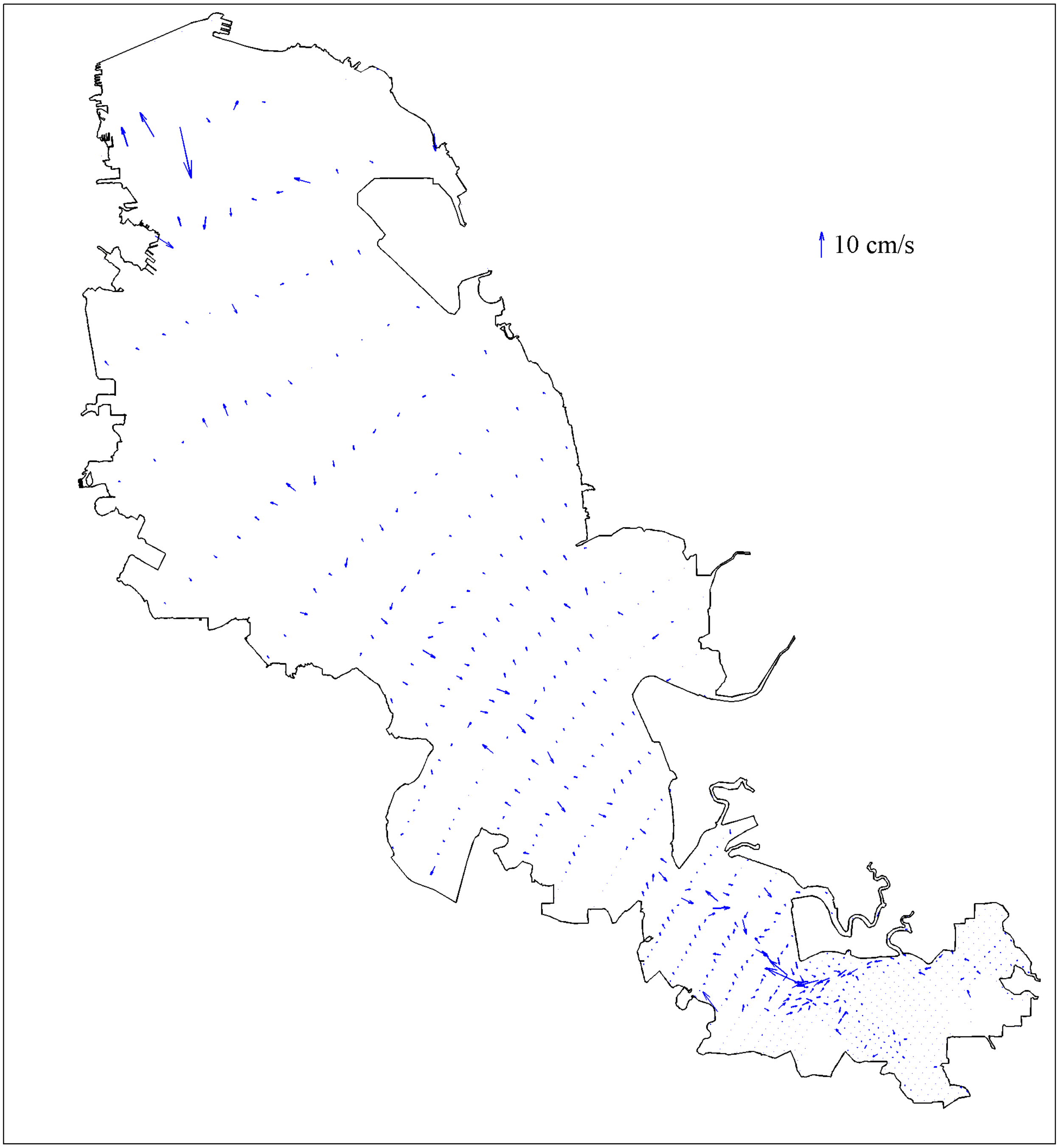

South Bay Residual Circulation (cm/s)

figure 6-96

South Bay Salt Pond Restoration Project

South Bay Residual Circulation, Alt A, Year 50, Summer

PWA

Difference (Alt A, Year 50 - Baseline)

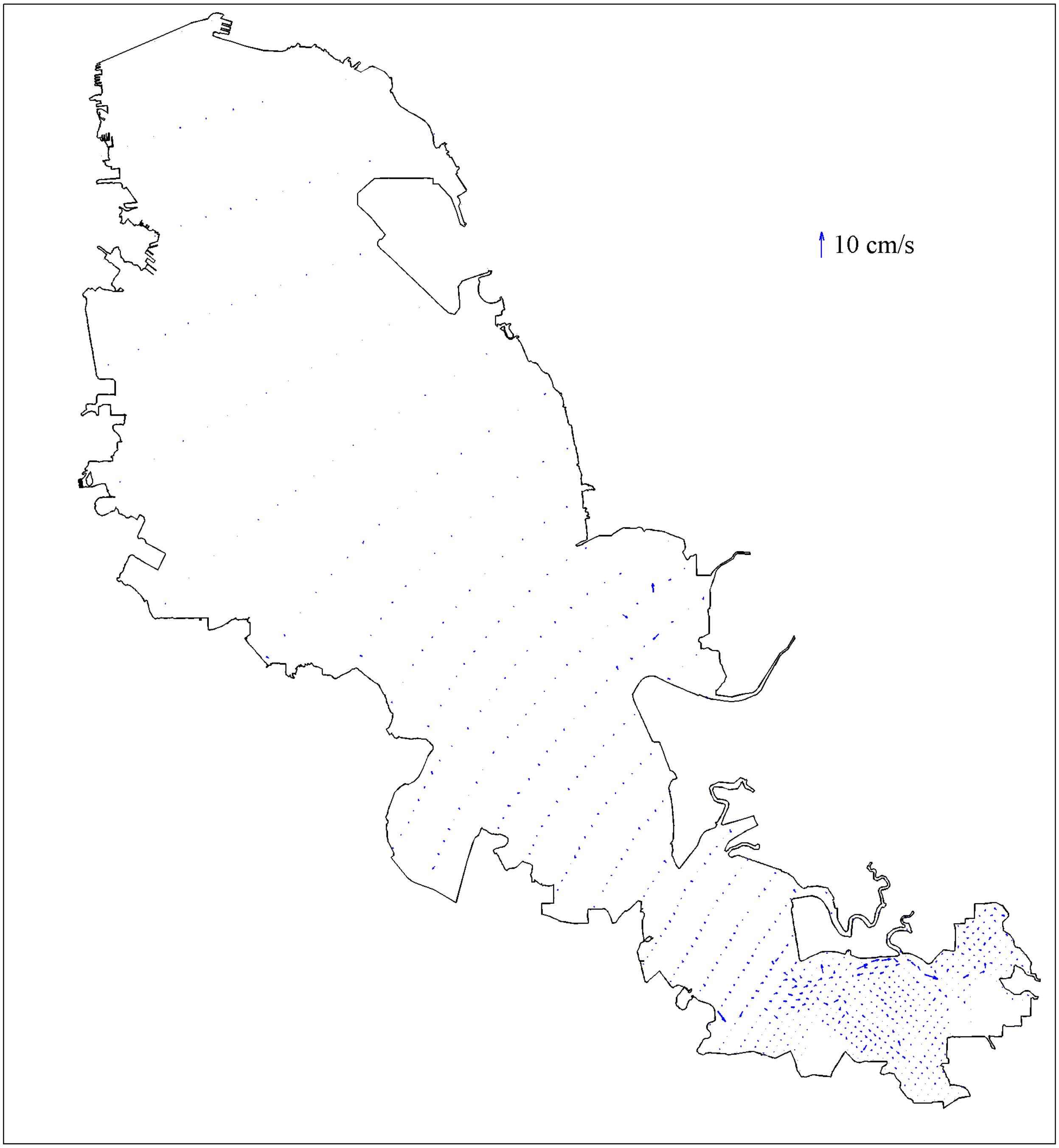

South Bay Residual Circulation Difference (cm/s)

figure 6-97

South Bay Salt Pond Restoration Project

South Bay Residual Circulation, Difference, Year 50, Summer

PWA

Baseline, Summer

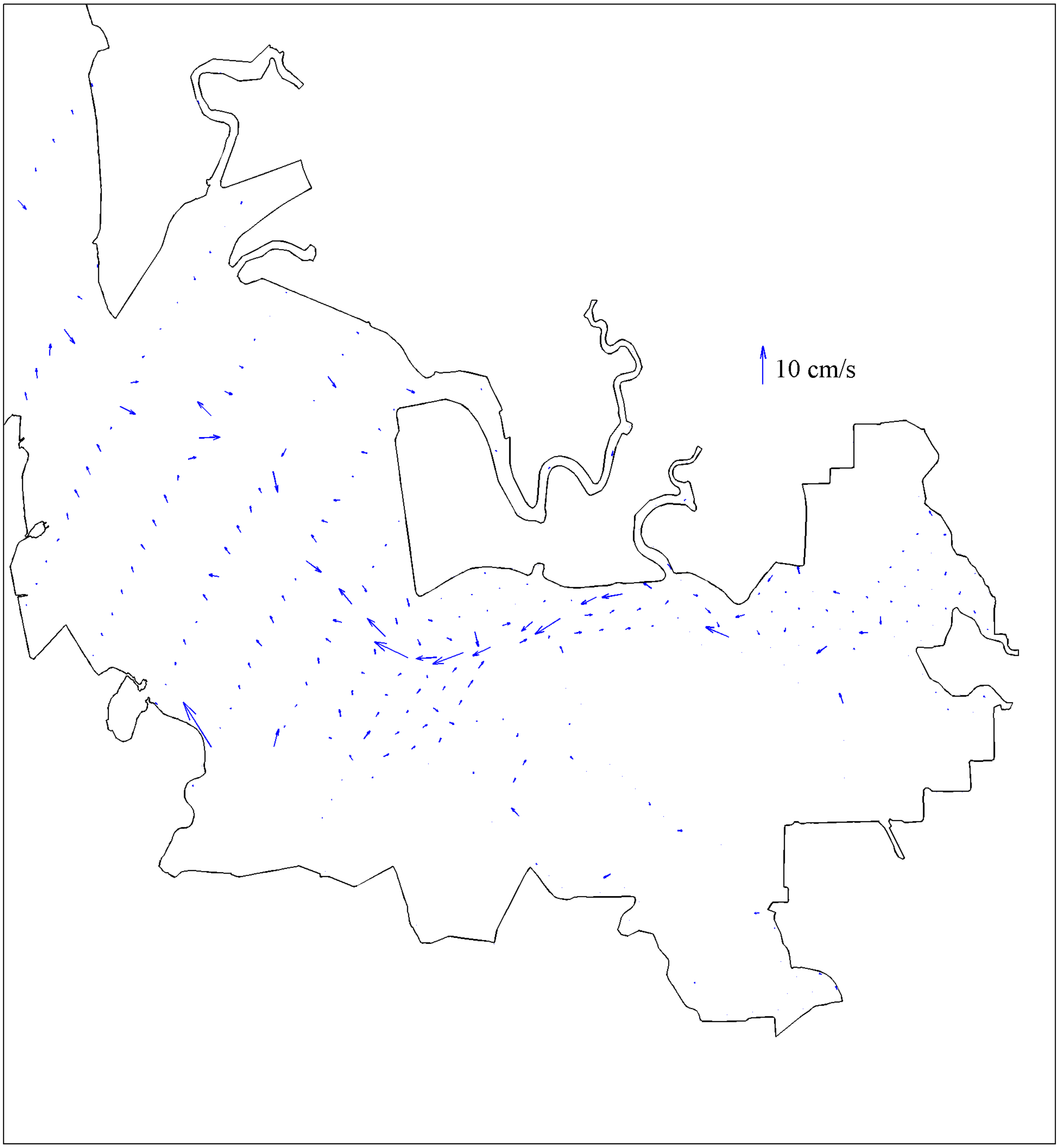

Far South Bay Residual Circulation (cm/s)

figure 6-98

South Bay Salt Pond Restoration Project

Far South Bay Residual Circulation, Baseline, Summer

PWA

Alternative A, Summer, Year 50

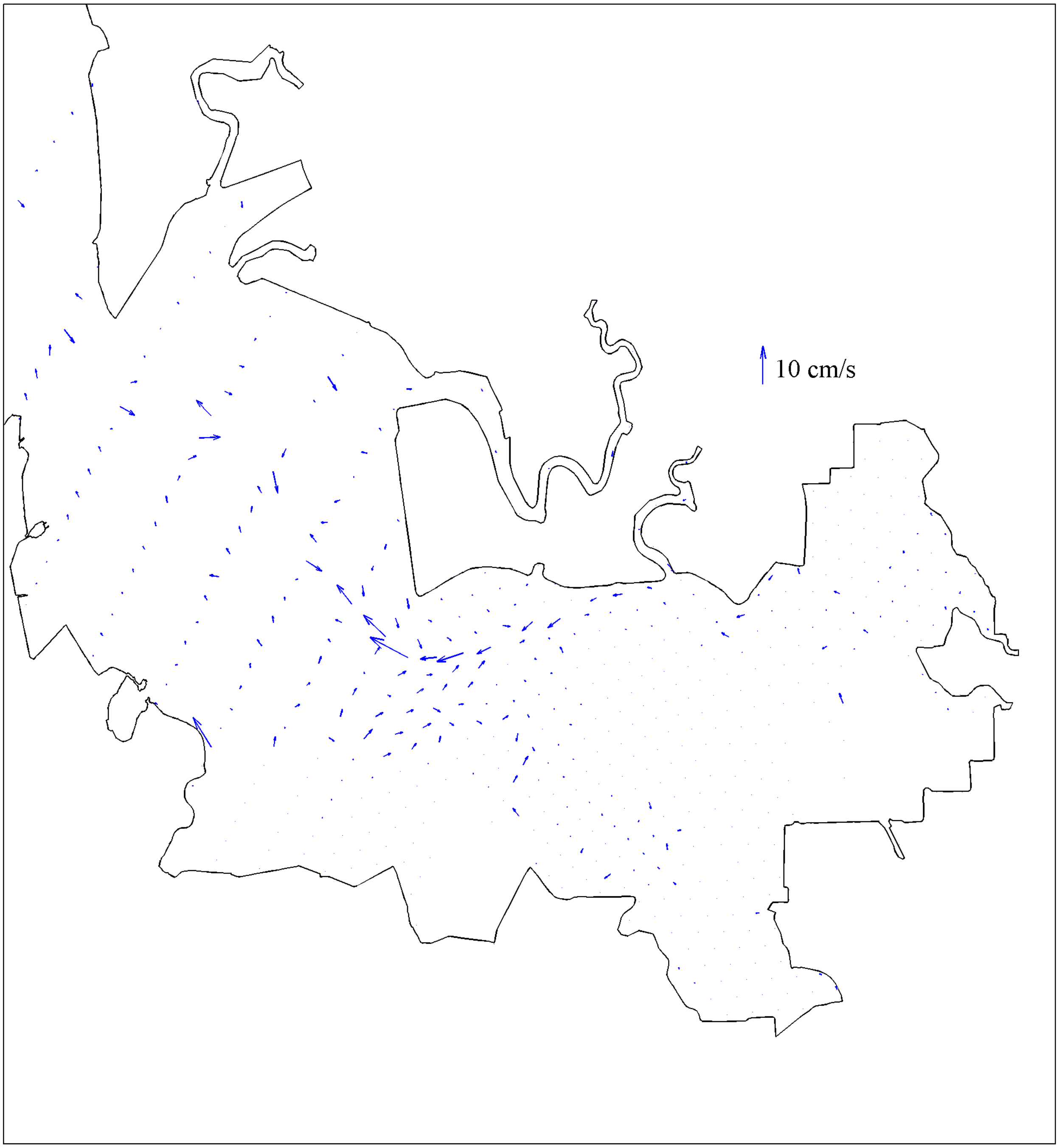

Far South Bay Residual Circulation (cm/s)

figure 6-99

South Bay Salt Pond Restoration Project

Far South Bay Residual Circulation, Alt A, Year 50, Summer

PWA

Difference (Alt A, Year 50 - Baseline)

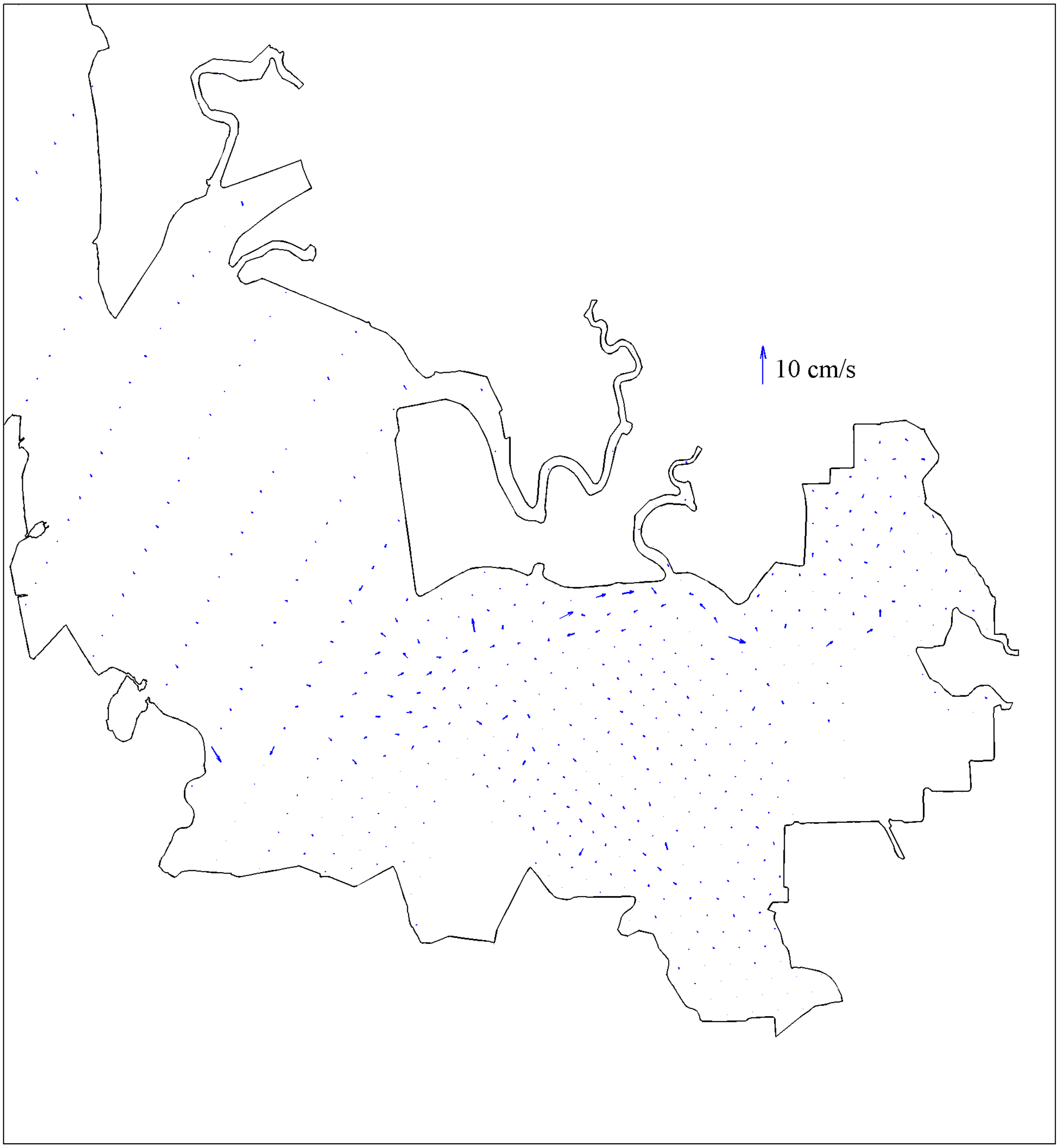

Far South Bay Residual Circulation Difference (cm/s)

figure 6-100

South Bay Salt Pond Restoration Project

Far South Bay Residual Circulation, Difference, Year 50, Summer

PWA

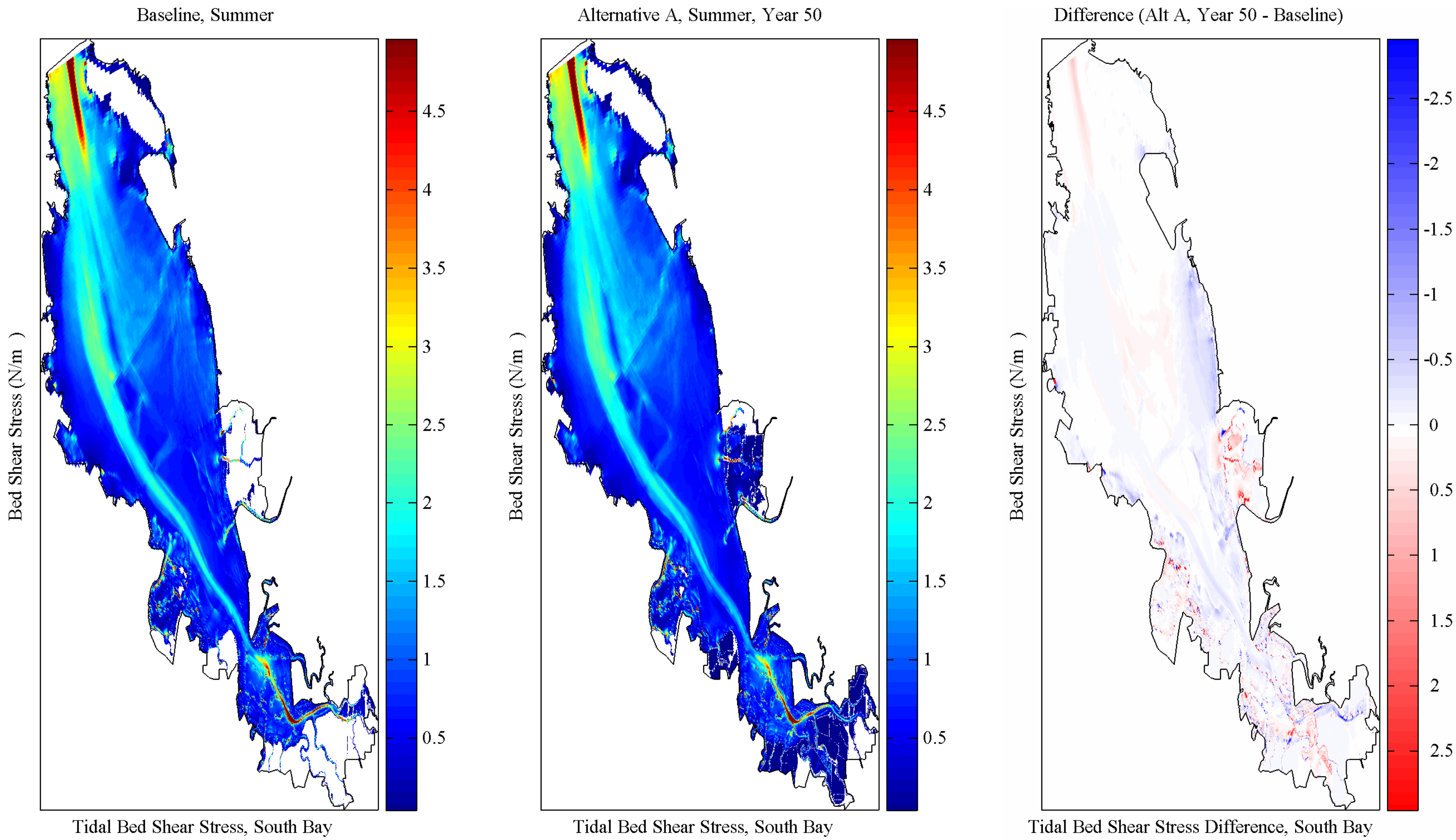

figure 6-101

South Bay Salt Pond Restoration Project

Tidal Bed Shear Stress, South Bay, Alt A, Year 50, Summer

PWA

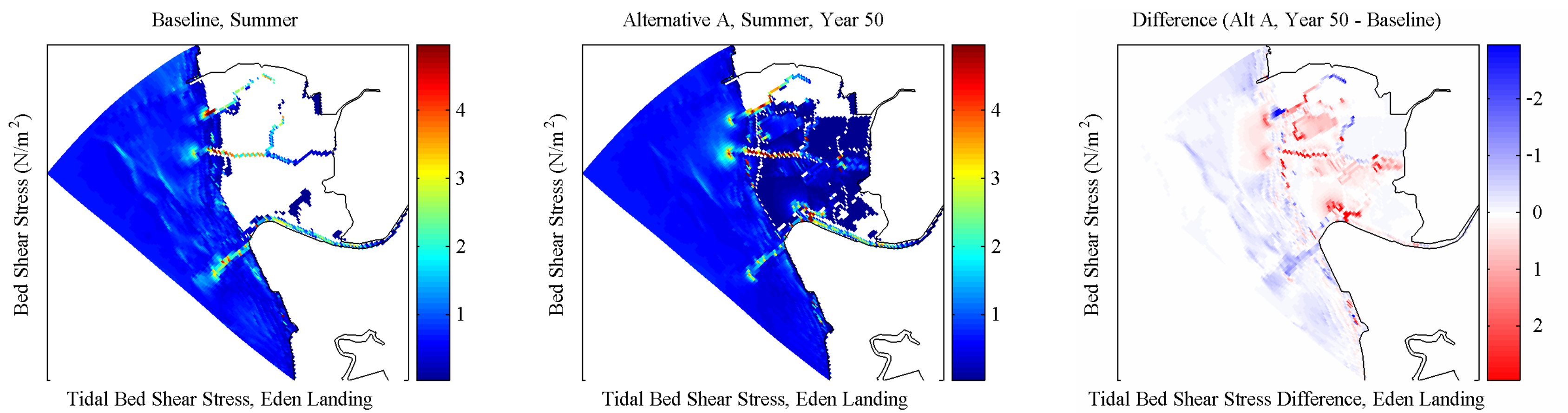

figure 6-102

South Bay Salt Pond Restoration Project

Tidal Bed Shear Stress, Eden Landing, Alt A, Year 50, Summer

PWA

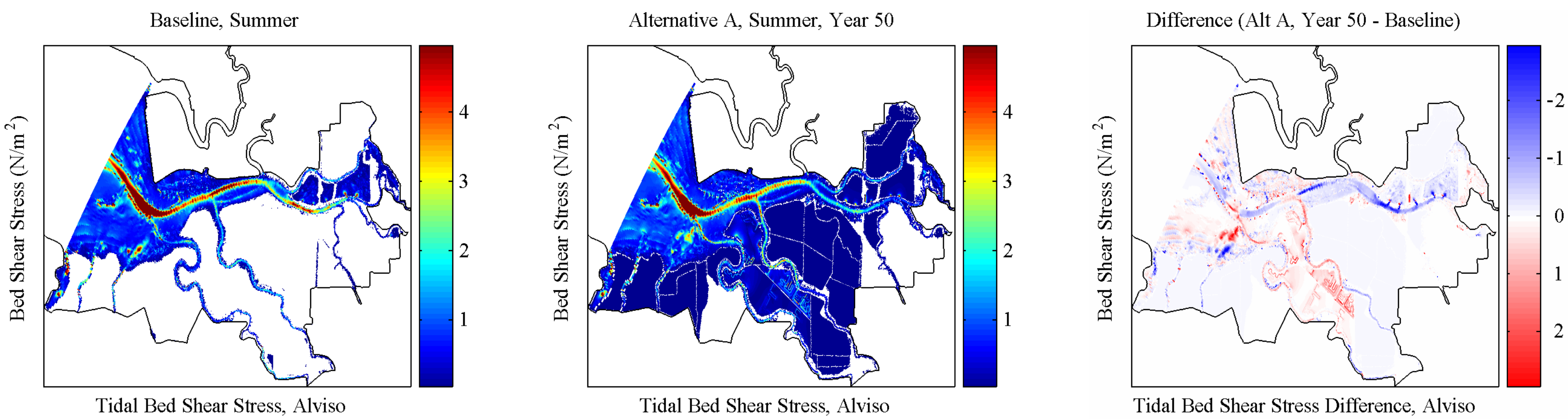

figure 6-103

South Bay Salt Pond Restoration Project

Tidal Bed Shear Stress, Alviso, Alt A, Year 50, Summer

PWA

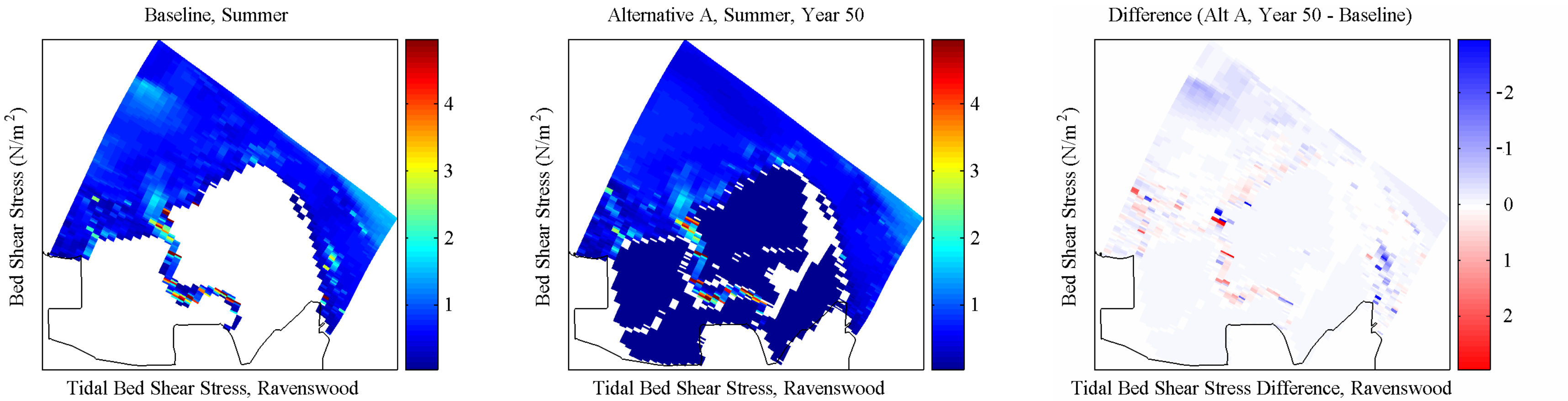

figure 6-104

South Bay Salt Pond Restoration Project

Tidal Bed Shear Stress, Ravenswood, Alt A, Year 50, Summer

PWA

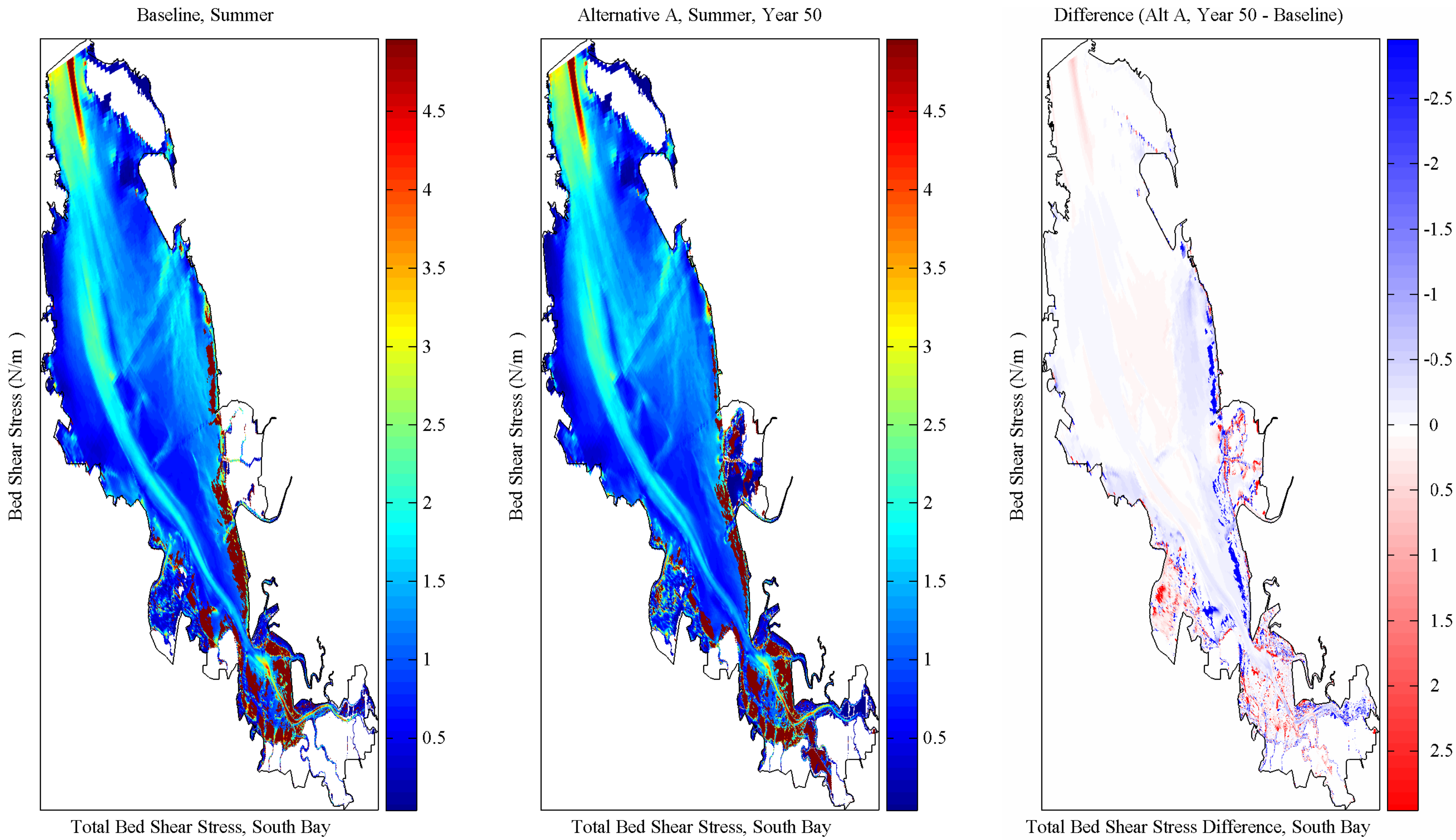

figure 6-105

South Bay Salt Pond Restoration Project

Total Bed Shear Stress, South Bay, Alt A, Year 50, Summer

PWA

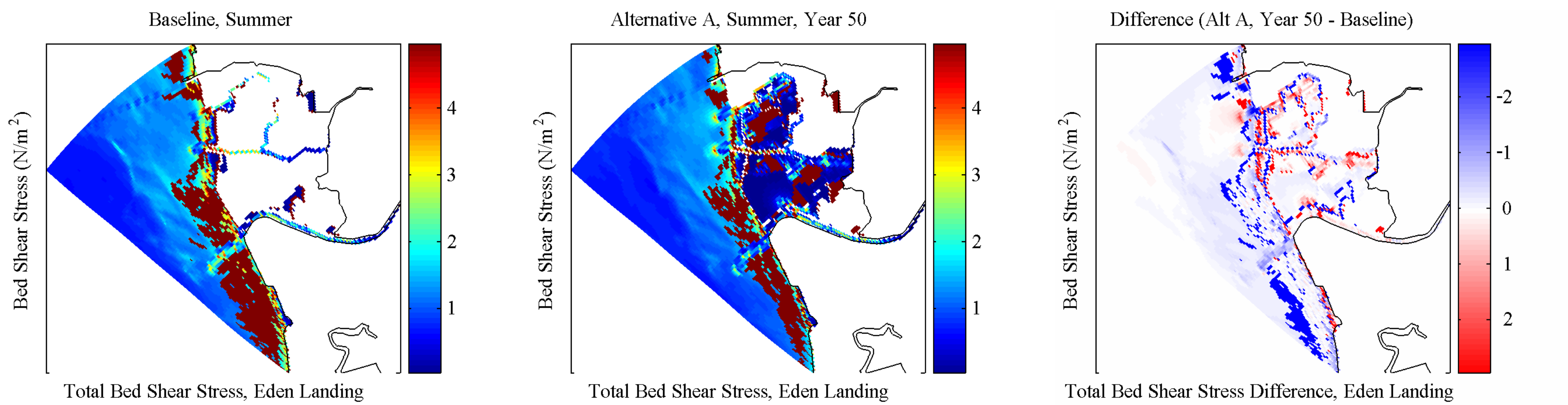

figure *6-106*

South Bay Salt Pond Restoration Project

Total Bed Shear Stress, Eden Landing, Alt A, Year 50, Summer

PWA

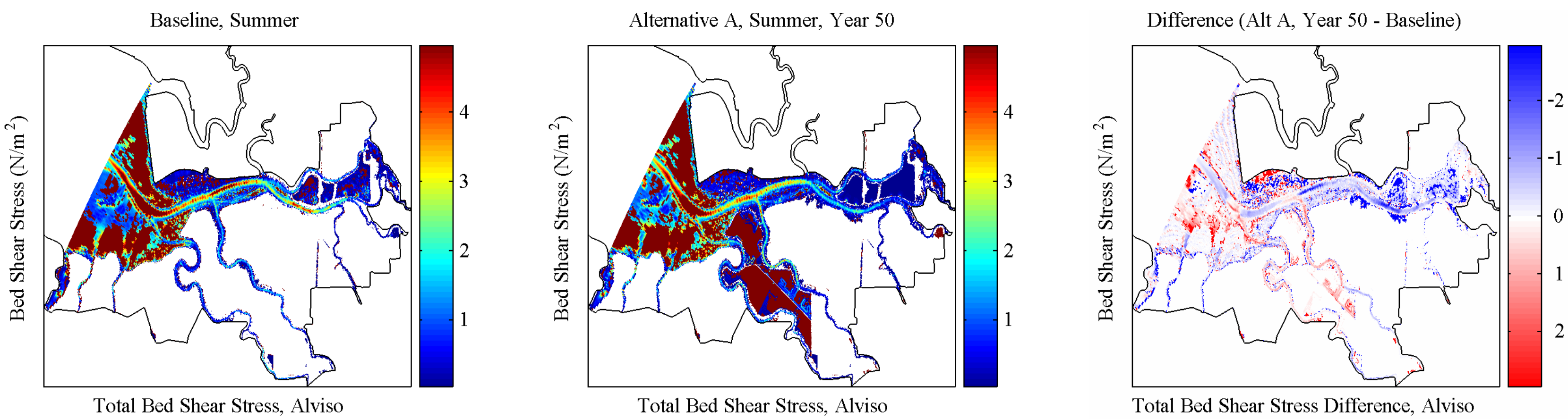

figure 6-107

South Bay Salt Pond Restoration Project

Total Bed Shear Stress, Alviso, Alt A, Year 50, Summer

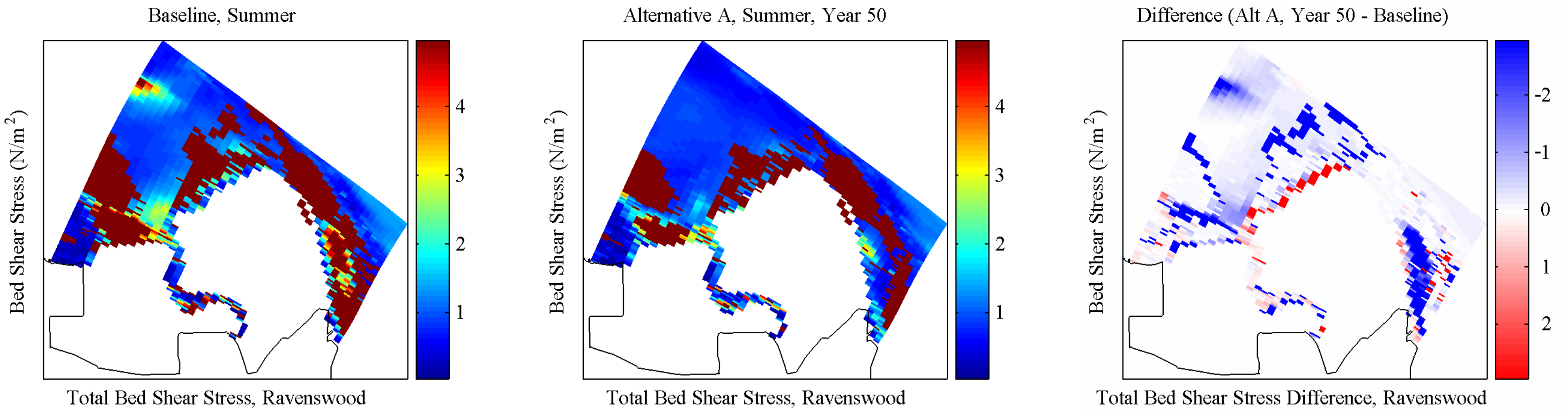

figure 6-108

South Bay Salt Pond Restoration Project

Total Bed Shear Stress, Ravenswood, Alt A, Year 50, Summer

PWA

7. ALTERNATIVE C, YEAR 50, SUMMER CONDITIONS

This section presents the results of the Alternative C, year 50, simulation under summer conditions, including a comparison with baseline summer conditions, where baseline represents present conditions, not the Alternative C, year 0 conditions presented in Section 4. The analysis presented utilizes the same approach presented in Section 4 for ease of comparison between simulations. The model predictions are analyzed using time series at stations throughout the South Bay. Figure 4-1 through Figure 4-4 show the station locations for the South Bay and the three pond complexes. The model predictions are also analyzed at specific snapshots in time for the entire South Bay and the pond complexes. Figure 4-5 shows where in the analysis period the snapshots were taken with respect to the spring-neap tidal cycle. The sections below present the results with respect to water levels, tidal prism, salinity, circulation and bed shear stress.

7.1 Water Levels

This section presents the model results with respect to water levels in the South Bay and the tidal sloughs under Alternative C, year 50, summer conditions (a.k.a. Alternative C, long-term conditions). The model predictions are compared to baseline summer predictions in order to assess the long-term impacts associated with opening 90 percent of the ponds to tidal action.

7.1.1 South Bay

Table 7-1 shows the water surface elevation and phase difference for the South Bay under Alternative C, long-term, summer conditions. Positive values in Table 7-1 represent an increase in water surface elevation when compared with baseline conditions, and negative values represent a decrease in water surface elevation. Positive phase values correspond to a slower arrival time under Alternative C, long-term conditions, or a phase lag when compared with baseline conditions, whereas negative values represent that modeled water levels under Alternative C are leading baseline conditions.

In the South Bay, the modeled water levels at the San Mateo Bridge increase on all phases of the daily tidal cycle relative to baseline conditions, and the increase is largely representative of the modeled rate of seal-level rise of 15 cm over 50 years (Figure 7-1). The change in water surface elevation is greatest at LLW when the water surface increases approximately 20 cm. Compared with Alternative A, long-term conditions (Figure 6-1), the water surface elevation is approximately 1 cm higher under Alternative C, long-term conditions for much of the diurnal tidal cycle, and approximately 3 cm higher at LLW.

At the Dumbarton Bridge (Figure 7-2), the water level increase under Alternative C, long-term conditions, when compared with baseline conditions, is approximately equal to sea-level rise throughout the analysis period with the exception of LLW during spring tide. Water levels decrease by approximately 25 to 30 cm at LLW during spring tide conditions. The Dumbarton Bridge station is located on the eastern edge of the main South Bay channel, and this station is completely dry when the water surface elevation drops below approximately -0.4 m NAVD88 under baseline conditions. At year 50, scour is predicted to occur along the edges of the main South Bay channel; therefore the water level at LLW is no longer constrained by the bed elevation. The change in water surface elevation at the Dumbarton Bridge is slightly lower (-1 cm) than that predicted under Alternative A long-term conditions at low water, with slightly higher water levels (+ 2 cm) predicted at HHW under neap tide conditions.

At Channel Marker 17 (Figure 7-3), located near the mouth of Coyote Creek, water levels increase on all phases of the tide when compared with baseline conditions. The increases at HHW are of similar magnitude to the rate of sea-level rise; however, the tidal restoration under Alternative C tempers the water level increase. In other words, the increase in HHW could be larger in the absence of the tidal restoration. The increase in HHW water surface elevations is slightly higher (+ 2 to 3 cm) under Alternative C, long-term conditions than predicted under Alternative A, long-term conditions. LLW increases by approximately 20 cm under neap tide and 25 cm under spring tide conditions in response to sea-level rise, the increase in tidal prism associated with the tidal restoration in the Alviso pond complex, and the erosion of the intertidal mudflats predicted to occur in the far South Bay.

The long-term trend in increased water levels leads to an increase in the MLLW and MHHW tidal datums. Table 7-2 presents the increase in MLLW and MHHW tidal datums relative to baseline conditions for both Alternative C and Alternative A, long-term conditions. Figure 7-4 depicts the change in MLLW at year 50. The increase in MLLW is most pronounced in the far South Bay where MLLW increases approximately 18 – 19 cm. This trend is similar to that observed under Alternative A, long-term conditions; however, the increase in MLLW in the far South Bay is approximately 1 cm greater under Alternative C. Conversely, the increase in MHHW is approximately 1 cm less under Alternative C, long-term conditions than predicted under Alternative A. MHHW increases by approximately 15 cm throughout most of the South Bay (Figure 7-5), with a slightly smaller increase on the order of 12 cm occurring in the far South Bay.

Harmonic analysis was performed on water levels at several stations along the main South Bay channel, and the computed phase and amplitudes of the M_2 and K_1 tidal constituents for baseline and Alternative C year 50 conditions are compared in order to assess how the alternative is affecting tidal propagation within the South Bay (Figure 7-6). Figure 7-6a presents the computed phase of the M_2 and K_1 tidal constituents. There is a small reduction in phase relative to baseline conditions for both tidal constituents under Alternative C, year 50 conditions. Figure 7-6b presents the computed amplitude of the M_2 and K_1 tidal constituents. As the tides propagate into the South Bay, the amplitude of both tidal constituents is decreased, with a more marked difference observed in the M_2 tidal constituent in the far South Bay. This difference is smaller than observed under Alternative C, year 0 conditions (Figure 4-11).

Table 7-1. South Bay Water Surface Elevation and Phase Differences under Alt C, Year 50, Summer
(Water surface elevation differences in cm, phase differences in minutes. June 13 = neap tide, June 22 = spring tide.)

Station Name	June 13 LLW		June 13 HHW		June 22 LLW		June 22 HHW	
	WSE	Phase	WSE	Phase	WSE	Phase	WSE	Phase
San Mateo Bridge, Figure 7-1	16	0	15	0	20	0	15	0
Dumbarton Bridge, Figure 7-2	16	10	14	0	-26	-30	14	0
Channel Marker 17, Figure 7-3	19	30	14	0	26	10	13	0

Table 7-2. South Bay Tidal Datums Differences under Alt C, Year 50, Summer and Alt A, Year 50, Summer
(All differences are increases relative to baseline conditions in cm)

South Bay Station	Alternative A, year 50		Alternative C, year 50	
	MLLW	MHHW	MLLW	MHHW
Oakland-Bay Bridge	15.0	15.0	15.0	15.0
San Mateo Bridge	16.2	14.6	18.2	14.9
Dumbarton Bridge	18.1	13.7	17.9	14.0
Channel Marker 17	21.8	13.7	23.0	13.6

7.1.2 Tidal Sloughs

Under Alternative C, approximately 90 percent of the SBSP Restoration Project Area would be restored to tidal action, and over the 50-year horizon, the restored ponds are assumed to develop into mature salt marsh (see Section 3.4). The ponds restored to tidal marsh are shown in Figure 3-7, Figure 3-8 and Figure 3-9 for each pond complex. In response to the increase in tidal prism associated with this conversion, the tidal sloughs are expected to scour and deepen as they approach equilibrium conditions, potentially lessening the tidal damping effect seen under the Alternative C, year 0 simulations in the absence of channel scour (Section 4). Table 3-7 presents the predicted increase in channel depth for the tidal sloughs located within the SBSP Restoration Project Area. The tidal sloughs outside of the project area are assumed to retain their existing bathymetry.

Table 7-3 presents the water surface elevation and phase difference under Alternative C long-term conditions at both upstream and downstream stations in each tidal slough. Positive water surface elevation values in Table 7-3 represent an increase in water level when compared with baseline conditions, and negative values represent a decrease in water level. Positive phase values correspond to a slower arrival time under Alternative C, or a phase lag when compared with baseline conditions, whereas negative values represent that modeled water levels under Alternative C are leading baseline conditions.

The sloughs that are predicted to have the greatest channel scour (downstream in ACFCC, Old Alameda Creek, Charleston Slough, Mountain View Slough, Stevens Creek and Ravenswood Slough) all exhibit an increase in tidal range – low water levels decrease and high water levels increase under Alternative C, long-term conditions. In contrast, under Alternative C, year 0 conditions where no channel scour was assumed, tidal damping was predicted in these sloughs. In the sloughs predicted to have a lesser amount of channel scour (upstream in ACFCC, Coyote Creek, downstream in Alviso and Guadalupe Sloughs, and Mud Slough), water levels increase on all phases of the tide – low water levels and high water levels increase, with the increase in low water levels greater than the increase in high water levels.

Upstream in Alviso Slough (Figure 7-18), Guadalupe Slough (Figure 7-20) and the Moffett Channel (Figure 7-21), tidal damping is predicted – low water levels increase and high water levels decrease. Compared with the year 0 simulation (Section 4), the increase in low water levels under long-term conditions is approximately half that predicted at year 0, and the increase in high water levels is approximately one-half to three-quarters of the year 0 prediction. In general for all tidal sloughs, the increase in high water levels is less than the predicted rate of sea-level rise of 15 cm, and the increase is smaller than that predicted for Alternative A, long-term conditions.

Phasing changes are relatively small in most tidal sloughs, with a phase lag on the order of 30 minutes throughout the SBSP Restoration Project Area. Larger phase changes are observed in the tidal sloughs predicted to have the most channel scour, such as ACFCC, Old Alameda Creek, Charleston Slough, Mountain View Slough, Stevens Creek and Ravenswood Slough. In these sloughs, the tide is predicted to arrive one to two hours faster at LLW, with less significant deviations associated with high water levels. However, as discussed in Section 2.3.5, with the exception of the ACFCC, the slough widths associated with these sloughs are oversized in the model due to grid resolution limitations; therefore, the faster arrival times and greater tidal range predicted for these sloughs may be overstated by the model results.

Table 7-3. Tidal Slough Water Surface Elevation and Phase Differences under Alt C, Year 50, Summer
(Water surface elevation differences in cm, phase differences in minutes. June 13 = neap tide, June 22 = spring tide.)

Station Name	June 13 LLW		June 13 HHW		June 22 LLW		June 22 HHW	
	WSE	**Phase**	**WSE**	**Phase**	**WSE**	**Phase**	**WSE**	**Phase**
Eden Landing pond complex								
ACFCC Downstream, Figure 7-7	-33	-90	18	-10	-96	-80	12	10
ACFCC Upstream, Figure 7-8	-4	40	26	-40	7	-90	18	-10
Old Alameda Creek Downstream, Figure 7-9	-7	-60	13	30	-37	-40	12	40
Old Alameda Creek Upstream, Figure 7-10	-14	-60	13	30	-37	-40	12	40
Alviso pond complex								
Coyote Creek Power Tower, Figure 7-11	25	30	11	10	23	80	10	0
Coyote Creek Railroad Bridge, Figure 7-12	21	30	14	0	18	30	13	0
Coyote Creek/Island Ponds , Figure 7-13	21	20	12	10	17	20	11	0
Coyote Creek Upstream, Figure 7-14	22	30	11	10	18	20	8	0
Mud Slough Downstream, Figure 7-15	21	20	7	20	19	20	9	0
Mud Slough Upstream, Figure 7-16	25	20	8	30	24	20	7	0
Alviso Slough Downstream, Figure 7-17	25	30	8	10	36	30	6	10
Alviso Slough Upstream, Figure 7-18	38	80	-13	90	55	90	-19	80
Guadalupe Slough Downstream, Figure 7-19	23	30	13	0	36	30	13	0
Guadalupe Slough Upstream, Figure 7-20	37	40	-9	60	48	50	-11	50
Moffett Channel, Figure 7-21	37	50	-8	60	48	50	-11	50
Stevens Creek Downstream, Figure 7-22	-19	-70	13	10	-15	-50	11	10
Stevens Creek Upstream, Figure 7-23	-23	-90	12	10	-15	-60	10	10
Mountain View Slough Downstream, Figure 7-24	-30	-90	15	0	-33	-60	15	20
Mountain View Slough Upstream, Figure 7-25	-31	-110	15	0	-34	-70	15	20
Charleston Slough Downstream, Figure 7-26	-41	-100	22	-50	-63	-80	14	20
Charleston Slough Upstream, Figure 7-27	-45	-70	21	-60	-56	-50	13	20
Ravenswood pond complex								
Ravenswood Slough Downstream, Figure 7-28	-36	-100	15	10	-38	-60	12	20
Ravenswood Slough Upstream, Figure 7-29	-27	-90	14	0	-30	-50	14	10

7.2 Tidal Prism

A comparison of the estimates of modeled tidal prism between baseline and Alternative C, year 50, summer conditions is summarized in Table 7-4. As discussed in Section 4.2, tidal prism has been estimated as the volume of water crossing a cross-section during a flood tide for the basis of comparing tidal prism estimates with previous studies.

Under Alternative C, long-term conditions, the modeled tidal prism at the San Mateo and Dumbarton Bridge cross-sections is predicted to increase approximately ten to fifteen percent. This increase results from the increase in tidal prism from the tidally-restored ponds and the mudflat erosion predicted to occur in the South Bay (see Section 3.4.3). Figure 7-30 presents the modeled flux of water across both bridge cross-sections under baseline and Alternative C, long-term conditions, and the relative increase and decrease in tidal prism are evident. Within the far South Bay, the tidal prism and the associated modeled flux of water relative to baseline conditions increases, as shown on Figure 7-31. At Calaveras Point, the modeled tidal prism increases approximately 36 percent (Table 7-4).

Within the Eden Landing pond complex, tidal prism is predicted to increase approximately 130 to 250 percent as a result of Alternative C, long-term conditions. This tidal prism increase is associated with the slough scour in response to the tidal restoration (see Section 3.4.2), and the establishment of a mature marsh channel network within the tidally-restored ponds. Although the depth of scour matches the hydraulic geometry estimates, the tidal sloughs in the Eden Landing pond complex are oversized in the model due to the grid resolution limitations discussed in Section 2.3.5; therefore, the volume of scour may be over-estimated in the model. The oversized nature of the sloughs, coupled with an overestimation of the volume of potential slough scour, leads to an over-estimation of the potential long-term increase in tidal prism. Although the magnitudes of tidal prism increase are probably overstated in the Eden Landing pond complex, the trend of increasing tidal prism is consistent with the addition of intertidal area. This trend in increasing tidal prism is also evident in the comparisons of the modeled flux of water under baseline and Alternative C, long-term conditions near the slough mouths of the ACFCC and Old Alameda Creek (Figure 7-32).

All tidal sloughs within the Alviso pond complex are predicted to experience an increase in tidal prism under Alternative C, long-term conditions. The magnitude of the potential increase for a particular slough depends upon the number of tidally-restored ponds along the slough, the location of the slough within the pond complex, and the slough's existing conveyance capacity. Cross-sections in the upper reaches of Coyote Creek, such as at the Railroad Bridge and east of the Island Ponds, exhibit a moderate increase in tidal prism (Figure 7-33). Under Alternative C, year 0 conditions, the tidal prism was predicted to decreases at these cross sections (Section 4.2). However, under Alternative C, long-term conditions, the Island Ponds are assumed to develop into mature salt marsh over the 50-year horizon, therefore water previously captured by the Island Ponds under year 0 conditions can propagate into the upper reaches of Coyote Creek under long-term conditions.

Mud Slough, a tributary of Coyote Creek, exhibits a tidal prism increase of approximately 60 percent under Alternative C, long-term conditions. This increase is associated with the tidal restoration of Ponds A22 and A23 at the upper end of Mud Slough, the development of mature salt marsh within the Island Ponds and sea-level rise.

The remaining sloughs in the Alviso pond complex exhibit increases in tidal prism associated with the development of mature marsh channel networks within the tidally-restored ponds, the sloughs' existing conveyance capacity, estimate of long-term channel scour and sea-level rise. For example, the tidal prism in Guadalupe Slough is predicted to by 62 percent under Alternative C, year 50. Under Alternative C, year 0 conditions, the tidal prism within Guadalupe Sough is predicted to increase by approximately 160 percent (Table 4-4). The lesser increase under long-term conditions occurs because the tidally-restored ponds develop into mature salt marsh, reducing the volume of added tidal prism associated with the ponds. The tidal prism of Alviso Slough and Artesian Slough evolve similarly with time. Figure 7-34 presents the modeled flux of water near the mouths of Guadalupe and Alviso Sloughs under baseline and Alternative C, long-term conditions. The lesser tidal prism increase than that associated with year 0 conditions is evident upon visual inspection of Figure 7-34 and Figure 4-49, which presents the same results for Alternative C, year 0 conditions.

In contrast, the long-term tidal prism associated with Stevens Creek, Mountain View Slough and Charleston Slough is predicted to increase from year 0 to year 50. These sloughs are oversized in the model, as discussed in Section 2.3.5, therefore the relative increase in tidal prism associated with the predicted increase in channel scour is likely overstated in the model results. The sloughs also experience increases in tidal prism associated with sea-level rise. The predicted tidal prism increase in Ravenswood Slough in the Ravenswood pond complex is likely overstated as well for the same reasons. Although the predicted increases in tidal prism within these sloughs are likely overstated, the general trend of increasing tidal prism is expected. The comparison of modeled flux between baseline and Alternative C, long-term conditions at the mouth of Stevens Creek and Mountain View Slough (Figure 7-35) and Charleston and Ravenswood Soughs (Figure 7-36) is likely also overstated due the oversized representation of the sloughs in the model and the associated overestimation of the volume of slough scour.

Non-project sloughs north of the Dumbarton, i.e. Corkscrew Slough, Redwood Creek, and Westpoint Slough exhibit tidal prism increases on the order of 15 percent under Alternative C, long-term conditions. This increase is similar to that predicted for Alternative A, long-term conditions; therefore, this increase is likely largely associated with the predicted rate of sea-level rise.

The non-project sloughs in the far South Bay, i.e. Mowry Slough, Plummer Slough and Newark Slough, exhibit larger increases in tidal prism relative to baseline conditions than predicted for Alternative A, long-term conditions. This increase in tidal prism is therefore likely associated with sea-level rise and the mudflat erosion predicted to occur in the far South Bay. However, the slough mouths were eroded using the same routine applied to the far South Bay, therefore the predicted tidal prism increase is likely overstated. If these sloughs were subject to continued sedimentation over the 50-year horizon, the sloughs would experience a decrease in tidal prism.

Table 7-4. Comparison of Tidal Prism between Baseline and Alternative C, year 50, summer

Transect location	Tidal prism (millions of cubic meters)		
	Baseline summer	Alternative C yr 50, summer	% change baseline to Alt. C
South Bay			
San Mateo Bridge	270	290	9.2%
Dumbarton Bridge	71	80	14%
Eden Landing pond complex			
ACFCC	1.4	3.3	130%
Old Alameda Creek	1.4	4.5	220%
Mount Eden Creek	0.58	2.0	250%
Ravenswood pond complex			
Ravenswood Slough	0.53	2.2	310%
Alviso pond complex			
Calaveras Point	14	19	36%
Coyote Creek at Power Tower	6.8	10	48%
Coyote Creek at RR Bridge	2.2	2.3	1.8%
Coyote Creek east of Island Ponds	0.53	0.81	54%
Charleston Slough	0.55	0.94	73%
Mountain View Slough	0.21	0.85	300%
Stevens Creek	0.11	0.53	380%
Guadalupe Slough	1.1	1.8	62%
Alviso Slough	1.1	2.4	110%
Artesian Slough	0.48	0.63	30%
Mud Slough	0.79	1.3	59%
Non-project Sloughs			
Corkscrew Slough	3.4	3.9	12%
Redwood Creek	16	18	16%
Westpoint Slough	2.9	3.3	14%
Mowry Slough	0.41	0.60	47%
Plummer Slough	0.32	0.36	13%
Newark Slough	0.86	1.1	27%

7.3 Salinity

This section presents the model results with respect to salinity in the South Bay and the tidal sloughs under Alternative C, year 50, summer conditions. The model predictions are compared to baseline summer predictions in order to assess the impact of restoring 90 percent of the SBSP Restoration Project Area to tidal action on the South Bay and the tidal sloughs, as presented below.

7.3.1 South Bay

Under Alternative C, long-term conditions, little change is observed with respect to salinity north of the Dumbarton Bridge (Table 7-5). Positive values in Table 7-5 represent an increase in salinities relative to the baseline, and negative values represent a decrease in salinities relative to baseline conditions. At the San Mateo and Dumbarton Bridges, there is no significant difference in salinity when compared with baseline conditions (Figure 7-37 and Figure 7-38, respectively). Higher salinity differences are observed at Channel Marker 17 (Figure 7-39), with salinity increases on the order of 3 – 5 ppt observed at LLW.

Figure 7-40 displays the salinities in the South Bay during spring tide conditions at HHW, representing peak salinity conditions during the analysis period. As can be seen, little difference in peak South Bay salinities occurs under summer conditions with respect to long-term, Alternative C conditions. The largest changes in salinity are confined to the tidal sloughs. Figure 7-41 displays South Bay salinities at LLW during spring tide conditions. At low water, the observed differences are higher downstream of the tidal sloughs and in the subtidal channels in the South Bay. The salinity in the tidal sloughs is higher under Alternative C, long-term conditions than baseline conditions; therefore, the water drawn into the Bay from the tidal sloughs on ebb tide is more saline.

Table 7-5. South Bay Salinity Differences under Alt C, Year 50, Summer

(Salinity differences in ppt. June 13 = neap tide, June 22 = spring tide.)

Station Name	**June 13 LLW**	**June 13 HHW**	**June 22 LLW**	**June 22 HHW**
San Mateo Bridge, Figure 7-37	-0.2	-0.1	-0.1	0.0
Dumbarton Bridge, Figure 7-38	0.0	-0.1	-0.1	-0.1
Channel Marker 17, Figure 7-39	3.0	0.1	4.4	0.4

7.3.2 Tidal Sloughs

Table 6-5 shows the salinity difference between Alternative C, long-term conditions and baseline conditions during neap and spring tide summer conditions. Positive values represent an increase in salinities relative to the baseline, and negative values represent a decrease in salinities relative to baseline conditions.

In the Eden Landing pond complex, salinities increase in the downstream reach of the ACFCC in response to the increased tidal exchange and mixing associated with the deeper channel and the increased tidal prism (Figure 7-42). At high water levels, only a moderate salinity increase of 0 – 2 ppt is observed; however, low water salinities increase up to 10 ppt. This increase in downstream salinities shifts the salinity gradient upstream, and salinities at the upstream station in ACFCC are 4 – 8 ppt higher throughout the analysis period (Figure 7-43). Salinities in Old Alameda Creek exhibit little change with respect to baseline salinities (Figure 7-44 and Figure 7-45). As discussed in the previous sections, the potential changes to the salinity regime in Old Alameda Creek is likely underestimated due to the oversized representation of Old Alameda Creek in the model. The salinity trends in the Eden Landing pond complex are similar to those observed under Alternative A, long-term conditions, although under Alternative C, long-term conditions, salinities downstream are approximately 2 ppt higher, and salinities upstream are approximately 2 ppt lower.

Figure 7-46 and Figure 7-47 present the peak salinities in the Eden Landing pond complex during spring HHW and LLW conditions, respectively. As can be seen, the largest salinity changes are observed in the ACFCC and in the South Bay directly downstream of the ACFCC.

In the Alviso pond complex, salinities increase both upstream and downstream in all tidal sloughs. At the Power Tower downstream in Coyote Creek, salinities increase approximately 5 ppt at LLW and less than 0.5 ppt at HHW on both spring and neap tide (Figure 7-48). Farther upstream in Coyote Creek, salinities increase approximately 3 – 5 ppt on all phases of the tide (Figure 7-49, Figure 7-50, and Figure 7-51). This increase in salinity is due to the increased tidal prism associated with restoring the Pond A9 system (Ponds A9 through A17), as well as the estimates of long-term bathymetric change. Moderate channel scour is predicted to occur in Coyote Creek (Table 3-7), therefore unlike Alternative A, long-term conditions, tidal exchange is not restricted due to continuing channel sedimentation.

Alviso Slough and Guadalupe Slough both experience salinity increases on the order of 4 – 10 ppt. At the downstream stations (Figure 7-54 and Figure 7-56, respectively), salinities at LLW increase 4 – 9 ppt, while salinities at HHW increase approximately 0 – 1 ppt. At the upstream stations, salinities increase across all phases of the tide (Figure 7-55 and Figure 7-57, respectively). Stevens Creek, Mountain View Slough, Charleston Slough and Ravenswood Slough exhibit slight increases in salinity on the order of 0 – 1.5 ppt. As discussed in the previous sections, these sloughs are represented in the model at approximately twice their physical width; therefore they are more hydraulically connected to the Bay in the model. This could result in an underestimation of the potential changes in the salinity regime in these sloughs.

Table 7-6. Tidal Slough Salinity Differences under Alt C, Year 50, Summer

(Salinity differences in ppt. June 13 = neap tide, June 22 = spring tide.)

Station Name	June 13 LLW	June 13 HHW	June 22 LLW	June 22 HHW
Eden Landing pond complex				
ACFCC Downstream, Figure 7-42	9.8	1.1	7.5	0.2
ACFCC Upstream, Figure 7-43	4.6	4.3	7.9	2.8
Old Alameda Creek Downstream, Figure 7-44	0.0	-0.2	0.0	0.0
Old Alameda Creek Upstream, Figure 7-45	-0.4	-0.5	-0.5	-0.5
Alviso pond complex				
Coyote Creek Power Tower, Figure 7-48	5.6	0.2	5.1	0.4
Coyote Creek Railroad Bridge, Figure 7-49	2.8	3.4	3.2	0.4
Coyote Creek/Island Ponds , Figure 7-50	2.7	5.2	3.7	7.3
Coyote Creek Upstream, Figure 7-51	2.4	2.4	3.9	3.8
Mud Slough Downstream, Figure 7-52	3.1	8.3	5.5	2.7
Mud Slough Upstream, Figure 7-53	2.8	3.1	4.6	4.5
Alviso Slough Downstream, Figure 7-54	7.2	0.7	8.9	0.6
Alviso Slough Upstream, Figure 7-55	5.1	5.8	7.1	8.4
Guadalupe Slough Downstream, Figure 7-56	4.4	0.6	5.9	0.9
Guadalupe Slough Upstream, Figure 7-57	6.2	8.1	7.6	10.9
Moffett Channel, Figure 7-58	5.6	6.4	7.0	8.8
Stevens Creek Downstream, Figure 7-59	0.4	0.1	1.1	1.3
Stevens Creek Upstream, Figure 7-60	1.3	1.0	1.0	1.0
Mountain View Slough Downstream, Figure 7-61	0.2	0.0	0.4	0.7
Mountain View Slough Upstream, Figure 7-62	0.6	0.4	0.7	0.7
Charleston Slough Downstream, Figure 7-63	0.1	0.1	0.3	0.3
Charleston Slough Upstream, Figure 7-64	0.2	0.1	0.0	0.2
Ravenswood pond complex				
Ravenswood Slough Downstream, Figure 7-67	-0.2	-0.2	-0.1	0.3
Ravenswood Slough Upstream, Figure 7-68	0.2	0.0	0.4	0.6

7.4 Circulation

As discussed previously, the most important factor influencing circulation patterns in South Bay is bathymetry (Cheng and Gartner 1985). At year 50, significant large-scale bathymetric change is assumed to have occurred under Alternative C. Mudflat erosion is assumed to have occurred in both the far South Bay and in the region between the San Mateo and Dumbarton Bridges, the tidally-restored ponds are assumed to have developed into mature salt marsh with corresponding marsh channel networks, and the tidal sloughs within the SBSP Restoration Project Area are assumed to have scoured in response to restoration efforts.

7.4.1 Current Velocity

South Bay

Table 7-7 shows the peak velocity magnitudes at the San Mateo and Dumbarton Bridge stations and Channel Marker 17 under baseline and Alternative C long-term conditions. Positive values indicate a higher modeled velocity under Alternative C, and negative values indicate a decrease in current velocity under Alternative C. At the San Mateo Bridge station, velocities increase approximately 0 – 10 cm/s on strong flood tides (Figure 7-71). At the Dumbarton Bridge station, velocities increase less than 10 cm/s on all phases of the tide. These velocity increases are in response to the tidal restoration, and the predicted estimates of mudflat erosion and sea-level rise.

At Channel Marker 17 (Figure 7-73), velocity magnitudes increase 5 – 15 cm/s on strong ebb tide and decrease 0 – 5 cm/s on weak ebb tide. The increase in velocities under Alternative C, long-term conditions is less than predicted under Alternative A, long-term conditions due to the predictions of mudflat erosion rather than mudflat accretion. A larger cross-sectional area is available to carry the ebbing flow due to the higher elevation of MLLW relative to the bathymetry.

Figure 7-74 and Figure 7-75 present velocity magnitudes within the South Bay under peak flood and peak ebb conditions under baseline and Alternative C long-term conditions, as well as the difference between the two model predictions. The differences are minor, and the greatest change occurs in the subtidal channels under ebb tide conditions.

Table 7-7. South Bay Peak Velocity Magnitude Comparisons: Alt C, Year 50, Summer vs. Baseline, Summer

(All velocities in cm/s)

Station Name	Baseline	Alt C	Difference
San Mateo Bridge, Figure 7-71	102	104	2
Dumbarton Bridge, Figure 7-72	34	37	3
Channel Marker 17, Figure 7-73	67	79	12

Tidal Sloughs

In the South Bay, modeled velocities within the tidal sloughs experience significant changes in response to the restoration, estimates of large-scale bathymetric change, and sea-level rise. Table 7-8 shows the peak velocity magnitudes at the downstream stations in the tidal sloughs under baseline and Alternative C, long-term conditions. Positive values indicate a higher modeled velocity under Alternative C, and negative values indicate a decrease in current velocity under Alternative C.

In the Eden Landing pond complex, velocity magnitudes in both the ACFCC and Old Alameda Creek increase on all phases of the tide. In the ACFCC, the velocity magnitude increase on ebb and flood tides is similar (Figure 7-76). In Old Alameda Creek, the velocity magnitude increase is largest on strong ebb tide under spring tide conditions (Figure 7-77). Figure 7-78 and Figure 7-79 depict the tidal slough velocity magnitudes within the Eden Landing pond complex at both strong flood and strong ebb, respectively. At strong flood, the largest velocity magnitude differences relative to baseline conditions are seen in the downstream reaches of the sloughs. At strong ebb, the largest differences are seen in the South Bay just beyond the slough mouth.

In the Alviso pond complex, velocity magnitudes increase in the Coyote Creek/Mud Slough region, with the exception of the Coyote Creek Railroad Bridge station (Figure 7-81). A portion of the tidal prism in this region under baseline conditions is captured by the tidally-restored ponds along Alviso Slough and the Pond A9 system (Ponds A9 through A 17) under Alternative C long-term conditions. Channel scour is also predicted to occur in Coyote Creek under Alternative C, long-term conditions, compared with continued sedimentation under Alternative A, long-term conditions, and therefore the cross-sectional area under Alternative C is larger, leading to the potential for a velocity decrease.

Velocity magnitudes increase in both Alviso Slough (Figure 7-84) and Guadalupe Sough (Figure 7-85), with a larger increase predicted in Alviso Sough to due the larger increase in tidal prism. In Stevens Creek (Figure 7-87), Mountain View Slough (Figure 7-88) and Charleston Slough (Figure 7-89), velocity magnitudes exhibit lesser differences when compared with baseline conditions. These sloughs are predicted to scour in response to the tidal restoration (see Table 3-6 and Table 3-7 for the respective increases in tidal prism and channel depth), and the increase in channel cross-sectional area nearly compensates for the increase in tidal flows. However, under baseline conditions, the sloughs exhibit a higher degree of flood-ebb asymmetry (higher velocities on flood tide) than predicted under Alternative C long-term conditions.

Figure 7-90 and Figure 7-91 depict the tidal slough velocity magnitudes within the Alviso pond complex at both strong flood and strong ebb, respectively. As with the Eden Landing pond complex, the largest differences under strong ebb conditions are seen in the far South Bay just beyond the slough mouth. At strong flood, the largest velocity differences relative to baseline conditions are seen in the downstream reaches of the tidal sloughs.

In Ravenswood Slough in the Ravenswood pond complex, velocities decrease 0 – 5 cm/s on flood tide, and increase 0 – 15 cm/s on ebb tide, decreasing some of the flood-ebb asymmetry observed under baseline conditions (Figure 7-92). Figure 7-93 and Figure 7-94 depict the tidal slough velocity magnitudes within the Ravenswood pond complex at both strong flood and strong ebb, respectively. As with the other pond complexes, the largest differences under strong ebb conditions are seen in the far South Bay just beyond the slough mouth. At strong flood, the largest velocity magnitude differences relative to baseline conditions are seen in the downstream reach of the slough.

Table 7-8. Tidal Slough Peak Velocity Magnitude Comparisons: Alt C, Year 50, Summer vs. Baseline, Summer

(All velocities in cm/s)

Station Name	Baseline	Alt C	Difference
ACFCC Downstream, Figure 7-76	45	66	21
Old Alameda Creek Downstream, Figure 7-77	53	91	38
Coyote Creek Power Tower, Figure 7-80	76	93	17
Coyote Creek Railroad Bridge, Figure 7-81	82	77	-5
Coyote Creek/Island Ponds, Figure 7-82	39	57	19
Mud Slough Downstream, Figure 7-83	46	67	22
Alviso Slough Downstream, Figure 7-84	49	76	27
Guadalupe Slough Downstream, Figure 7-85	46	53	7
Moffett Channel , Figure 7-86	5	2	-2
Stevens Creek Downstream, Figure 7-87	51	49	-3
Mountain View Slough Downstream, Figure 7-88	49	58	9
Charleston Slough Downstream, Figure 7-89	77	76	-1
Ravenswood Slough Downstream, Figure 7-92	38	35	-3

7.4.2 Residual Circulation

The total residual current observed in the South Bay is a product of tidally-driven residual currents, as well as wind-driven and density-driven circulation patterns. The long-term conditions under Alternative C, including large-scale tidal restoration, bathymetric change and sea-level rise, have the potential to alter residual circulation patterns within the South Bay.

Figure 7-95 displays the 29-day residual circulation under summer baseline conditions. Figure 7-96 displays the 29-day residual circulation for long-term, Alternative C conditions, and Figure 7-97 displays the difference between the predicted residual circulation under baseline and Alternative C conditions (Alternative C, year 50 minus baseline). Little change is observed in the South Bay north of the Dumbarton Bridge.

More noticeable changes are observed in the far South Bay, south of the Dumbarton Bridge. Figure 7-98 displays the 29-day residual circulation under summer baseline conditions for the far South Bay, Figure 7-99 displays the same for long-term, Alternative C conditions, and Figure 7-100 displays the difference. The largest difference in residual circulation pattern is observed in the main South Bay subtidal channel near the mouth Coyote Creek. Under Alternative C, long-term conditions, there is a stronger net-northward residual current in the downstream reach of Coyote Creek, and there is a small increase in the net-northward flux through the Dumbarton Narrows.

7.5 Bed Shear Stress

Potential impacts to sediment erosion and deposition patterns are inferred based on comparisons of total bed shear stress both before and after tidal restoration, where total bed shear stress is a function of both tidal currents and locally-generated wind-waves. Section 4.5 provides a description of the methodology used to generate and compare the total combined wind- and tidally-induced bed shear stress.

7.5.1 South Bay

The changes in water levels and tidal datums associated with sea-level rise and large-scale bathymetric change result in minor decreases in tidally-induced bed shear stresses in the shallow regions of the South Bay, including the eastern and western shoals. The increase in tidal prism and tidal flows also leads to slight increases in the tidally-induced bed shear stress in the subtidal areas and in the main South Bay channel (Figure 7-101). The difference map shown on Figure 7-101 depicts red regions where the erosive potential increases (bed shear stresses are higher under Alternative C long-term conditions relative to baseline conditions), and the areas depicted in blue correspond to regions with a potential for increased deposition. However, the red and blue areas are for illustrative purposes only and do not predict erosion or deposition under Alternative C long-term conditions. The critical shear stresses for erosion are not well known within the South Bay, and they vary spatially and temporally depending on the sediment characteristics and level of compaction of the substrate. In addition, such an inference would assume that the erodibility of the bed remains constant over the 50-year horizon. The benthic community strongly affects erodibility and the benthic community is likely to change in the next 50 years, therefore an assumption of constant erodibility would be poor.

When the combined wind-wave- and tidally-induced shear stress is considered in the South Bay, additional changes become apparent. MLLW and MHHW are higher under Alternative C long-term conditions (Figure 7-4 and Figure 7-5, respectively). Because wind-wave-driven bed shear stress is a function of water depth, and the erosive potential decreases with increasing water depth, the reduction in tidal amplitude leads to additional reductions in the total bed shear stress in the shallow areas of the South Bay (Figure 7-105), including the shallows in the far South Bay (Figure 7-107) and the eastern and western shoals north of the Dumbarton Bridge (Figure 7-108 and Figure 7-106, respectively).

7.5.2 Tidal Sloughs

Within and adjacent to the Eden Landing pond complex (Figure 7-102), the maximum tidally-induced bed shear stress is increased downstream of tidal breaches, corresponding to the increased tidal prism, and decreased upstream of the tidal breaches because a portion of the flow upstream in the tidal slough under baseline conditions is captured within the tidally-restored ponds under restored conditions. Within and adjacent to the Alviso pond complex (Figure 7-103) and the Ravenswood pond complex (Figure 7-104), the dynamic is similar to that observed in the Eden Landing pond complex. Tidally-induced bed shear stresses increase downstream of tidal breaches and decrease upstream of tidal breaches.

The primary effect of the combined wind-wave- and tidally-induced shear stress is evident in the South Bay rather than in the tidal sloughs as wind-induced waves require sufficient fetch to develop.

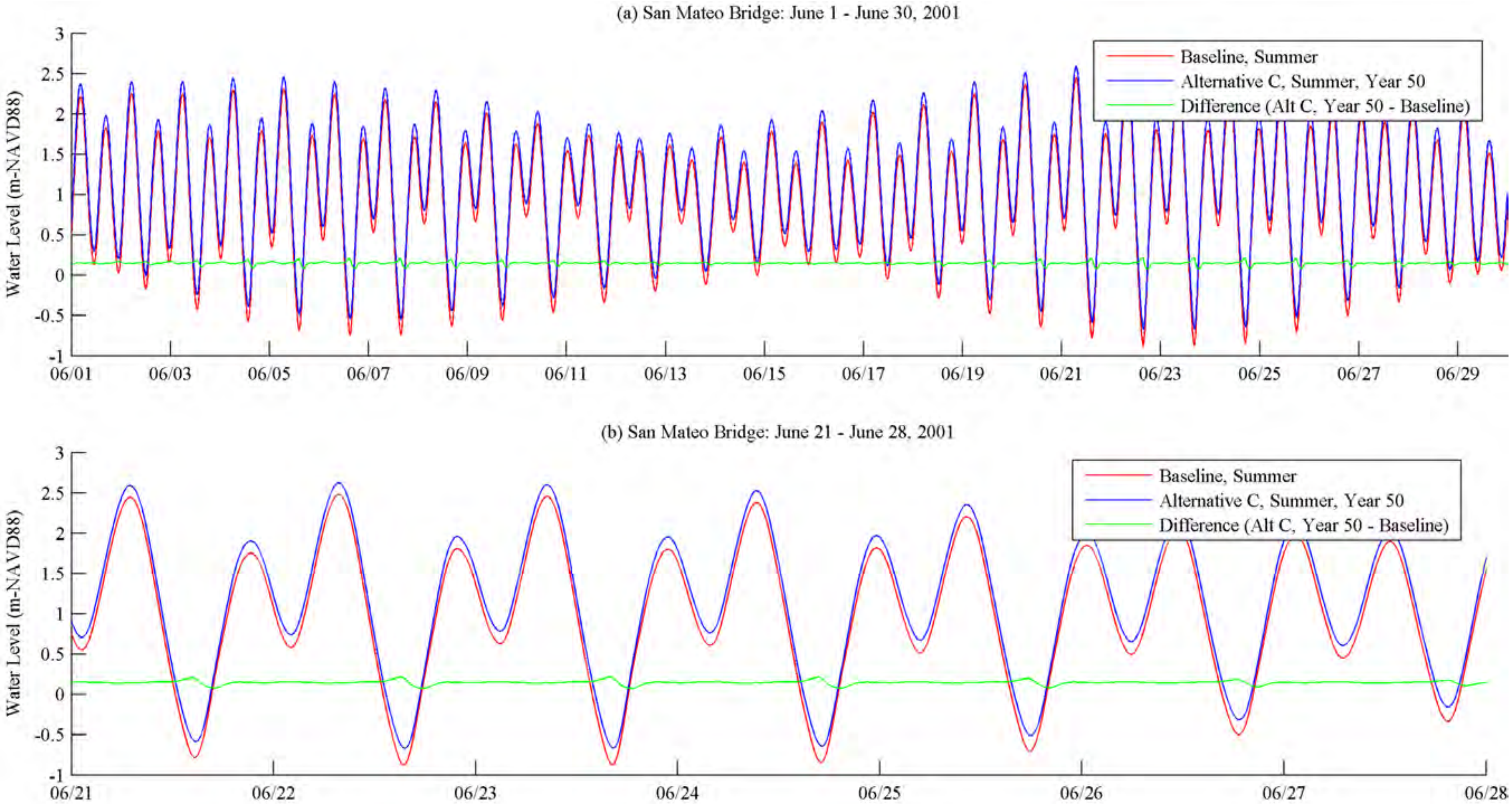

figure 7-1

South Bay Salt Pond Restoration Project

Water Levels, San Mateo Bridge, Alt C, Year 50, Summer

PWA

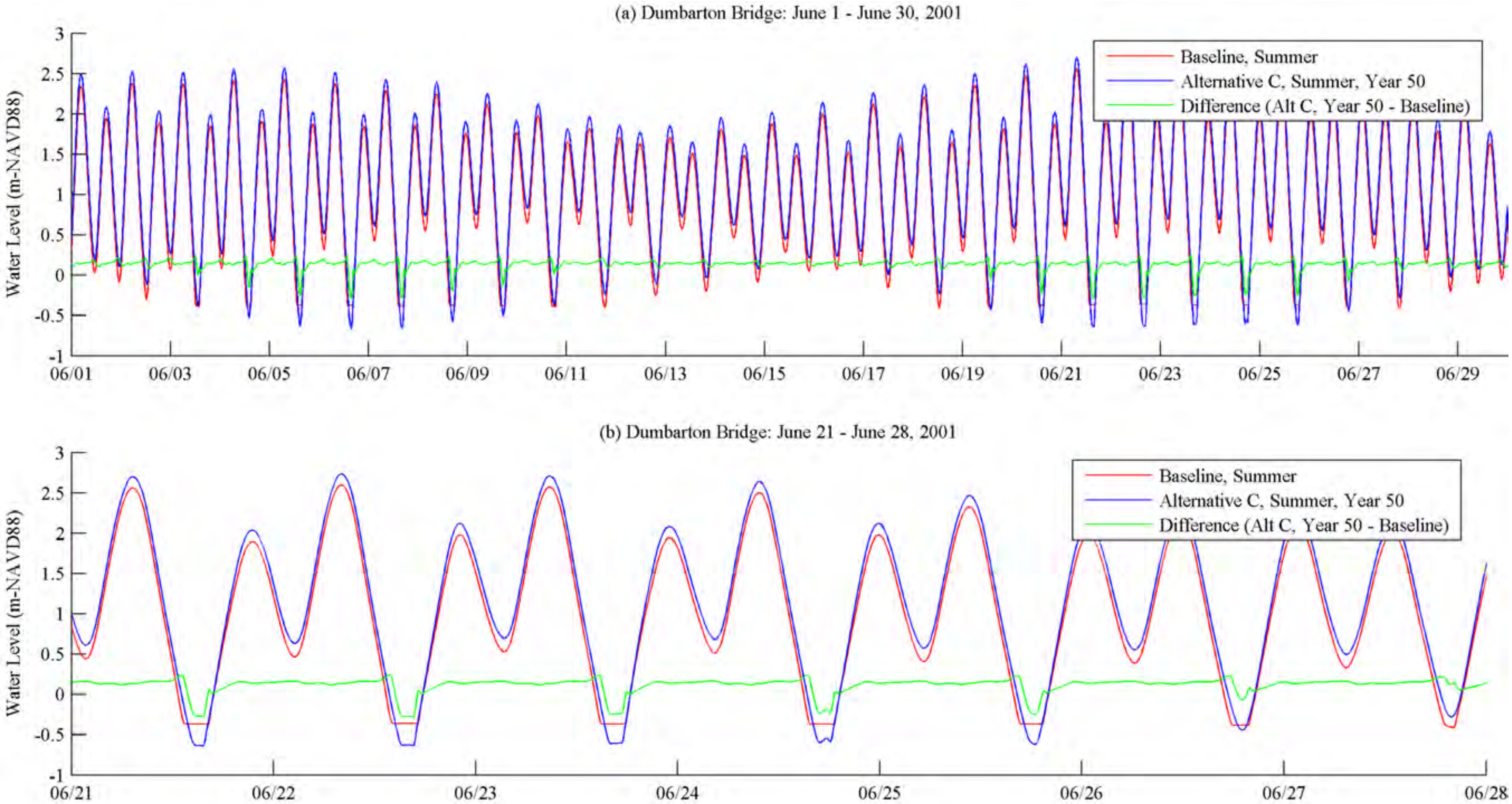

figure *7-2*

South Bay Salt Pond Restoration Project

Water Levels, Dumbarton Bridge, Alt C, Year 50, Summer

PWA

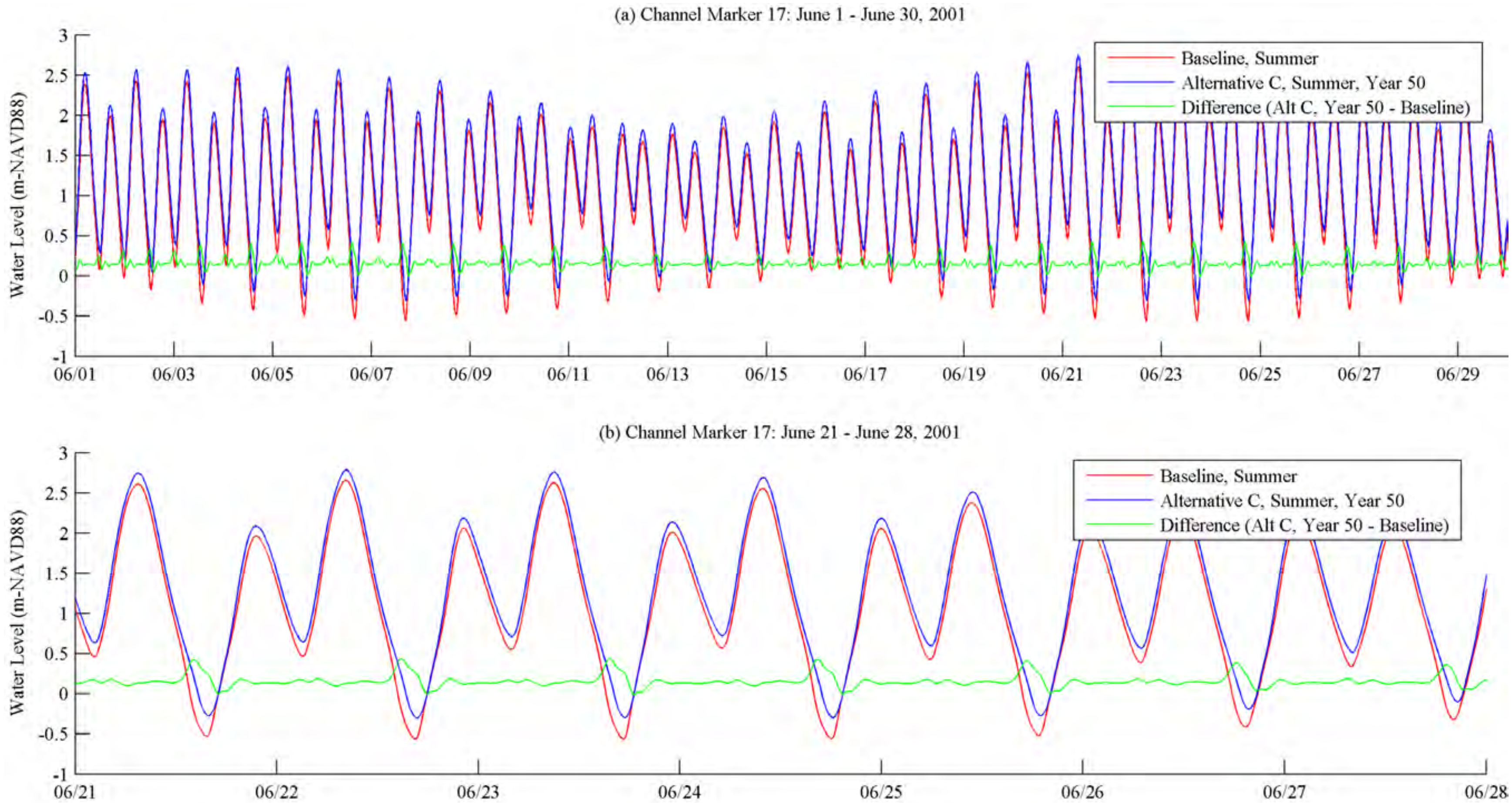

figure 7-3

South Bay Salt Pond Restoration Project

Water Levels, Channel Marker 17, Alt C, Year 50, Summer

PWA

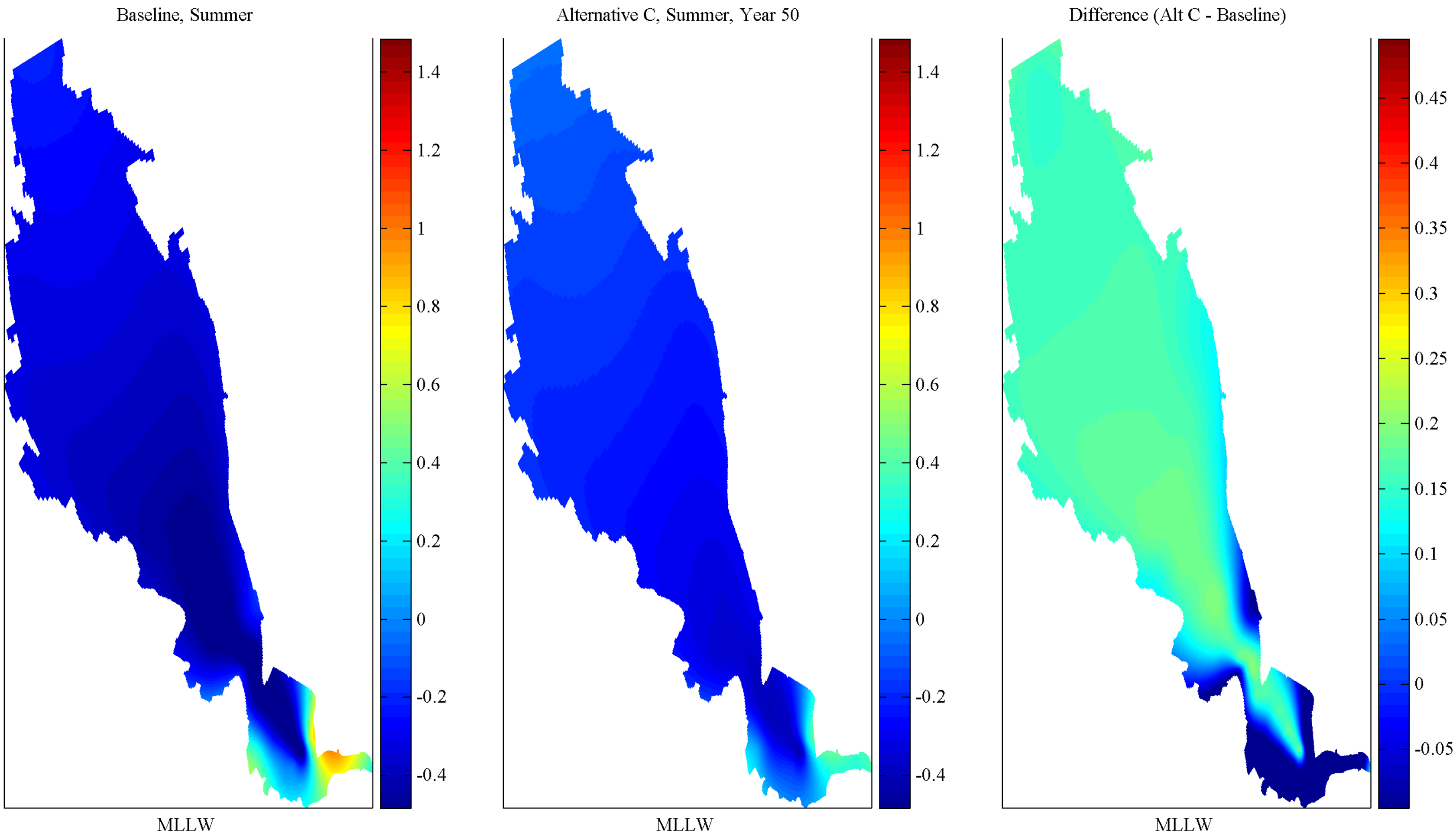

Note: Units shown are m-NAVD88, difference units are m

figure 7-4

South Bay Salt Pond Restoration Project

Changes in MLLW, Alt C, Year 50, Summer

PWA

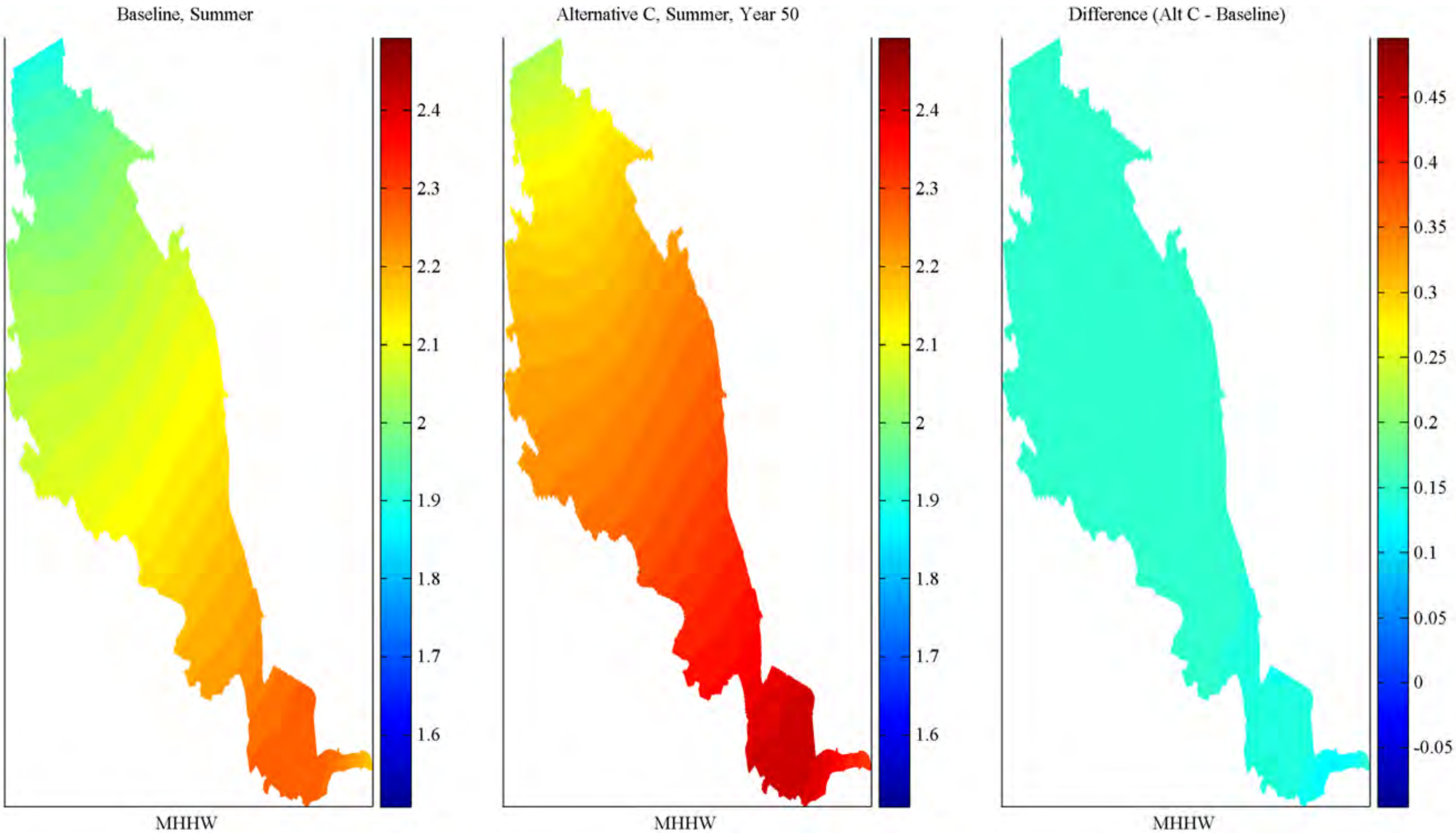

Note: Units shown are m-NAVD88, difference units are m

figure *7-5*

South Bay Salt Pond Restoration Project

Changes in MHHW, Alt C, Year 50, Summer

PWA

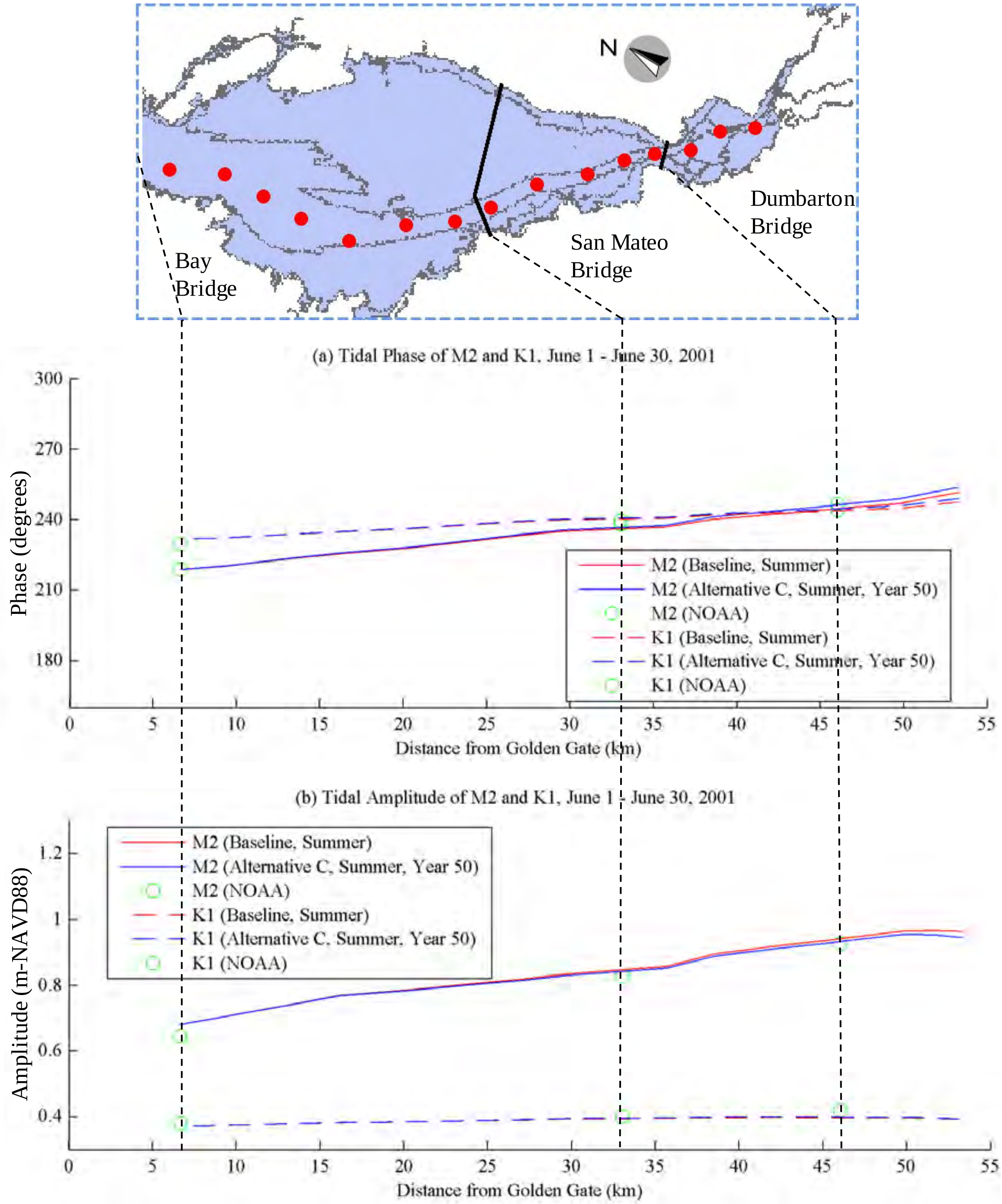

This figure shows the phase and amplitude of the M2 and K1 tidal components, calculated from harmonic analysis of the model. The green data points represent phase and amplitude values calculated by NOAA at the Bay Bridge (Pier 22), San Mateo Bridge, and Dumbarton Bridge.

figure *7-6*

South Bay Salt Pond Restoration Project

Changes in Tidal Propagation, Alt C, Year 50, Summer

PWA

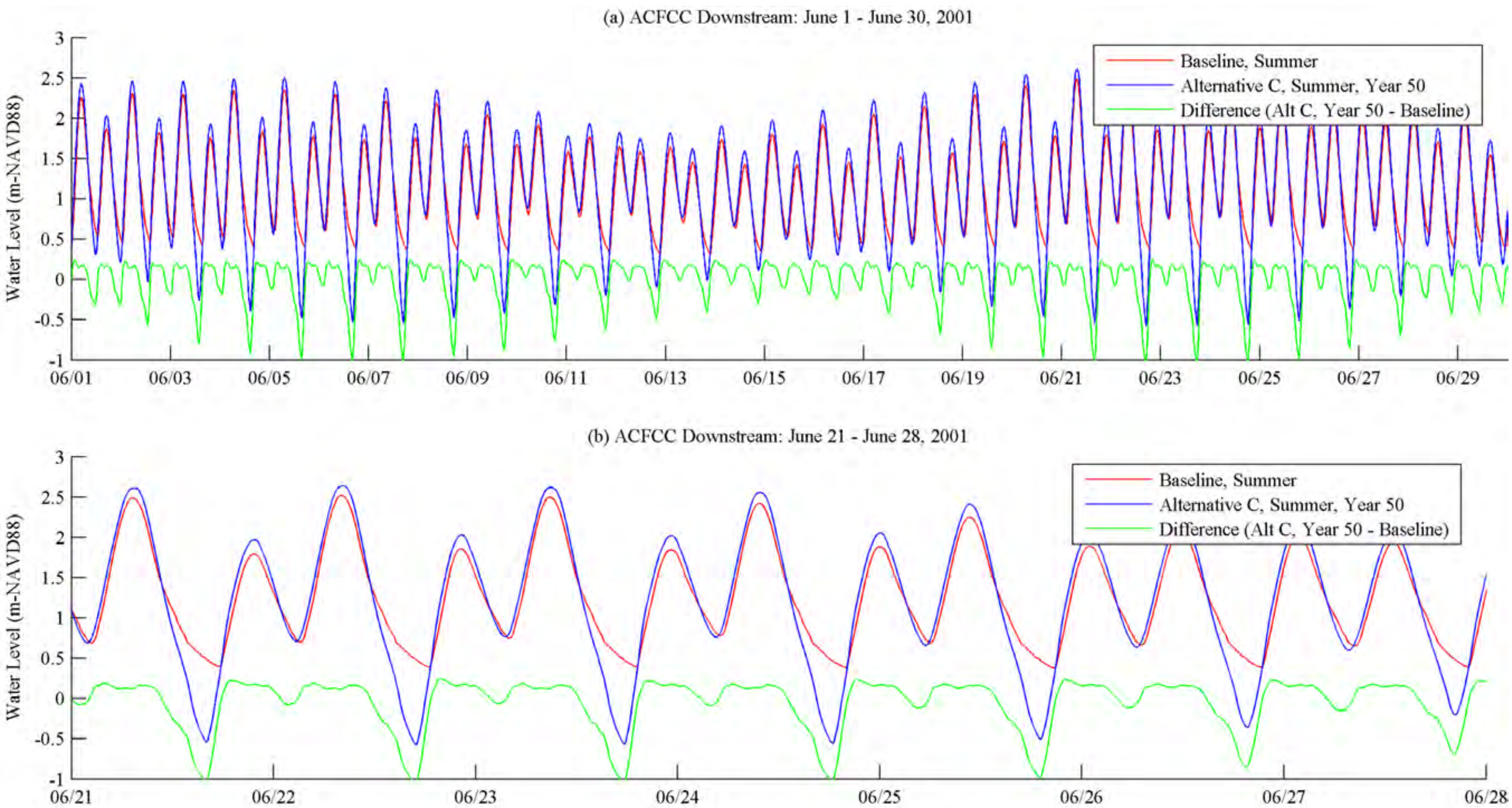

figure *7-7*

South Bay Salt Pond Restoration Project

Water Levels, ACFCC Downstream, Alt C, Year 50, Summer

PWA

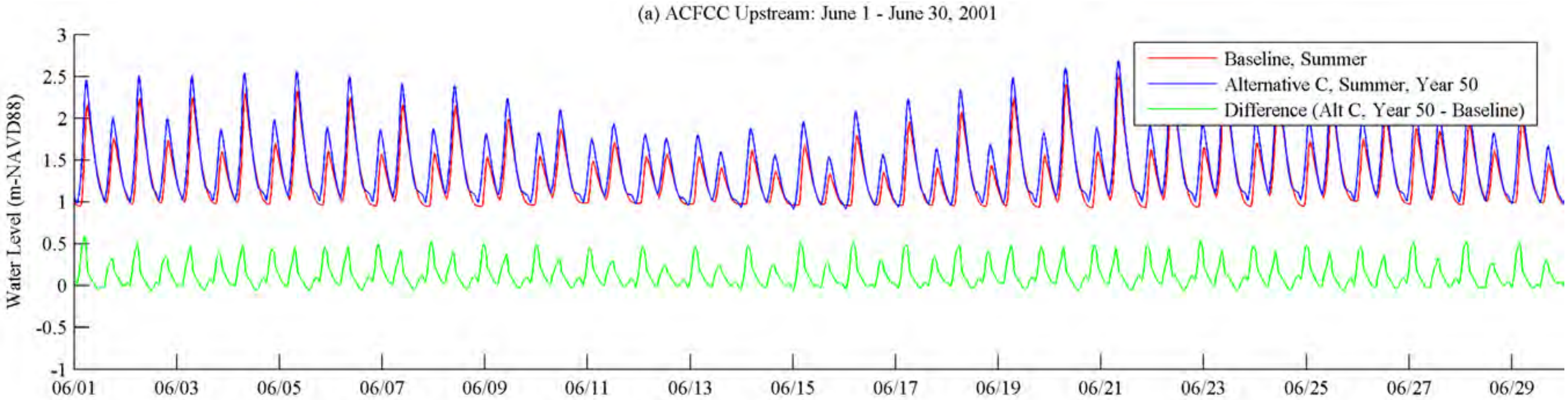

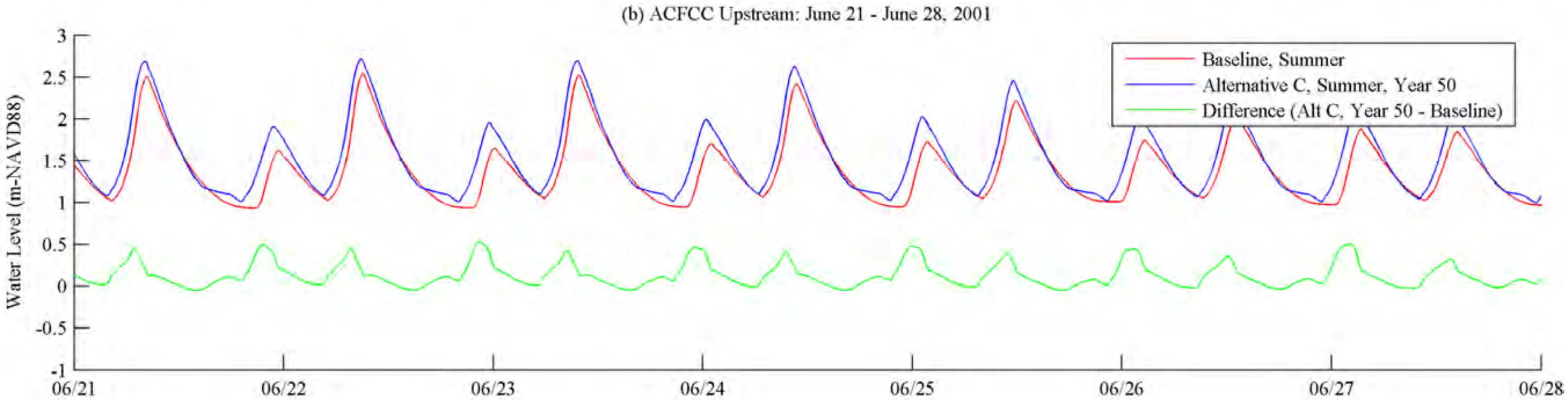

figure 7-8

South Bay Salt Pond Restoration Project

Water Levels, ACFCC Upstream, Alt C, Year 50, Summer

PWA

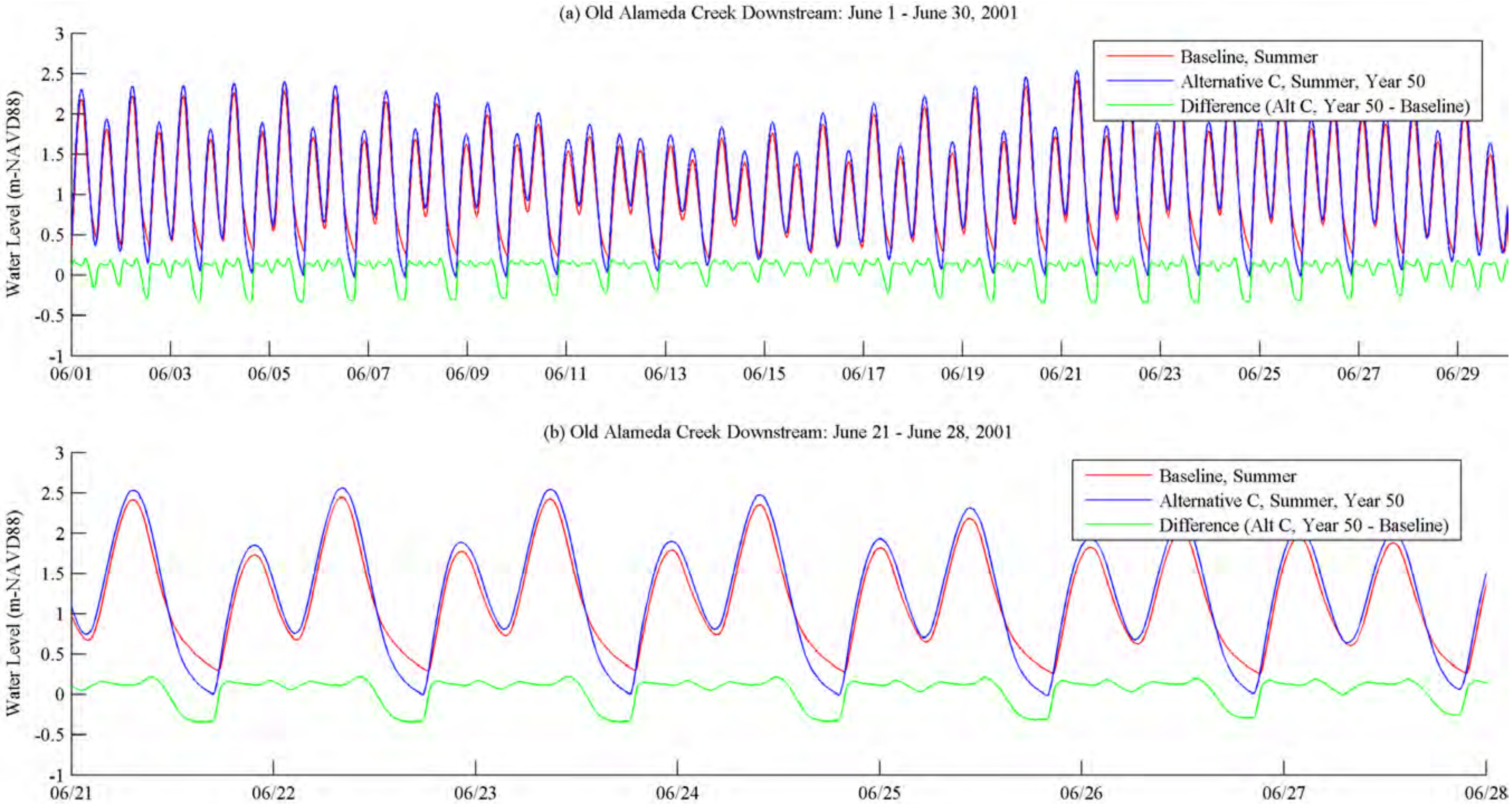

figure 7-9

South Bay Salt Pond Restoration Project

Water Levels, Old Alameda Creek Downstream, Alt C, Year 50, Summer

PWA

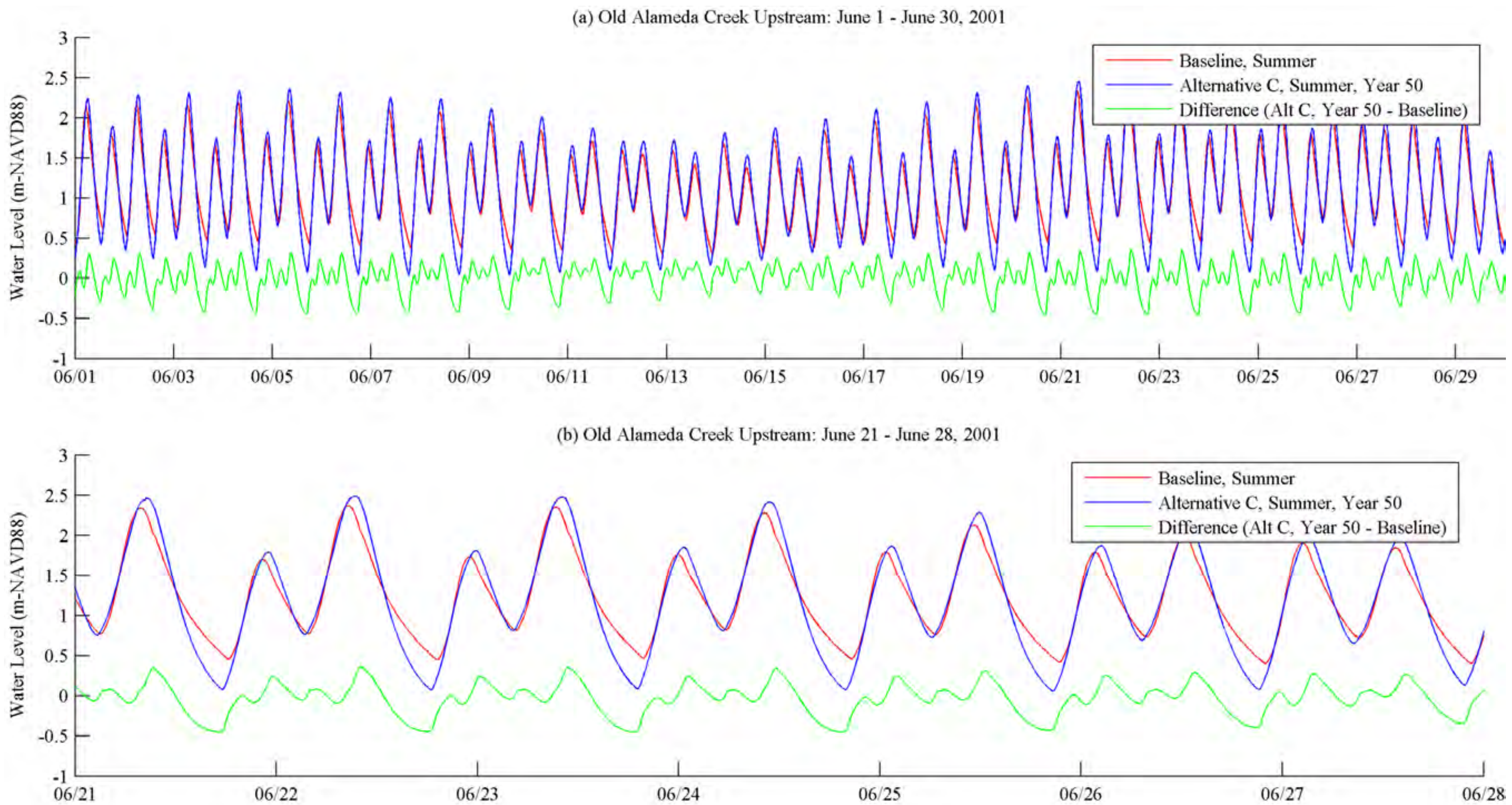

figure 7-10

South Bay Salt Pond Restoration Project

Water Levels, Old Alameda Creek Upstream, Alt C, Year 50, Summer

PWA

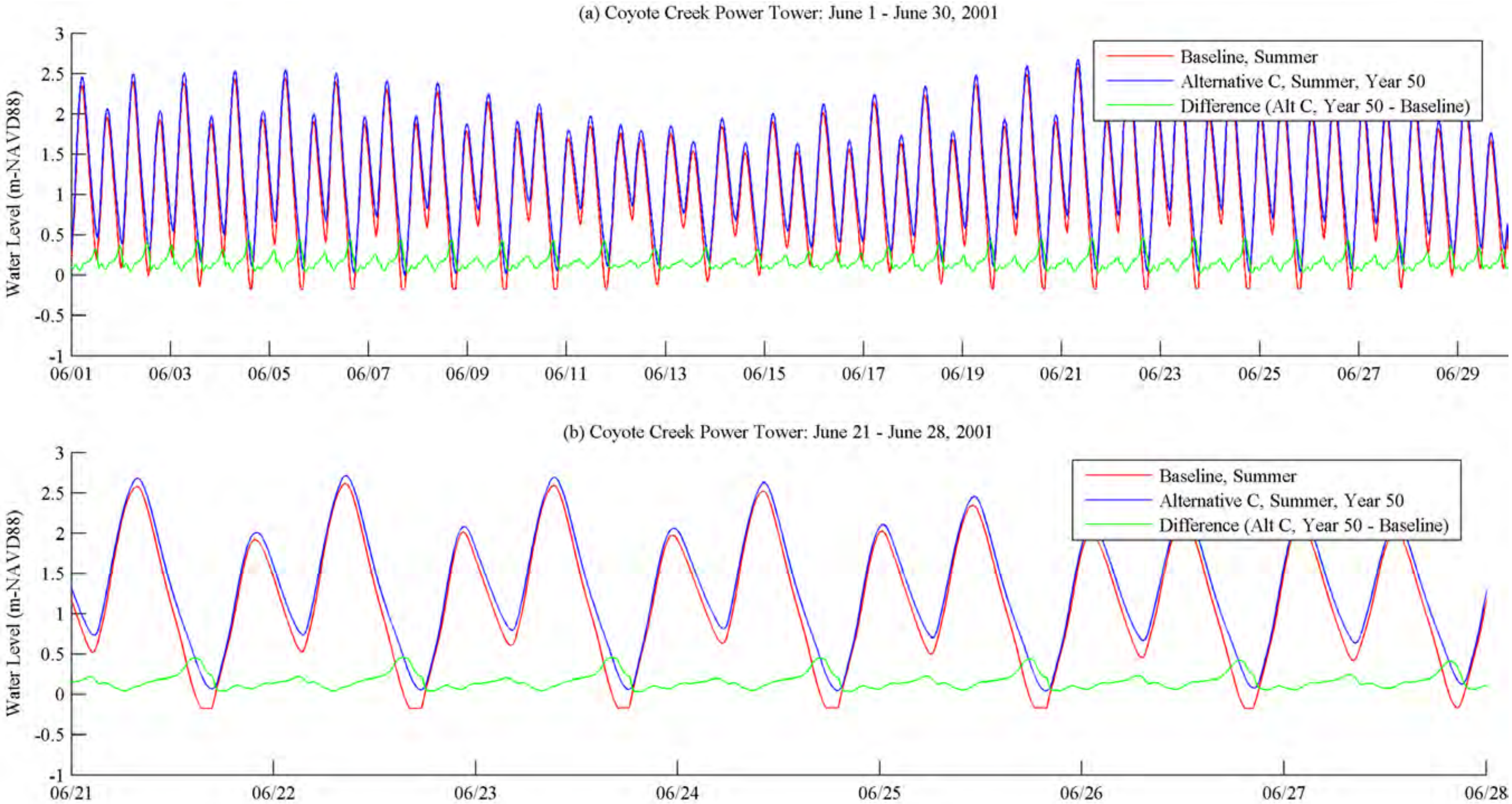

figure 7-11

South Bay Salt Pond Restoration Project

Water Levels, Coyote Creek Power Tower, Alt C, Year 50, Summer

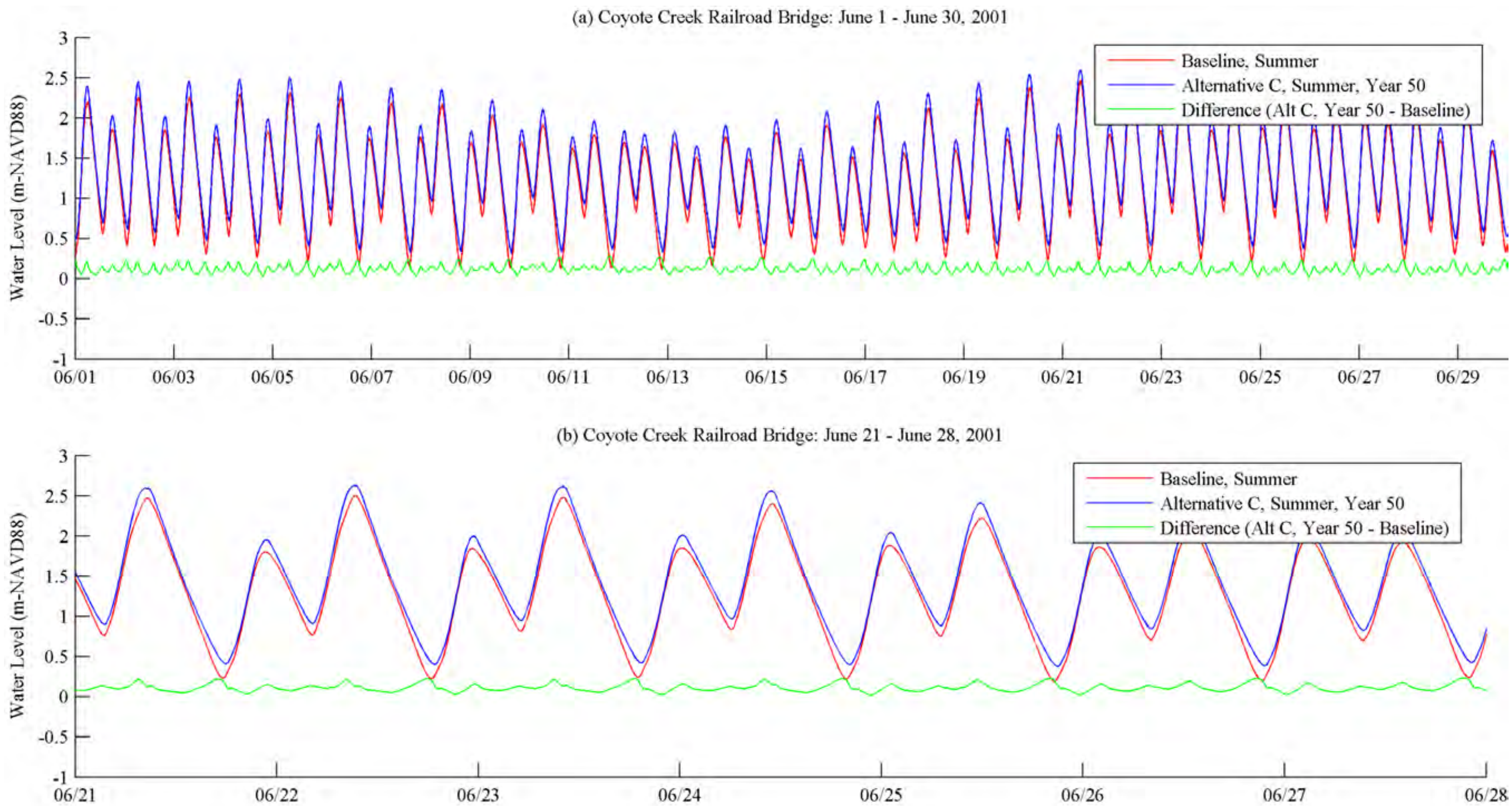

figure 7-12

South Bay Salt Pond Restoration Project

Water Levels, Coyote Creek Railroad Bridge, Alt C, Year 50, Summer

PWA

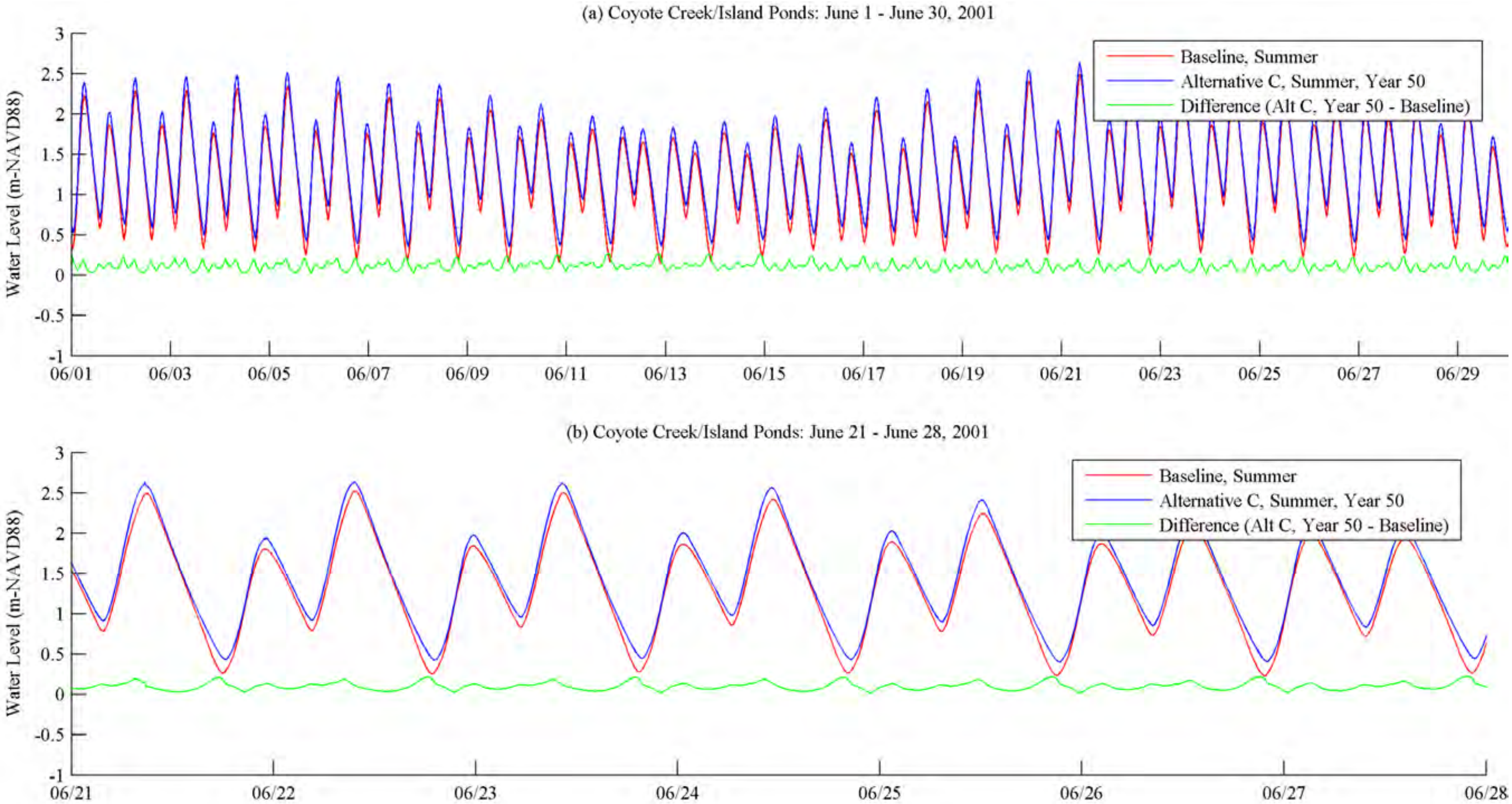

figure *7-13*

South Bay Salt Pond Restoration Project

Water Levels, Coyote Creek/Island Ponds, Year 50, Summer

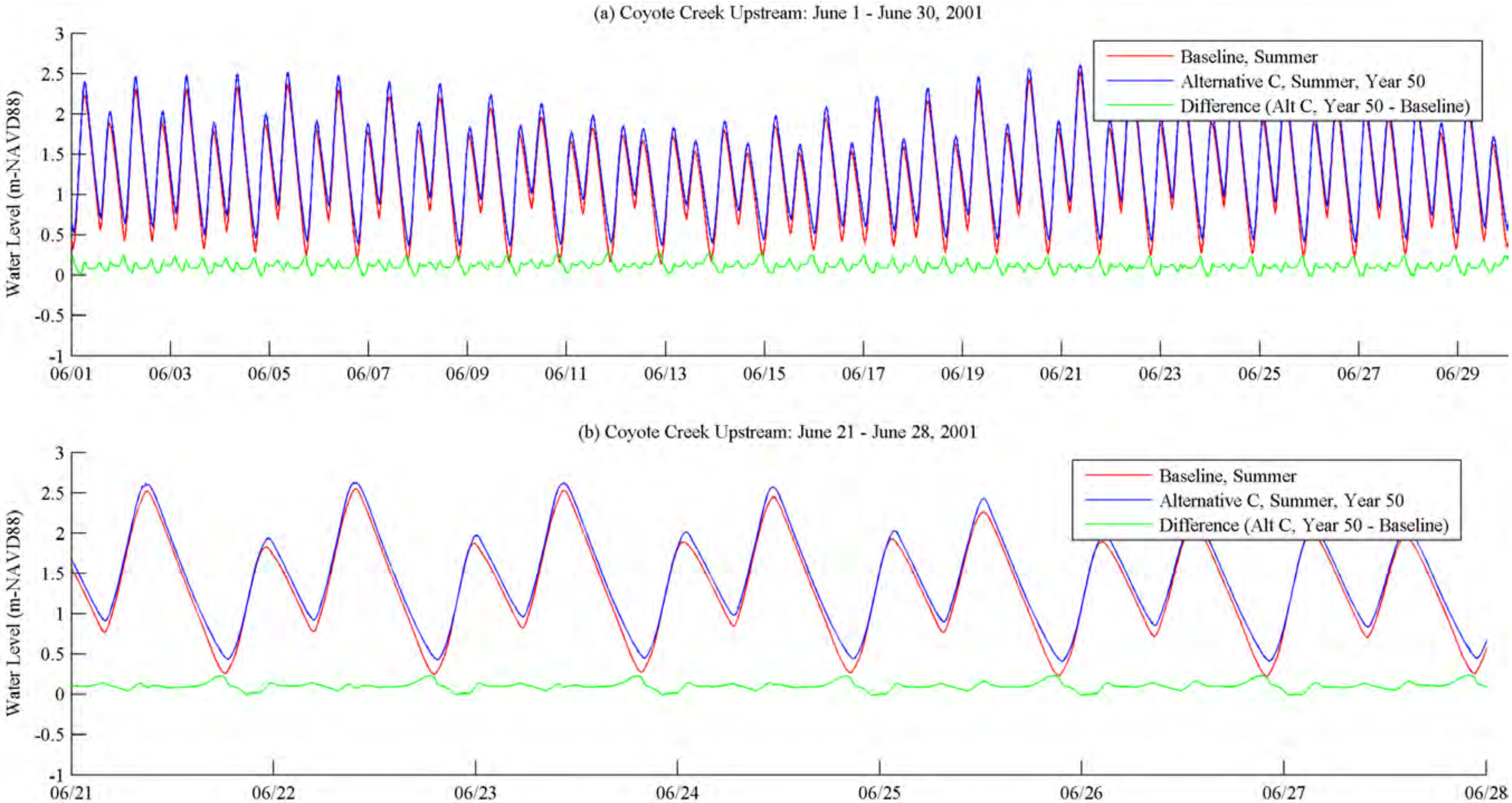

figure *7-14*

South Bay Salt Pond Restoration Project

Water Levels, Coyote Creek Upstream, Year 50, Summer

PWA

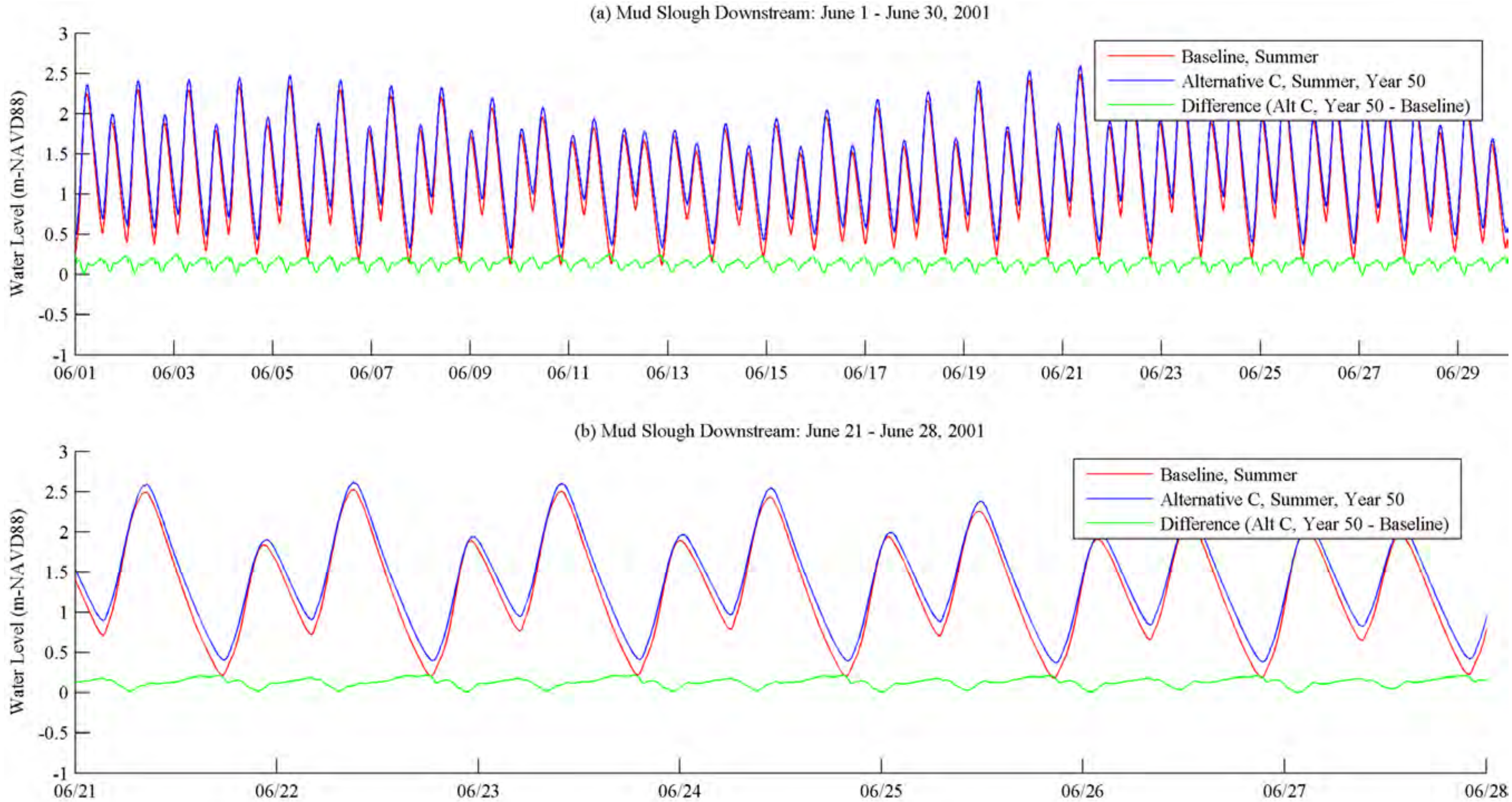

figure 7-15

South Bay Salt Pond Restoration Project

Water Levels, Mud Slough Downstream, Alt C, Year 50, Summer

PWA

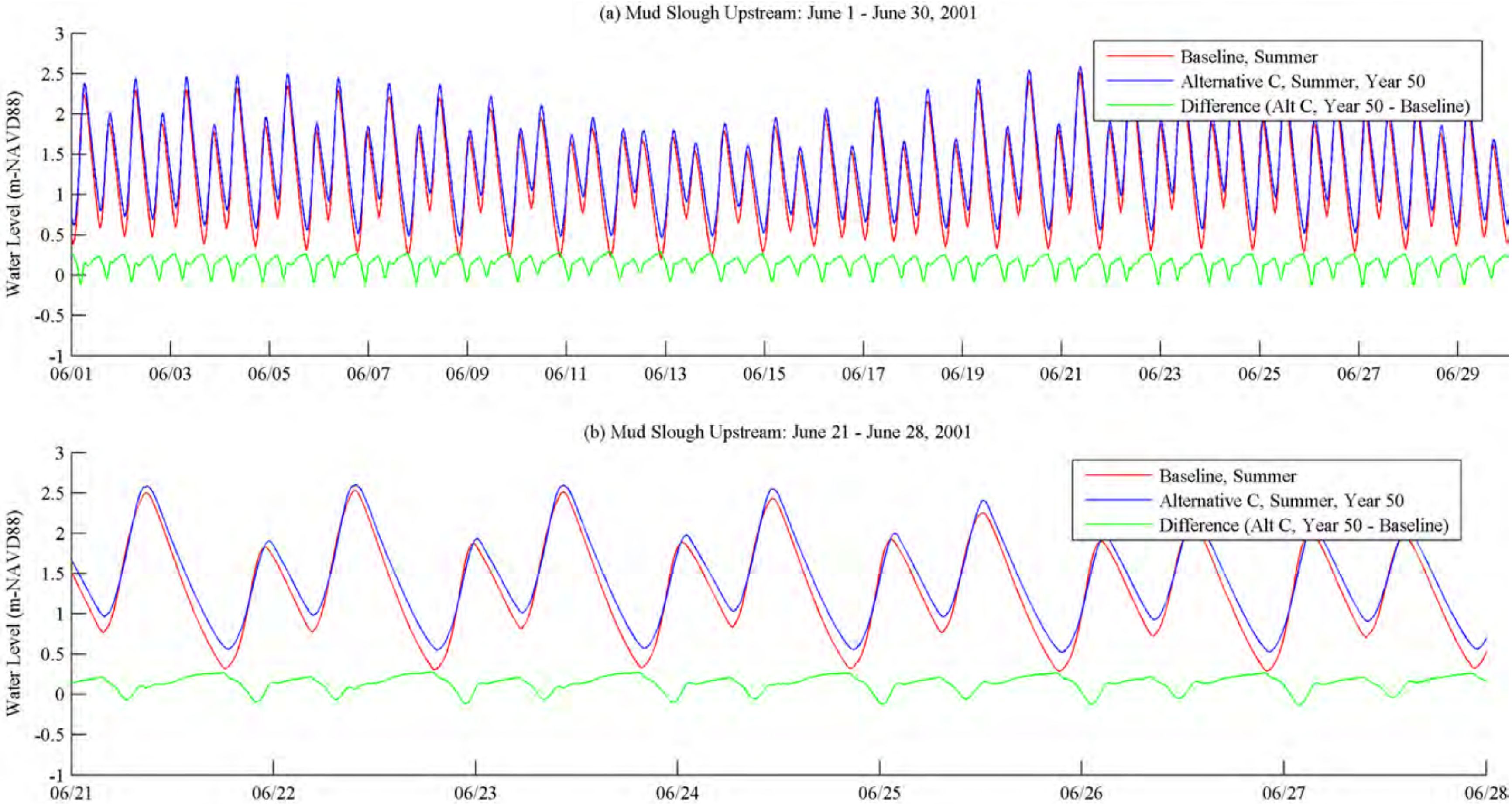

figure 7-16

South Bay Salt Pond Restoration Project

Water Levels, Mud Slough Upstream, Alt C, Year 50, Summer

PWA

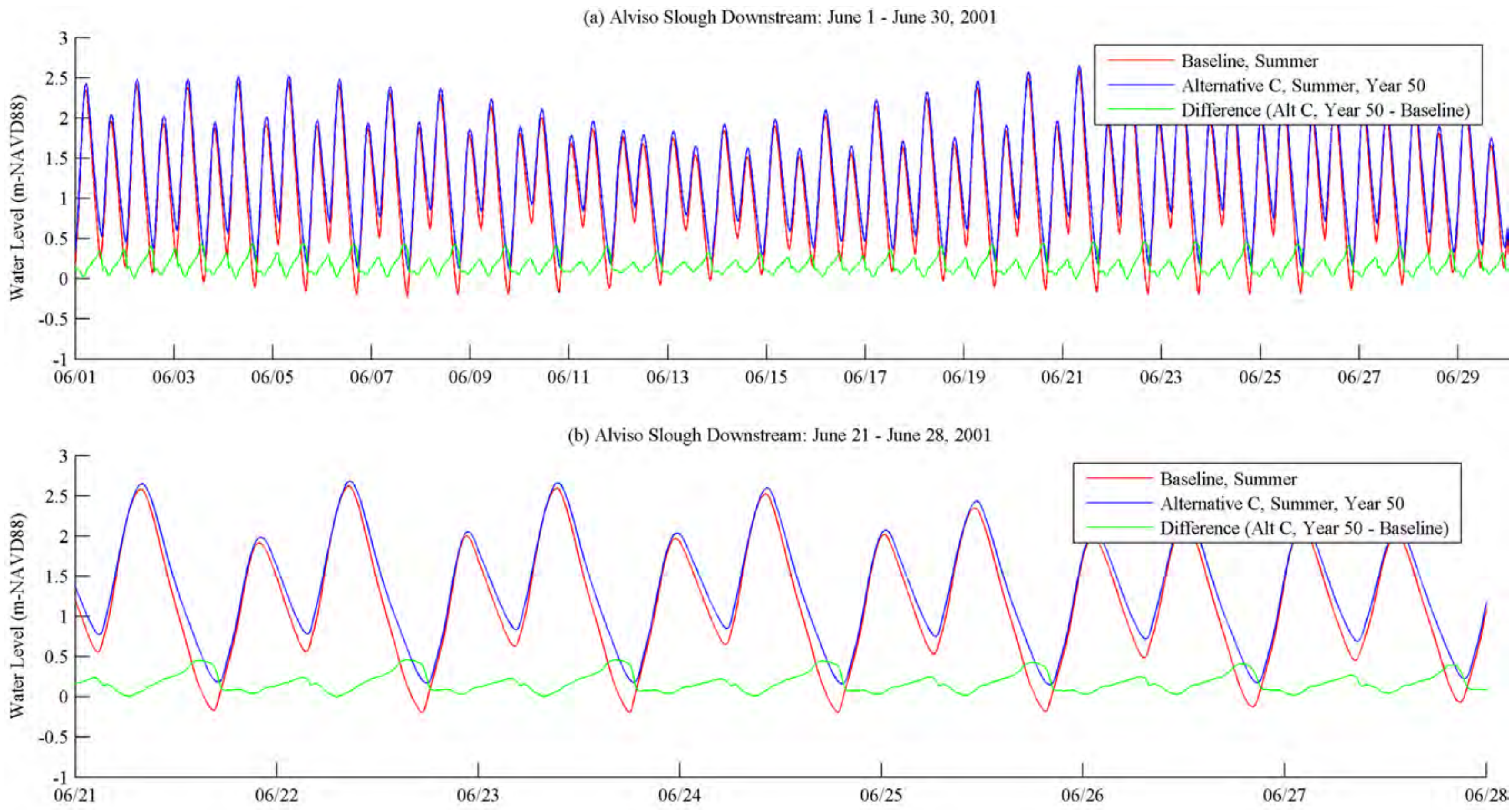

figure *7-17*

South Bay Salt Pond Restoration Project

Water Levels, Alviso Slough Downstream, Alt C, Year 50, Summer

PWA

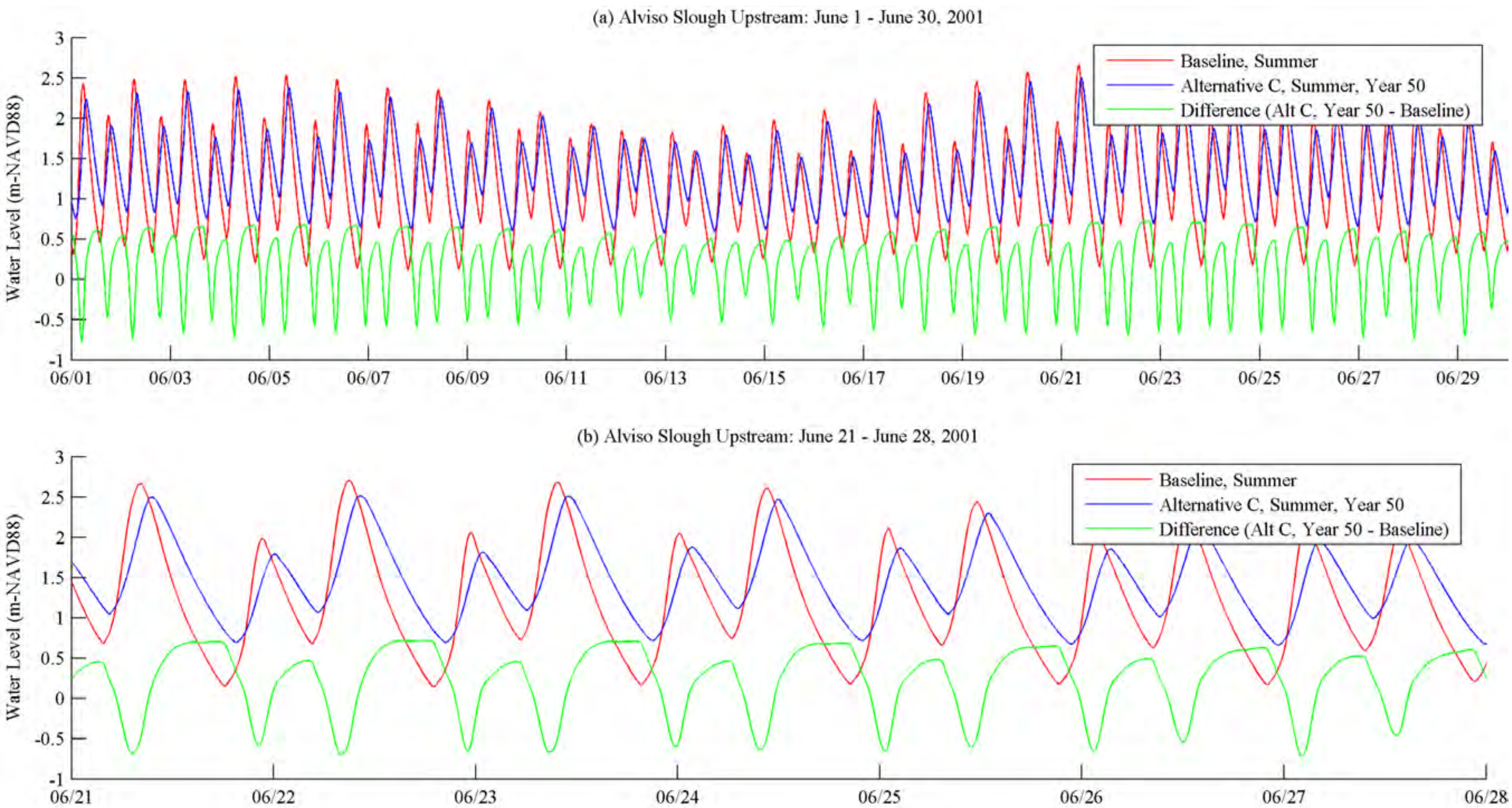

figure 7-18

South Bay Salt Pond Restoration Project

Water Levels, Alviso Slough Upstream, Alt C, Year 50, Summer

PWA

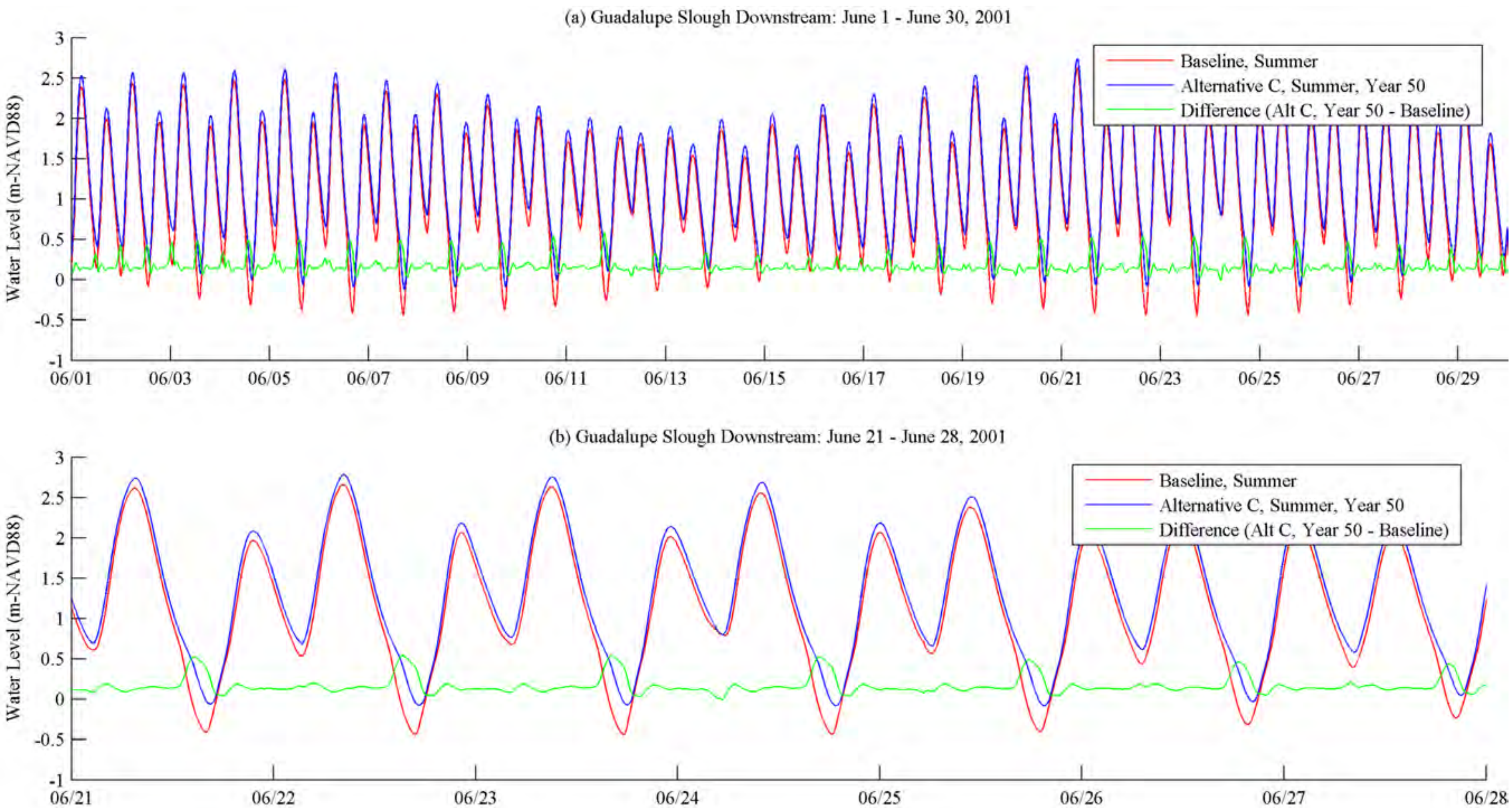

figure 7-19

South Bay Salt Pond Restoration Project

Water Levels, Guadalupe Slough Downstream, Alt C, Year 50, Summer

PWA

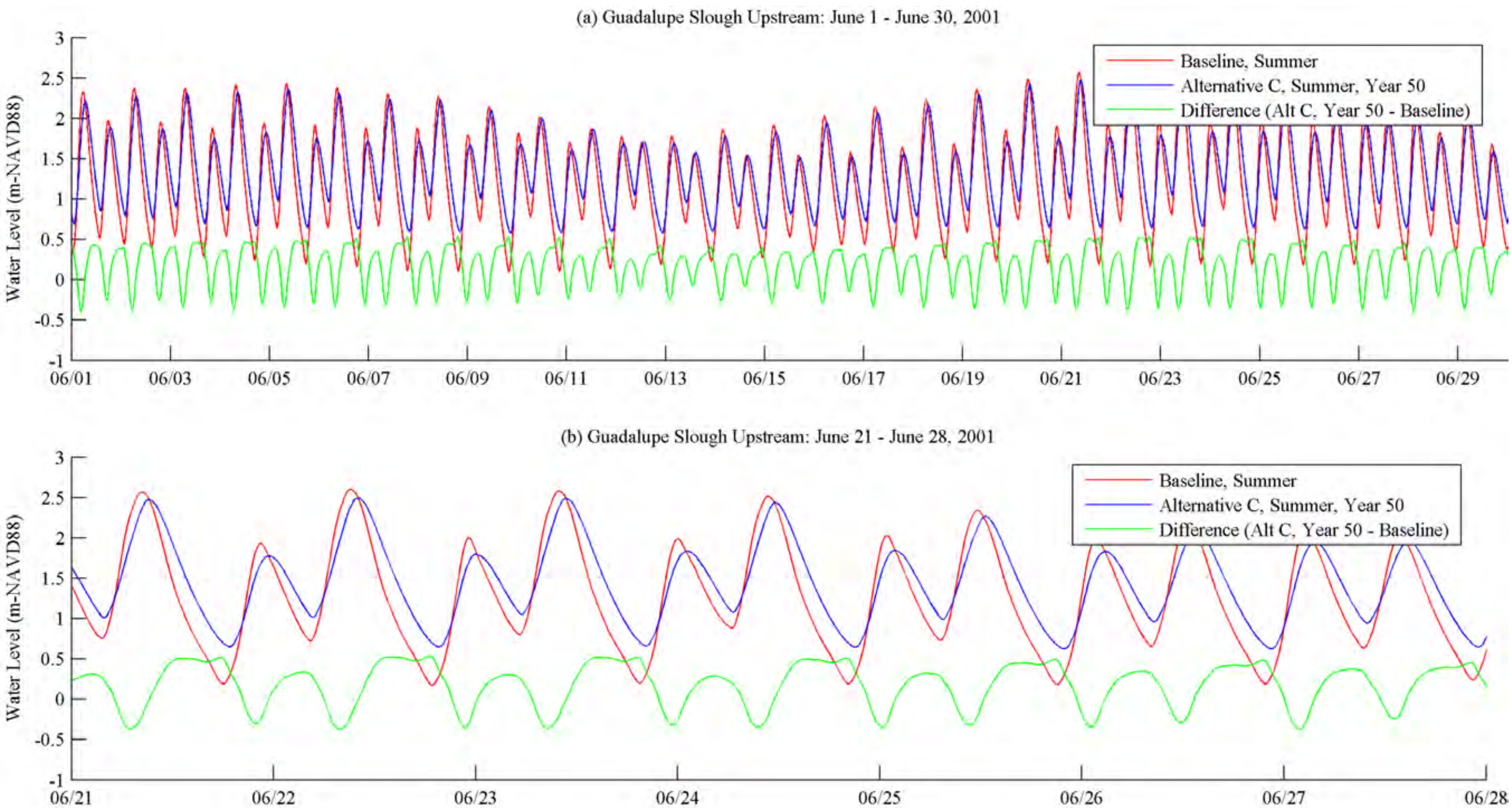

figure 7-20

South Bay Salt Pond Restoration Project

Water Levels, Guadalupe Slough Upstream, Alt C, Year 50, Summer

PWA

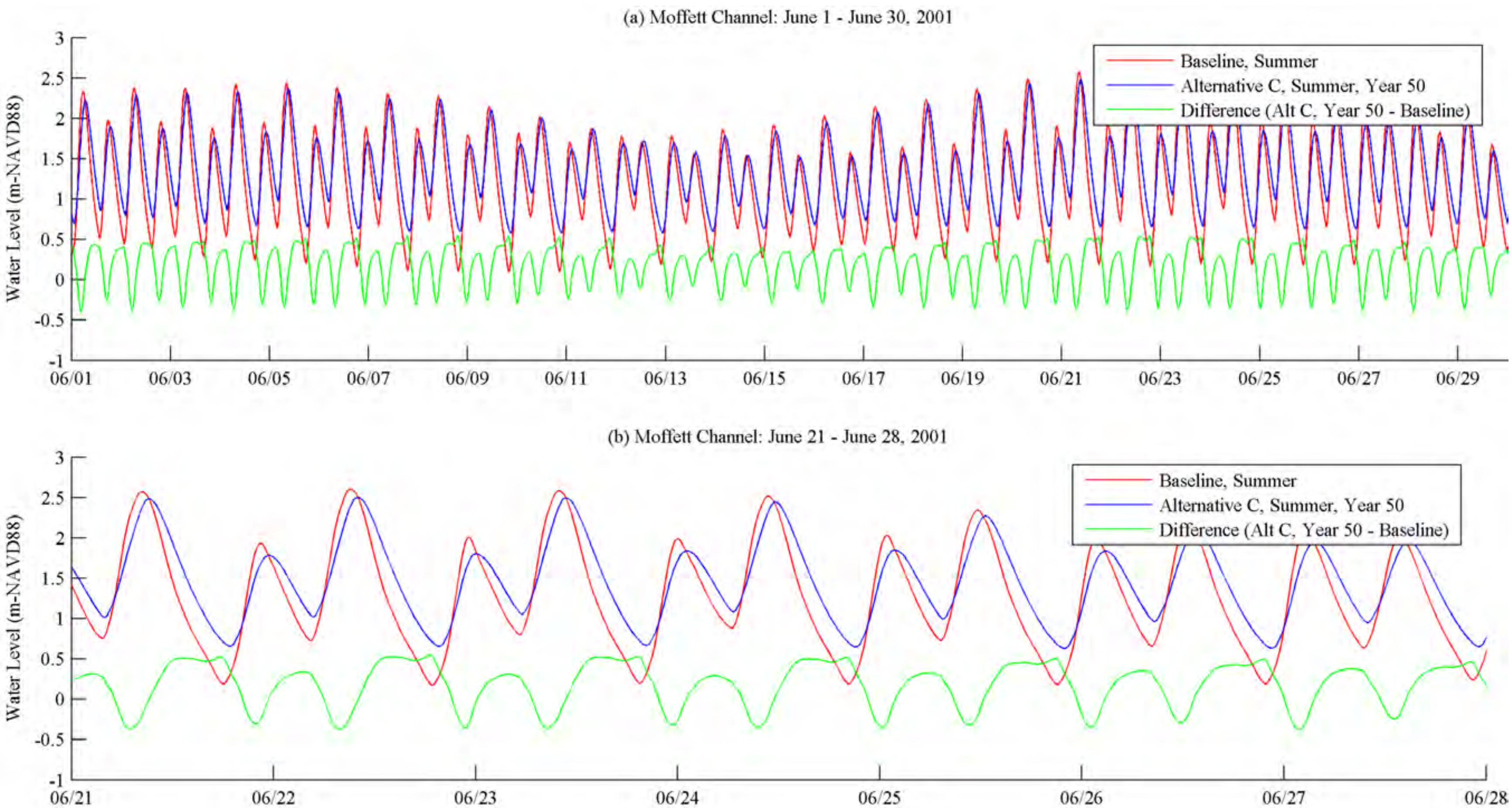

figure *7-21*

South Bay Salt Pond Restoration Project

Water Levels, Moffett Channel, Alt C, Year 50, Summer

PWA

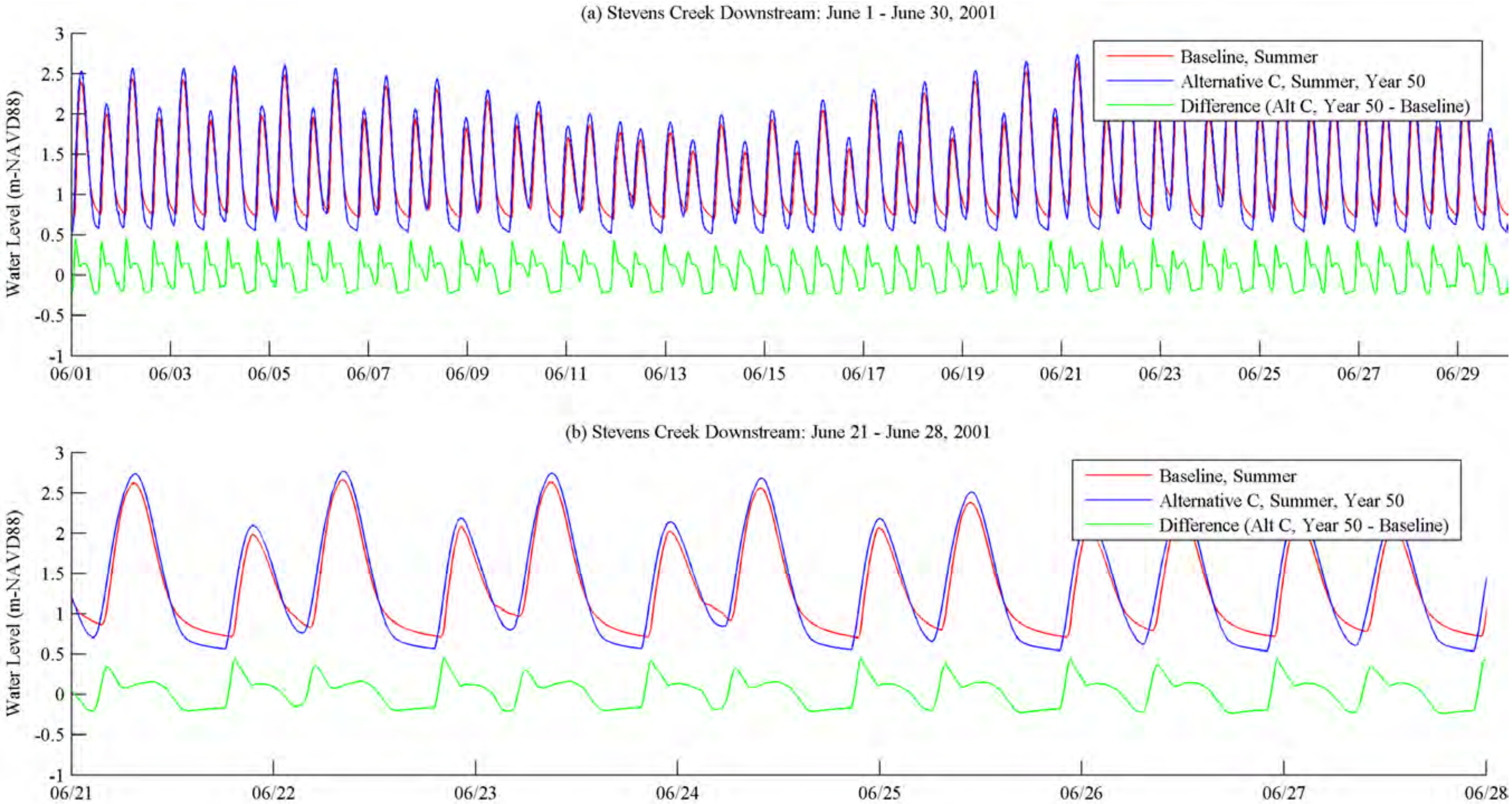

figure 7-22

South Bay Salt Pond Restoration Project

Water Levels, Steven Creek Downstream, Alt C, Year 50, Summer

PWA

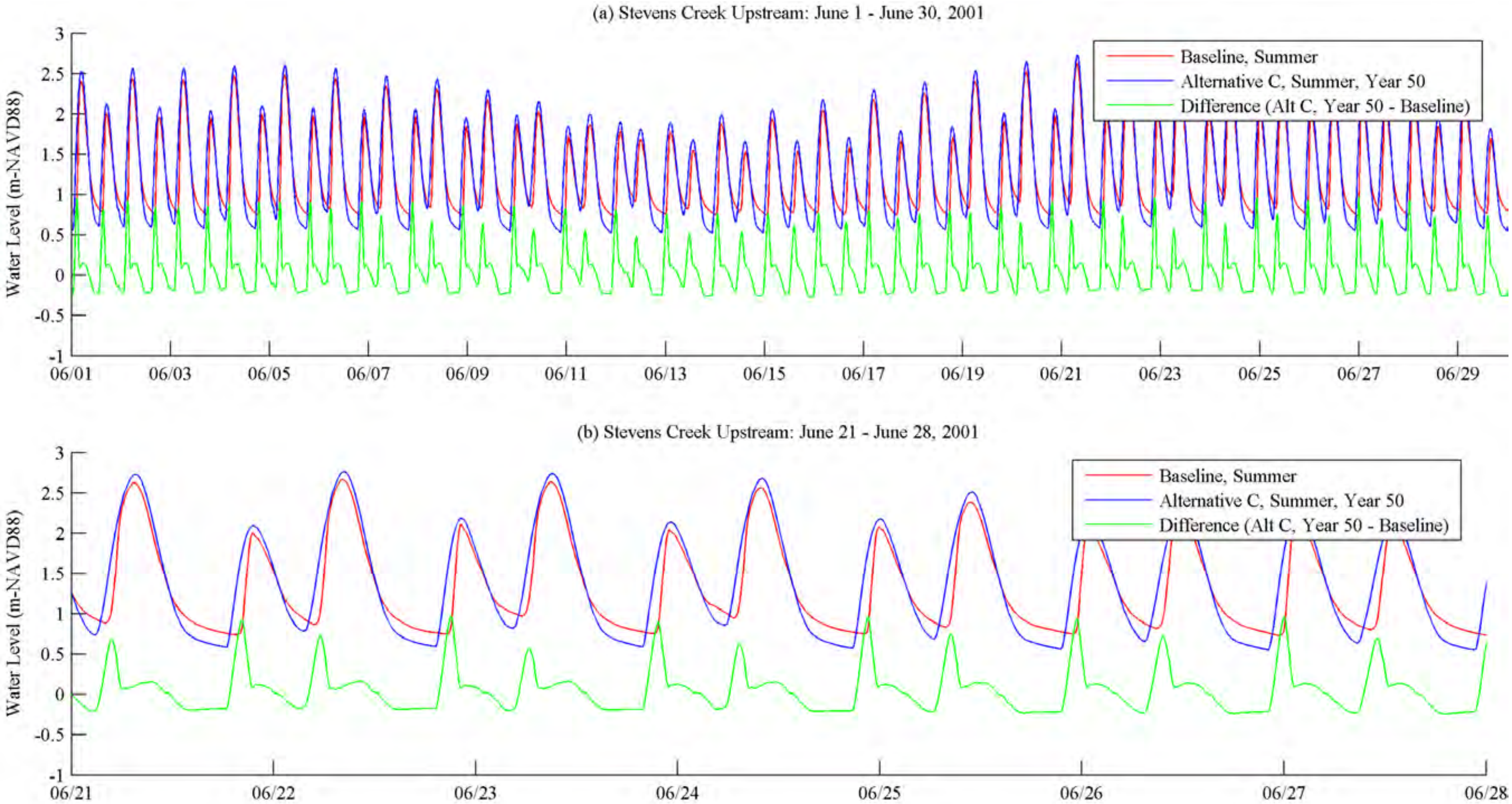

figure 7-23

South Bay Salt Pond Restoration Project

Water Levels, Stevens Creek Upstream, Alt C, Year 50, Summer

PWA

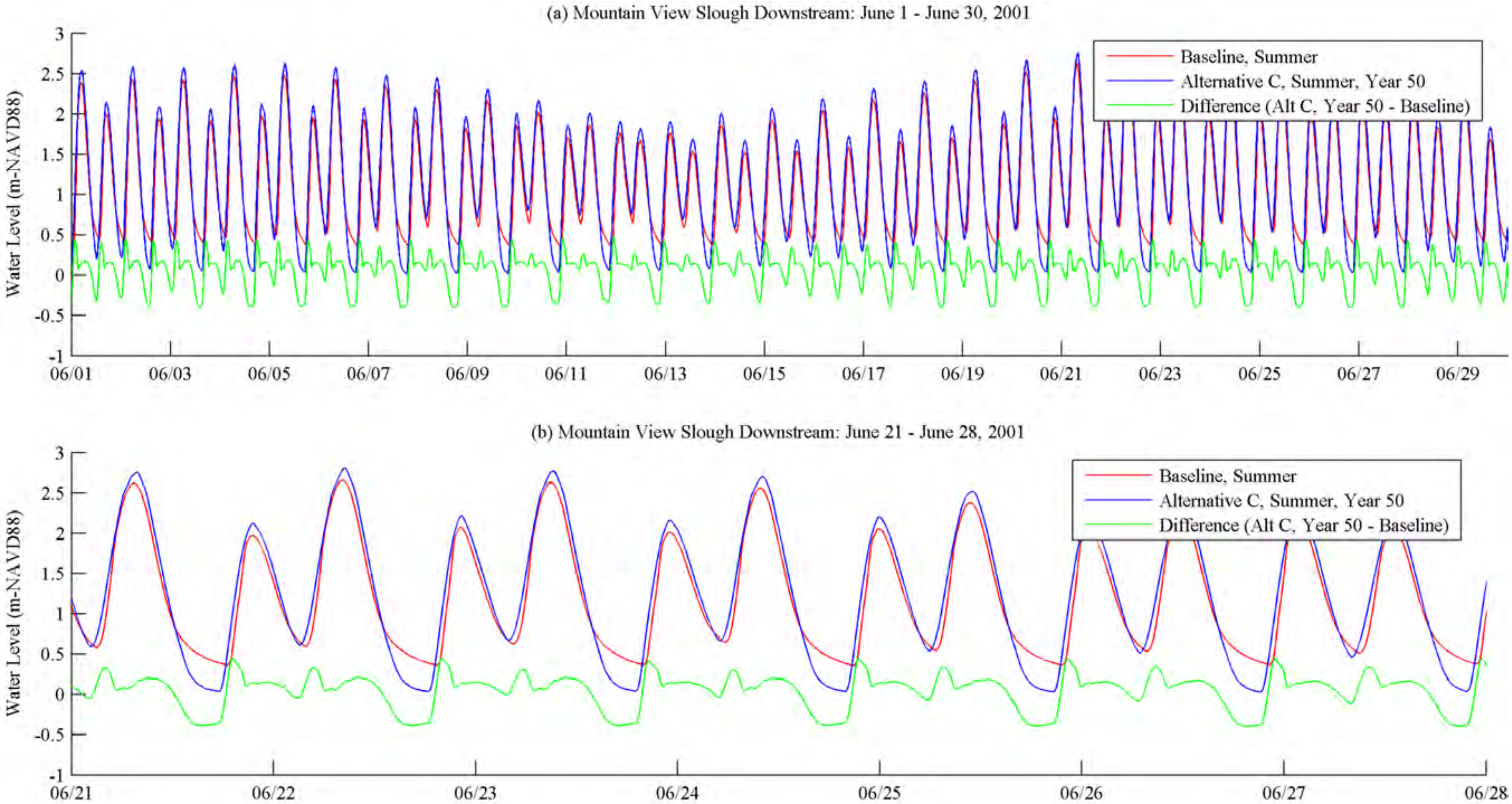

figure 7-24

South Bay Salt Pond Restoration Project

Water Levels, Mountain View Slough Downstream, Alt C, Year 50, Summer

PWA

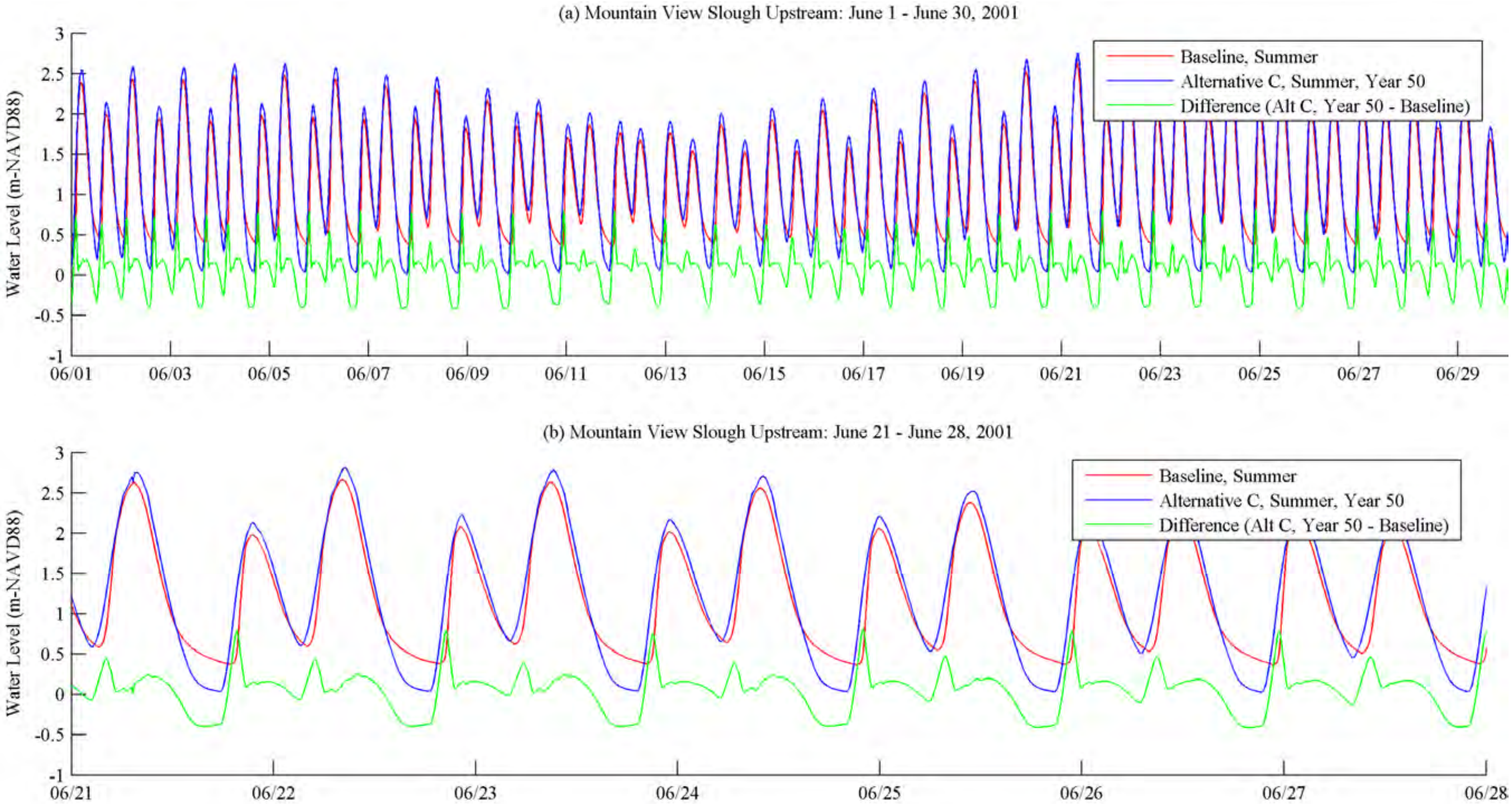

figure 7-25

South Bay Salt Pond Restoration Project

Water Levels, Mountain View Slough Upstream, Alt C, Year 50, Summer

PWA

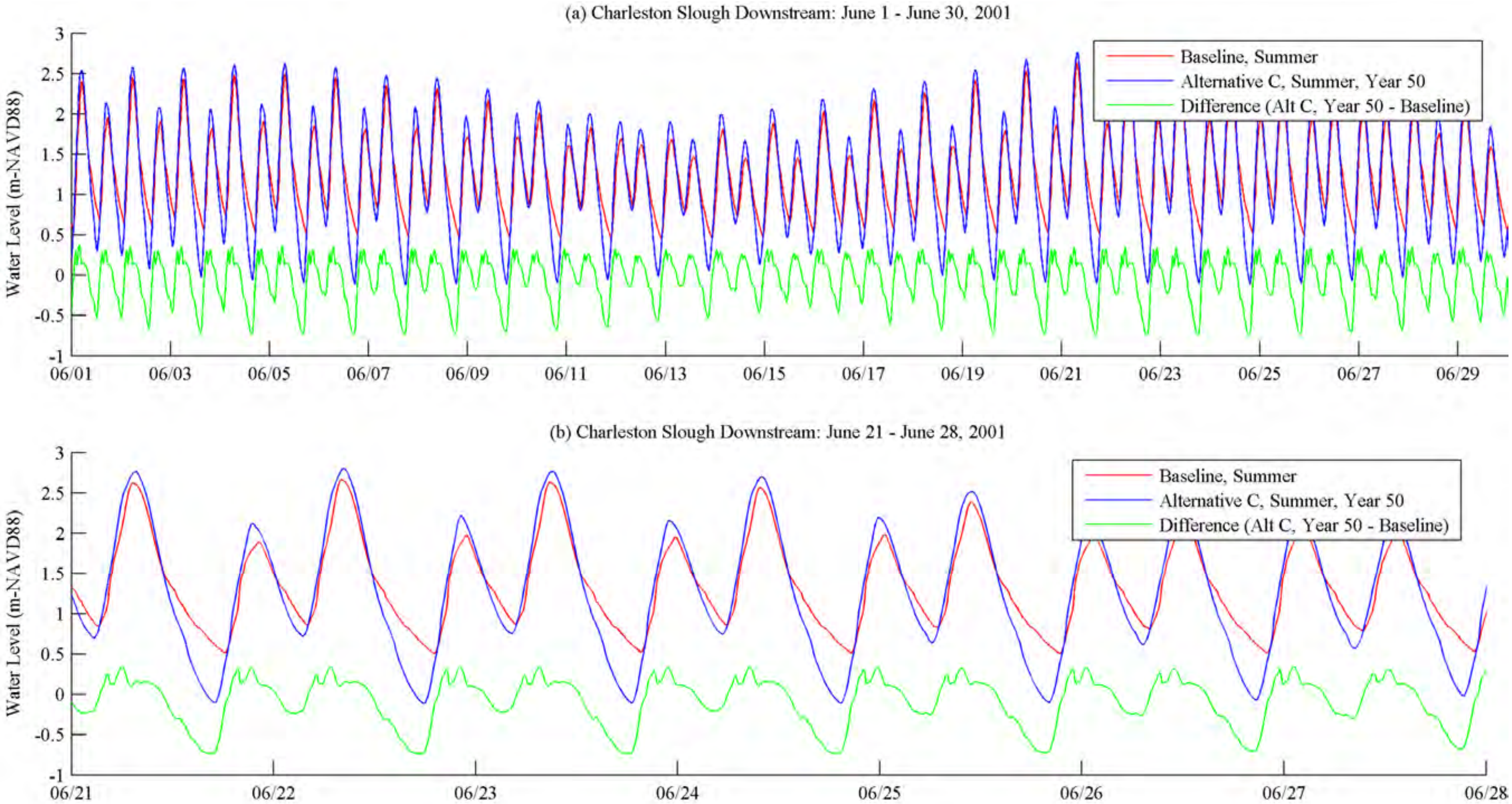

figure 7-26

South Bay Salt Pond Restoration Project

Water Levels, Charleston Slough Downstream, Alt C, Year 50, Summer

PWA

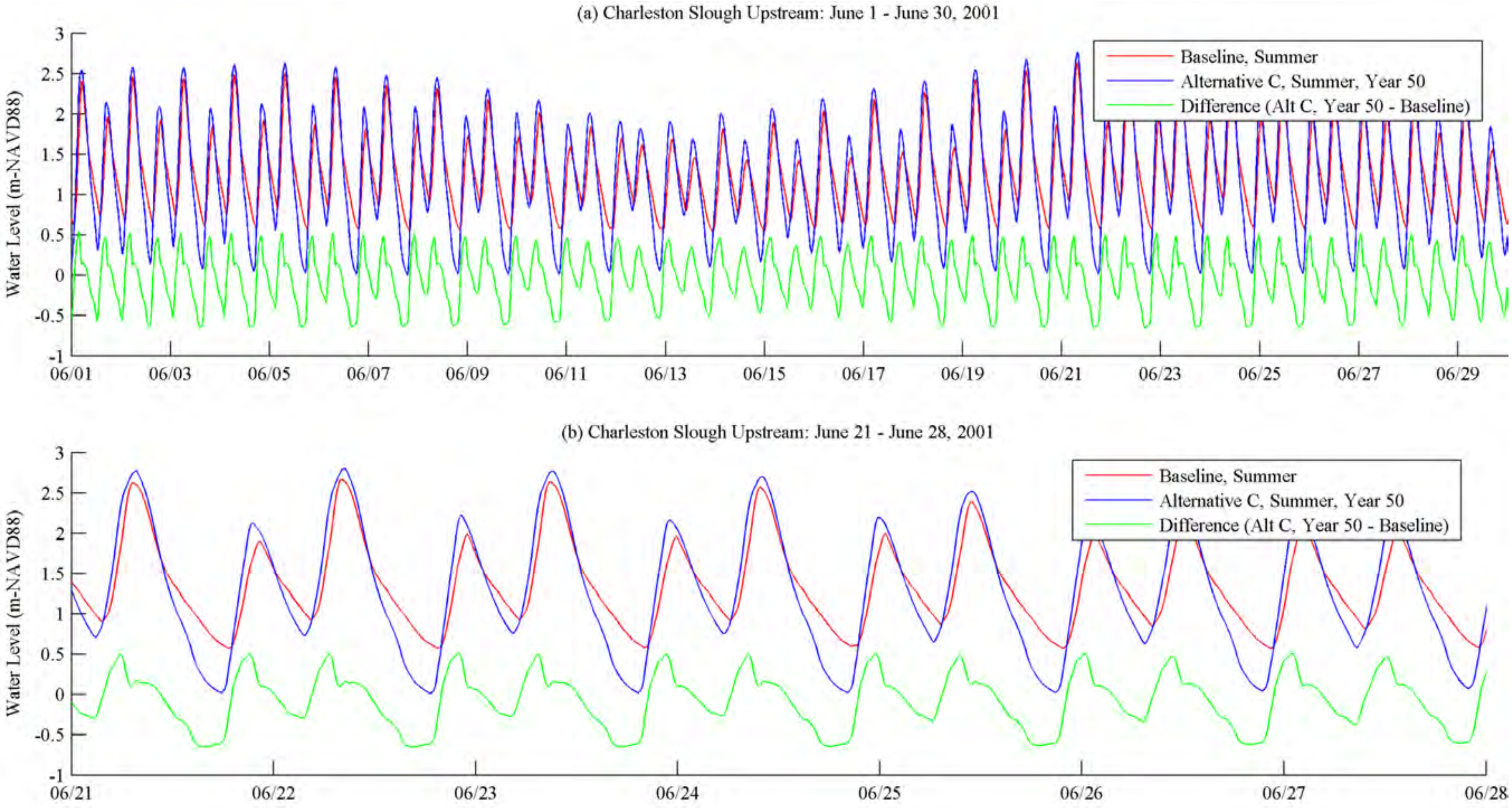

figure 7-27

South Bay Salt Pond Restoration Project

Water Levels, Charleston Slough Upstream, Alt C, Year 50, Summer

PWA

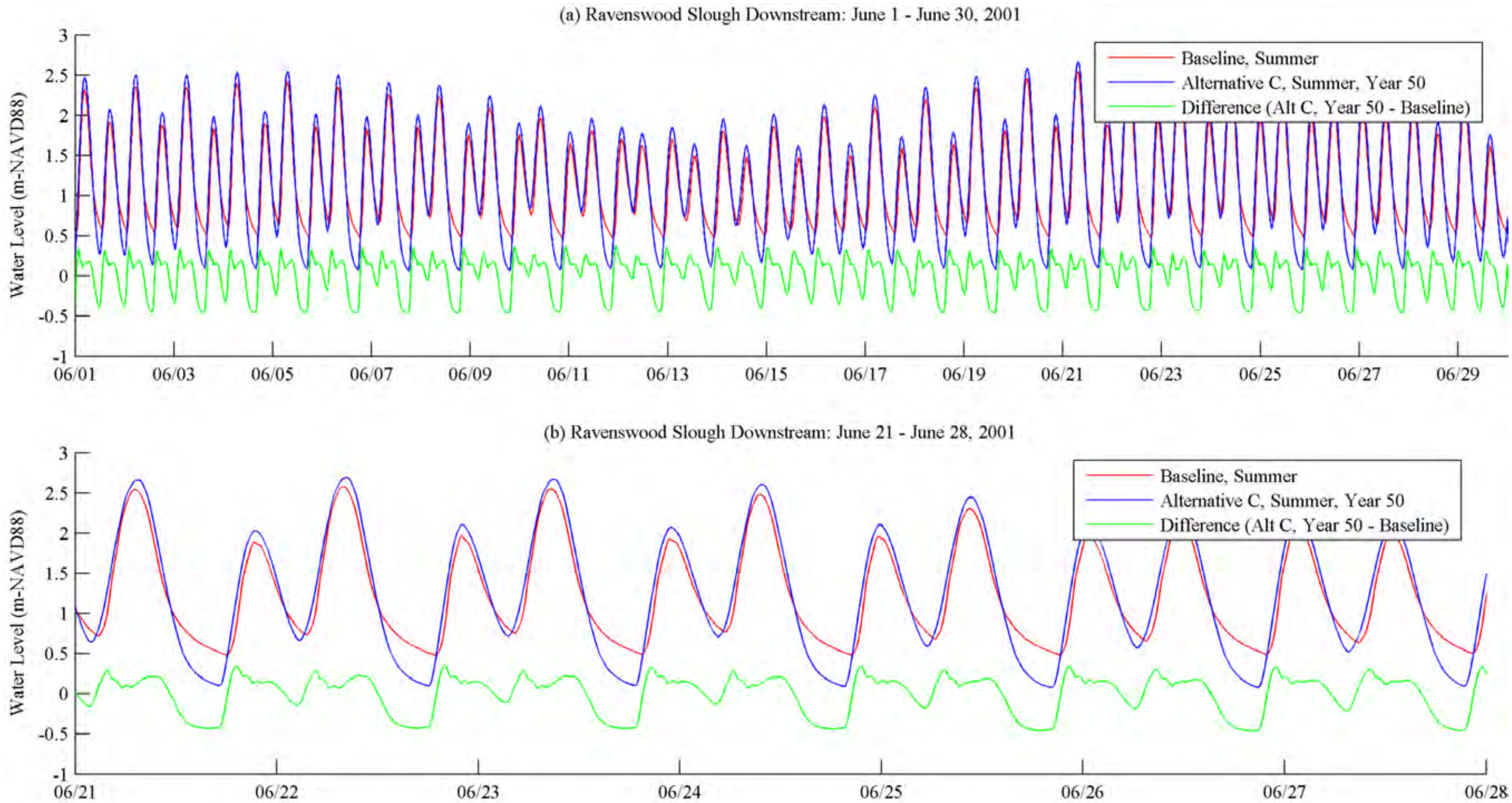

figure 7-28

South Bay Salt Pond Restoration Project

Water Levels, Ravenswood Slough Downstream, Alt C, Year 50, Summer

PWA

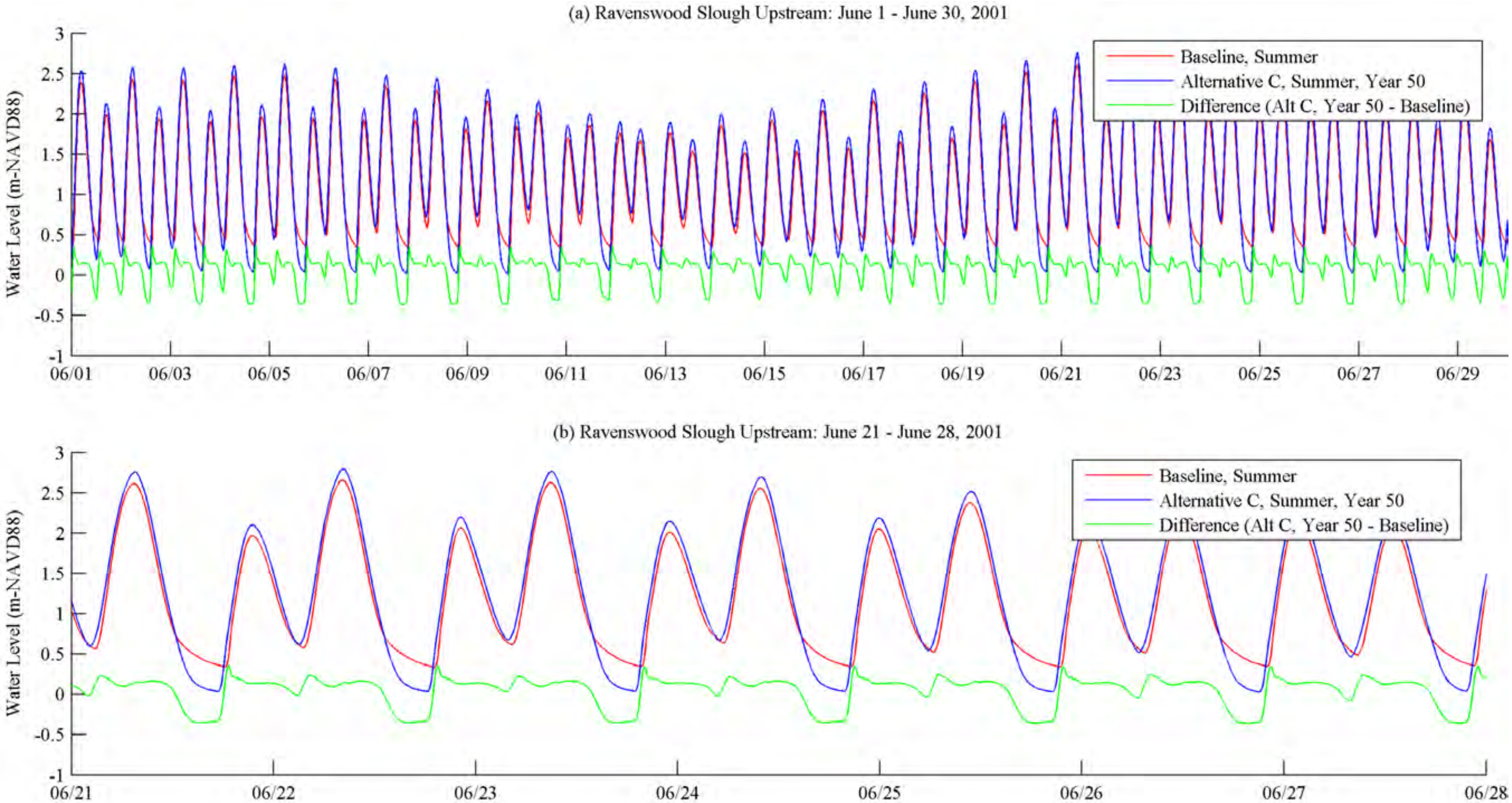

figure 7-29

South Bay Salt Pond Restoration Project

Water Levels, Ravenswood Slough Upstream, Alt C, Year 50, Summer

PWA

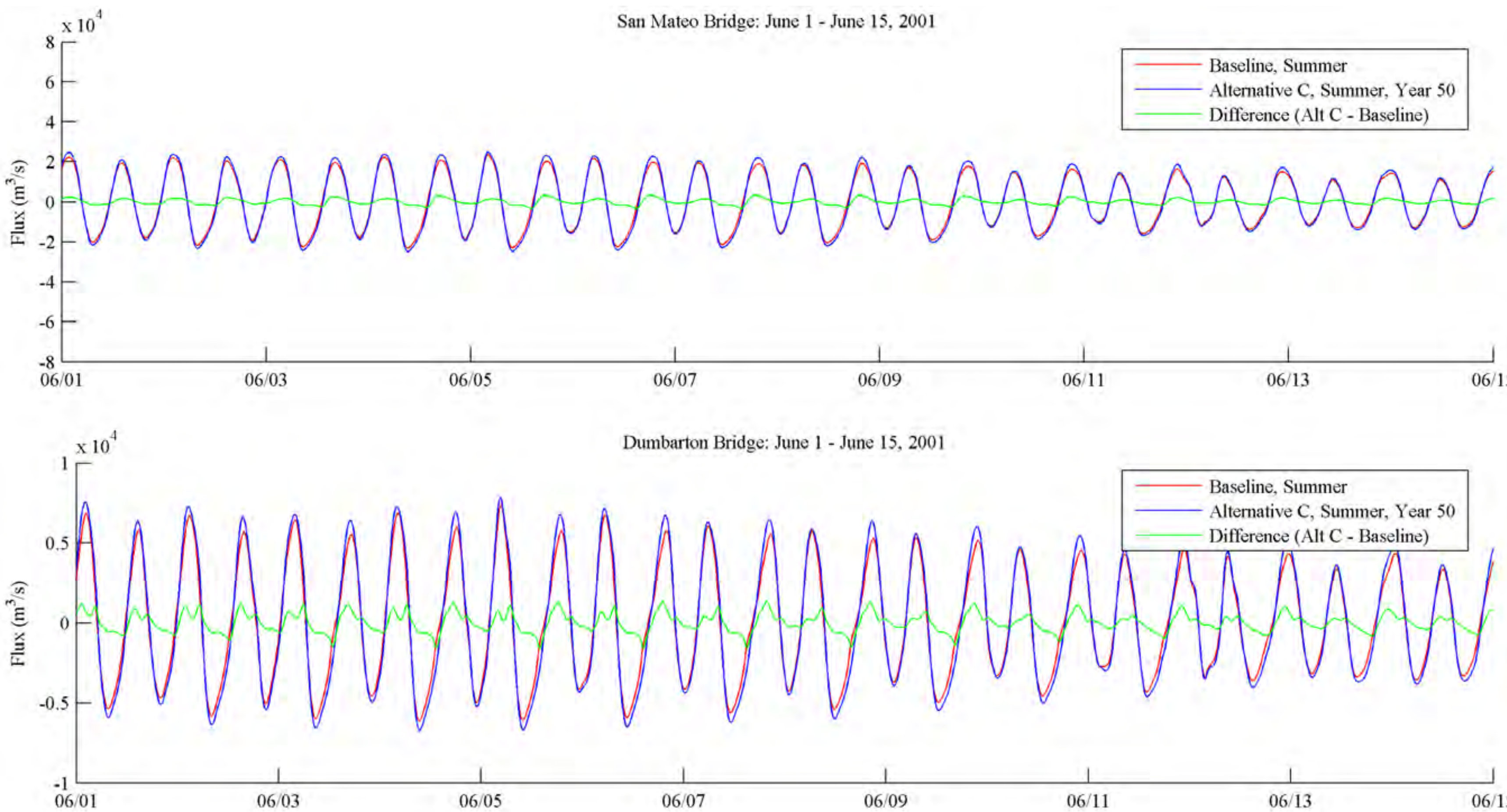

figure 7-30

South Bay Salt Pond Restoration Project

Tidal Prism, San Mateo and Dumbarton Bridges, Alt C, Year 50, Summer

PWA

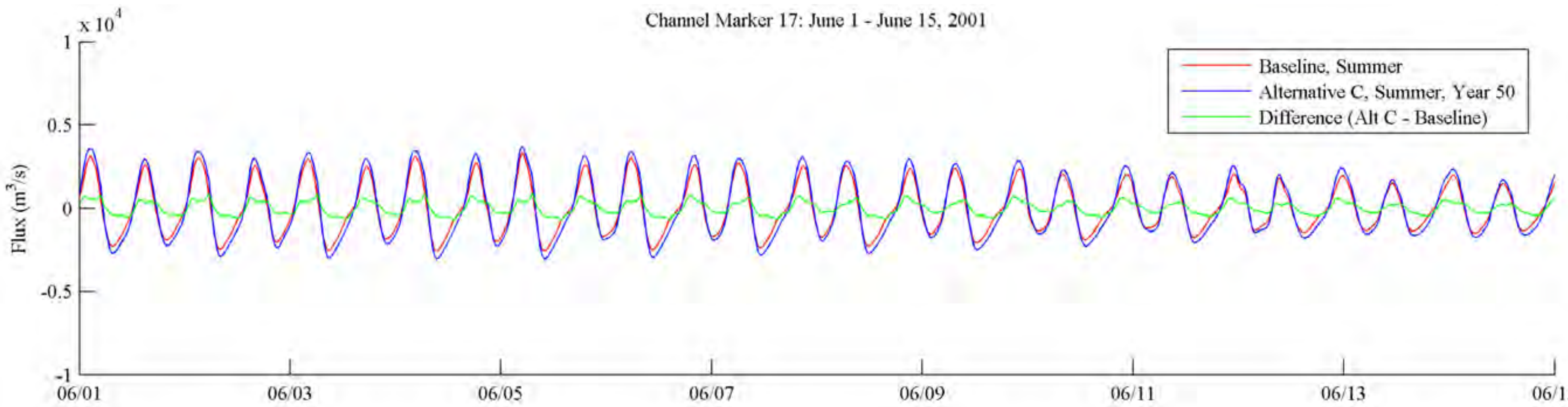

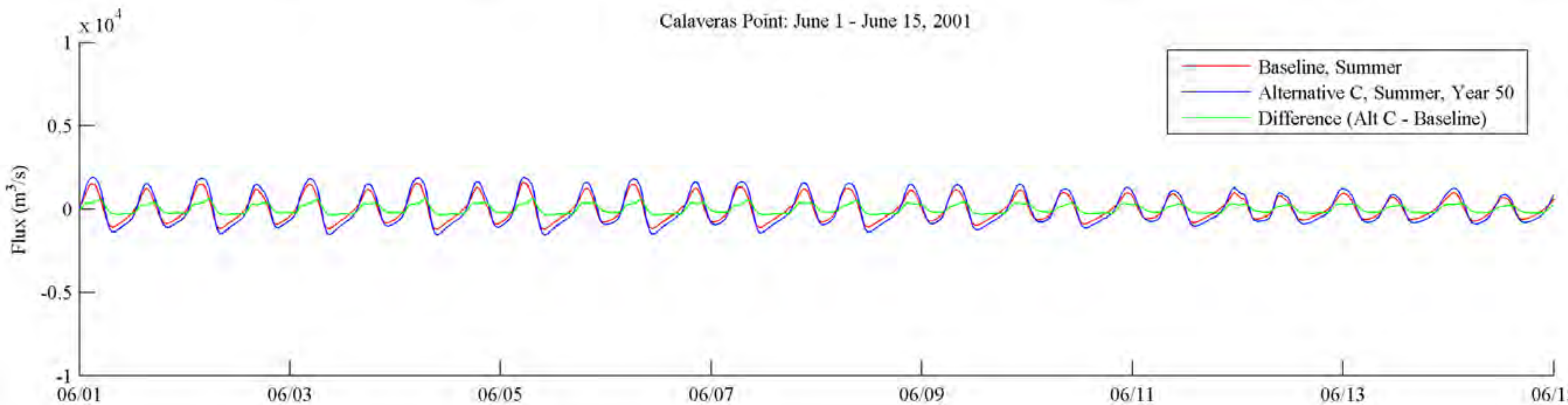

figure 7-31

South Bay Salt Pond Restoration Project

Tidal Prism, Channel Marker 17 and Calaveras Point, Alt C, Year 50, Summer

PWA

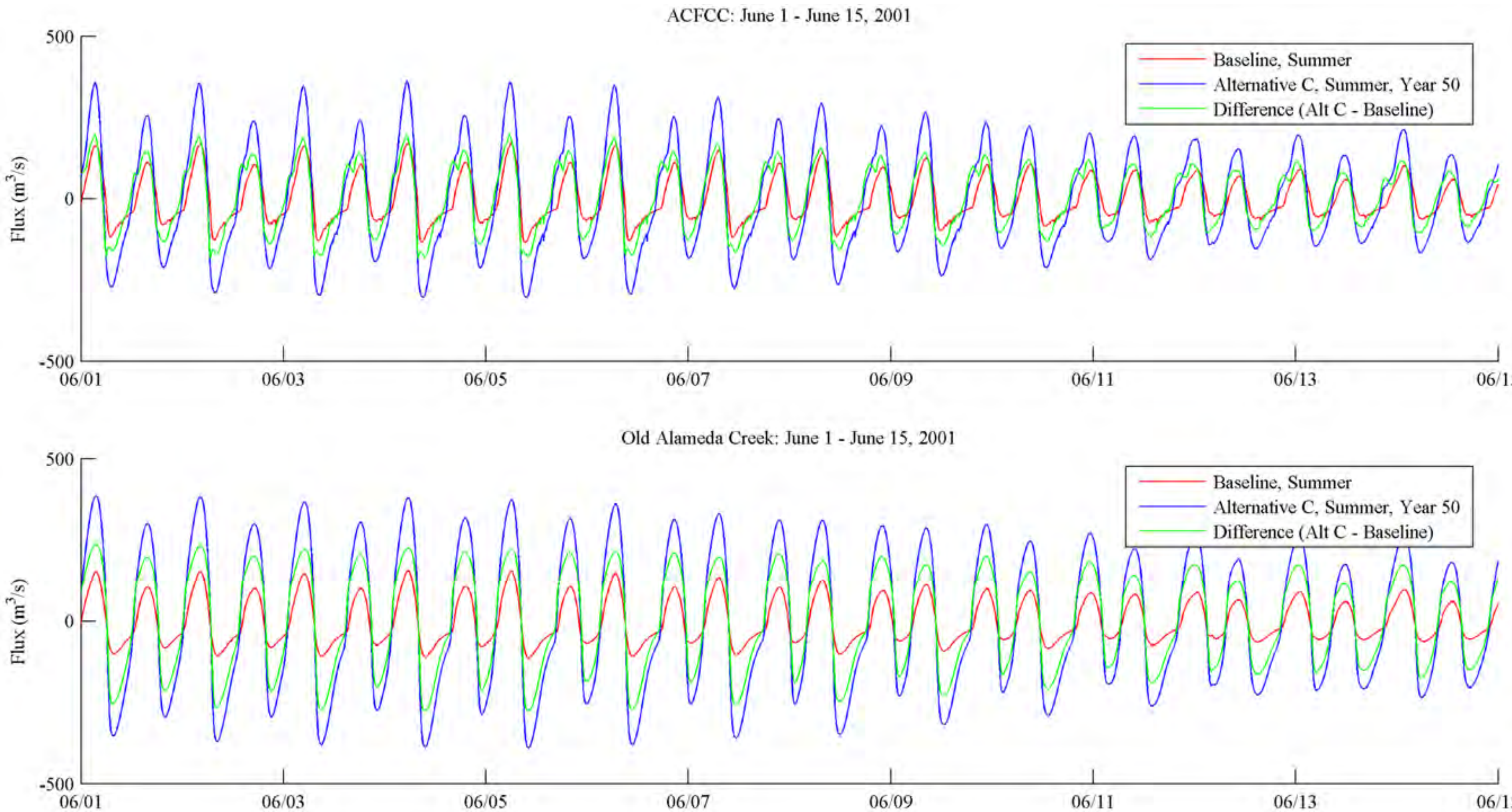

figure 7-32

South Bay Salt Pond Restoration Project

Tidal Prism, ACFCC and Old Alameda Creek, Alt C, Year 50, Summer

PWA

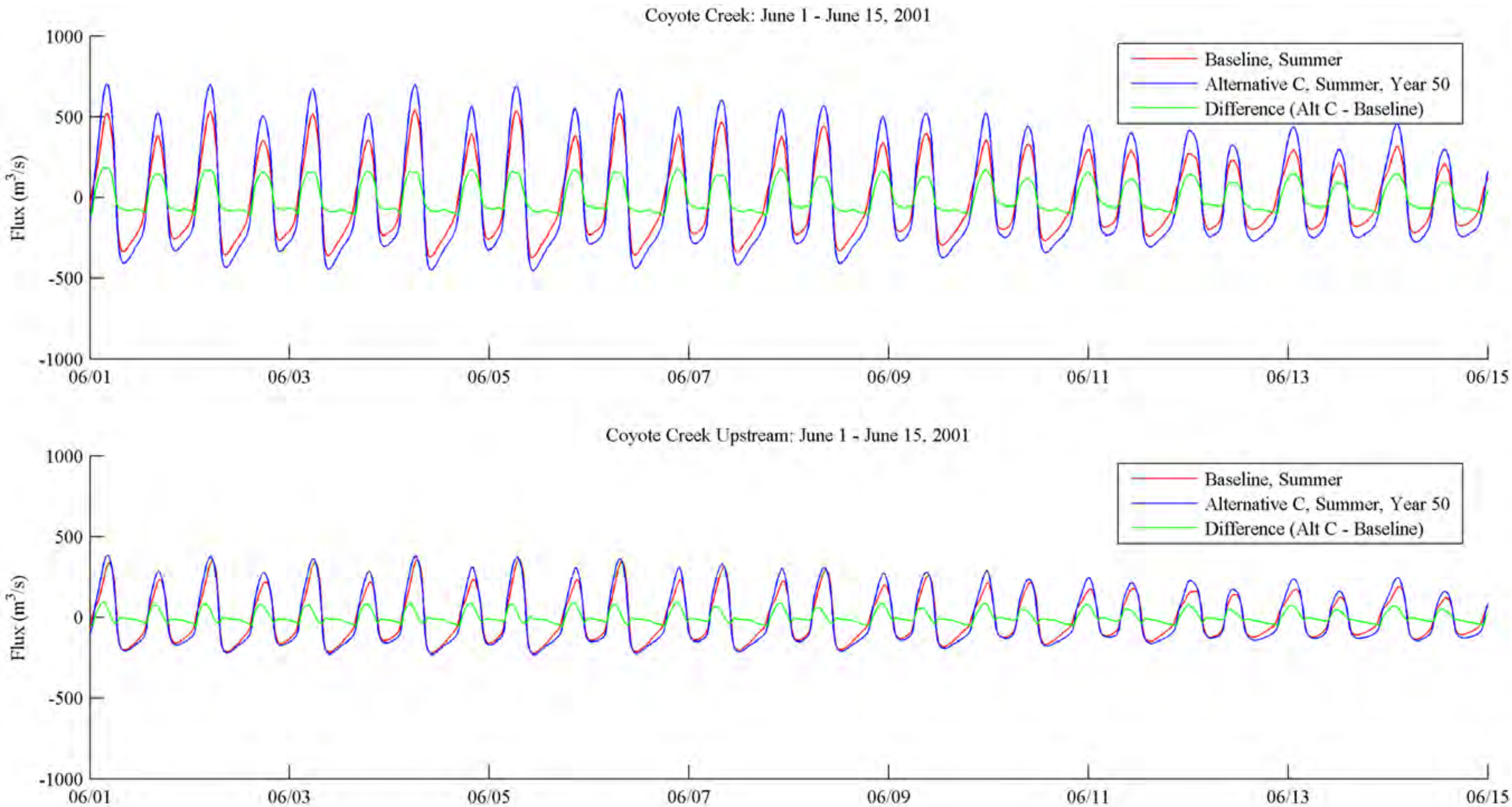

figure 7-33

South Bay Salt Pond Restoration Project

Tidal Prism, Coyote Creek, Alt C, Year 50, Summer

PWA

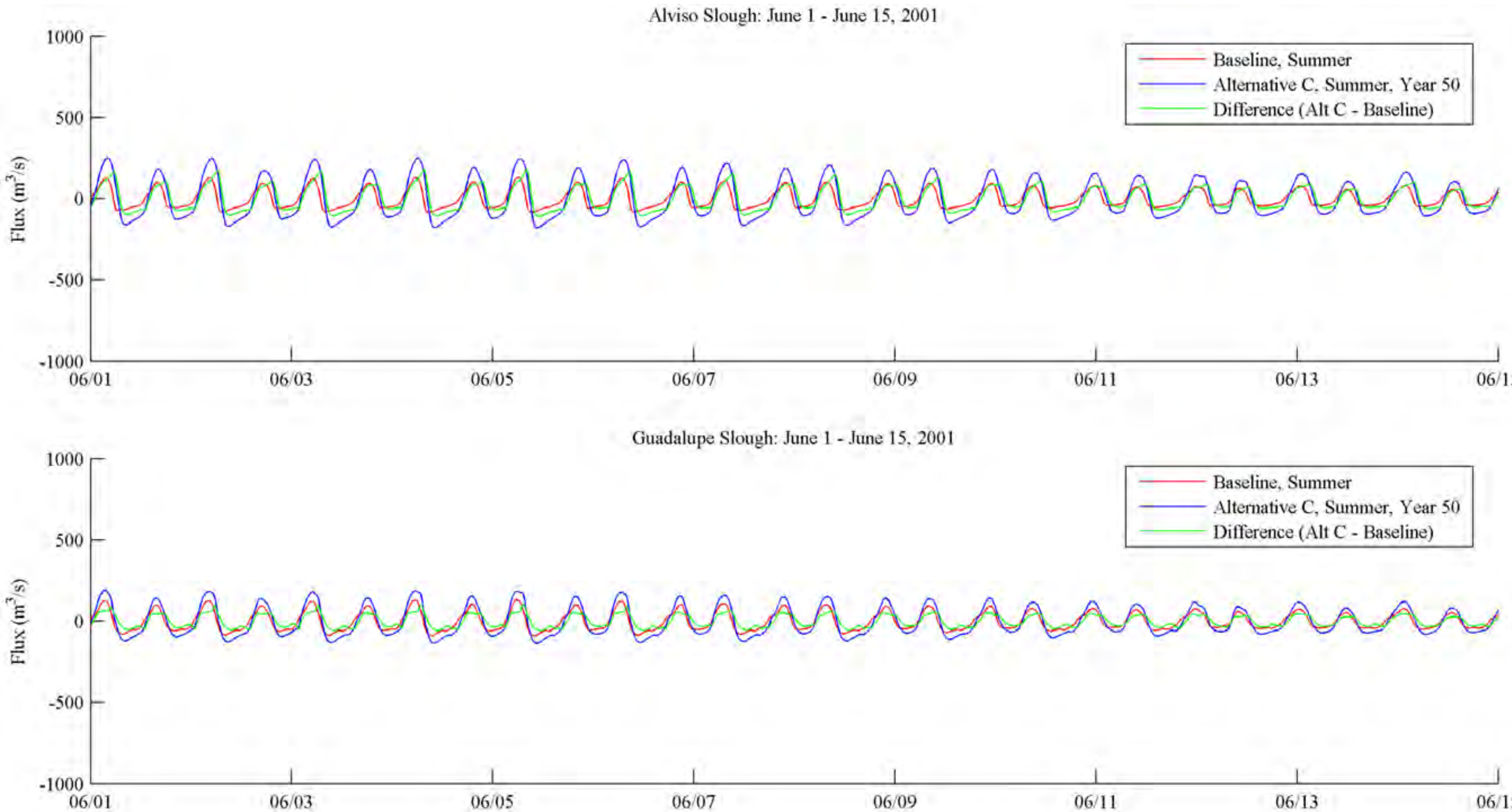

figure 7-34

South Bay Salt Pond Restoration Project

Tidal Prism, Alviso and Guadalupe Sloughs, Alt C, Year 50, Summer

PWA

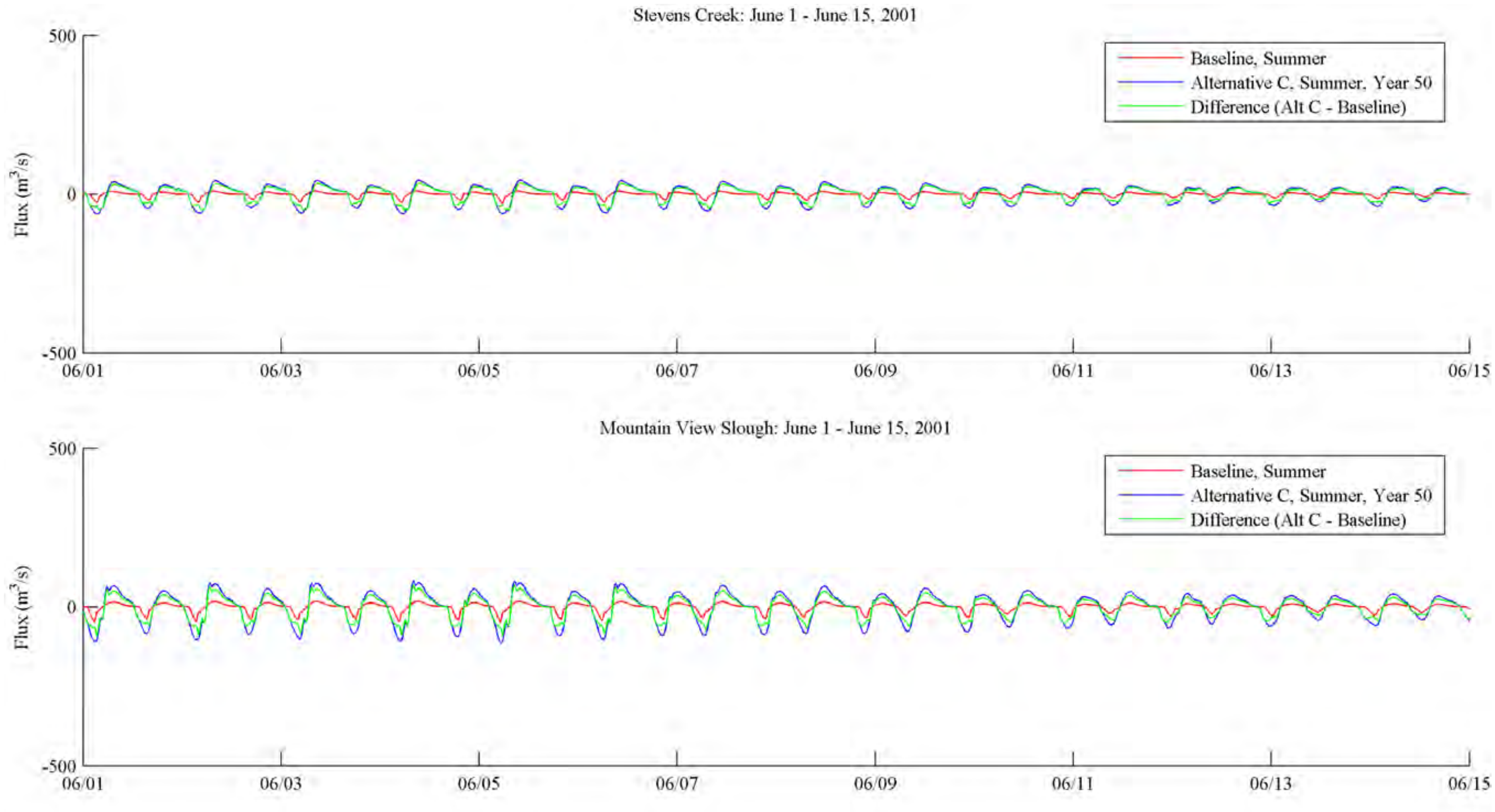

figure 7-35

South Bay Salt Pond Restoration Project

Tidal Prism, Stevens Creek and Mountain View Slough, Alt C, Year 50, Summer

PWA

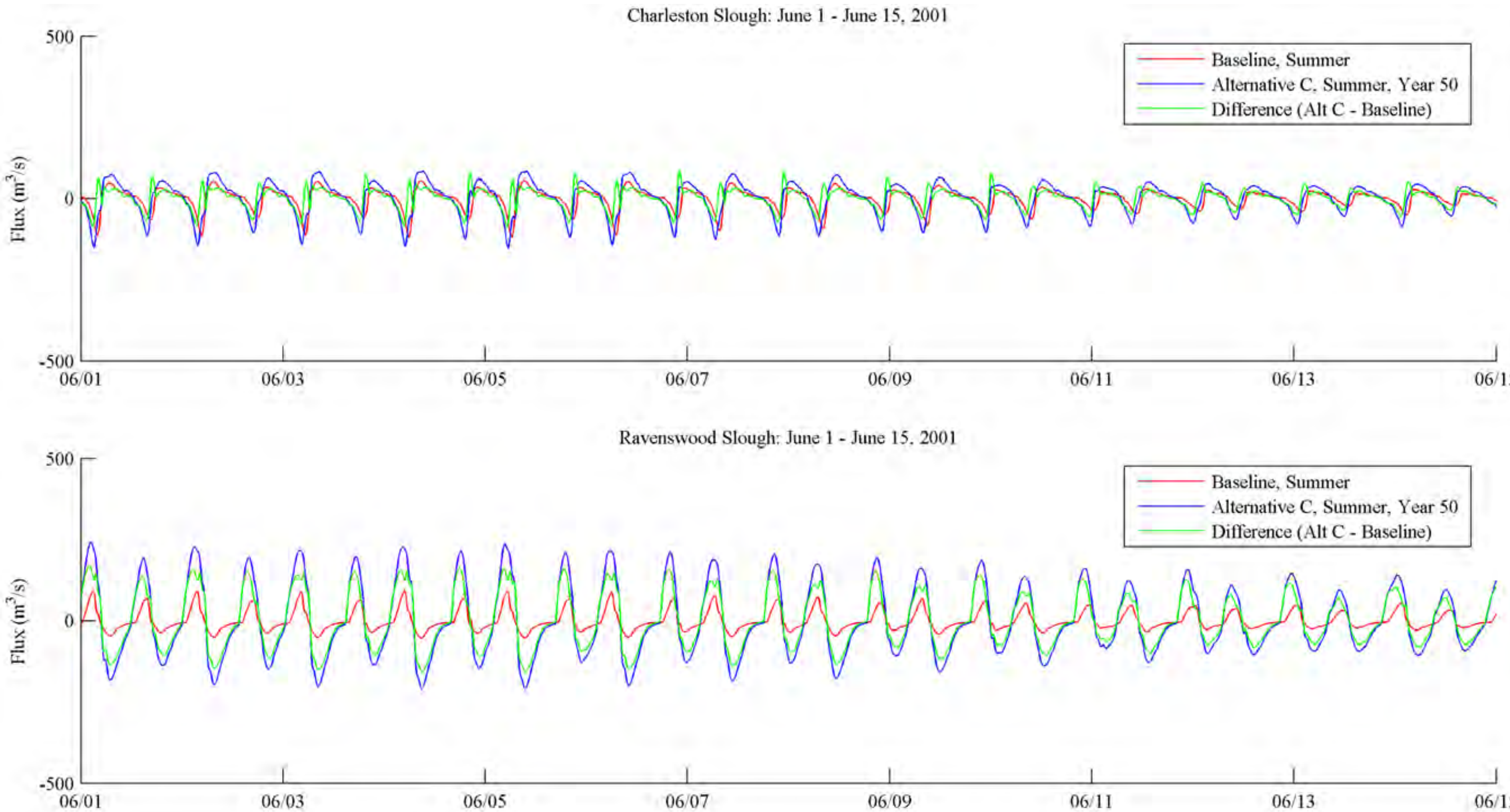

figure 7-36

South Bay Salt Pond Restoration Project

Tidal Prism, Charleston and Ravenswood Sloughs, Alt C, Year 50, Summer

PWA

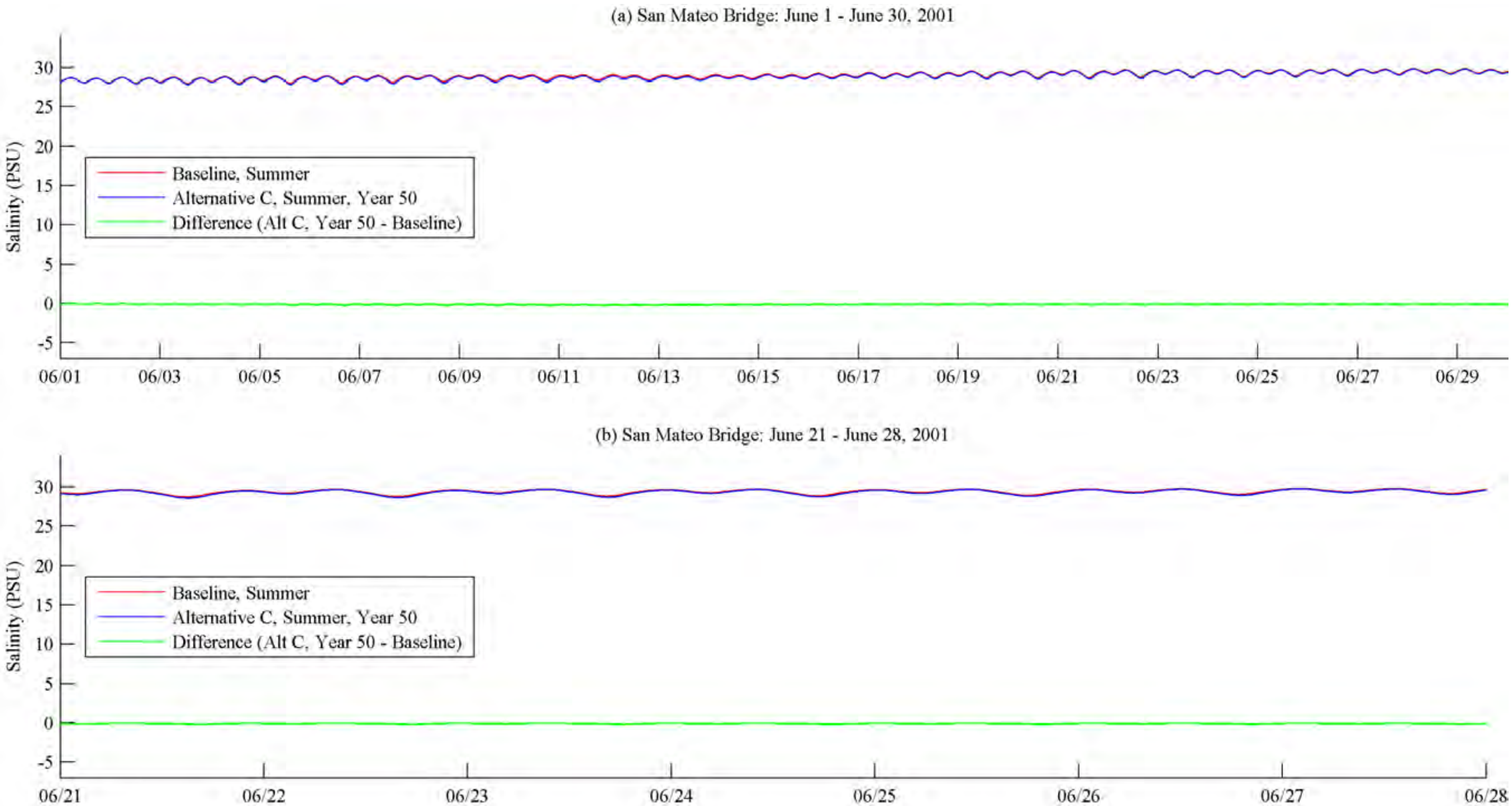

figure 7-37

South Bay Salt Pond Restoration Project

Salinity, San Mateo Bridge, Alt C, Year 50, Summer

PWA

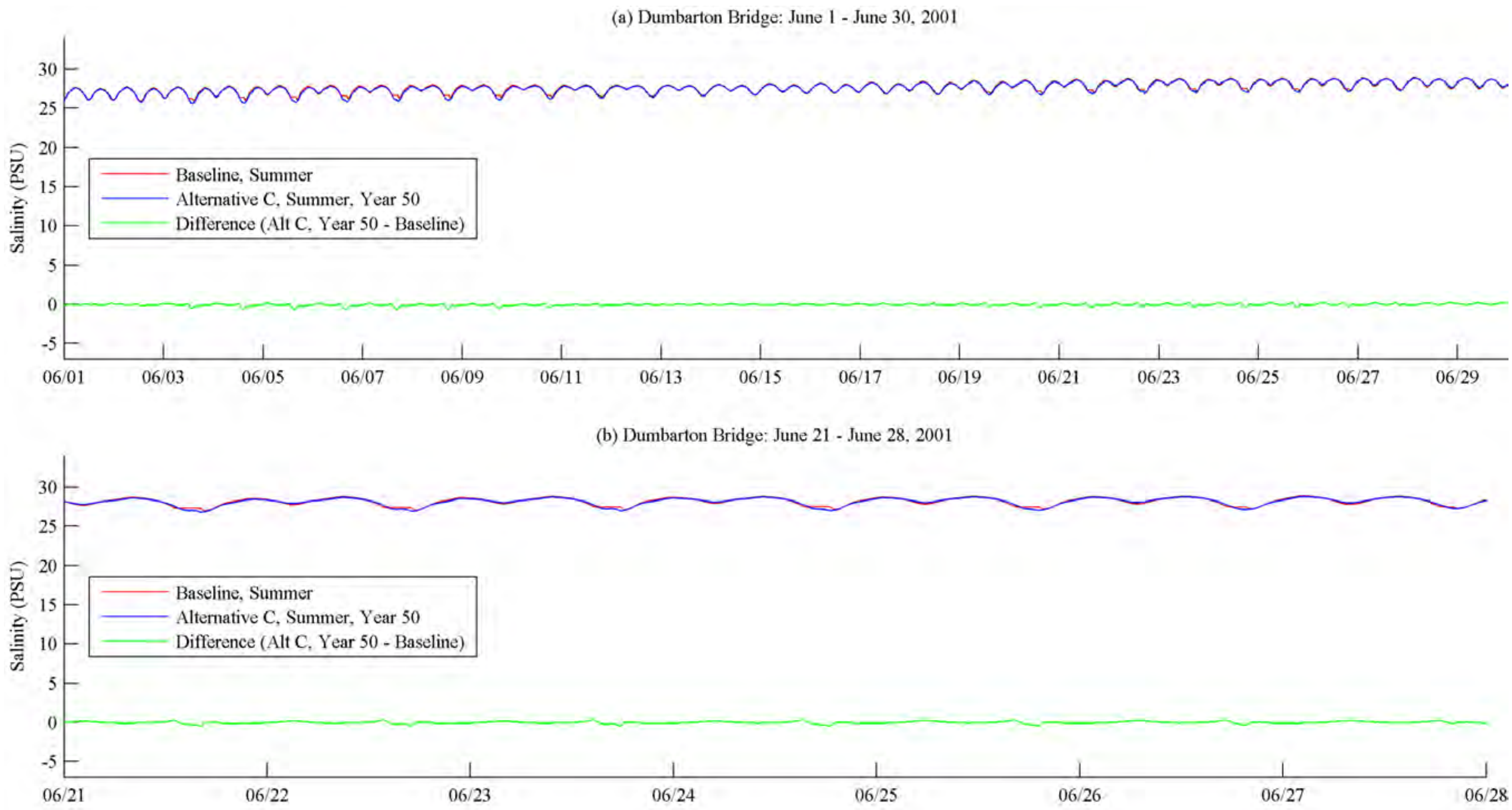

figure 7-38

South Bay Salt Pond Restoration Project

Salinity, Dumbarton Bridge, Alt C, Year 50, Summer

PWA

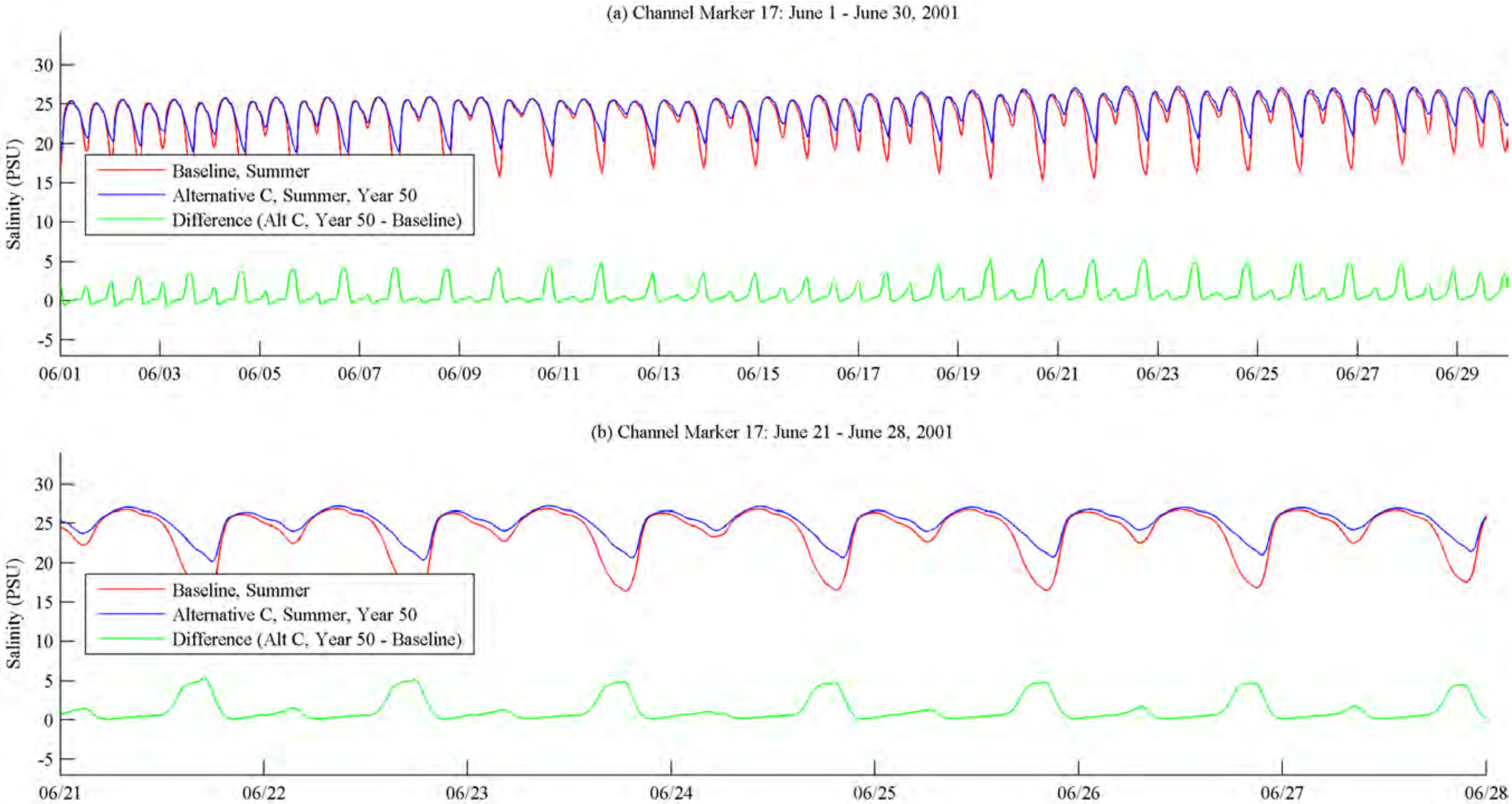

figure 7-39

South Bay Salt Pond Restoration Project

Salinity, Channel Marker 17, Alt C, Year 50, Summer

PWA

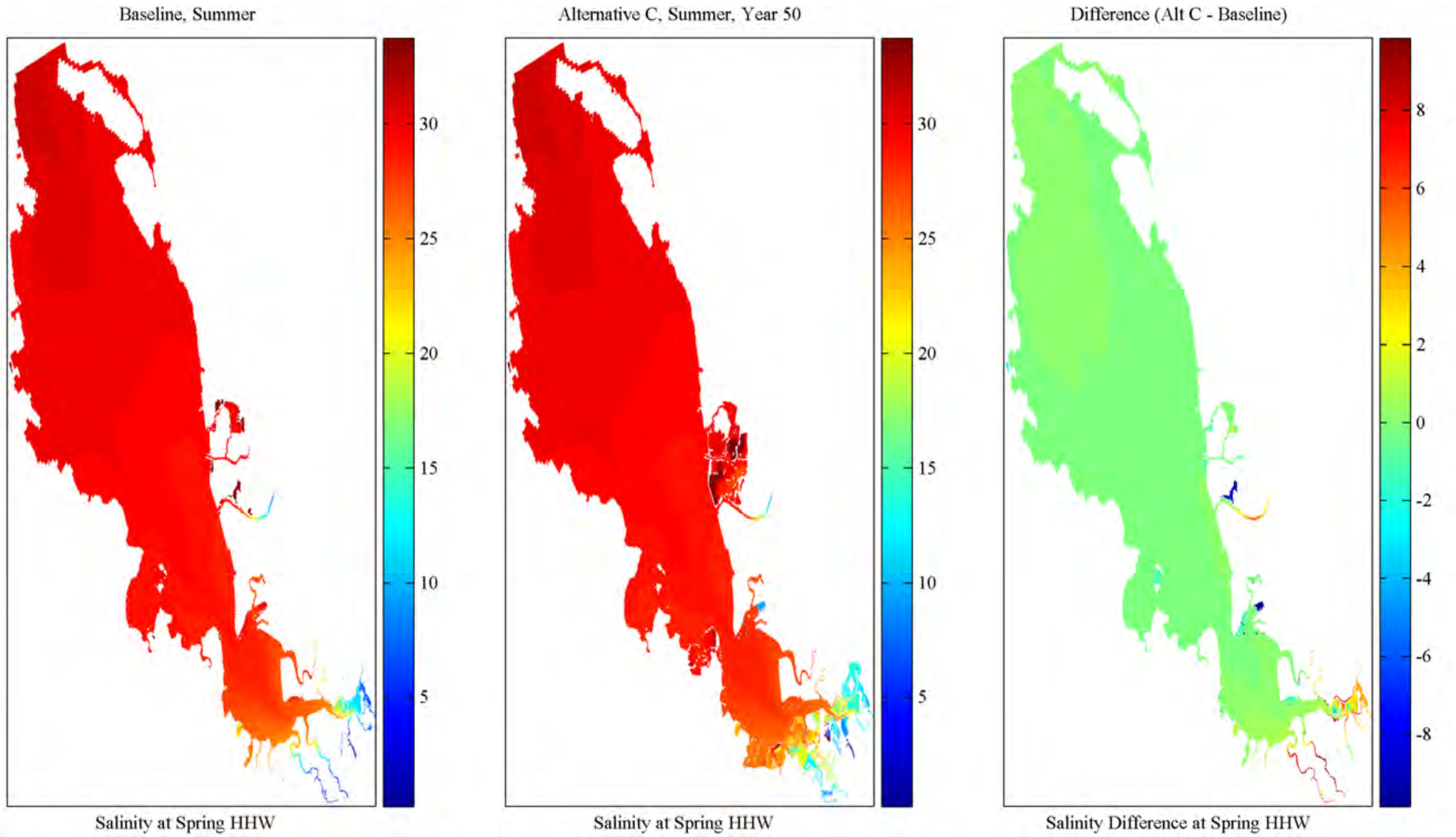

Note: Units shown are PSU

figure 7-40

South Bay Salt Pond Restoration Project

Salinity at Spring HHW, Alt C, Year 50, Summer

PWA

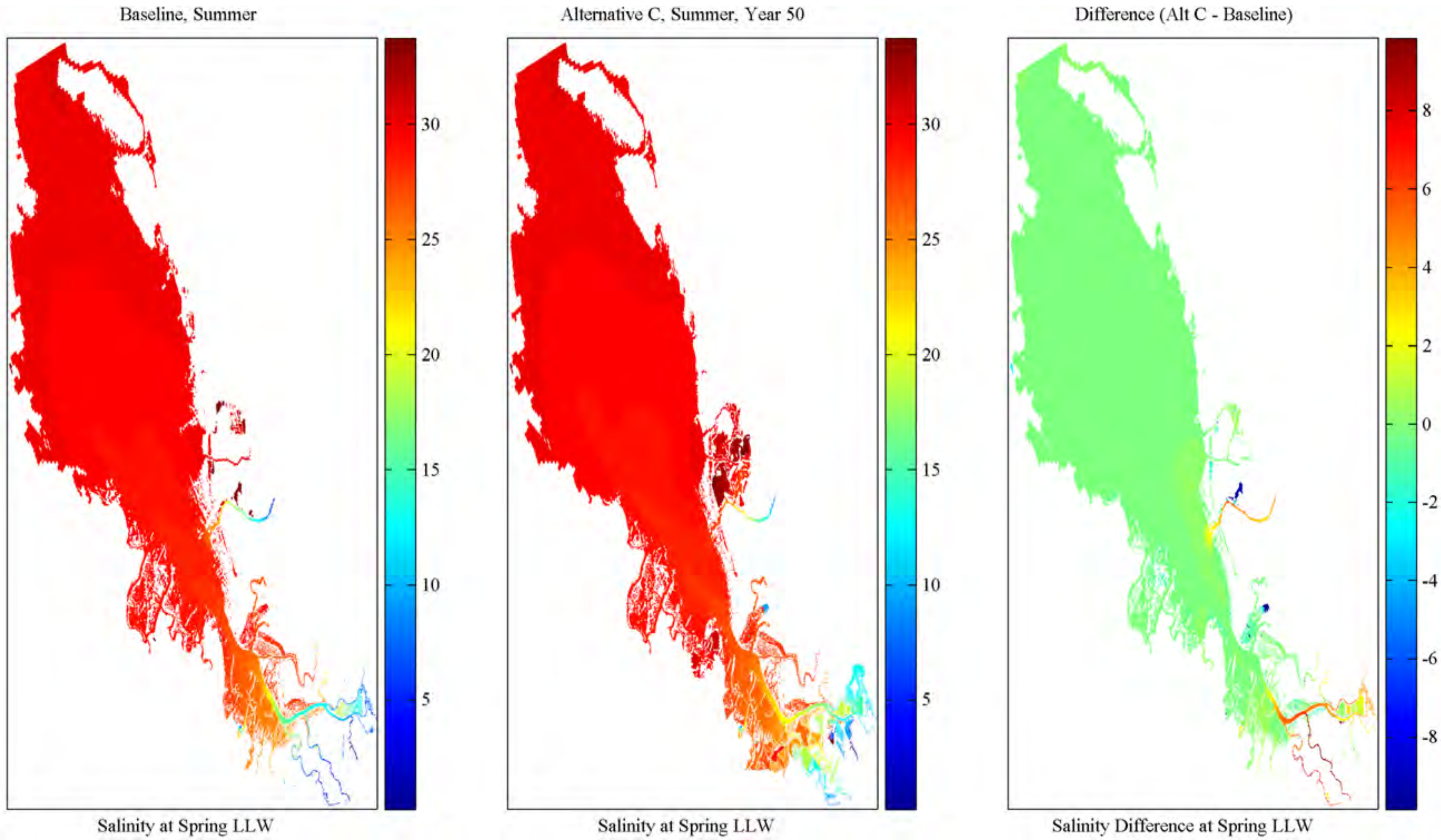

Note: Units shown are PSU

figure 7-41

South Bay Salt Pond Restoration Project

Salinity at Spring LLW, Alt C, Year 50, Summer

PWA

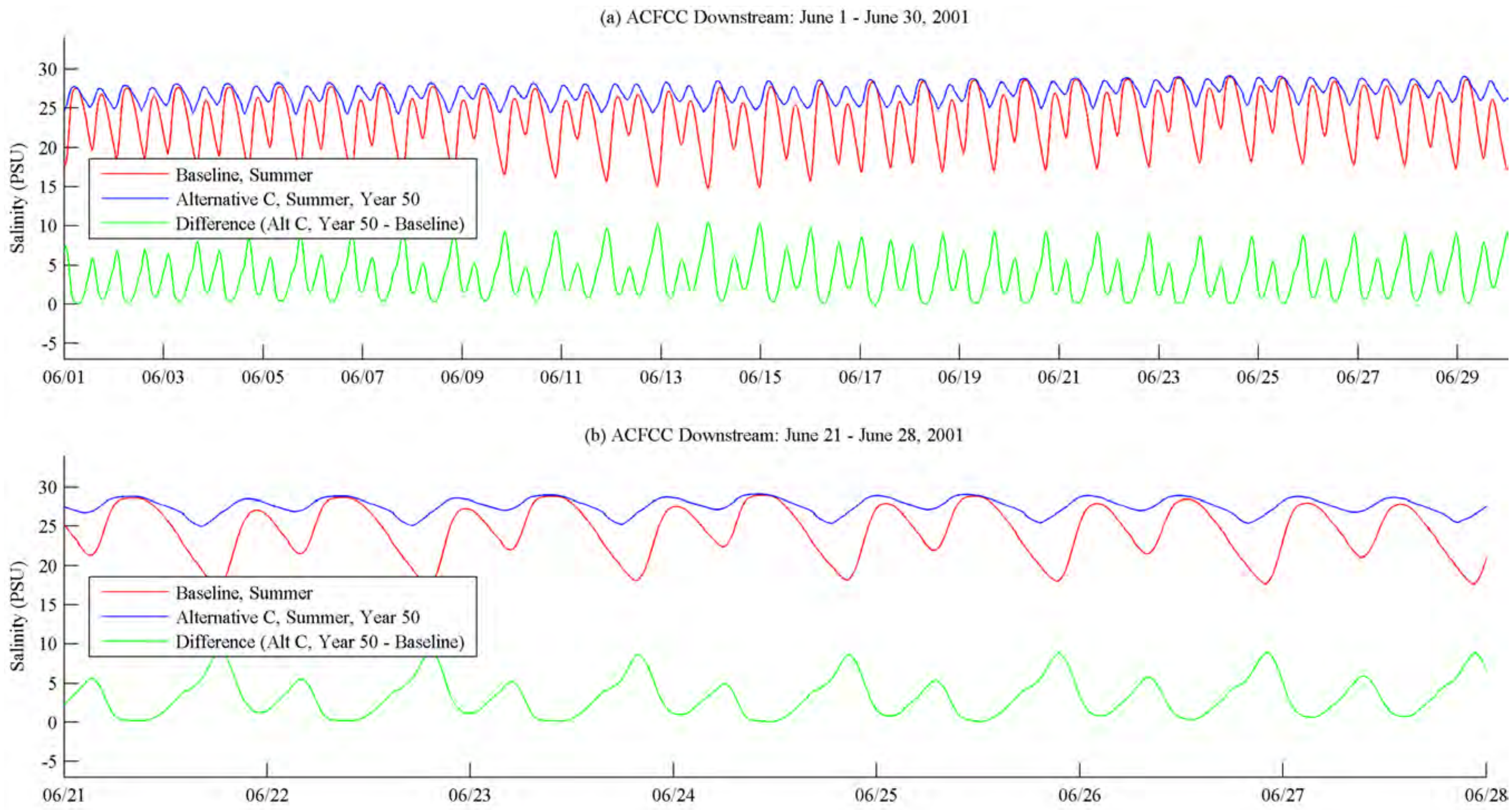

figure *7-42*

South Bay Salt Pond Restoration Project

Salinity, ACFCC Downstream, Alt C, Year 50, Summer

PWA

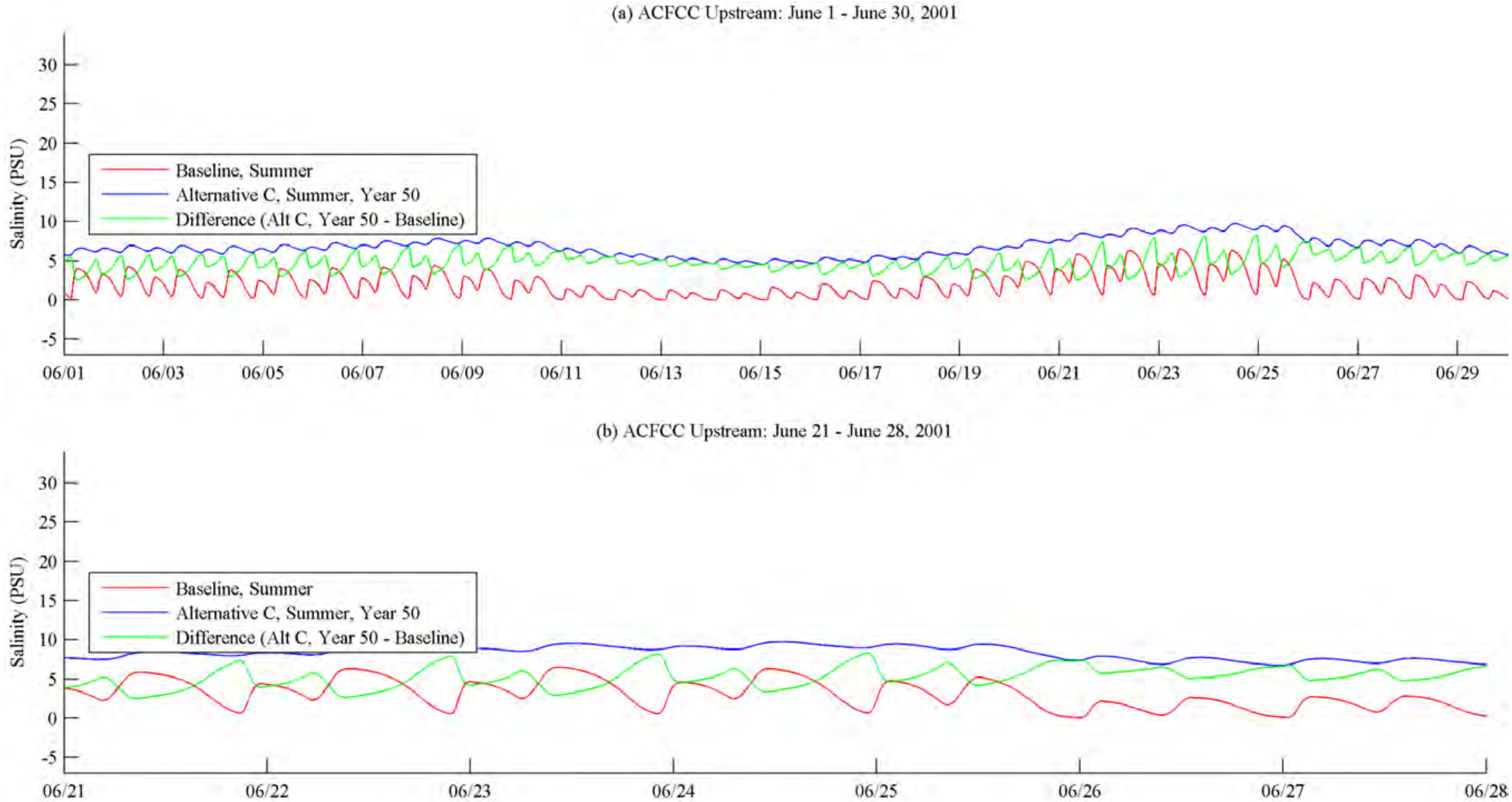

figure 7-43

South Bay Salt Pond Restoration Project

Salinity, ACFCC Upstream, Alt C, Year 50, Summer

PWA

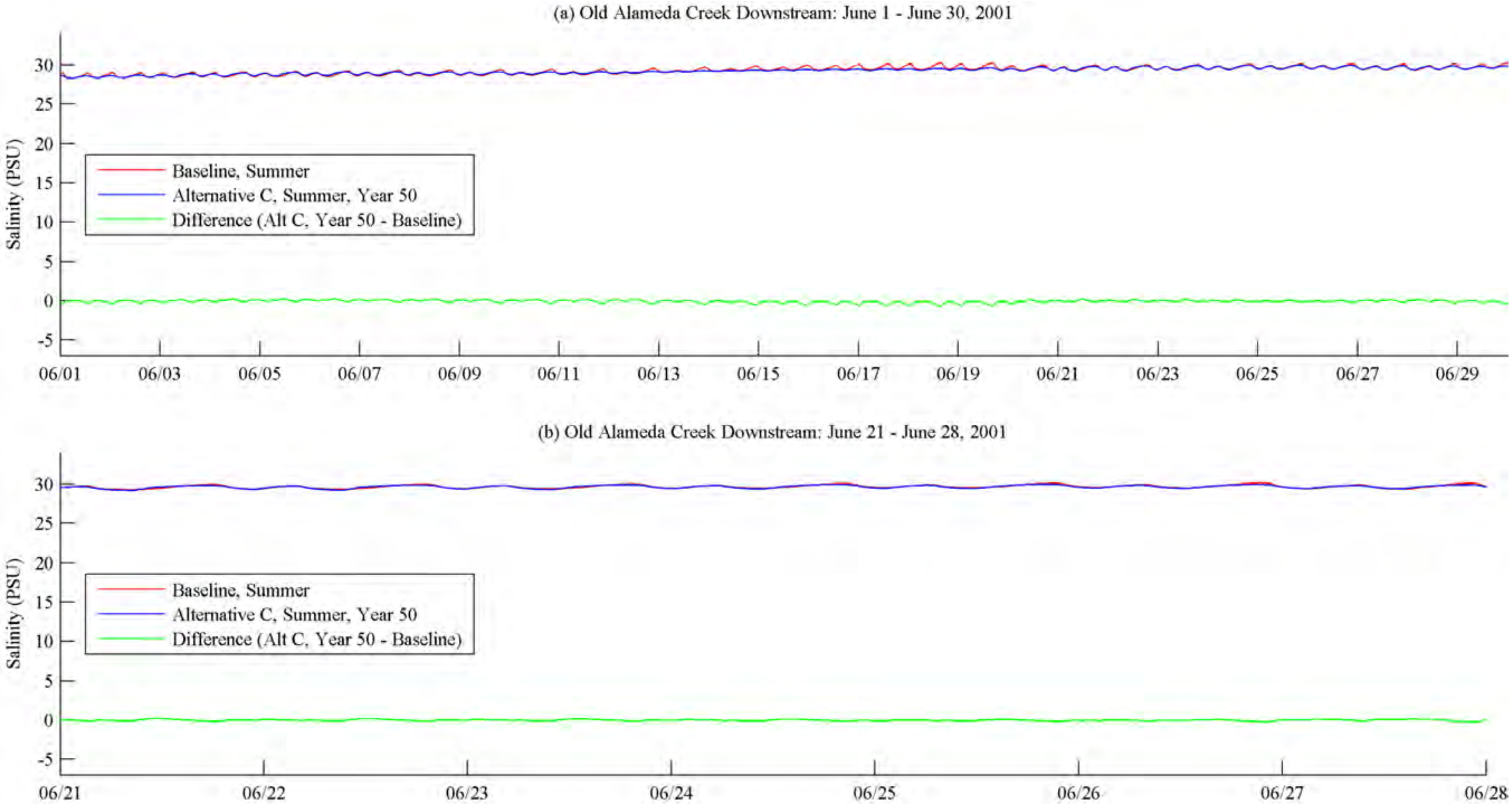

figure *7-44*

South Bay Salt Pond Restoration Project

Salinity, Old Alameda Creek Downstream, Alt C, Year 50, Summer

PWA

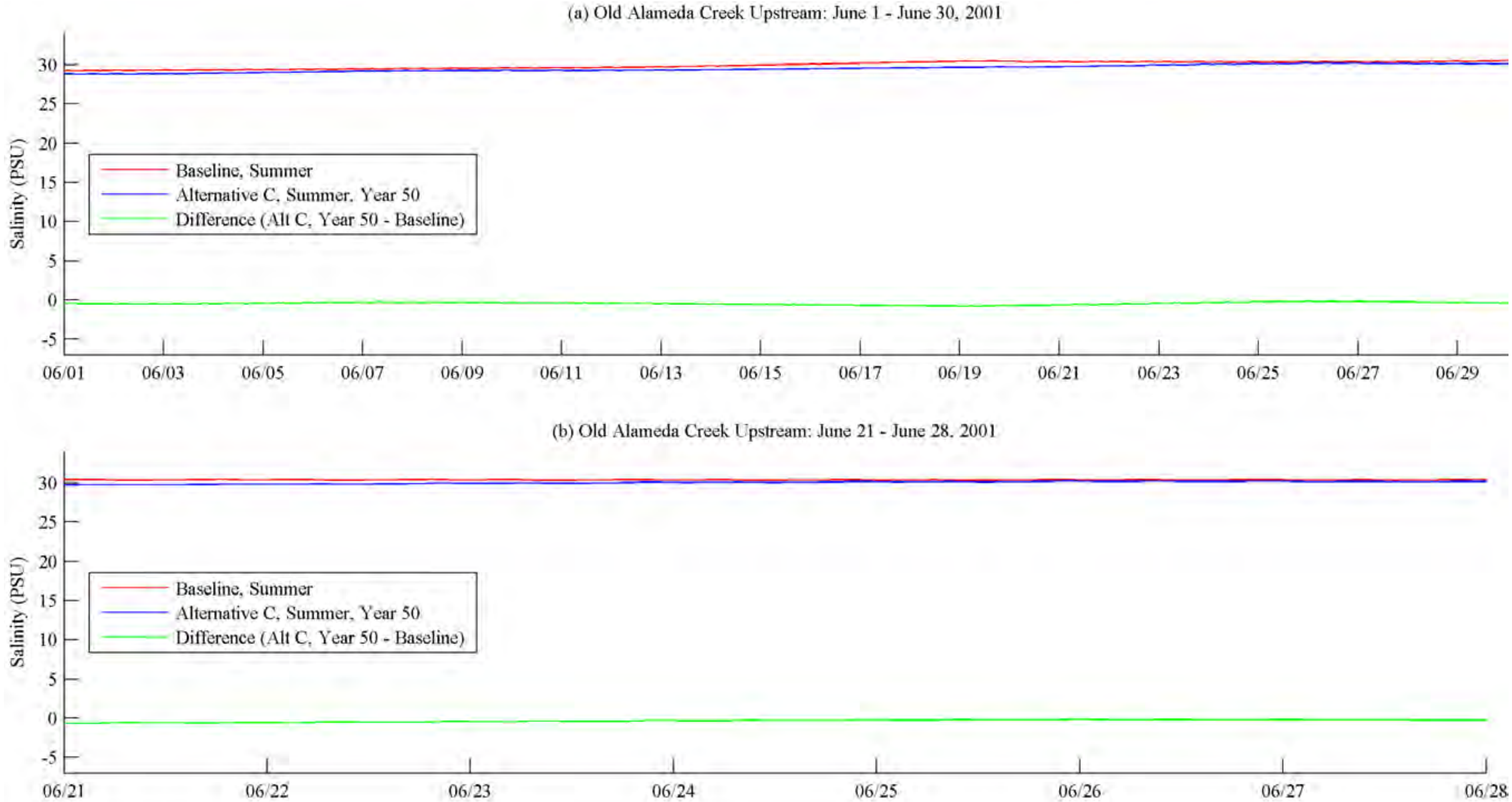

figure *7-45*

South Bay Salt Pond Restoration Project

Salinity, Old Alameda Creek Upstream, Alt C, Year 50, Summer

PWA

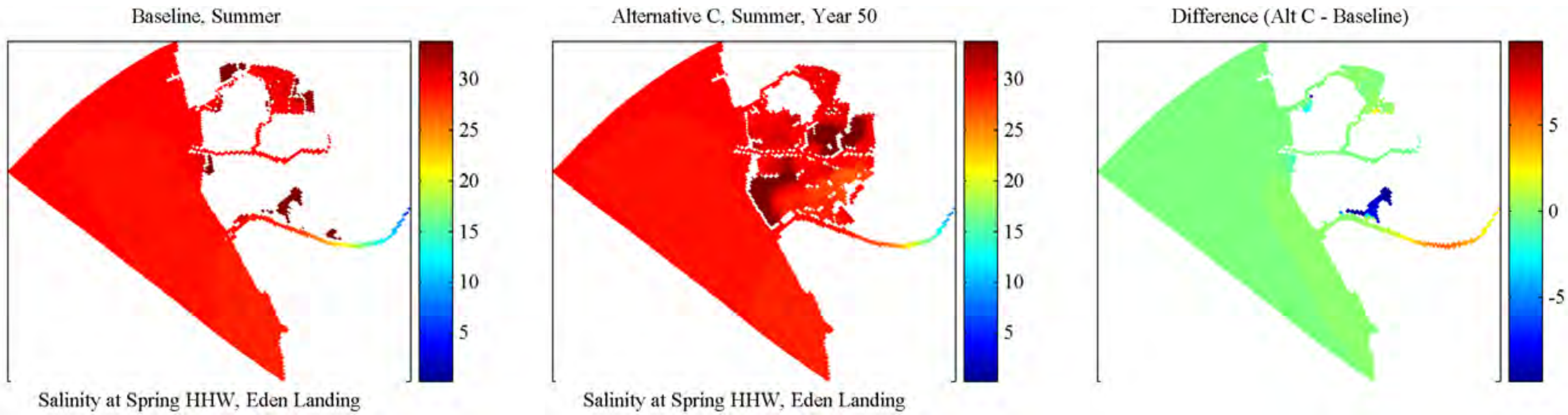

Note: Units shown are PSU

figure 7-46

South Bay Salt Pond Restoration Project

Salinity at Spring HHW, Eden Landing, Alt C, Year 50, Summer

PWA

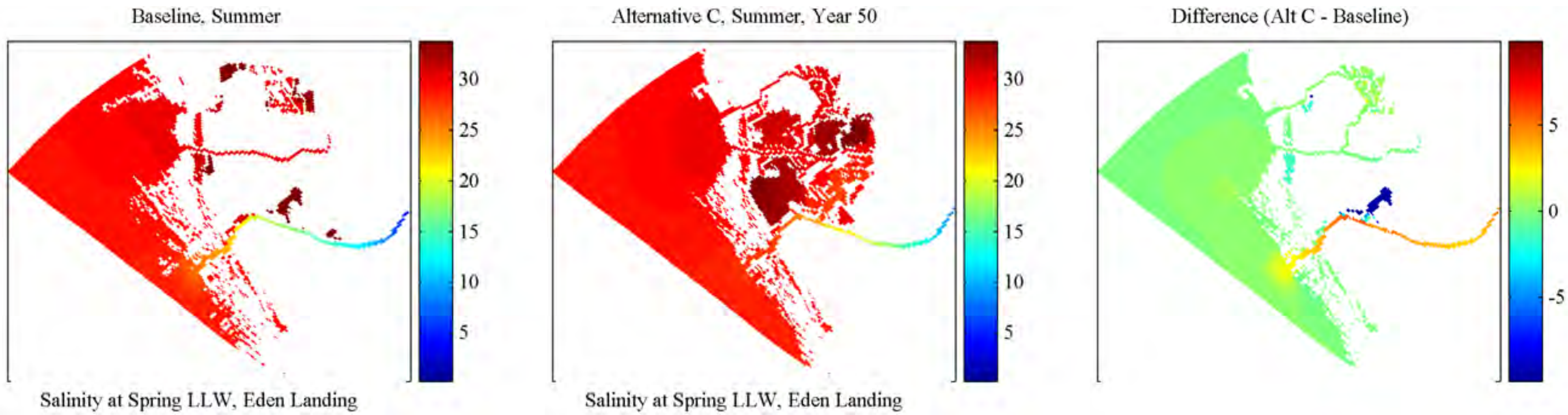

Note: Units shown are PSU

figure 7-47

South Bay Salt Pond Restoration Project

Salinity at Spring LLW, Eden Landing, Alt C, Year 50, Summer

PWA

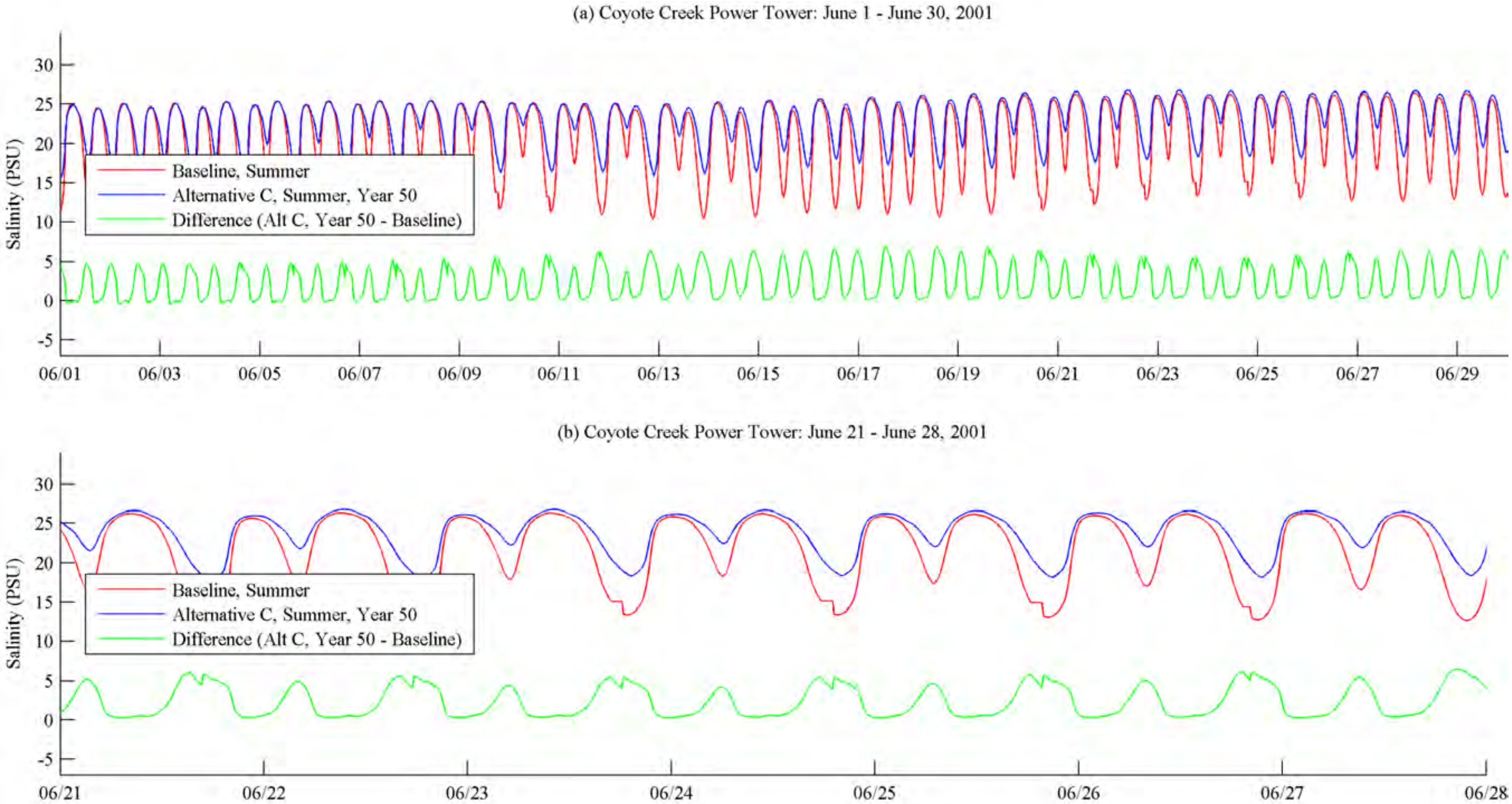

figure 7-48

South Bay Salt Pond Restoration Project

Salinity, Coyote Creek Power Tower, Alt C, Year 50, Summer

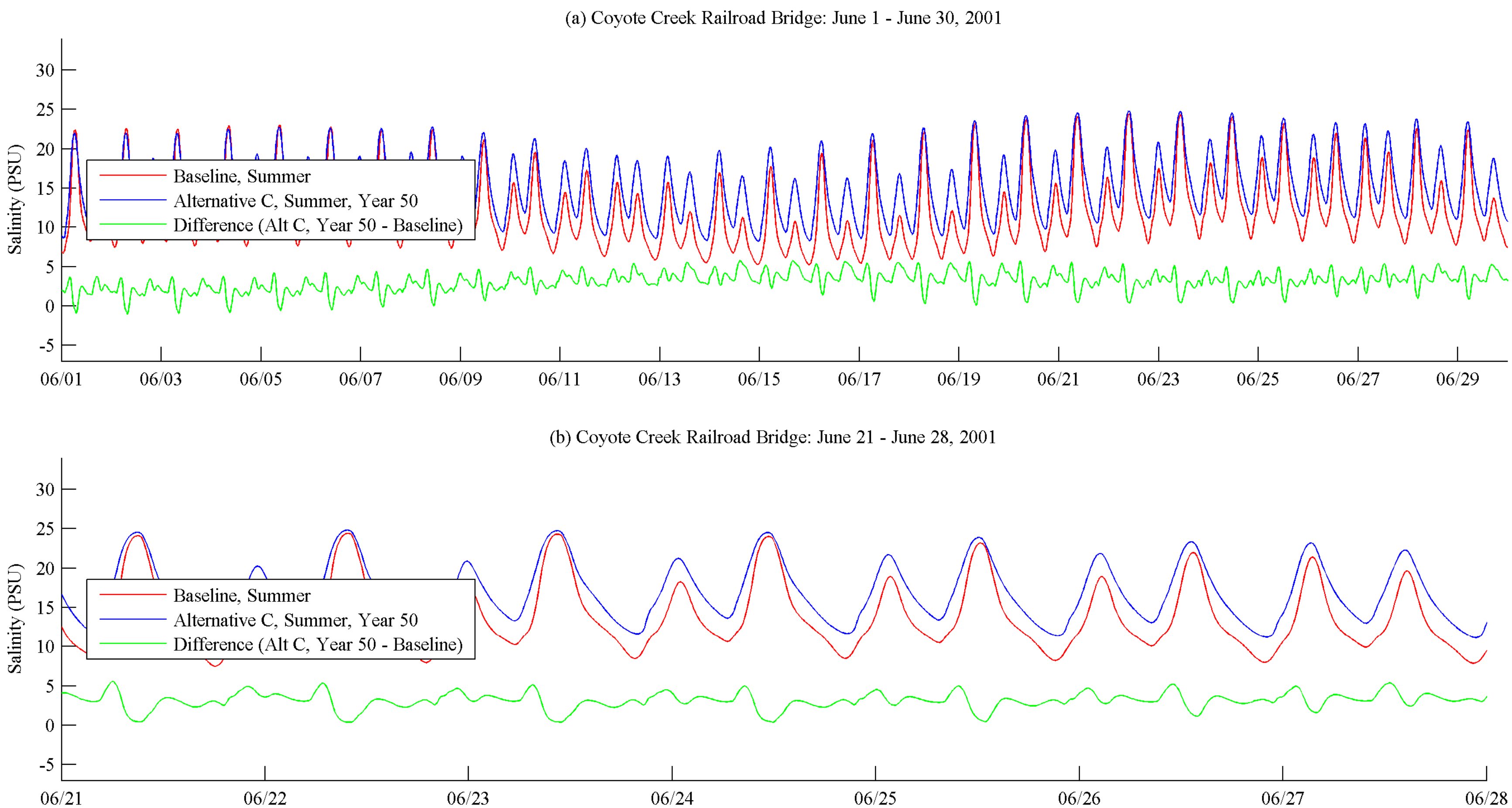

figure *7-49*

South Bay Salt Pond Restoration Project

Salinity, Coyote Creek Railroad Bridge, Alt C, Year 50, Summer

PWA

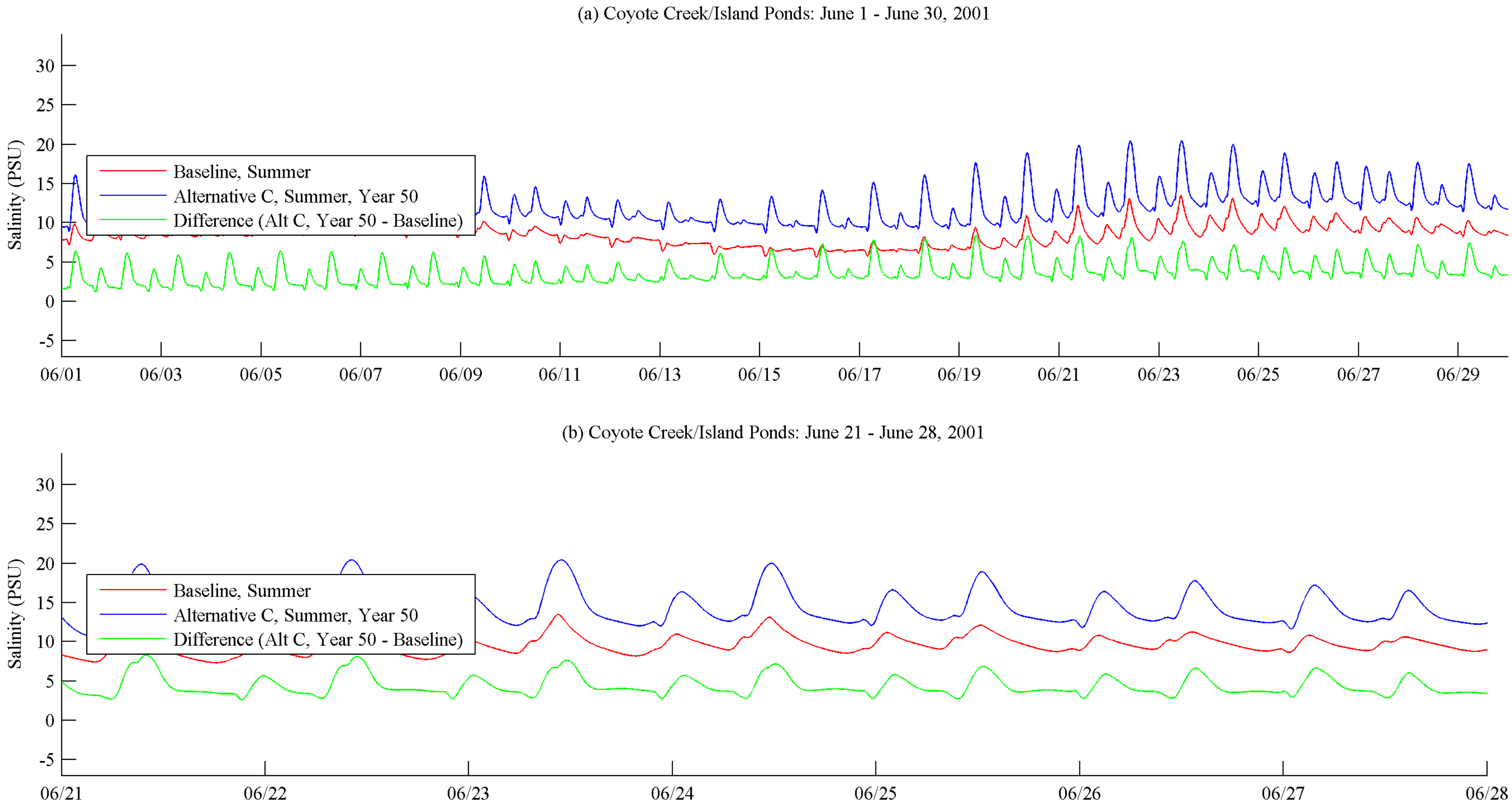

figure 7-50

South Bay Salt Pond Restoration Project

Salinity, Coyote Creek/Island Ponds, Year 50, Summer

PWA

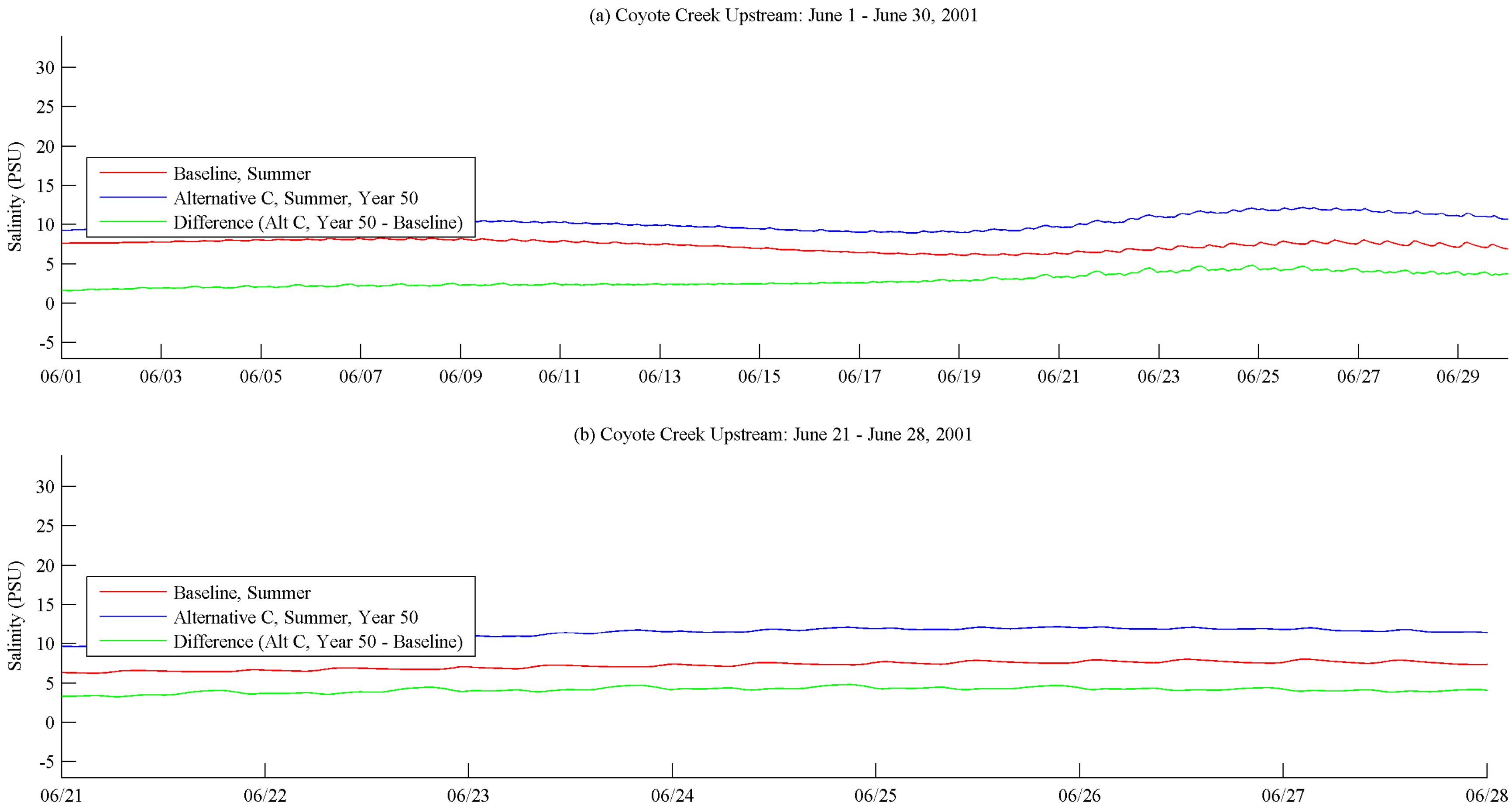

figure *7-51*

South Bay Salt Pond Restoration Project

Salinity, Coyote Creek Upstream, Year 50, Summer

PWA

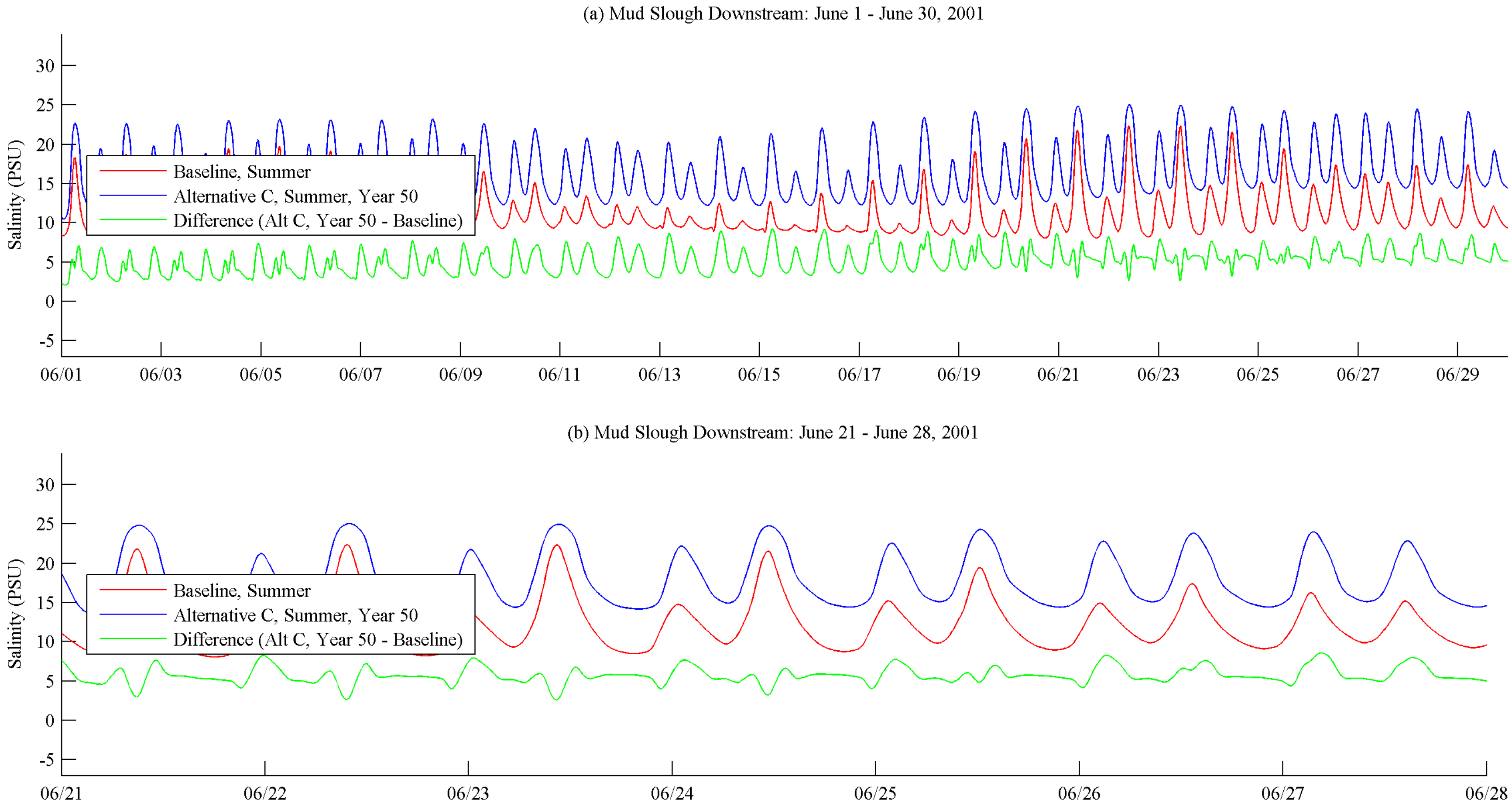

figure *7-52*

South Bay Salt Pond Restoration Project

Salinity, Mud Slough Downstream, Alt C, Year 50, Summer

PWA

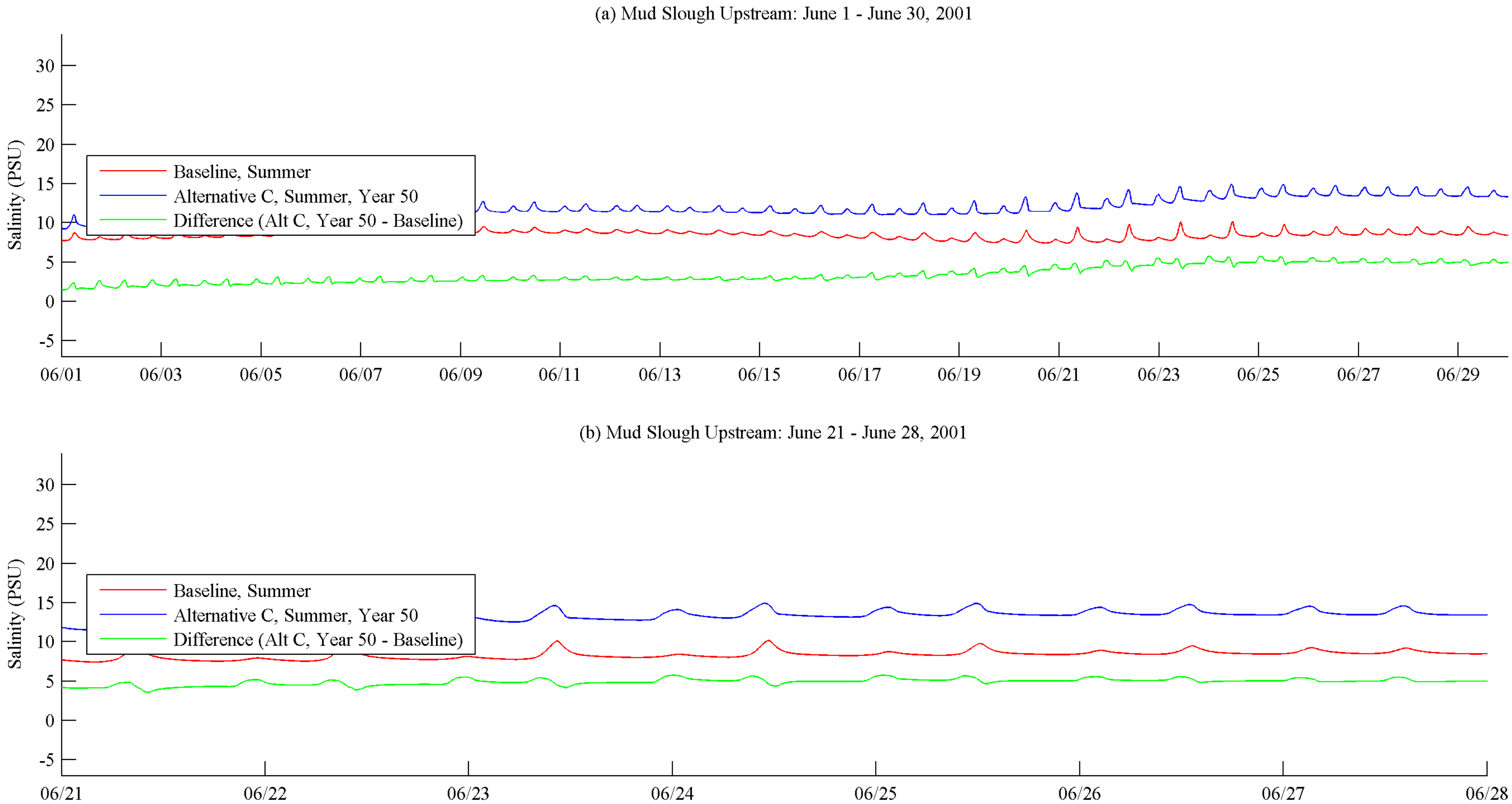

figure 7-53

South Bay Salt Pond Restoration Project

Salinity, Mud Slough Upstream, Alt C, Year 50, Summer

PWA

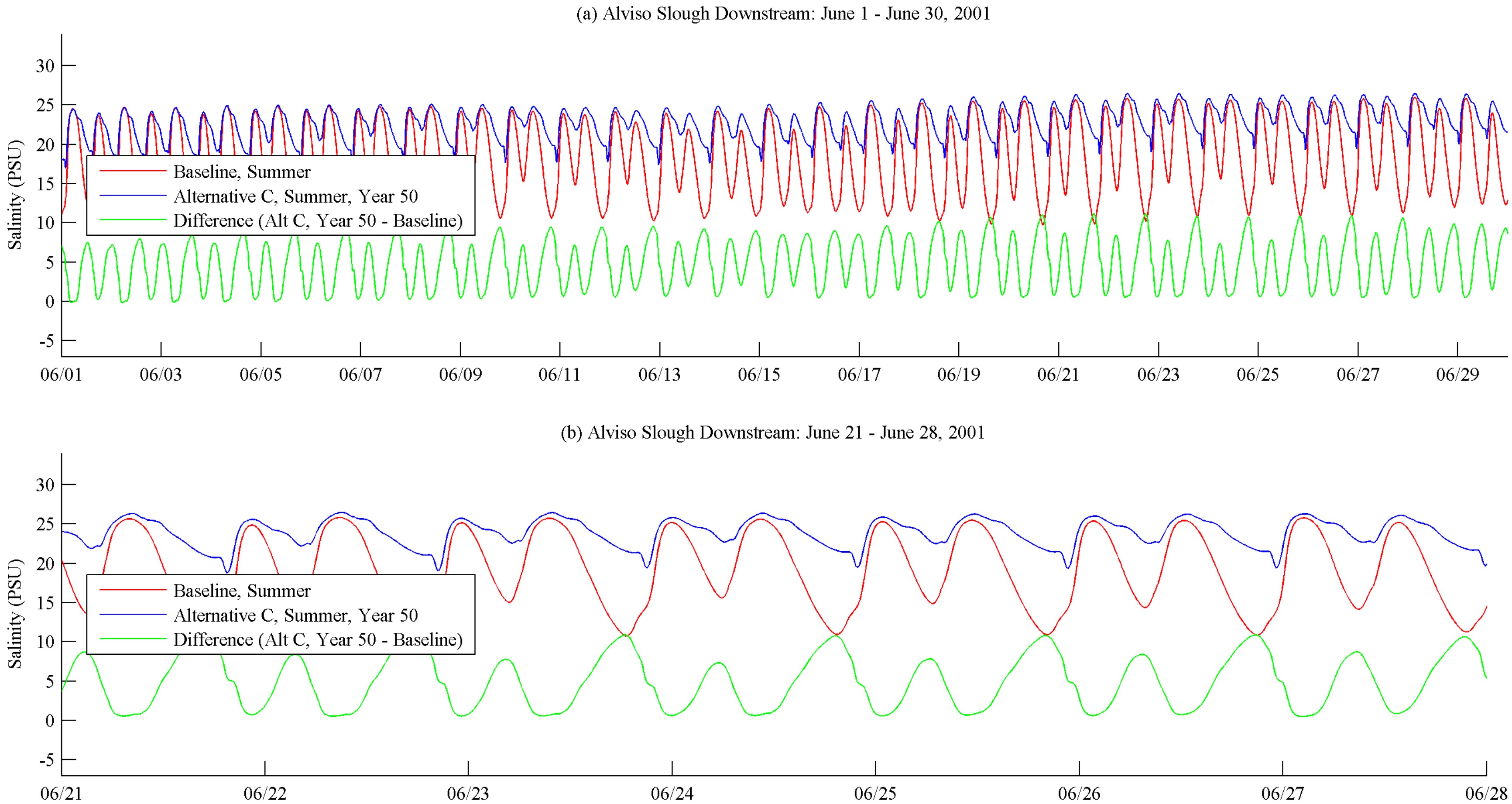

figure *7-54*

South Bay Salt Pond Restoration Project

Salinity, Alviso Slough Downstream, Alt C, Year 50, Summer

PWA

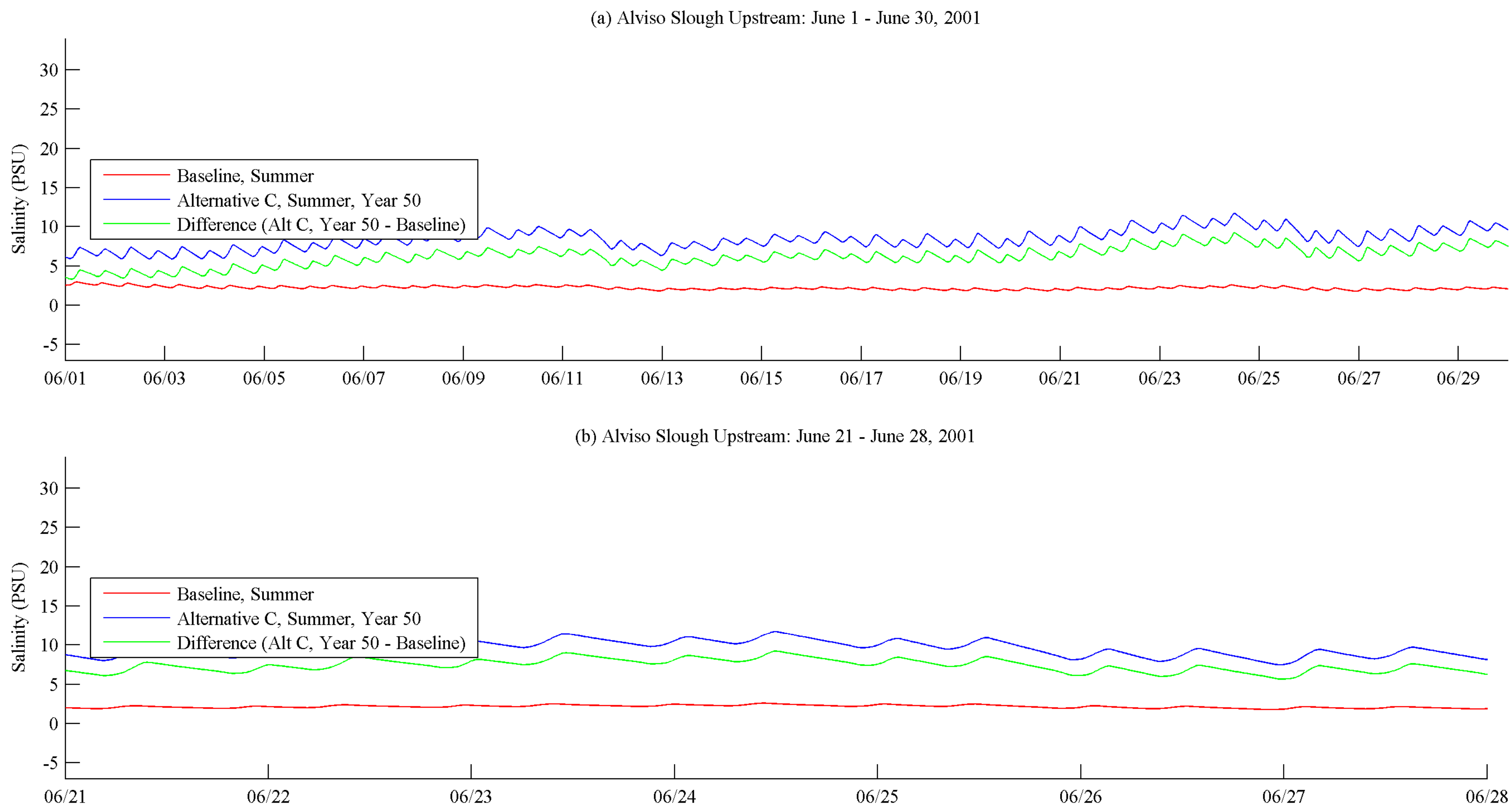

figure 7-55

South Bay Salt Pond Restoration Project

Salinity, Alviso Slough Upstream, Alt C, Year 50, Summer

PWA

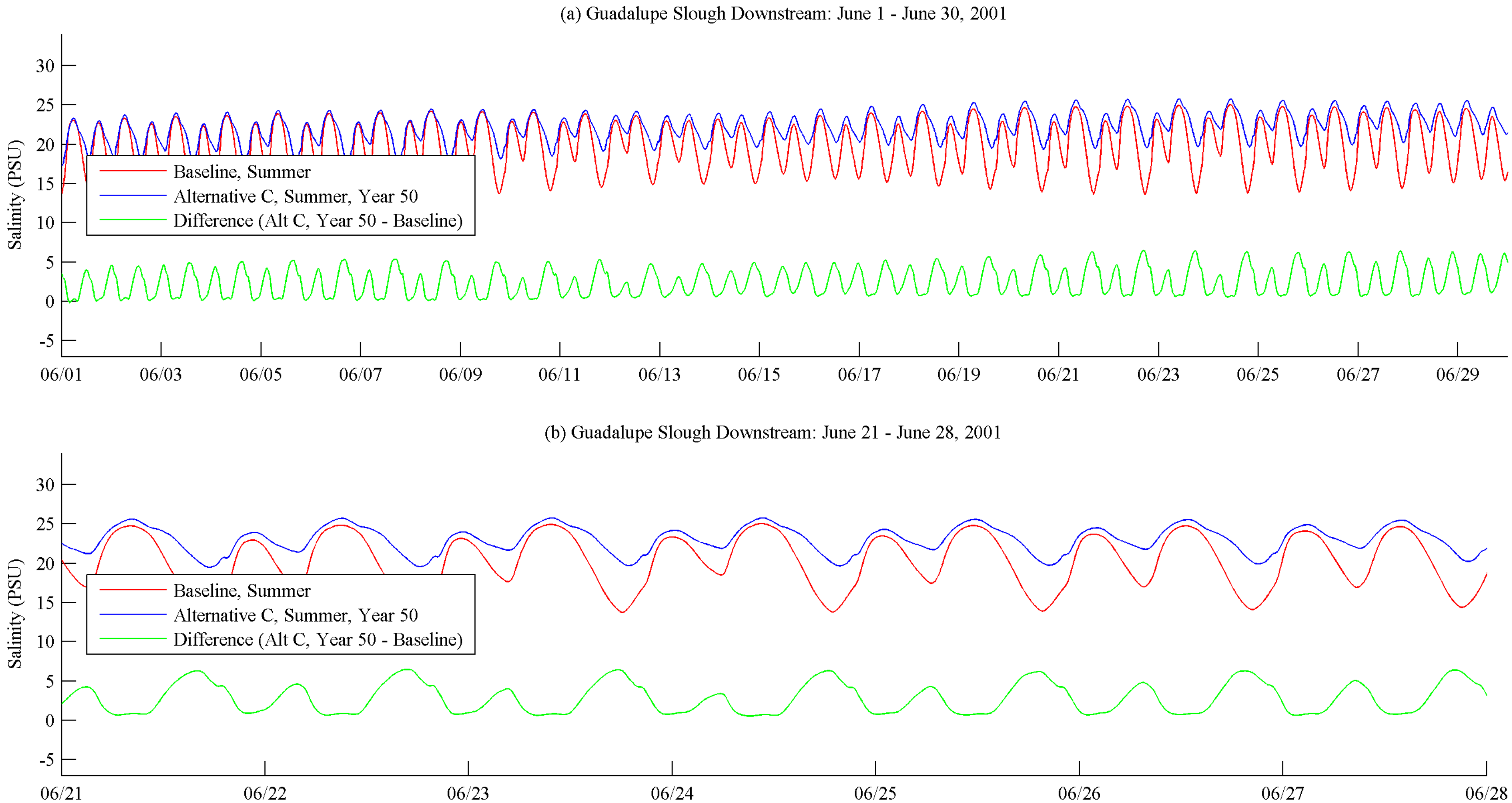

figure 7-56

South Bay Salt Pond Restoration Project

Salinity, Guadalupe Slough Downstream, Alt C, Year 50, Summer

PWA

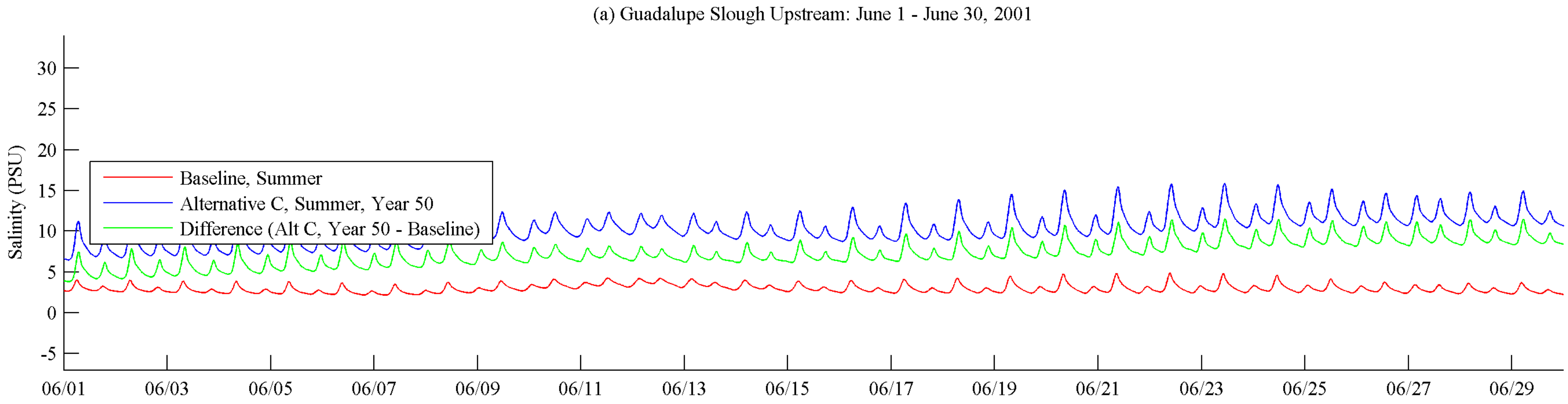

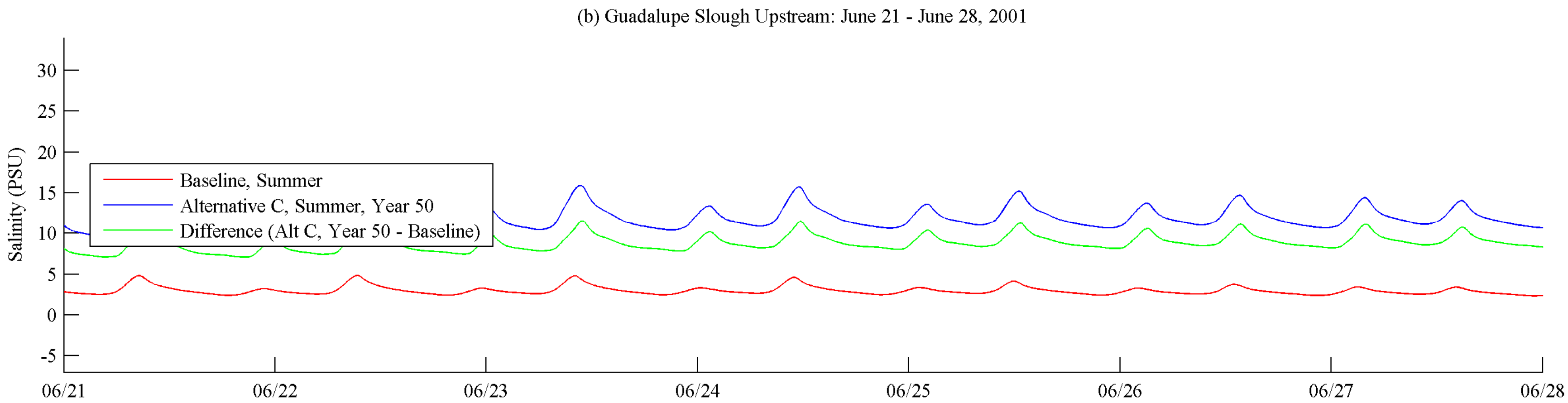

figure 7-57

South Bay Salt Pond Restoration Project

Salinity, Guadalupe Slough Upstream, Alt C, Year 50, Summer

PWA

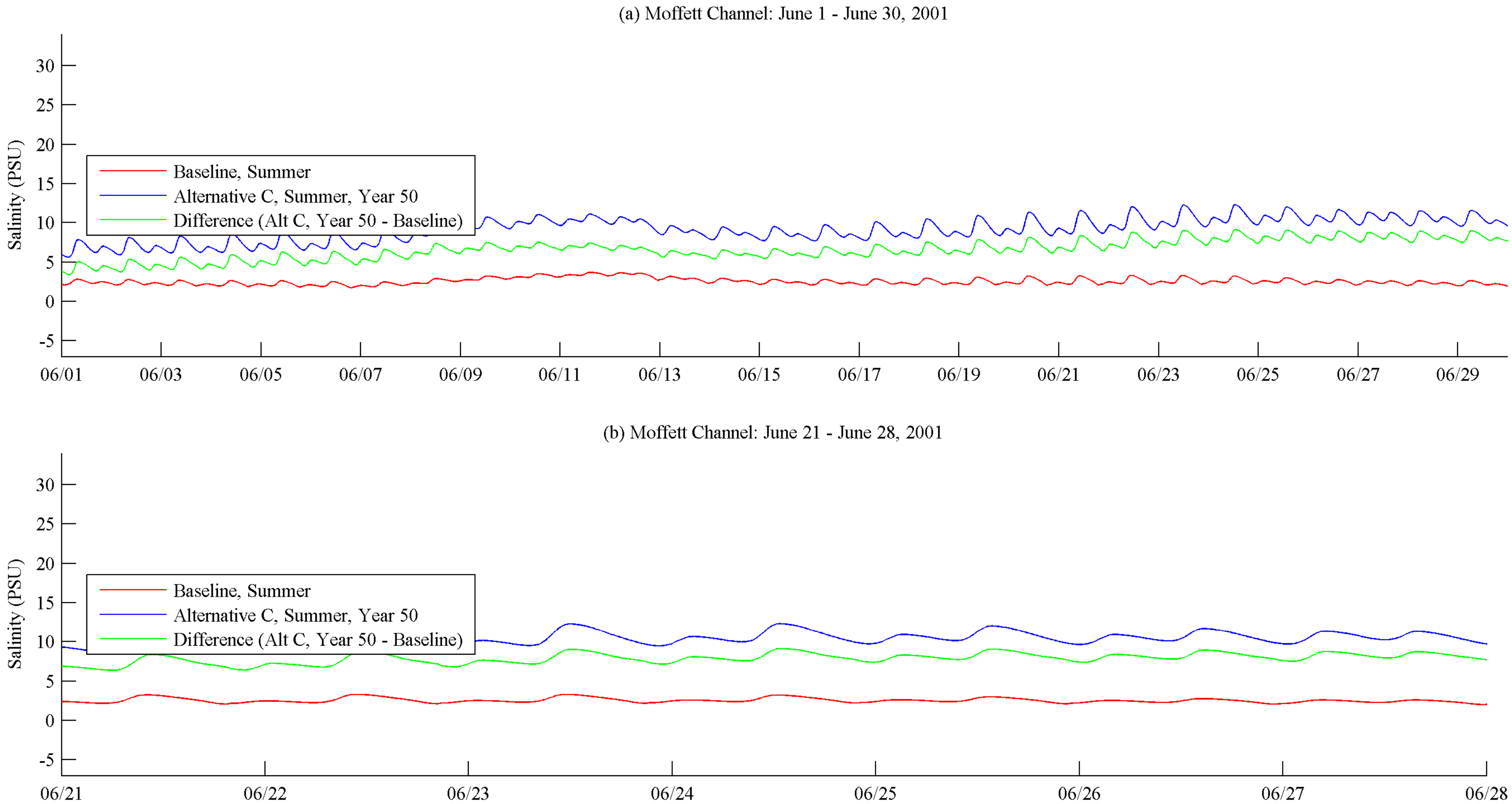

figure *7-58*

South Bay Salt Pond Restoration Project

Salinity, Moffett Channel, Alt C, Year 50, Summer

PWA

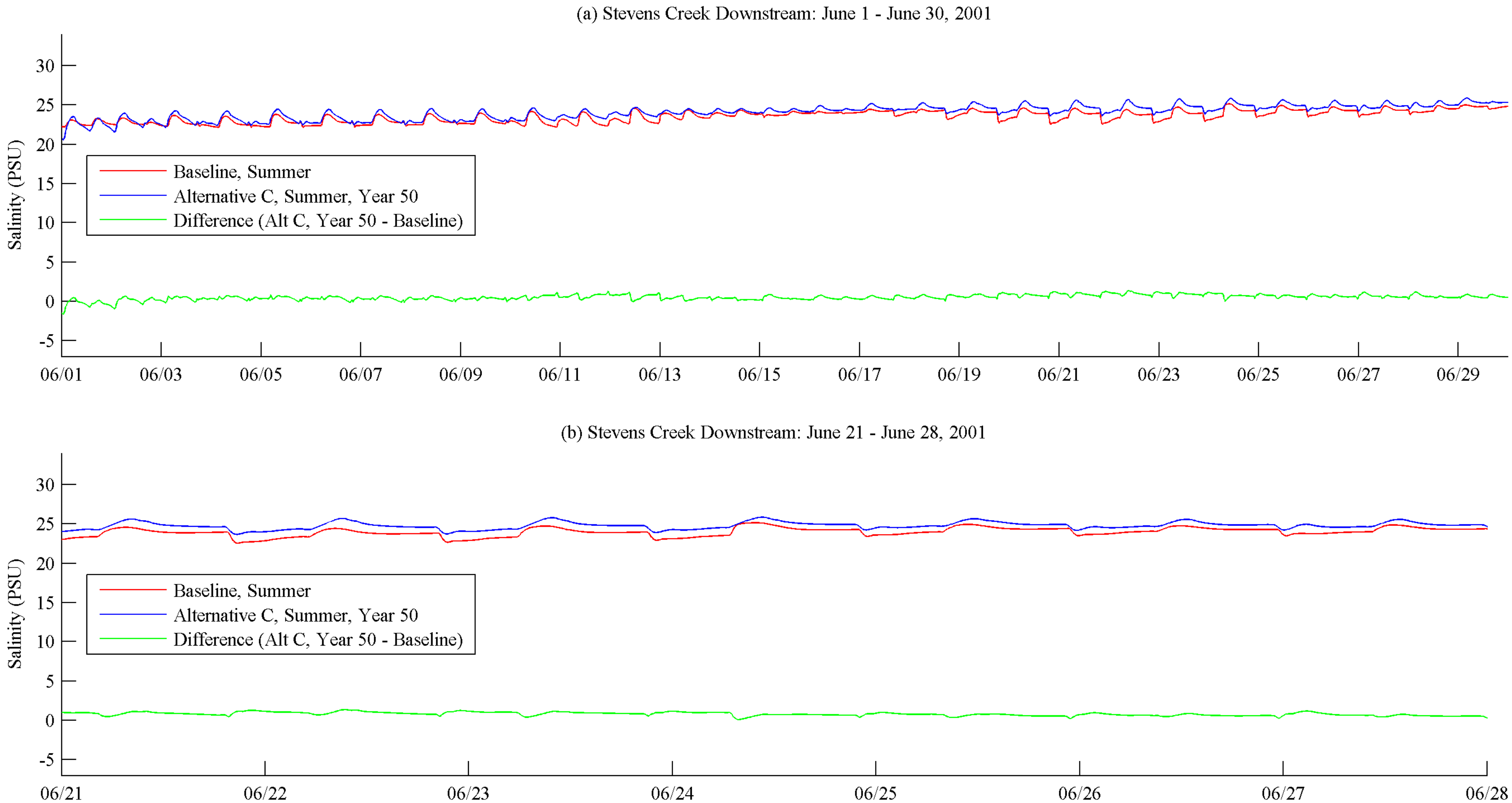

figure 7-59

South Bay Salt Pond Restoration Project

Salinity, Steven Creek Downstream, Alt C, Year 50, Summer

PWA

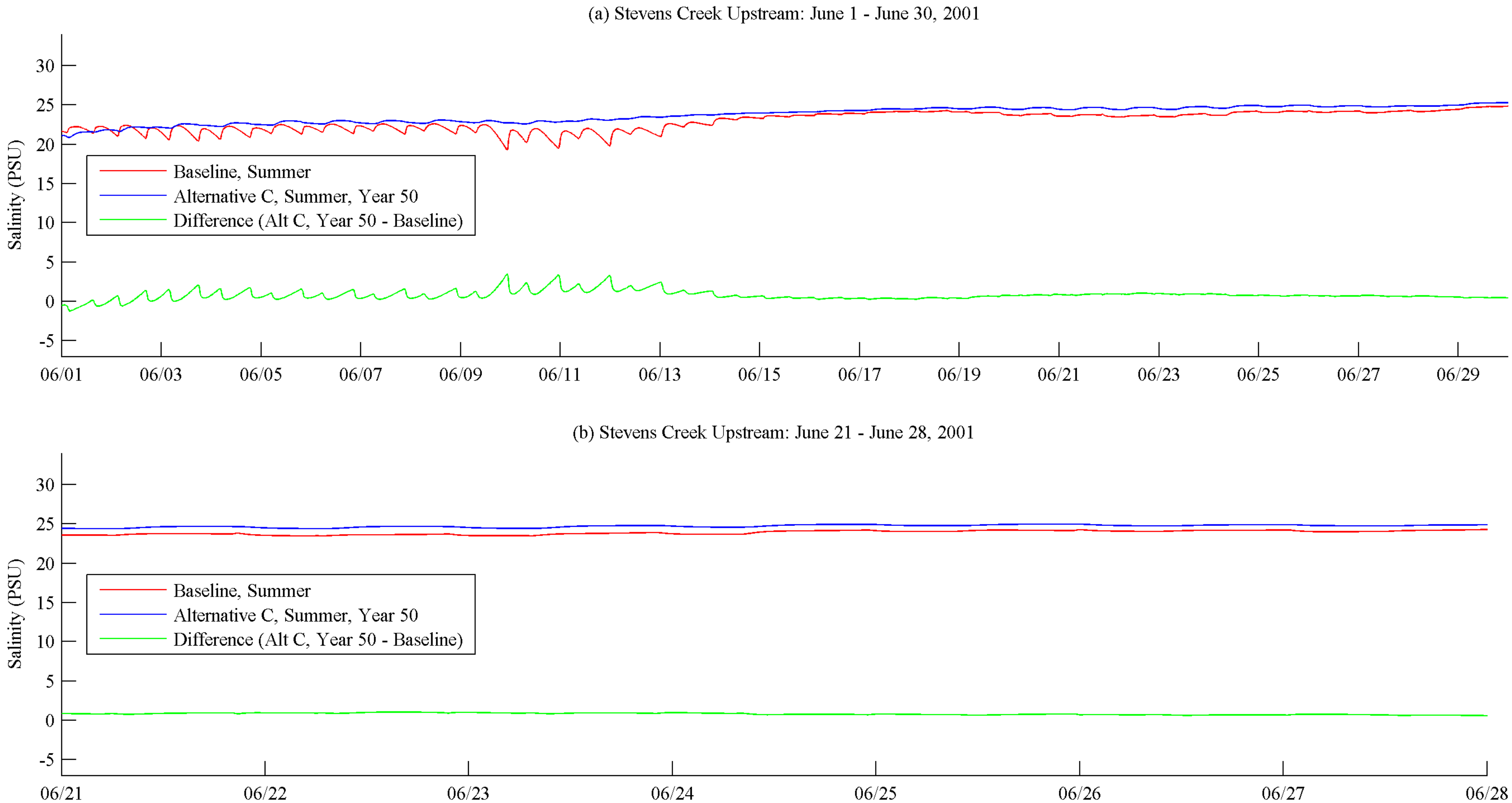

figure 7-60

South Bay Salt Pond Restoration Project

Salinity, Stevens Creek Upstream, Alt C, Year 50, Summer

PWA

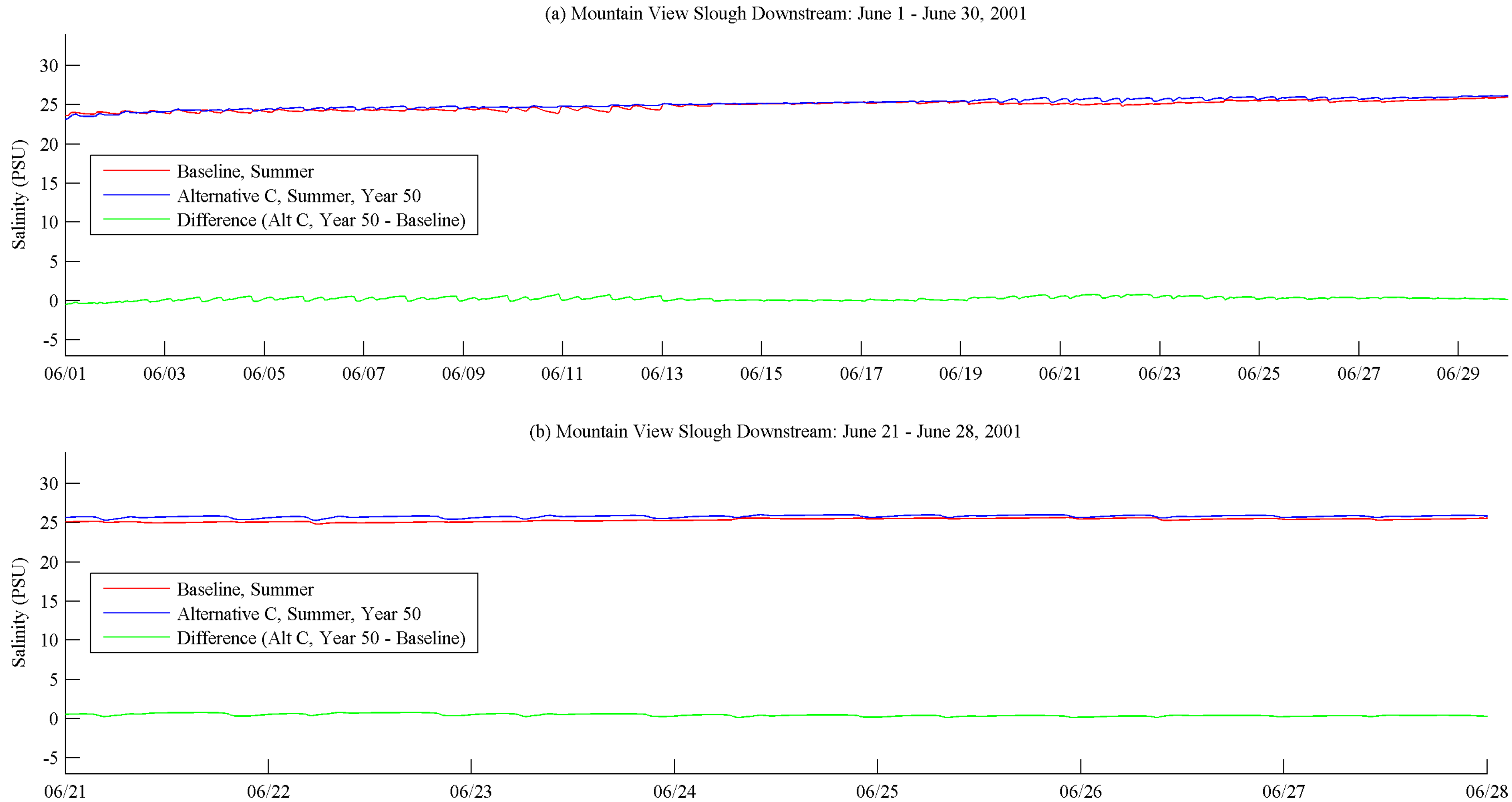

figure 7-61

South Bay Salt Pond Restoration Project

Salinity, Mountain View Slough Downstream, Alt C, Year 50, Summer

PWA

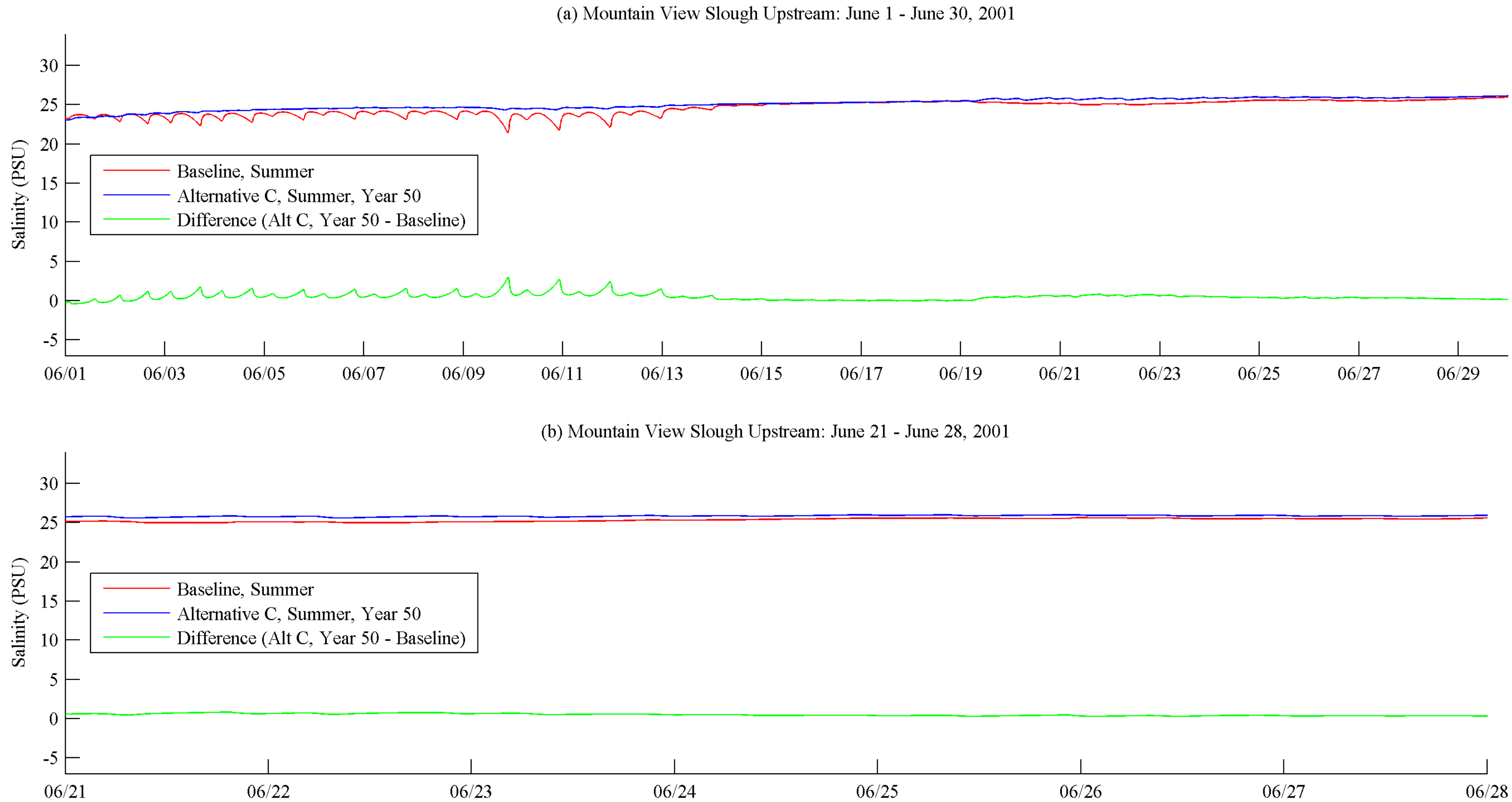

figure 7-62

South Bay Salt Pond Restoration Project

Salinity, Mountain View Slough Upstream, Alt C, Year 50, Summer

PWA

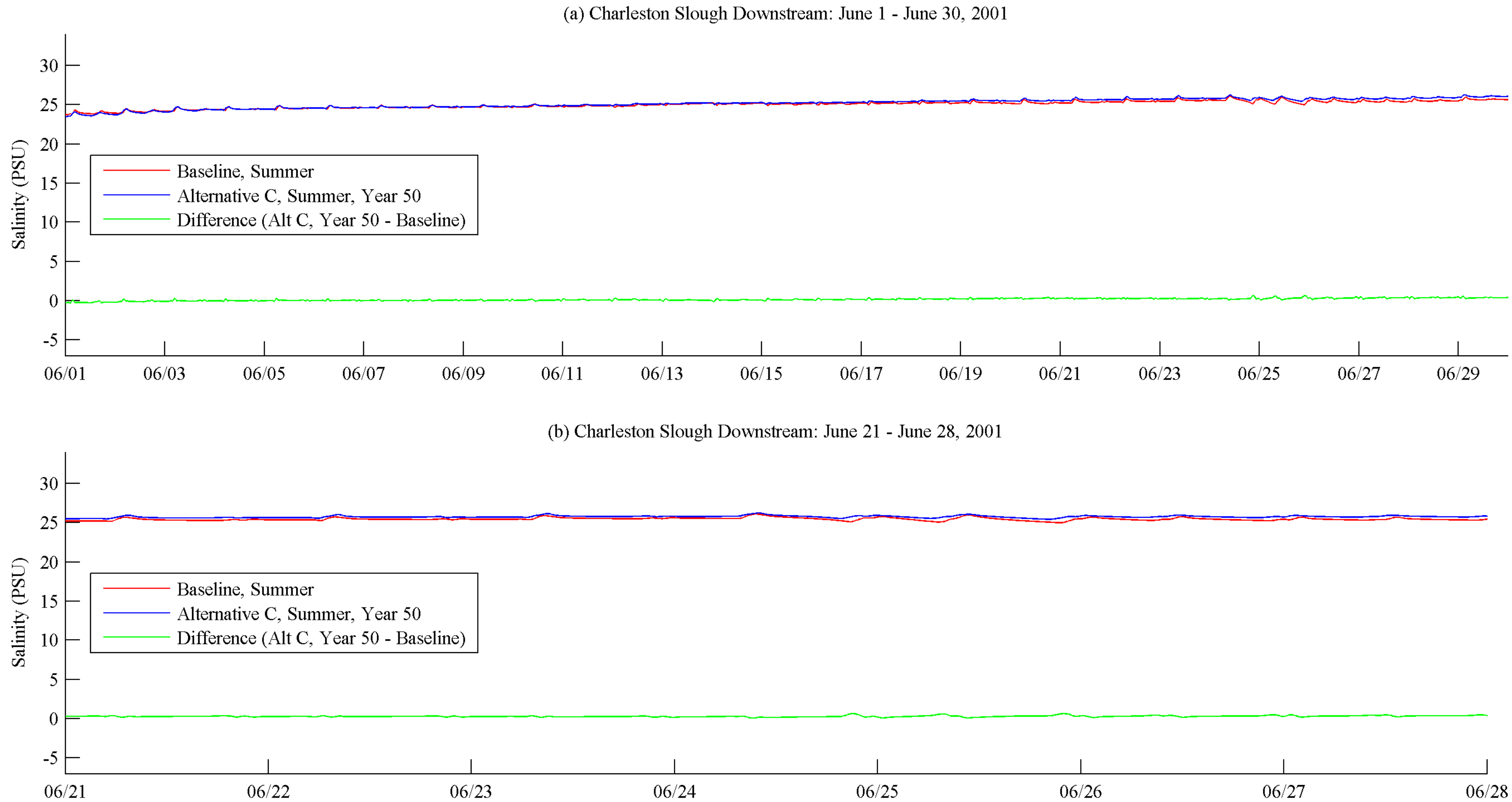

figure *7-63*

South Bay Salt Pond Restoration Project

Salinity, Charleston Slough Downstream, Alt C, Year 50, Summer

PWA

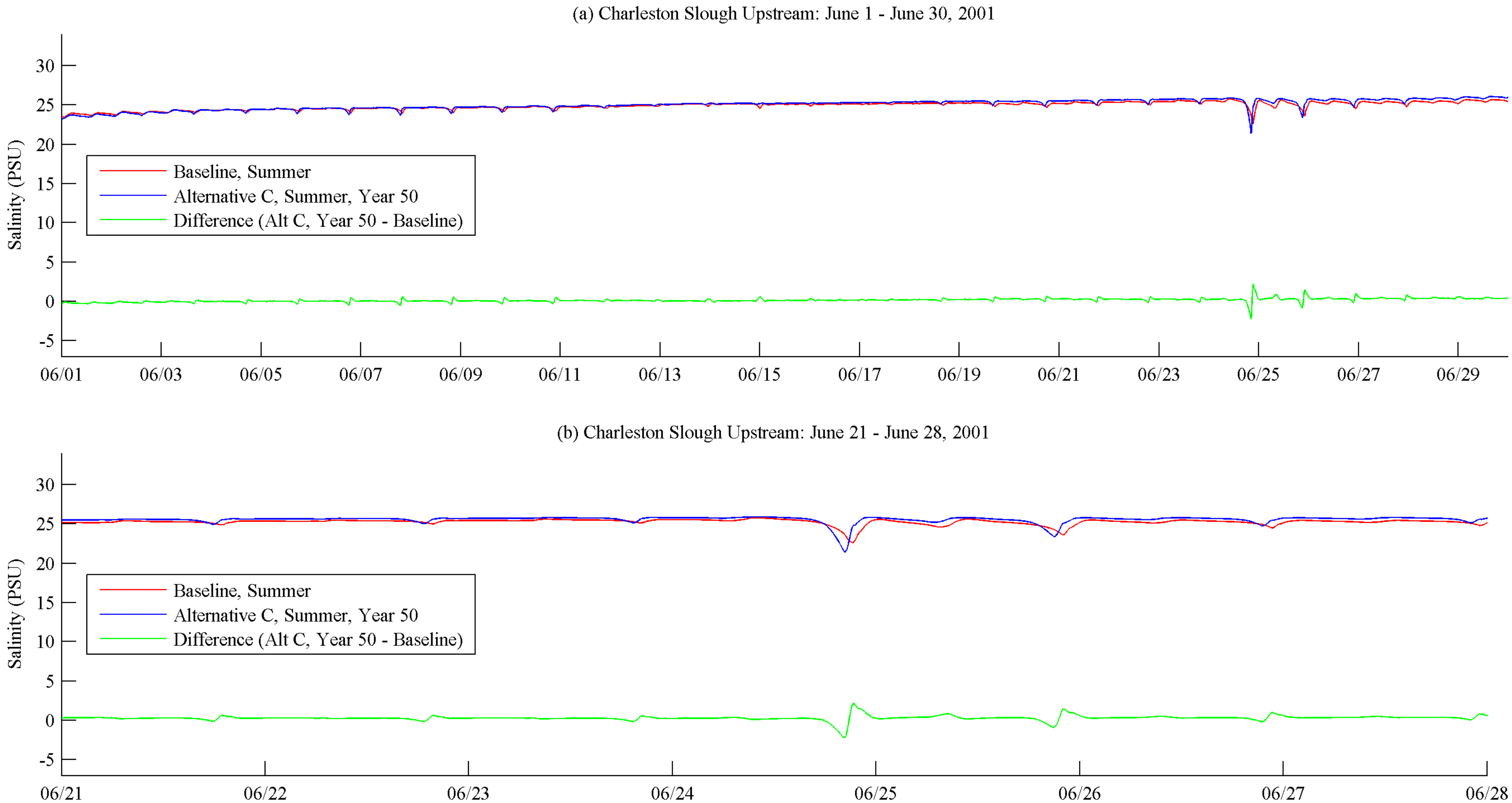

figure 7-64

South Bay Salt Pond Restoration Project

Salinity, Charleston Slough Upstream, Alt C, Year 50, Summer

PWA

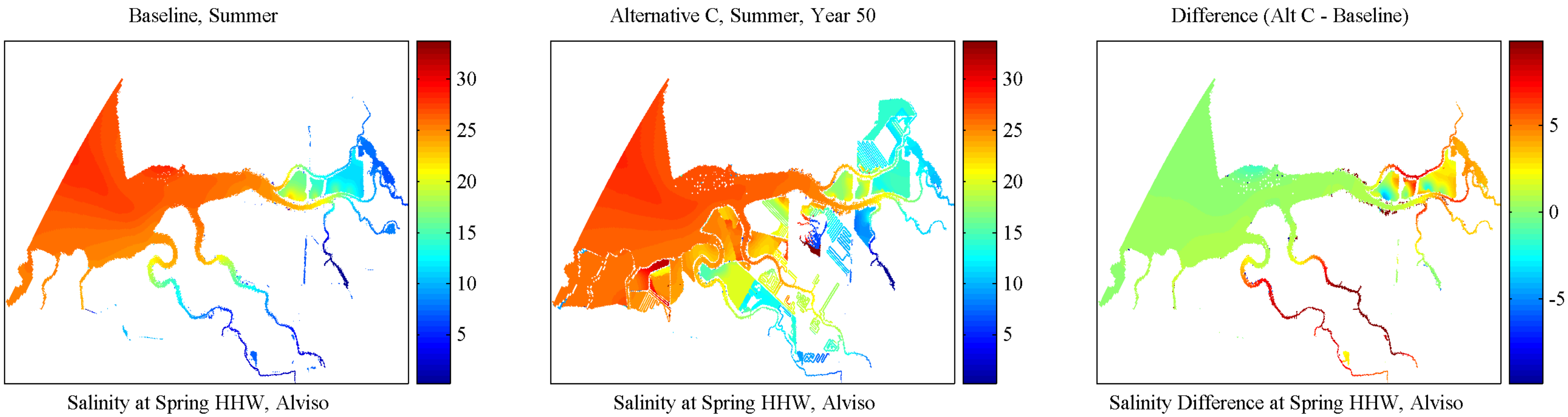

Note: Units shown are PSU

figure 7-65

South Bay Salt Pond Restoration Project

Salinity at Spring HHW, Alt C, Alviso, Year 50, Summer

PWA

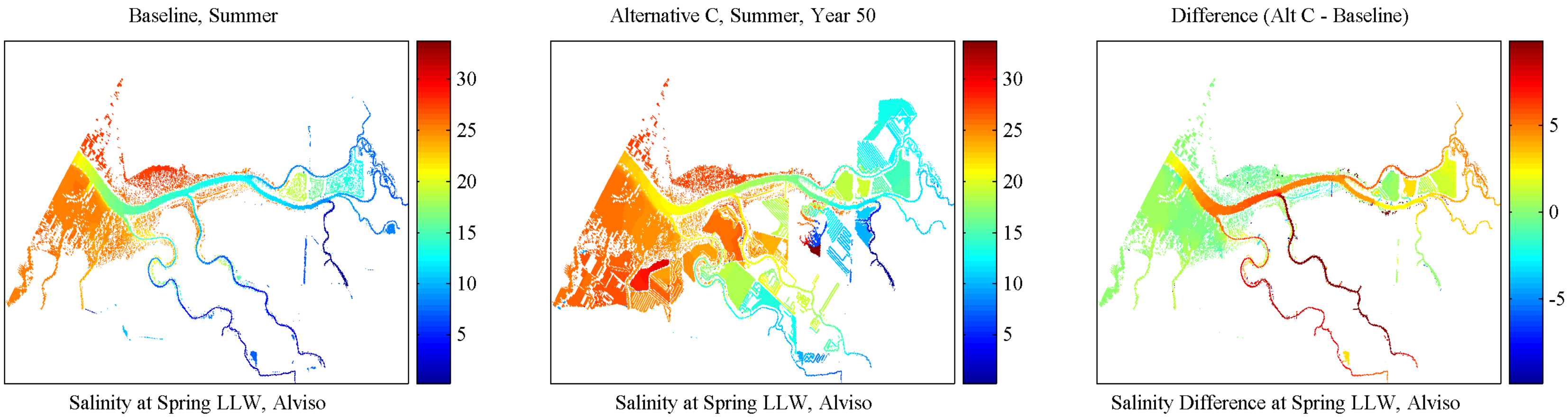

Note: Units shown are PSU

figure 7-66

South Bay Salt Pond Restoration Project

Salinity at Spring LLW, Alt C, Alviso, Year 50, Summer

PWA

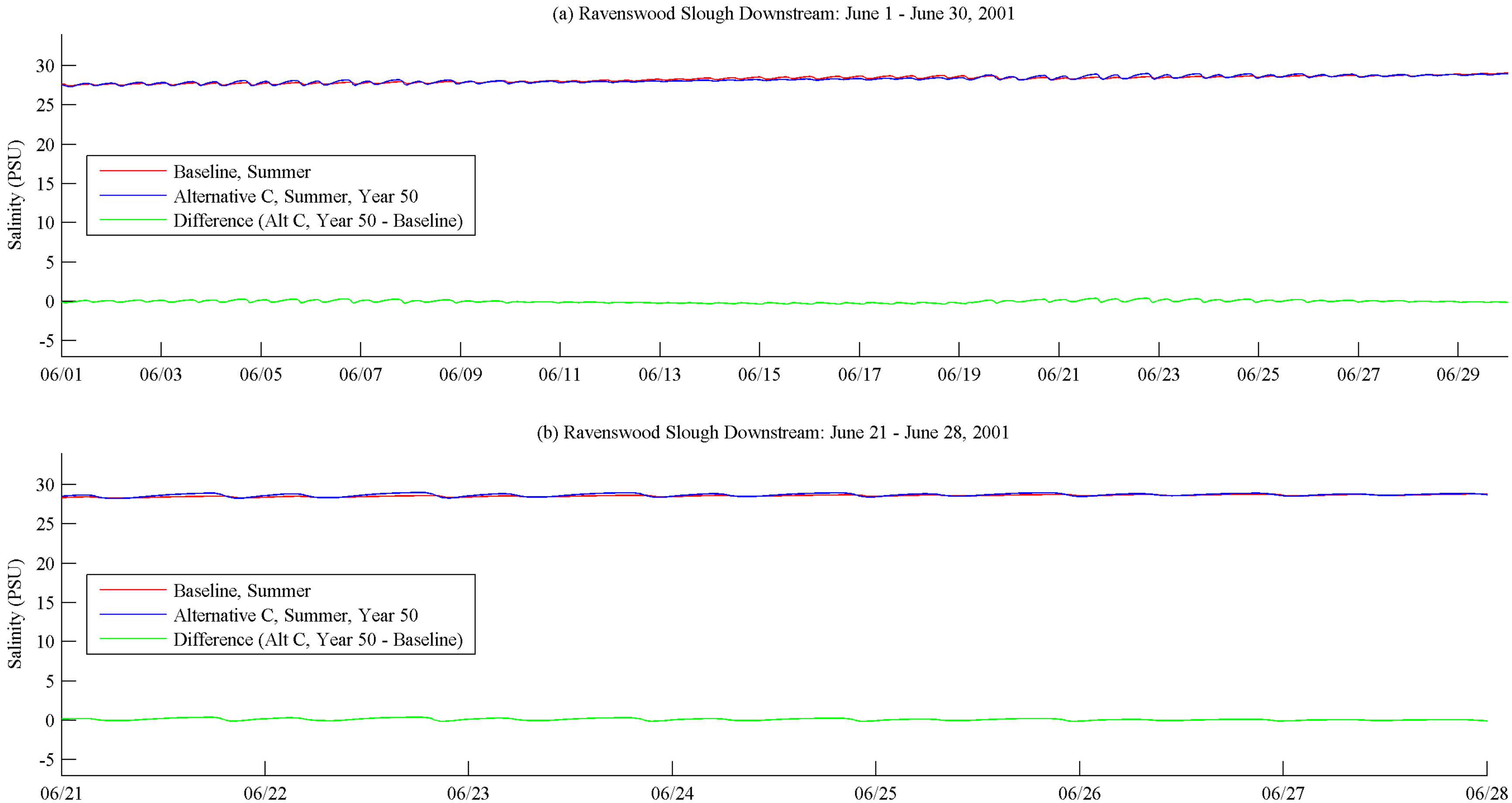

figure 7-67

South Bay Salt Pond Restoration Project

Salinity, Ravenswood Slough Downstream, Ravenswood, Alt C, Year 50, Summer

PWA

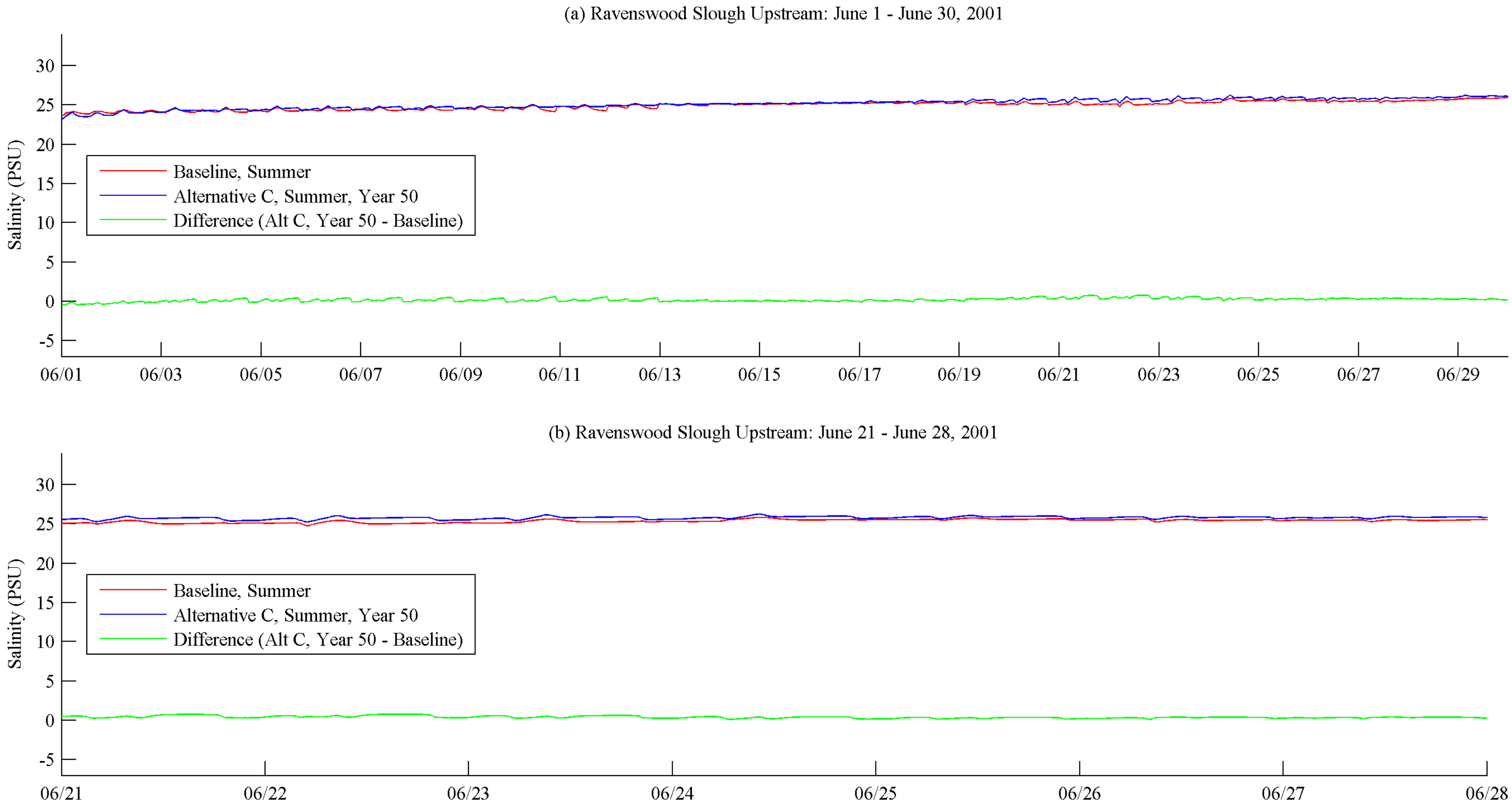

figure *7-68*

South Bay Salt Pond Restoration Project

Salinity, Ravenswood Slough Upstream, Ravenswood, Alt C, Year 50, Summer

PWA

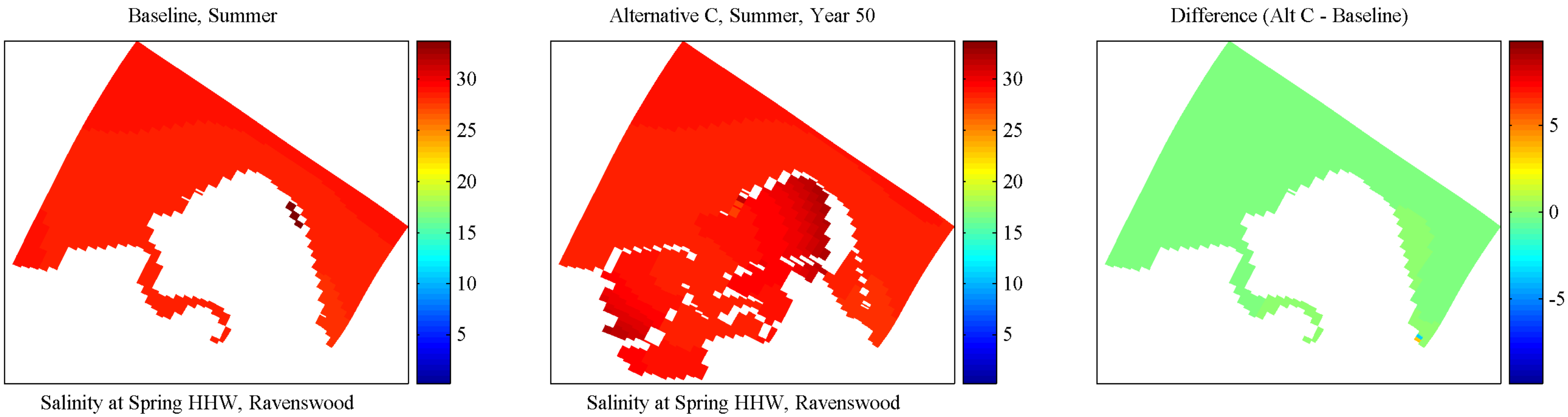

Note: Units shown are PSU

figure 7-69

South Bay Salt Pond Restoration Project

Salinity at Spring HHW, Ravenswood, Alt C, Year 50, Summer

PWA

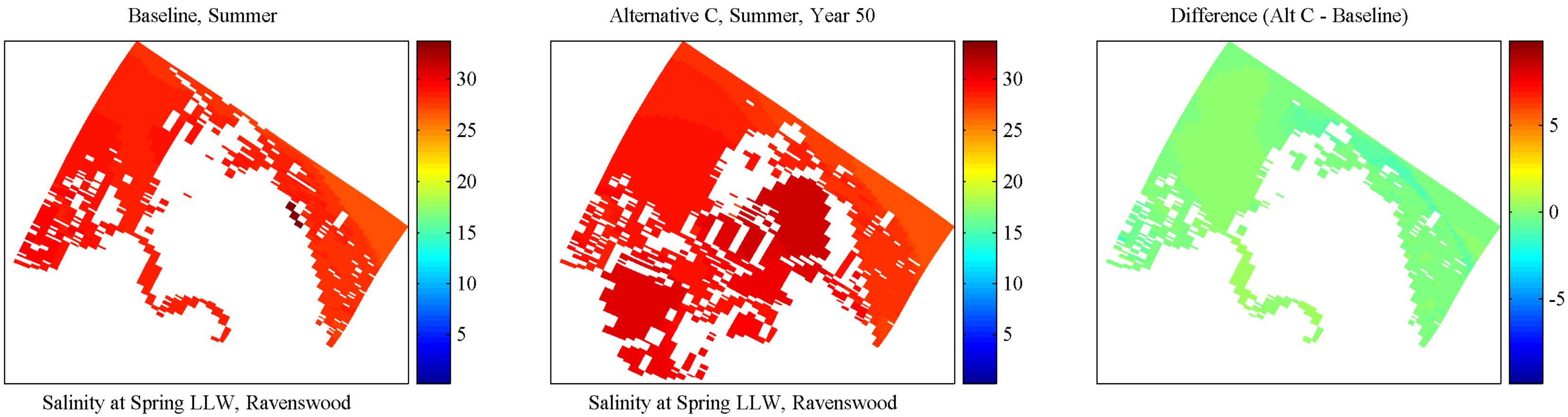

Note: Units shown are PSU

figure *7-70*

South Bay Salt Pond Restoration Project

Salinity at Spring LLW, Ravenswood, Alt C, Year 50, Summer

PWA

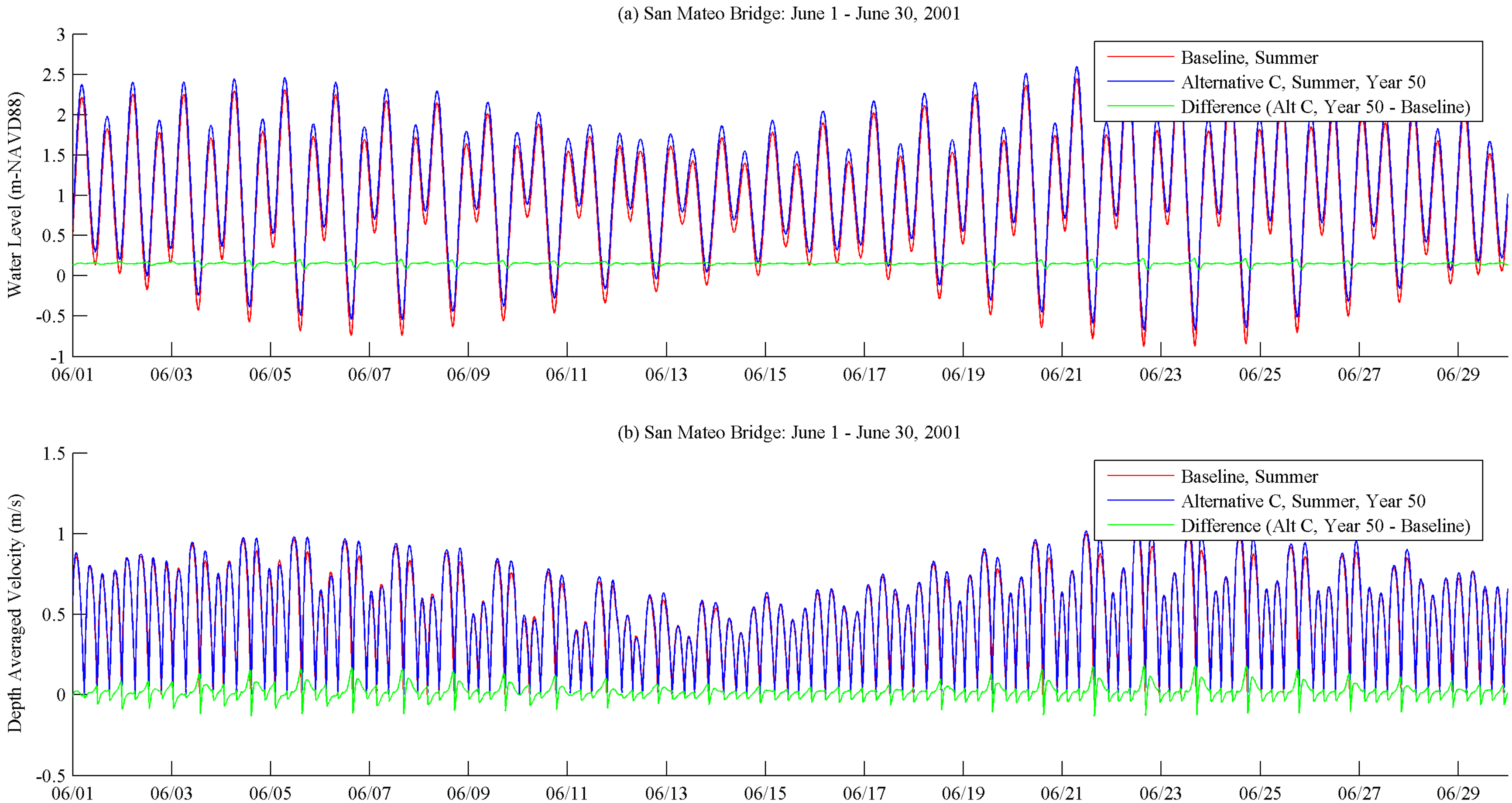

The depth-averaged velocity is calculated as $v = (u^2 + v^2)^{1/2}$, where u and v are the horizontal depth-averaged velocity components.

figure 7-71

South Bay Salt Pond Restoration Project

Velocity, San Mateo Bridge, Alt C, Year 50, Summer

PWA

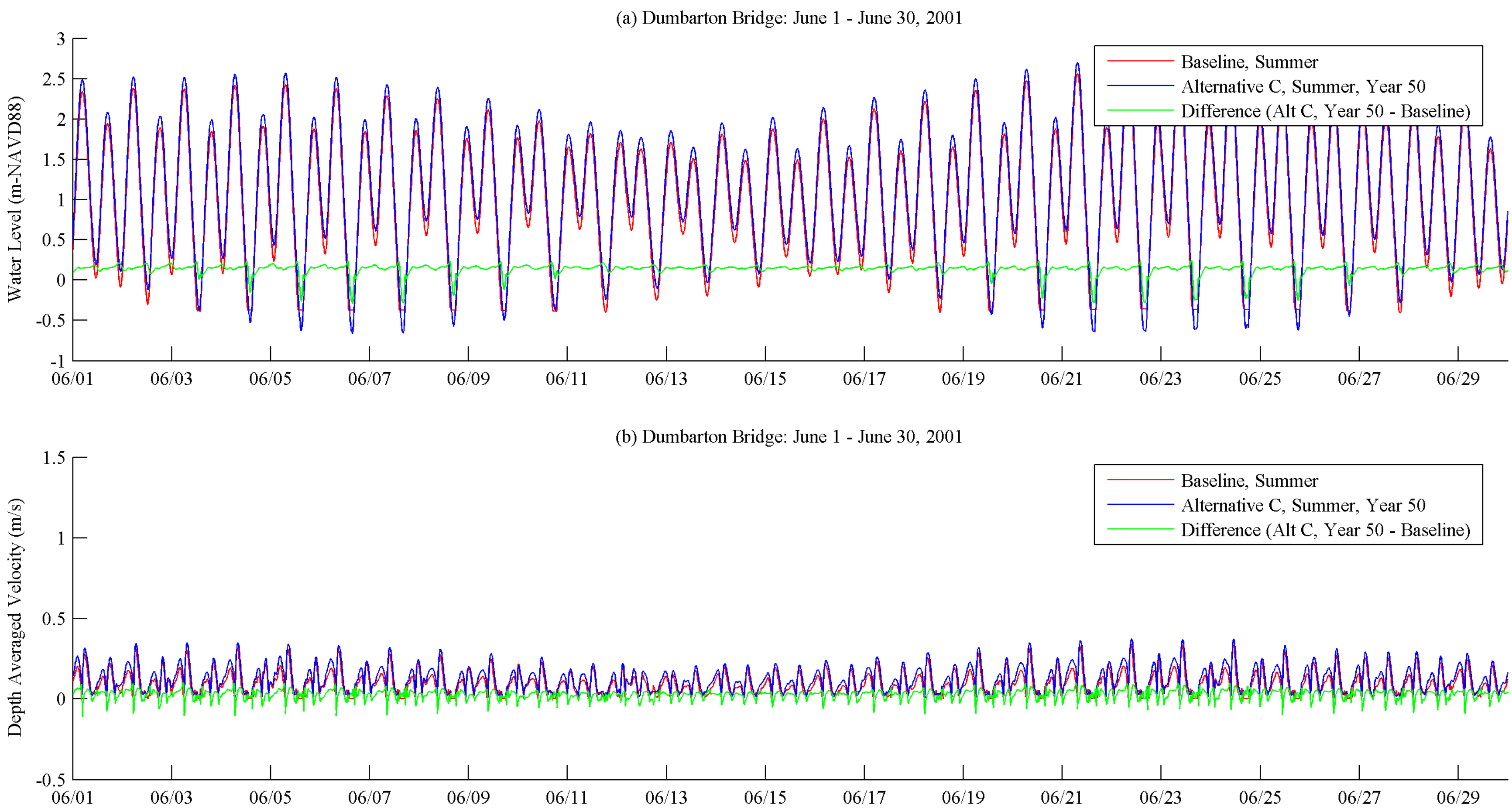

The depth-averaged velocity is calculated as $v = (u^2 + v^2)^{1/2}$, where u and v are the horizontal depth-averaged velocity components.

figure 7-72

South Bay Salt Pond Restoration Project

Velocity, Dumbarton Bridge, Alt C, Year 50, Summer

PWA

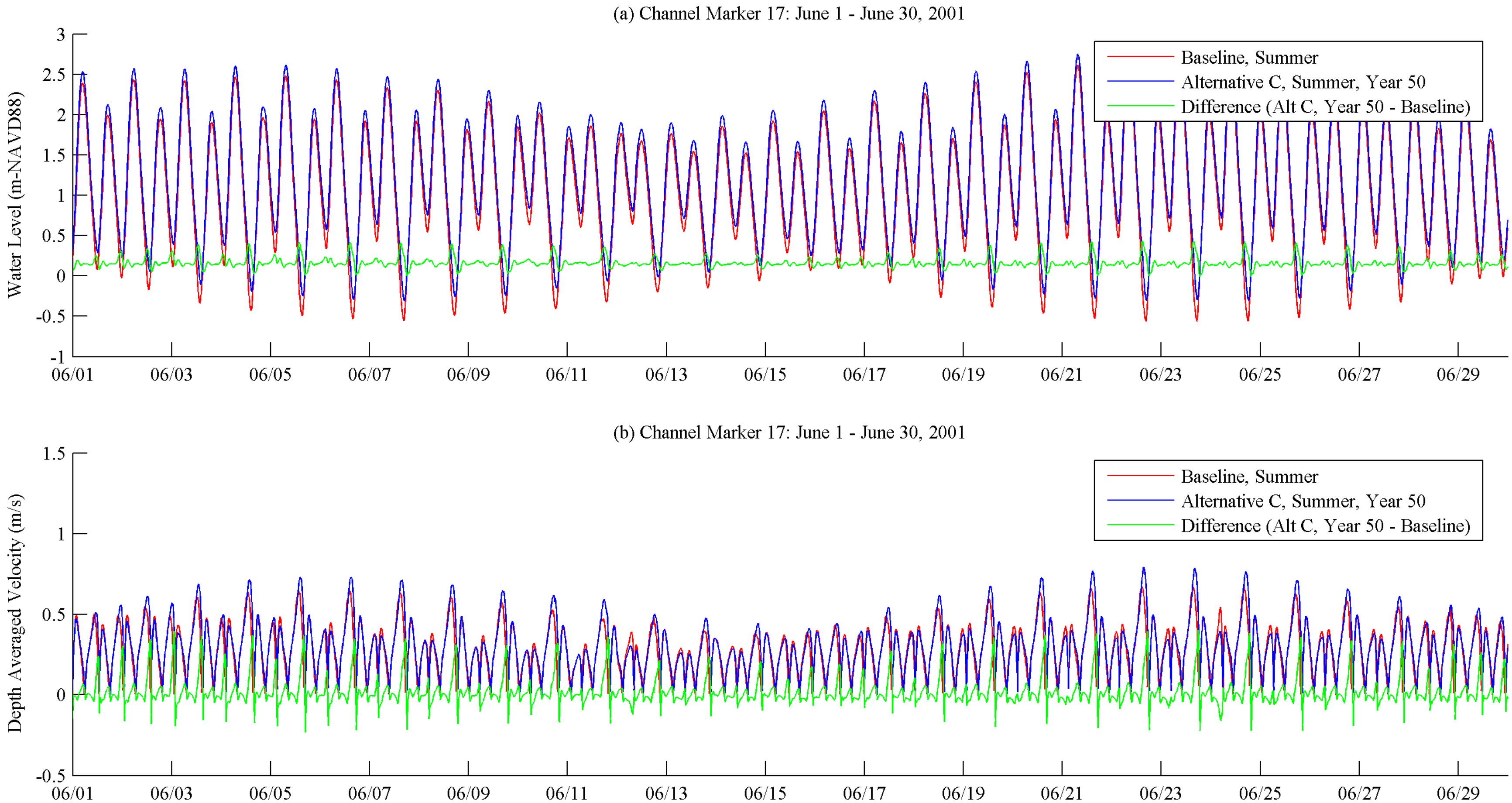

The depth-averaged velocity is calculated as $v = (u^2 + v^2)^{1/2}$, where u and v are the horizontal depth-averaged velocity components.

figure 7-73

South Bay Salt Pond Restoration Project

Velocity, Channel Marker 17, Alt C, Year 50, Summer

PWA

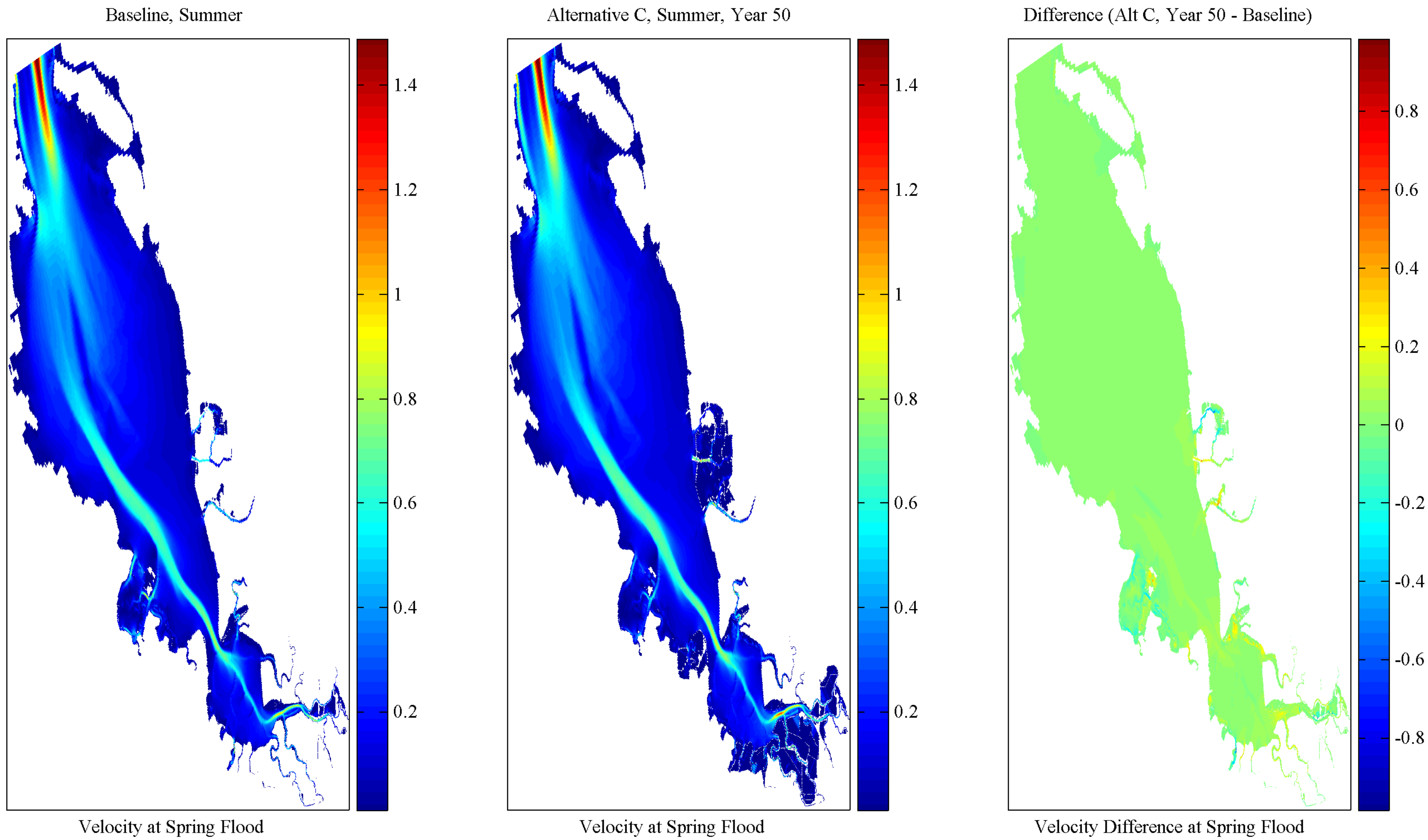

Note: Units shown are m/s

figure 7-74

South Bay Salt Pond Restoration Project

Velocity at Spring Flood, Alt C, Year 50, Summer

PWA

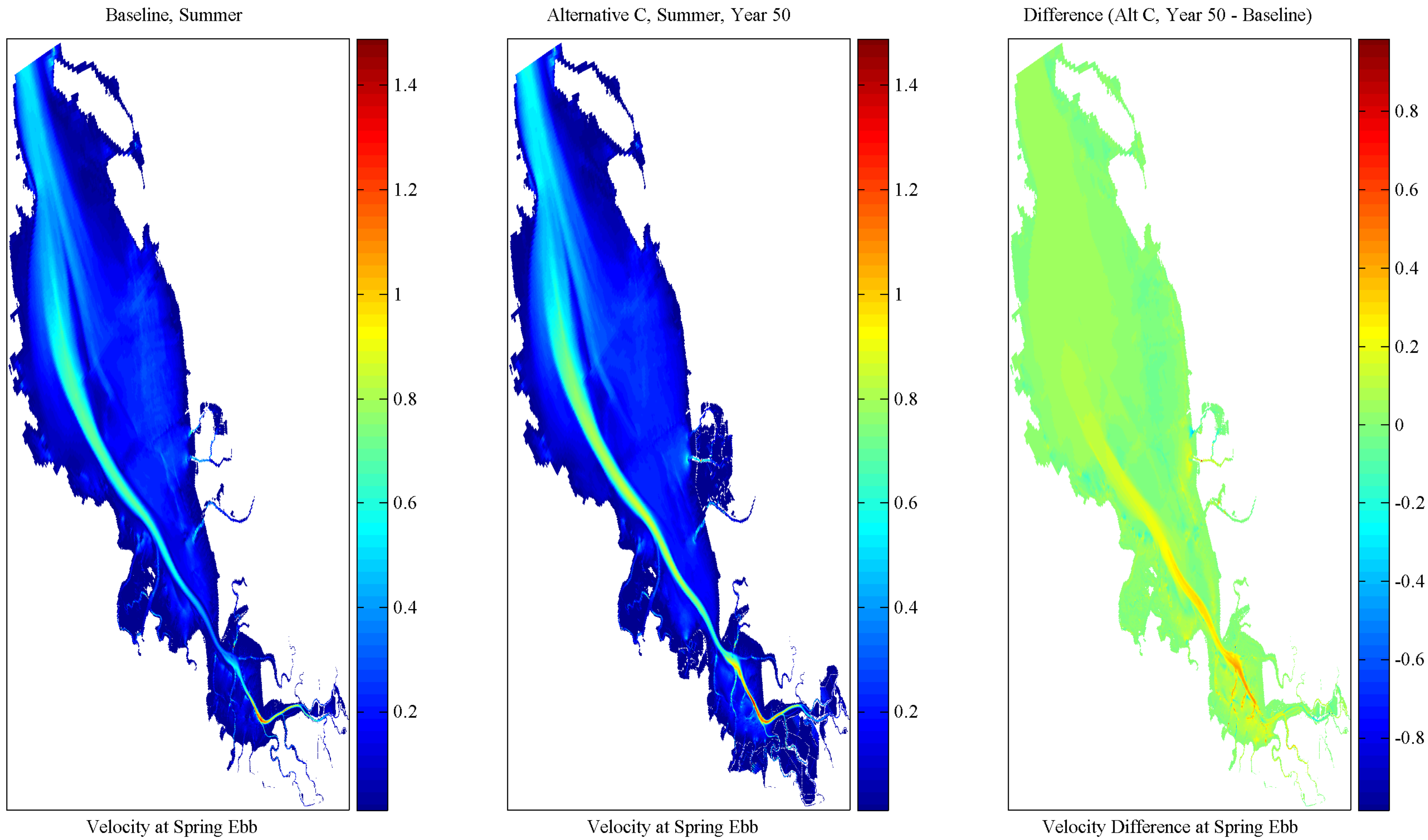

Note: Units shown are m/s

figure 7-75

South Bay Salt Pond Restoration Project

Velocity at Spring Ebb, Alt C, Year 50, Summer

PWA

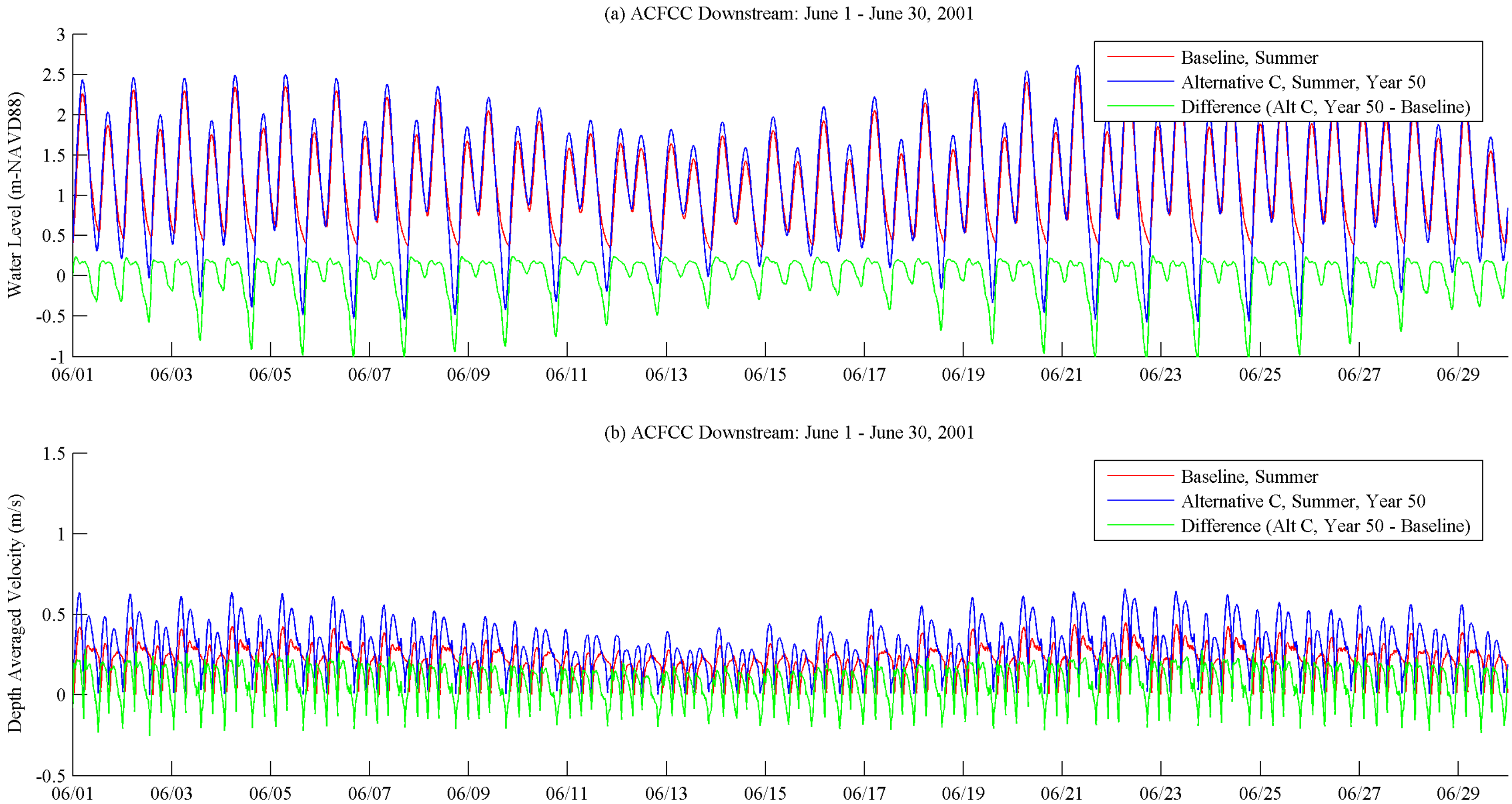

The depth-averaged velocity is calculated as $v = (u^2 + v^2)^{1/2}$, where u and v are the horizontal depth-averaged velocity components.

figure *7-76*

South Bay Salt Pond Restoration Project

Velocity, ACFCC Downstream, Alt C, Year 50, Summer

PWA

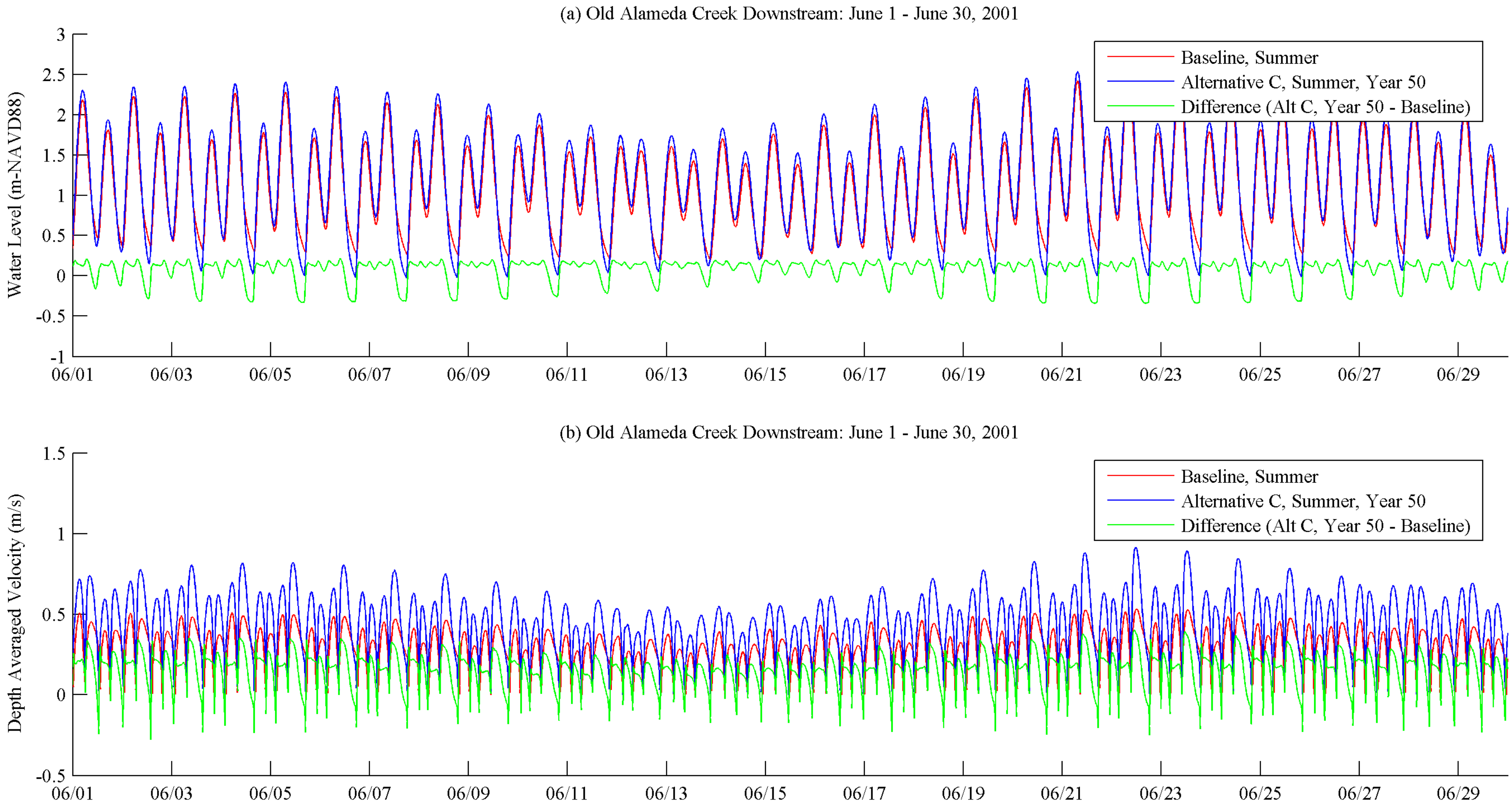

The depth-averaged velocity is calculated as $v = (u^2 + v^2)^{1/2}$, where u and v are the horizontal depth-averaged velocity components.

figure 7-77

South Bay Salt Pond Restoration Project

Velocity, Old Alameda Creek Downstream, Alt C, Year 50, Summer

PWA

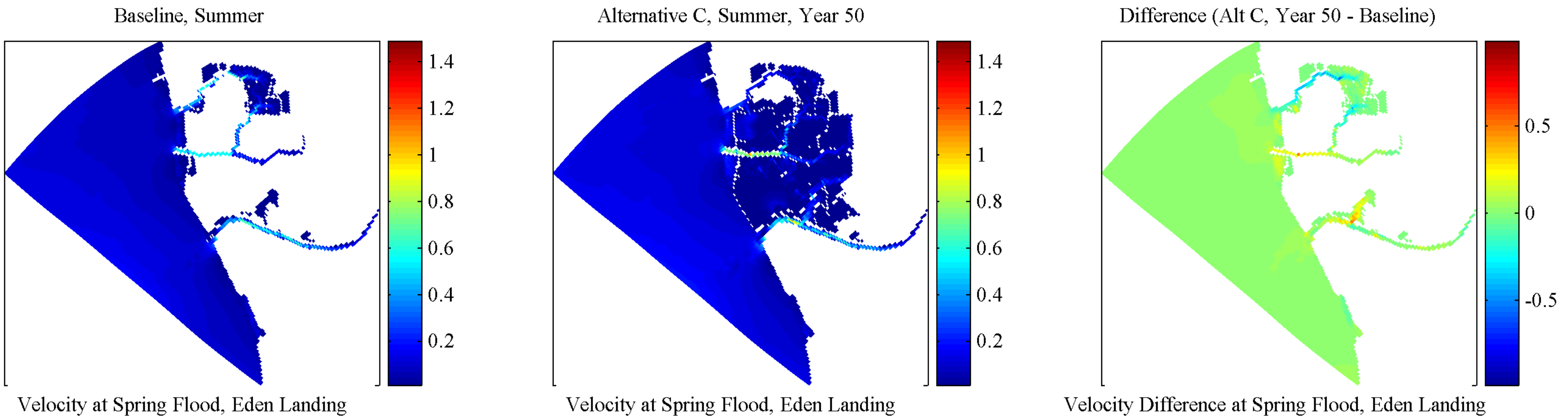

Note: Units shown are m/s

figure 7-78

South Bay Salt Pond Restoration Project

Velocity at Spring Flood, Eden Landing, Alt C, Year 50, Summer

PWA

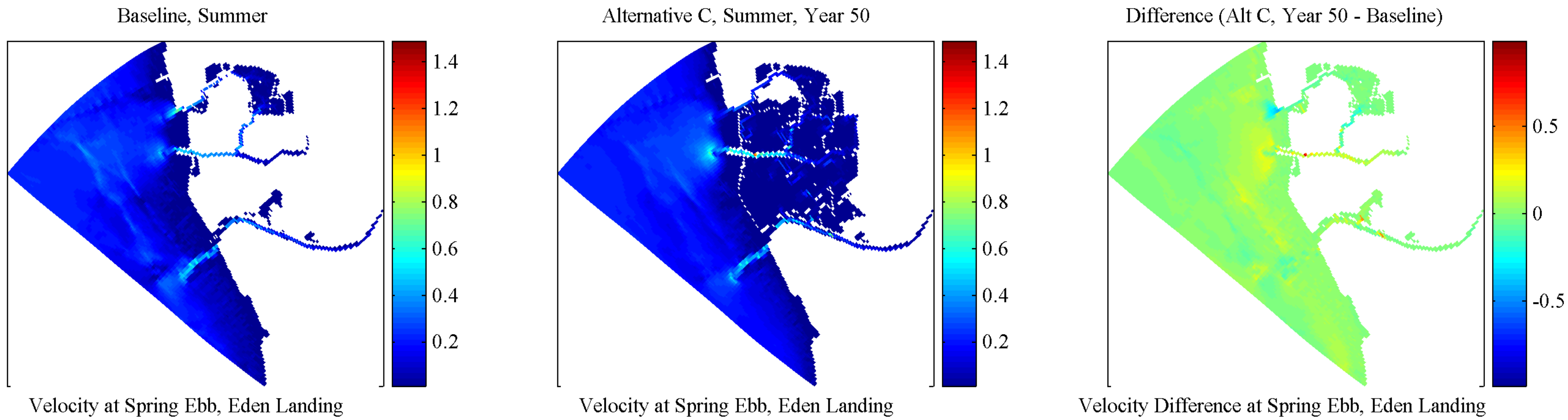

Note: Units shown are m/s

figure 7-79

South Bay Salt Pond Restoration Project

Velocity at Spring Ebb, Eden Landing, Alt C, Year 50, Summer

PWA

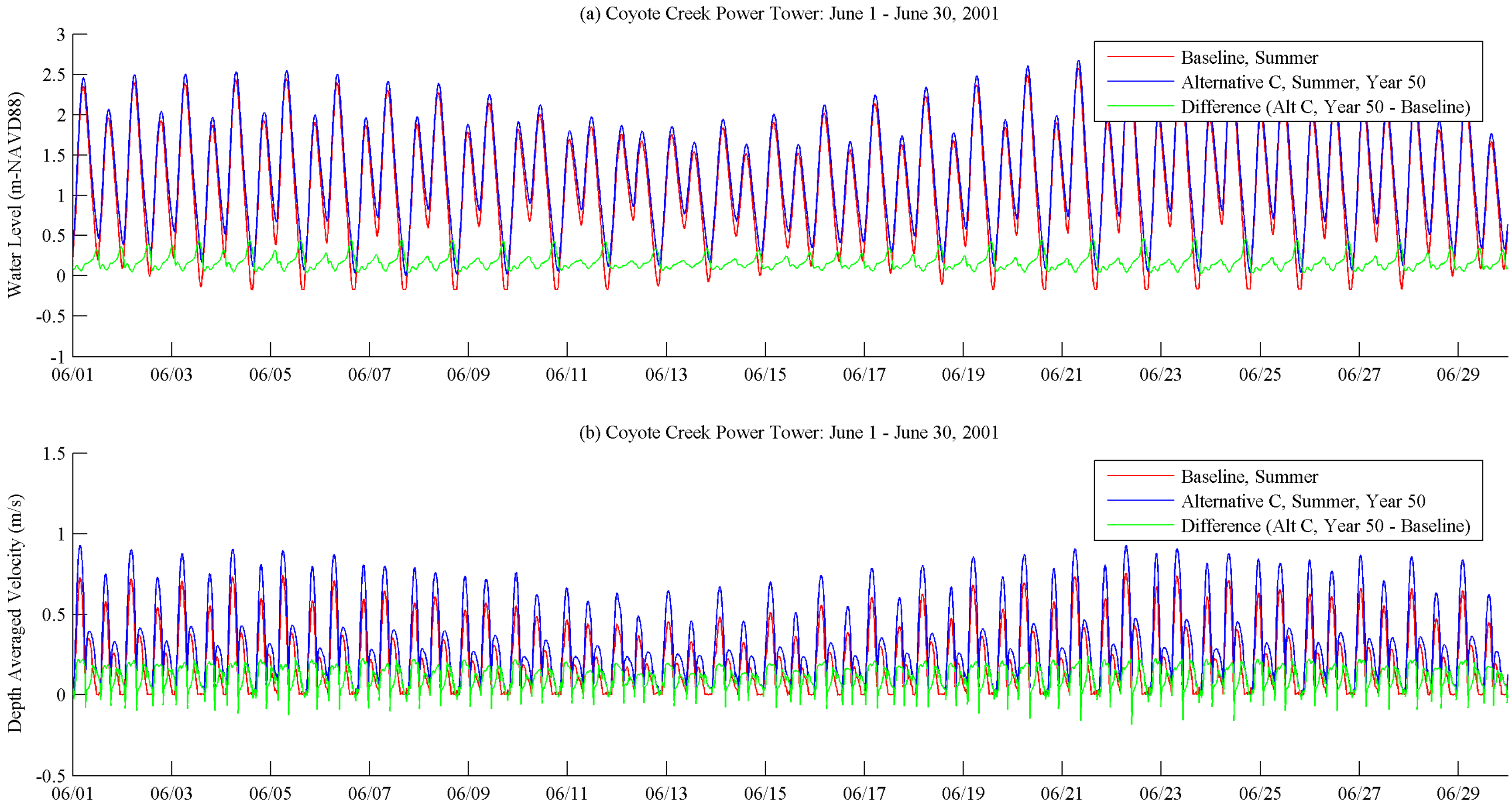

The depth-averaged velocity is calculated as $v = (u^2 + v^2)^{1/2}$, where u and v are the horizontal depth-averaged velocity components.

figure *7-80*

South Bay Salt Pond Restoration Project

Velocity, Coyote Creek Power Tower, Alt C, Year 50, Summer

PWA

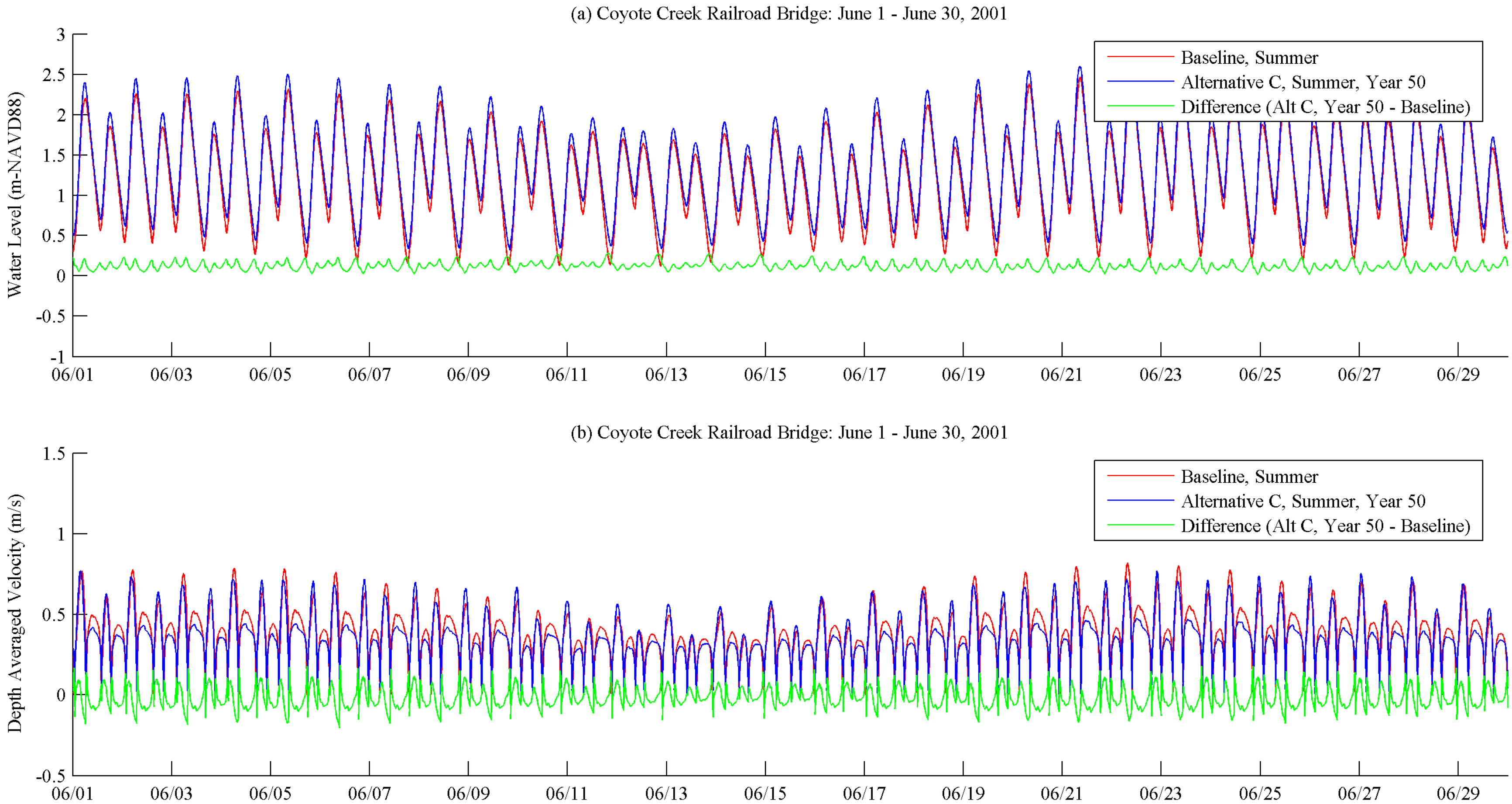

The depth-averaged velocity is calculated as $v = (u^2 + v^2)^{1/2}$, where u and v are the horizontal depth-averaged velocity components.

figure 7-81

South Bay Salt Pond Restoration Project

Velocity, Coyote Creek Railroad Bridge, Alt C, Year 50, Summer

PWA

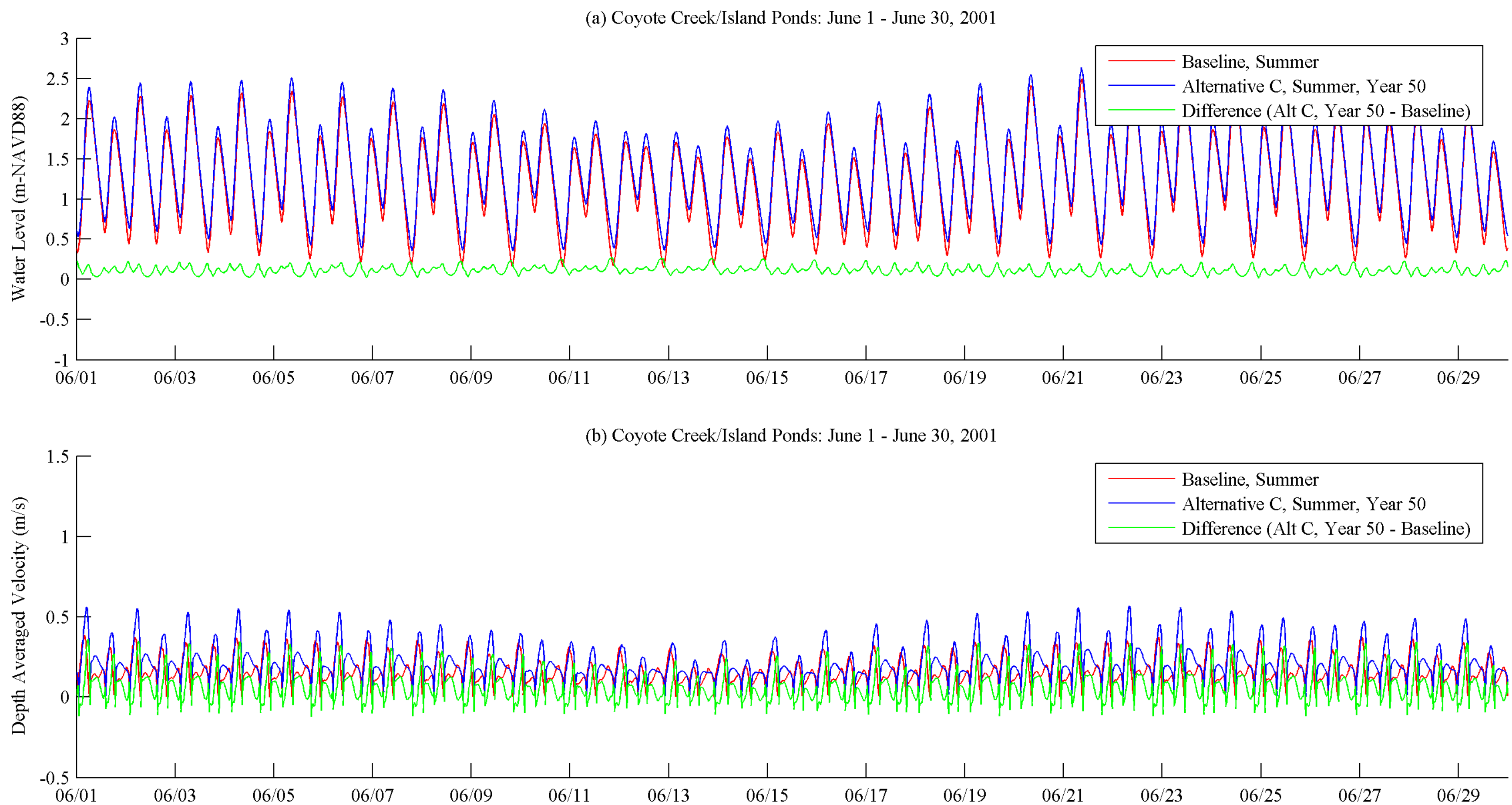

The depth-averaged velocity is calculated as $v = (u^2 + v^2)^{1/2}$, where u and v are the horizontal depth-averaged velocity components.

figure 7-82

South Bay Salt Pond Restoration Project

Velocity, Coyote Creek/Island Ponds, Year 50, Summer

PWA

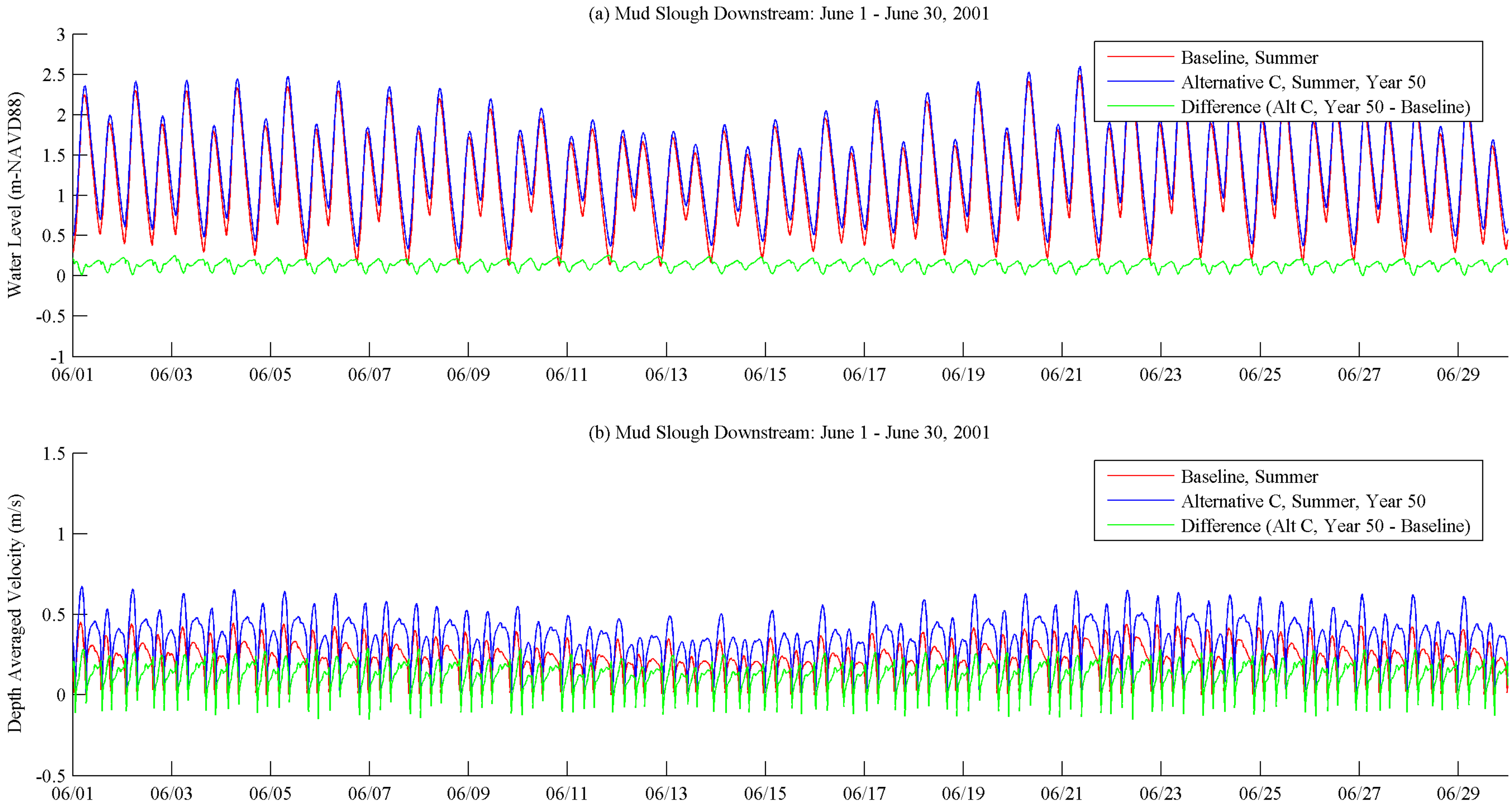

The depth-averaged velocity is calculated as $v = (u^2 + v^2)^{1/2}$, where u and v are the horizontal depth-averaged velocity components.

figure 7-83

South Bay Salt Pond Restoration Project

Velocity, Mud Slough Downstream, Alt C, Year 50, Summer

PWA

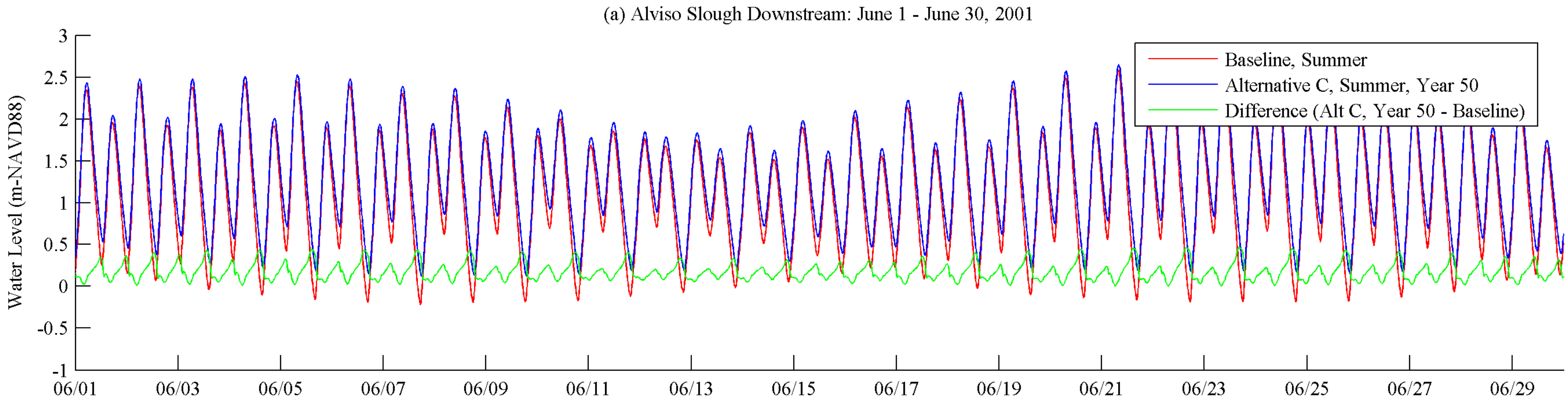

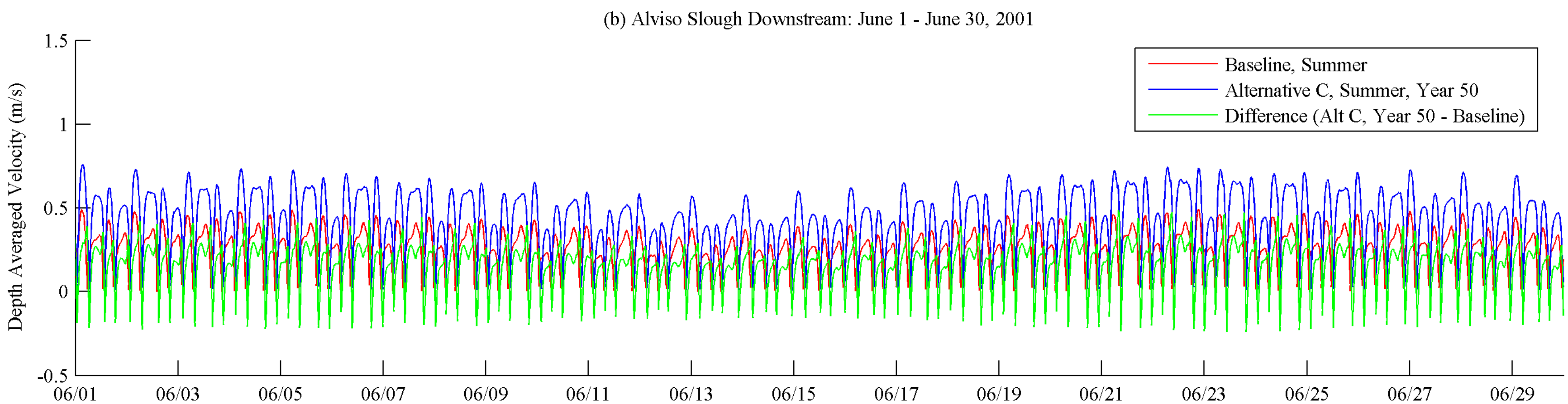

The depth-averaged velocity is calculated as $v = (u^2 + v^2)^{1/2}$, where u and v are the horizontal depth-averaged velocity components.

figure 7-84

South Bay Salt Pond Restoration Project

Velocity, Alviso Slough Downstream, Alt C, Year 50, Summer

PWA

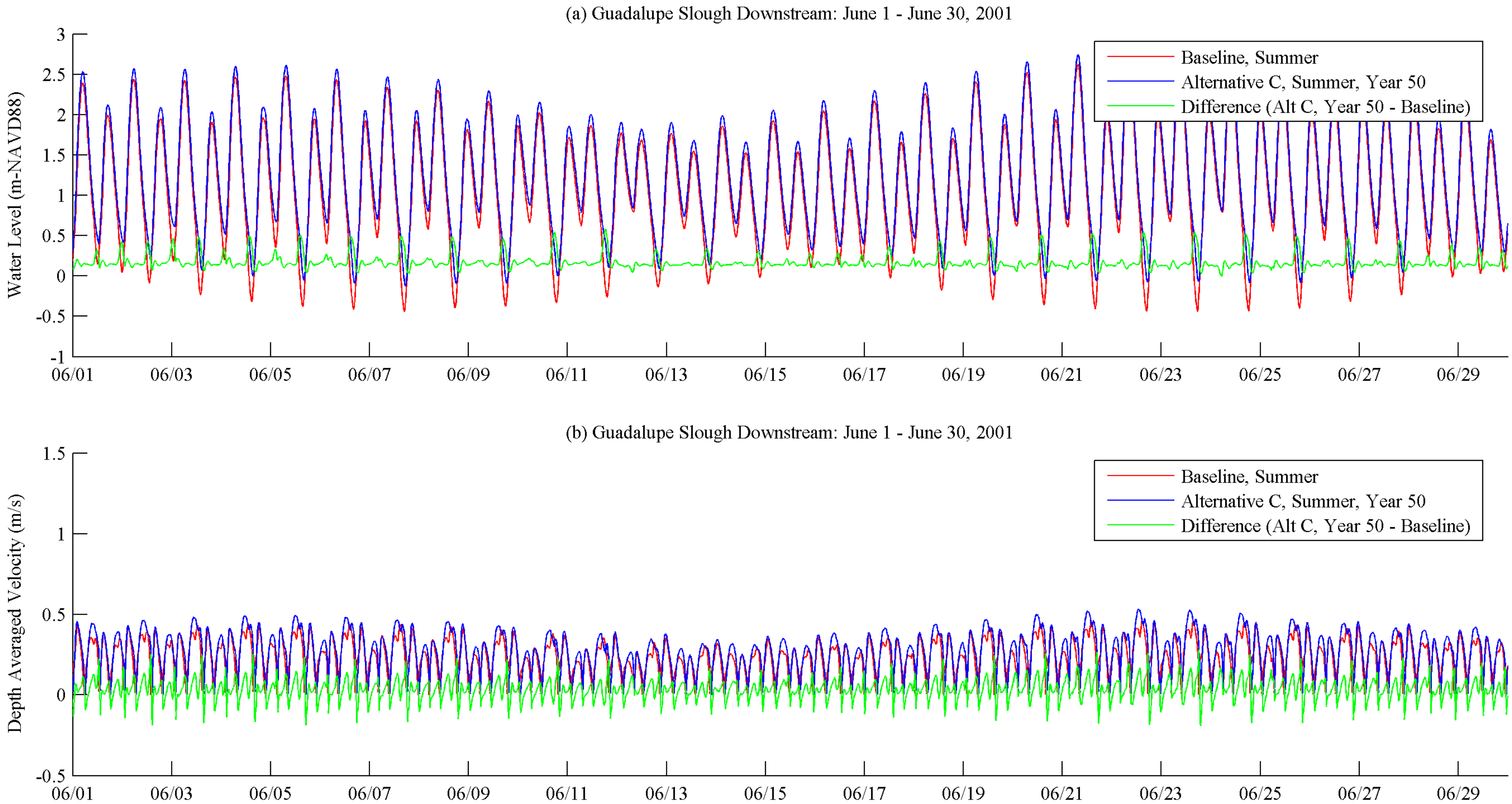

The depth-averaged velocity is calculated as $v = (u^2 + v^2)^{1/2}$, where u and v are the horizontal depth-averaged velocity components.

figure 7-85

South Bay Salt Pond Restoration Project

Velocity, Guadalupe Slough Downstream, Alt C, Year 50, Summer

PWA

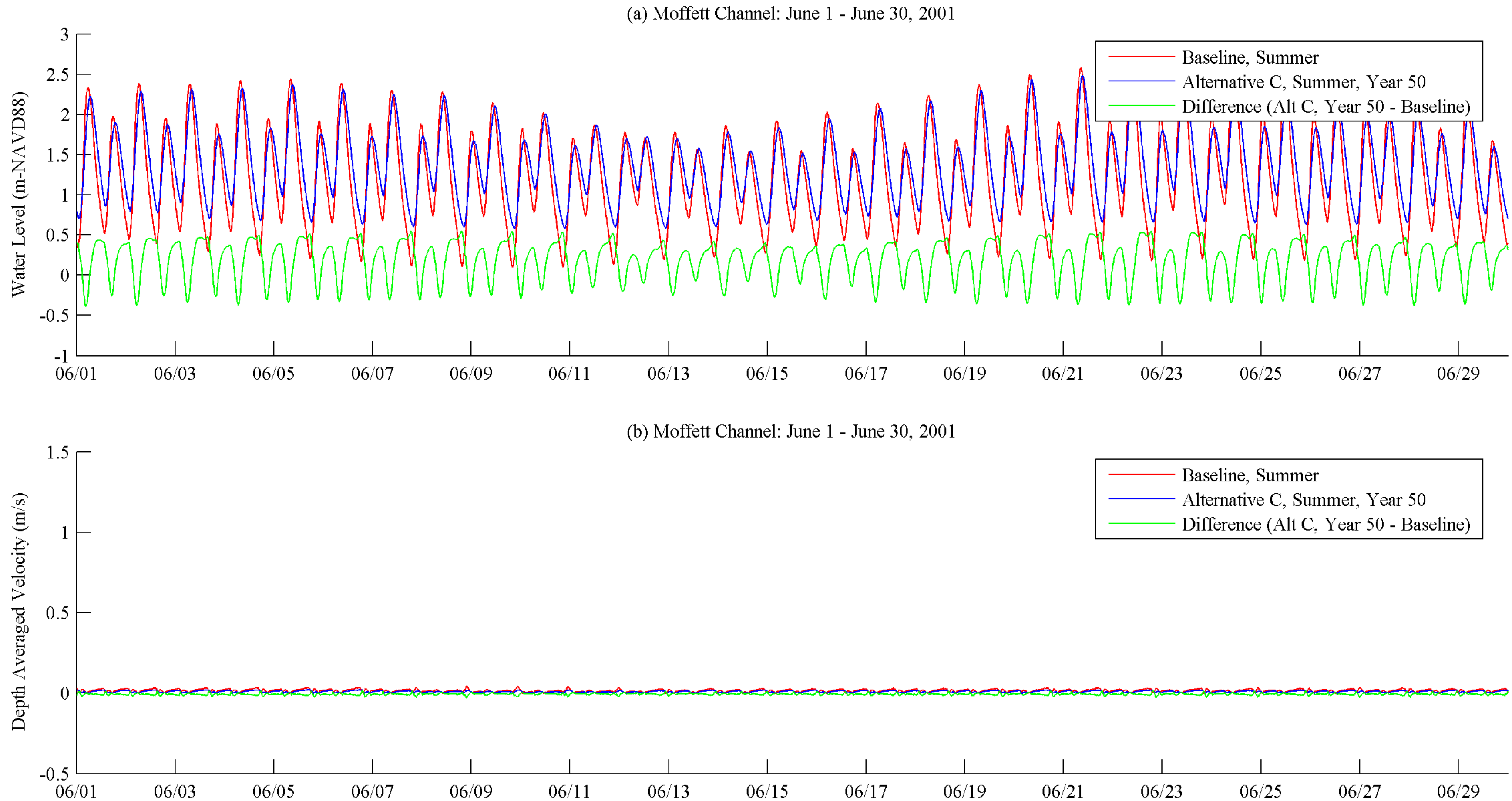

The depth-averaged velocity is calculated as $v = (u^2 + v^2)^{1/2}$, where u and v are the horizontal depth-averaged velocity components.

figure 7-86

South Bay Salt Pond Restoration Project

Velocity, Moffett Channel, Alt C, Year 50, Summer

PWA

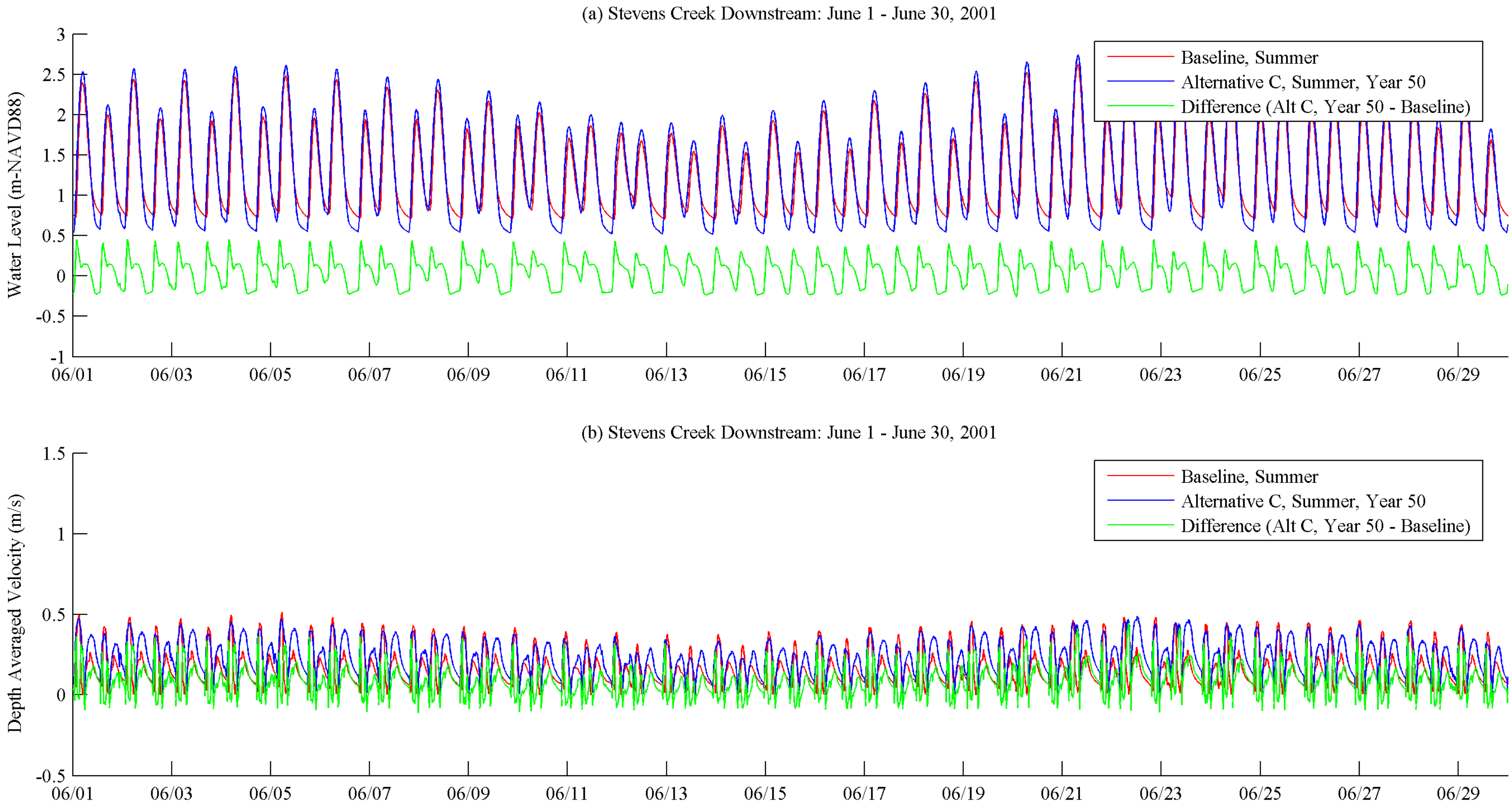

The depth-averaged velocity is calculated as $v = (u^2 + v^2)^{1/2}$, where u and v are the horizontal depth-averaged velocity components.

figure 7-87

South Bay Salt Pond Restoration Project

Velocity, Stevens Creek Downstream, Alt C, Year 50, Summer

PWA

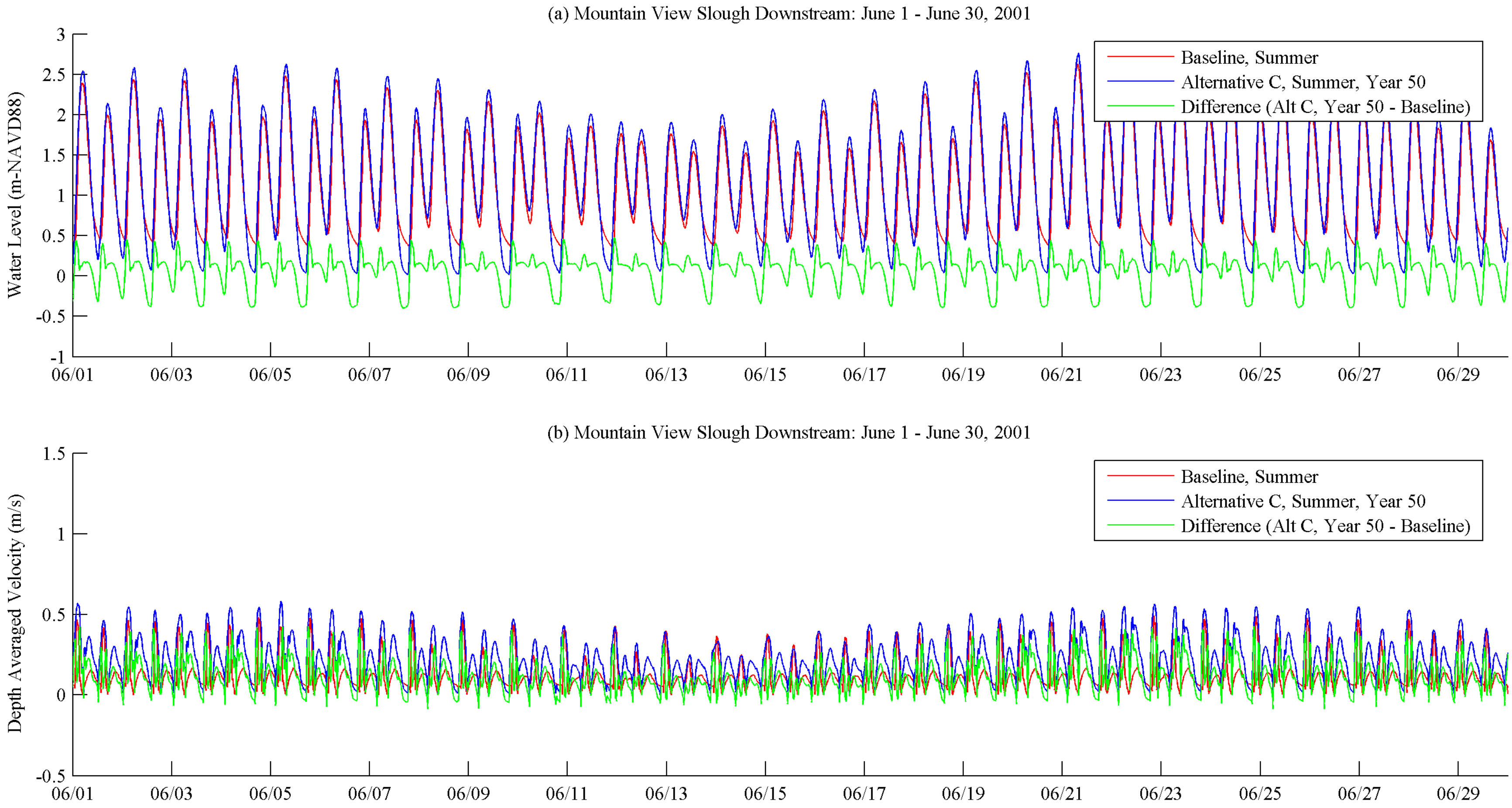

The depth-averaged velocity is calculated as $v = (u^2 + v^2)^{1/2}$, where u and v are the horizontal depth-averaged velocity components.

figure 7-88

South Bay Salt Pond Restoration Project

Velocity, Mountain View Slough Downstream, Alt C, Year 50, Summer

PWA

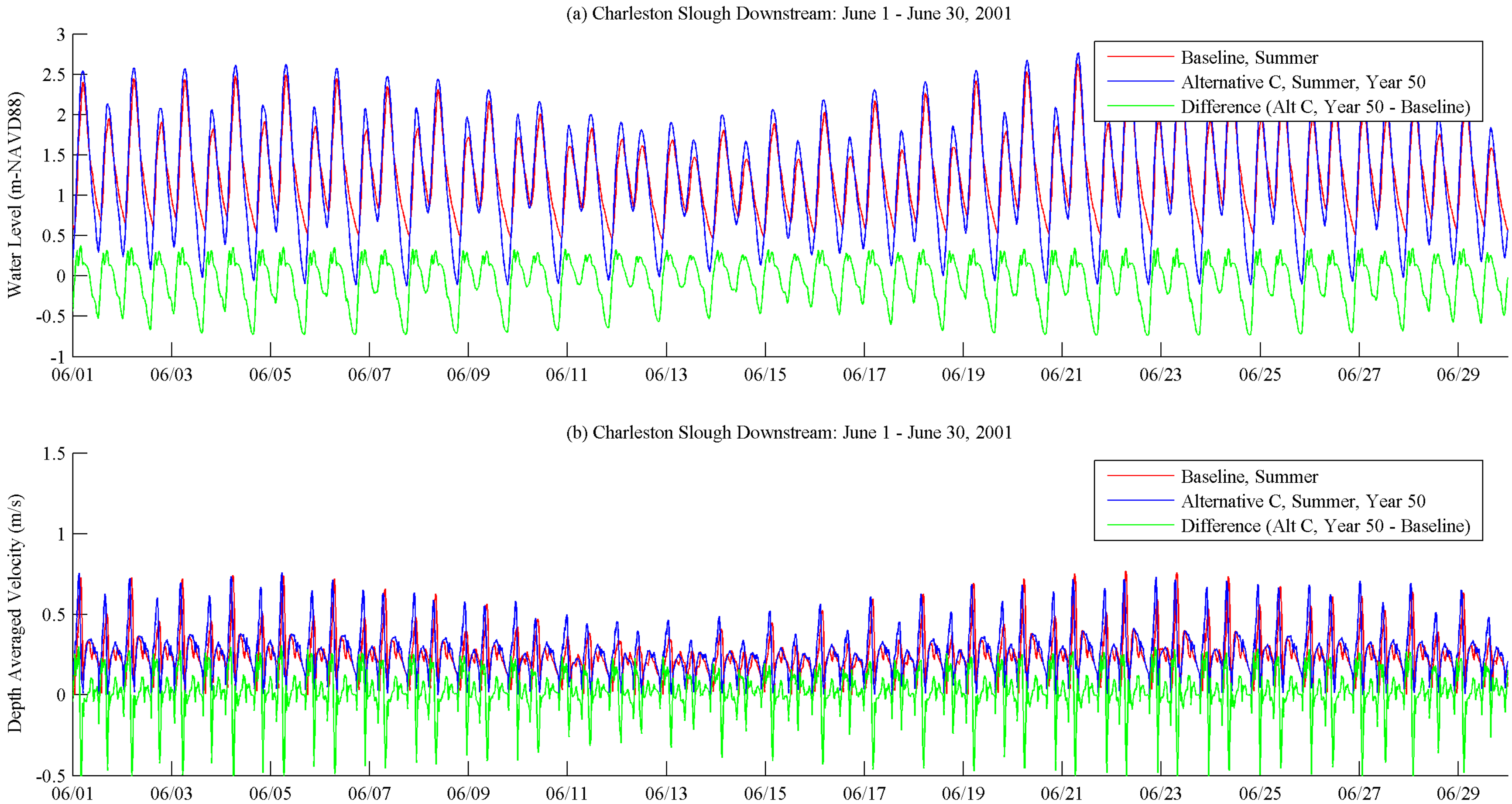

The depth-averaged velocity is calculated as $v = (u^2 + v^2)^{1/2}$, where u and v are the horizontal depth-averaged velocity components.

figure *7-89*

South Bay Salt Pond Restoration Project

Velocity, Charleston Slough Downstream, Alt C, Year 50, Summer

PWA

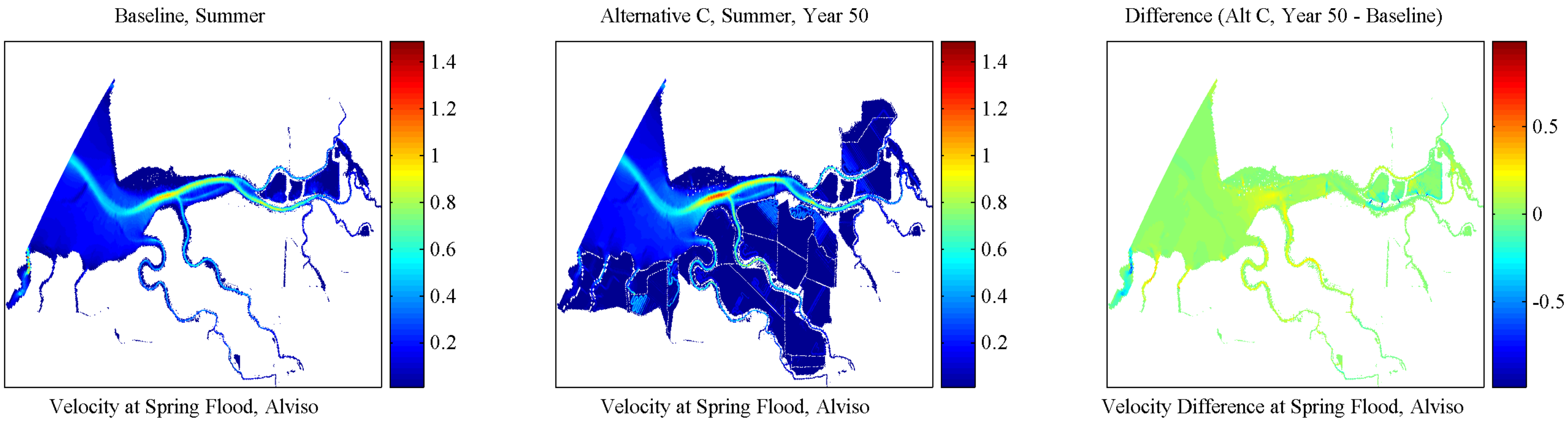

Note: Units shown are m/s

figure 7-90

South Bay Salt Pond Restoration Project

Velocity at Spring Flood, Alviso, Alt C, Year 50, Summer

PWA

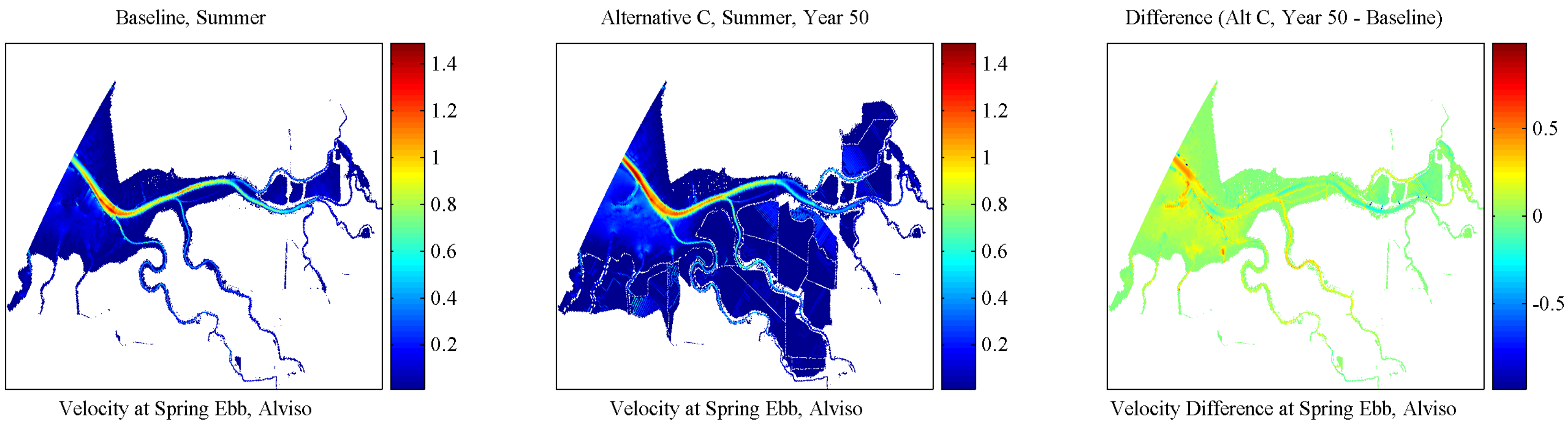

Note: Units shown are m/s

figure 7-91

South Bay Salt Pond Restoration Project

Velocity at Spring Ebb, Alviso, Alt C, Year 50, Summer

PWA

The depth-averaged velocity is calculated as $v = (u^2 + v^2)^{1/2}$, where u and v are the horizontal depth-averaged velocity components.

figure *7-92*

South Bay Salt Pond Restoration Project

Velocity, Ravenswood Slough Downstream, Alt C, Year 50, Summer

PWA

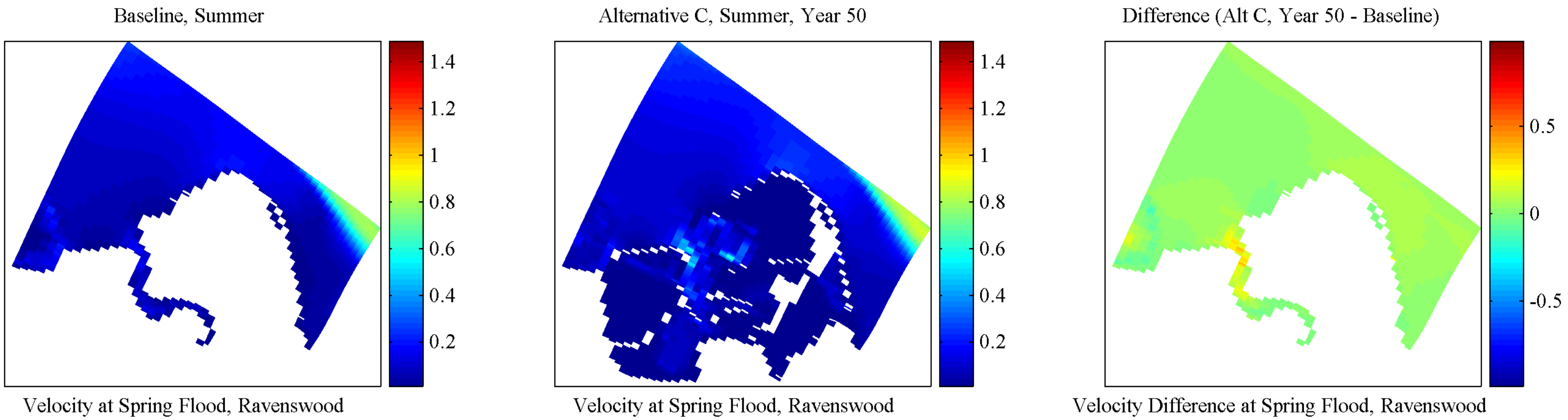

Note: Units shown are m/s

figure 7-93

South Bay Salt Pond Restoration Project

Velocity at Spring Flood, Ravenswood, Alt C, Year 50, Summer

PWA

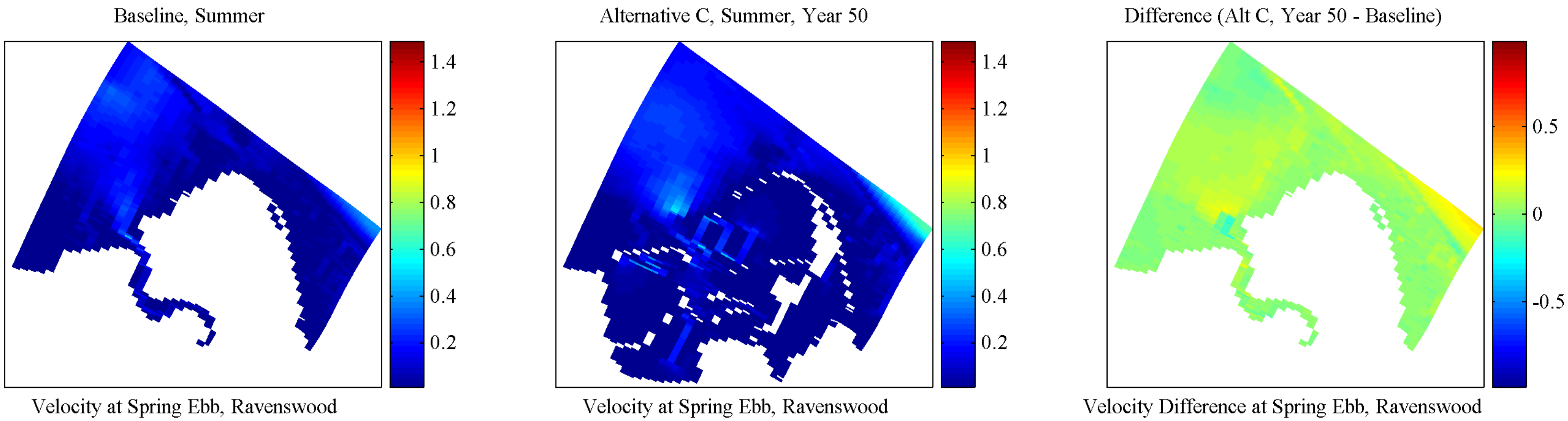

Note: Units shown are m/s

figure *7-94*

South Bay Salt Pond Restoration Project

Velocity at Spring Ebb, Ravenswood, Alt C, Year 50, Summer

PWA

Baseline, Summer

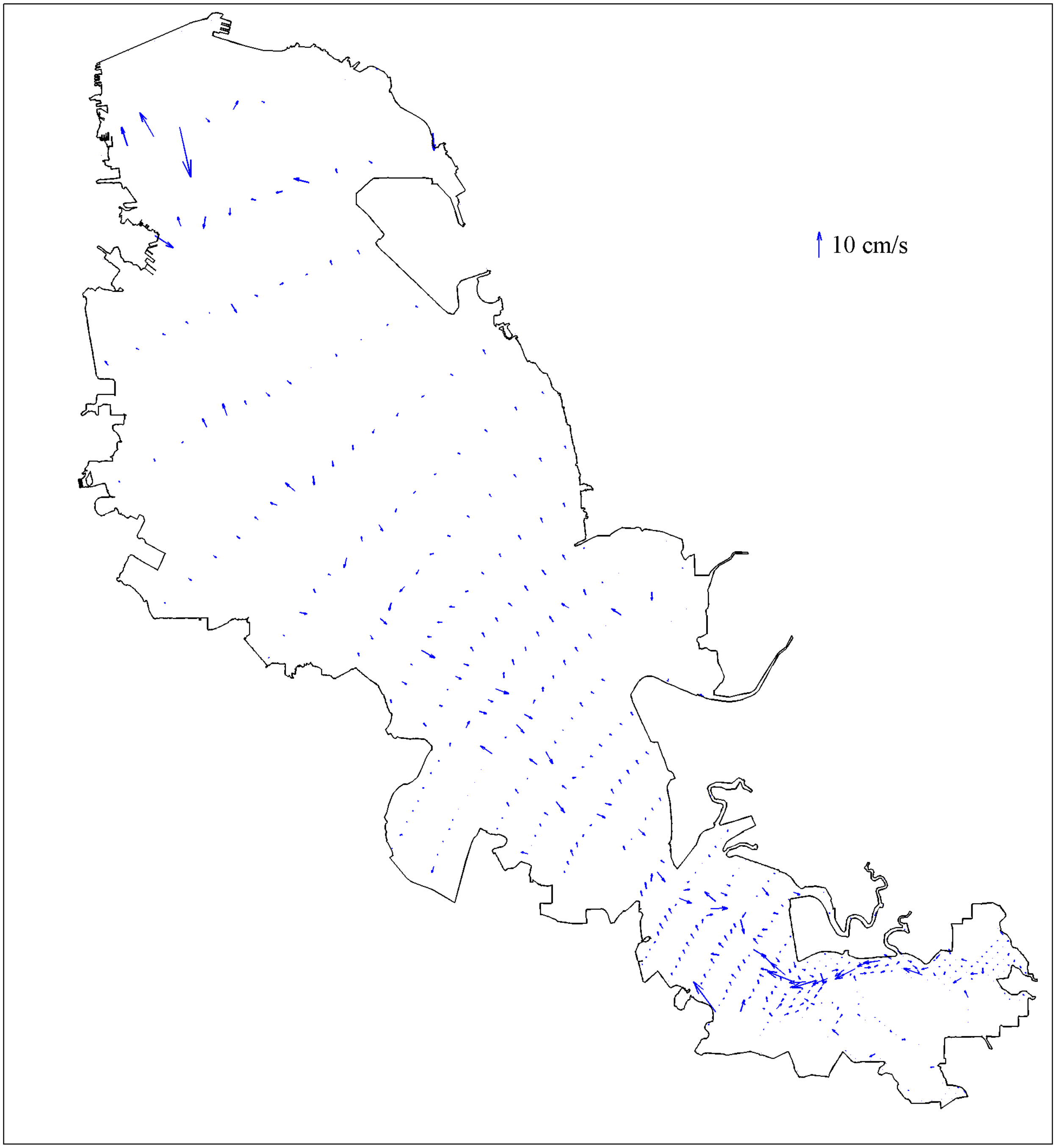

South Bay Residual Circulation (cm/s)

figure 7-95

South Bay Salt Pond Restoration Project

South Bay Residual Circulation, Baseline, Summer

PWA

Alternative C, Summer, Year 50

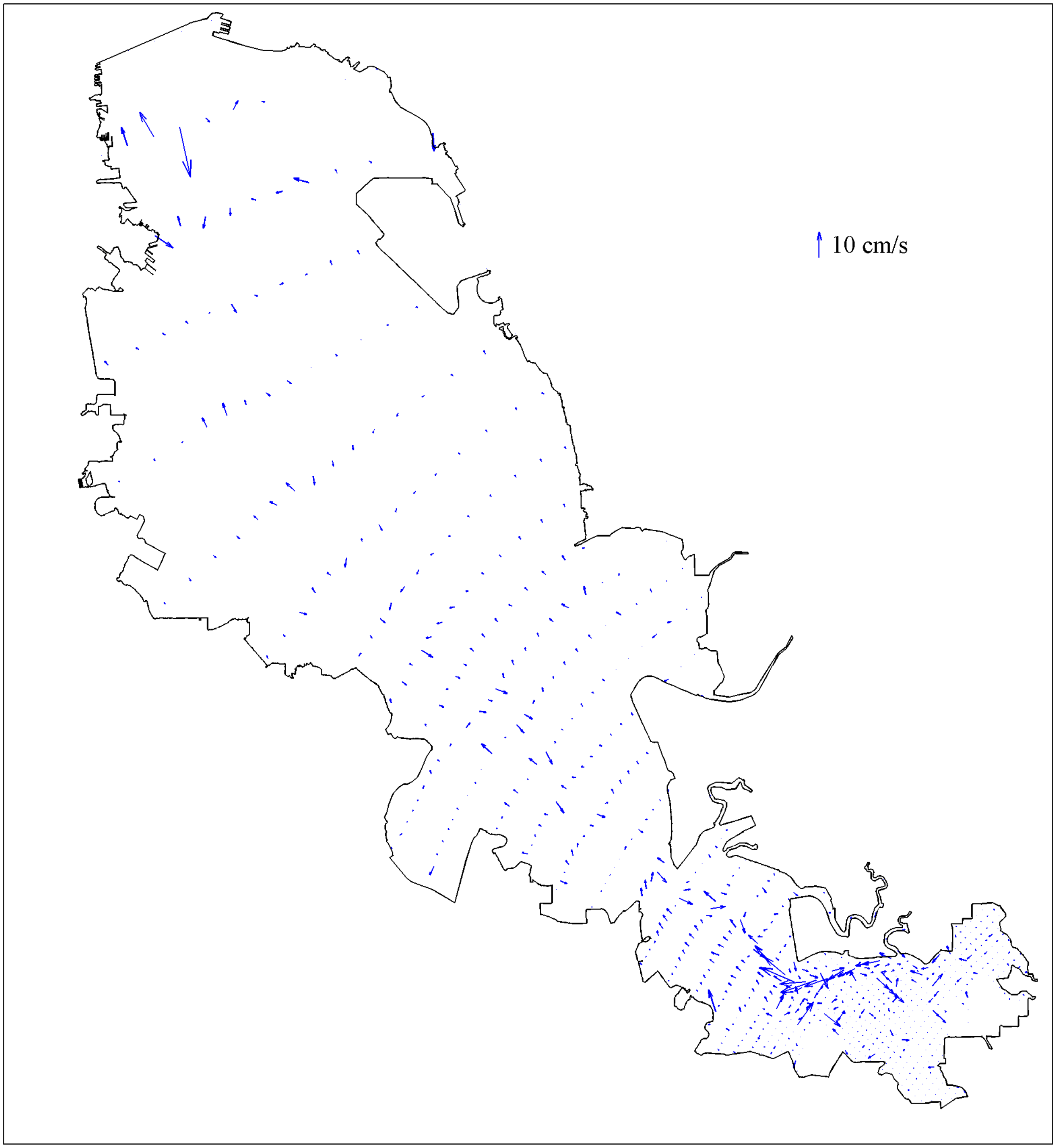

South Bay Residual Circulation (cm/s)

figure 7-96

South Bay Salt Pond Restoration Project

South Bay Residual Circulation, Alt C, Year 50, Summer

PWA

Difference (Alt C - Baseline)

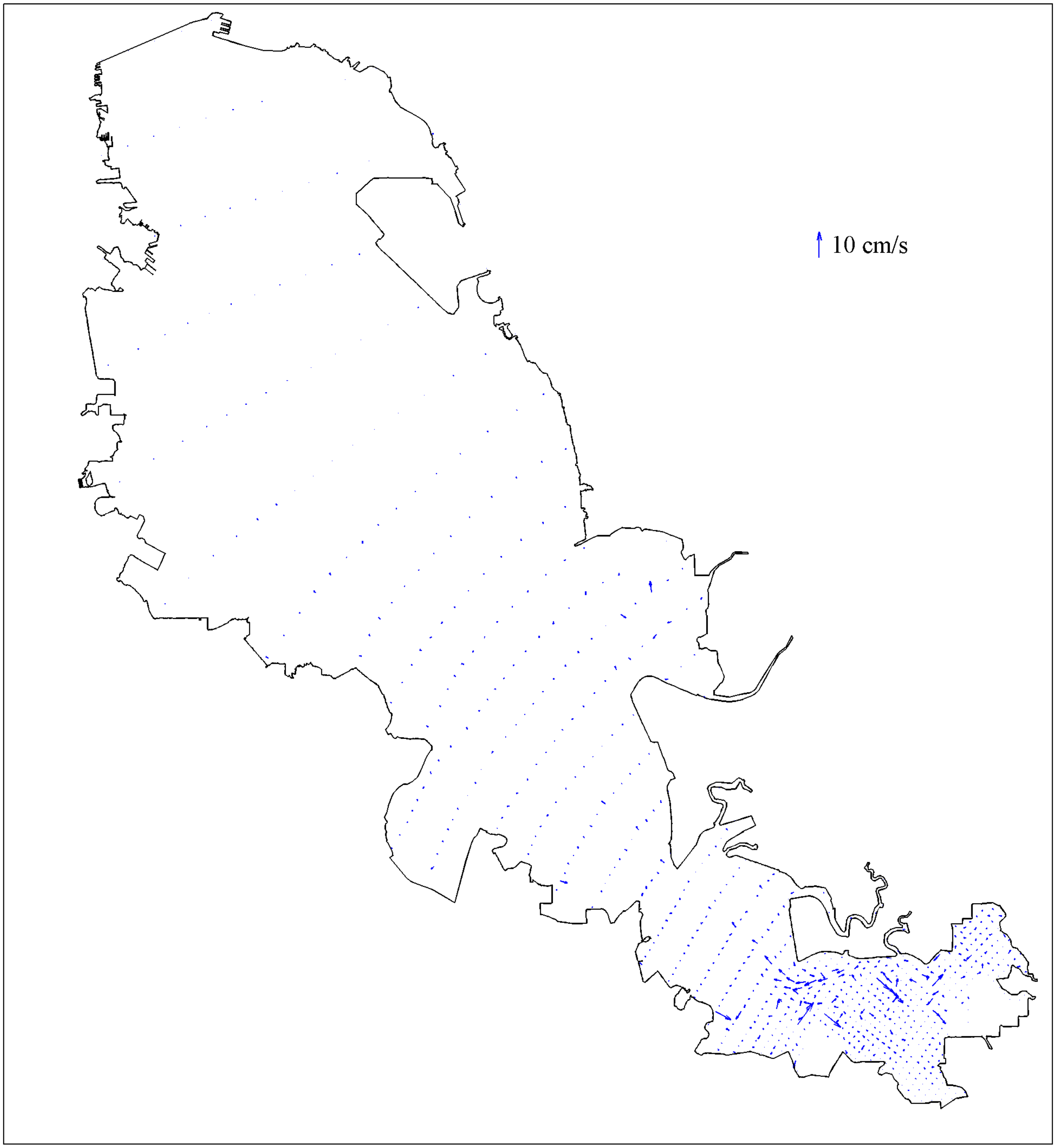

South Bay Residual Circulation Difference (cm/s)

figure 7-97

South Bay Salt Pond Restoration Project

South Bay Residual Circulation, Difference, Year 50, Summer

PWA

Baseline, Summer

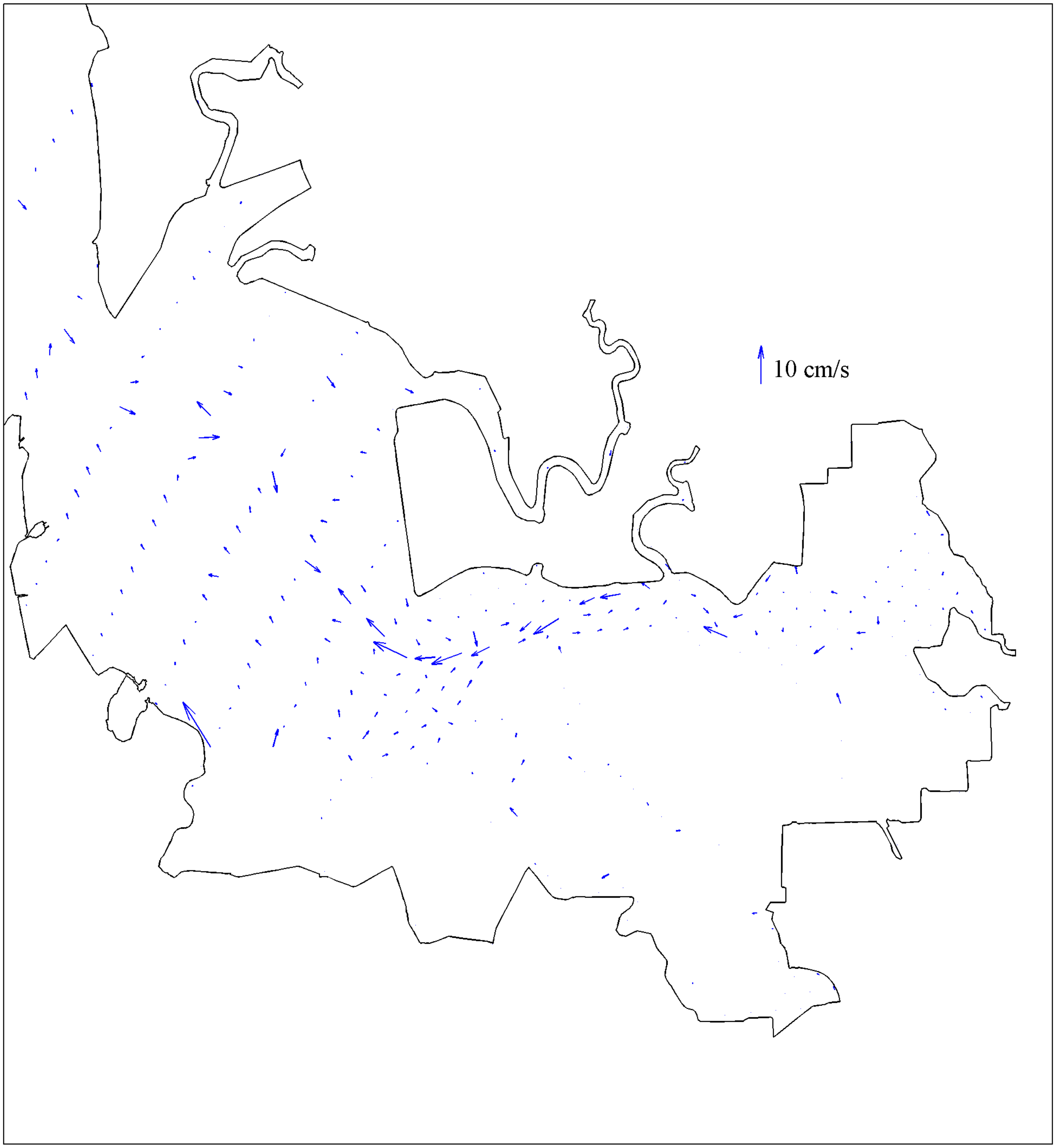

Far South Bay Residual Circulation (cm/s)

figure 7-98

South Bay Salt Pond Restoration Project

Far South Bay Residual Circulation, Baseline, Summer

PWA

Alternative C, Summer, Year 50

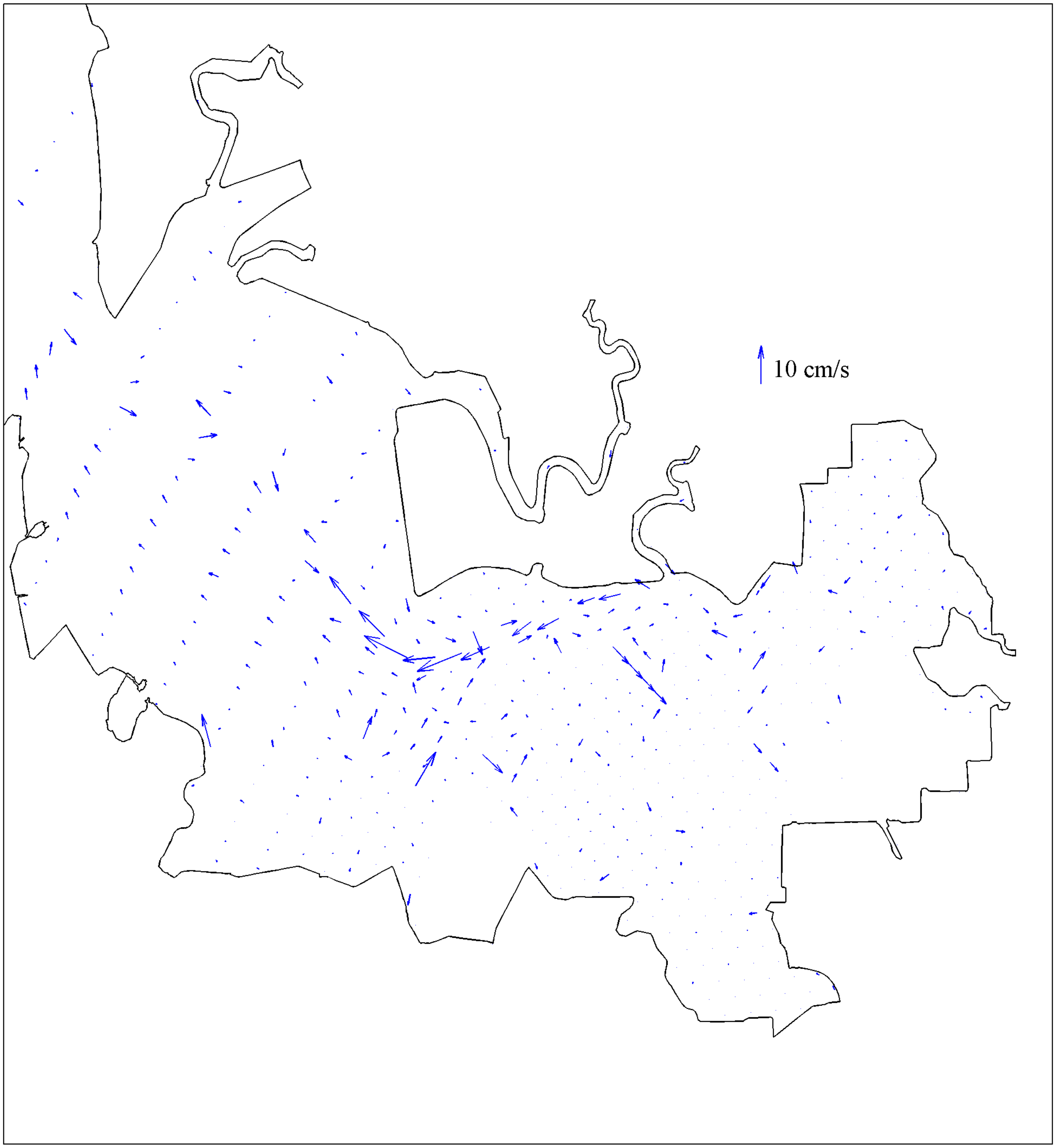

Far South Bay Residual Circulation (cm/s)

figure 7-99

South Bay Salt Pond Restoration Project

Far South Bay Residual Circulation, Alt C, Year 50, Summer

PWA

Difference (Alt C - Baseline)

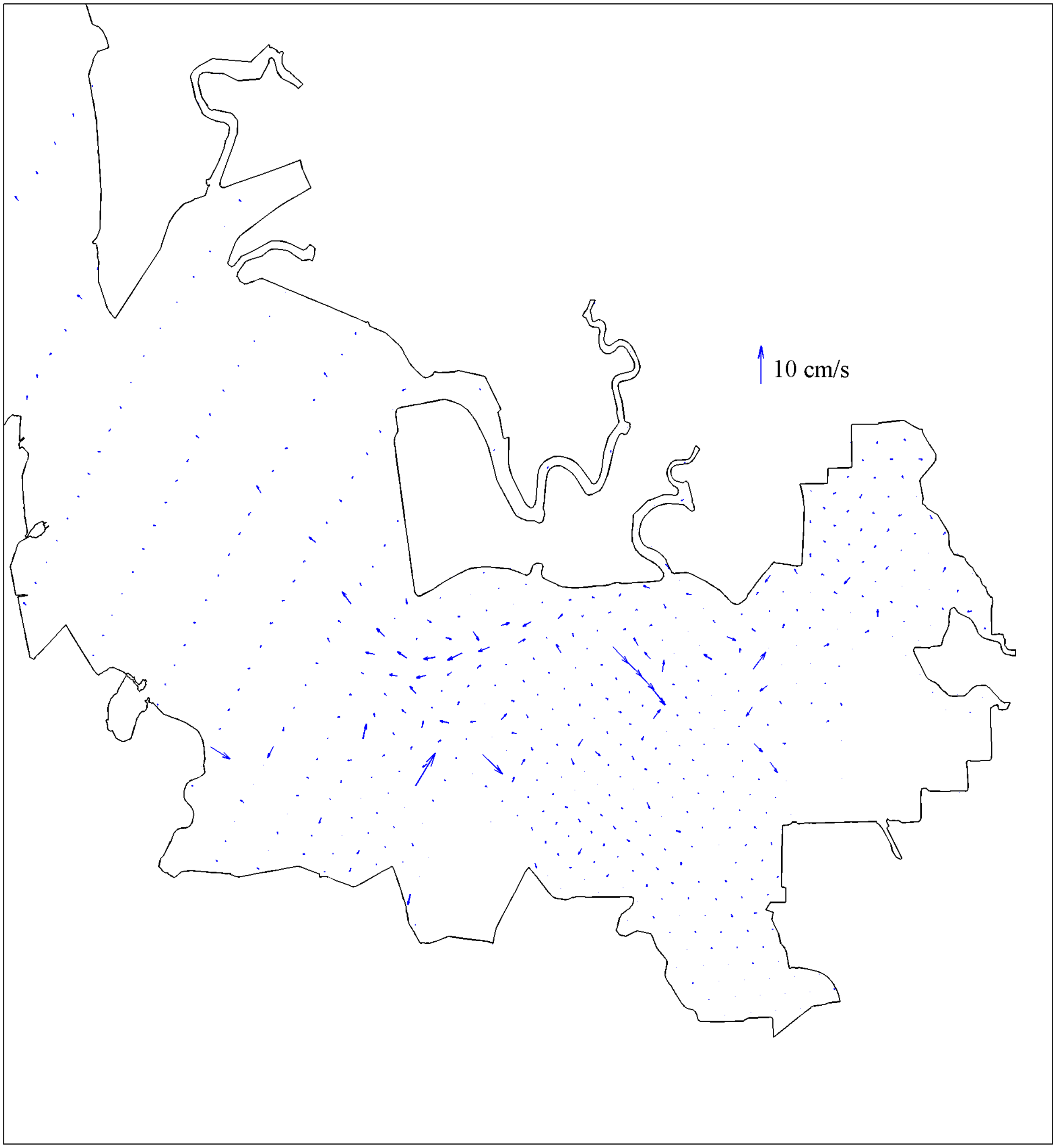

Far South Bay Residual Circulation Difference (cm/s)

figure 7-100

South Bay Salt Pond Restoration Project

Far South Bay Residual Circulation, Difference, Summer

PWA

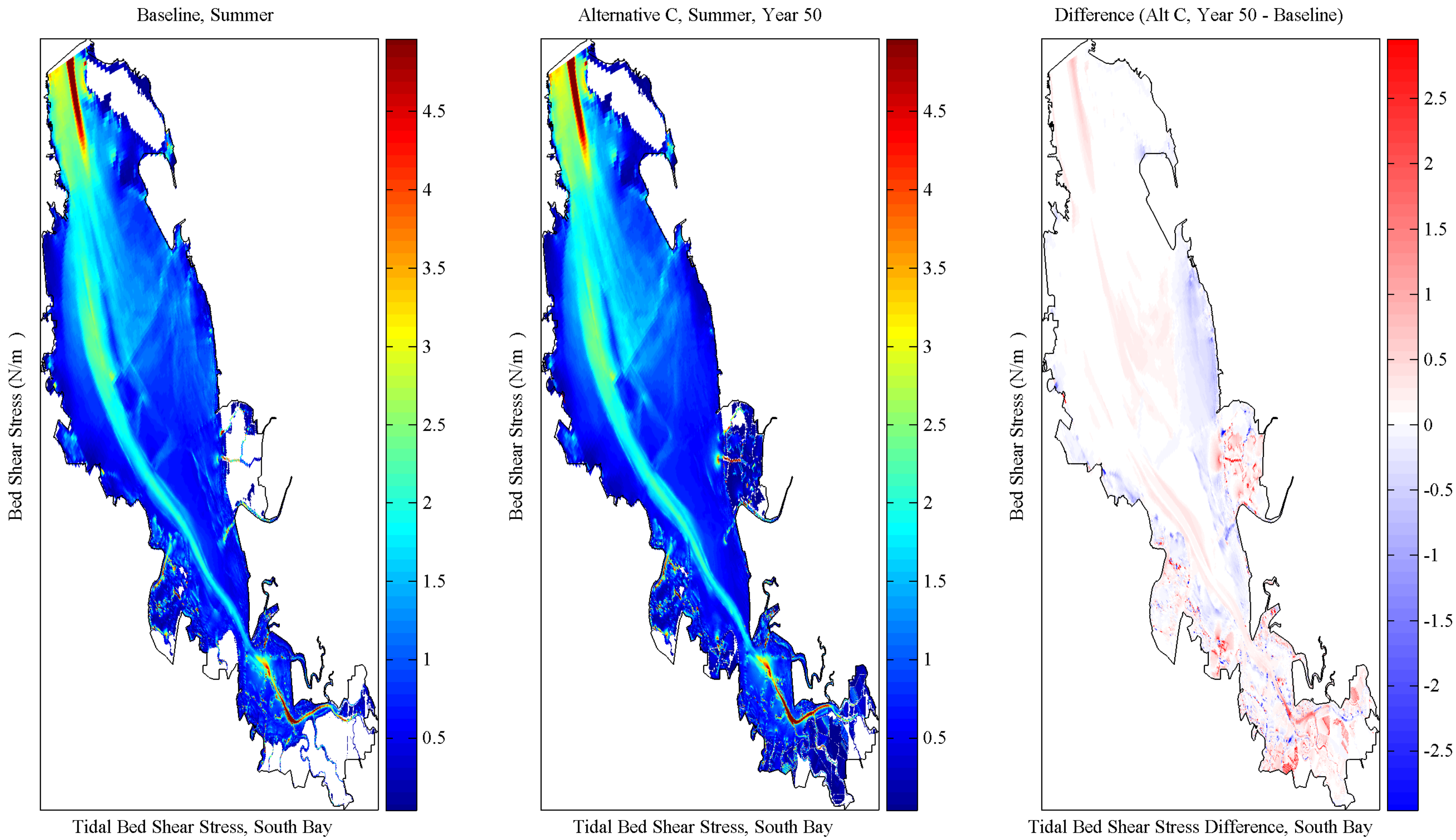

figure 7-101

South Bay Salt Pond Restoration Project

Tidal Bed Shear Stress, South Bay, Alt C, Year 50, Summer

PWA

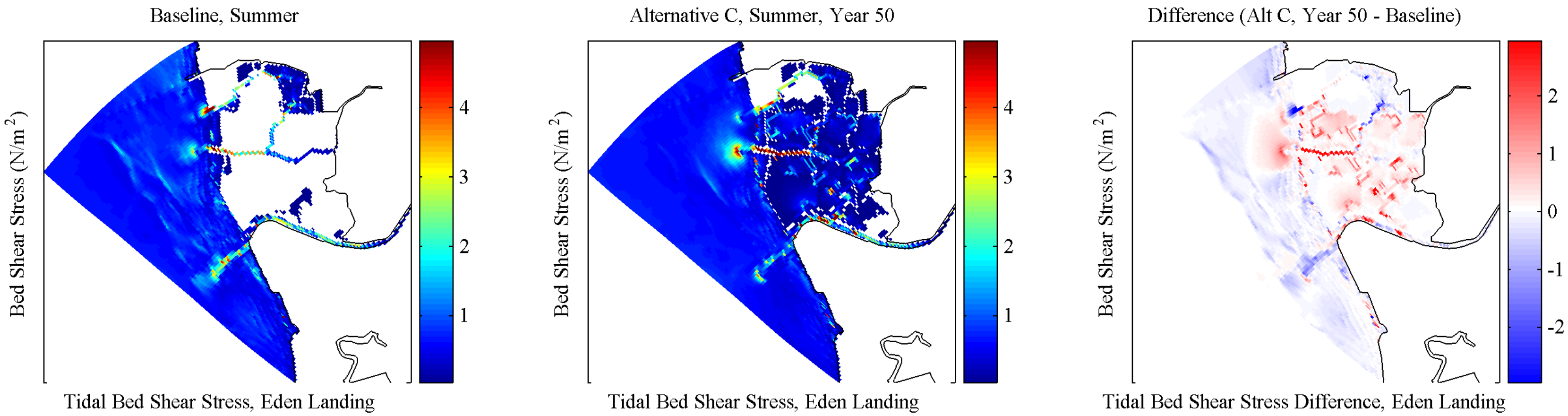

figure 7-102

South Bay Salt Pond Restoration Project

Tidal Bed Shear Stress, Eden Landing, Alt C, Year 50, Summer

PWA

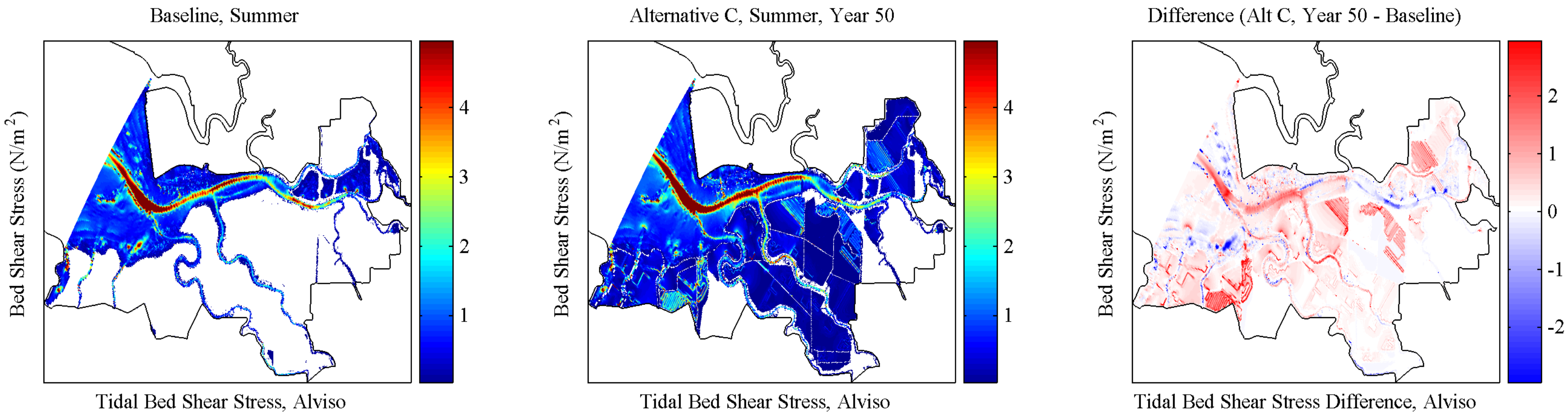

figure 7-103

South Bay Salt Pond Restoration Project

Tidal Bed Shear Stress, Alviso, Alt C, Year 50, Summer

PWA

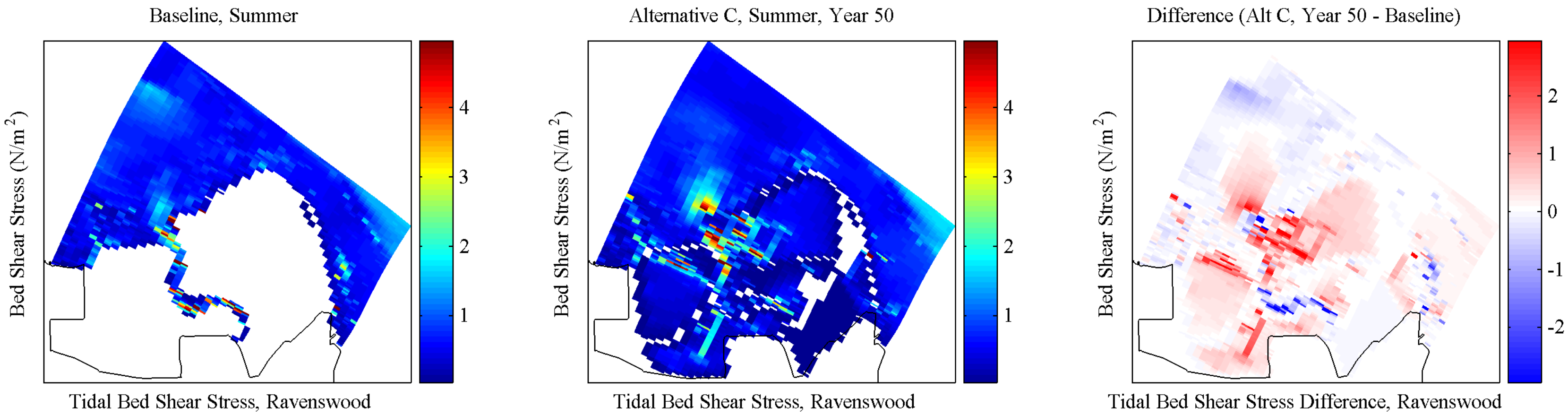

figure 7-104

South Bay Salt Pond Restoration Project

Tidal Bed Shear Stress, Ravenswood, Alt C, Year 50, Summer

PWA

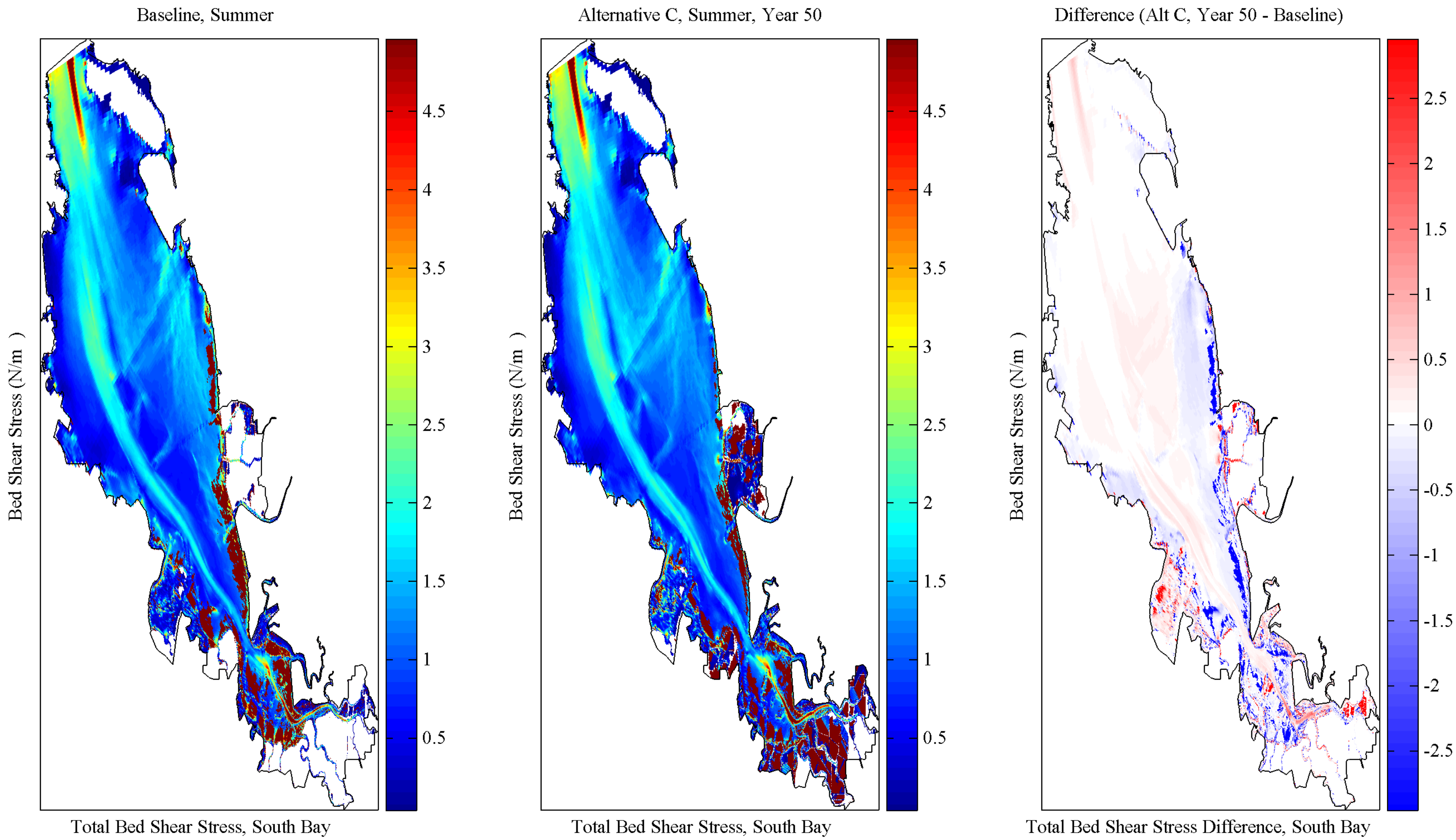

figure *7-105*

South Bay Salt Pond Restoration Project

Total Bed Shear Stress, South Bay, Alt C, Year 50, Summer

PWA

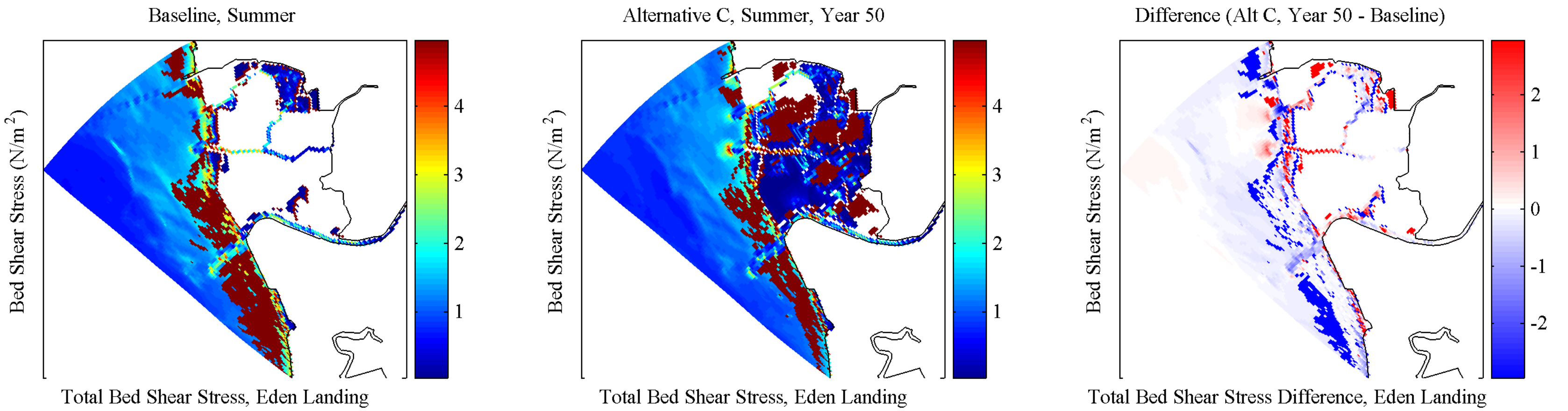

figure 7-106

South Bay Salt Pond Restoration Project

Total Bed Shear Stress, Eden Landing, Alt C, Year 50, Summer

PWA

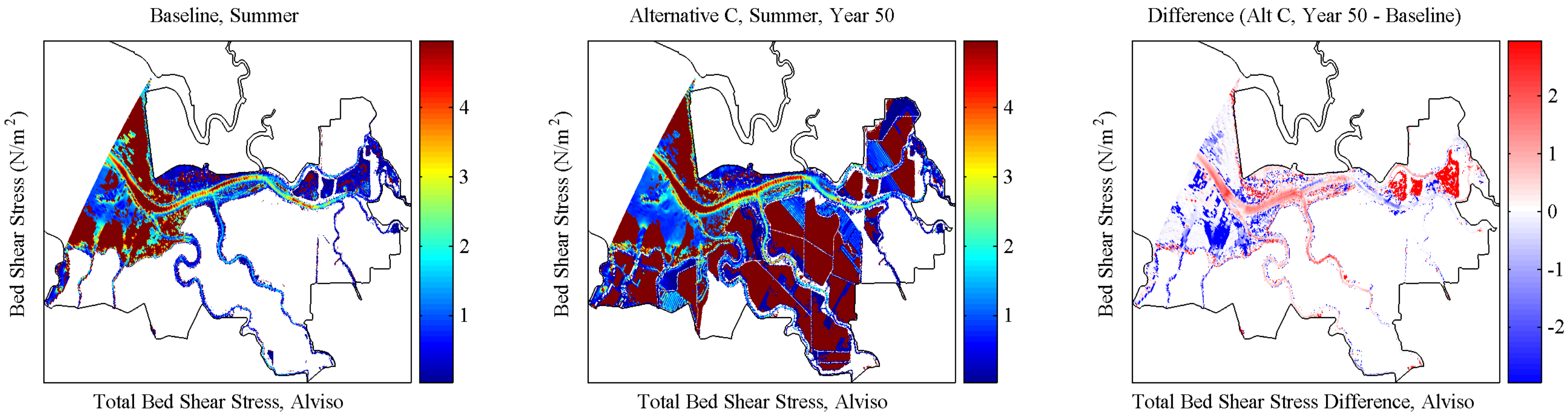

figure *7-107*

South Bay Salt Pond Restoration Project

Total Bed Shear Stress, Alviso, Alt C, Year 50, Summer

PWA

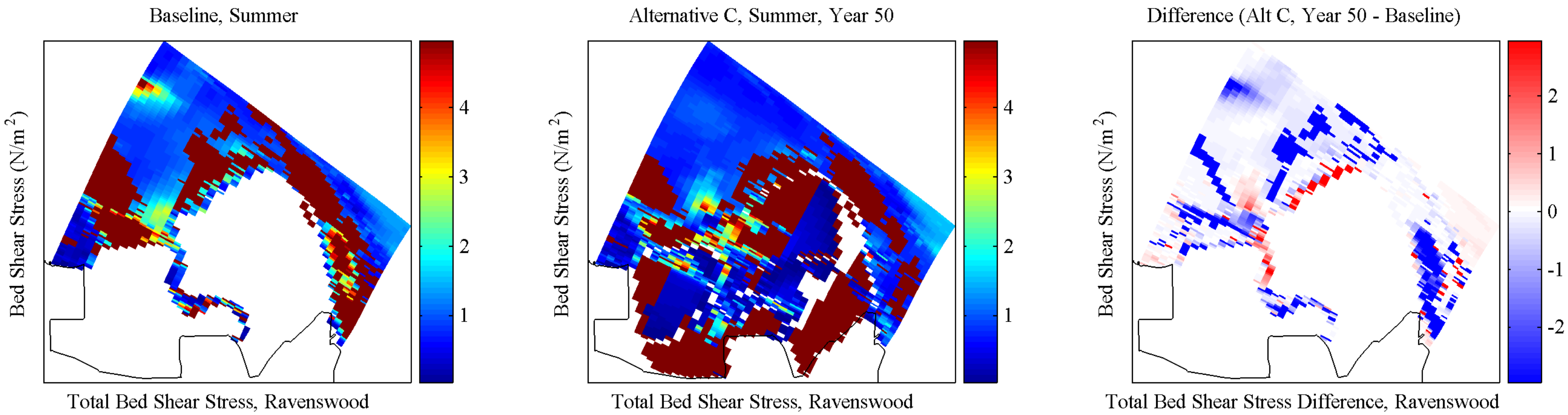

figure 7-108

South Bay Salt Pond Restoration Project

Total Bed Shear Stress, Ravenswood, Alt C, Year 50, Summer

PWA

8. REFERENCES

Barnard P, Lescinski J, Hanes D, Eshleman J, Lesser GR. in press. Toward a validated 2-D hydrodynamic model for the mouth of San Francisco Bay. U.S.G.S. Open-File Report. 40 pp p.

Booij N, Ris R, Holthuijsen L. 1999. A third-generation wave model for coastal regions, 1. Model description and validation. Journal of Geophysical Research - Oceans 104(C4):7649-7666.

California Department of Fish and Game. 2005. 2004 Self-Monitoring Report Baumberg Complex. Order No. R2-2004-0018, WDID No. 2 019438001. Hayward, CA.

Cheng R, Casulli V. 1982. On lagrangian residual currents with applications in South San Francisco Bay, California. Water Resources Research 18(6):1652-1662.

Cheng RT, Casulli V, Gartner JW. 1993. Tidal, residual, intertidal mudflat (TRIM) model and its applications to San-Francisco Bay, California. Estuarine, Coastal, and Shelf Science 36(3):p235-280.

Cheng RT, Gartner JW. 1985. Harmonic Analysis of tides and tidal Currents in South San Francisco Bay, California. Estuarine, Coastal, and Shelf Science 21:p57-74.

Cloern J, Powell T, Huzzey L. 1989. Spatial and temporal variability in South San Francisco Bay (USA). 2. Temporal changes in salinity, suspended sediments, and phytoplankton biomass and productivity over tidal time scales. Estuarine, Coastal and Shelf Science 28(6):599-613.

Fischer HB, List EJ, Koh RCY, Imberger J, Brooks NH. 1979. Mixing Inland and Coastal Water: Academic Press. 483 pp. p.

Foxgrover AC, Higgins SA, Ingraca MK, Jaffe BE, Smith RE. 2004. Deposition, erosion, and bathymetric change in South San Francisco Bay: 1858-1983.: U.S. Geologic Survey Open-File Report 2004-1192. 25 p.

Grant WD, Madsen OS. 1979. Combined wave and current interaction with a rough bottom. Journal of Geophysical Research 84(C4):1791-1808.

Gross E. 1997. Numerical modeling of hydrodynamics and scalar transport in an estuary [PhD Thesis]. Stanford, CA: Stanford University. 331 p.

Gross E, Schaaf & Wheeler. 2003a. Alviso Island Pond Breach Initial Stewardship Plan Study. South Bay Salt Ponds Initial Stewardship Plan, Draft Environmental Impact Report/Environmental Impact Statement, Technical Appendix K.: California Department of Fish and Game and U.S. Fish and Wildlife Service,.

Gross ES, Schaaf & Wheeler. 2003b. South Bay Salt Ponds Initial Stewardship Plan: South San Francisco Bay Hydrodynamic Model Results Report. Prepared for Cargill Salt.

IPCC. 2001. Climate Change 2001: The Scientific Basis. Contribution of Working Group I to the Third Assessment Report of the Intergovernmental Panel on Climate Change. Houghton JT, Y. Ding, D.J. Griggs, M. Noguer, P.J. van der Linden, X. Dai, K. Maskell, C.A. Johnson (eds.), editor. Cambridge: Cambridge University Press. 881 p.

Jaffe BE, Foxgrover AC. 2006a. A History of intertidal flat area in South San Francisco Bay, California: 1858 to 2005. U.S. Geological Survey Open-File Report 2006-1262. 32 p.

Jaffe BE, Foxgrover AC. 2006b. Sediment Deposition and Erosion in South San Francisco Bay, California from 1956 to 2005. U.S. Geological Survey Open-File Report 2006-1287. Report nr Open File Report. 24 p.

Jaffe BE, Fregoso T. in progress. Bulk density of near-surface sediments of South San Francisco Bay, California. U.S. Geological Survey. Report nr Open File Report.

Jones & Stokes. 2004a. Napa-Sonoma River Salt Marsh Restoration Project, Final Environmental Impact Report. Prepared for California State Coastal Conservancy, Oakland, CA, and California Department of Fish and Game, Napa, CA. Sacramento, CA.

Jones & Stokes. 2004b. Napa-Sonoma River Salt Marsh Restoration Project, Final Environmental Impact Statement. Prepared for California State Coastal Conservancy, Oakland, CA, and California Department of Fish and Game, Napa, CA. Sacramento, CA.

Kamman Hydrology and Engineering. 2004. Technical studies of the Giacomini Restoration Project. Point Reyes, CA: National Park Service, Point Reyes CA.

Lucas L. 1997. A numerical investigation of coupled hydrodynamic and phytoplankton dynamics in shallow estuaries [PhD Thesis]. Stanford, CA: Stanford University.

Madsen OS, Wikramanayake PN. 1991. Simple models for turbulent wave-current bottom boundary layer flow. Vicksburg, MS: U.S. Army Corps of Engineers Waterways Experiment Station. Report nr DRP-91-1. 150 p.

Monsen NE, Cloem JE, Lucas LV. 2002. A comment on the use of flushing time, residence time, and age as transport time scales. Limnol Oceanogr 47(5):1545-1553.

PWA. 2005. Modeling Methods and Strategy Report: Hydrodynamics, Coastal Flood and Fluvial Flood Analyses. San Francisco, CA.: Prepared for: California State Coastal Conservancy, U.S. Fish and Wildlife Service, California Department of Fish and Game.

PWA. 2006a. Hydrodynamic Modeling Calibration Report. San Francisco, CA.: Prepared for: California State Coastal Conservancy, U.S. Fish and Wildlife Service, California Department of Fish and Game.

PWA. 2006b. South Bay Geomorphic Assessment. San Francisco, CA.: Prepared for: California State Coastal Conservancy, U.S. Fish and Wildlife Service, California Department of Fish and Game.

PWA, H. T. Harvey & Associates, EDAW, Brown and Caldwell. 2005. Hydrodynamics and Sediment Dynamics Existing Conditions Report. San Francisco, CA.: Prepared for: California State Coastal Conservancy, U.S. Fish and Wildlife Service, California Department of Fish and Game.

PWA, H. T. Harvey & Associates, EDAW, Brown and Caldwell. 2006. Final Alternatives Report. San Francisco, CA.: Prepared for: California State Coastal Conservancy, U.S. Fish and Wildlife Service, California Department of Fish and Game.

Schaaf & Wheeler. 2004. Alviso Slough Tidal Prism Enhancement Project

Draft Technical Report. Santa Clara, California: Santa Clara Valley Water District.

Schemel LE. 1995. Measurements of salinity, temperature, and tides in South San Francisco Bay, California, at Dumbarton Bridge: 1990-1993 water years. US Geological Survey. Report nr Open-File Report 98-650.

Schoellhamer D. 1996. Factors affecting suspended-solids concentrations in South San Francisco Bay, California. Journal of Geophysical Research - Oceans 101(C5):12087-12095.

Sheldon JE, Alber M. 2006. The calculationof estuarine turnover times using freshwater fraction and tidal prism models: A critical evaluation. Estuaries and Coasts 29(1):133-146.

U.S. Army Corps of Engineers. 1984. Shore Protection Manual. Washington D.C. Vol.1 p.

U.S. Fish and Wildlife Service. 2005. 2004 Annual Self-Monitoring Report for Alviso Ponds within South San Francisco Bay Low Salinity Salt Ponds. Alameda, Santa Clara, and San Mateo Counties. Order No. R2-2004-0018, WDID No. 2 019438007.

U.S. Fish and Wildlife Service. 2006. 2005 Self Monitoring Program for Alviso Ponds WIthin South San Francisco Bay Low Salinity Ponds. Alameda, Santa Clara, & San Mateo Counties, California: California Regional Water Quality Control Board, San Francisco Bay Region. Report nr Order No. R2-2004-0018.

U.S. Fish and Wildlife Service, California Department of Fish and Game, David J Powers & Associates, H. T. Harvey & Associates, Philip Williams & Associates L. 2004. Draft Environmental Impact Statement, Environmental Impact Report: Bair Island Restoration and Management Plan, Don Edwards San Francisco Bay National Wildlife Refuge, Bair Island Ecological Preserve. San Mateo, California.

U.S. Fish and Wildlife Service, Santa Clara Valley Water District. 2006. Restoration and mitigation monitoring plan for the Island Ponds Restoration Project.

van Rijn LC. 1993. Principles of Sediment Transport in Rivers, Estuaries, and Coastal Seas. The Netherlands: Aqua Publications.
Walters RA, Cheng RT, Conomos TJ. 1985. Time scales of circulation and mixing processes of San Francisco Bay waters. Hydrobiologia 129: p13-36.
Wilcock P, Iverson R. 2003. Prediction in Geomorphology. In: Wilcock P, Iverson, RM, editor. Prediction in Geomorphology. Washington D.C.: American Geophysical Union.
Williams PB, Orr MK, Garrity NJ. 2002. Hydraulic geometry: A geomorphic design tool for tidal marsh channel evolution in wetland restoration projects. Restoration Ecology 10(3):577-590.
WL | Delft Hydraulics. 2003. Delft3D-FLOW, Simulation of multi-dimensional hydrodynamic flows and transport phenomena, including sediments. Delft, NL.

<This page intentionally left blank>

9. LIST OF PREPARERS

The following Team members assisted in preparation of this document:

Kris May, PWA
Gaurav Misra, PWA
Matt Brennan, PWA
Don Danmeier, PWA
Nick Garrity, PWA
Julie Stephenson, PWA
Matt Wickland, PWA
Phil Williams, PWA
David Brew, PWA

Source files for this report are located at PWA:
\\orca\projects\1750_SBSP\Task03c_Hydrodynamic_Modeling\Modeling_Report\Final_Draft

<This page intentionally left blank>

10. APPENDIX A – MODEL CALIBRATION SUMMARY

This section provides a summary of the calibration and validation results for both the GSFB and South Bay Models. The details with respect to both models and the complete calibration and validation are documented in the Hydrodynamic Model Calibration Report (PWA 2006a)

10.1 GSFB Model Calibration and Validation Summary

Model calibration for the GSFB Model was conducted using data from 2001 and 1980. Water level and salinity calibration was conducted using data from 2001; calibration of current velocities was conducted using data collected during 1980. The model was validated for summer 2000 and winter 2004 conditions. During each period, water levels were analyzed through the use of time series comparisons, statistical correlations and harmonic analysis. Predicted salinity was compared to observed salinity at fixed stations and predicted salinity transects were compared to USGS monitoring data.

During the 2001 calibration period the predicted water levels from the GSFB Model shows very good agreement with observed water levels based on the time series comparisons, correlations and harmonic analysis at all four stations analyzed. Similarly, the predicted salinity at the Oakland-Bay Bridge shows good agreement with observed salinity; slightly higher than observed salinity is predicted at the San Mateo Bridge. The predicted salinity transects show good agreement with observed salinity for the nine days during the simulation period when observation data were available.

During the 1980 simulation period, predicted water levels show a similar level of agreement with observed water levels as shown during the calibration period. Current velocities were compared against observed velocities at eleven stations in the South Bay. The predicted current velocities show good agreement with observed current velocities in terms of speed, direction, spring-neap variability, and trends in current velocity between deeper and shallower stations.

The water level comparisons for the summer 2000 validation period show a similar level of agreement to that achieved for the calibration period. Limited salinity data is available for validation during the summer 2000 period. Based on the limited data available, the GSFB Model tends to slightly under predict salinity relative to observations in summer 2000.

During the 2004 period the correlation between predicted and observed water levels is slightly lower than during the other periods, but relatively good agreement between predicted phase and amplitude of the major harmonic constituents is still achieved. The GSFB Model slightly over predicts salinity at San Mateo Bridge during the analysis period but shows better agreement at Dumbarton Bridge and Channel Marker 17.

Since the GSFB Model is run for a period of two to three months prior to each analysis period to demonstrate that the salinity field is fully spun-up, it is possible to assess the capacity of the GSFB Model to predict longer-term salinity trends. In this regard, the 2001 period shows relatively constant salinity at the Oakland-Bay Bridge and throughout the South Bay with only a very gradual increase in salinity during the simulation period. The GSFB Model predicts salinity exceptionally well during this period (Figure 10-1 through Figure 10-5). The 2000 simulation period begins with relatively fresh conditions in much of South Bay and salinity increases by more than 5 ppt in much of the South Bay during the simulation period. The GSFB Model captures some of this trend but tends to slightly under predict salinity by the end of the simulation period (Figure 10-6 through Figure 10-9). In contrast, during the 2004 simulation period the salinity in the South Bay starts relatively high and tends to become fresher as the simulation progresses (Figure 10-10 through Figure 10-14) as a result of flow events during the simulation period. Although the model tends to over predict salinity somewhat at the end of the simulation period, much of this freshening trend is captured in the predicted salinity. Given the limited grid resolution—particularly south of Dumbarton Bridge in the GSFB Model (Figure 2-2) with grid cell sizes ranging from 300 to 400 m in this region—the predicted salinity in the far South Bay compares reasonably well with observed salinities.

Overall the GSFB Model shows good agreement with observed water levels, salinity, and current velocities under the range of conditions simulated. In particular, the GSFB Model shows very good agreement with observed water levels near the Oakland-Bay Bridge which demonstrates that it provides a suitable boundary condition for the South Bay Model. The predicted salinity fields from the GSFB Model show reasonable agreement with observed salinity during most periods and can therefore provide a suitable initial salinity condition for the South Bay Model.

10.2 South Bay Model Calibration and Validation Summary

Model calibration for the South Bay Model was conducted using data from 2001 and 1980. Water level and salinity calibration was conducted using data from 2001; calibration of current velocities was conducted using data collected during 1980. The model was validated for summer 2000 and winter 2004 conditions. During each period, water levels were analyzed through the use of time series comparisons, statistical correlations and harmonic analysis. Predicted salinity was compared to observed salinity at fixed stations and predicted salinity transects were compared to USGS monitoring data. The 2001, 2000 and 2004 South Bay simulations span a period of six weeks, with two weeks for spin-up preceding each 29-day analysis period.

During the 2001 calibration period, the predicted water levels from the South Bay period show very good agreement with observed water levels at the Alameda, Redwood City, and Channel Marker 20 stations. At the Railroad Bridge station, the predicted tides tend to lag the observed tides somewhat and there is some damping of tidal amplitude, particularly near low water. Overall the predicted water levels from the South Bay show a similar to better agreement with predicted water levels from the GSFB Model for the same calibration period.

During the South Bay Model 1980 simulation period, predicted water levels show a similar level agreement with observed water levels as during the calibration period. Current velocities were compared against observed velocities at eleven stations in the South Bay. The predicted current velocities show good agreement with observed current velocities in terms of speed, direction, spring-neap variability, and trends in current velocity between deeper and shallower stations. A similar level of agreement with observed current velocities was achieved in the South Bay Model to that achieved in the GSFB Model for the same period.

The water level comparisons for the South Bay Model during the summer 2000 validation period show a similar level of agreement to that achieved for the calibration period. Based on the limited salinity data available for validation during the summer 2000 period, the South Bay Model shows a similar tendency as the GSFB Model to slightly under predict salinity relative to observations during the summer 2000 analysis period. Much of this may result from the initial condition transferred from the GSFB Model.

During the 2004 period, the correlation between predicted and observed water levels in the South Bay Model is slightly lower than during the other periods, which is the same trend observed in the GSFB Model. Overall, relatively good agreement between predicted phase and amplitude of the major harmonic constituents is achieved. The 2004 validation period offered the most extensive available salinity data in the far South Bay of any of the simulated periods. In addition, two freshwater flow events during this period provide an opportunity to evaluate the model's response to varying flow conditions. Although some differences exist between predicted and observed salinity, overall, the South Bay Model salinity comparisons for the 2004 period (Figure 10-15 through Figure 10-22) demonstrate that the South Bay Model is predicting a reasonable salinity range, similar semi-diurnal variability, and a similar response to flow events in much of the far South Bay. Given the limitations in accurately predicting salinity using a 2D model, a reasonable level of agreement between observed and predicted salinities is achieved over the three different analysis periods.

Overall, the South Bay Model shows very similar results to the GSFB Model in much of the South Bay. However, the South Bay Model provides significantly higher grid resolution in the far South Bay and therefore allows for more accurate predictions in areas not well-resolved in the GSFB Model. As a result, the South Bay Model calibration and validation made use of data in the far South Bay for both water level and salinity comparisons which were not used in the GSFB Model comparisons. In general the South Bay Model agrees favorably with predicted water levels and salinity in the far South Bay. However, the comparisons of observed and predicted water levels at the Railroad Bridge in Coyote Creek highlight that some damping of tidal amplitude occurs in the far South Bay, particularly near low water. In particular, the solution scheme used in DELFT3D appears to result in energy dissipation in channels which are not aligned with the grid (i.e. "stair-step" channels) when the channel is only one cell wide. This effect is most dominant at low water when only a single row of channel cells are wet and can lead to an under prediction of tidal range in narrow sloughs with increasing distance from the Bay. The use of finer grid resolution for project-level modeling would allow for more grid resolution across slough channels and help to reduce this effect.

<This page intentionally left blank>

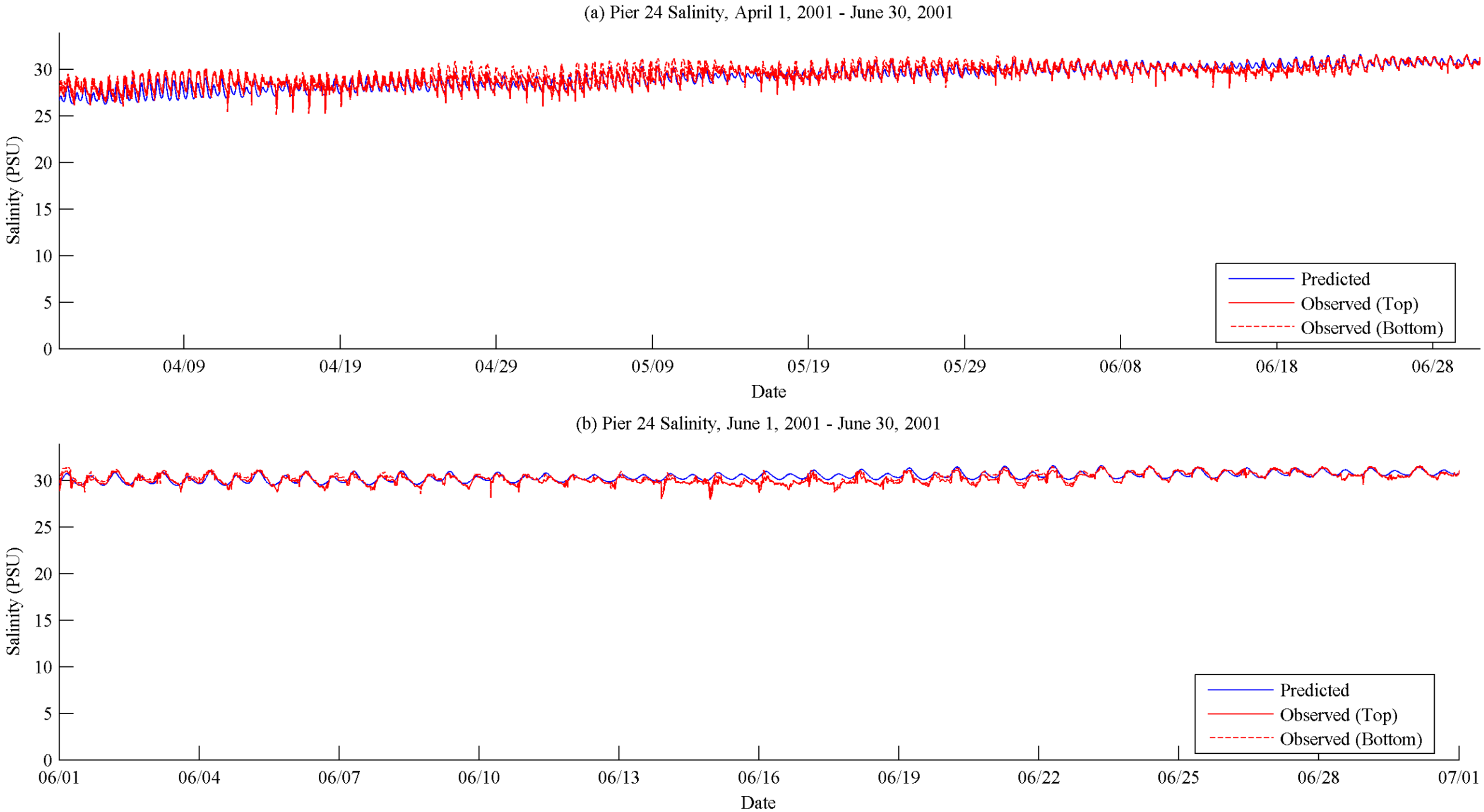

These plots compare model predicted and measured salinities at the Pier 24 station, located at the western end of the Bay Bridge. (A) shows the full time series of the calibration run, excluding one month of spin-up time. (B) shows greater detail, focusing only on the one month analysis period

figure 10-1

South Bay Salt Pond Restoration Project

GSFB Summer 2001 Salinity, Pier 24/Bay Bridge

PWA

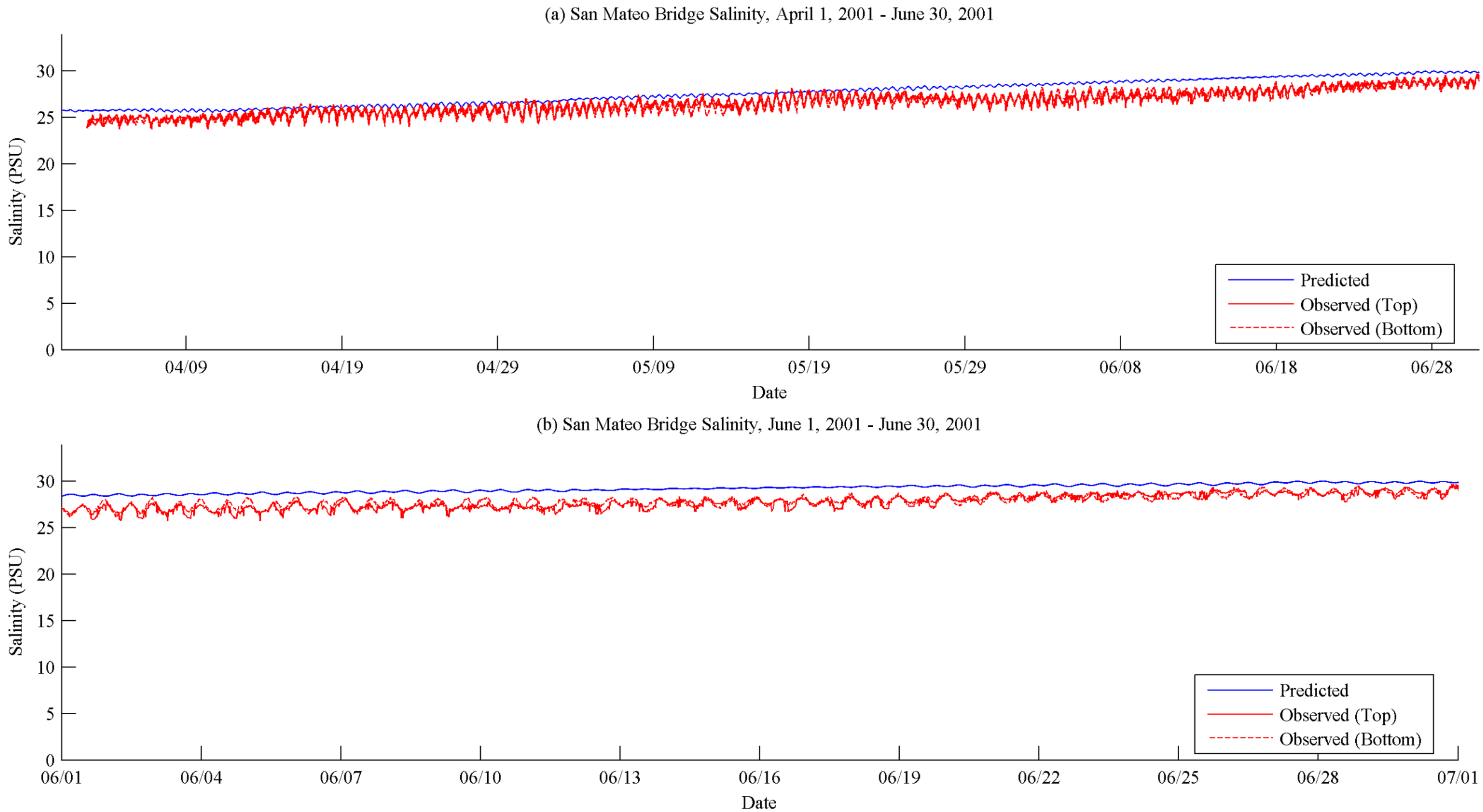

These plots compare model predicted and measured salinities at the San Mateo Bridge station. (A) shows the full time series of the calibration run, excluding one month of spin-up time. (B) shows greater detail, focusing only on the one month analysis period..

figure 10-2

South Bay Salt Pond Restoration Project

GSFB Summer 2001 Salinity, San Mateo Bridge

PWA

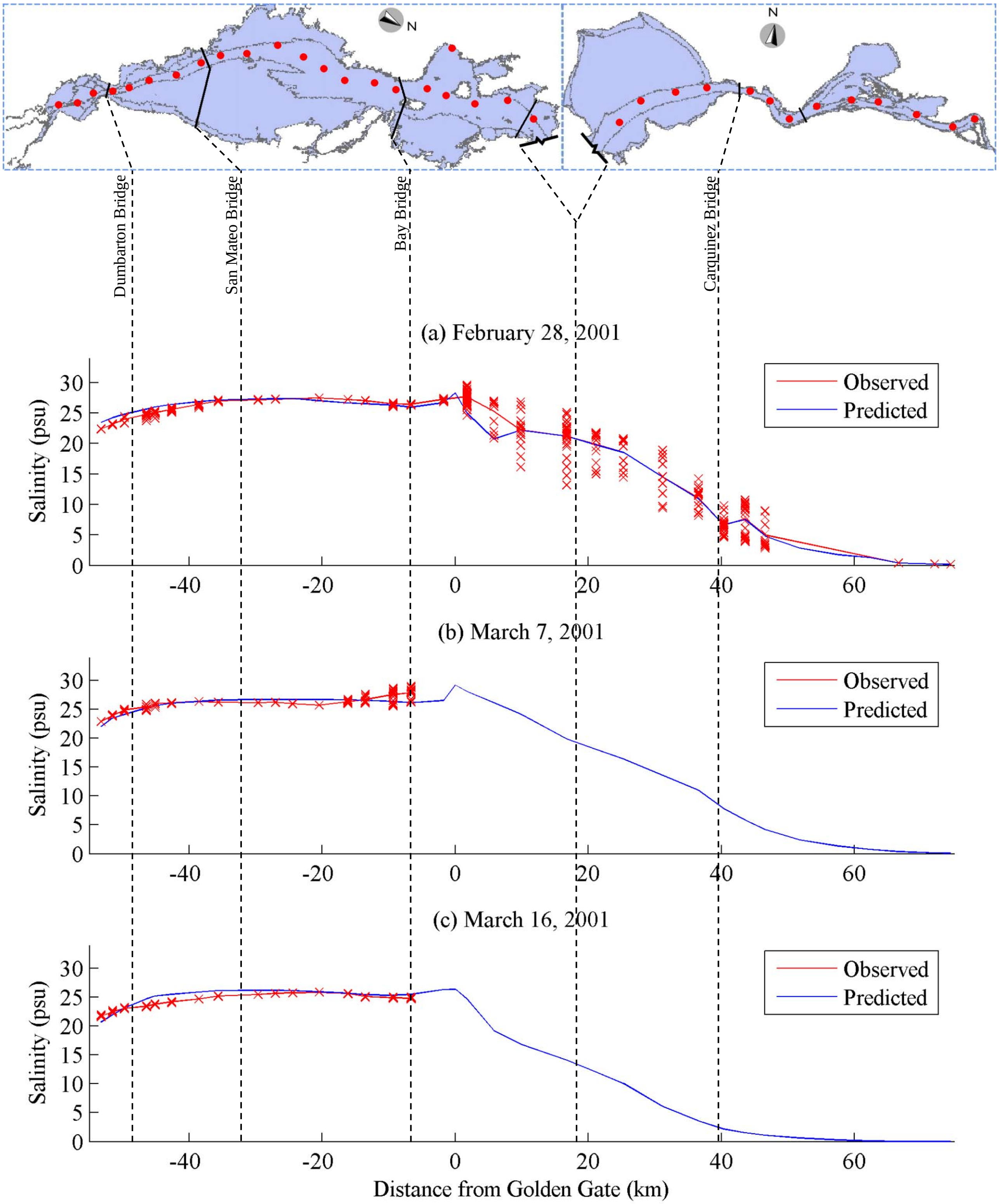

This figure compares salinity data collected by the USGS San Francisco Bay Water Quality Monitoring Program against modeled predictions at the same stations. The observation data shows all samples collected during the USGS depth transect; the observed line is plotted through the depth-averaged values.

figure 10-3

South Bay Salt Pond Restoration Project

GSFB Summer 2001 Salinity Transect

PWA

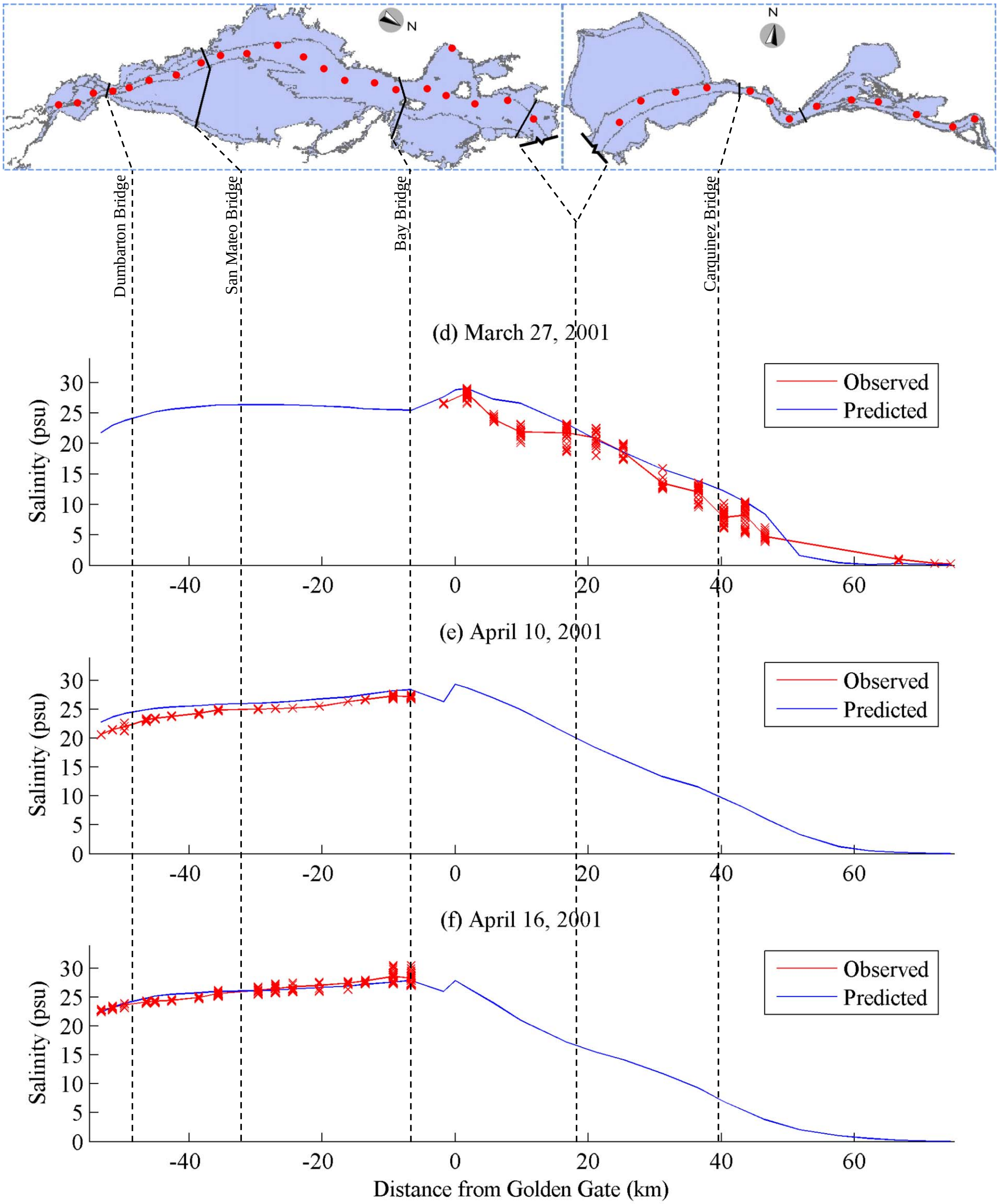

This figure compares salinity data collected by the USGS San Francisco Bay Water Quality Monitoring Program against modeled predictions at the same stations. The observation data shows all samples collected during the USGS depth transect; the observed line is plotted through the depth-averaged values.

figure 10-4

South Bay Salt Pond Restoration Project

GSFB Summer 2001 Salinity Transect

PWA

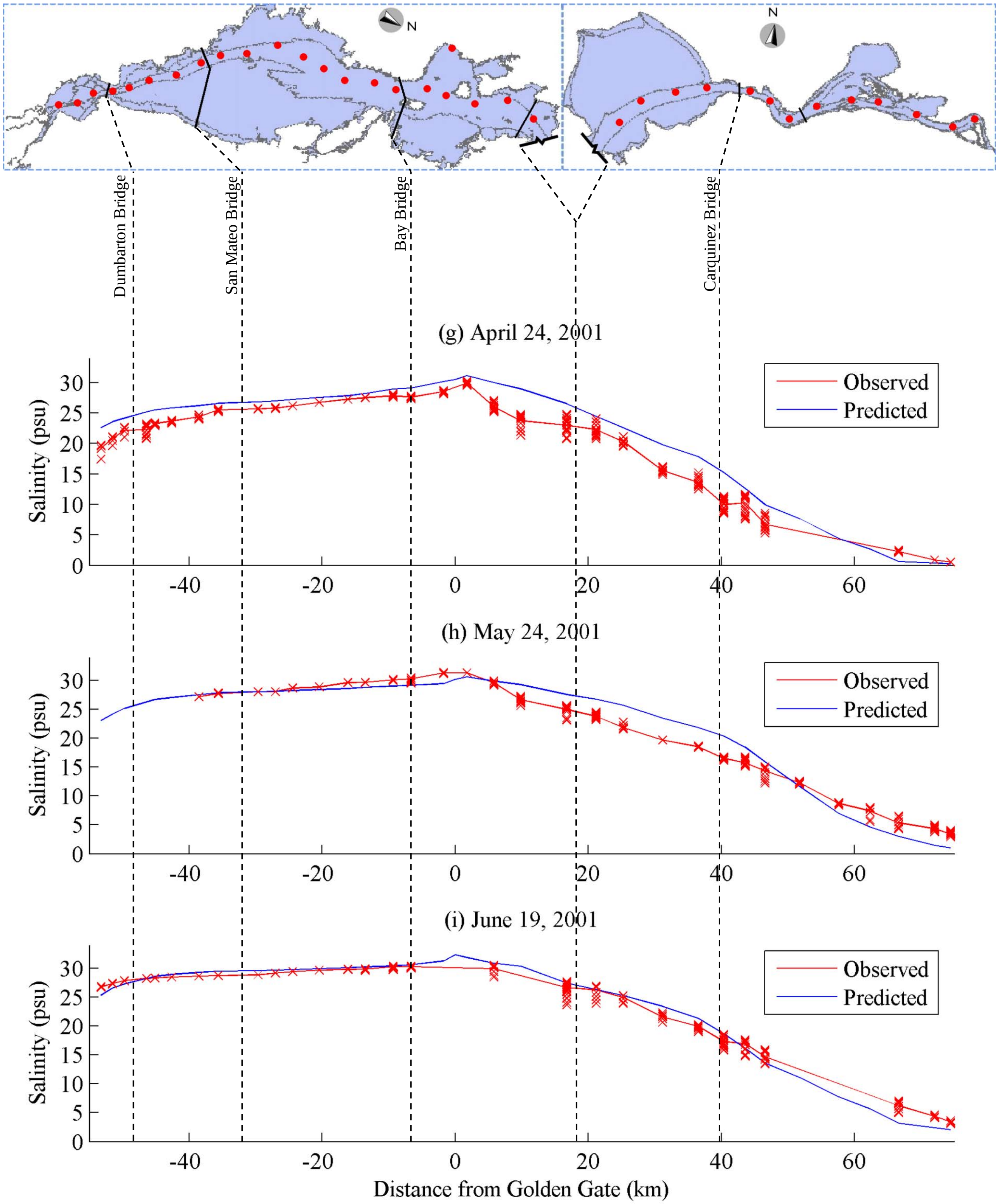

This figure compares salinity data collected by the USGS San Francisco Bay Water Quality Monitoring Program against modeled predictions at the same stations. The observation data shows all samples collected during the USGS depth transect; the observed line is plotted through the depth-averaged values.

figure 10-5

South Bay Salt Pond Restoration Project

GSFB Summer 2001 Salinity Transect

PWA

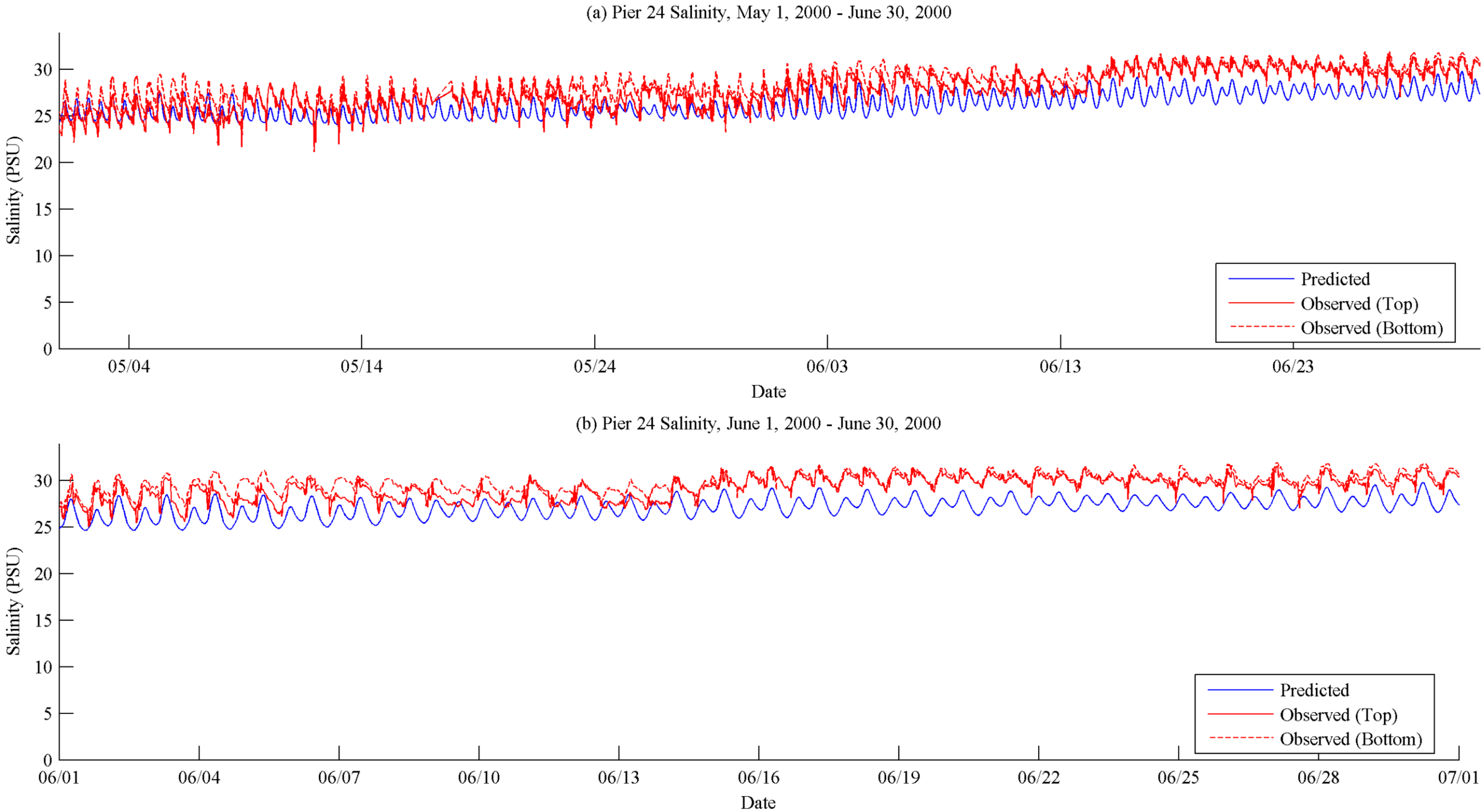

These plots compare model predicted and measured salinities at the Pier 24 station, located at the western end of the Bay Bridge. (A) shows the full time series of the calibration run, excluding one month of spin-up time. (B) shows greater detail, focusing only on the one month analysis period..

figure 10-6

South Bay Salt Pond Restoration Project

GSFB Summer 2000 Salinity, Pier 24/Bay Bridge

PWA

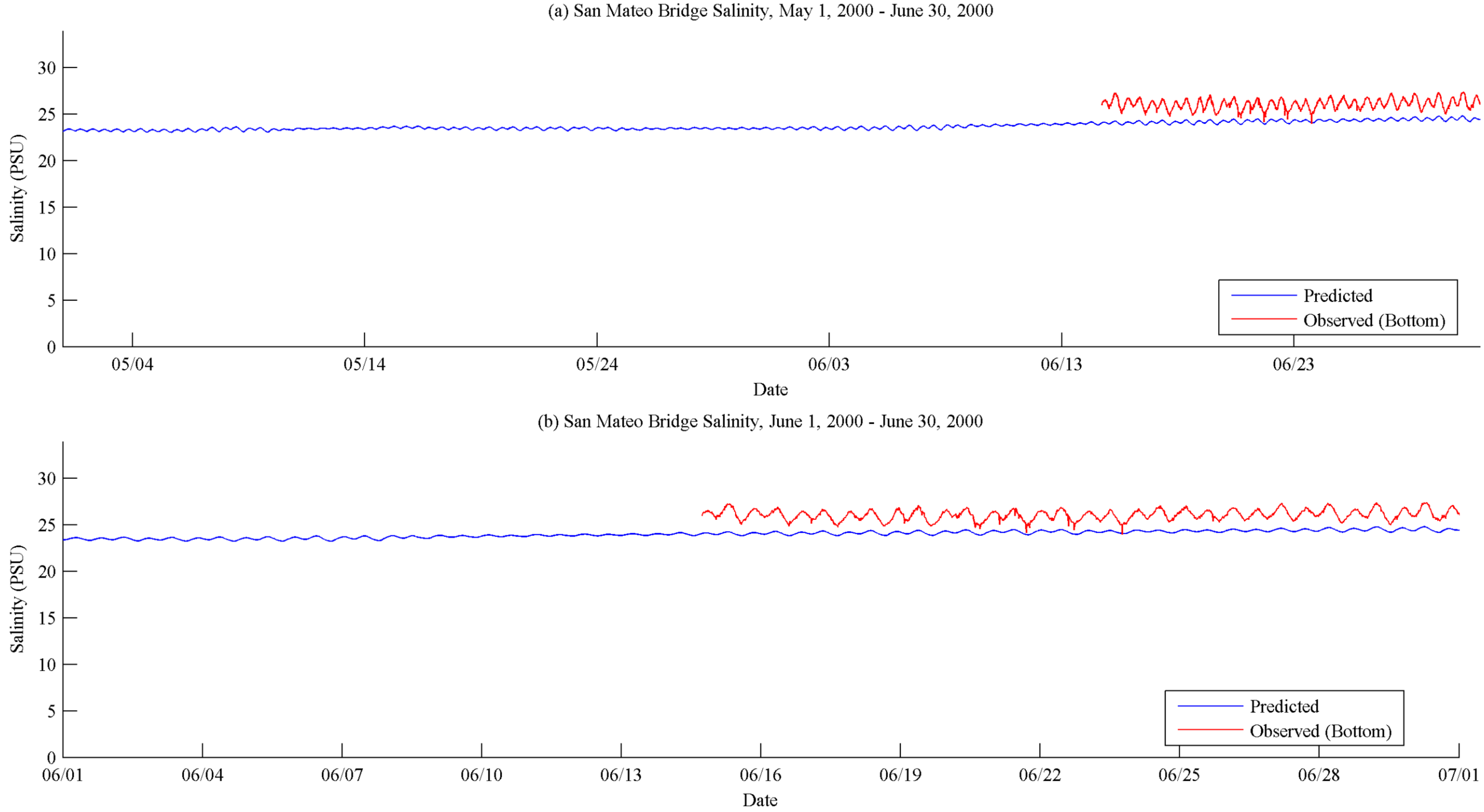

These plots compare model predicted and measured salinities at the San Mateo Bridge station. (A) shows the full time series of the calibration run, excluding one month of spin-up time. (B) shows greater detail, focusing only on the one month analysis period.

figure *10-7*

South Bay Salt Pond Restoration Project

GSFB Summer 2000 Salinity, San Mateo Bridge

PWA

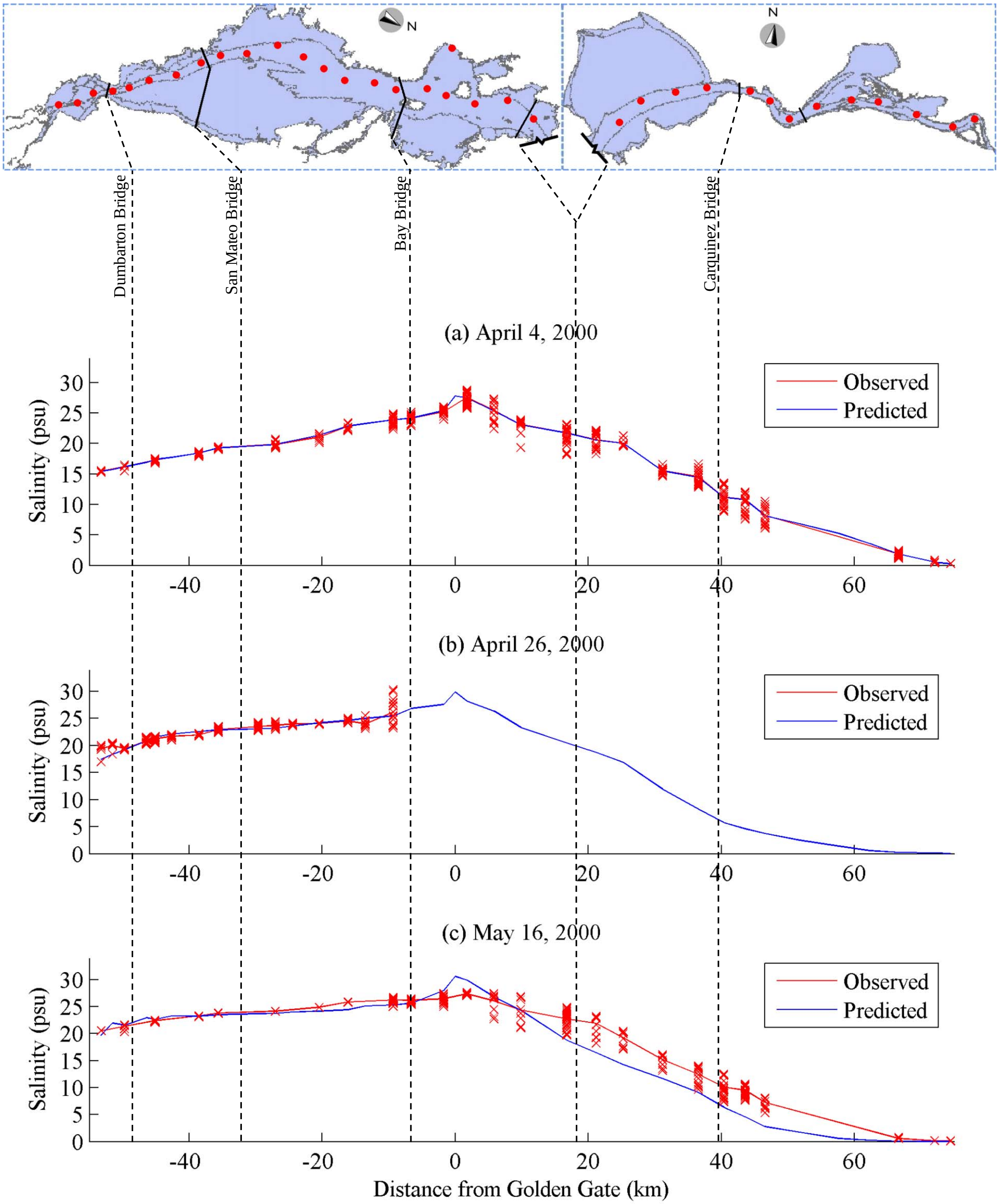

This figure compares salinity data collected by the USGS San Francisco Bay Water Quality Monitoring Program against modeled predictions at the same stations. The observation data shows all samples collected during the USGS depth transect; the observed line is plotted through the depth-averaged values.

figure 10-8

South Bay Salt Pond Restoration Project

GSFB Summer 2000 Salinity Transect

PWA

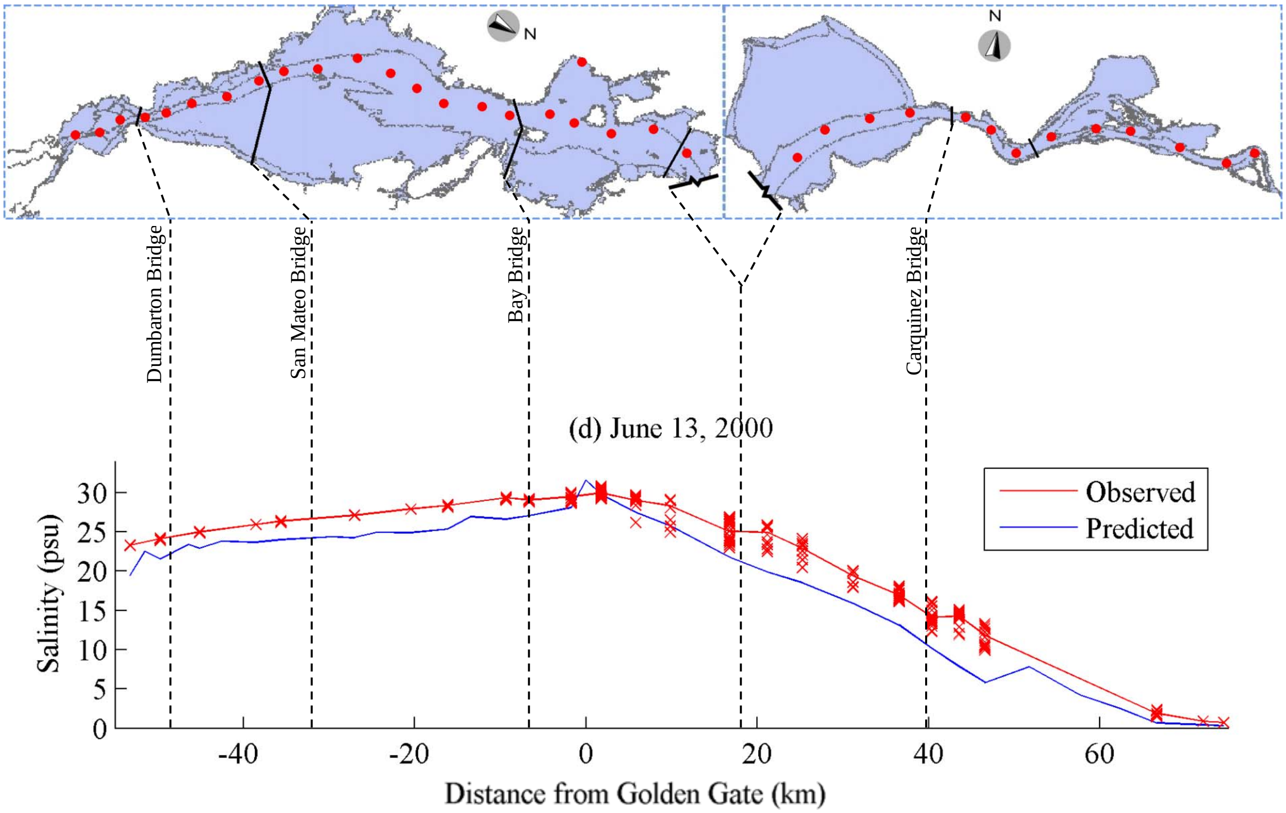

This figure compares salinity data collected by the USGS San Francisco Bay Water Quality Monitoring Program against modeled predictions at the same stations. The observation data shows all samples collected during the USGS depth transect; the observed line is plotted through the depth-averaged values.

figure 10-9

South Bay Salt Pond Restoration Project

GSFB Summer 2000 Salinity Transect

PWA

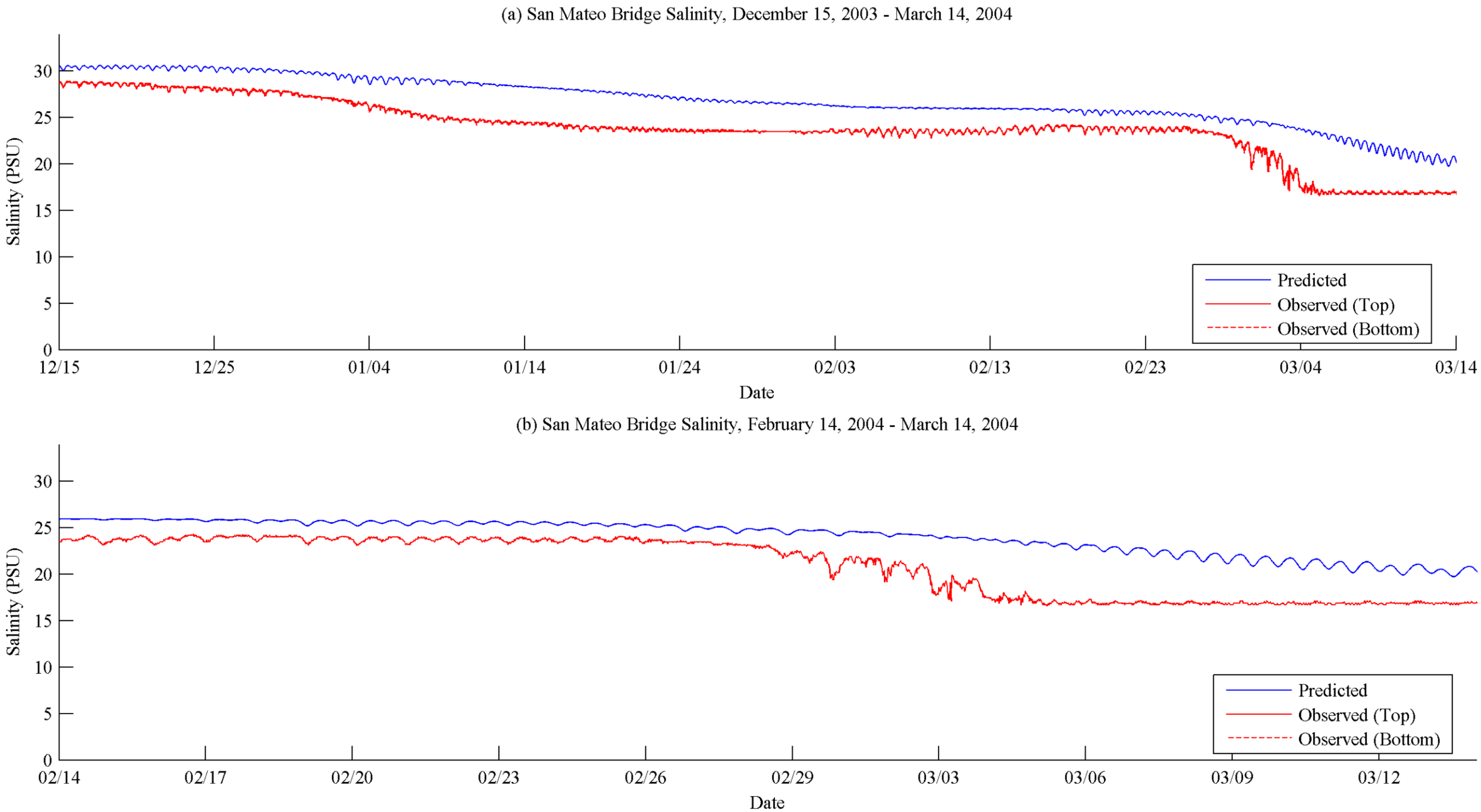

These plots compare model predicted and measured salinities at the San Mateo Bridge station. (A) shows the full time series of the calibration run, excluding one month of spin-up time. (B) shows greater detail, focusing only on the one month analysis period.

figure *10-10*

South Bay Salt Pond Restoration Project

GSFB Winter 2004 Salinity, San Mateo Bridge

PWA

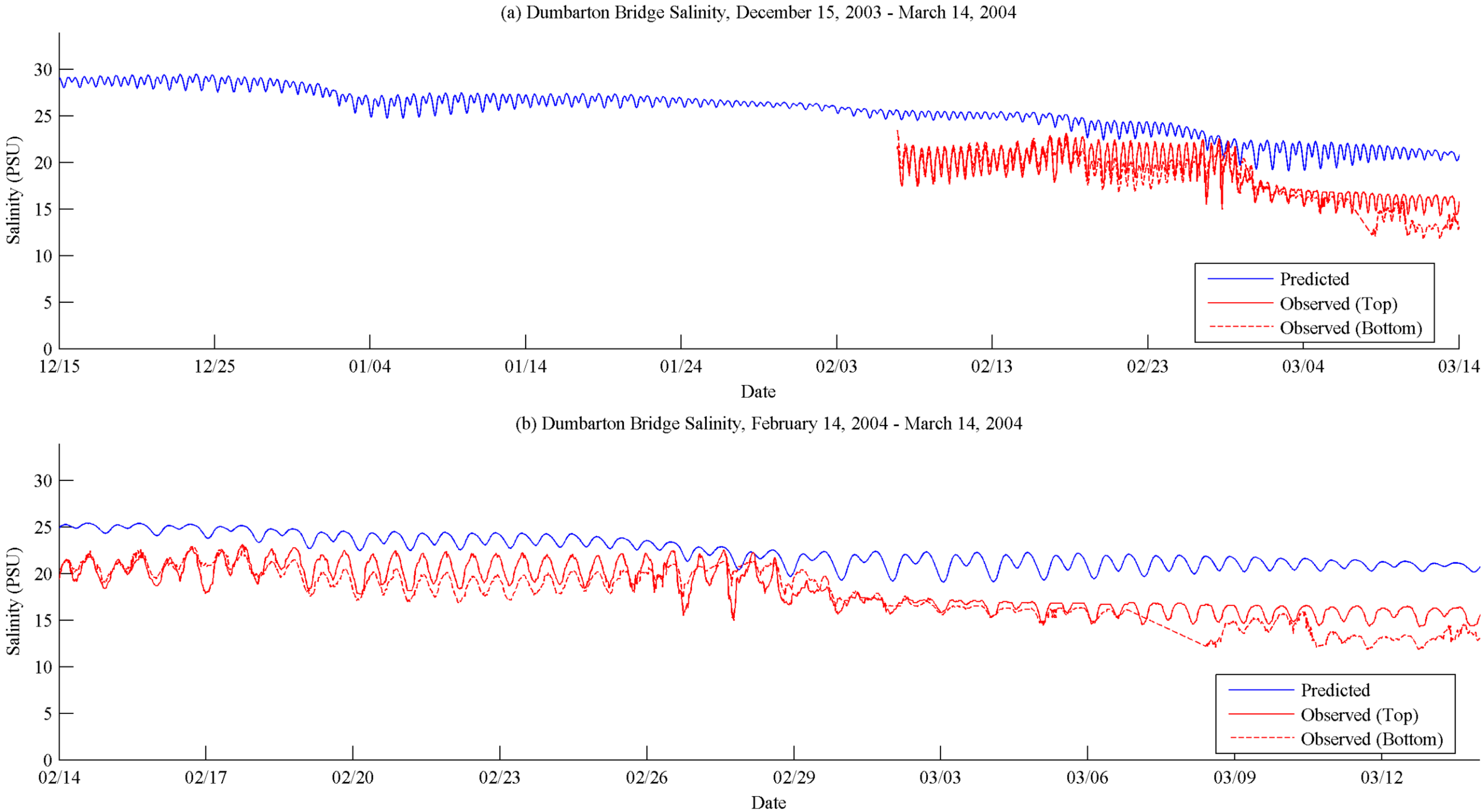

These plots compare model predicted and measured salinities at the Channel Marker 17 station. (A) shows the full time series of the calibration run, excluding one month of spin-up time. (B) shows greater detail, focusing only on the one month analysis period.

figure 10-11

South Bay Salt Pond Restoration Project

GSFB Winter 2004 Salinity, Dumbarton Bridge

PWA

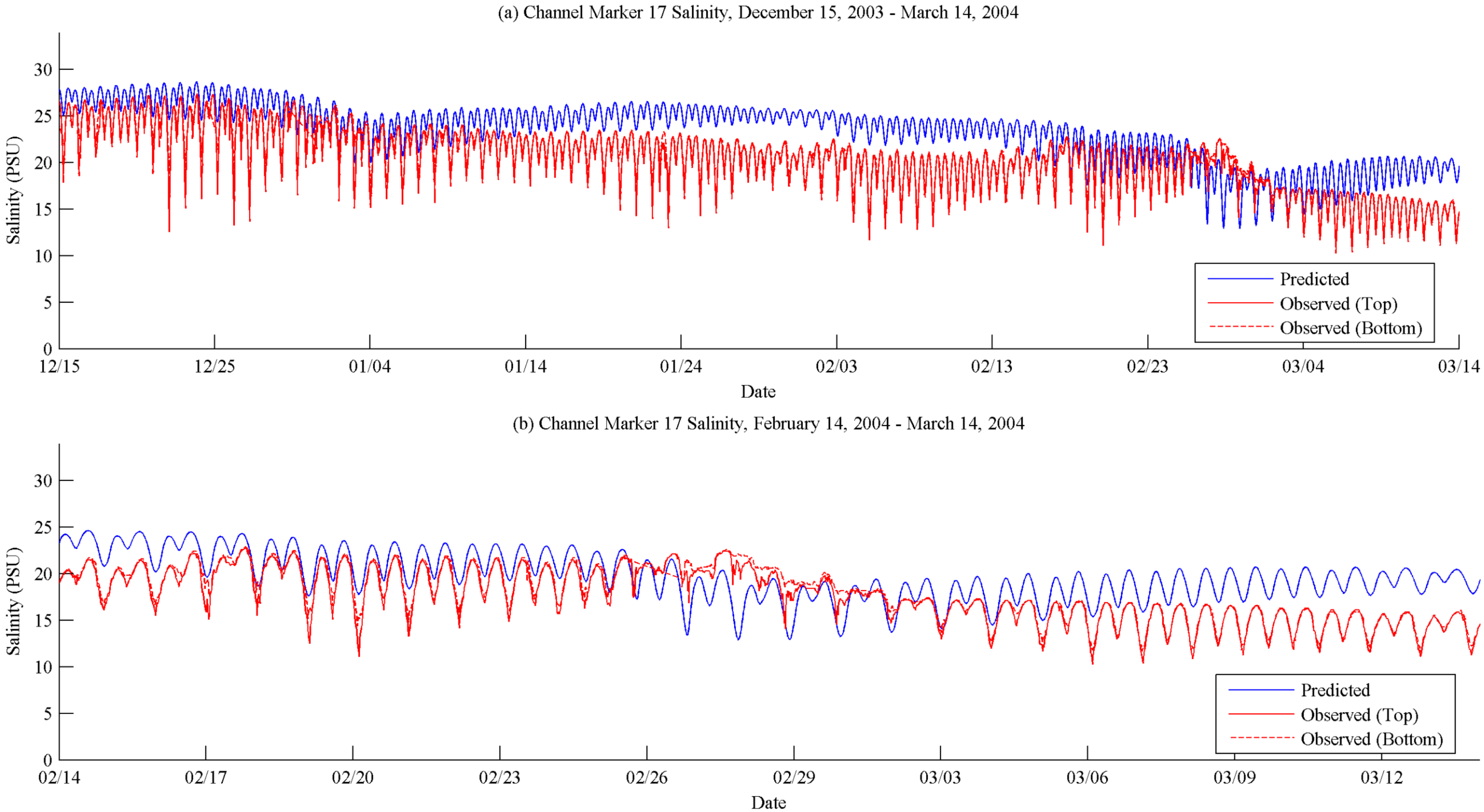

These plots compare model predicted and measured salinities at the Channel Marker 17 station. (A) shows the full time series of the calibration run, excluding one month of spin-up time. (B) shows greater detail, focusing only on the one month analysis period.

figure 10-12

South Bay Salt Pond Restoration Project

GSFB Winter 2004 Salinity, Channel Marker 17

PWA

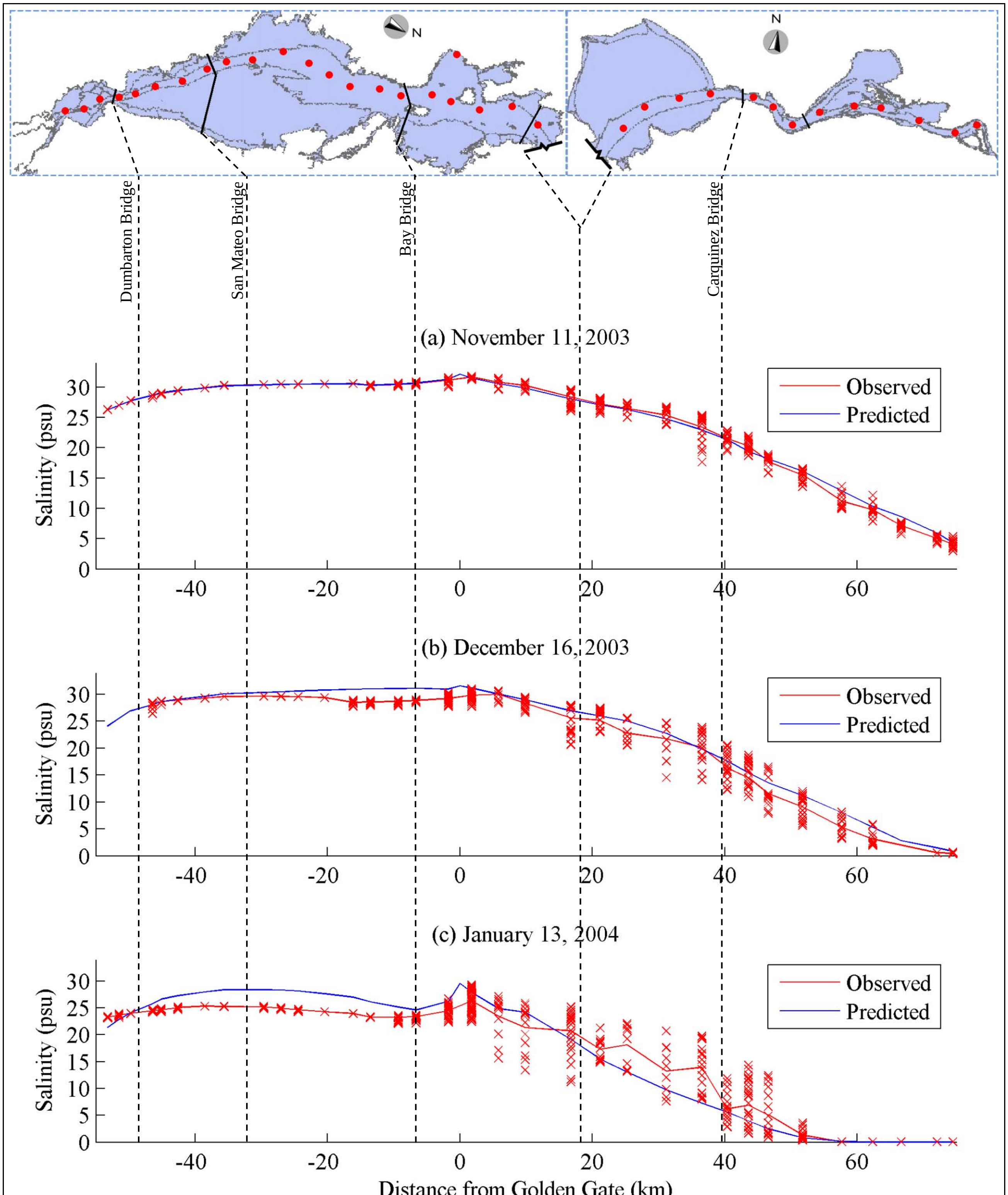

This figure compares salinity data collected by the USGS San Francisco Bay Water Quality Monitoring Program against modeled predictions at the same stations. The observation data shows all samples collected during the USGS depth transect; the observed line is plotted through the depth-averaged values.

figure 10-13

South Bay Salt Pond Restoration Project

GSFB Winter 2004 Salinity Transect

PWA

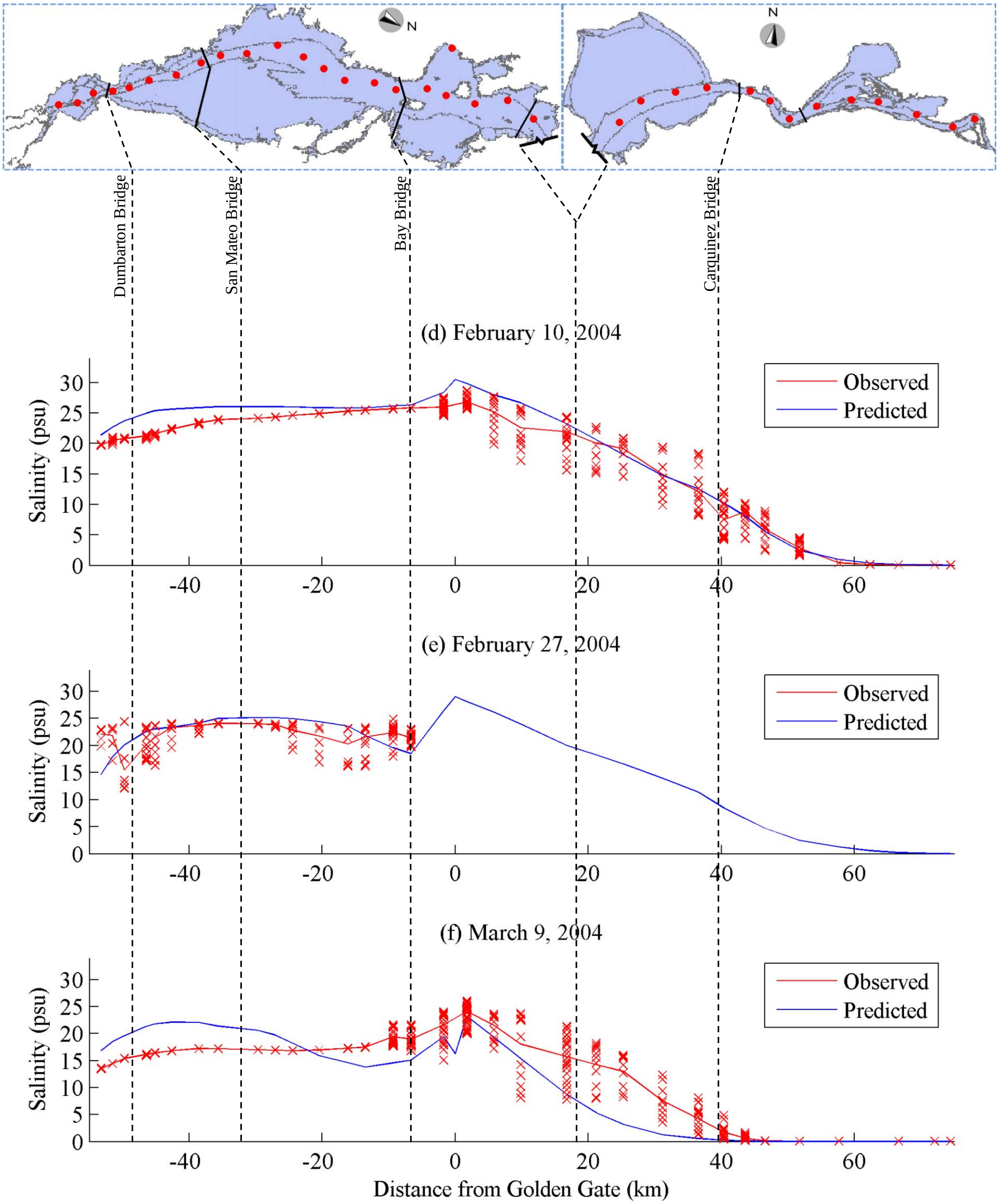

This figure compares salinity data collected by the USGS San Francisco Bay Water Quality Monitoring Program against modeled predictions at the same stations. The observation data shows all samples collected during the USGS depth transect; the observed line is plotted through the depth-averaged values.

figure 10-14

South Bay Salt Pond Restoration Project

GSFB Winter 2004 Salinity Transect

PWA

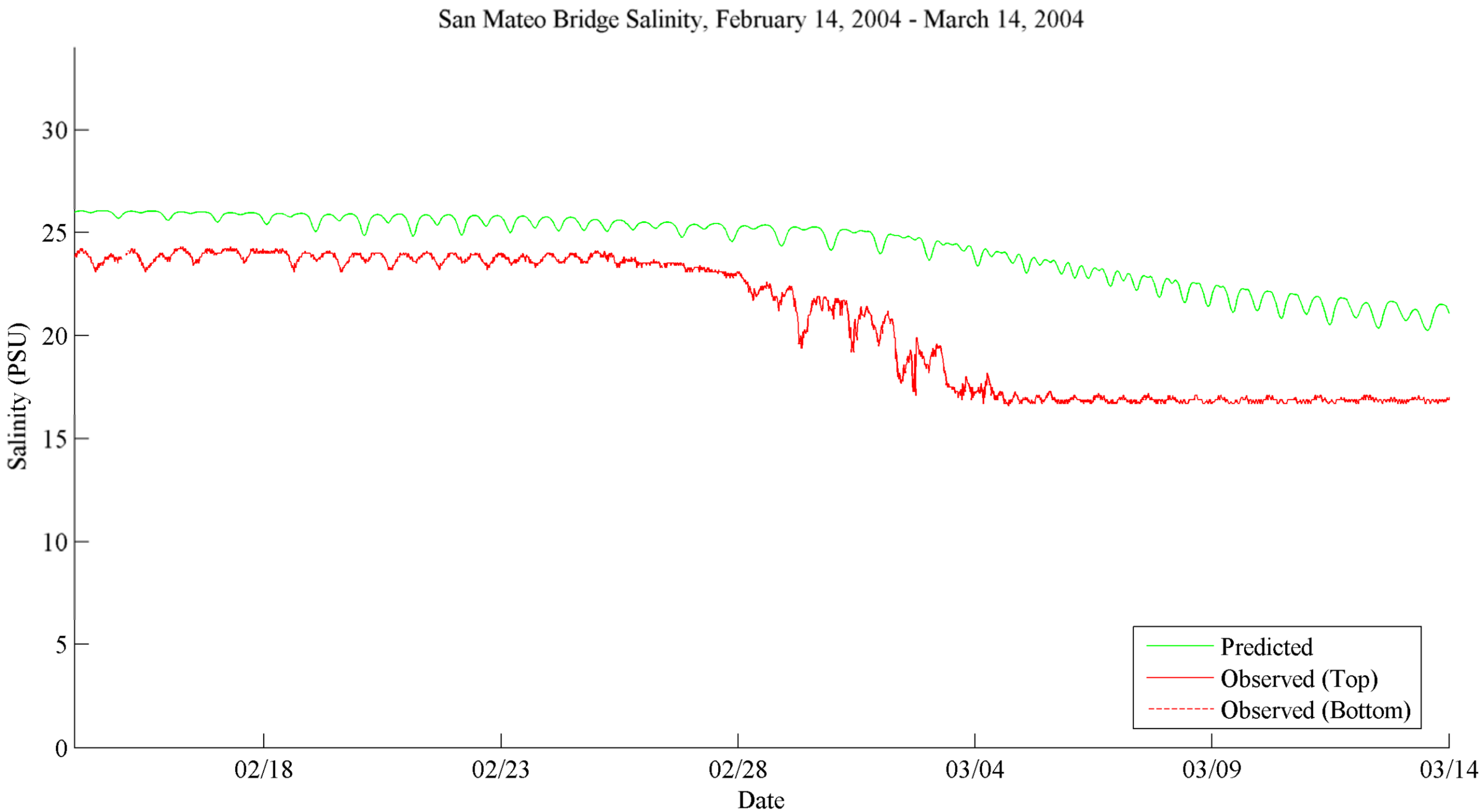

South San Francisco Bay Model

These plots compare model predicted and measured salinities at the San Mateo Bridge station.

figure 10-15

South Bay Salt Pond Restoration Project

South Bay Winter 2004 Salinity, San Mateo Bridge

PWA

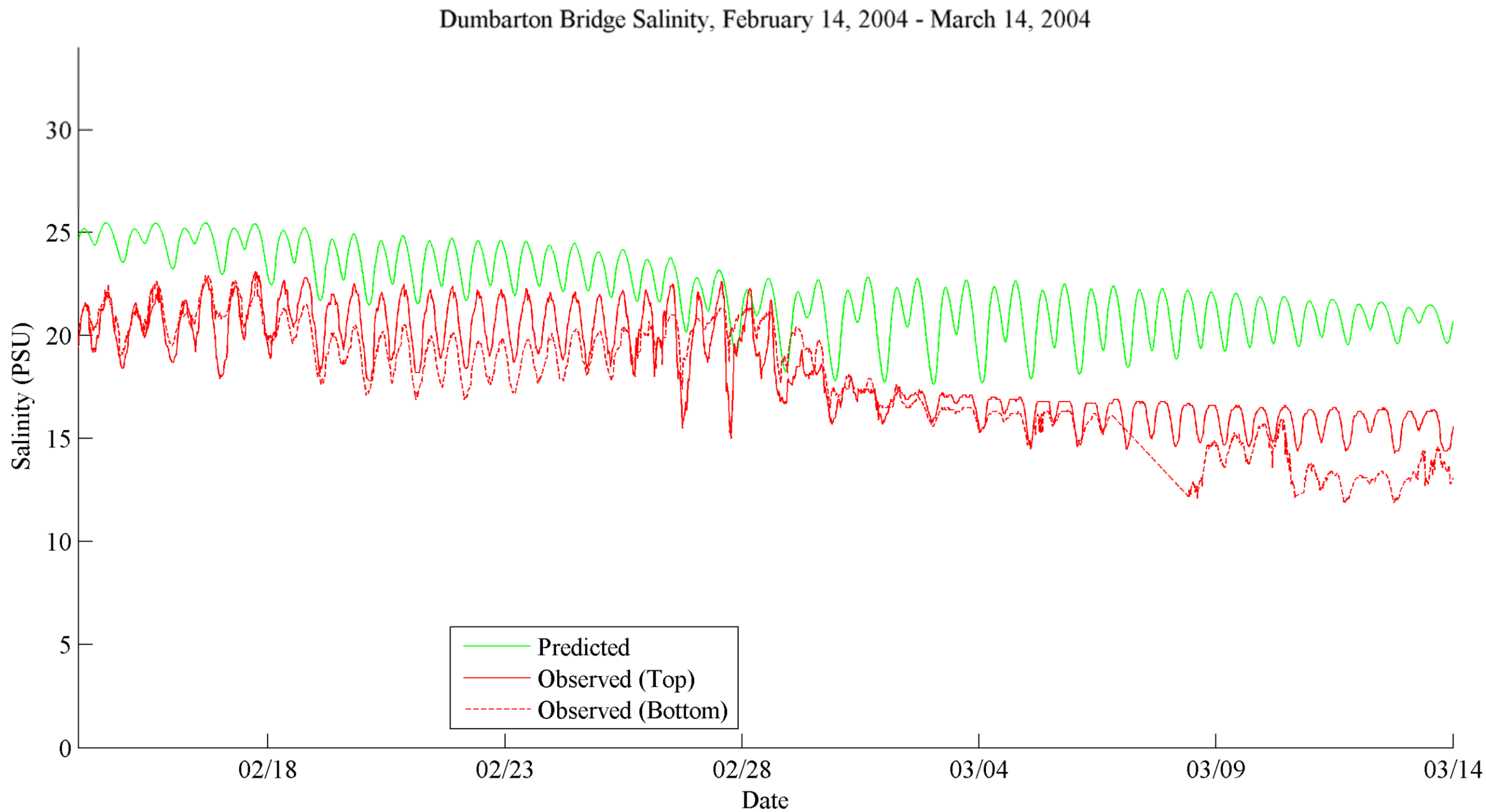

South San Francisco Bay Model

These plots compare model predicted and measured salinities at the Dumbarton Bridge station.

figure 10-16

South Bay Salt Pond Restoration Project

South Bay Winter 2004 Salinity, Dumbarton Bridge

PWA

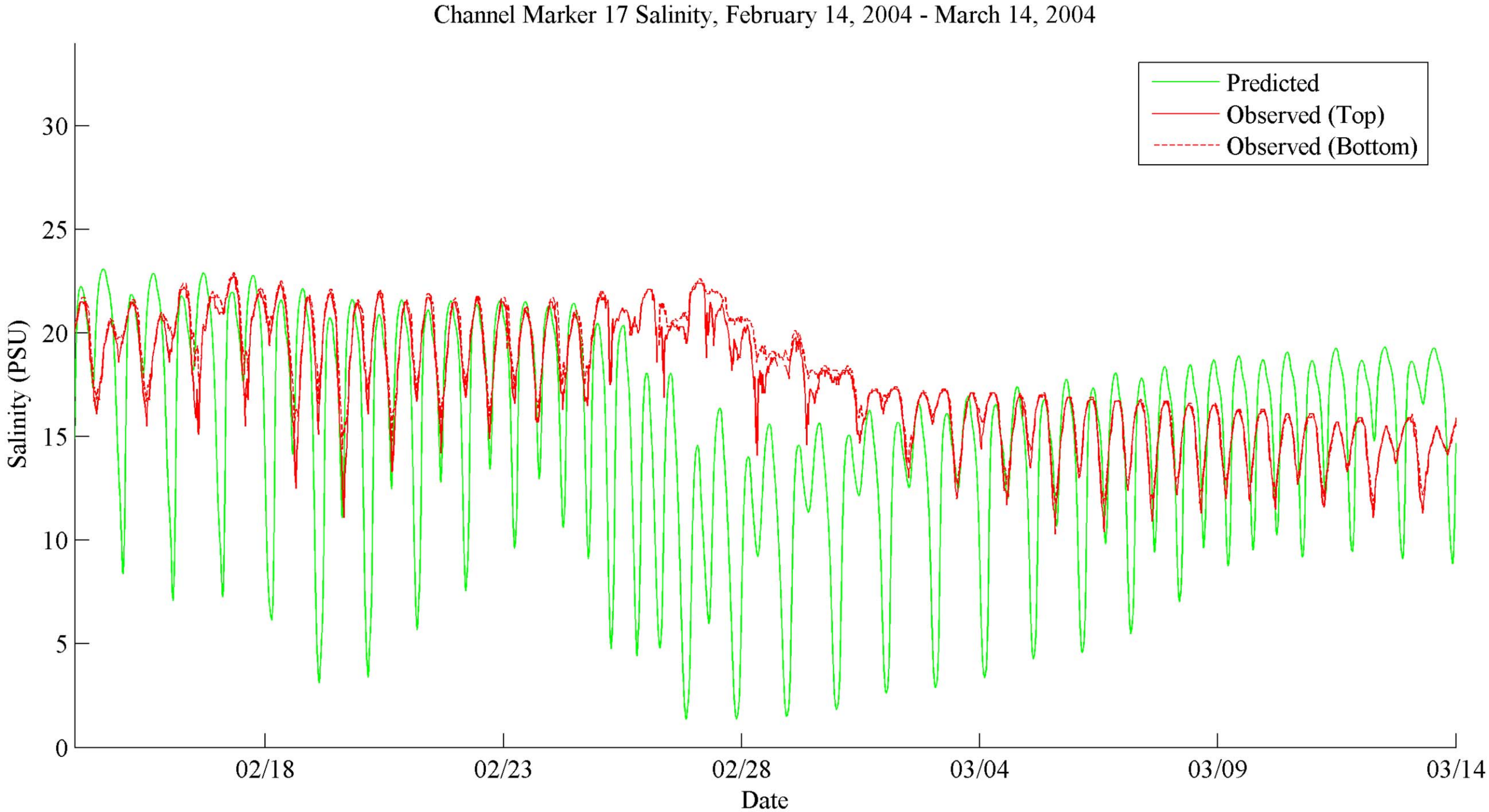

South San Francisco Bay Model

These plots compare model predicted and measured salinities at the Channel Marker 17 station.

figure 10-17

South Bay Salt Pond Restoration Project

South Bay Winter 2004 Salinity, Channel Marker 17

PWA

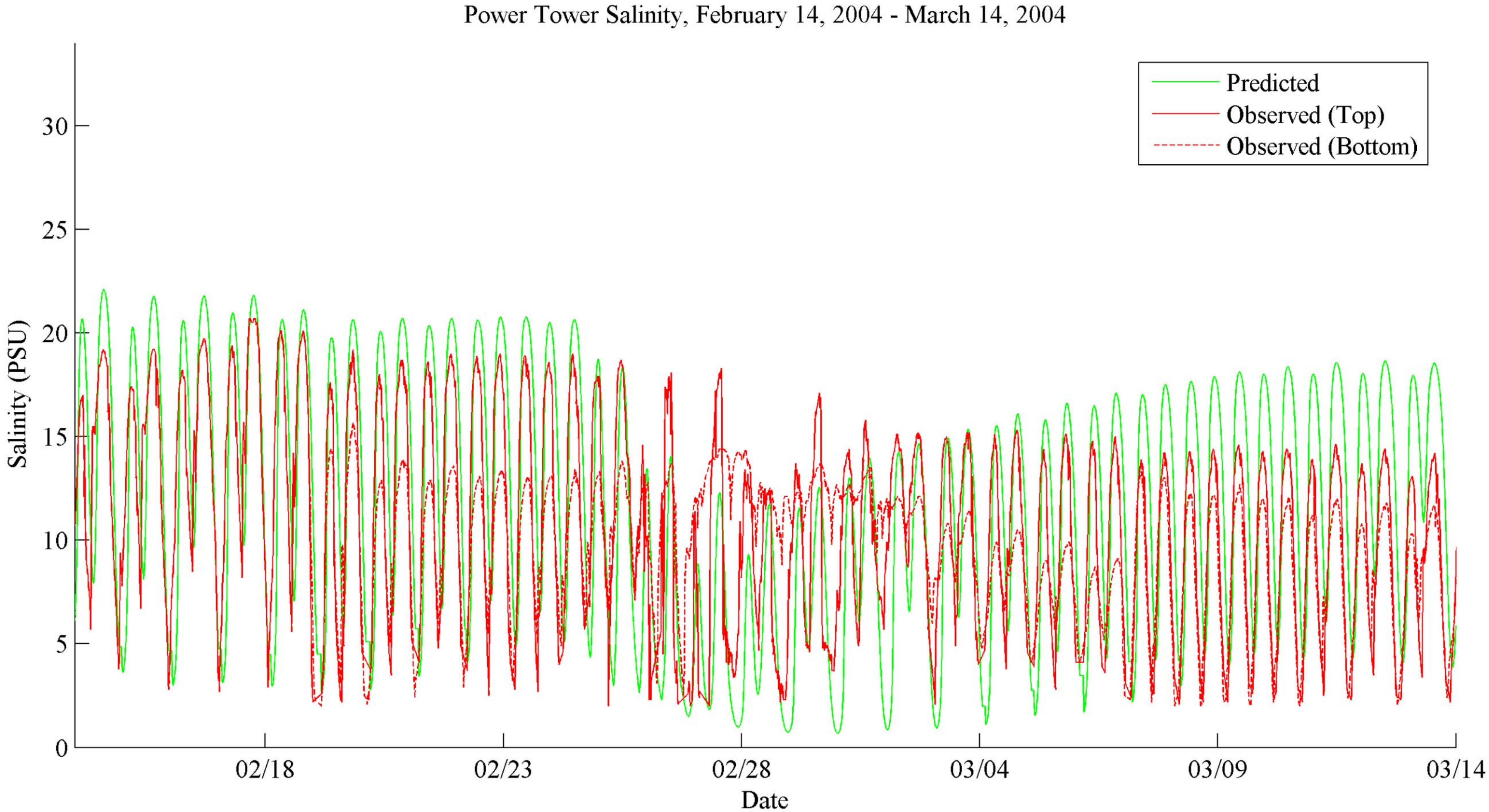

South San Francisco Bay Model

These plots compare model predicted and measured salinities at the Power Tower station.

figure 10-18

South Bay Salt Pond Restoration Project

South Bay Winter 2004 Salinity, Power Tower

PWA

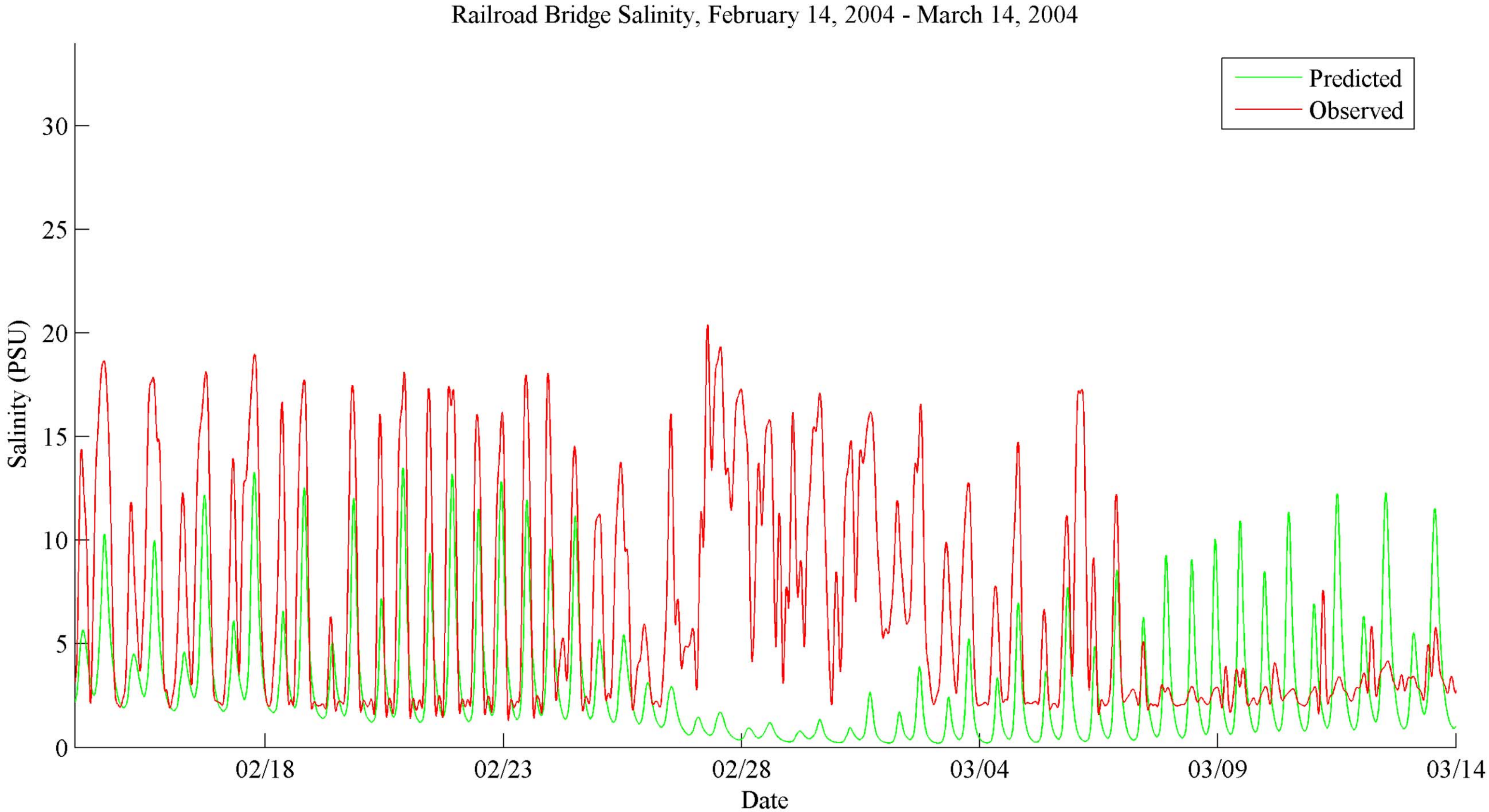

South San Francisco Bay Model

These plots compare model predicted and measured salinities at the Railroad Bridge station.

figure 10-19

South Bay Salt Pond Restoration Project

South Bay Winter 2004 Salinity, Railroad Bridge

PWA

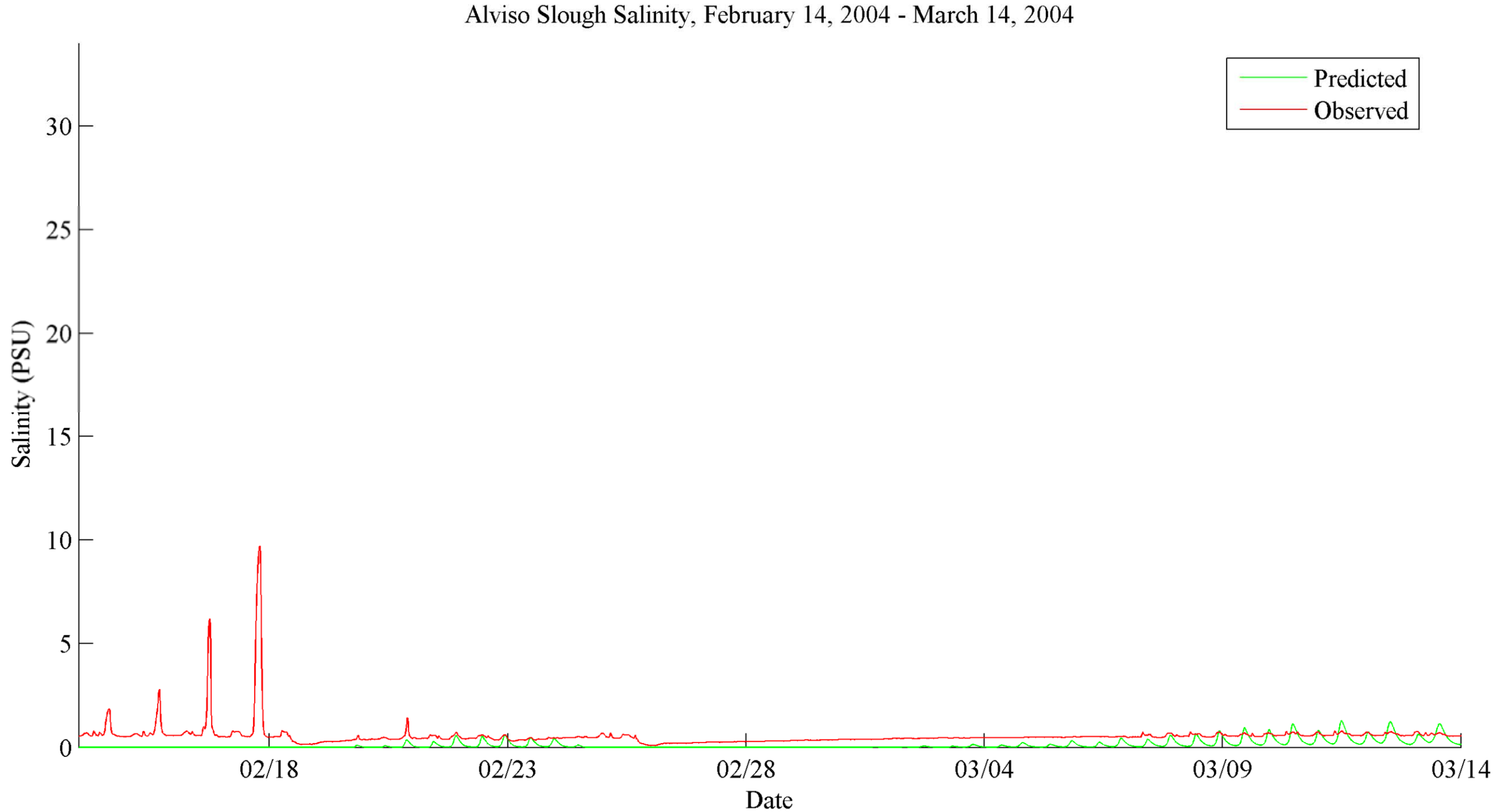

South San Francisco Bay Model

These plots compare model predicted and measured salinities at the Alviso Slough station.

figure 10-20

South Bay Salt Pond Restoration Project

South Bay Winter 2004 Salinity, Alviso Slough

PWA

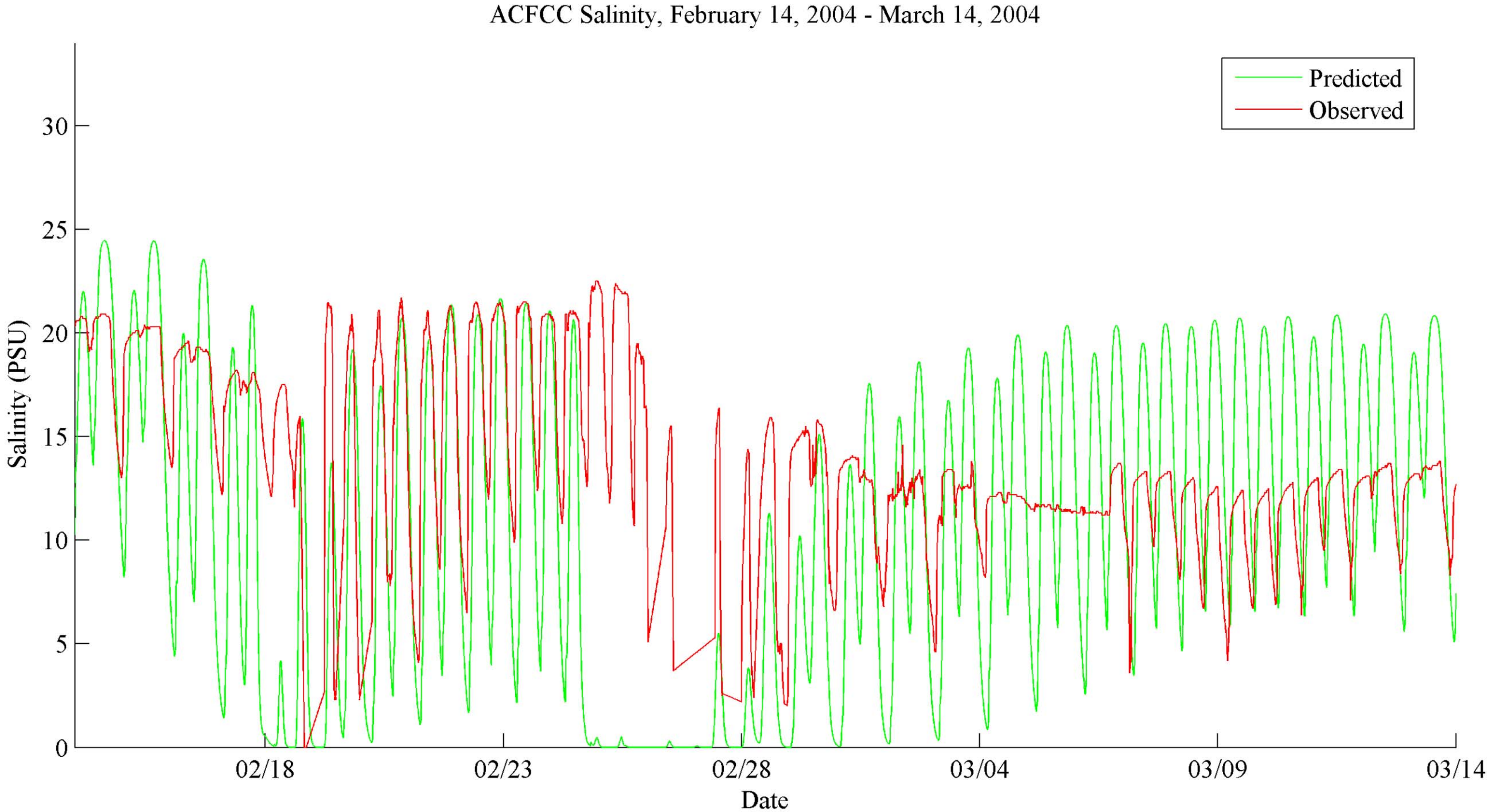

South San Francisco Bay Model

These plots compare model predicted and measured salinities at the Alameda County Flood Control Channel (ACFCC) station.

figure 10-21

South Bay Salt Pond Restoration Project

South Bay Winter 2004 Salinity, ACFCC

PWA

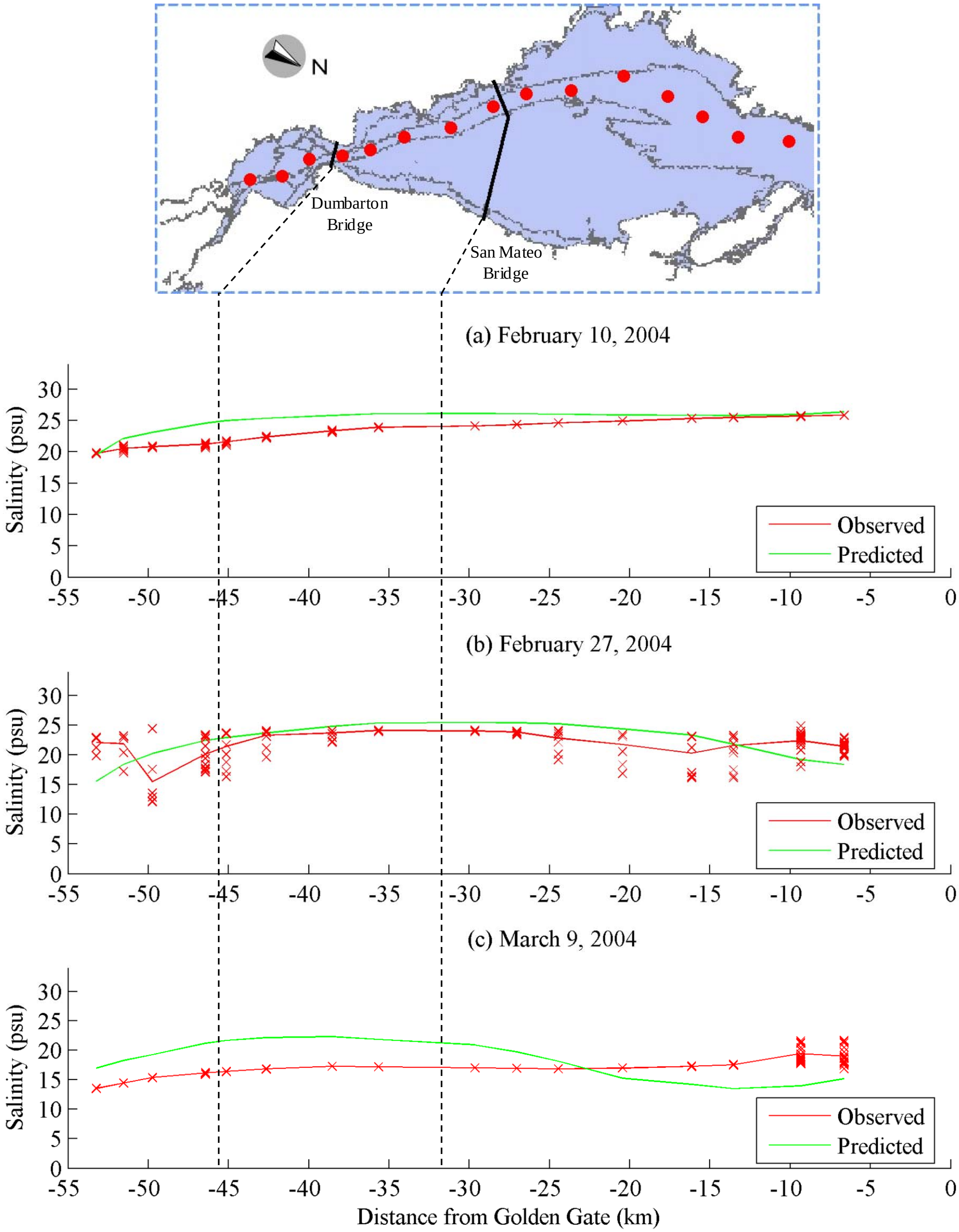

This figure compares salinity data collected by the USGS San Francisco Bay Water Quality Monitoring Program against modeled predictions at the same stations. The observation data shows all samples collected during the USGS depth transect; the observed line is plotted through the depth-averaged values.

figure 10-22

South Bay Salt Pond Restoration Project

South Bay Winter 2004 Salinity Transect

PWA